



Dipl.-Ing Jakov Ivković

**Studies Towards the Structure-based Design of Inhibitors of
Dipeptidyl Peptidase-3 and Rhodesain**

DOCTORAL THESIS

to achieve the university degree of

Doktor der Naturwissenschaften

submitted to

Graz University of Technology

Supervisor

Univ.-Prof. Dipl.-Ing. Dr.rer.nat. R. Breinbauer
Institute of Organic Chemistry

Univ.-Prof. Dr.rer.nat. P. Macheroux
Institute of Biochemistry

Graz, December 2015

AFFIDAVIT

I declare that I have authored this thesis independently, that I have not used other than declared sources/resources, and that I have explicitly indicated all material which has been quoted either literally or by content from the sources used. The text document uploaded to TUGRAZonline is identical to the present doctoral thesis.

Date

Signature

The primary part of this PhD thesis, titled “Studies Towards the Structure-based Design and Synthesis of Peptidomimetic Transition State Mimicking Inhibitors of Dipeptidyl Peptidase-3”, was completed under supervision of Univ. Prof. Dipl.-Ing. Dr. rer. nat. Rolf Breinbauer at the Institute of Organic Chemistry and the Institute of Biochemistry at the Faculty of Technical Chemistry, Chemical & Process Engineering and Biotechnology at Graz University of Technology between August 2011 and October 2015.

The second part, titled “Synthesis of New Triazine Nitrile Inhibitors of Rhodesain and hCatL for Probing of Amide- π Stacking Interactions” was completed under supervision of Prof. Dr. François Diederich and Maude Giroud at the Department of Chemistry and Applied Biosciences, Laboratory of Organic Chemistry, ETH Zurich between July and December 2014.

*To my family
Mome ćáci, mami, seki i braci*

Acknowledgments

Making my PhD research in Graz was an amazing experience, which wouldn't be anywhere near completion without some great people and many pleasant experiences with them.

First of all I would like to thank my supervisor Prof. Rolf Breinbauer for drafting me into the DK Molecular Enzymology to do an exciting research in his group. Thank you for all the guidance, motivation and invaluable experience that you shared with me and everything else that I have learned from you, especially how to present better!

Special gratitude goes to the most awesome doctoral programme, DK Molecular Enzymology, which provided me with the financial and administrative means to undertake my studies and research in Graz. Special thanks to Prof. Ellen Zechner as the speaker of the organization and Dr. Kristina Schild, who so kindly and promptly responded to my requests and calls for help with the administrative stuff and more.

I would like to express my gratitude to the members of my thesis committee for all the constructive guidance through my efforts in performing the research: Prof. Peter Macheroux, Prof. Karl Gruber, Prof. Robert Zimmermann and Prof. Wolfgang Kroutil. I am also grateful to members of their research groups for help and patience in explaining me the complex world of structural biology, pharmacology and the aspects of biochemistry which were required to enhance my work. Particularly, I would like to thank Prashant Kumar, Shalinee Jha, Sylvia Wallner and Alexandra Binter for great contribution to my project and for kind support. Thank you!

I am thankful to Prof. Hansjörg Weber and Ing. Carina Illaszewicz-Trattner for immense help with the measurement of very demanding NMR-spectra, which were required in this project. I am grateful to Pal Wiliam Wallace for being a good friend, a football match mate, and for putting in his good will into recording and evaluation of 27 HRMS spectra of superb accuracy within 5 hours, for just a crate of beer. I am very thankful to Ing. Peter Plachota for the skillful technical intervention in solving all problems regarding our computer and software resources. I would like to thank Gernot Strohmeier for his patient support and providing helpful knowledge in HPLC-MS troubleshooting.

I would like to thank Astrid Nauta and Annemarie Portschy for their outstanding help in explaining and solving various administrative formalities, helping to fill in a great deal of documents and forms. They were very kind and they were cheerful faces even on most cloudy days.

I am very grateful to the whole Institute of Organic Chemistry, TU Graz for providing a friendly atmosphere and support in research activities.

Probably the most important factor in life at the Institute were my colleagues from the Breinbauer group. Thank you very, very much for existing there, having fun, helping me in experiments, sharing useful thoughts on research, making superb cakes, helping to clean out mess, bringing me a reviving shot of coffee, mental support in rough times, mumbling or whistling some cheerful tunes, giving compliments I didn't deserve, etc.

After one year in the group, I was both very glad and sad that Joanna Wroblewski already finished her PhD and needed to move. I thank her for a lot of support, motivation, help and pleasant moments with our common ally coffee and other friends. Special thanks to a great friend Jakob Pletz for relaxing and creative talks, exquisite tea selections from around the world, for always having supportive words for me, and a sincere constructive critique when necessary. I thank the good Chinese spirit of the Institute, Xuepu Yu, for often having interesting stories to break the daily routine with some thoughts about far eastern societies, sometimes accompanied by his own handmade Chinese dumplings or other delicacies. Big thanks to Mario Faber for great company and timely alerts for low caffeine levels.

Thank you, Mario Leypold, for those awesome Styrian wines and four years of conditioning in understanding Styrian dialects! Of course, right (or left, in the social room) next to Mario one should thank Melanie Trobe, the master of cakes! I thank Kathrin Heckenbichler for relaxing chats, support in the lab, having always nice words and for really pleasant welcome whenever I was back at the Institute after some trips. Danke, werte Kollegen, Marko Kljaić, Patrick Dobrounig und Felix Anderl, für Spass mit Puntis! Thank you, Carina Doler, for Steven King's "*Das Mädchen*"! Thank you too, Nikolaus Guttenberger, Christian Pichler and Julia Blesl!

A share of gratitude certainly needs to be given to my students who skillfully worked on their theses: Christian Leypold, Marina Toplak and Christian Lembacher-Fadum. I thank also the lab project students and guest researchers for their contributions: Manuel Hollauf, Haitham Hassan, Ivana Rajković, Marina Kovačević and Jovana Trifunović.

I was glad to share some nice moments with the German team of PhDs who were in here, during my initial period in the group: Nicole Mayer, Martin Peters, Jana Rentner and Hilmar Schröder. They have also provided significant technical and friendly support.

I am grateful to Prof. Dr. François Diederich from ETH Zürich for hosting me for my abroad research stay in his research group. In his group I have gained invaluable knowledge and skills which contributed to the success of my PhD project. I am very grateful to the most kind secretary in the universe, Mrs. Irma Näf, for taking care of administration in advance and during my stay in Zürich. Massive thanks to Maude Giroud, for having me assisting on her project and for providing a great company in coffee breaks, beach volleyball sessions at Höggerberg, and other memorable occasions. The view, the mood, the productivity and apéros (the most important research enhancing activities at ETH) on the top of the hill above Zürich wouldn't be so engaging without Jovana Milić, Oliver Dumele, Elke Persch, Tristan Reekie, Çağatay Dengiz, Haraldur Gardarsson, Michael Harder, Etienne Donckele, Geoffrey Schwertz and other members of the Diederich group and guests from the neighbouring floors. Special thanks to Prof. Jack D. Dunitz for honoring me with his pleasant and inspirational company during the Diederich group Christmas dinner 2014, and for the courtesy of the first-hand account on life and great achievements of Vladimir Prelog.

I would like to thank all my dear friends that I have got to know in Graz for the unforgettable moments: I want to thank Heikki Tolvanen, Zalina Magomedova, Altijana Hromić, Anđela Đorđić, Domen Zafred, Vid Flis, Hrvoje Turčić, Pašo Sivro, Venugopal Gudipati, and some pictures of Monica Bellucci. During my time in Graz I had a real privilege of being just three hours from Zagreb. I thank Trpimir Ivšić and Elena Primorac for philosophical and even some spiritual guidance. I thank Mario Kovač and his future wife Iva Keser for great company on numerous occasions, and for computer- and textile-related favors. I thank Toni and Ivana Drazenović for some nice time in Zürich. I thank my friends from the “Znanost na eteru” crew: Ana Knezović and Bojan Markičević. Great thanks to friends and ex coworkers from Pliva Zagreb: Sanela Mutka, Jelena Sruck and Mislav Runje. Big thanks also to my previous principal investigators Nikola Basarić and Prof. Kata Majerski, and colleagues and coworkers from IRB: Jelena Veljković, Vesna Bregović and Marija Renić, Enidija Luksa, Marina Šekutor, Tatjana Ramljak and Nikola Cindro. I express big gratitude to Prof. Nenad Judaš, Prof. Ernest Meštrović, Prof. Marina Cindrić and Prof. Srđanka Tomić-Pisarović for their support and believing in me.

The most important support was provided by my family, my parents and my sister and brother, who unconditionally supported me my whole life in ideas and actions which brought me to the point where I am now and where I am heading to. Fala vam neizmjereno, tata, mama, sestri i brate! Vi ste posvetili veliki dio sebe meni. Ja vama posvećujem ovaj rad.

*“Es ist überall nichts in der Welt, ja überhaupt auch außer derselben zu denken
möglich, was ohne Einschränkung für gut könnte gehalten werden, als allein ein
guter Wille.”*

Immanuel Kant, 1724–1804

Abstract

The majority of metalloproteases have a zinc cation cofactor coordinated by conserved amino acid residues. In terms of abundance and essential roles these enzymes are among the dominant classes of enzymes in all living organisms. These molecular machines maintain homeostasis of various sorts of proteins and peptides performing important roles.

A zinc metallopeptidase called dipeptidyl peptidase-3 (DPP3), which degrades shorter peptides with 4–12 amino acid residues, has a particular affinity to opioid peptides and some of the vasoconstrictor peptides from renin-angiotensin-aldosterone system. It has been associated with pain signaling, cardiovascular pressure regulation and enhancement of cancer cell defense against oxidative stress. The precise role of DPP3 is still unknown.

The availability of the first cocrystal structure of human DPP3 (hDPP3) with a peptide substrate provided the foundation of structure-based design of selective inhibitors for this enzyme. The main objective is creation of small-molecule inhibitors as tools for chemical probing of the role of DPP3 *in vivo*. In this thesis the development of peptidomimetic transition state mimicking inhibitors is presented. The hydroxyethylene transition state isostere was used to replace the scissile peptide bond in the peptide substrate mimetic inhibitors, instead of conventionally used zinc-chelating moieties. Two epimers of hydroxyethylene based mimetics have been synthesized and they successfully inhibited recombinant hDPP3 at low micromolar concentrations. This case represents the first demonstration of efficient inhibition of a metalloprotease by a hydroxyethylene pseudopeptide. Among smaller synthesized peptidomimetic analogues, an *N*-terminal niacin ketomethylene pseudopeptide was found as a new lead molecule for further design in the direction of bioavailable inhibitors.

Additionally, in the scope of synthesis of the peptidomimetic inhibitors a new rapid and efficient method for the synthesis of chiral α -amino aldehydes from proteinogenic α -amino acids has been developed.

In another project a selection of triazine nitrile inhibitors of a cysteine protease have been synthesized. This protease, rhodesain, is a target for fighting African Sleeping Sickness. The nitrile inhibitors will serve for characterization of amide- π stacking interactions in the design of enzyme inhibitors.

Zusammenfassung

Die Mehrheit aller Metalloproteasen besitzt ein Zink-Kation als Cofaktor, das durch konservierte Aminosäurereste koordiniert ist. Diese Proteasen gehören zu einer der wichtigsten Klassen von Enzymen in allen lebenden Organismen. Als molekulare Maschinen erhalten sie die Homöostase verschiedener Proteine und Peptide.

Dipeptidylpeptidase-3 (DPP3) ist eine Zink-Metallopeptidase mit Affinität zu Opioidpeptiden und einigen Vasokonstriktor-Peptiden aus dem Renin-Angiotensin-Aldosteron-System, die kürzere Peptide mit 4–12 Aminosäureresten hydrolysiert. Die genaue Rolle von DPP3 ist jedoch noch unbekannt, aber es wird angenommen, dass sie in Zusammenhang mit der Schmerzweiterleitung, der Regelung des Blutdrucks und der Fähigkeit von Krebszellen steht, sich verstärkt gegen oxidativen Stress zu verteidigen.

Durch die Verfügbarkeit der ersten Co-Kristallstruktur menschlicher DPP3 (hDPP3) mit einem Peptidsubstrat ist es möglich, selektive Inhibitoren für dieses Enzym zu designen. Das Hauptziel ist die Herstellung niedermolekularer Inhibitoren, die als Werkzeug für die chemische Untersuchung der Rolle von DPP3 *in vivo* dienen. In dieser Arbeit wird die Entwicklung von Inhibitoren auf Basis von Peptidmimetika vorgestellt, die den Übergangszustand der Peptidhydrolyse nachahmen. Ein Hydroxyethylen-Isoster wurde verwendet, um die spaltbare Peptidbindung des Substratmimetikums anstelle des herkömmlich verwendeten Zink-chelatbildenden Rests zu ersetzen. Zwei Epimere der Hydroxyethylen-basierenden Mimetika wurden synthetisiert und erwiesen sich als erfolgreiche Inhibitoren von rekombinanter hDPP3 bei niedrig-mikromolaren Konzentrationen. Dieses Beispiel stellt die erste effiziente Hemmung einer Metalloprotease durch ein Hydroxyethylen-Pseudopeptid dar. Für die weitere Gestaltung von bioverfügbaren Inhibitoren wurde ein Ketomethylen-Pseudopeptid mit *N*-terminalem Niacinrest als neues Lead-Molekül gefunden, das kleiner ist als die zuvor synthetisierten peptidomimetischen Analoga.

Im Rahmen der Synthese peptidomimetischer Inhibitoren wurde zusätzlich ein neues, schnelles und effizientes Verfahren für die Synthese chiraler α -Aminoaldehyde aus proteinogenen α -Aminosäuren entwickelt.

In einem anderen Projekt wurde eine Auswahl an Triazinnitril-Inhibitoren für eine Cysteinprotease synthetisiert. Diese Cysteinprotease, Rhodesain, stellt ein Zielprotein für die

Bekämpfung der Afrikanischen Schlafkrankheit dar. Die Triazinnitril-Inhibitoren dienen zur Charakterisierung von Amid- π Wechselwirkungen beim Design der Enzyminhibitoren.

Part of this thesis has been published in

“A Rapid and Efficient One-pot Method for the Reduction of N-Protected α -Amino Acids to Chiral α -Amino Aldehydes Using CDI/DIBAL-H” J. Ivković, C. Lembacher-Fadum, R. Breinbauer, *Org. Biomol. Chem.* **2015**, *13*, 10456–10460.

DOI: 10.1039/C5OB01838B

TABLE OF CONTENT

1	Studies Towards the Structure-based Design and Synthesis of Peptidomimetic Transition State Mimicking Inhibitors of Dipeptidyl Peptidase-3.....	1
1.1	Introduction.....	2
1.2	State of the Art	4
1.2.1	Zinc Metalloproteases	4
1.2.1.1	Carboxypeptidase A.....	5
1.2.1.2	Thermolysin	7
1.2.1.3	Other Zinc Metallopeptidases	9
1.2.2	Dipeptidyl Peptidase-3 (DPP3).....	11
1.2.2.1	Discovery.....	11
1.2.2.2	Pathophysiological Indications.....	12
1.2.2.2.1	Protein Turnover.....	12
1.2.2.2.2	Nociception.....	12
1.2.2.2.3	Inflammation and Blood Pressure Regulation.....	13
1.2.2.2.4	Defense Against Oxidative Stress - Cancer Related Implications.....	13
1.2.2.3	Structure of hDPP3	15
1.2.2.4	Structure of hDPP3 in Complex with Opioid Peptide Tynorphin.....	16
1.2.2.5	Mechanism of Action of DPP3	18
1.2.2.6	Known Substrates and Inhibitors.....	21
1.2.3	Structure-based Approaches in Inhibitor Drug Design.....	26
1.2.3.1	General Aspects	26
1.2.3.2	Historical Milestones in Structure-based Design.....	27
1.2.3.3	Lead Compound Design via Extensive Database Searches	28
1.2.3.4	Peptidomimetics.....	30
1.2.3.5	Inhibitors of metalloproteases	36
1.2.3.5.1	Development of Inhibitors of Angiotensin Converting Enzyme	36
1.2.3.5.2	Development of Matrix Metalloprotease Inhibitors	40
1.2.3.6	Inhibitors of Serine Proteases	46
1.2.3.6.1	Inhibitors of Thrombin.....	48
1.2.3.6.2	Saxagliptin - Case Study in Inhibition of DPP4.....	51
1.2.3.7	Inhibitors of Cysteine Proteases	53
1.2.3.8	Inhibitors of Aspartic Proteases.....	58
1.2.3.8.1	Development of HIV-1 Protease Inhibitors.....	62
1.3	Aims of Work	66
1.4	Results and Discussion.....	68
1.4.1	Structure-based Design of Inhibitors of hDPP3	68
1.4.1.1	Hydroxyethylene-based Transition State Mimetics of Tynorphin	68
1.4.2	Synthesis of (S)-Hydroxyethylene Pseudopeptide.....	70
1.4.2.1	Retrosynthetic Analysis	70
1.4.2.2	Preparation of Boc-Pro-Trp-OMe Dipeptide.....	71
1.4.2.3	Stereoselective Synthesis of the Core Pseudodipeptide.....	72
1.4.2.4	Completion of the (S)-Hydroxyethylene Pseudopentapeptide.....	77
1.4.2.5	Summary of the Synthesis of SHE	81

1.4.3	Synthesis of (<i>R</i>)-Hydroxyethylene Pseudopeptide	82
1.4.3.1	Summary of the Synthesis of <i>HER</i>	86
1.4.4	Design and Synthesis of Smaller Pseudopeptide Analogues	87
1.4.4.1	Short Hydroxyethylene Pseudopeptide Analogues	87
1.4.4.2	Synthesis of the Short Hydroxyethylene Analogues	89
1.4.4.3	Short Ketomethylene Pseudopeptide Analogues	91
1.4.5	Development of CDI/DIBAL-H Method for the Synthesis of Chiral α -Amino Aldehydes from α -Amino Acids	94
1.4.5.1	Existing Methods for Synthesis of α -Amino Acids	94
1.4.5.2	Development of CDI/DIBAL-H Method	95
1.4.6	<i>In Vitro</i> Evaluation of the Proposed Peptidomimetic Inhibitors	102
1.4.6.1	Isothermal Microcalorimetry Assay	102
1.4.6.2	Inhibition of hDPP3 with Hydroxyethylene Transition State Mimetics	104
1.4.6.3	Inhibition of hDPP3 with Shorter Peptidomimetic Hydroxyethylene and Ketomethylene Transition State Mimetics	105
1.4.7	Structure of hDPP3 in Complex with the Hydroxyethylene Transition State Mimicking Inhibitors	108
1.4.7.1	X-ray Crystallographic Structure of hDPP3-SHE Complex	108
1.4.7.2	Computer-assisted Molecular Modelling	111
1.5	Summary	114
1.6	Outlook	119
1.6.1	Lead Optimization	119
1.6.1.1	Structure-activity Relationship for Use in the Design of New Inhibitors	119
1.6.1.2	Quick and Scalable Approaches for the Synthesis of Next Generation of hDPP3 Inhibitors	123
1.6.2	Efficient Design of hDPP3 Inhibitors for <i>In Vivo</i> Studies	125
1.7	Experimental Section	127
1.7.1	Organic Chemistry Experiments	127
1.7.2	Synthesis of SHE	131
1.7.2.1	<i>tert</i> -Butyl <i>N</i> -[(2 <i>S</i>)-3-methyl-1-oxobutan-2-yl]carbamate (2)	131
1.7.2.2	Racemic <i>tert</i> -butyl <i>N</i> -[(2 <i>S</i>)-3-methyl-1-oxobutan-2-yl]carbamate (<i>rac</i> -2)	132
1.7.2.3	Ethyl (5 <i>S</i>)-5-[[<i>tert</i> -butoxy]carbonyl]amino]-4-hydroxy-6-methylhept-2-ynoate (3)	133
1.7.2.4	<i>tert</i> -Butyl <i>N</i> -[(1 <i>S</i>)-2-methyl-1-[(2 <i>S</i>)-5-oxooxolan-2-yl]propyl]carbamate (4) and <i>tert</i> -butyl <i>N</i> -[(1 <i>S</i>)-2-methyl-1-[(2 <i>R</i>)-5-oxooxolan-2-yl]propyl]carbamate (5)	134
1.7.2.5	<i>tert</i> -Butyl <i>N</i> -[(1 <i>S</i>)-1-[(2 <i>S</i> ,4 <i>R</i>)-4-benzyl-5-oxooxolan-2-yl]-2-methylpropyl]carbamate (6)	136
1.7.2.6	(2 <i>R</i> ,4 <i>S</i> ,5 <i>S</i>)-2-Benzyl-5-[[<i>tert</i> -butoxy]carbonyl]amino]-4-[(<i>tert</i> -butyldimethylsilyloxy)-6-methylheptanoic acid (7)	138
1.7.2.7	<i>tert</i> -Butyl (2 <i>S</i>)-2-[[[(2 <i>S</i>)-3-(1 <i>H</i> -indol-3-yl)-1-methoxy-1-oxopropan-2-yl]carbonyl]pyrrolidine-1-carboxylate (1)	140
1.7.2.8	Methyl (2 <i>S</i>)-2-[[[(2 <i>S</i>)-1-[(2 <i>R</i> ,4 <i>S</i> ,5 <i>S</i>)-2-benzyl-5-[[<i>tert</i> -butoxy]carbonyl]amino]-4-[(<i>tert</i> -butyldimethylsilyloxy)-6-methylheptanoyl]pyrrolidin-2-yl]formamido]-3-(1 <i>H</i> -indol-3-yl)propanoate (8)	141
1.7.2.9	Methyl (2 <i>S</i>)-2-[[[(2 <i>S</i>)-1-[(2 <i>R</i> ,4 <i>S</i> ,5 <i>S</i>)-2-benzyl-5-[(2 <i>S</i>)-2-[[<i>tert</i> -butoxy]carbonyl]amino]-3-methylbutanamido]-4-hydroxy-6-methylheptanoyl]pyrrolidin-2-yl]formamido]-3-(1 <i>H</i> -indol-3-yl)propanoate (9)	143
1.7.2.10	Reference epimer mixture microsynthesis:	146
1.7.2.11	(2 <i>S</i>)-2-[[[(2 <i>S</i>)-1-[(2 <i>R</i> ,4 <i>S</i> ,5 <i>S</i>)-5-[(2 <i>S</i>)-2-azaniumyl-3-methylbutanamido]-2-benzyl-4-hydroxy-6-methylheptanoyl]pyrrolidin-2-yl]formamido]-3-(1 <i>H</i> -indol-3-yl)propanoate (10)	147
1.7.3	Synthesis of <i>HER</i>	149
1.7.3.1	<i>tert</i> -Butyl <i>N</i> -[(1 <i>S</i>)-1-[(2 <i>R</i> ,4 <i>R</i>)-4-benzyl-5-oxooxolan-2-yl]-2-methylpropyl]carbamate (11)	149
1.7.3.2	(2 <i>R</i> ,4 <i>R</i> ,5 <i>S</i>)-2-Benzyl-5-[[<i>tert</i> -butoxy]carbonyl]amino]-4-[(<i>tert</i> -butyldimethylsilyloxy)-6-methylheptanoic acid (12)	151
1.7.3.3	Methyl (2 <i>R</i>)-2-[[[(2 <i>S</i>)-1-[(2 <i>R</i> ,4 <i>S</i> ,5 <i>S</i>)-2-benzyl-5-[[<i>tert</i> -butoxy]carbonyl]amino]-4-[(<i>tert</i> -butyldimethylsilyloxy)-6-methylheptanoyl]pyrrolidin-2-yl]formamido]-3-(1 <i>H</i> -indol-3-yl)propanoate (13)	153
1.7.3.4	Methyl (2 <i>R</i>)-2-[[[(2 <i>S</i>)-1-[(2 <i>R</i> ,4 <i>S</i> ,5 <i>S</i>)-2-benzyl-5-[(2 <i>S</i>)-2-[[<i>tert</i> -butoxy]carbonyl]amino]-3-methylbutanamido]-4-hydroxy-6-methylheptanoyl]pyrrolidin-2-yl]formamido]-3-(1 <i>H</i> -indol-3-yl)propanoate (14)	155
1.7.3.5	(2 <i>S</i>)-2-[[[(2 <i>S</i>)-1-[(2 <i>R</i> ,4 <i>R</i> ,5 <i>S</i>)-5-[(2 <i>S</i>)-2-Azaniumyl-3-methylbutanamido]-2-benzyl-4-hydroxy-6-methylheptanoyl]pyrrolidin-2-yl]formamido]-3-(1 <i>H</i> -indol-3-yl)propanoate (15)	157

1.7.4	Synthesis of Shorter Peptidomimetics.....	160
1.7.4.1	(4 <i>S</i> ,5 <i>S</i>)-5-[(<i>tert</i> -Butoxy)carbonyl]amino]-4-[(<i>tert</i> -butyldimethylsilyloxy)]-6-methylheptanoic acid (16)	160
1.7.4.2	<i>tert</i> -Butyl <i>N</i> -[(3 <i>S</i> ,4 <i>S</i>)-4-[(<i>tert</i> -butyldimethylsilyloxy)]-6-[[<i>(1S)</i> -1-carbamoyl-2-phenylethyl]carbamoyl]-2-methylhexan-3-yl]carbamate (17)	162
1.7.4.3	<i>tert</i> -Butyl ((2 <i>S</i> ,3 <i>S</i>)-1-(((3 <i>S</i> ,4 <i>S</i>)-7-(((<i>S</i>)-1-amino-1-oxo-3-phenylpropan-2-yl)amino)-4-hydroxy-2-methyl-7-oxoheptan-3-yl)amino)-3-methyl-1-oxopentan-2-yl)carbamate (18).....	163
1.7.4.4	(2 <i>S</i> ,3 <i>S</i>)-1-(((3 <i>S</i> ,4 <i>S</i>)-7-(((<i>S</i>)-1-Amino-1-oxo-3-phenylpropan-2-yl)amino)-4-hydroxy-2-methyl-7-oxoheptan-3-yl)amino)-3-methyl-1-oxopentan-2-aminium 2,2,2-trifluoroacetate (19)	165
1.7.4.5	(2 <i>S</i> ,3 <i>S</i>)-2-Hydroxy-3-methylpentanoic acid (20)	166
1.7.4.6	(4 <i>S</i> ,5 <i>S</i>)- <i>N</i> -((<i>S</i>)-1-Amino-1-oxo-3-phenylpropan-2-yl)-4-hydroxy-5-((2 <i>S</i> ,3 <i>S</i>)-2-hydroxy-3-methylpentanamido)-6-methylheptanamide (21).....	167
1.7.4.7	Methyl 5-bromo-4-oxopentanoate (22)	169
1.7.4.8	Methyl 5-azido-4-oxopentanoate (23)	170
1.7.4.9	Methyl 5-((<i>tert</i> -butoxycarbonyl)amino)-4-oxopentanoate (24).....	171
1.7.4.10	5-((<i>tert</i> -Butoxycarbonyl)amino)-4-oxopentanoic acid (25).....	172
1.7.4.11	<i>tert</i> -Butyl <i>N</i> -(4-[[<i>(1S)</i> -1-carbamoyl-2-phenylethyl]carbamoyl]-2-oxobutyl)carbamate (26)	173
1.7.4.12	(2 <i>S</i> ,3 <i>S</i>)- <i>N</i> -(4-[[<i>(1S)</i> -1-Carbamoyl-2-phenylethyl]carbamoyl]-2-oxobutyl)-2-hydroxy-3-methylpentanamide (27).....	174
1.7.4.13	<i>N</i> -[(<i>1S</i>)-1-Carbamoyl-2-phenylethyl]-4-oxo-5-(pyridin-3-ylformamido)pentanamide (28)	176
1.7.4.14	<i>N</i> -[(<i>1S</i>)-1-Carbamoyl-2-phenylethyl]-5-methanesulfonamido-4-oxopentanamide (29)	178
1.7.4.15	<i>N</i> -[(<i>1S</i>)-1-Carbamoyl-2-phenylethyl]-4-oxo-5-(2,2,2-trifluoroethanesulfonamido)pentanamide (30).....	179
1.7.5	Synthesis of Chiral <i>N</i> -protected α -Amino Aldehydes via CDI/DIBAL-H Method	182
1.7.5.1	Purification of CDI (1,1'-carbonyldiimidazole)	182
1.7.5.2	General procedure for one-pot conversion of <i>N</i> -protected α -amino acids to <i>N</i> -protected α -amino aldehydes	182
1.7.5.3	<i>tert</i> -Butyl (<i>S</i>)-(1-oxopropan-2-yl)carbamate (32).....	183
1.7.5.4	<i>tert</i> -Butyl (<i>S</i>)-(1-oxo-3-phenylpropan-2-yl)carbamate (33).....	184
1.7.5.5	Racemic <i>tert</i> -butyl (1-oxo-3-phenylpropan-2-yl)carbamate (rac-33)	185
1.7.5.6	<i>tert</i> -Butyl (<i>S</i>)-2-formylpyrrolidine-1-carboxylate (34)	186
1.7.5.7	<i>tert</i> -Butyl (2 <i>S</i>)-2-(hydroxymethyl)pyrrolidine-1-carboxylate (44)	187
1.7.5.8	Racemic <i>tert</i> -butyl 2-(hydroxymethyl)pyrrolidine-1-carboxylate (rac-44).....	188
1.7.5.9	<i>tert</i> -Butyl (<i>S</i>)-(4-(methylthio)-1-oxobutan-2-yl)carbamate (35).....	189
1.7.5.10	Racemic <i>tert</i> -butyl (4-(methylthio)-1-oxobutan-2-yl)carbamate (rac-35).....	190
1.7.5.11	<i>tert</i> -Butyl ((2 <i>S</i> ,3 <i>S</i>)-3-methyl-1-oxopentan-2-yl)carbamate (36)	190
1.7.5.12	Partial epimerization of <i>tert</i> -butyl ((2 <i>S</i> ,3 <i>S</i>)-3-methyl-1-oxopentan-2-yl)carbamate ((2 <i>S</i> ,3 <i>S</i>)-36) to <i>tert</i> -butyl ((2 <i>R</i> ,3 <i>S</i>)-3-methyl-1-oxopentan-2-yl)carbamate ((2 <i>R</i> ,3 <i>S</i>)-36).....	191
1.7.5.13	Methyl (<i>S</i>)-3-((<i>tert</i> -butoxycarbonyl)amino)-4-oxobutanoate (37)	193
1.7.5.14	Benzyl (<i>S</i>)-(4-methyl-1-oxopentan-2-yl)carbamate (38)	194
1.7.5.15	Racemic benzyl (4-methyl-1-oxopentan-2-yl)carbamate (rac-38).....	195
1.7.5.16	Benzyl (<i>S</i>)-(1-oxo-3-phenylpropan-2-yl)carbamate (39).....	195
1.7.5.17	Benzyl (<i>S</i>)-(1-hydroxy-3-phenylpropan-2-yl)carbamate (45).....	196
1.7.5.18	Racemic benzyl (1-hydroxy-3-phenylpropan-2-yl)carbamate (rac-45).....	198
1.7.5.19	Benzyl (<i>S</i>)-(1-oxopropan-2-yl)carbamate (40)	199
1.7.5.20	Benzyl <i>N</i> -[(2 <i>S</i>)-1-hydroxypropan-2-yl]carbamate (46)	200
1.7.5.21	Racemic benzyl <i>N</i> -[1-hydroxypropan-2-yl]carbamate (rac-46).....	201
1.7.5.22	(9 <i>H</i> -Fluoren-9-yl)methyl (<i>S</i>)-2-formylpyrrolidine-1-carboxylate (41)	202
1.7.5.23	9 <i>H</i> -Fluoren-9-ylmethyl (2 <i>S</i>)-2-(hydroxymethyl)pyrrolidine-1-carboxylate (47).....	203
1.7.5.24	Racemic 9 <i>H</i> -fluoren-9-ylmethyl (2 <i>S</i>)-2-(hydroxymethyl)pyrrolidine-1-carboxylate (rac-47).....	204
1.7.5.25	(9 <i>H</i> -Fluoren-9-yl)methyl benzyl (6-oxohexane-1,5-diyl)(<i>S</i>)-dicarbamate (42)	205
1.7.5.26	<i>tert</i> -Butyl (<i>S</i>)-(2-oxo-1-phenylethyl)carbamate (43)	207

1.7.5.27	Racemic <i>tert</i> -butyl (2-oxo-1-phenylethyl)carbamate (rac-43)	208
1.7.6	Biological Assays	209
1.7.6.1	Isothermal Microcalorimetry	209
1.7.6.1.1	Binding of SHE to hDPP3	209
1.7.6.2	Fluorescence-based Inhibition Assays	211
1.7.6.3	X-ray Structure Determination	212
2	Synthesis of New Triazine Nitrile Inhibitors of Rhodesain and hCatL for Probing of Amide-π Stacking Interactions	213
2.1	Introduction	214
2.2	State of the Art	215
2.2.1	Noncovalent Interactions in Molecular Recognition	215
2.2.1.1	Amide- π Stacking	215
2.2.2	Inhibitors for Targeting African Sleeping Sickness	218
2.2.2.1	African Sleeping Sickness	218
2.2.2.2	Cysteine Proteases Targeted in African Sleeping Sickness	218
2.2.3	Chemistry of Selected Heterocycles	220
2.2.3.1	Triazines	220
2.2.3.2	Indazoles	223
2.3	Aims of Work	227
2.4	Synthesis of Triazine Nitrile Inhibitors	229
2.4.1	Structure and Synthesis of the Triazine Nitrile Scaffold	229
2.4.2	Synthesis of Indazole Series of Target Compounds	231
2.4.2.1	Bromomethyl Indazoles	231
2.4.2.2	Completion of the Indazole Series	232
2.4.3	Synthesis of an Imidazopyridine Derivative	234
2.4.3.1	The Imidazopyridine Aldehyde	234
2.4.3.2	Completion of the Imidazopyridine Derivative	234
2.4.4	Synthesis of a Pyridazine Derivative	235
2.4.4.1	The Pyridazine Aldehyde	235
2.4.4.2	Completion of the Pyridazine Derivative	236
2.4.5	Synthesis of Fluoropyridine Derivatives	237
2.4.5.1	Reductive Amination Towards Fluoropyridine Amines	237
2.4.5.2	Methodology Adaptation for Selective Triazine Substitution	238
2.4.5.3	Completion of Fluoropyridine Derivatives	241
2.5	Results and Discussion	242
2.5.1	Inhibition Assays with Rhodesain and hCatL	242
2.5.2	Computer Assisted Molecular Modelling	243
2.6	Summary and Outlook	250
2.7	Experimental Section	251
2.7.1	General procedures	251
2.7.1.1	General Procedure A (methylindazoles)	251
2.7.1.2	General Procedure B (N-Boc-methylindazoles)	251
2.7.1.3	General Procedure C (N-Boc-bromomethylindazoles)	251
2.7.1.4	General Procedure D (N-Boc-bromomethylindazoles)	252
2.7.1.5	General Procedure E (protected indazole triazine nitriles)	252
2.7.1.6	General Procedure F (indazole triazine nitriles)	252

2.7.1.7	General Procedure G (fluoropyridinyl(cyclopentyl)amine):	253
2.7.1.8	General Procedure H (fluoropyridinyl triazine chlorides):	253
2.7.2	Synthesized compounds	254
2.7.2.1	3-Methyl-1 <i>H</i> -indazole (52a)	254
2.7.2.2	4-Methyl-1 <i>H</i> -indazole (52b)	255
2.7.2.3	7-Methyl-1 <i>H</i> -indazole (52e)	256
2.7.2.4	6-Methyl-1 <i>H</i> -indazole (52d)	257
2.7.2.5	5-Methyl-1 <i>H</i> -indazole (52c)	258
2.7.2.6	2-Methyl-2-propanyl 3-methyl-1 <i>H</i> -indazole-1-carboxylate/	259
2.7.2.7	2-Methyl-2-propanyl 4-methyl-1 <i>H</i> -indazole-1-carboxylate/	260
2.7.2.8	2-Methyl-2-propanyl 7-methyl-2 <i>H</i> -indazole-2-carboxylate	261
2.7.2.9	2-Methyl-2-propanyl 6-methyl-1 <i>H</i> -indazole-1-carboxylate	262
2.7.2.10	2-Methyl-2-propanyl 5-methyl-1 <i>H</i> -indazole-1-carboxylate/	263
2.7.2.11	2-Methyl-2-propanyl 3-(bromomethyl)-1 <i>H</i> -indazole-1-carboxylate (54a)	264
2.7.2.12	2-Methyl-2-propanyl 4-(bromomethyl)-1 <i>H</i> -indazole-1-carboxylate (54b)	265
2.7.2.13	2-Methyl-2-propanyl 7-(bromomethyl)-1 <i>H</i> -indazole-1-carboxylate/	266
2.7.2.14	2-Methyl-2-propanyl 6-(bromomethyl)-1 <i>H</i> -indazole-1-carboxylate/	267
2.7.2.15	2-Methyl-2-propanyl 5-(bromomethyl)-1 <i>H</i> -indazole-1-carboxylate/	268
2.7.2.16	2-Methyl-2-propanyl-3-({[4-cyano-6-(4-morpholinyl)-1,3,5-triazin-2-yl](cyclopentyl)amino}methyl)-1 <i>H</i> -indazole-1-carboxylate (55a)	269
2.7.2.17	2-Methyl-2-propanyl-4-({[4-cyano-6-(4-morpholinyl)-1,3,5-triazin-2-yl](cyclopentyl)amino}methyl)-1 <i>H</i> -indazole-1-carboxylate (55b)	270
2.7.2.18	2-Methyl-2-propanyl 7-({[4-cyano-6-(4-morpholinyl)-1,3,5-triazin-2-yl](cyclopentyl)amino}methyl)-1 <i>H</i> -indazole-1-carboxylate (55e)	272
2.7.2.19	2-Methyl-2-propanyl 6-({[4-cyano-6-(4-morpholinyl)-1,3,5-triazin-2-yl](cyclopentyl)amino}methyl)-1 <i>H</i> -indazole-1-carboxylate (55d)	273
2.7.2.20	2-Methyl-2-propanyl 5-({[4-cyano-6-(4-morpholinyl)-1,3,5-triazin-2-yl](cyclopentyl)amino}methyl)-1 <i>H</i> -indazole-1-carboxylate (55c)	274
2.7.2.21	4-[Cyclopentyl(1 <i>H</i> -indazol-3-ylmethyl)amino]-6-(4-morpholinyl)-1,3,5-triazine-2-carbonitrile (56a)	276
2.7.2.22	4-[Cyclopentyl(1 <i>H</i> -indazol-4-ylmethyl)amino]-6-(4-morpholinyl)-1,3,5-triazine-2-carbonitrile (56b)	277
2.7.2.23	4-[Cyclopentyl(1 <i>H</i> -indazol-7-ylmethyl)amino]-6-(4-morpholinyl)-1,3,5-triazine-2-carbonitrile (56e)	278
2.7.2.24	4-[Cyclopentyl(1 <i>H</i> -indazol-6-ylmethyl)amino]-6-(4-morpholinyl)-1,3,5-triazine-2-carbonitrile (56d)	279
2.7.2.25	4-[Cyclopentyl(1 <i>H</i> -indazol-5-ylmethyl)amino]-6-(4-morpholinyl)-1,3,5-triazine-2-carbonitrile (56c)	281
2.7.2.26	Ethyl imidazo[1,2- <i>a</i>]pyridine-2-carboxylate (57)	282
2.7.2.27	Imidazo[1,2- <i>a</i>]pyridine-2-carbaldehyde (58)	283
2.7.2.28	<i>N</i> -(Imidazo[1,2- <i>a</i>]pyridin-2-ylmethyl)cyclopentanaminium acetate (59)	284
2.7.2.29	6-(4-Morpholinyl)-4-chloro- <i>N</i> -cyclopentyl- <i>N</i> -(imidazo[1,2- <i>a</i>]pyridin-2-ylmethyl)-1,3,5-triazin-2-amine (60)	285
2.7.2.30	4-[Cyclopentyl(imidazo[1,2- <i>a</i>]pyridin-2-ylmethyl)amino]-6-(4-morpholinyl)-1,3,5-triazine-2-carbonitrile (61)	287
2.7.2.31	(<i>E</i>)-3-styrylpyridazine (62)	288
2.7.2.32	Pyridazine-3-carbaldehyde (63)	289
2.7.2.33	<i>N</i> -(Pyridazin-3-ylmethyl)cyclopentanamine (64)	290
2.7.2.34	4-Chloro- <i>N</i> -cyclopentyl-6-(4-morpholinyl)- <i>N</i> -(pyridazin-3-ylmethyl)-1,3,5-triazin-2-amine (65)	291
2.7.2.35	4-[Cyclopentyl(pyridazin-3-ylmethyl)amino]-6-(4-morpholinyl)-1,3,5-triazine-2-carbonitrile (66)	292
2.7.2.36	<i>N</i> -[(3-Fluoropyridin-4-yl)methyl]cyclopentanamine (67a)	293
2.7.2.37	<i>N</i> -[(5-Fluoropyridin-3-yl)methyl]cyclopentanamine (67b)	295
2.7.2.38	<i>N</i> -[(3-Fluoropyridin-2-yl)methyl]cyclopentanamine (67c)	296
2.7.2.39	4-Chloro- <i>N</i> -cyclopentyl- <i>N</i> -[(3-fluoropyridin-4-yl)methyl]-6-(4-morpholinyl)-1,3,5-triazin-2-amine (68a)	297
2.7.2.40	4-Chloro- <i>N</i> -cyclopentyl- <i>N</i> -[(5-fluoropyridin-3-yl)methyl]-6-(4-morpholinyl)-1,3,5-triazin-2-amine (68b)	298

2.7.2.41	4-Chloro- <i>N</i> -cyclopentyl- <i>N</i> -[(3-fluoropyridin-2-yl)methyl]-6-(4-morpholinyl)-1,3,5-triazin-2-amine (68c).....	299
2.7.2.42	4-{Cyclopentyl[(3-fluoropyridin-4-yl)methyl]amino}-6-(morpholin-4-yl)-1,3,5-triazine-2-carbonitrile (69a).....	301
2.7.2.43	4-{Cyclopentyl[(5-fluoropyridin-3-yl)methyl]amino}-6-(morpholin-4-yl)-1,3,5-triazine-2-carbonitrile (69b).....	302
2.7.2.44	4-{Cyclopentyl[(3-fluoropyridin-2-yl)methyl]amino}-6-(morpholin-4-yl)-1,3,5-triazine-2-carbonitrile (69c).....	303
3	References	304
4	Abbreviations	329
5	Appendix	335
5.1	Bibliographic Data	335
5.2	Curriculum Vitae	335
5.3	List of Publications	337

1

**Studies Towards the Structure-based Design and
Synthesis of Peptidomimetic Transition State
Mimicking Inhibitors of Dipeptidyl Peptidase-3**

1.1 Introduction

The development of enzyme inhibitors is driven by the necessity of investigating the roles of enzymes in organisms, and for the purpose of validating enzymes as drug targets. It is most intensely performed in the early stages of drug development. Many drugs on the market are enzyme inhibitors, and the average cost to develop a drug is currently 2.6 billion USD.^[1] To effectively find inhibitor drug candidates, it is important to establish reliable structure-activity relationships on how the drug reaches and binds the target.^[2]

New scientific breakthroughs in investigations of characteristics which make a good ligand to a receptor in biological systems, are some of the major factors that can accelerate the rational development of good enzyme inhibitors. When an interesting new protein is validated as a potential drug target, it is usually possible to obtain the related structural data. Structural biology methods are being constantly developed and improved, e.g. x-ray crystallography and cryoelectron microscopy.^[3,4] Once the structural basis of the function of a macromolecule is known, medicinal chemists can engage in structure-based design of molecules that will address the known binding site.

Aspects that need to be addressed are shape complementarity and the thermodynamics of noncovalent interactions.^[5,6] A good ligand will fill in the binding site as much as possible, have as many as possible noncovalent interactions to the receptor, and the enthalpy of those interactions should greatly overcome the enthalpy of solvation of the ligand in the environment outside the binding site. The role of water is one important factor to consider on its own right, since it is omnipresent as the solvent and ligand.^[7]

Structural research on metallopeptidases intensified from the middle of the 20th century, when prominent scientists, like the Nobel laureate William N. Lipscomb, started their work on metalloenzymes. For over 50 years it has led to a vast literature output in zinc enzymology. Zinc is the second most abundant metal in biology (following iron), represented in all classes of metalloenzymes, especially metalloproteases.^[8] Our present knowledge about metalloproteases is very far from being complete and surprising new enzymes in the class are still being discovered. Many of them have been validated as drug targets and are being subject of intense drug development.^[9,10]

An interesting group of zinc metallopeptidases was found to be associated with the degradation of enkephalins – opioid peptides involved in signaling related to pain perception (Figure 1). The enzymes, collectively labelled as enkephalinases, are aminopeptidase N (APN, recently also associated to malignant development), neutral endopeptidase (NEP, neprilysin, enkephalinase A) and dipeptidyl peptidase-3 (DPP3, enkephalinase B). While roles and structures of APN and neprilysin have been subject of intense research and drug development efforts,^[8,11–14] DPP3 is still considerably uninvestigated,^[15] with fewer structures available,^[16,17] indications in involvement in opioid peptide signalling and progression of cancer,^[18] and no presently confirmed phenotype. These very important indications make DPP3 a very interesting physiological player and a potential, latent drug target.

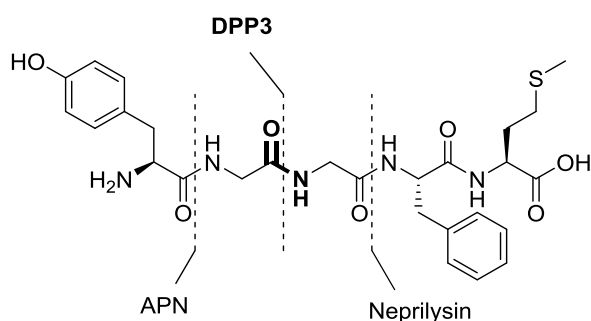


Figure 1 Enkephalinase enzymes and the corresponding cleavage sites on Met-enkephalin.

The present knowledge about DPP3 shows a general lack of inhibitors for the enzyme. In particular there are no inhibitors specifically designed to be selective for this enzyme, except for substrate inhibitor peptides which are being degraded by the enzyme itself and have very short lifetimes in blood serum.^[17,19–21] In order to provide the supporting tools to the efforts in DPP3 enzymology, the current knowledge prompted us to develop small-molecule inhibitors of DPP3.

1.2 State of the Art

1.2.1 Zinc Metalloproteases

Involvement in cell proliferation, differentiation of the extracellular matrix (ECM) to vascularization and cell migration are just some of the aspects of importance of metalloproteases in the biology of eukaryotes. These events occur multiple times during organogenesis in normal cellular development and in tumor progression. There are several modes of metalloprotease action in this context.^[22] Growth factors become available to cells which are not in direct physical contact through proteolytic cleavage by metalloproteases. Metalloproteases degrade the ECM to enable mobility of the founder cells across tissues into nearby stroma. A very important role of these enzymes is also found in regulated receptor cleavage to terminate migratory signaling. The precisely organized interplay of matrix metalloproteases (MMPs)^[9] or metalloprotease-disintegrins (ADAMs)^[23] and natural tissue inhibitors of metalloproteases (TIMPs)^[24] is required for balance in the aforementioned processes.

In the second half of the 20th century, continuous advancements in metalloprotease enzymology revealed that the degradation of constituents of the extracellular matrix represents only a fraction of the roles of these enzymes, and has uncovered their highly important roles in immunity. Metalloproteases are involved in immune cell development, migration, effector function, and ligand–receptor interactions.^[25]

Metalloproteases hydrolyze proteins and peptides via a distinct activating role of a metal ion in their active site in the hydrolysis of peptide bonds.^[26] The most common metal they utilize by far is the divalent zinc cation.^[27] In the active sites of metalloproteases other transition metals have been found, e.g. Co^{2+} and Mn^{2+} , and some are often used to restore function in zinc-metalloproteases in which the Zn^{2+} ion has been lost.^[28] Generally, metal ions are bound in nearly tetrahedral coordination at the active site. Configuration of the zinc complex in the active sites usually consists of three amino acid ligands and one water molecule, acting as a hydrolytic nucleophile.^[29]

Metalloproteases are divided into two major groups, named after the region of the substrate where the peptide cleavage is being performed: metalloendopeptidases and metalloexopeptidases.

Subdivisions in these groups are defined by target-specific localization sites in tissues and evolutionary conservation of residues which differentiate enzymes into specific roles.^[8,26,27] Among the large number of zinc metalloproteases, carboxypeptidase A and thermolysin are considered prototypical.^[8]

1.2.1.1 Carboxypeptidase A

A prototypical zinc peptidase^[30] from the zinc hydrolase family is carboxypeptidase A (CPA).^[31] Isolated in 1929 from bovine pancreas tissue, carboxypeptidase A is an exopeptidase which hydrolyses *C*-terminal peptide bonds and esters, exhibiting preference for big hydrophobic side chains. In metabolism, CPA contributes to the breakdown of proteins. It is commercially used for processing of cheese whey protein and production of protein hydrolysates used in nutritional products for people suffering from phenylketonuria.^[32]

The zinc ion of the active site in CPA is bound to two histidines (His69 and His196), one glutamate (Glu72) sidechain, and a water molecule. The activated water molecule in CPA is bound to the ion and held in the attack position by Glu270 (Figure 2).

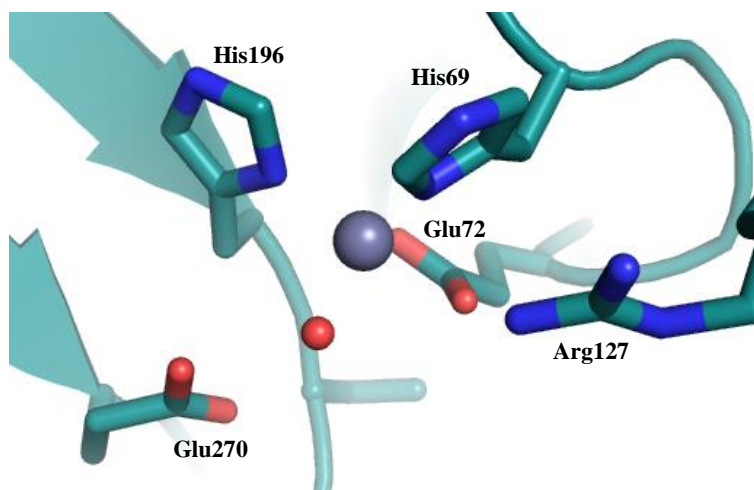


Figure 2 Structure of the active site of carboxypeptidase A.

There is experimental evidence for two different mechanisms,^[33] both supported by high-level QM/MM calculations and used to describe how this enzyme acts. One is the “promoted-

water pathway”, known as the “general base-general acid pathway”,^[34] and the “nucleophilic pathway”, or “anhydride pathway”.

Precise positioning of the substrate is ensured through interactions with at least five other side chains (Arg127, Asn144, Arg145, Tyr248, and Arg71). Glu270 acts as a general base, deprotonating the water molecule which then attacks the carbonyl carbon of the ester/peptide, reaching a stabilized transition state (TS1) and subsequently producing a tetrahedral intermediate (Figure 3A). The Glu270 residue shuttles the proton from the nucleophile-acting water molecule to the leaving group, destabilizing the C–O (ester substrate) or C–N (peptide substrate) bond, which is broken through the second transition state. In CPA Arg127 provides an “oxyanion hole” for stabilization of the first transition state and intermediate.

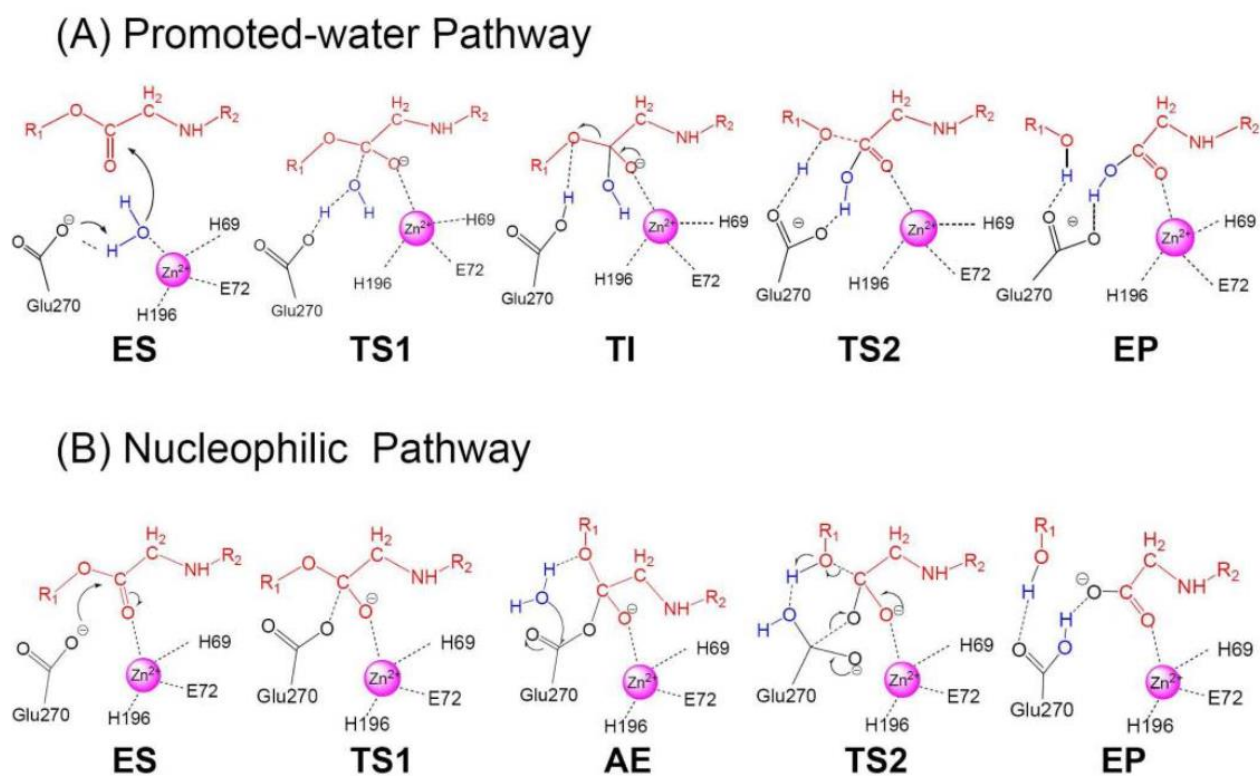


Figure 3 Two different proposed mechanisms of hydrolysis of substrates in carboxypeptidase A. Picture taken from ref. 33.

The second proposed pathway recruits the carboxylate of the Glu270 as a nucleophile (Figure 3B).^[33] The mechanism is used to describe the cleavage of esters and it is considered not to be viable in case of the peptide bond cleavage. It emphasizes complexation of the carbonyl

oxygen with zinc ion in the initial state (ES) upon substrate binding. The carbonyl oxygen is polarized by zinc, raising the electrophilicity to enable the nucleophilic attack by the properly positioned carboxylate of Glu270. This gives rise to the first transition state (TS1) and the formation of an acyl-enzyme intermediate (AE). In the generated conditions, the water molecule hydrolyzes the anhydride-type acyl-enzyme intermediate by attacking the carboxylate carbon of Glu270. Deacylation via the second transition state (TS2) ultimately leads to the product.

Computational evidence suggests that in regards to proteolysis, the general base-general acid pathway, or the “promoted-water” pathway, is the feasible pathway of the two.^[30,33] However, the anhydride pathway still seems to compete in ester hydrolysis reactions. Additionally, Breslow and Wernick disputed the anhydride pathway via ¹⁸O-labelling experiments to show that the formation of the acyl-enzyme intermediate of the anhydride pathway is unlikely.^[35,36]

1.2.1.2 Thermolysin

The first ever sequenced metalloprotease was thermolysin, a bacterial zinc metalloendopeptidase, discovered in *Bacillus thermoproteolyticus*.^[37,38] It is a virulence factor which bacteria use for digestion of exogenous proteins enabling colonization of hosts and tissue degradation.^[39,40] Thermolysin hydrolyses internal peptide bonds, recognizing the *N*-terminal side of large hydrophobic residues like leucine, isoleucine, or phenylalanine. Thermolysin has important applications in peptide sequencing and industrial use in the production of the artificial sweetener aspartame (Figure 4B).^[41]

The structure of thermolysin consists of 316 amino acids. Its two domains can be described as the *N*-terminal domain containing mostly β -sheets, and the *C*-terminal domain having mostly α -helices.^[38] The active site of the enzyme is located at the interface of the domains. The zinc ion is bound in a tetrahedral complex via His142, His146, Glu166 and a water molecule in the active site (Figure 4A).

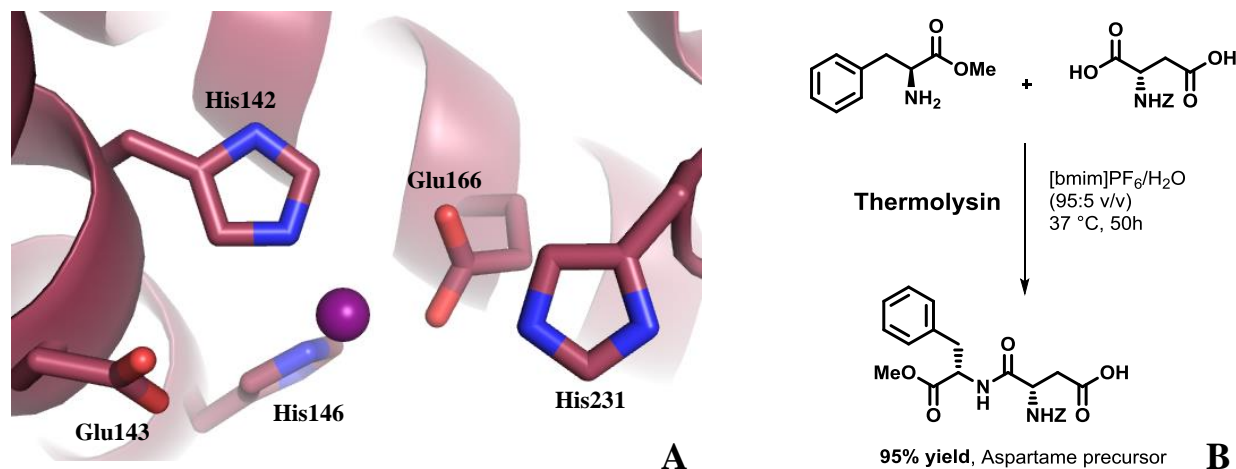
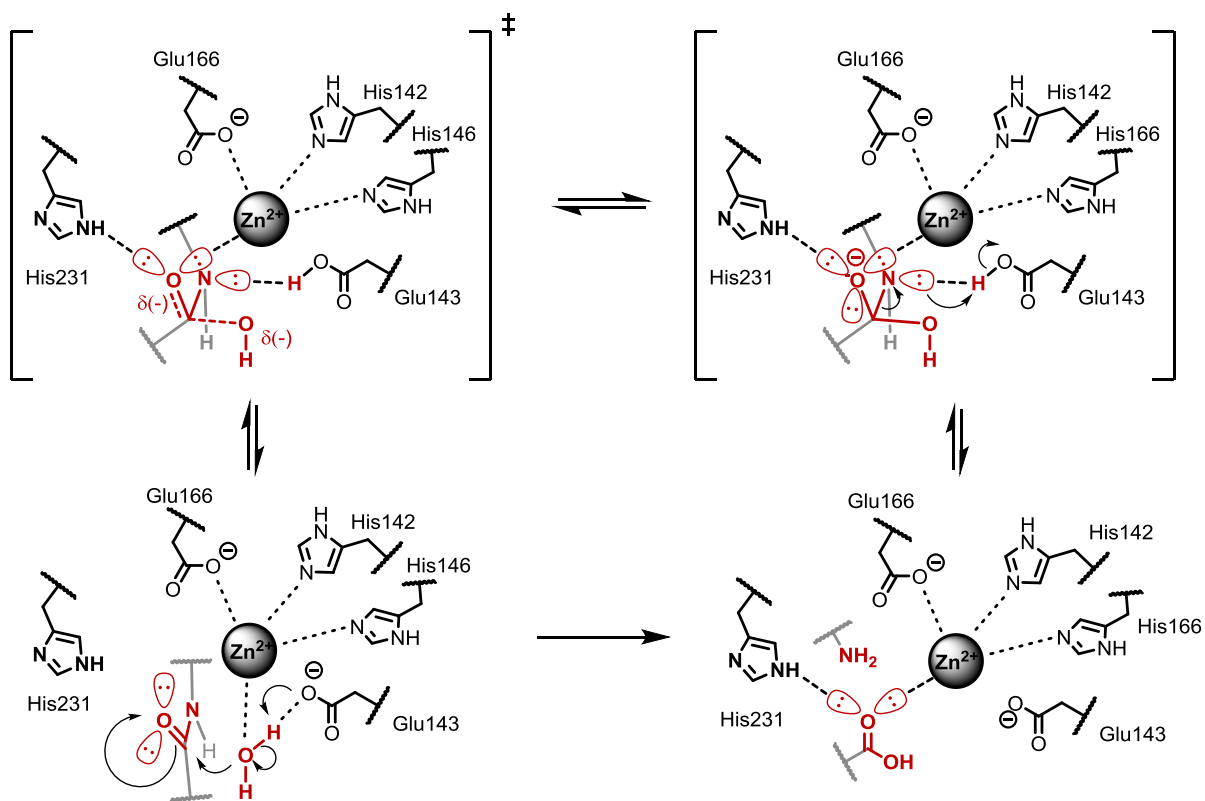


Figure 4 A: Active site of thermolysin. **B:** Aspartame precursor synthesis catalyzed by thermolysin.

The coordinating sidechains represent a conserved binding motif of **HEXXH**.^[42,43] A distinct characteristic of thermolysin is its impressive thermal stability, arguably enabled by four associated Ca^{2+} ions in the structure.^[38]

Several mechanisms for thermolysin-mediated peptide cleavage have been proposed in respect to the roles of catalytic residues Glu143 and His231. One of them is the generally accepted mechanism which is supported by high-level calculations.^[44] It is the general acid-base pathway mechanism proceeding as in the case of carboxypeptidase A. Upon binding of the peptide substrate, zinc ion complexation and deprotonation by Glu143 activate a water molecule for nucleophilic attack on carbonyl of the peptide bond. The produced transition state is stabilized by His231 via a hydrogen bond. The transition state proceeds to formation of a geminal diolate. Through the process all of the atoms in the peptide bond have changed their orbital hybridization, which results in increasing electron localization and basicity on the nitrogen atom. The nitrogen atom is conveniently positioned next to Glu143, where it gets protonated, causing destabilization of the C–N bond and reorganization of the geminal diolate into carboxylate, finishing the process (Scheme 1).



Scheme 1 The general acid-base mechanism of action of thermolysin in hydrolysis of peptides.

The catalytic activity of thermolysin depends on temperature and pH.^[45] The maximum activity has been found at pH = 7.2.^[46] Its thermal stability prevents the loss of activity up to the temperature of 70 °C.^[45,47]

1.2.1.3 Other Zinc Metallopeptidases

Historically, subsequent to the structures of carboxypeptidase A and thermolysin, structures of other mononuclear zinc peptidases have become available, in particular those of matrix metalloproteases and snake venom proteases (reprolysins).

Reprolysins are proteases functionally very similar to matrix metalloproteases and they are among the most toxic snake venom components.^[48] Both matrix metalloproteases and reprolysins are classified under a higher order group called metzincins, and they are all zinc endopeptidases. Metzincins are structurally differentiated from thermolysin-like proteases by having a third

histidine as the third ligand of zinc instead of glutamate. While thermolysin-like proteases have a **HEXXH** binding motif, metzincins have **HEXXHXXGXXH**. They have a conserved methionine residue in vicinity to the active site, presumably important for stabilization.^[49] Another important feature of many of them is a cysteine switch, in form of a cysteine residue coordinated into the zinc ion.^[50] This cysteine residue is removed from the complex by different means (posttranslational modification of cysteine, proteolysis of a proenzyme, conformational changes induced by physical factors), leading to activation of the enzyme, as studied on one of the matrix metalloproteases, stromelysin-1.^[51]

Many zinc proteases are related to thermolysin, but also a great number of mononuclear zinc proteases are known which evolved independently, including carboxypeptidase A. All of these proteases show a remarkably similar active site according to the complexation pattern of zinc and recruitment of a water molecule in substrate cleavage. Researchers were surprised when a typical zinc protease site was found in the crystal structure of Sonic hedgehog protein, which is investigated for its role in cell signaling and embryonic development. To this date it is still unknown whether this protein, which is an important morphogen in the tissue development, acts also as a protease, regardless of its obvious structural characteristics.^[10,52]

1.2.2 Dipeptidyl Peptidase-3 (DPP3)

1.2.2.1 Discovery

Dipeptidyl peptidase-3 (DPP3, classified as EC 3.4.14.4) named after being the third enzyme with dipeptidyl aminopeptidase activity ever discovered, was first isolated from bovine pituitary by Ellis and Nuenke.^[53] To date, eight dipeptidyl peptidases are known, almost all of them being serine peptidases, except DPP1 and DPP3. DPP1 is a lysosomal cysteine protease, involved in immune response.^[54] DPP3 is distinctive among dipeptidyl peptidases as the only zinc metallopeptidase, and also among zinc metalloproteases, as the only dipeptidyl peptidase in this huge class.

Depending on localization it was named also dipeptidyl aryl amidase III^[53] and dipeptidyl aminopeptidase III, enkephalinase B^[55] and red blood cell angiotensinase.^[56] After its early discovery,^[53] the progress slowed down for a long time.^[57] It was later found that it could be connected to pathophysiological processes such as inflammation,^[58] cardiovascular regulation,^[56,59–61] and pain modulation.^[20,62,63] Most recent developments bring DPP3 in connection with cancer. Activity in histological aggressiveness of human ovarian carcinoma,^[64,65] and a genomic discovery of DPP3 as a primary inhibitor of KEAP1-mediated ubiquitination of Nrf2, supporting cancer cell defense against oxidative stress.^[18] Synthetic peptides were used in an attempt to identify the biological significance of DPP3.^[55,56,58,62]

X-ray crystal structure has been determined. First the structures of yeast ortholog and the human DPP3 (hDPP3),^[16] and subsequently a surprising cocrystal structure of an inactive mutant of the human DPP3, in complex with a pentapeptide, displaying huge conformational change and an entropy-driven substrate binding process.^[17]

After the first discovery in bovine pituitary, homologues of DPP3 were identified from a variety of prokaryotic and eukaryotic species. It has been found in human erythrocytes,^[56] neutrophils,^[58] placenta^[66], seminal plasma,^[67] muscle,^[68] skin,^[69] cerebrospinal fluid,^[70] eye lens extracts,^[71] neuroblastoma cells (IMR 32 cells),^[72] rat liver,^[73] brain,^[55,74] erythrocytes,^[75] spinal cord dorsal horn^[63] *Drosophila melanogaster*,^[76] *Dictyostelium discoideum*,^[77] *S. cerevisiae*,^[78]

and many others. Its identification across kingdoms and species indicate DPP3 to be a ubiquitous enzyme, emphasizing its biological significance of an evolutionarily conserved protein.

1.2.2.2 Pathophysiological Indications

1.2.2.2.1 Protein Turnover

Proteins marked with ubiquitin for degradation are degraded by the ubiquitin proteasome system. 3–24 amino acid residues peptides are released into the cytosol. This peptidome is being further processed by various cytosolic peptidases. Longer peptides are degraded by tripeptidyl peptidase II^[79] (peptides longer than 16 residues) and thimet oligopeptidase (6–17 residues).^[80,81] Shorter peptides are degraded down to the level of amino acids mostly by action of terminal aminopeptidases such as aminopeptidase B, leukotriene A4 hydrolase, bleomycin hydrolase and puromycin-sensitive aminopeptidase.^[82–84]

DPP3 is very likely a contributor to the cytosolic protein turnover. The peptidome portion consisting of peptides of 4–8 amino acid residues are within the typical substrate length of DPP3.^[56] The lack of substrate specificity and the post-proline activity of DPP3^[63] additionally support the protein turnover role, because proline containing peptides are resistant to most aminopeptidases involved.

1.2.2.2.2 Nociception

Peptides have roles in diverse physiological process. These include signal transduction,^[85–87] nociception/antinociception,^[88] blood pressure regulation,^[89,90] immunomodulation,^[91,92] reproduction,^[93] and emotional and behavioural balance.^[94,95] These peptides include opioid peptides, e.g. enkephalins, endorphins, dynorphins, endomorphins (EM-1 and EM-2), angiotensins (angiotensin II, angiotensin III and angiotensin IV) and hemopressins.^[96] They have been found both colocalized with the targets or released into the blood stream and body fluids for remote effect.

DPP3 has a high affinity for angiotensins, enkephalins and endomorphins and cleaves them at physiological pH. Their colocalization in body fluids such as serum, cerebrospinal fluid and seminal plasma indicates the disposition of these peptides to DPP3, thereby contributing to their homeostasis.

It is reported for both *Drosophila melanogaster* and cockroaches that DPP3 degrades their insect neuropeptide proctolin due to their colocalization in the central nervous system.^[62,76] Enkephalins are endogenous δ -opioid receptor agonists, secreted by enkephalinergic cells of the neuroendocrine system^[97] and create an antinociceptive (pain diminishing) effect upon binding. Synaptic membrane localization of mammalian DPP3 in mouse brain has been reported.^[68] Together with findings that enkephalins are among better substrates of DPP3,^[17,56,61] it was proposed that the enzyme could be involved in pain signalling. Endomorphins (EM-1 and EM-2) are class of endogenous opioid peptides which are also substrates of DPP3.^[63]

1.2.2.2.3 Inflammation and Blood Pressure Regulation

Spinorphin, a known endogenous peptide inhibitor of DPP3, relieves rats from bradykinin-induced pain.^[98] Since spinorphin inhibits all enkephalinases, further work using specific DPP3 inhibitors is necessary to confirm any role in inflammation.

Angiotensins are the key peptide vasoconstrictors of the renin-angiotensin-aldosterone system.^[99] Angiotensin II is regarded as more potent than angiotensin III. Since angiotensin II is much more quickly degraded by angiotensinases, it is still not clear which one plays the dominant role in renin-angiotensin-aldosterone system.^[100] Human DPP3 isolated from erythrocytes cleaves angiotensin II and angiotensin III.^[56] In fact, it degrades angiotensin III with higher affinity than Leu-enkephalin. This implicates a potentially important role of hDPP3 in cardiovascular events and a connection to the renin-angiotensin-aldosterone system.

1.2.2.2.4 Defense Against Oxidative Stress - Cancer Related Implications

Transcription factor Nrf2 or NF-E2 (Nuclear Factor Erythroid-derived 2) related factor 2^[101] is a basic leucine zipper protein.^[102] In the events of high cellular oxidative stress it

activates transcription of genes encoding for phase II detoxifying enzymes.^[103,104] Nuclear migration of Nrf2 in response to overexpression of DPP3 in neuroblastoma cells (IMR-32 cells) has been reported. DPP3 overexpression efficiently attenuates the toxic effects of H₂O₂ and rotenone, demonstrating the cytoprotective effect of DPP3 against oxidative stress.^[72] Expression of DPP3 has been reported to increase with the histological aggressiveness of human ovarian primary carcinomas.^[65] In ovarian cancer cells tumor induced release of H₂O₂ transcriptionally upregulates the expression of Ets-1, a critical regulator of DPP3 expression.^[105]

Many tumors display high Nrf2 activity, rendering cancer cells resistant to oxidative stress. Until recently, it was not known how this occurs in the absence of mutations on KEAP1, ubiquitin ligase which is marking Nrf2 for degradation. In the most recent investigation proteomic analysis of KEAP1 interaction network and comparison to genomic profiles of 178 squamous cell lung carcinomas revealed amplification and mRNA overexpression of the DPP3 gene in tumors with high Nrf2 activity.^[18] The findings support competitive binding of DPP3 to KEAP1 ligase, via its **ETGE** amino acid sequence motif, which Nrf2 uses for binding to KEAP1 (Figure 5).

Based on these findings, and the large structural changes in hDPP3 upon small-molecule binding to the active site,^[106] it is legitimate to examine the potential of allosteric inhibition of hDPP3-KEAP1 interaction, via small-molecule inhibitors. This could cause downregulation of cytoprotective genes and lowering the resistance of cancer cells to oxidative stress.

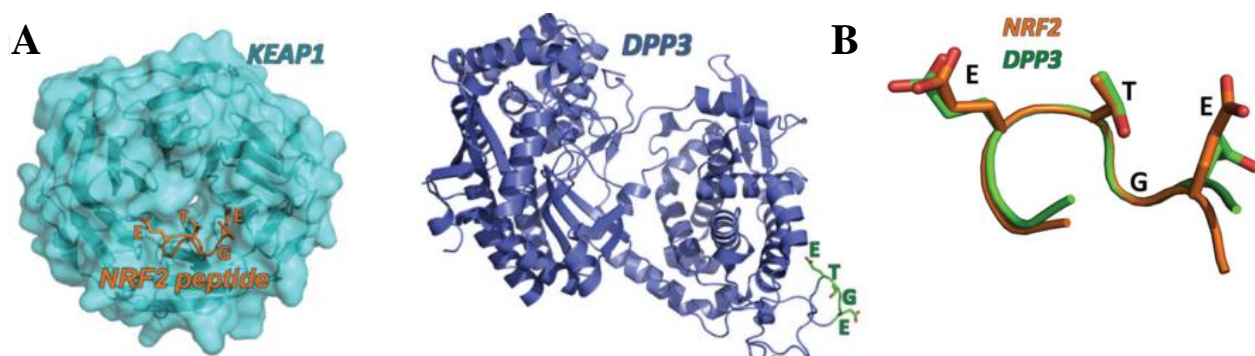


Figure 5 A: Structures of KEAP1 and hDPP3, and emphasis to the ETGE motif and its binding site in KEAP1. **B:** The structures of ETGE motif from Nrf2 and hDPP3 have a good overlap. Pictures taken from the ref. 18.

1.2.2.3 Structure of hDPP3

The first structure of hDPP3 uncovered two big lobe-like domains with a large cleft in between.^[16] Both domains are composed mostly of α -helices, but have also a smaller β -sheet portion in the lower domain. Bezerra et al. published the second structure, having a peptide ligand bound in the active site. It revealed a large collapse of the two lobes, encapsulating the ligand completely (Figure 6).^[17]

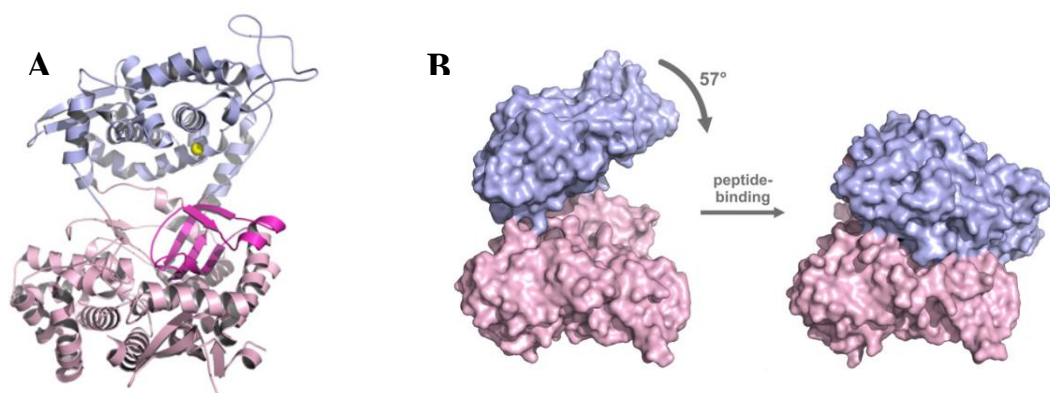


Figure 6 Structure of hDPP3. **A:** Structure without a ligand (PDB: 3FVY). **B:** Large conformational change upon substrate binding (PDB: 3T6B). Pictures taken from the ref. 17.

The most abundant metalloprotease clan, including the prototypical thermolysin, has a characteristic catalytic motif **HEXXH**.^[42] The two histidines and a glutamate residue from a neighboring α -helix are bound in complex with a zinc ion (there are rare examples of such proteases with Mn^{2+} , Co^{2+} , Ni^{2+} or even Cu^{2+}).^[107] The complex and the glutamate residue from the **HEXXH** motif activate a water molecule thereby increasing its nucleophilicity. The discovery of DPP3 introduced a very similar but unique longer motif **HEXXGH**, opening a new metallopeptidase family – M49. On the basis of published structures it is believed to have the same function.^[16,17] Additionally, the conserved motif **EEXRAE/D** provides the glutamate residue which coordinates zinc together with the two histidines. Amino acid sequence alignment of DPP3 from different species identified a number of conserved residues in hDPP3.^[15]

1.2.2.4 Structure of hDPP3 in Complex with Opioid Peptide Tynorphin

The structure of an inactive point mutant hDPP3 in complex with tynorphin (PDB code: 3T6B)^[17] reveals how a peptide binds to this enzyme. The general remark is that the binding mode resembles an extended β -sheet (Figure 7A). The first three amino-terminal amino acid units form a typical β -sheet hydrogen bonding network. The *N*-terminus of the peptide is charged and ion-paired and hydrogen-bound to the Glu316 side chain of the enzyme (Figure 7B). It also makes two more hydrogen bonds with Asn394 and Asn391. This very tight interaction most probably represents an ammonium cation recognition site, since there is no other amino acid residue that can be positively charged in the vicinity of Glu316, and provide the necessary stabilization in the closed, ligand bound conformation, where this subsite is not exposed to the solvent.

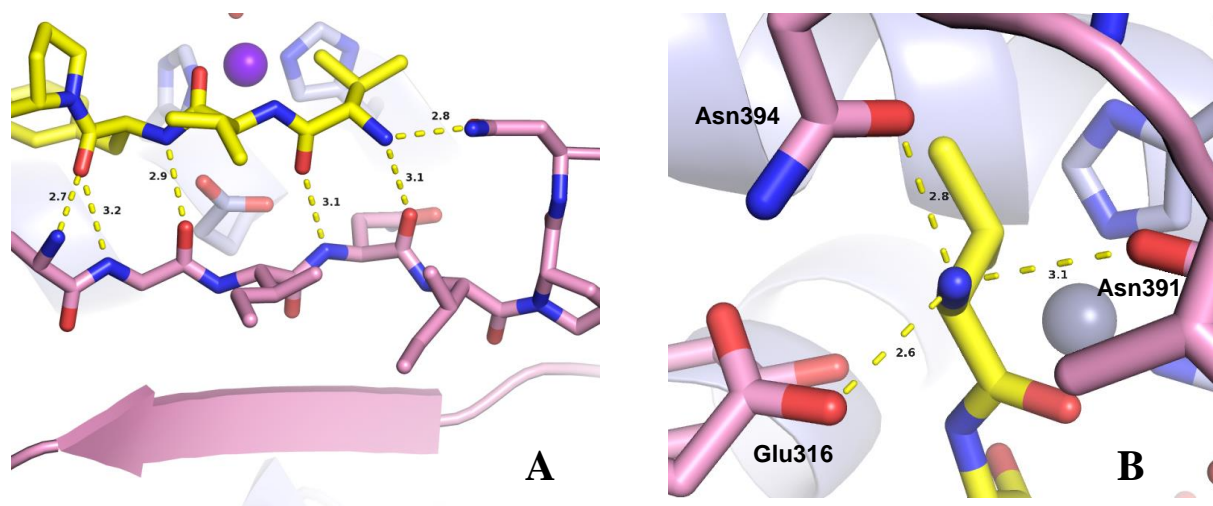


Figure 7 Binding mode of tynorphin. The Zn-ion and the cat. Glu451 residue were added and force field optimized with molecular modelling software MOLOC.^[108] A: an extended β -sheet; B: amino-terminal ammonium group of the ligand is bound very tightly via three hydrogen bonds and a salt bridge to the Glu316 residue.

The *C*-terminal tryptophan residue, along with two hydrogen bonds, adds also a pincer-like cation- π interaction with Lys670 and Arg669 residues within the enzyme (Figure 8). The cation- π interaction is well characterized as one of the strongest noncovalent interactions in protein environments. It is electrostatic in nature, robust in its stereoelectronic determinants, boasting interaction energies on average comparable to hydrogen bonding, but much less spatially limited.^[109–111] This additional localized set of tight interactions in the tynorphin-DPP3

complex is the probable cause of the higher affinity of binding and the substrate inhibition ability, compared to the other peptide substrates of DPP3 (e.g. enkephalins, which have Leu or Met as a C-terminal residue, or endomorphins, which are shorter by one amino acid unit and thus can hardly interact with this site).

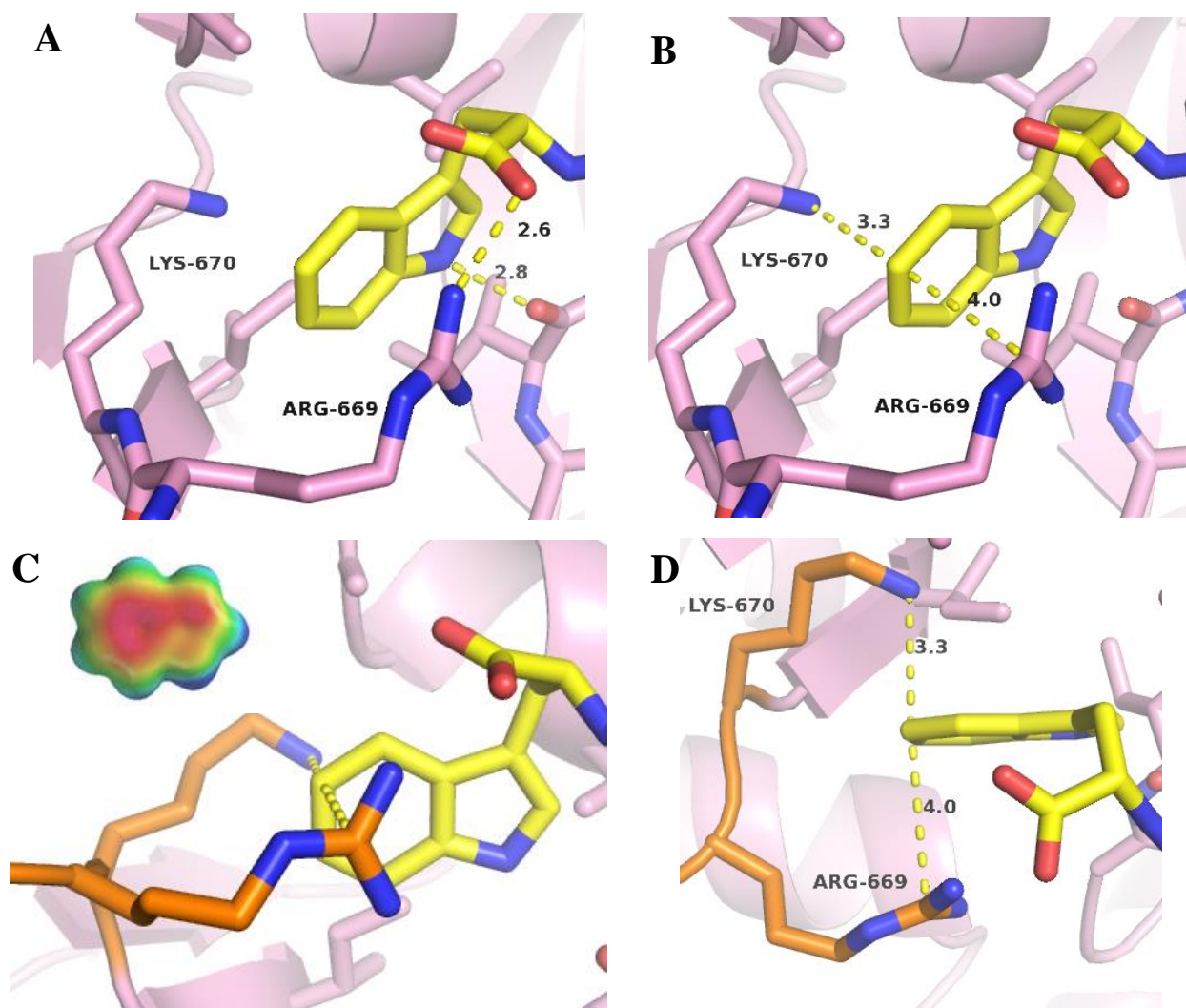


Figure 8 Binding mode of tynorphin: the C-terminus of the ligand is tightly bound via two hydrogen bonds (A) and a dual cation- π interaction "pincer" (B, C and D); Electrostatic potential map of indole residue is displayed for consideration (C, upper left corner).

The second peptide bond is subject to nucleophilic attack in the wild type enzyme. It is surrounded by the catalytic apparatus, consisting of four ligands complexing Zn-ion (a molecule of water, Glu508, His450 and His 455) and the Glu451, and two additional residues involved in precise substrate positioning and stabilization of the transition state. Tyr318 has been reported as an important conserved residue in the family of DPP3 enzymes. Mutation of this residue leads to

a decrease of the k_{cat} -value by two orders of magnitude.^[106,112] Tyr318 forms hydrogen bonds to the first amide bond of the peptide ligand and Glu508, thus bringing together the catalytic apparatus and the peptide substrate backbone. His568 apparently has the major role in stabilization of the transition state. From the X-ray structure of the complex, it can be observed that it is in the range of hydrogen bonding distances to the carbonyl oxygen of the cleavable peptide bond, but the interaction is weak, because lone electron pair orbitals are positioned orthogonally to the N–H donor of the His568 (Figure 9).

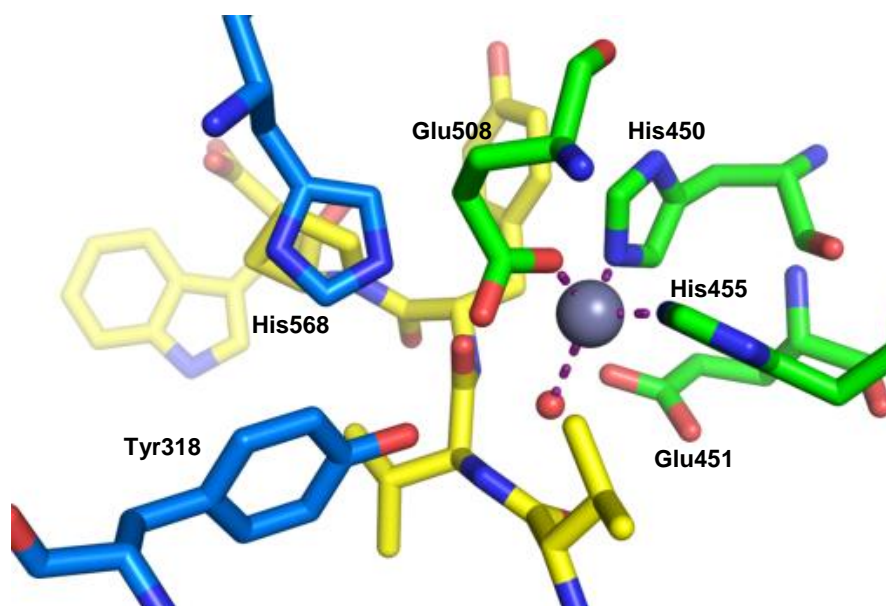


Figure 9 The structure of the active site of hDPP3 with a bound substrate, created by molecular modelling and force field based structural optimization, using MOLOC software^[108] and the cocrystal X-ray-based structure of tynorphin in complex with hDPP3 (PDB code 3T6B).^[17]

1.2.2.5 Mechanism of Action of DPP3

Thermolysin is one of the best studied zinc metalloproteases.^[113] The relative topology of the residues of the active site of thermolysin and hDPP3 is very similar. Thermolysin has also two histidines (His142 and His146) and a glutamate (Glu166) which coordinate the catalytic zinc ion. One more glutamate takes the role of base (Glu143), and one more histidine residue (His231)

provides a hydrogen bond donor for stabilization of the transition state oxyanion, which was indicated in QM/MM computational studies.^[44] The Glu143 that acts as the base for deprotonation of a water molecule, was also found to shuttle this proton to the nitrogen atom of the amide bond which is being hydrolyzed.

Since the arrangement of the active site residues in hDPP3 is almost identical to thermolysin (Figure 10) in respect to the zinc complex with the water molecule and the general acid/base Glu451, a mechanism analogous to thermolysin has been proposed. In the first crystal structure (ligand-free), the electron density of a water molecule was observed, coordinated to zinc, supporting the “promoted water” or “general acid/base” mechanism (Scheme 2).^[33,44]

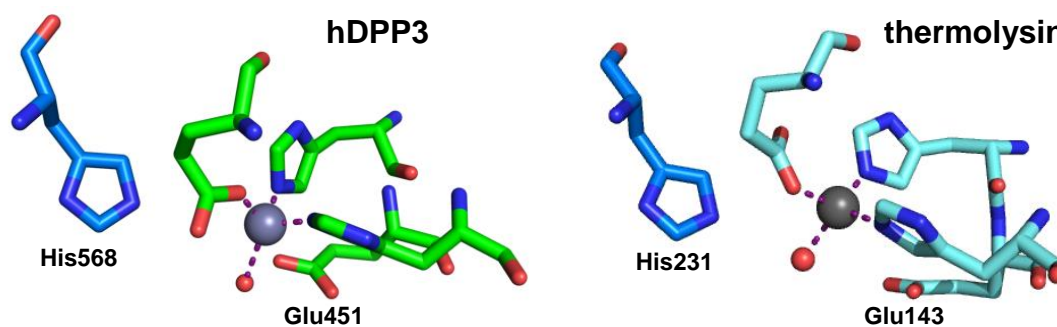
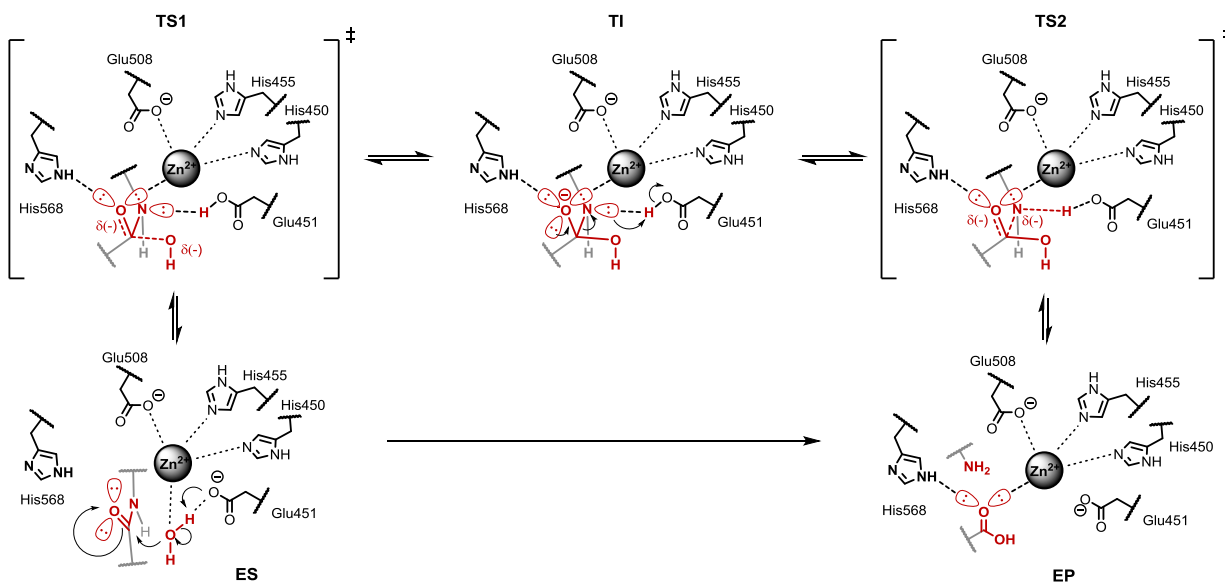


Figure 10 Active site catalytic machineries of hDPP3 (left)^[16] and thermolysin (right).^[42]

In the enzyme-substrate complex (ES) a bound peptide substrate is precisely positioned for the nucleophilic attack by a water molecule in the following way: the carbonyl of the peptide bond interacts with zinc ion. There are three residues which are anchoring the *N*-terminus of the peptide (Asn394, Asn391, Glu316). The conserved Tyr318 residue makes hydrogen bonds both to the substrate and the zinc-binding ligand Glu508. Glu451 deprotonates the water molecule. The water molecule attacks the peptide bond, leading to transition state 1 (TS1) and formation of an amino-gem-diolate intermediate (TI), stabilized by zinc ion and a hydrogen bond to His568. The protonated Glu451 shuttles the proton originating from the water molecule to the conveniently positioned nitrogen atom from the substrate, which now has tetrahedral sp^3 hybridization and is much more basic. This destabilizes the C–N bond and produces the products of the hydrolysis along transition state 2 (TS2).



Scheme 2 The general acid/base mechanism of action of hDPP3 in the hydrolysis of peptides. **ES**: Enzyme-substrate complex; **TS1**: transition state 1; **TI**: transition intermediate (amino-gem-diolate); **TS2**: transition state 2; **EP**: enzyme-product complex. Free electron pairs and their lobes are emphasized on the atoms of the peptide bond and its transition structures.

In the hDPP3-catalyzed hydrolysis the transition state 1 is reached, where hybridization is being changed on C, O and N atoms within the cleavable peptide bond, so their orbitals are getting more p-character and their orbital configurations pyramidal. The pyramidalization upon approach of a nucleophile to a carbonyl has been investigated by Hans-Beat Bürgi and Jack D. Dunitz with crystallographic “snapshots” of this phenomenon.^[114,115] The positive charge on the zinc ion drives newly enabled rotation around the C–O axis of the transition state, so that one of the electron pairs on oxygen complexes into d-orbitals of the zinc ion, and the second electron pair facilitates a hydrogen bond with His568 (thus having the same role as the His143 in thermolysin). These two interactions provide the required stabilization of the transition state. Upon pyramidalization the π -electrons originally shared in the amide bond are being retrieved back to nitrogen into an orbital ideally positioned for abstraction of the proton that is being shuttled by Glu451. Protonation of nitrogen destabilizes the C–N bond, which breaks and its electrons are taken by nitrogen. This causes the negative charge built up on the stabilized oxygen to collapse into a newly formed carboxylic acid. After the cycle, the products are formed and released, and the catalytic complex is brought to the initial resting state.

1.2.2.6 Known Substrates and Inhibitors

Over the years, a number of publications reported characterization of DPP3 of bovine, porcine, monkey, rat, human, insect, yeast and other organisms, and examined its activity with important endogenous peptide hormones. In all of the relevant studies, competitive inhibition of hydrolysis of Arg-Arg-amide substrates was used to provide a quantitative measure of affinity to the enzyme (Table 1).

Entry	Peptide of physiological importance	AA composition	Activity (K_i [μ M])	References
<u>Angiotensins</u>				
1	Angiotensin II	Asp-Arg- -Val-Tyr-Ile-His-Pro-Phe	0.34, 3.6	55, 56
2	Angiotensin III	Arg-Val- -Tyr-Ile-His-Pro-Phe	0.22, 0.05	55, 56
3	Proctolin (insect neuropeptide)	Arg-Tyr- -Leu-Pro-Thr	1.2	56
<u>Enkephalins (δ-opioid receptor agonists)</u>				
4	Leu-enkephalin	Tyr-Gly- -Gly-Phe-Leu	6.6, 125.5, 3.65	55, 56, 63
5	Met-enkephalin	Tyr-Gly- -Gly-Phe-Met	9.2	55, 56
<u>Endomorphins (μ-opioid receptor agonists)</u>				
6	Endomorphin-1	Tyr-Pro- -Trp-Phe-NH ₂	5.00	63
7	Endomorphin-2	Tyr-Pro- -Phe-Phe-NH ₂	2.49	63
8	Human β -casomorphin	Tyr-Pro- -Phe-Val-Glu-Pro-Ile	0.56	63
<u>Dipeptidyl amides for assays</u>				
9	Standard DPP3 assay substrate	Arg-Arg- - β NA	-	53
10		Arg-Arg- -NH-Mec	-	57

Table 1 DPP3 substrates of physiological importance. Cleavage site is indicated with a vertical line. K_i values were obtained from competitive substrate inhibition assays, measuring fluorescence in the hydrolysis of test substrates of Arg-Arg-amide type (entries 9 and 10).

One can notice by assessment of the collected data, that DPP3 has good affinities to angiotensins and opioid peptides. This is generally taken as a foundation of the possible connection of DPP3 with the opioid signaling processes and regulation of cardiovascular events in connection to the renin-angiotensin-aldosterone system. It needs to be pointed out that the

affinities to angiotensins II and III are an order of magnitude stronger than the values for opioid peptides, pushing the emphasis of potential role of DPP3 more in the direction of blood pressure regulation.^[55,56]

An interesting peptide, named spinorphin, was found in bovine spinal cord, and characterized as a potent peptide inhibitor of enkephalin degrading peptides.^[116] Inspired by the potency of spinorphin in inhibition of enkephalinases (including DPP3) research was performed in order to find spinorphin/haemorphin derivatives that are specifically inhibiting activity of DPP3.^[20] The results of competitive substrate inhibition are summarized in the Table 2.

Entry	Competitive substrate inhibitor	AA composition	Activity (K_i , [μM])	References
1	Spinorphin (VVYPWT)	Leu-Val- -Val-Tyr-Pro-Trp-Thr	6.67, 2.42	20, 19
2	Tynorphin (VVYPW)	Val-Val- -Tyr-Pro-Trp	2.67, 0.075	20, 19
3	LVYPW	Leu-Val- -Tyr-Pro-Trp	1.35	20
4	YVYPW	Tyr-Val- -Tyr-Pro-Trp	0.42	20
5	FVYPW	Phe-Val- -Tyr-Pro-Trp	0.28	20
6	WVYPW	Trp-Val- -Tyr-Pro-Trp	0.24	20
7	IVYPW	Ile-Val- -Tyr-Pro-Trp	0.16	20
8	Valorphin (VVYPWTQ)	Val-Val- -Tyr-Pro-Trp-Thr-Gln	0.049	63
9	LVV-haemorphin-7 (LVVYPWTQRF)	not tested as a substrate of DPP3	n/a	117, 119

Table 2 Haemorphin/Spinorphin derived synthetic inhibitory peptide substrates of DPP3. Cleavage site is indicated with a vertical line. The affinity was quantified indirectly, via K_i values from competitive substrate inhibition, measuring fluorescence in the hydrolysis of standard test substrates of Arg-Arg-amide type. Rat DPP3 was used for assays. LVV-haemorphin-7 sequence is provided for comparison.

The authors of the spinorphin and tynorphin discovery study^[19] fail to mention that spinorphin is actually a subsequence of the known opioid peptides LVV-haemorphin-7 and VV-haemorphin-5 (valorphin),^[117] which was later indicated in the investigation of tynorphin derivatives by Chiba *et al.*^[20] These two haemorphins are opioid peptide metabolites of the β -chain of hemoglobin (numbered 32–41, sequence: LVVYPWTQRY(F)), and their signaling and release is thought to be started by hemoglobin degradation events, e.g. hemolysis.^[87,118] Specifically, μ -opioid receptor related analgesic activity of valorphin was demonstrated by hot plate and tail flick tests on mice, and Randall-Selitto test on rats. The highest affinities among

substrates/inhibitors of DPP3 have been demonstrated for angiotensins II and III, valorphin and valorphin/spinorphin derived pentapeptides. They indicate that a complex role of DPP3 can be expected, connecting opioid signaling and renin-angiotensin-aldosterone blood pressure regulation system.

Moreover, structural features of these substrates and the X-ray structure based mode of binding support this correlation. In the cocrystal structure of hDPP3 with tynorphin it was found that tynorphin binds with its first three *N*-terminal amino acids in a manner of β -sheet extension (Figure 7A). Valorphin, tynorphin, tynorphin-like pentapeptides, and angiotensin III actually have shared structural motif in these three amino acid residues. The first amino acid is variable, but the second and the third are the same (XVY). This common structure-activity relationship feature could be an indication of evolutionary training of DPP3 to recognize such sequences with higher selectivity. Additionally, the fact that Arg-Arg- β NA is by far the best dipeptidyl substrate of DPP3,^[53] provides additional support to the blood pressure regulation related hypothesis, since angiotensin III has Arg as the *N*-terminal residue, and angiotensin II has Arg as the second residue from the *N*-terminus.

Interestingly, angiotensin IV (VYIHPF) – a metabolite of angiotensin II long considered to have no particular role – is the product of degradation of angiotensin II by DPP3. Both angiotensin IV as well as LVV-haemorphin-7 were found to bind to the same specific receptor type (AT₄).^[87] Agonism of AT₄ receptors triggers increase of cerebral artery blood flow in rabbits, renal cortical blood flow in rats, and manifests enhancement of memory recall in passive avoidance studies in rats.^[119]

Besides competitive peptide substrates known nonpeptide inhibitors of DPP3 are nonselective and not designed for DPP3. They encompass general cysteine,^[53,56,73,75,120] serine^[57,67,75,121–123] and aminopeptidase inhibitors,^[57,73,75] heavy metals,^[67,73,75,76,124] metal chelating agents,^[53,57,67,73,75,76,121,122] and microbial broth extracts (Table 3).^[125] Certain general enkephalinase inhibitors have also been developed. Although some of them inhibit DPP3, they were focused on inhibition of aminopeptidase N and neprilysin.^[21]

Inhibitor	IC ₅₀ [μM]	References
Serine protease inhibitors		
PMSF	2170 (human placenta)	57, 67, 75, 120, 121
DFP	n/a	120, 122
TPCK	100 (human erythrocytes)	67, 120, 121
DCI	4.54 (human placenta)	75
Leupeptin	100 (human erythrocytes)	55
Cysteine protease inhibitors		
<i>p</i> CMB	n/a	57, 120
<i>p</i> CMS	20 (rat brain)	53, 55
<i>p</i> HMB	10 ⁻⁶ (human erythrocytes)	121
<i>p</i> CMBS	n/a	73
4-PDS	10 ⁻⁶ (rat erythrocytes)	56, 121
DTNB	10 ⁻⁵ (human erythrocytes)	67, 121
iodoacetamide	2300 (rat brain)	55, 57, 67, 73, 121
PCMPS	3.30 (human placenta)	75
NEM	6330 (human placenta)	53, 55, 57, 67, 75
Aminopeptidase inhibitors		
bestatin, amastatin, probestatin, bacitracin, captopril, arphamenine B, promycin	no effect	57, 73, 75
Actinonin	20 (rat liver)	73
Metal chelators		
EDTA	298 (human placenta)	53, 57, 67, 73, 75, 121, 122
EGTA	n/a	76
1,10-phenanthroline	240 (human erythrocytes)	55, 57, 67, 75, 120
8-hydroxyquinoline	n/a	57
Heavy metals		
Cd ²⁺ , Cu ²⁺ , Mn ²⁺	n/a	
Zn ²⁺	31.6 (human erythrocytes)	75, 76
Hg ²⁺ , Pb ²⁺ , Ni ²⁺ , Co ²⁺		67, 73, 75, 124
Microbial broth extracts		
fluostatin A	0.44 ug/mL (human placenta)	120
fluostatin B	24 ug/mL (human placenta)	120

Table 3 The general inhibitors employed in characterization of DPP3.

Twelve synthesized amidino benzimidazole compounds were tested as inhibitors of DPP3, solely on the basis of bioisosterism of amidino groups to arginine guanidine residues from the DPP3 test substrate Arg-Arg- β NA and were found to inactivate the enzyme.^[126] A mechanism of the observed inactivation and structure characterization have not been provided.

1.2.3 Structure-based Approaches in Inhibitor Drug Design

1.2.3.1 General Aspects

In recent years there has been an exponential rise in the number of determined protein structures.^[127,128] This was enabled by great advancements in genetics, protein biochemistry, and structural biology. Thanks to the advancements a structure of a protein involved in an interesting process can be determined in shorter time than ever before, most importantly in the early stage of drug development. Developments in genomics are driving forward discovery of new proteins. Completion of sequencing of the human genome was a milestone achievement.^[129] Structural genomics will bring significant amount of new precious information on sequence-structure-function relationship of proteins. It is expected that many new drug targets will be found through these efforts.

New opportunities for bioorganic and medicinal chemists are rising for new lead structures for probing newly discovered targets. In lead compound discovery the presently dominant methods are high throughput screening of large compound libraries, computational virtual screening, and *de novo* design.^[130-132] In *de novo* design knowledge about structural features of the binding site is a prerequisite. Based on shape complementarity and synthetic viability molecular scaffolds are proposed which can favorably interact with the functional groups in the binding site of the target.^[127] First lead structures require optimization to achieve high-affinity binding and sufficient selectivity/specificity. The optimization process is performed iteratively, cycling through structure design, synthesis of proposed molecules and structural determination. In order to succeed in optimization, it is necessary to understand the factors ruling the binding affinity.

1.2.3.2 Historical Milestones in Structure-based Design

The first reported structure-based design was authored by Beddell and Goodford in 1973 at Wellcome Laboratories of UK.^[133,134] During that period, hemoglobin was a target of choice, as the only example of pharmacological relevance with a determined crystal structure. The researchers were aiming to produce a ligand that acts similarly to the endogenous allosteric modulator 2,3-bisphosphoglycerate. The natural effector binds to hemoglobin enhancing its affinity to oxygen. Based on 2,3-bisphosphoglycerate, dialdehyde derivatives and their bisulfite adducts were designed (Figure 11). These artificial molecules successfully modulated the affinity of oxygen to hemoglobin.

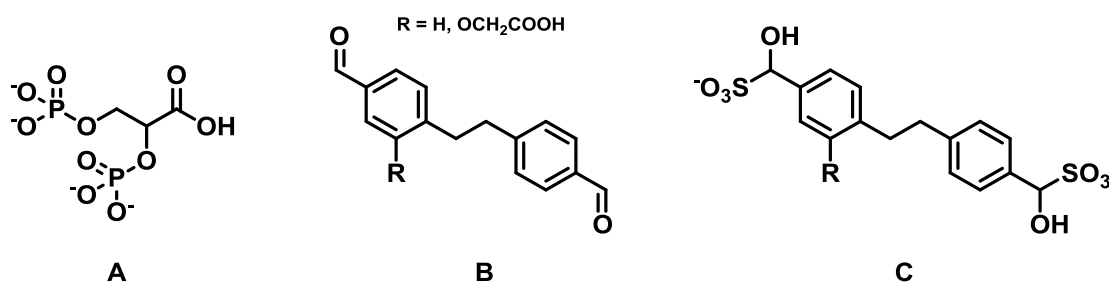


Figure 11 A: 2,3-bisphosphoglycerate; B: the synthetic dialdehyde hemoglobin effector; C: the bisulfite adduct of B.

The first drug which was developed based on the protein structural data was marketed in the following years. Captopril (Figure 12) is an antihypertensive designed to inhibit the angiotensin-I-converting enzyme (ACE). A peptide lead compound from snake venom was already long known, but Squibb scientists decided to use structural data. In the 1970s, T. Steitz and W. Lipscomb determined the structure of the binding site of carboxypeptidase A,^[135] and according to all available sequence and characterization data, it had to be a zinc metallopeptidase very similar to ACE. Cushman et al.^[136] at Squibb used the structure of carboxypeptidase A to model the active site of ACE. Over the last 30 years a great number of therapeutically important targets were structurally characterized and this led to successful new drug applications.^[127,128,137,138] Perhaps the greatest and most convincing example of the demonstrated

power of structure-based design is HIV-1 protease inhibitor drugs, thanks to which millions of people worldwide infected with HIV virus can live normal lives.

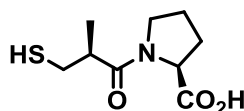
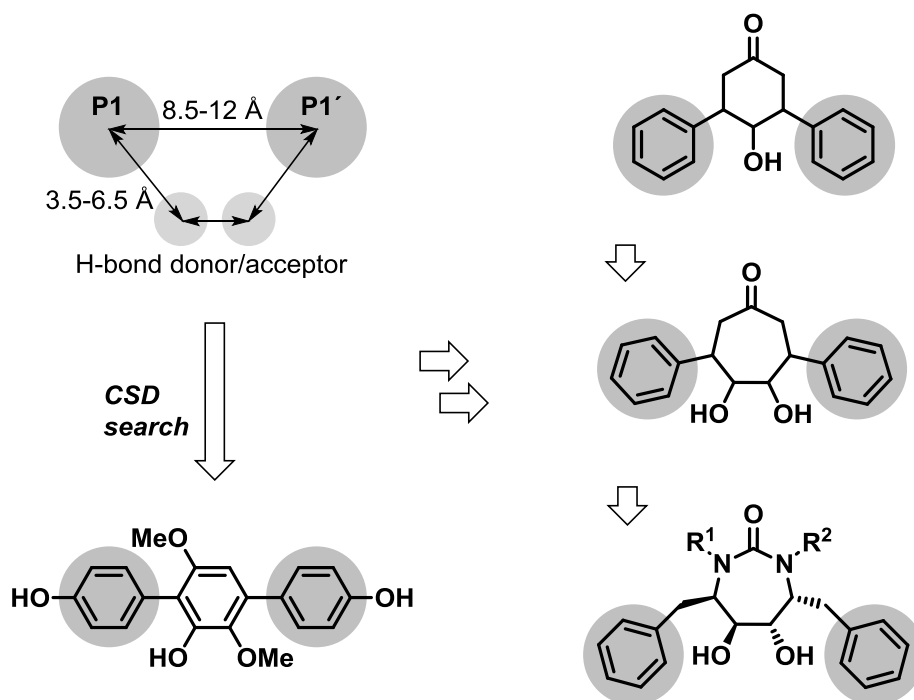


Figure 12 Structural formula of captopril.

1.2.3.3 Lead Compound Design via Extensive Database Searches

The AIDS syndrome is caused by human immunodeficiency virus. HIV-1 protease is essential in development of AIDS and the virus cannot replicate without its function. Inhibition of HIV-1 protease thus stops the replication of the virus.^[139] The existence of HIV-1 protease was proposed in mid-1980s. It was soon characterized in 1988 and – most importantly – its crystal structure was revealed in 1989. Knowledge about the structure of the active site, especially in respect to positioning of the catalytic aspartate residues, provided the foundation for structure-based design. The drug design group of Dupont-Merck has established a pharmacophore model based on the arrangement of amino acid residues in the active site.^[140] According to the model, two lipophilic moieties have to be placed in the site, separated by 8.5–12 Å (Scheme 3). Additionally, in C₂-symmetric arrangement, hydrogen bond donor/acceptor groups have to be positioned around at the distance of 3.5–6.5 Å.



Scheme 3 The Dupont-Merck structure-based pharmacophore model, leading to the design of first HIV-1 protease inhibitors.

With the pharmacophore model established, the researchers extensively searched the Cambridge Structural Database, using the preset parameters based on the model. A substituted phenol compound was found as a putative lead scaffold.^[141] Additional computational development involving input from synthetic chemists led to a C₂-symmetric cyclic urea as a new core design, inspired partially by the C₂ symmetry of the enzyme structure itself. The cyclic ureas were potent inhibitors of HIV-1 protease and some of them entered clinical trials. A later obtained cocrystal structure showed that the designed ligand indeed binds in the proposed way, so that the two hydroxyl functions form a network of hydrogen bonds with the catalytic aspartate residues, and that the carbonyl oxygen of the inhibitor replaces the structurally important water molecule, unique to HIV-1 protease and usually called “flap water” in this context.

1.2.3.4 Peptidomimetics

A great number of enzymes is involved in the production and catabolism of peptides. Peptides have important roles as neurotransmitters and hormones.^[142] Peptides such as endorphins, enkephalins, substance P, cholecystokinin, oxytocin, vasopressin, and somatostatin serve as neuropeptides or peptide hormones with diverse activities, e.g. analgesia,^[143] blood pressure regulation,^[144] some of them being even antitumor agents.^[145] There are also various antibiotic peptides in plants and animals.^[146]

On the other hand peptides are generally not good drug candidates. Orally administered peptides are rapidly proteolyzed in the gastrointestinal tract and serums and are poorly bioavailable. They still provide useful information for the design of drugs with more favorable properties. Peptides can be redesigned into compounds which mimic or counteract the biological effect via interactions with receptors or enzymes. The design principle in which the undesirable characteristics of peptides are removed by carefully considered structural modifications is called peptidomimetics.^[147]

Inhibiting an enzyme in the pathway of peptide biosynthesis is one of the strategies to counter action of a peptide in the organism. The strategy was used to develop inhibitors of angiotensin-I-converting enzyme (ACE), which converts peptide angiotensin I into its active metabolite angiotensin II. Preventing production of angiotensin II results in antihypertensive effect. As mentioned previously, the first orally active ACE inhibitor sold as a blockbuster antihypertensive drug (captopril) was designed as a hybrid peptidomimetics of angiotensin I and snake venom peptides, targeting also the zinc ion in the active site since ACE is a zinc metallopeptidase.^[136,148] Invention of peptidomimetics provided a way to improving the peptide lead properties without having traditional HTS nonpeptide leads.

Morphine and similar compounds (Figure 13) are potent agonists of the μ -opioid receptor. It was demonstrated in the 1970s that the opioid peptides enkephalins and β -endorphin bind to the same opioid receptor.^[149] The *N*-terminal tyrosine structure was soon brought into connection with the morphine phenol ring substructure, implicating the possible structural basis of interaction with the same receptor.^[150]

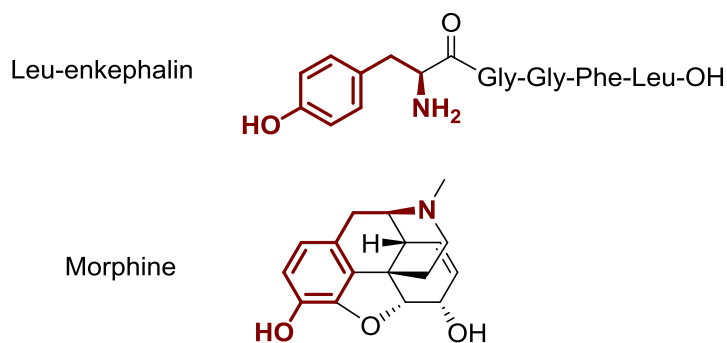


Figure 13 Comparison of Leu-enkephalin and morphine. The common pharmacophore feature is highlighted.

Optimization of lead compounds quite often includes conformational restriction based analogs, repositioning the pharmacophores in the three-dimensional configuration required for binding to the targeted receptor.^[151] Conformational constraints in single amino acids are exemplified on phenylalanine in Figure 14.^[152–154] Such constraints can be applied to connect different parts of the peptide backbone, e.g. two adjacent amino acid residues (Figure 15).^[151,155]

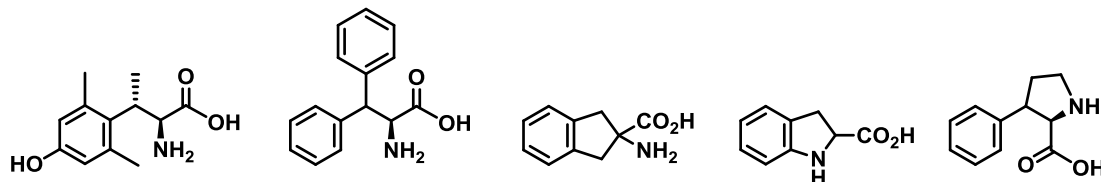


Figure 14 Examples of conformational constraints introduced in phenylalanine.

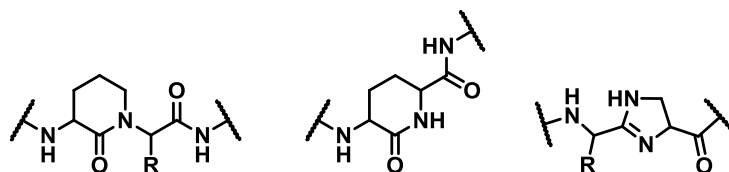


Figure 15 Examples of conformational constraints via bridging adjacent amino acid residues.

Further levels of conformational restrictions apply in the design of secondary structure mimetics (Figure 16), e.g. β -turns (A),^[156,157] α -helices (B),^[158] Ω -loops (C),^[159] and β -strands (D).^[160]

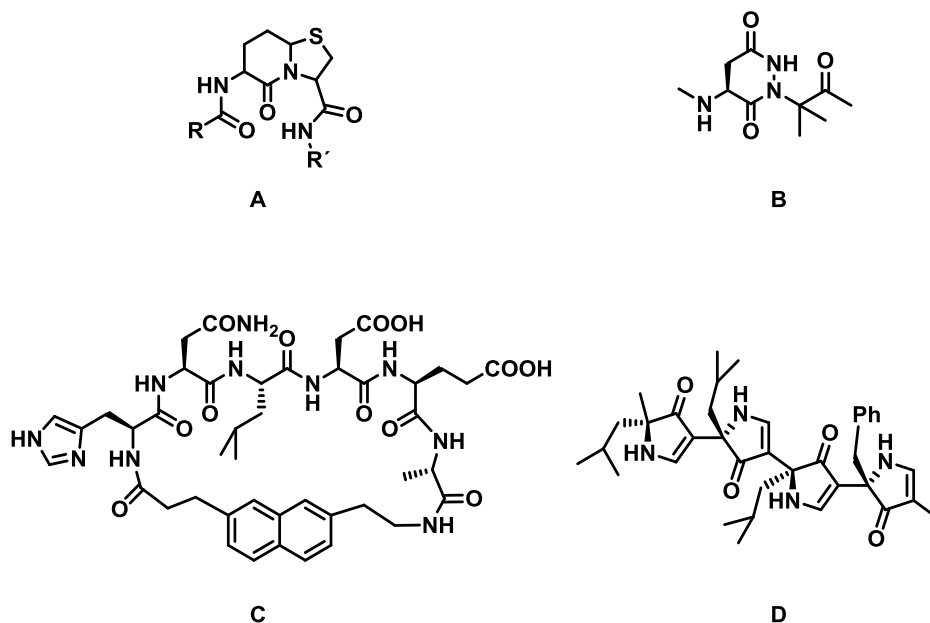


Figure 16 Selected examples of secondary structure mimetics.

Higher level of peptidomimetics is also achieved in the form of what is called scaffold peptidomimetics. A rigid template core is selected and it is decorated with pharmacophore residues in such way that they are ordered in the binding configuration. Platelet aggregation can be prevented through action of antagonists of fibrinogen. They act via binding to the same receptor, the glycoprotein IIb/IIIa (GPIIb/IIIa).^[161] Protein sequence binding to this receptor is organized into a β -turn and it was discovered that the Arg–Gly–Asp sequence (shortened to RGD in amino acid letter-code) carries the required pharmacophore residues. Researchers have produced a number of RGD-based scaffold mimetics. In some examples Gly was replaced by rigid moieties to produce potent antagonists for this receptor (Figure 17).^[162–164]

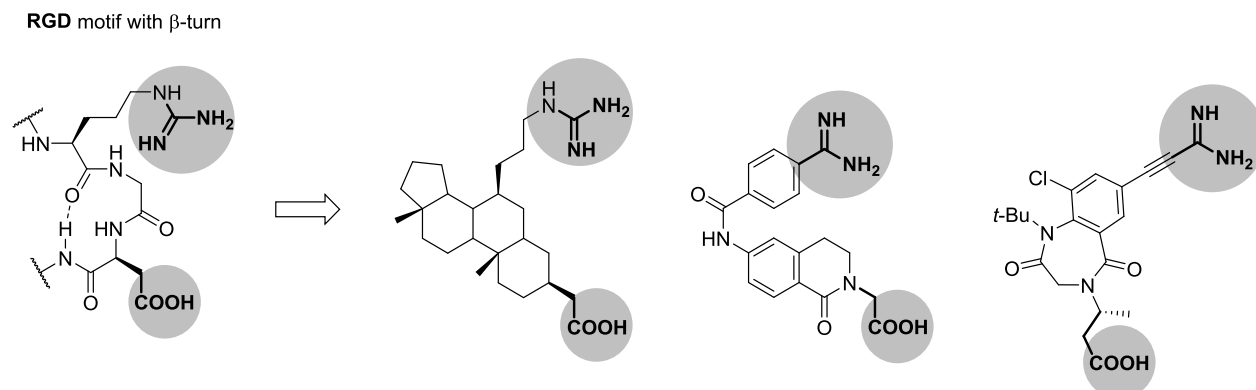


Figure 17 Scaffold peptidomimetics for GPIIb/IIIa receptor binding RGD motif.

A potent somatostatin agonist has been designed using β -D-glucose as a core scaffold decorated by the recognized pharmacophore substituents of somatostatin (Figure 18).^[165] Alzheimer disease still greatly puzzles scientists all over the world, and effective therapies are almost nonexistent. Scaffold peptidomimetics has been applied to develop an antagonist for one of the related signaling molecules, a thyrotropin-releasing hormone peptide.^[166,167]

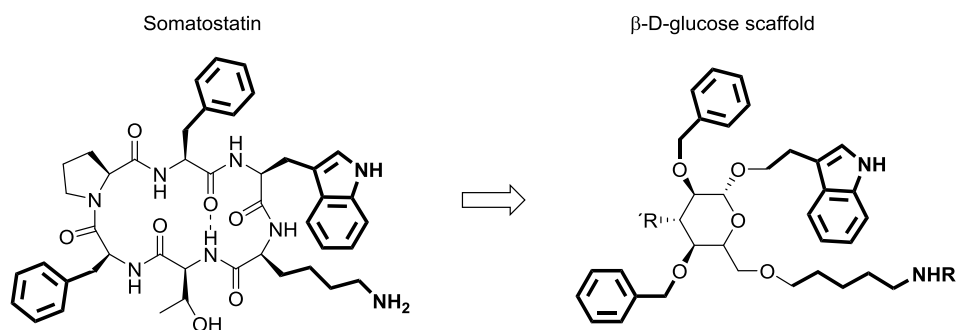


Figure 18 Scaffold mimetics of somatostatin, using substituted β -D-glucose.

It was mentioned previously that peptides are generally not good lead compounds. Probably the major reason for that is the vulnerability of their backbone to proteolytic enzymes. Accordingly, in peptidomimetics this is addressed via replacement of the peptide backbone with suitable isosteres, simultaneously preserving pharmacophore elements, preferably with lipophilic groups which generally enhance bioavailability. Peptidomimetic modifications where peptide bonds are exchanged for isosteres are called pseudopeptides.^[168] Those replacements can be retro-inverso amide bonds, hydroxyethylenes, ketomethylenes, alkenes, ethylenes, trifluoromethylamines, phosphonates etc. (Figure 19A). If one or more α -carbons are replaced with nitrogen atom, such mimetics are called azapeptides (Figure 19B).^[169] Those of them with all α -carbons replaced with N are azatides^[170] and peptoids.^[171]

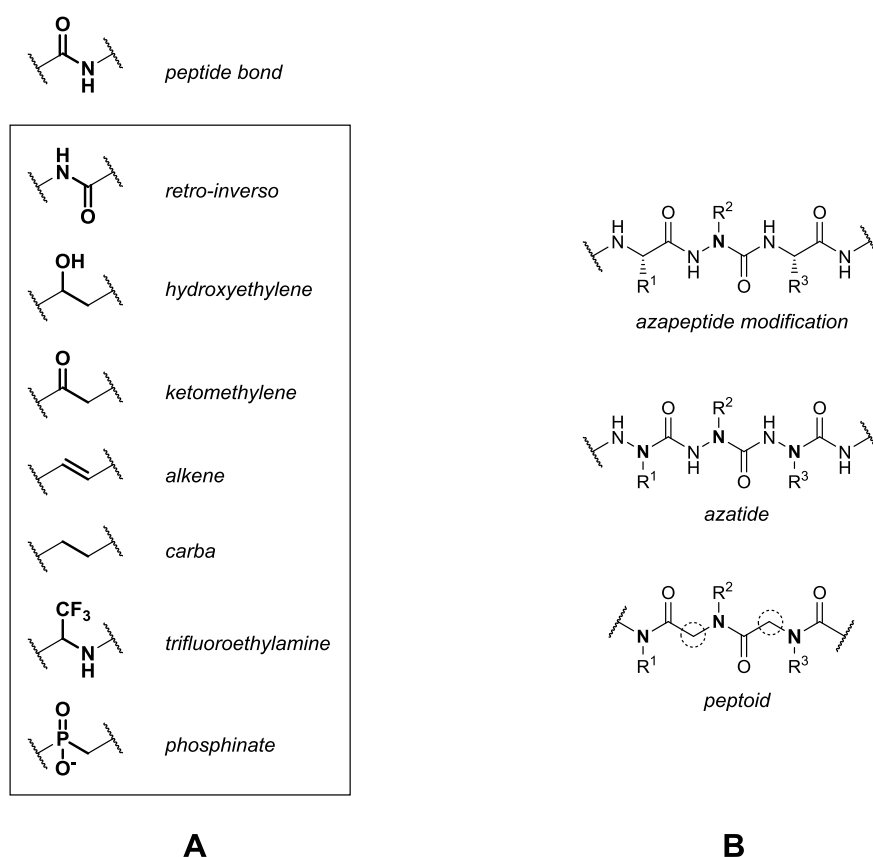


Figure 19 A: Peptide bond isosteres; B: Azapeptides.

Discovery and commercial launch of human immunodeficiency virus protease inhibitors is a famous success in drug development history. Besides the early database-driven approach of Dupont-Merck scientists, HIV-1 protease inhibitors resulting from peptidomimetic approaches are still the most popular weapon against AIDS. The main feature of peptidomimetic HIV-1 protease inhibitors is a noncleavable isostere that substitutes the peptide bond which is hydrolyzed by the enzyme.^[172-174] In most cases that replacement is the hydroxyethylene isostere. The hydroxyethylene isostere is also a transition state mimetics, mimicking the tetrahedral transition state stabilized by the enzyme during the hydrolysis event (Figure 20).

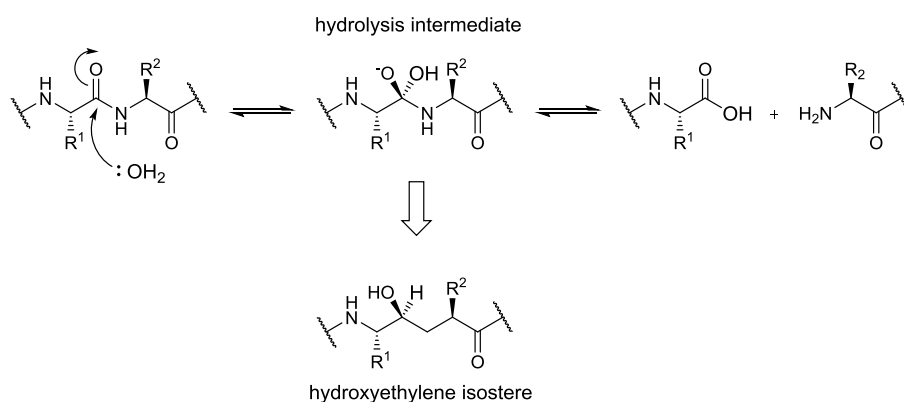


Figure 20 Comparison of the tetrahedral transition intermediate in the peptide bond hydrolysis with the hydroxyethylene isostere.

In contrast to the successful cases of peptidomimetic drugs for targeting ACE and viral enzymes, attempts to develop efficient opioid receptor agonists/antagonists based on peptide mimetics, have not been successful. For example, good substitutes for μ -opioid receptor binding narcotics, like morphine and its potent derivatives, are still sought for.

1.2.3.5 Inhibitors of metalloproteases

1.2.3.5.1 Development of Inhibitors of Angiotensin Converting Enzyme

In terms of drug development, the best studied zinc metalloprotease by far is angiotensin-I-converting enzyme (ACE). In clinical blood pressure management inhibiting this enzyme is the most important course of action. A considerable collection of compounds has been produced to explore the structure-activity relationship before the structure of ACE has become available.^[175] Although effective peptidomimetic inhibitor drugs for ACE have been designed much earlier based on structure homology with carboxypeptidase A, the first structure of human ACE has been determined only a decade ago.^[176]

An important lead was found in 1965 among peptides from the venom of the *Bothrops jararaca* species of snakes. It was discovered that the snake venom peptides have dual action: inhibition of conversion of angiotensin I into angiotensin II (vasoconstrictor) and inhibition of degradation of bradykinin (vasodilator).^[177,178] Among the identified peptides, the nonapeptide Pyr-Trp-Pro-Arg-Pro-Gln-Ile-Pro-Pro or teprotide, had the greatest in vivo potency and was effective in lowering blood pressure. Cushman and Ondetti of Squibb used these peptides as a starting point for the design of captopril as the first commercial antihypertensive drug.^[179]

The known structure of the zinc metalloprotease carboxypeptidase A was brought into connection with the probable structural characteristics of ACE, providing the grounds for postulation of the same mechanism.^[135,180] The most important subsites which are binding peptides in carboxypeptidase A are a carboxylate-binding subsite which accommodates the C-terminal amino acid residue, and the zinc ion which interacts with the carbonyl of the substrate peptide bond (Figure 21A).^[136] A simple and potent inhibitor of carboxypeptidase A was found in (*R*)-2-benzylsuccinic acid, which complies to all of these requirements, but its exceptional potency was attributed to mimetics of products of substrate hydrolysis (Figure 21B).^[181]

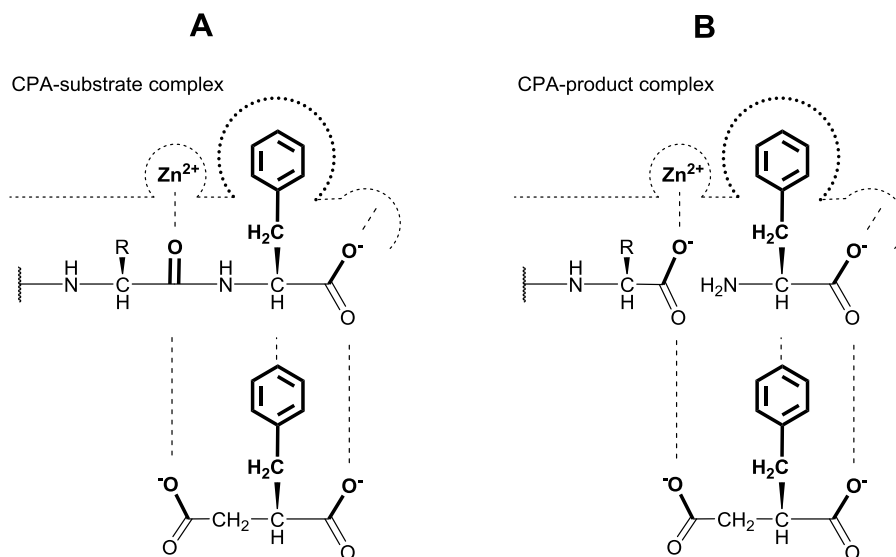


Figure 21 (*R*)-2-benzylsuccinate as peptidomimetic ligand for carboxypeptidase A (CPA). **A**: comparison of the mimetics with the enzyme-substrate complex; **B**: comparison of the mimetics with the enzyme-product complex.

The carboxypeptidase A-based structural model of interactions and the prominent feature of a C-terminal proline in ACE inhibition by the snake venom peptides led to a series of peptidomimetic carboxyalkanoylproline derivatives as prototype inhibitors of ACE. The N-terminal amino group was substituted by isosteric functional groups in order to reduce the number of peptide features and to enhance the stability. Unfortunately, these molecules displayed poor inhibition of ACE. Ultimately introduction of a thiol group as a strong zinc complexing ligand enhanced the inhibition significantly resulting in potent inhibitors of angiotensin-converting enzyme (Figure 22).^[136] A binding mode for inhibitors of ACE was proposed considering the difference between the two enzymes where carboxypeptidase A acts as an exopeptidase (cleaving a single C-terminal amino acid) and ACE acts as endopeptidase – or more precisely as a dipeptidyl carboxypeptidase. Hence, there is one additional binding subsite between zinc ion and the subsite binding the C-terminal carboxylate (Figure 22 right).

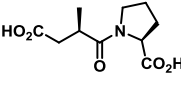
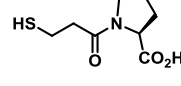
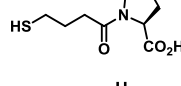
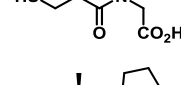
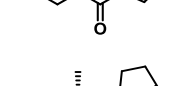
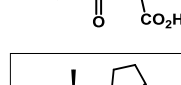
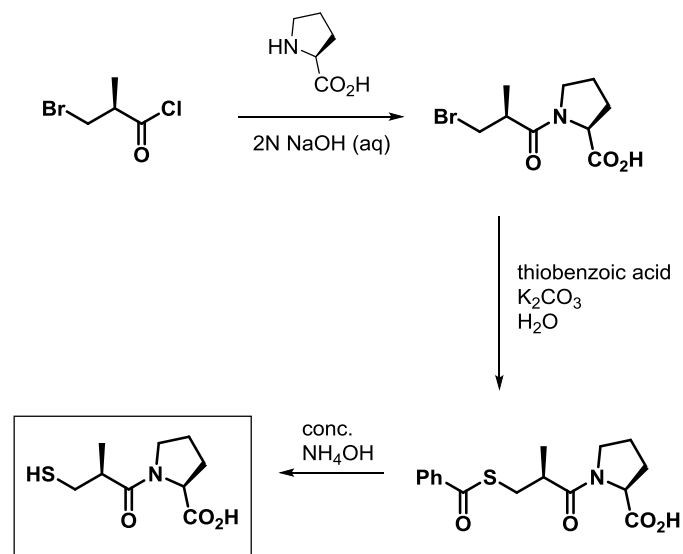
Compound	Relative K_i [nM]
	1100
	10
	12000
	120
	12500
	120
 captopril	1

Table 4 Relative inhibition potencies of captopril and selected derivatives.



Scheme 4 First synthesis of captopril.

Two decades later the cocrystal structure of captopril in complex with the testicular ACE confirmed the postulated binding mode and provided more precise insights into the crucial interactions (Figure 23).^[176,184]

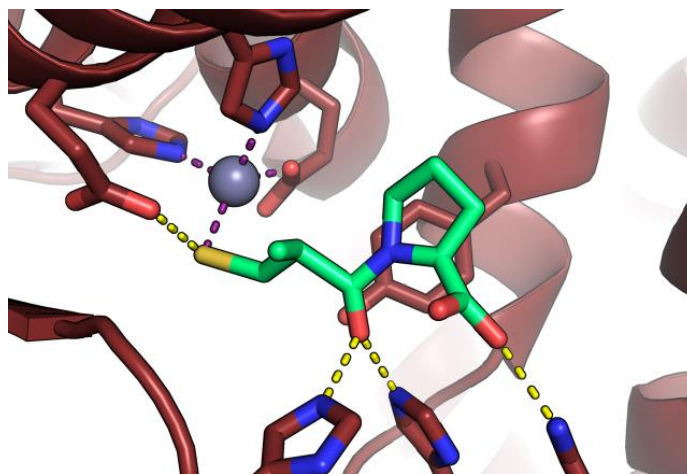


Figure 23 Binding mode of captopril in testicular ACE (tACE). Picture rendered from PDB entry 1UZF.^[184]

1.2.3.5.2 Development of Matrix Metalloprotease Inhibitors

Matrix metalloproteases (MMPs) operate in the extracellular matrix, where they participate in the reshaping of connective tissue. The whole group displays proteolytic activity on practically all peptides and proteins of the extracellular matrix.^[185,186] Due to such extensive activity, they are tightly regulated through transcriptional regulation by cytokines and growth factors, requiring activation as proenzymes and inhibition by specific tissue inhibitors of matrix metalloproteases (TIMPs). Certain clinical states involving uncontrolled degradation of connective tissue, e.g. arthritis and tumor invasion and metastasis, are consequences of misregulation of MMPs. Among human MMPs, fourteen have been characterized. These include collagenases, stromelysins, gelatinases, matrilysin, metalloelastase, and a small number of MMP isozymes (Table 5).

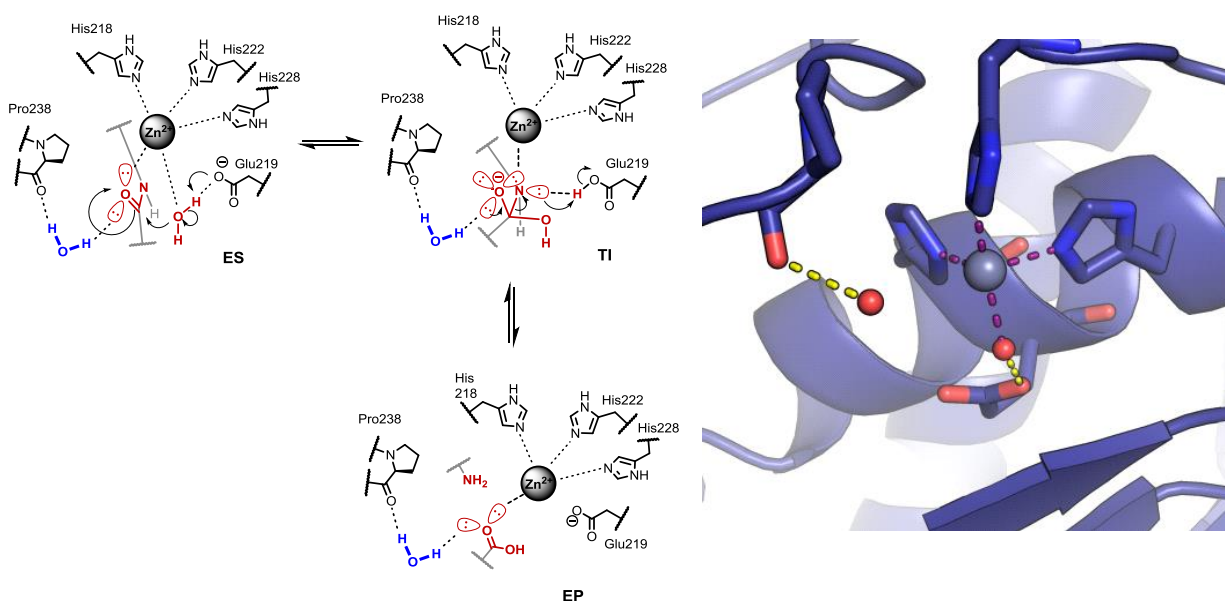
	Name	Indications
MMP-1	fibroblast collagenase (HFC), collagenase-1	cancer, arthritis
MMP-2	gelatinase A (Gel A), 72 kD gelatinase, type IV collagenase, human fibroblast gelatinase (HFG)	cancer, MS, stroke
MMP-3	stromelysin-1 (HSl1)	cancer, arthritis
MMP-7	matrilysin	cancer
MMP-8	neutrophil collagenase (HNC), collagenase-2	
MMP-9	gelatinase B (Gel B), 92 kD gelatinase, human neutrophil gelatinase (HNG)	cancer, MS, stroke
MMP-10	stromelysin-2	
MMP-11	stromelysin-3	cancer
MMP-12	metalloelastase	emphiseama
MMP-13	collagenase-3	arthritis
MMP-14–17	membrane-type MMPs	cancer

Table 5 Characterized matrix metalloproteases.

Although there are big differences in the determined structures between MMPs, the structures of their active sites are equivalent. However, differences in their surface loops, differentiating mostly their S1' subsite^[187] result in different substrate specificity. For human MMPs a number of active site residues are conserved. Histidines His218, His222, and His228 coordinate the zinc ion. Like in most metalloproteases, Glu219 in MMPs is acting as a general

acid-base at the catalytic site. Ala182, Leu181, Tyr240, Pro238 and Ala234 conserved residues participate in the spatial definition of the subsites and in the substrate positioning interactions.^[188–192]

A major structural difference between MMPs and prototypical metalloproteases like thermolysin and carboxypeptidase A is the absence of an “oxyanion” hydrogen bond donor.^[8,193] Determination of the structure of MMP-7 in complexes with inhibitors uncovered a constitutional water molecule positioned to serve as an equivalent hydrogen bond donor stabilizer of the transition intermediate oxyanion.^[191] Based on the observation the authors propose a general acid-base hydrolysis mechanism equivalent to those of thermolysin,^[44] CPA,^[30,35] DPP3,^[16,106] and ACE,^[176,184] with the exception of having a conserved water molecule which assists in stabilization of the transition intermediate (Scheme 5).



Scheme 5 Left: the general acid/base mechanism of action of MMP-7 (matrilysin) in hydrolysis of peptides.^[191] **ES:** Enzyme-substrate complex; **TI:** transition intermediate (amino-gem-diolate); **EP:** enzyme-product complex. Free electron pairs and their lobes are emphasized on the atoms of the peptide bond and its transition structures. **Right:** Structure of the active site of matrilysin (rendered from PDB entry 1MMQ).

Because of their pharmacologically interesting implications MMPs are subject of drug development. A large number of inhibitor candidates has been produced. The most of them are

pseudopeptides.^[128] Most MMP-targeting peptidomimetics have a zinc-binding function (ZBF) installed on one end. They are divided into three classes.

Class I inhibitors are constructed so that they have two sp^3 carbons between the first peptide bond and the ZBF. Their ZBF is designed to chelate zinc in the fashion of the tetrahedral hydrolysis intermediate. The most effective ones are hydroxamates and succinamide carboxylates. Class II MMP inhibitors have three sp^3 -hybridized atoms between the ZBF and the first peptide bond. The most notable ones are (*R*)-carboxyalkylamino amides and glutaramide carboxylates. Their design is mimicking the enzyme-product complex, or also the secondary peptide hydrolysis intermediate, having a protonated amine (Figure 24).

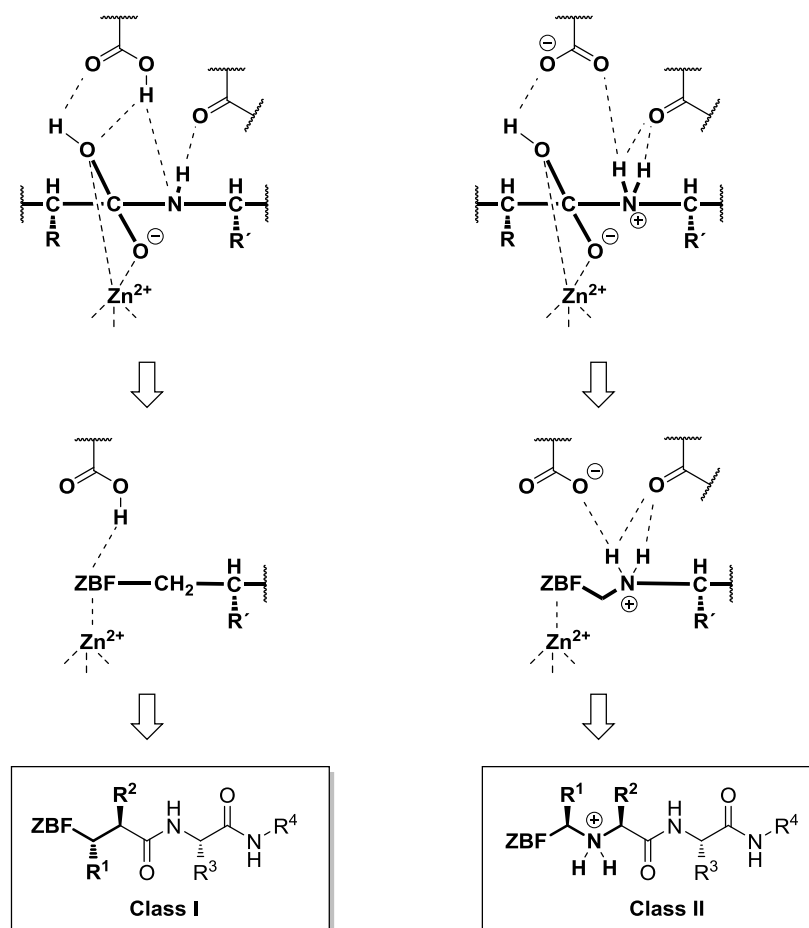


Figure 24 The design of class I and class II inhibitors of matrix metalloproteases.

Class I hydroxamate inhibitors with isobutyl group as R² and amide capping at R⁴ potentially inhibit all MMPs (K_i range is 1–100 nM). Bigger groups at R² generally increase potency, except in the cases of MMP-1 and MMP-7.^[194,195] Introduction of tryptophan as R³ and macrocyclization with C₆-alkyl chain between its two nitrogens result in somewhat increased potency, but introduces higher selectivity to some MMPs. The succinamide carboxylate derivatives have generally 100–2000-fold lower potencies (Figure 25).^[194,196]

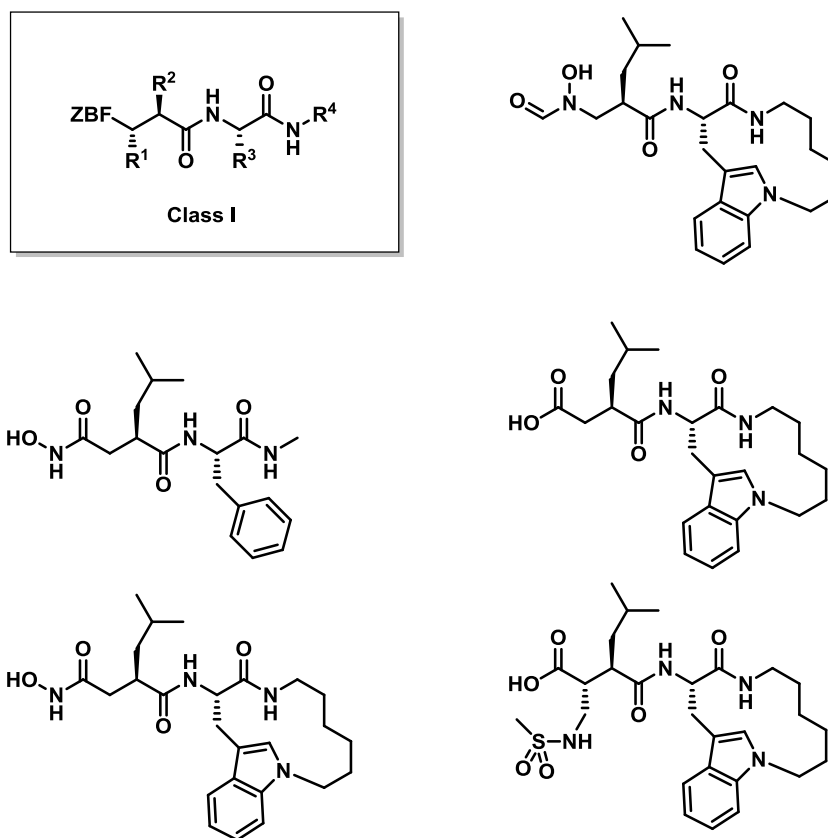


Figure 25 Examples of class I inhibitors of matrix metalloproteases.

Compounds of the structural class II have been relatively successful inhibitors of ACE, and for that reason class II has been explored in inhibition of matrix metalloproteases. From ACE inhibition investigations (Figure 26A) it was known that an alkyl substituent at the R¹-position enhanced inhibition dramatically, while the unsubstituted version was of comparable potency to the analogous class I carboxylate. Introduction of the (*S*)-configured R¹-methyl group increased

inhibitory potency 50-fold against ACE.^[175] In the case of the MMPs, the use of an equivalent scaffold produced potent inhibitors, but equivalent R¹-substitution patterns caused just a modest increase in potency (Figure 26B).^[197]

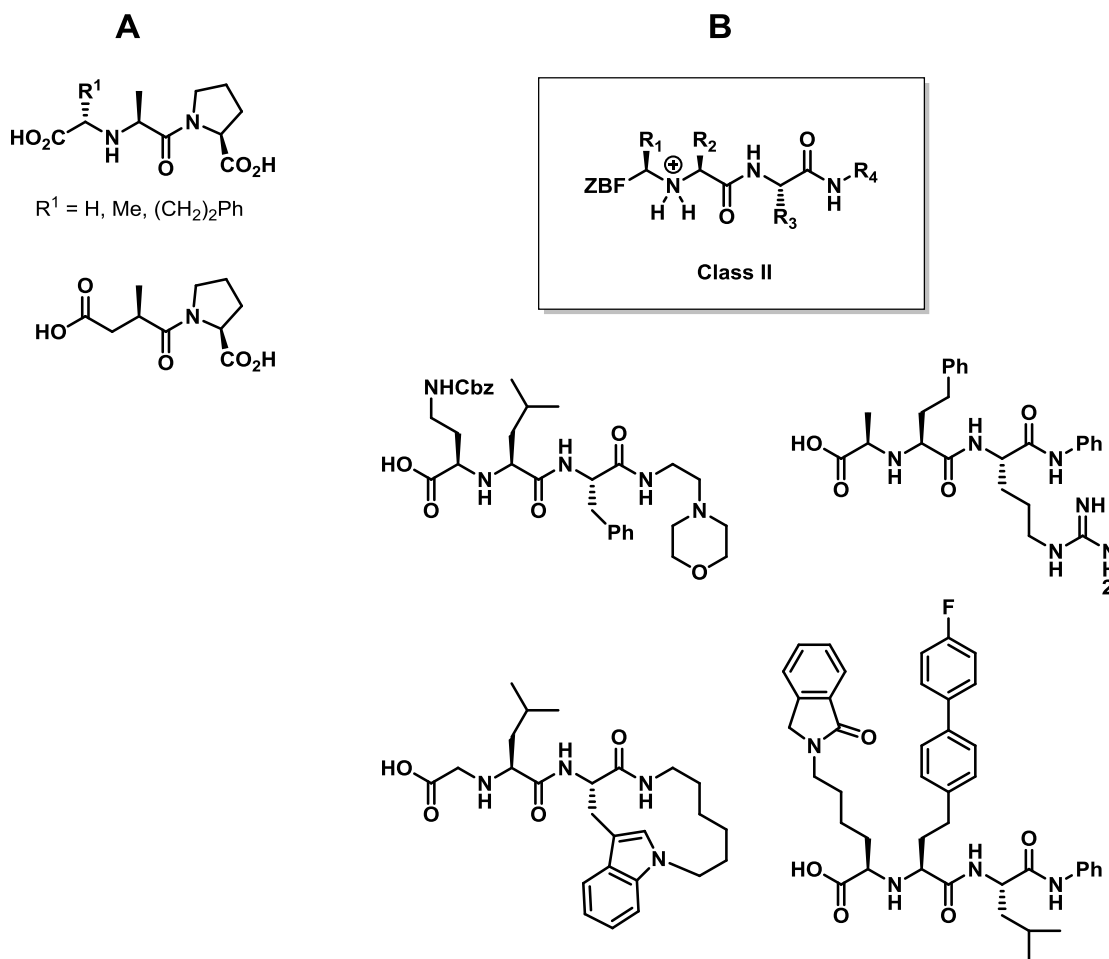


Figure 26 A: Class I and class II inhibitor scaffold used in inhibition of ACE; **B:** examples of class II inhibitors of matrix metalloproteases inspired by carboxylate inhibitors of ACE.

The cocrystal structures of both class I and class II MMP inhibitors are available.^[51,191] These structures from different research groups display almost identical binding topologies and clearly illustrate that the ZBF in both classes are involved in key interactions in the active site (Figure 27).

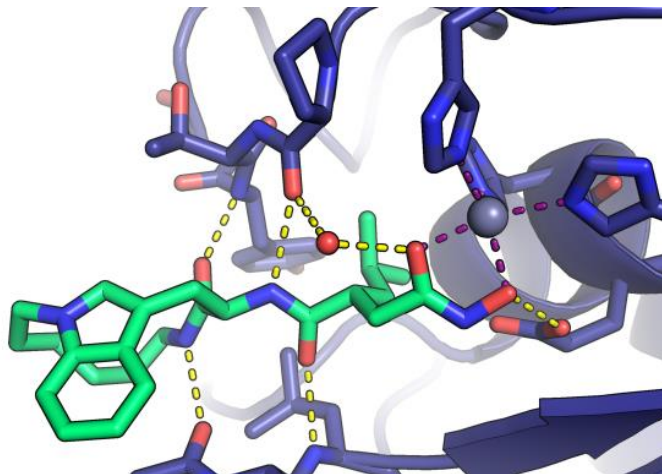


Figure 27 Class I hydroxamate pseudopeptide MMP inhibitor in complex with MMP-7 (matrilysin). Picture rendered from PDB entry 1MMQ.^[191]

Due to long-known issues with lack of specificity and off-targeting with the classical pseudopeptide hydroxamate MMP inhibitors, recently more attempts have been made to develop completely nonpeptidic MMP inhibitors, which consider binding secondary sites (exosites), out of the typical peptide binding subsites (Figure 28).^[198]

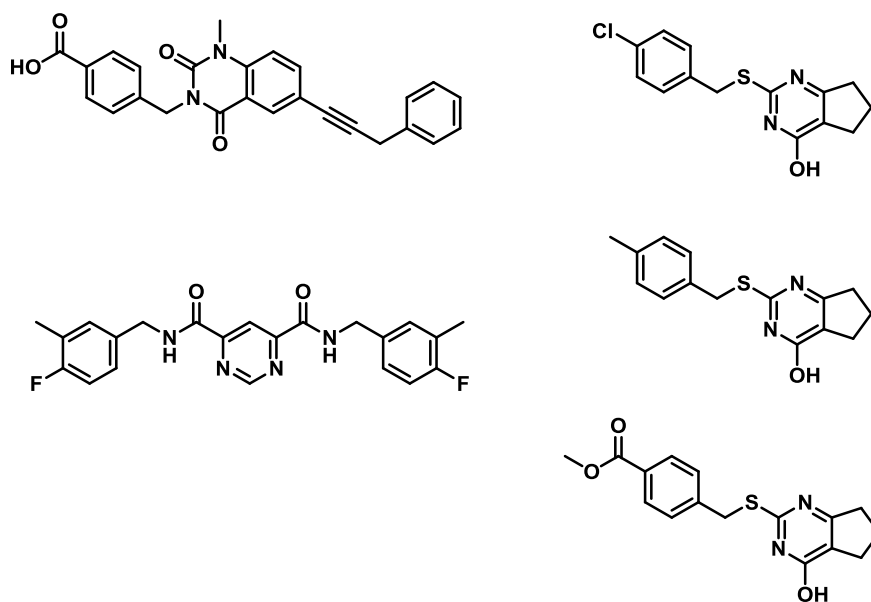
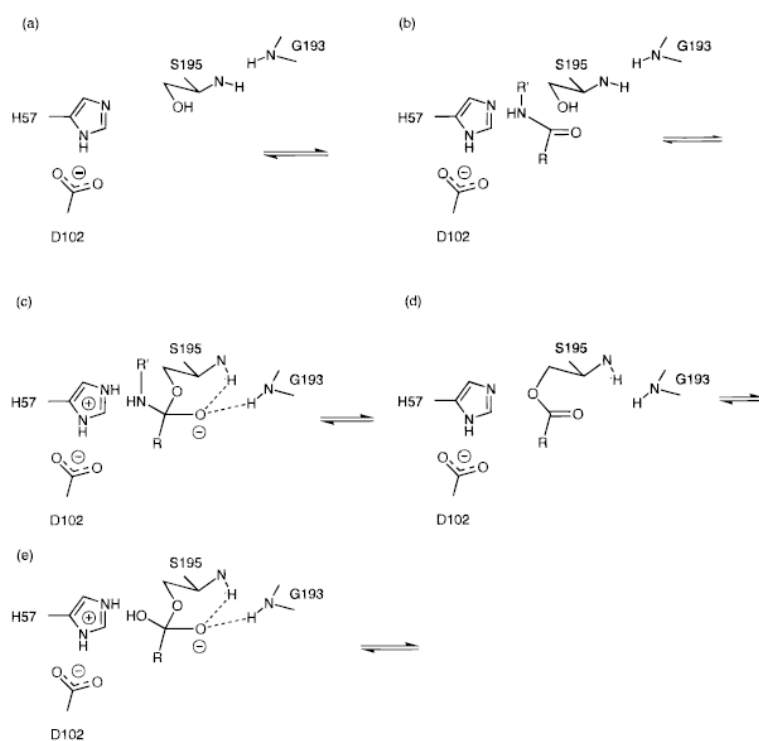


Figure 28 New generation of nonpeptidic inhibitors of MMPs.

1.2.3.6 Inhibitors of Serine Proteases

One of the best studied families of enzymes is serine protease family. The trypsin/chymotrypsin class is the most characterized among them.^[199] Human neutral elastase and thrombin were specifically interesting for drug development.

In mechanistic terms, they dispose the classic arrangement of a catalytic triad of Ser-His-Asp and an “oxyanion hole”. The catalytic triad is represented by Ser195 as nucleophile, His57 as the general acid/base, and Asp102 for stabilization and orientation of His57. The stabilization of transition state and the intermediate is facilitated by the oxyanion hole composed of the backbone amide hydrogen bond donors of Gly193 and Ser195.



Scheme 6 Mechanism of peptide hydrolysis catalyzed by a serine protease. Picture taken from ref. 199.

Upon substrate binding event, the Ser195 hydroxyl nucleophile performs the nucleophilic attack on the carbonyl of the substrate peptide bond, while the basic His57 simultaneously

removes the proton from the nucleophile (Scheme 6). The attack results in formation of the tetrahedral intermediate, whose oxyanion gets stabilized by the oxyanion hole hydrogen bond donors. His57 protonates the nitrogen atom of the intermediate, and the C–N bond breaks down so that the covalent acyl enzyme complex remains. The acyl-enzyme complex is attacked by a water molecule, which is supported by His57 and Asp102 in an equal way. The second intermediate breaks down too, producing a free carboxylic acid and releases Ser195 to the resting state.

Chymotrypsin can perform hydrolysis of benzoyl-L-arginine amide. Kinetic experiments were performed for this case using ^{15}N -labeling. The determined kinetic isotope effect was close to unity, implicating stability of the C–N bond in the main transition state.^[200] The transition state in catalysis is evidently very similar to the tetrahedral intermediate.

Among natural products which inhibit various serine proteases are chymostatin^[201] and leupeptin (Figure 29).^[202] Cocrystal structures with their proteases have been determined: chymostatin bound to *Streptomyces griseus* protease A,^[203] and leupeptin bound to trypsin.^[204]

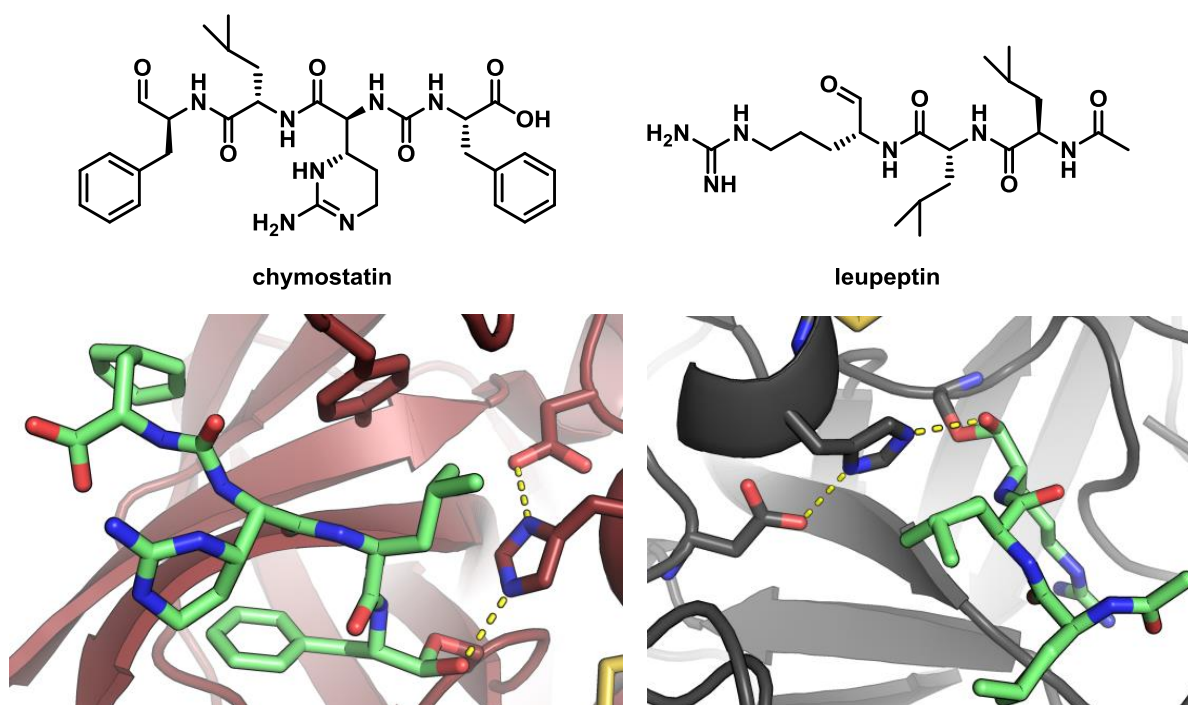


Figure 29 Cocrystal structures of chymostatin with chymotrypsin (left, PDB: 1SGC), and leupeptin with trypsin (right, PDB: 1JRT).

Streptomyces griseus protease A (SGPA) has a large hydrophobic S1 specificity pocket, just like the related chymotrypsin. From both cocrystal structures it is apparent that the aldehyde has been attacked by Ser195 and it forms a covalent adduct. The phenyl group of chymostatin is in close complementary contact with the large hydrophobic S1 subsite of chymotrypsin, and in the case of leupeptin-trypsin complex, the equivalent position is held by the Arg residue of leupeptin, where polar interactions are dominant in trypsin. The backbone amides of both the inhibitors bind as extensions to the β -sheet of the corresponding proteins. The terminal carboxylate of chymostatin in complex with chymotrypsin remains exposed to the solvent. In both complexes the hydrogen bonding interactions between the residues of the catalytic triad have been emphasized in Figure 29.

1.2.3.6.1 Inhibitors of Thrombin

Thrombin is the serine protease responsible for the cleavage of soluble fibrinogen. It converts fibrinogen into insoluble fibrin. This occurs in steps of the coagulation cascade. Targeting thrombin provides means of inhibiting unwanted blood clots. Consequently, inhibitors for this protease have been developed into medical anticoagulants.^[205] The most potent natural inhibitor of thrombin was known as a small protein isolated from the leech *Hirudo medicinalis* and named hirudin accordingly.^[206] It is so potent that it inhibits thrombin with a $K_i = 22$ pM. Hirudin binds in a manner considerably different from that of the fibrinogen substrate. The *N*-terminus binds to the active site and the peptide chain spreads along so that its *C*-terminal region interacts with thrombin in the fibrinogen recognition exosite.^[207,208]

The α -chloro ketone PPACK is a potent irreversible inhibitor of thrombin.^[209] This type of inhibitor is mechanism-based and forms an irreversible covalent attachment to one of the catalytic residues. The crystal structure displays that the ketone carbonyl forms a hemiketal upon the nucleophilic attack by Ser195, and His57 gets alkylated by displacement of the chloride from the inhibitor. The hemiketal hydroxyl group points into the oxyanion hole with the distances of 3.2 Å to both hydrogen bond donating N–H functions of Ser195 and Gly193.

It is proposed that histidine alkylation can mechanistically occur in two ways (Figure 30). Either His57 nitrogen is alkylated by the alkyl chloride after the formation of hemiketal, or the

hemiketal oxyanion performs an intramolecular attack to form an epoxide which is immediately opened by the attack of His57. The PPACK action on thrombin represents a typical case of inhibition of serine proteases by α -chloro ketones.

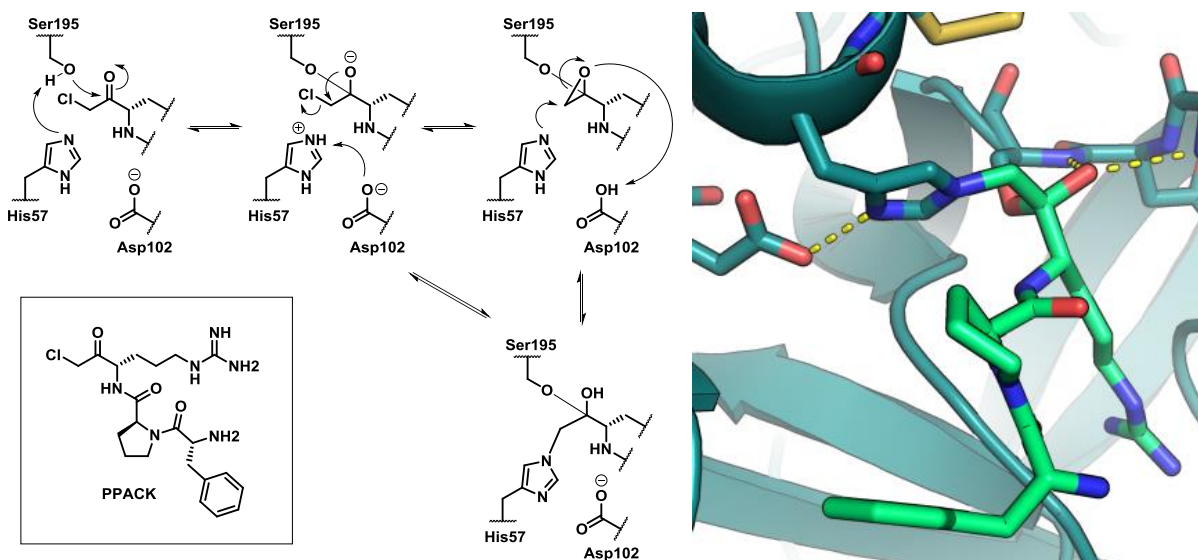


Figure 30 Left: two proposed pathways of inactivation of thrombin by PPACK; Right: crystal structure of PPACK-thrombin adduct (PDB: 1PPB).^[209]

A potent boronic acid derivative thrombin inhibitor (DuP714, $K_i = 40$ pM) was developed by DuPont-Merck scientists.^[210] The cocrystal structure has been solved. A covalent bond between the boron atom of the inhibitor and the hydroxyl oxygen of Ser-195 results in a type I complex, which was not surprising based on the previous knowledge about complexes of boronic acids with serine proteases.^[128] The inhibitor binds in an equivalent manner to how PPACK binds to thrombin, but the boron shows a more trigonal than tetrahedral geometry in complex with four donors.

This investigation was a great contribution to the general SAR knowledge about thrombin. Amidine, lysine, ornithine, and homolysine analogs of DuP714 were prepared, and assayed and cocrystallized with thrombin (Figure 31). The detailed stereoelectronic data on interactions in the S1 subsite of thrombin have been acquired.^[210]

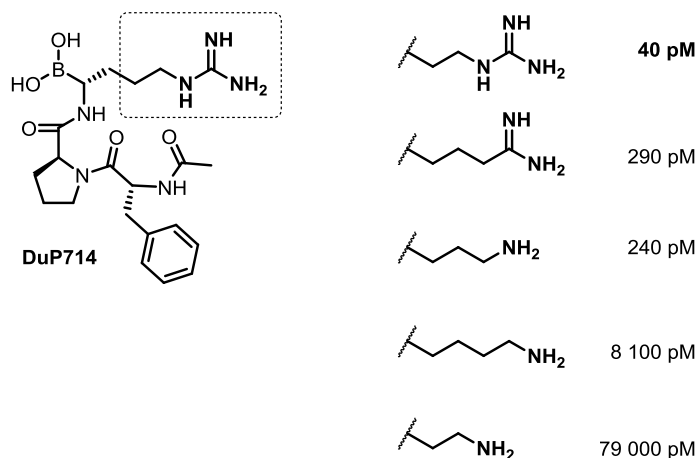


Figure 31 The Dupont-Merck series of boronic acid derivatives of PPACK for inhibition of thrombin.

One of the medicinal chemistry campaigns in development of thrombin inhibitors identified and used an *N*-tosylated arginine as a lead compound based on its substrate inhibition behavior. Potent reversible derivatives argatroban (MD-805, $K_i = 19 \text{ nM}$)^[211] and NAPAP ($K_i = 6.6 \text{ nM}$)^[212] have been found (Figure 32).

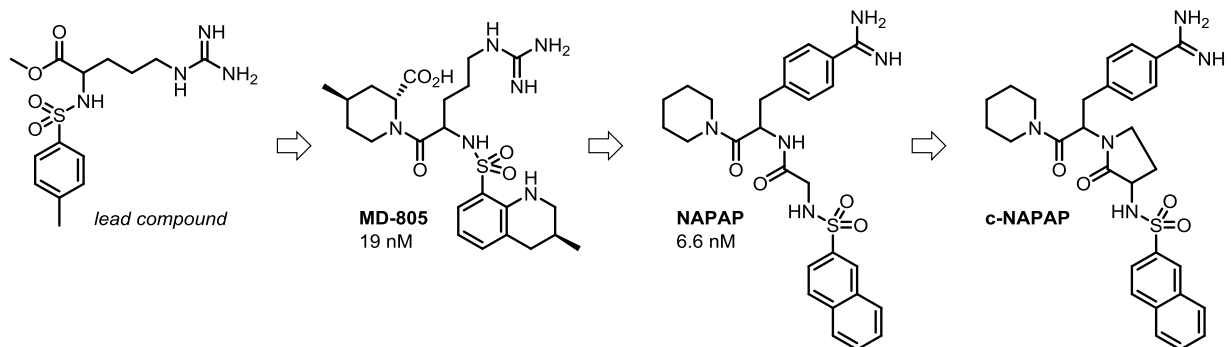


Figure 32 The development of *N*-tosyl arginine mimetic inhibitors of thrombin.

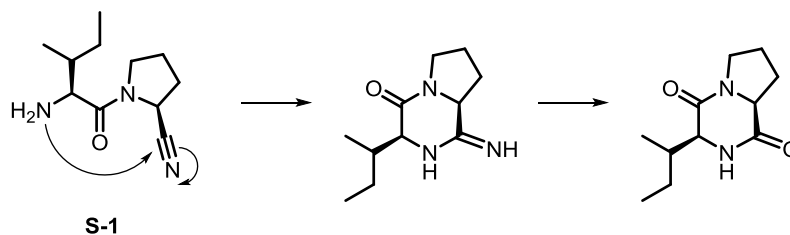
The molecules have been cocrystallized with thrombin and the structures determined.^[209,213–215] Previous modeling studies^[216] gave grounds to propose a substrate-like binding mode, but the crystal structure revealed that the arginine side chain occupied the S1 subsite in a considerably different way than what is observed for binding of PPACK.

1.2.3.6.2 Saxagliptin - Case Study in Inhibition of DPP4

Peptide hormone insulin produced in the pancreas modulates the blood sugar level. Defects in insulin-based regulation lead to high blood glucose levels. This is caused by a disease known as diabetes. The most common type is type 2 diabetes, manifesting in elevated plasma glucose and glycosylated hemoglobin. It is the most prominent cause of blindness, renal failure, and limb amputations.^[217]

Two gastrointestinal hormones, known as glucagon-like peptide-1 (GLP-1) and glucose-dependent insulintropic polypeptide are inducing an increase in insulin secretion from the pancreas. The half-life of GLP-1 is very short, because it is rapidly degraded by the serine protease dipeptidyl peptidase-4 (DPP4). This knowledge invoked big medicinal campaigns in search for DPP4 targeting drugs.^[218,219]

In one of the most successful DPP4-related medicinal chemistry efforts, researchers of Bristol Myers Squibb (BMS) elaborated a cyanopyrrolidine amide lead scaffold (**S-1**, Scheme 7). Ferring Research reported this molecule as a potent inhibitor of DPP4,^[220] with medium-lasting pharmacokinetic profile and instability due to intramolecular cyclization (Scheme 7). This prompted a search for conformationally restricted analogs, which were found by Phenomix (compound **S-2**, Figure 33), demonstrating that this undesired cyclization can indeed be prevented. Due to IP issues, and in order to obtain efficient conformationally restricted inhibitors, BMS cleverly fused a cyclopropane ring into each pyrrolidine ring, examining the impact of different stereoisomers too. The molecules with the best stability and pharmacokinetic profile were found via **S-3** scaffold, having one cyclopropane-annulated pyrrolidine ring and one free amino acid side chain R.



Scheme 7 Intramolecular cyclization issue with the cyanopyrrolidine inhibitors of DPP4.

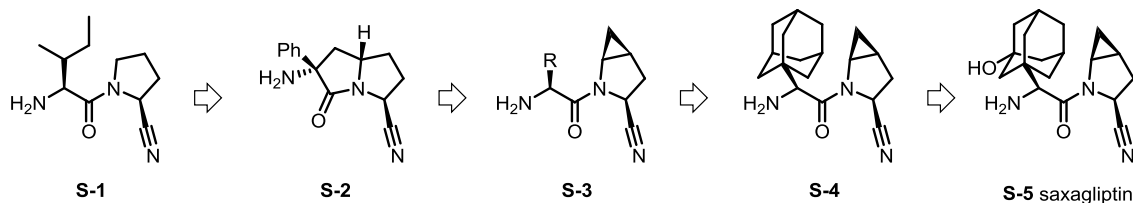
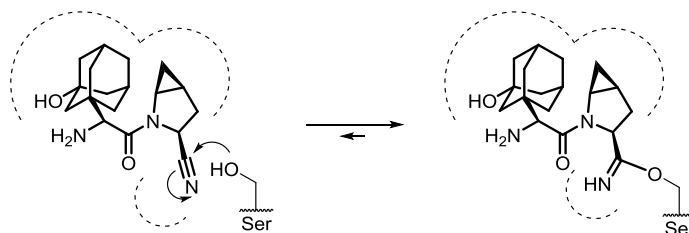


Figure 33 Chemical evolution of cyanopyrrolidine scaffold toward the marketed inhibitor drug for DPP4.

Additional enhancements in solution stability and overall potency were achieved with bigger steric bulk of R. For example, the R = *t*-butyl derivative of **S-3** inhibited DPP4 with $K_i = 7$ nM and had excellent pharmacokinetic properties (>50% oral bioavailability in rats). BMS examined further the impact of larger groups. Adamantyl derivative (**S-4**) was found to be the most potent, having $K_i = 0.9$ nM. It was a disappointing discovery that it was rapidly metabolized *in vivo*, due to the liver microsomal oxidation by cytochromes. The problem was solved with hydroxyadamantyl derivative **S-5**, named saxagliptin, which was almost equally potent, but had much better bioavailability and pharmacokinetic properties. After phase III clinical trials it was approved for treatment of type 2 diabetes and marketed under trade name Onglyza[®] by Bristol Myers Squibb.^[221,222]

Kinetic analysis showed that saxagliptin is a slow, tight-binding inhibitor of dipeptidyl peptidase-4. Two structural characteristics were brought into connection with this ligand behavior. The adamantyl substituent replaces a water molecule at the active site, resulting in the slow entropy-driven binding. The second aspect is formation of a reversible, covalent bond of nitrile with the catalytic serine residue of the active site, producing a slow enthalpic off-rate effect. The cocrystal structure of saxagliptin bound to DPP4 clearly displayed the covalent bond between the catalytic serine and the nitrile carbon atom (Scheme 8). To confirm the reversibility of the

formation of the adduct, dialysis was performed, showing that the enzyme was completely reactivated upon removal of the ligand.^[222]



Scheme 8 Formation of reversible covalent imidate adduct between saxagliptin and DPP4.

1.2.3.7 Inhibitors of Cysteine Proteases

Papains, the ICE class and the picornavirus 3C-proteases class represent the three characterized structural families of cysteine proteases.^[223–225] Cysteine proteases use the enhanced nucleophilicity of their active site cysteine thiol function to perform catalytic cleavage of peptide bonds.

The protease mechanism of papain is related to the protease mechanism of chymotrypsin. The nucleophile attacks the carbonyl of the substrate to give a tetrahedral intermediate. The intermediate breaks down, releasing the amine product to give an acyl enzyme intermediate. A water molecule attacks the acyl enzyme intermediate, producing the carboxylic acid. In papain catalyzed peptide hydrolysis, the $^{14}\text{N}/^{15}\text{N}$ kinetic isotope effect observed for labeled benzoyl-L-arginine amide showed that, in difference to the analogous mechanistic insights for serine proteases, the significant C–N bond cleavage occurs in the major transition state, suggesting that the breakdown of the tetrahedral intermediate is the rate limiting step.^[226] The same kinetic isotope effect for chymotrypsin indicated that both formation and breakdown of the transition intermediate contribute to the kinetics equally.^[200]

A lysosomal cysteine protease Cathepsin B has also been associated with pathophysiological conditions like inflammation, cancer progression, bone resorption, muscular dystrophy, and myocardial infarction. These indications prompted for Cathepsin B targeting

drugs.^[227] The plant cysteine protease papain is used as a model of cathepsin B due to very high homology in the active site. The protein fold is equivalent and structural characterization data favor equivalent catalytic mechanisms.^[228,229]

Leupeptin, a natural inhibitor of serine and cysteine proteases, was cocrystallized with papain and the reported structure (Figure 34)^[230] shows that the thiol function of Cys25 forms a hemithioacetal adduct upon the nucleophilic attack to the aldehyde function of leupeptin. Similar to serine proteases, the oxygen atom of the tetrahedral adduct binds to the oxyanion hole comprised of the backbone NH of Cys25 and the NH of the side chain of Gln19.

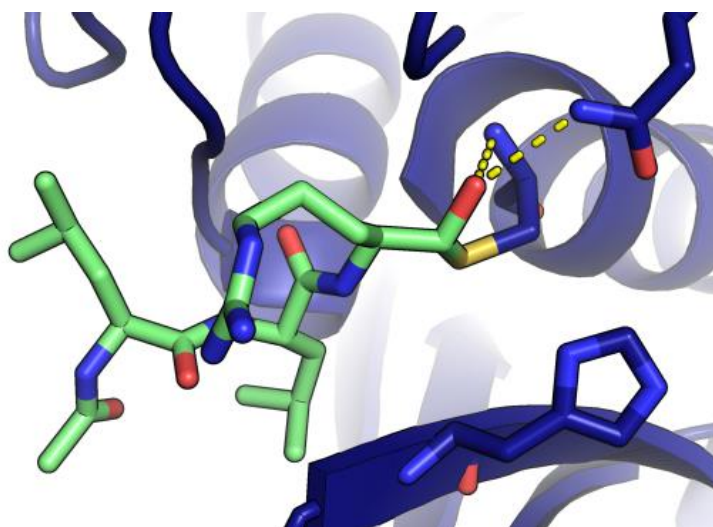
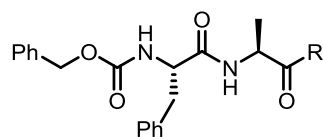


Figure 34 Binding mode of leupeptin in complex with papain (PDB: 1POP).^[230]

Leupeptin potently and reversibly inhibits cathepsin B, with a measured $K_i = 4.1$ nM, and its shorter peptide aldehyde analogue **P-1** ($R = H$) is slightly weaker with $K_i = 21$ nM (Figure 35). The dramatic loss in potency with ketone analogue **P-2** and trifluoromethyl ketone **P-3** indicates quite a different trend, as opposed to stronger inhibition of serine proteases.^[231]



		K_i [μM]
P-1	R = H	0.021
P-2	R = CH ₃	31
P-3	R = CF ₃	300

Figure 35 K_i values of inhibition of cathepsin B with three leupeptin analogs.

Although many nitrile compounds were ultimately not good inhibitors of serine proteases,^[232,233] they have still been very successfully used in inhibition of DPP4.^[220,221] In the case of cysteine proteases, nitrile function is widely used for covalent inhibitor design.^[234–236] It generally serves as an electrophile suitable for being attacked by the catalytic cysteine in the active site. ¹³C NMR experiments have been used to demonstrate that the inhibition of papain by a nitrile results in the enzyme bound thioimidate ester adduct (Figure 36A).^[237,238] These adducts are structural analogs of the acyl enzyme intermediate. Among the two simple covalent inhibitors **E-1** and **E-2** (Figure 36B), aldehyde derivative **E-1** ($K_i = 25 \mu\text{M}$) is a more potent inhibitor of papain than the nitrile derivative **E-2** ($K_i = 380 \mu\text{M}$).^[239] It is rationalized that papain can better stabilize a tetrahedral adduct formed with aldehyde, than the planar thioimidate in case of nitrile inhibitor. However, aldehydes are not the most desirable inhibitors due to instability. Upon introduction of a suitable subsite filling group, the nitrile inhibitor can get a significant boost in potency (**E-3**, $K_i = 0.73 \mu\text{M}$).

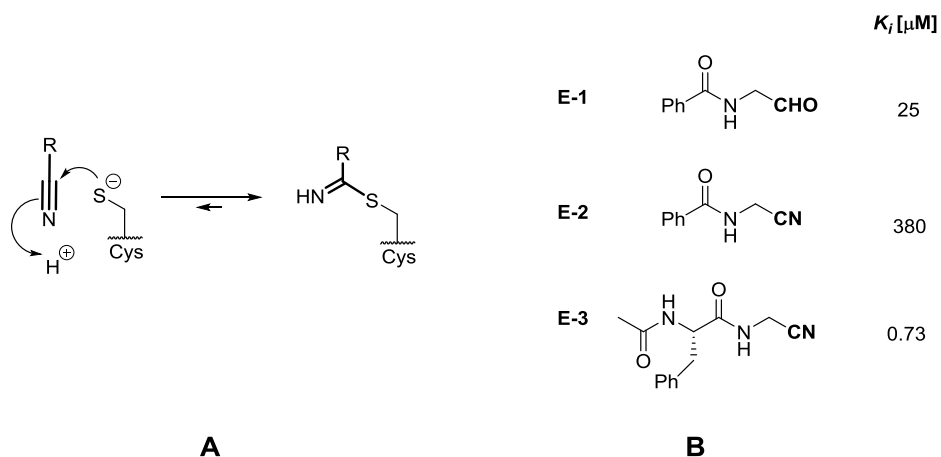


Figure 36 A: Formation of a reversible covalent thioimidate adduct between a nitrile inhibitor and a cysteine protease; **B:** Comparison of simple electrophilic, covalent inhibitors of papain.

Vinyl sulfones were designed as mechanism-based cysteine protease inhibitors (Figure 37A). Based on the active site geometry, it is proposed that vinyl sulfones engage in hydrogen bonding to the side chain NH_2 of the oxyanion hole Gln sidechain and the protonated His sidechain of the active site. This recognition pattern provides a convenient orientation to the vinyl sulfone in the active site, and proper positioning for the nucleophilic attack by the catalytic cysteine.^[240]

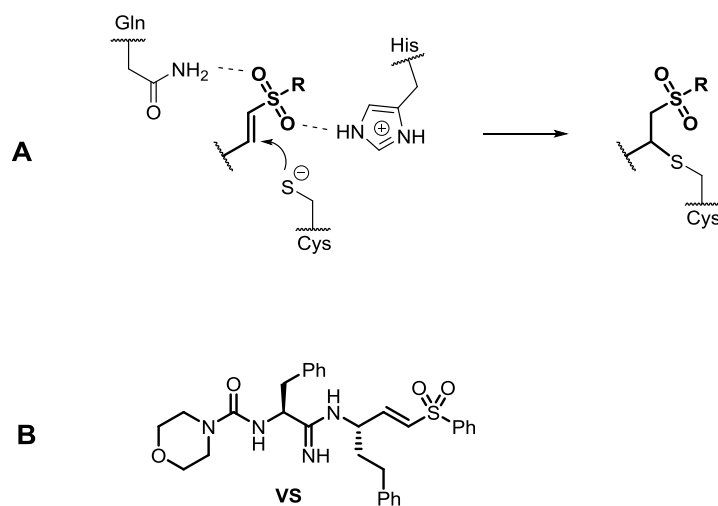


Figure 37 A: Formation of an irreversible covalent adduct between a vinyl sulfone inhibitor and a cysteine protease; **B:** A vinyl sulfone inhibitor of cathepsins and cruzain.

Vinyl sulfone derivatives like **VS** (Figure 37B) irreversibly inhibit cathepsins B, L, S, and O2 and cruzain, which is one of the important cysteine proteases in drug development efforts in fighting malarial parasites.^[235,241] Regardless of high structural homology between these enzymes, this class of compounds achieved some selectivity between the aforementioned cathepsins. In order to assess general reactivity to thiol nucleophiles, and thus possible risk of off-target reactivity, **VS** was tested with dithiothreitol. It was inert to it indicating that precise positioning is required in respect to thiol nucleophiles to react with them, e.g. when bound to the active site of cathepsins.

1.2.3.8 Inhibitors of Aspartic Proteases

Two members of the aspartic protease class of enzymes, renin and HIV-1 protease, have been the subjects of extensive research efforts to discover therapeutically useful inhibitors. Inhibitors of renin have high potential as antihypertensive agents,^[242] and have not yielded much success until only very recently, when aliskiren was approved for sales as the first, and still presently the only renin inhibitor drug.^[243] On another side, HIV-1 protease inhibitors have already been widely used in treatment of HIV infection.^[172,173,244] Aspartic proteases are endopeptidases. In this class the proteases have two different conserved Asp-Thr-Gly subsequences (for cathepsin D: Asp33-Thr34-Gly35 and Asp231-Thr232-Gly233). Cathepsin D can serve as a good example of a typical aspartic protease, showing these two chains closely positioned and oriented oppositely to each other. A water molecule which serves as a nucleophile in the protease catalyzed hydrolysis is bound mutually by the two aspartates (Figure 38B).

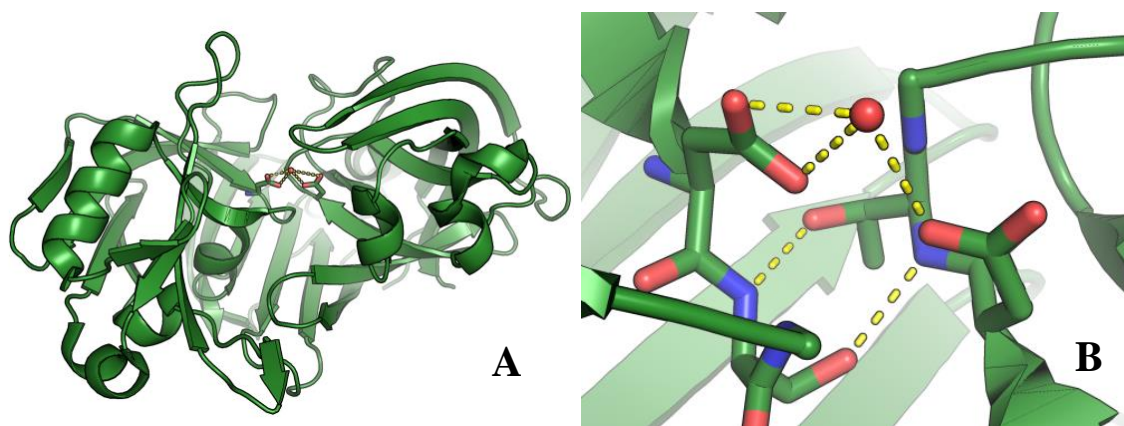
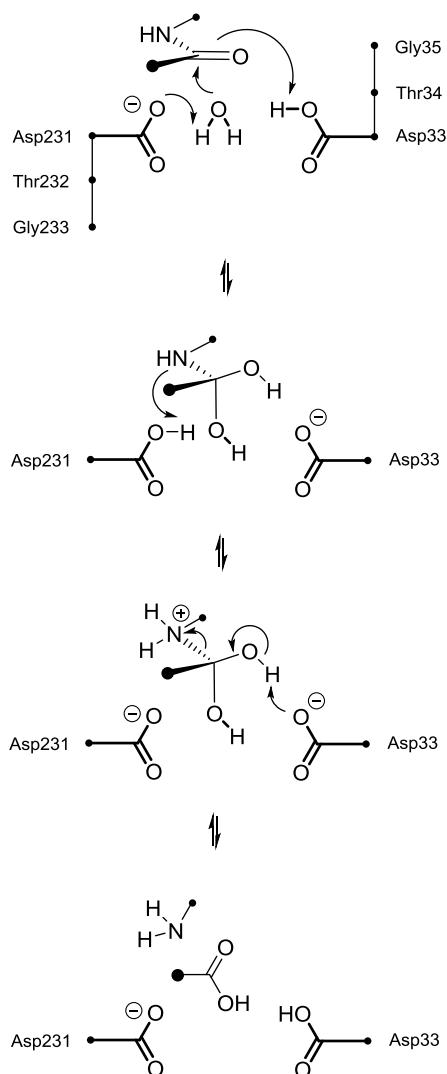


Figure 38 Structure of cathepsin D aspartic protease. **A:** The whole structure of the enzyme; **B:** active site and emphasis on the two conserved Asp-Thr-Gly subsequences in the opposing chains. The tight interaction network between the Thr residues keeping the chains together, and water-aspartate interactions are also depicted. The pictures were rendered from PDB entry 1LYA.

The consensus is that catalysis is initiated by the form of aspartic protease in which one aspartate is protonated and the other is deprotonated.^[245] A general acid/base-catalyzed hydrolysis mechanism type is proposed (Scheme 9). A water molecule attacks the scissile peptide

bond carbonyl and produces a tetrahedral intermediate. There is an intriguing report of a cocrystal structure of HIV-1 protease with the stabilized transition intermediate.^[246] Similar to metalloproteases, the nitrogen of the scissile bond gets protonated and the tetrahedral intermediate collapses, breaking apart into the peptide hydrolysis products.^[247,248]



Scheme 9 Mechanism of peptide hydrolysis catalyzed by an aspartic protease.

The natural product pepstatin was found in the 1970s to be a very potent pepsin inhibitor ($K_i = 56 \text{ pM}$).^[201] Pepstatin became known as a generic aspartic protease inhibitor. Its mode of binding and inhibition is considered a major blueprint for ligand binding to the aspartic protease

class enzymes. Structure-activity data and crystal structures of pepstatin and its derivatives with various aspartic proteases have greatly enhanced our understanding of this enzyme class.^[249]

The determined structure of pepstatin in complex with cathepsin D (Figure 39)^[250] uncovers very important structural features. The water molecule which is originally bound to the catalytic aspartate residues is displaced by the hydroxyl group of the (*S*)-configured stereogenic carbon atom of the central statine moiety of the inhibitor. The interaction network of statine with the catalytic aspartates is considered one of the crucial factors in the molecular recognition of this type of ligand and the manifestation of its inhibitory potency. The central statine unit contains a hydroxyethylene peptide bond isostere, thus mimicking the tetrahedral intermediate and a restricted conformation of a central dipeptide unit. It also naturally provides protection from the cleavage by the enzyme.

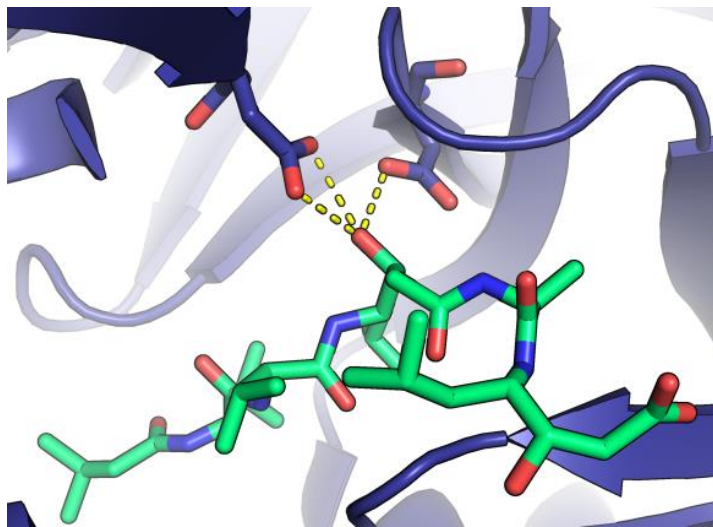


Figure 39 Structure of Cathepsin D in complex with pepstatin (PDB: 1LYB).^[250]

A lot of understanding in aspartic protease SAR was obtained through synthesis and evaluation of analogues of pepstatin with porcine pepsin enzyme. Considerable attention was dedicated to the central statine unit and its stereochemistry (Figure 40).^[251–254]

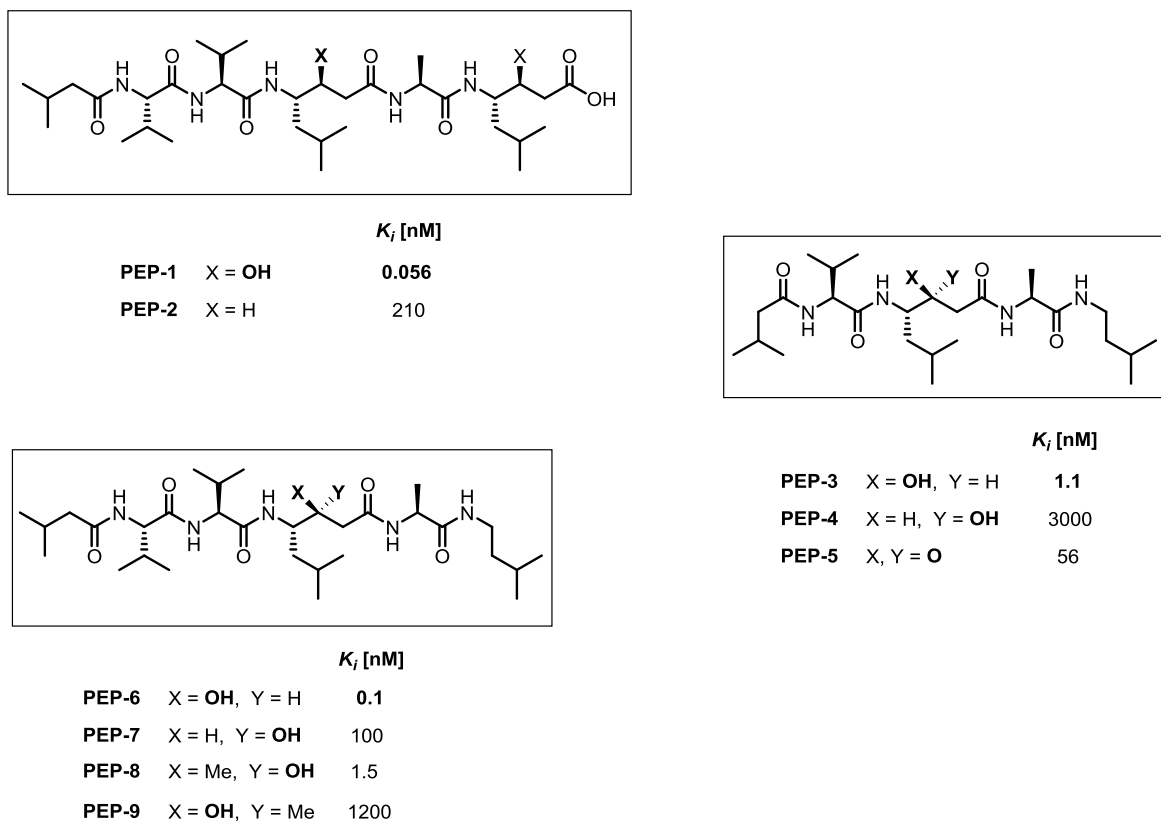


Figure 40 Inhibition of porcine pepsin with different pepstatin analogs.

As evident in the examples of analogues **PEP-1**, **PEP-3** and **PEP-6**, regardless of the size of the pepstatin analog, the configuration of the stereogenic carbon bearing the hydroxyl group has a dramatic impact on binding affinity. In those examples, the (*S*)-configuration of the hydroxyethylene moiety produces three orders of magnitude higher potency of inhibition than its hydroxyethylene epimer counterpart (*R*-configuration). Additionally, but not surprisingly, reduction in size by one sidechain reduces the potency. The exemplified SAR data obtained from pepstatin interactions with aspartic proteases, in conjunction with the X-ray structural information, guided the success in drug development of HIV-1 protease inhibitors.

1.2.3.8.1 Development of HIV-1 Protease Inhibitors

Development of urea based inhibitors of HIV-1 protease has already been described previously in the context of a structure-based design milestone, where extensive database searching was used as a powerful tool for the identification of a *de novo* designed lead scaffold (Chapter 1.2.3.3). In this section, an example will be given on the historical basis of structure-based peptidomimetic design of HIV-protease inhibitors.

Over the past two decades, a major research effort of a number of industrial and academic groups has been the design of effective drugs to target HIV-1 protease. The search resulted in reports of many structures of inhibitors in complex with HIV-1 protease. The first reported inhibitor of this aspartic protease was pepstatin.^[255] The first related cocrystal structure reported was a complex of acetyl-pepstatin with HIV-1 protease.^[256]

All the way from the 1970s, many research groups were struggling in attempts to provide an orally available inhibitor of renin aspartic protease which is another popular antihypertension target besides ACE.^[257] The major drawback in the existing designs of renin inhibitors was lack of oral bioavailability. This problem is associated with many unchanged peptide features in majority of the reported renin inhibitors. It took four decades until the first and currently only renin-targeting drug was approved and marketed in 2007.^[243]

Throughout the early phases of search for the renin inhibitor, the structure of renin was not known.^[258] On the other hand, the three-dimensional structure of HIV-1 protease was already published in the early stages along with validation of a drug target.^[259,260] In the design of HIV-1 protease inhibitors the foundations were set from the experience in development of renin inhibitors.

Two years after the first structures of HIV-1 protease have become available researchers from Upjohn Company and National Cancer Institute have developed the substrate-based pseudopeptide inhibitor **U-85548e**.^[261] Similar to pepstatin and its derivatives, the inhibitor contained a hydroxyethylene isostere replacement at the scissile bond which is mimicking the tetrahedral transition state of the substrate hydrolysis. The classic studies on aspartic protease inhibition by pepstatin guided the design of this potent inhibitor ($K_i < 1$ nM against HIV-1 protease). A cocrystal structure of **U-85548e** with HIV-1 protease was published by the Upjohn

and NCI groups (Figure 41).^[261] A detailed discussion of this structure is warranted since it is a large inhibitor, having a subsite binding span from P5 to P3' residues, and it illustrates many of the protein-ligand contacts available for inhibitors. The inhibitor is positioned within the large active site in an extended conformation and fills subsites S4 to S3'. The hydroxyl of the hydroxyethylene moiety is bound in a network of hydrogen bonds with two catalytic aspartate residues (Asp25 and Asp25'). It makes complementary electrostatic contacts in an equivalent manner that pepstatin does with cathepsin D. Much like in the case of pepstatin, the hydroxyethylene interactions are considered crucial to the tight binding of the complex.

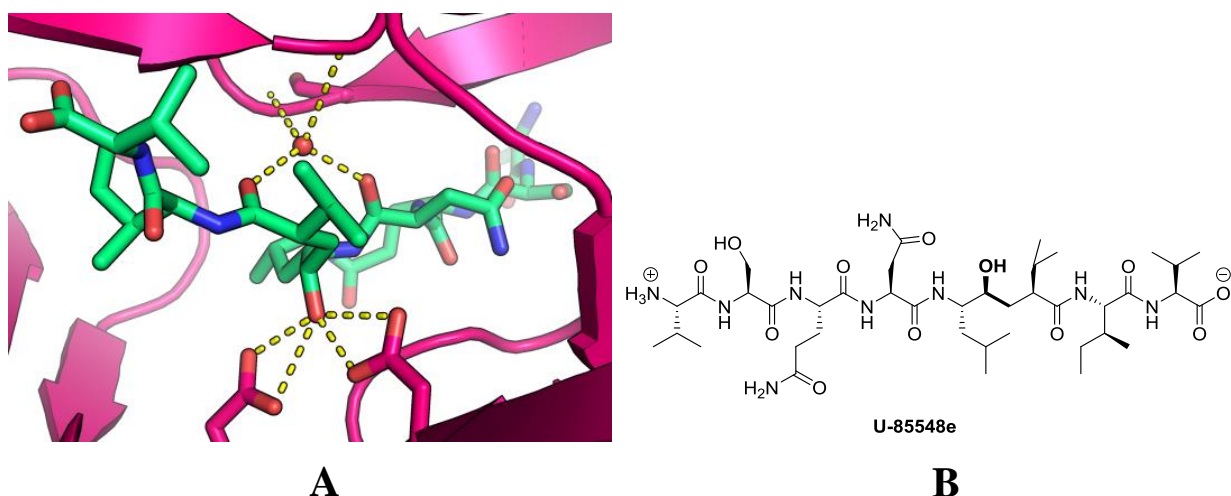


Figure 41 A: Structure of HIV-1 protease in complex with the hydroxyethylene pseudopeptide **U-85548e** (PDB: 8HVP). B: Structure of the hydroxyethylene pseudopeptide inhibitor **U-85548e**.^[261]

The peptide backbone of the inhibitor makes hydrogen bond contacts with the main chain of the protein. The most interesting feature in this complex is a tightly bound water molecule, bound by two carbonyls of inhibitor, flanking the hydroxyethylene. The water molecule completely saturates its hydrogen bond network by interacting with two NH hydrogen bond donors from the “flaps” of the enzyme. This water molecule has been called “flap water”.

In another case, in order to lower the risk of problems with bioavailability which most of the early renin inhibitors have, the Agouron group decided to dramatically reduce the amount of peptide features of their inhibitors.^[262–264] This resulted in the design of the compound **AG1132** ($K_i = 24 \mu\text{M}$). The cocrystal structure of complex with HIV-1 protease reveals that the hydroxyl group is interacting with the catalytic aspartates and hydrogen bond formation to the flap water

from the two carbonyl groups. (Figure 42) For each of the benzamide compounds, the *ortho*-substituent favors a nonconjugated amide and enables hydrogen bond formation to the flap water. The phenyl groups make van der Waals contacts with the S1 subsites and the *tert*-butyl substituents form similar contacts with the S2 subsites. The amide NH interacts with the enzyme via ordered water molecules.

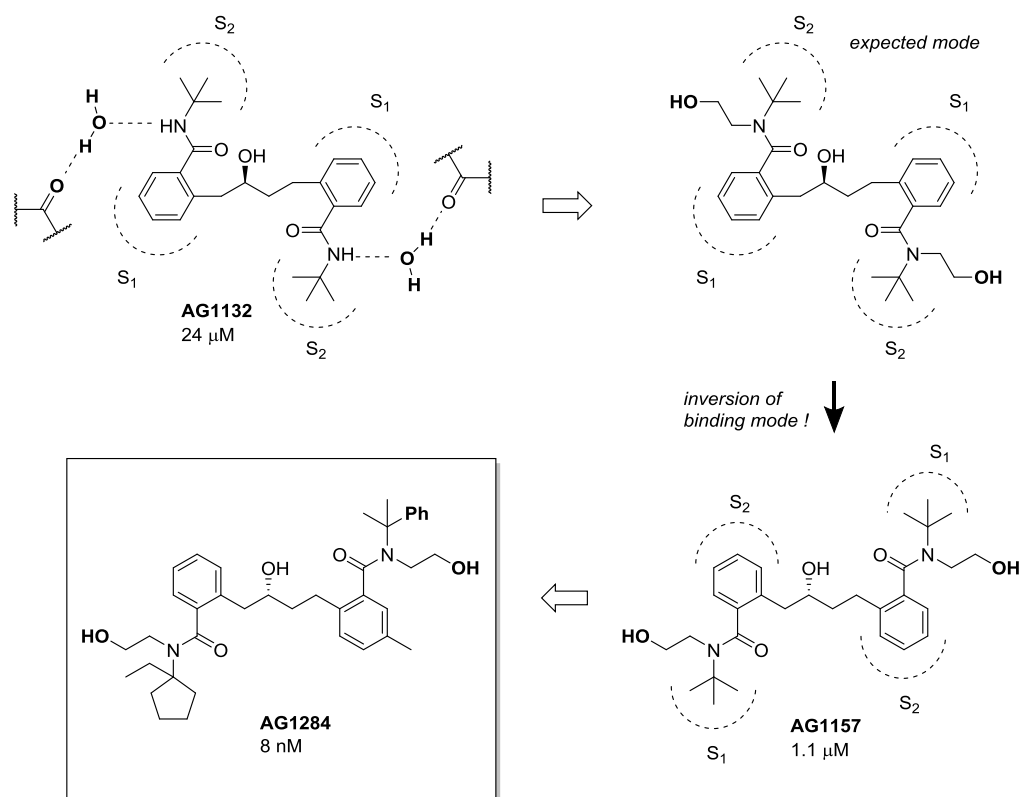


Figure 42 Development of benzamide inhibitors of HIV-1 protease by Agouron.

For more efficient interactions, attempting to mimick the ordered water molecules, the amide nitrogens were functionalized with hydroxyethyl substituents. The same binding mode was proposed, but the structural data surprisingly indicated that the binding mode was inverted with the introduction of new functionality. With the compound **AG1157** ($K_i = 1.1 \mu\text{M}$) a 20-fold improvement in potency was achieved in the new binding mode. The researchers then devised the strategy for optimization using the information of the novel binding mode of **AG1157**. The

lipophilic groups were increased to achieve more favorable spatial complementarity. The ultimate result of this design was the potent, orally available inhibitor compound **AG1284** ($K_i = 8$ nM), demonstrating the efficiency of the relatively simple effort to optimize van der Waals contacts.

A team at Roche UK reported in 1990 a potent HIV-1 protease inhibitor ($K_i = 0.12$ nM), **Ro 31-8959**, which contained a novel decahydroisoquinoline hydroxyethylamine isostere replacement for the Phe-Pro cleavage site.^[265,266] The structure of **Ro 31-8959** was surprising because it had (*R*)-configuration on its hydroxyl-functionalized carbon atom from the transition state mimicking isostere (Figure 43). The (*S*)-epimer of saquinavir was three orders of magnitude less potent. This was a great surprise at that time, when the canonical pepstatin-based design advocated using the (*S*)-configurations for favorable binding of hydroxyethylene-modified peptidomimetic inhibitors of aspartic proteases. This compound was the first HIV-1 protease drug approved by FDA, getting the generic name saquinavir.^[172,244]

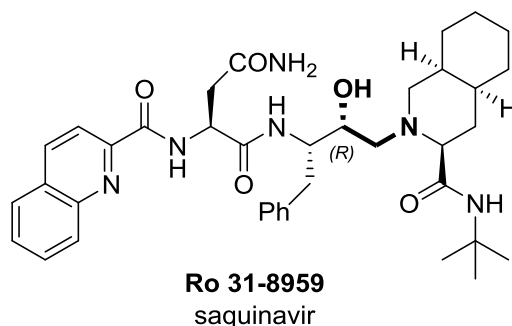


Figure 43 The first FDA-approved HIV-1 protease inhibitor drug, saquinavir.

1.3 Aims of Work

The general lack of specific inhibitors of DPP3 and the need for supporting tools to the efforts in DPP3 enzymology, prompted us to develop small-molecule inhibitors specifically for this enzyme.

Since the structure of DPP3 has been determined relatively recently, the researchers in the community have been testing various general protease inhibitors versus DPP3. Inhibitors reported up to date are not specific and can be categorized in several groups. These are general cysteine, serine and aminopeptidase inhibitors, metal chelators, heavy metals, peptides and microbial broth constituents.^[15] The substrate inhibitor peptides are being degraded by the enzyme itself and have very short lifetimes in blood serum.^[17,19–21] Two fluostatins which are moderate, nonselective inhibitors of DPP3, have been discovered in screening of activity of microbial broths.^[125] Their mode of inhibition is not known. There was one attempt of design of specific inhibitors. However, the design was not structure-guided and the inhibitors inactivate the enzyme via an unknown mechanism.^[126]

Until recently, only one crystal structure of DPP3 was reported, having no ligand in the active site, and displaying a large cleft without solid indication into possible binding interactions with the active site ligands.^[16] Fortunately, a structure of human DPP3 in complex with tynorphin peptide has been determined, revealing surprisingly large conformational changes upon binding, and indicating the very challenging plasticity of its relatively big binding site.

We have made the assessment of the binding mode of the peptide ligand in the cocrystal structure, and the crucial interactions that it makes with the binding subsites. Major objective of this project was to use tynorphin as a template for peptidomimetic design of pseudopeptide inhibitors of hDPP3, guided by the specific interactions displayed in the cocrystal structure of tynorphin-hDPP3 complex. In order to translate tynorphin from substrate into a true inhibitor of human dipeptidyl peptidase-3, noncleavable peptide bond isosteres are envisioned to replace the corresponding second *N*-terminal peptide bond which is subject to catalytic hydrolysis by the enzyme.

We have proposed the use of hydroxyethylene transition state mimetic isostere for the following reasons:

- it resembles the transient stereoelectronic features of the tetrahedral intermediate which is well recognized and stabilized by the favorable binding action of the enzyme;
- use of other transition state mimetics would involve generally much more polar isosteres like sulfonamides, phosphoramidites or phosphinates, and they would cause more undesirable polar peptide-like properties, which need to be gradually removed according to the principles of peptidomimetics (in respect to the desolvation penalty upon binding, and lower bioavailability of peptides);
- in contrast to chelating zinc-binding functions which are very often used in metallopeptidase inhibitor design, hydroxyethylene provides only one oxygen atom as a coordinating bond donor, which can be carefully placed in the design, to maximize the cooperative interactions with zinc ion and the neighboring structural features in the binding site.

An additional objective was the optimization of inhibitor design in the direction of bioavailable molecules. This should be accomplished by exchanging the peptide structural features for nonpeptidic ones, in accordance with the peptidomimetic principles and the structure-activity relationship information generated throughout the project, together with biologists who will perform *in vivo* studies.

The ultimate goal is a potent, selective and bioavailable inhibitor of human DPP3, suitable for use as a tool in dose-dependent and time-dependent studies of chemical interference with the role of the enzyme *in vivo*, which will provide a better understanding of the biological role of hDPP3 *in vivo*.

1.4 Results and Discussion

1.4.1 Structure-based Design of Inhibitors of hDPP3

1.4.1.1 Hydroxyethylene-based Transition State Mimetics of Tynorphin

The structural insights into the noncovalent interactions in the tynorphin-hDPP3 complex, present tynorphin as a defined lead structure for structure-based inhibitor design. The logical step to create a true inhibitor out of this slow converting substrate inhibitor is to make a modification which will render it inert to the action of hDPP3. We propose to incorporate a hydroxyethylene moiety instead of the cleavable peptide bond, as a noncleavable isostere resembling the transition state in the peptide bond hydrolysis. Hydroxyethylene has a tetrahedral geometry, equivalent to the geometry of the transition state. It has a stable chiral configuration, and it can be obtained in two different configurations, both viable for synthesis (Figure 44).

It can be predicted from the representations of both inhibitors in the binding site, that the (*S*)-hydroxyethylene could coordinate to the zinc ion with a lone electron pair from the hydroxyl substituent. On the other hand, (*R*)-hydroxyethylene is expected to form both a coordinative bond with zinc ion and a hydrogen bond to the His568, much like the transition state configuration during the peptide hydrolysis does. With one additional major noncovalent interaction, (*R*)-hydroxyethylene is expected to have a more favorable enthalpy of binding and stronger inhibitory effect.

We set out to produce both (*S*) and (*R*) epimers of hydroxyethylene transition state mimetics of tynorphin. To shorten our initial synthetic efforts, we left out the hydroxyl residue of the tyrosine side chain, and decided to produce the molecules containing a pseudo-phenylalanine instead (Figure 44). By examination of this residue in the enzyme cocrystal structure, we decided that leaving out this residue from the first generation of molecules is not likely to cause a dramatic loss of the affinity of binding. Using the main tynorphin scaffold is expected to provide

selectivity over other enkephalinases, as demonstrated in the research on endogenous peptides which inhibit DPP3.^[19]

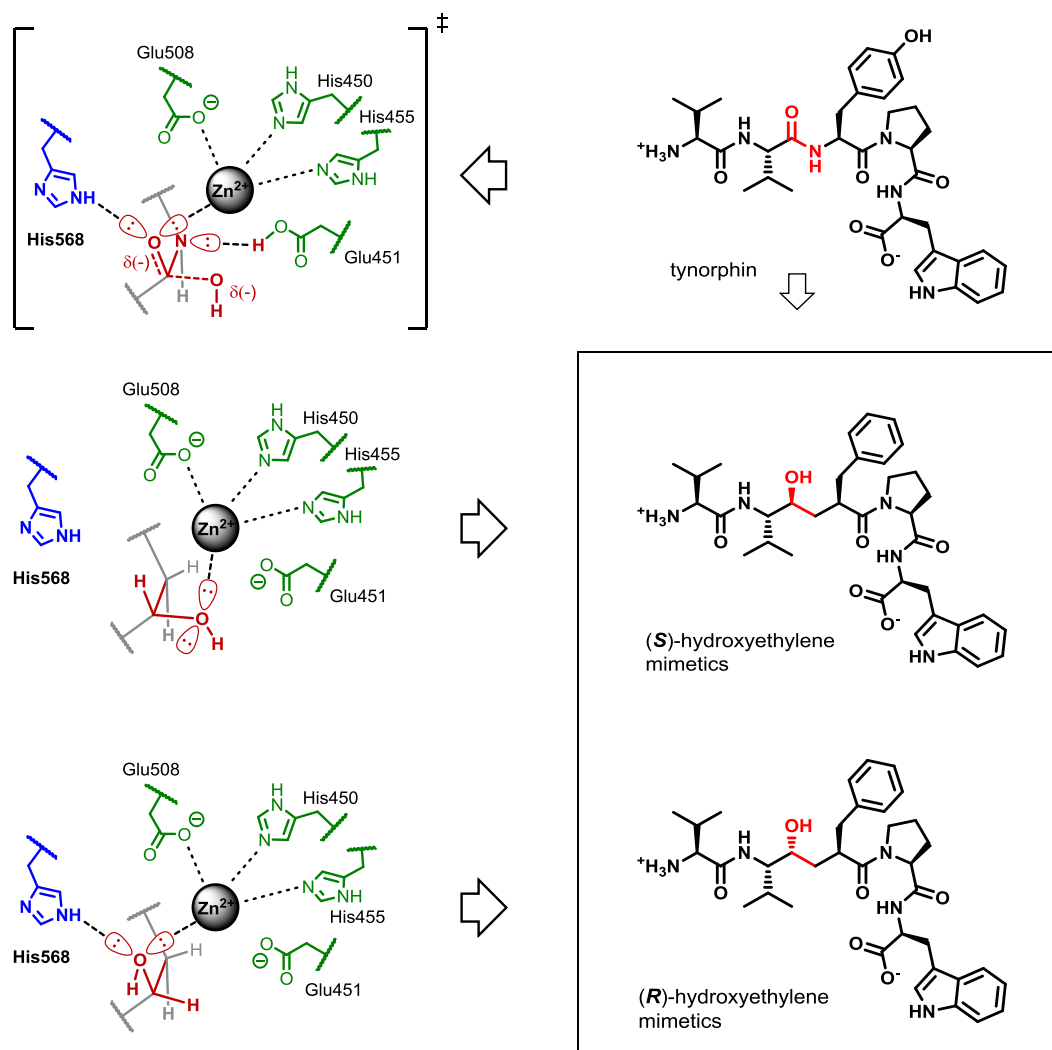
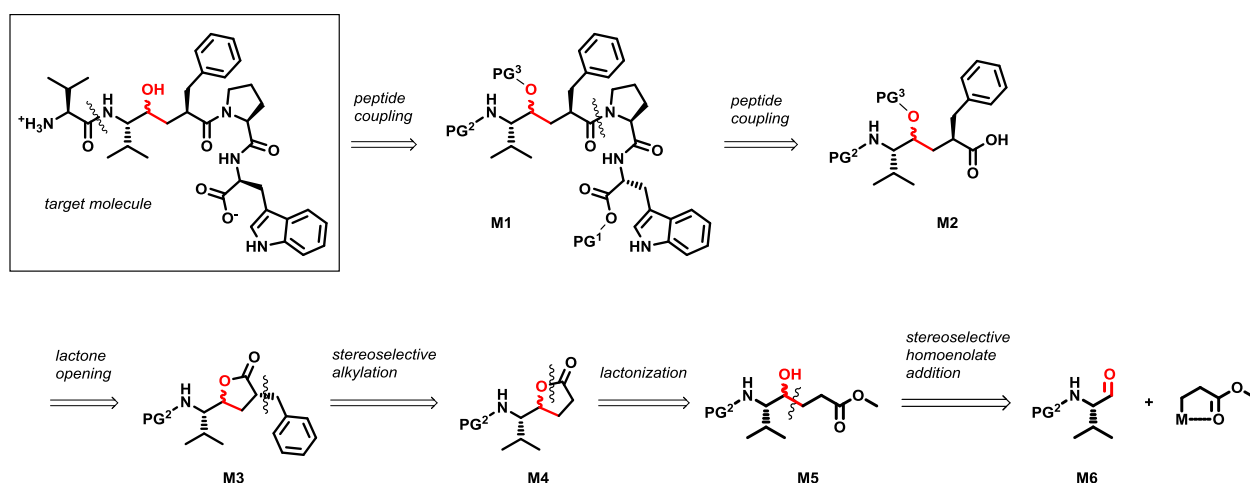


Figure 44 The proposed hydroxyethylene transition state mimetics, as the tynorphin-derived inhibitors of hDPP3.

1.4.2 Synthesis of (*S*)-Hydroxyethylene Pseudopeptide

1.4.2.1 Retrosynthetic Analysis

The first look at the structure of the target molecules suggests that the most obvious disconnection points would be peptide bonds. Peptide coupling methods are nowadays very well established, and are also very often used for the synthesis of complex natural products which contain one or more amide bonds. The first retrosynthetic proceeding involves three functional group interconversions, introducing protection groups on the *N*-terminus, *C*-terminus and the hydroxyl group (Scheme 10). The first disconnections have been made at the *N*-terminal valine peptide bond, and the second at the peptide bond connecting the Pro-Trp fragment to the rest of the molecule.



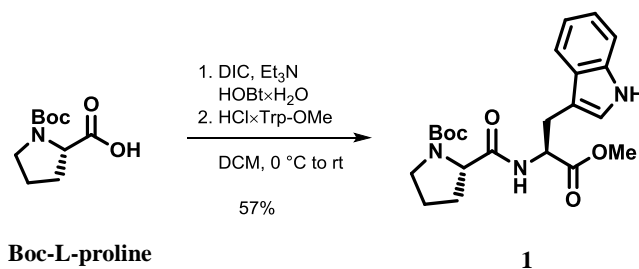
Scheme 10 Retrosynthetic analysis of the approach towards synthesis of hydroxyethylene pseudopeptide.

γ -Lactone **M3** have been recognized as a synthetic equivalent that would lead to the core intermediate, 4-oxyl acid **M2**. The lactone **M3** is disconnected into lactone enolate alkylation synthons. Subsequently, the γ -lactone **M4** is disconnected into a γ -hydroxy ester **M5**, which can be conveniently produced by addition of a homoenolate equivalent to aldehyde **M6**. This disconnection presents a chiral α -amino aldehyde as a convenient starting point in a linear

synthesis, since it can be easily produced from a natural L-amino acid. The chiral pool of a natural amino acid adds an advantage of controlling the stereoselectivity in the formation of the two stereogenic centers, defining the ultimate configuration of the hydroxyethylene motif and the pseudophenylalanine residue of the target molecule.

1.4.2.2 Preparation of Boc-Pro-Trp-OMe Dipeptide

The most facile part of the synthesis was coupling of two commercially available amino acids, *N*-Boc-protected proline and methyl ester protected tryptophan (Scheme 11). Since proline is not seen as a racemization prone amino acid, we have used the conventional amide coupling reagent diisopropylcarbodiimide to activate the amino acid. To avoid any potential of racemization we have used HOBt, which is a common peptide coupling racemization suppressant. The protected dipeptide **1** was obtained in 57% yield after recrystallization.



Scheme 11 Coupling of Boc-proline with tryptophan methyl ester.

For peptides containing tryptophan it is known that electron-rich aromatics like indole are prone to react with the *tert*-butyl carbocation produced during Boc-deprotection.^[267] To avoid risk of significant formation of an undesired byproduct, we have added ethanethiol to serve as a carbocation scavenger. Instead of classical additives like anisole or thioanisole, which are more useful in the solid phase peptide synthesis,^[268] we have tested ethanethiol (Table 6).

conditions	starting material (1) [%]	free amine (A) [%]	impurities [%]
TFA, rt	-	74	26
TFA, EtSH, rt	-	97	3
ZnBr ₂ , EtSH, DCM, rt	5	78	17

Table 6 Test experiments for *N*-Boc deprotection of the peptide **1**. Results were obtained based on HPLC-MS chromatogram using UV-detection at 210 nm.

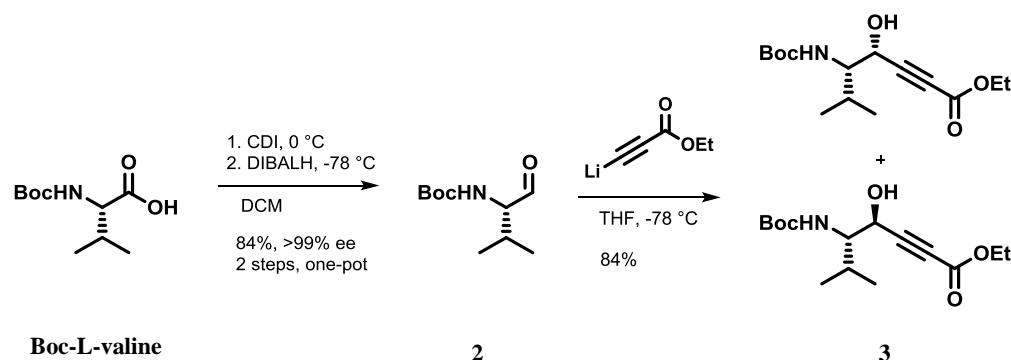
Ethanethiol ultimately produces *tert*-butyl methyl sulfide, which is a byproduct in the solution phase synthesis that is convenient to remove simply by evaporation. Two useful methods for *N*-Boc deprotection have been compared and ethanethiol was added to the mixture. ZnBr₂ was tested as a possible reagent, as it had been reported in milder methods for deprotections of Boc groups and *t*-Bu esters.^[269] The deprotection with TFA and ethanethiol as a scavenger gave the best result, generating minimum amount of byproducts. For further synthetic use, shortly before each coupling to other amino acids the dipeptide **1** was freshly deprotected in TFA with ethanethiol as an additive, and then evaporated and dried in high vacuum to constant mass.

1.4.2.3 Stereoselective Synthesis of the Core Pseudodipeptide

As described in the retrosynthetic analysis, the linear synthesis leading to the chiral core pseudodipeptide was started from a protected amino acid. Boc-protection was selected because the analysis indicated that steps involving strong bases would be used (organometallic reagents and intermediates, and enolate chemistry), along with the peptide coupling methodology. Boc is a robust *N*-protecting group, base-resistant, and frequently used in peptide chemistry and organic synthesis in general.^[270]

In the initial efforts we could obtain the required chiral amino aldehyde by a known method utilizing two isolated steps, which involved the relatively expensive formation of an amino acid Weinreb amide.^[271] This prompted us to develop a more convenient method.

Ultimately, *N*-Boc protected valine was converted to the corresponding chiral aldehyde using a rapid and robust, one-pot two-step methodology developed in this work and described in detail in a dedicated subsequent chapter. The amino acid was activated with Staab's reagent (1,1'-carbonyldiimidazole, CDI),^[272] and the resulting intermediate imidazolide was selectively reduced to the aldehyde **2** using DIBAL-H (Scheme 12). The aldehyde was isolated in 84% yield and >99% ee by an extractive workup, requiring no further purification.

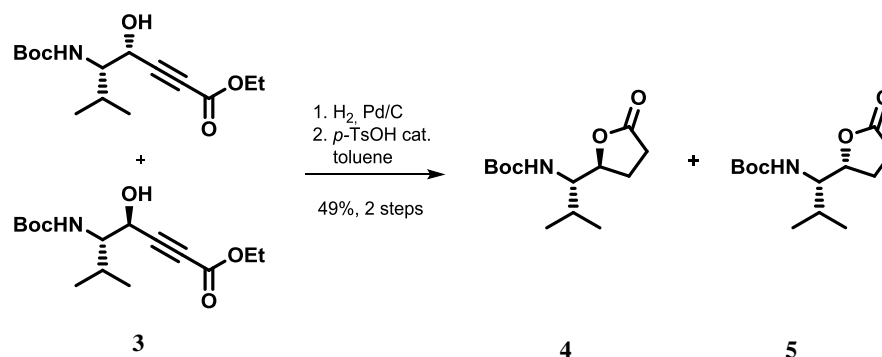


Scheme 12 Synthesis of Boc-valinal and the intermediate acetylenic alcohols.

Homoenolate chemistry has a range of established methods, but requires a great deal of optimization to obtain satisfactory yields and stereoselectivity. In the specific field of hydroxyethylene transition state mimetics synthesis, lithiated propiolate has been established as a reliable equivalent of homoenolate. The amino aldehyde **2** was reacted to the lithiated ethyl propiolate to obtain a mixture of two diastereomers of acetylenic alcohols **3**, which were unseparable at this stage.

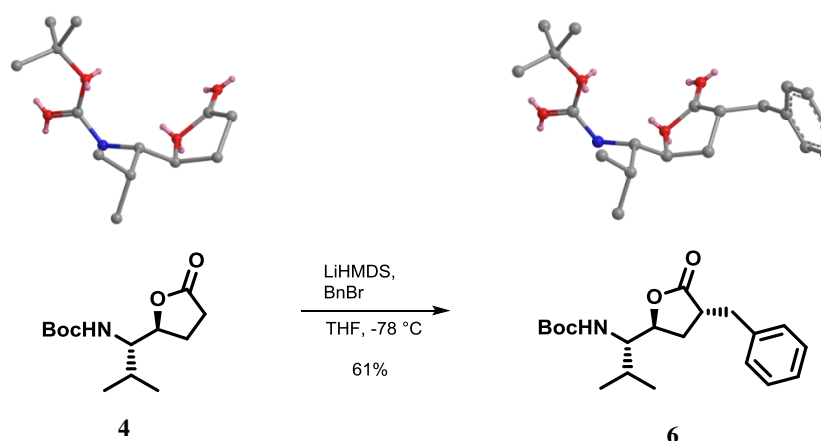
The alcohols **3** were catalytically hydrogenated with Pd/C, and the saturated intermediates were lactonized with catalytic amounts of *p*-toluenesulfonic acid (Scheme 13). The lactones **4** and **5** were readily separated by flash chromatography. The poor stereoselectivity in the formation of acetylenic alcohols was an advantage at this stage as we needed both diastereomers as intermediates for the synthesis of both (*S*)- and (*R*)-hydroxyethylene mimetics. The lactone **4**

has its 4-carboxyl-attached stereogenic center (*S*)-configured, as required to form the final product with the (*S*)-hydroxyethylene.



Scheme 13 Synthesis of γ -lactone intermediates via a hydrogenation/lactonization sequence.

Lactone **4** was enolized by deprotonation with LiHMDS at $-78\text{ }^\circ\text{C}$ and alkylated with benzyl bromide (Scheme 14). The *Si*-face of the ring of the enolate lactone **4** is hindered with a bulky substituent. This resulted in the approach of the electrophile preferentially from the *Re*-face. Accordingly, the benzylated lactone **6** was isolated in 61% yield without observation of significant amount of the diastereomer that would be formed from the attack of the opposite face. In a thought experiment, upon lactone opening this absolute configuration is topologically equivalent to the configuration of the natural dipeptide, which is required for the accurate peptide mimetics.



Scheme 14 Stereoselective alkylation of γ -lactone **4**. Perkin-Elmer Chem3D[®] software was used to acquire the force-field optimized 3D-models of molecules

With the stereoselectively alkylated lactone in hand, the pseudodipeptide can be produced by lactone opening. A synthesis of this sort of peptide mimetics with exactly the same residues and the absolute configuration has already been accomplished in the attempt to develop Severe Acute Respiratory Syndrome (SARS) protease targeting inhibitors.^[273] Ghosh and coworkers used slightly different methods to access the desired pseudodipeptide. The α -amino aldehyde was produced in two separate steps, via the Weinreb amide derivative, and the lactone enolization was performed with LDA. They have obtained a TBS-protected pseudodipeptide acid from the alkylated lactone **6** in two steps. Lactone was opened with LiOH, and the 4-hydroxyacid intermediate was silylated via standard silyl ether protection method developed by Corey, using TBSCl and imidazole.^[274,275]

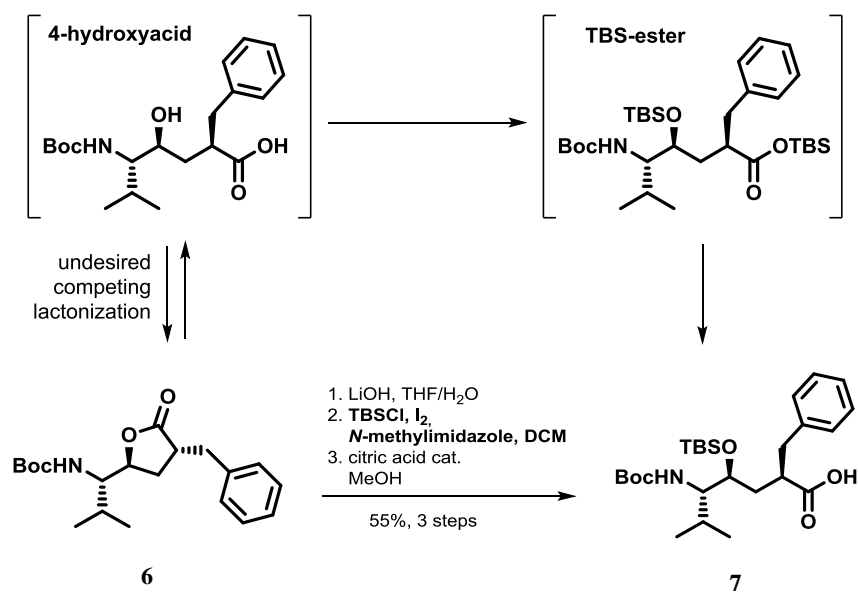
In our hands the lactone opening proceeded smoothly, with few major precautions that needed to be very carefully addressed. All of the lactone was completely opened by stirring for 1 h with at least 4.0 eq of LiOH in THF/H₂O. The 4-hydroxyacid intermediate appears to be very prone to spontaneous lactonization. The degree of unwanted lactonization was found to be highly dependent on the temperature and the acidity of the workup. The acidification was performed carefully, at 0 °C, using a 25% aqueous citric acid to adjust the pH value to 4. Also, it was found that if the temperature of the water bath used for the evaporation of solvents is >30 °C, the majority of the intermediate lactonized to the starting material.

Once these obstacles were solved, new problems were faced due to the high thermodynamic propensity for lactonization, and due to the known issues with the TBS-protection of sterically hindered secondary alcohols like the 4-hydroxyacid intermediate. Unfortunately, our efforts to utilize the TBSCl/imidazole method were unsuccessful. When using large excess of reagents according to the protocol of Ghosh,^[273,276] the reactions were extremely slow, very low yielding, and irreproducible.

In 2007 Bartoszewicz *et al.* published a new highly efficient method of silyl protection using only 1.1 eq TBSCl, TBDPSCI or TIPSCI for sterically demanding substrates.^[277] *N*-Methylimidazole was used as a base and iodine as an additive speeded up reactions dramatically, enabling even full TBDPS protection of 1-adamantanol, which did not occur to any extent under standard conditions. In contrast to the classical TBSCl/imidazole method, which works well only

in DMF, the TBSCl/*N*-methylimidazole/iodine method works remarkably well in THF, acetonitrile and DCM.

To our great satisfaction, we have found that this method successfully silylated our challenging substrate with good reproducibility. It outcompetes the thermodynamically favored lactonization and it is complete within 12 h (Scheme 15).

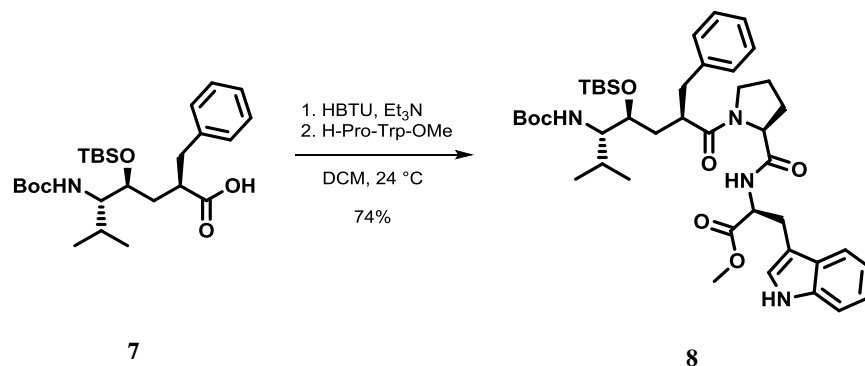


Scheme 15 Hydrolytic opening of the γ -lactone and subsequent TBS protection.

We were surprised to find that a simultaneously formed TBS-ester could not be readily deprotected just by short methanolysis as it was described in literature.^[273,276] After stirring in methanol at room temperature overnight, the TBS ester cleavage occurred to a negligible extent. When the treatment with methanol was performed with a catalytic amount of citric acid, the cleavage was completed selectively within 6 h without harming the TBS-ether.

1.4.2.4 Completion of the (*S*)-Hydroxyethylene Pseudopentapeptide

In order to complete the synthesis, the protected intermediate **7** was coupled with the H-Boc-Trp-OMe dipeptide fragment, which was obtained by facile deprotection of **1** in TFA. Since this was a coupling of dipeptide fragments, we have chosen a robust reagent for activation of the carboxylic acid. In the presence of triethylamine as a base, the use of HBTU resulted in 74% isolated yield of the pseudotetrapeptide intermediate **8** (Scheme 16). The potential of epimerization during this peptide coupling was excluded. The acid **7** should not be prone to epimerization due to the lower acidity of its α -C-H, because it cannot form an oxazolone intermediate which needs to be formed to increase the acidity enough for racemization to take place.^[278–280]



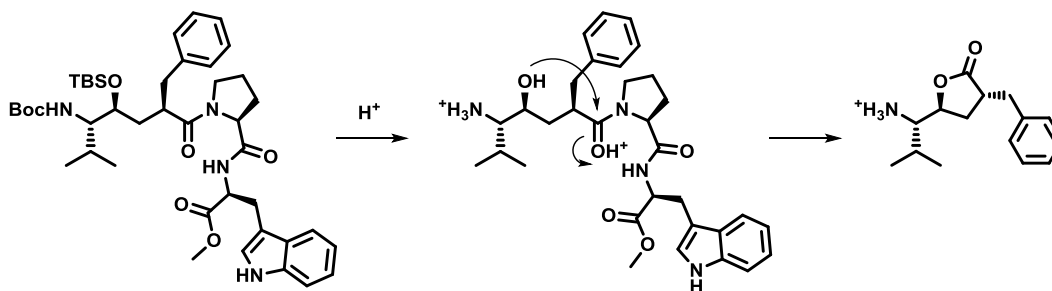
Scheme 16 Peptide coupling of the acid **7** with the dipeptide H-Pro-Trp-OMe, using HBTU as an activation reagent.

In order to complete the required pentapeptide-like scaffold, *N*-Boc deprotection of the peptide **8** and coupling with Boc-L-valine were necessary. Trials with different reagents for *N*-Boc deprotection were performed (Table 7).

conditions	8 [%]	A [%]	B [%]	C [%]	D [%]
ZnBr ₂ , EtSH, DCM	2	40	-	58	-
ZnBr ₂ , EtSH, CF₃CH₂OH	-	14	-	85	-
ZnBr ₂ , EtSH, MeCN	9	-	76	15	-
HCl/MeOH anhydrous	-	-	-	26	73
TFA, EtSH	-	95	-	4	-

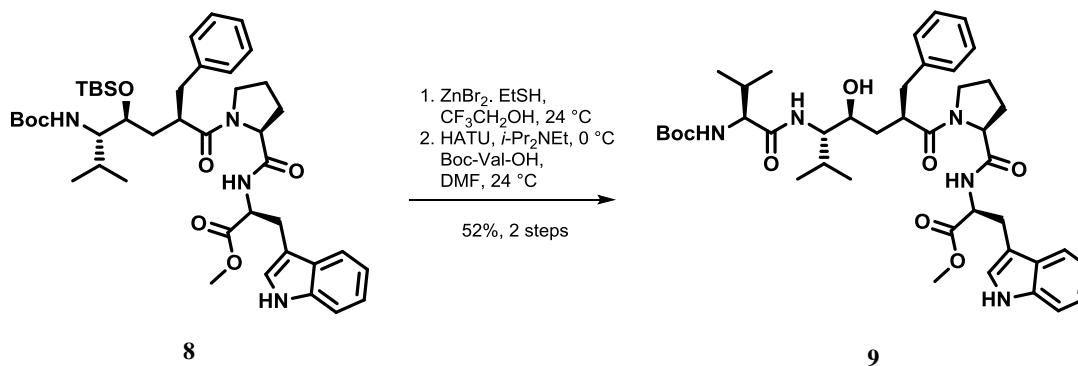
Table 7 Test experiments for finding an optimal method for deprotection of the peptide **8**. The trials were performed at room temperature and stopped after 60 min by a basic workup with 25% aqueous ammonia and extraction with EtOAc. Results were obtained based on HPLC-MS chromatogram using UV-detection at 280 nM. In the first three conditions 4.0 eq ZnBr₂ and 4.0 eq EtSH were used. Anhydrous HCl/MeOH was prepared by a dropwise addition of 20 vol% of AcCl into anhydrous MeOH at 0 °C and leaving it to react for 4 h before it was used for the deprotection. In the fifth trial TFA was used in large excess, as a solvent, and 4.0 eq EtSH were added.

The TFA/ethanethiol conditions resulted in a neat and selective *N*-Boc deprotection. Anhydrous HCl in the protic solvent resulted in rapid dual deprotection of both the Boc and TBS function, causing also a thermodynamically favoured, acid-catalyzed lactone cyclization “backbite” in the peptide (Scheme 17). Particularly interesting were the conditions with ZnBr₂ in 2,2,2-trifluoroethanol and acetonitrile. The use of 2,2,2-trifluoroethanol was inspired by a method for neat cleavage of Boc protecting groups under microwave-assisted conditions.^[281] ZnBr₂ in 2,2,2-trifluoroethanol with EtSH as an additive removed both Boc and TBS protections without generating byproducts. More surprisingly in acetonitrile within 60 min it selectively removed the TBS protection.



Scheme 17 Thermodynamically favoured, acid-catalyzed γ -lactone “backbite”.

Under peptide coupling conditions amines are much more nucleophilic than oxygen nucleophiles like alcohols, which need to be deprotonated to have comparable nucleophilicities to the amines.^[282,283] Hence, any competing *O*-nucleophilicity of the TBS-deprotected hydroxyethylene was not of concern. The conditions which cleave both the Boc and the TBS protection were convenient at this stage and we decided to use $\text{ZnBr}_2/\text{EtSH}/2,2,2$ -trifluoroethanol for the deprotection before the last coupling (Scheme 18). *N,O*-Deprotected pseudotetrapeptide afforded compound **9** in 52% isolated yield in two steps, with no observed ester coupling byproduct.



Scheme 18 Simultaneous *N*-Boc and TBS deprotection of **8**, and coupling to Boc-Valine, using HATU as an activation reagent.

Valine is one of the amino acids, alongside phenylalanine, notorious for its propensity to racemization due to the steric hindrance of its isopropyl residue. To ensure minimum risk of racemization we have used HATU as one of the most reliable peptide coupling activation reagents available. In order to measure the degree of racemization, we have prepared small amounts of the reference mixture of both related epimers of the peptide **9**. HPLC-MS measurement showed that no epimerization occurred during the coupling (Figure 45).

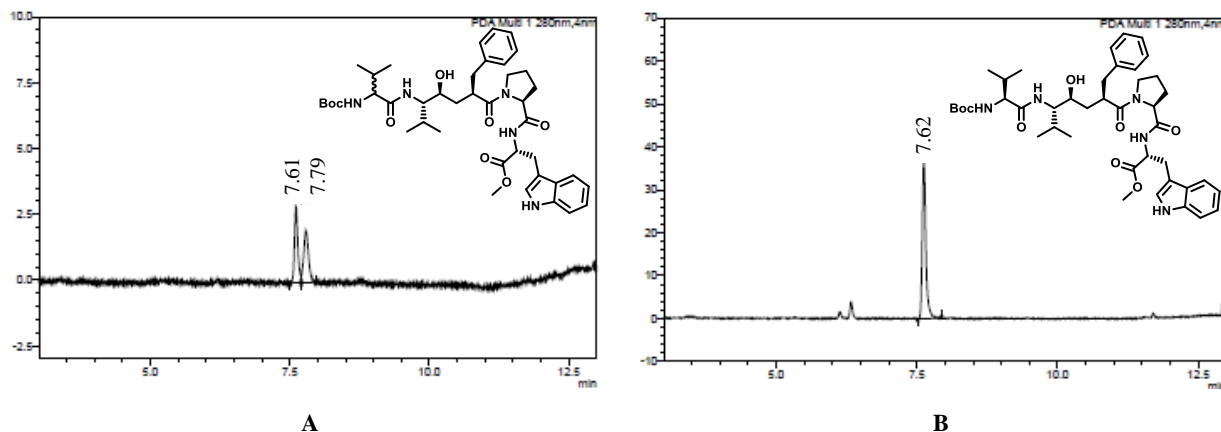
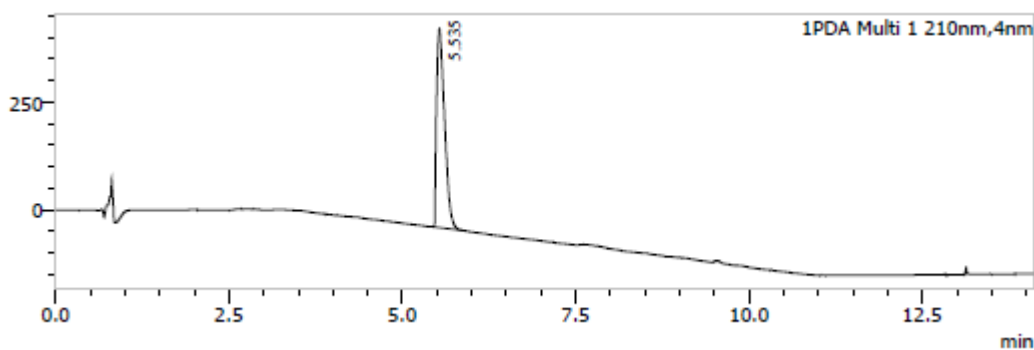
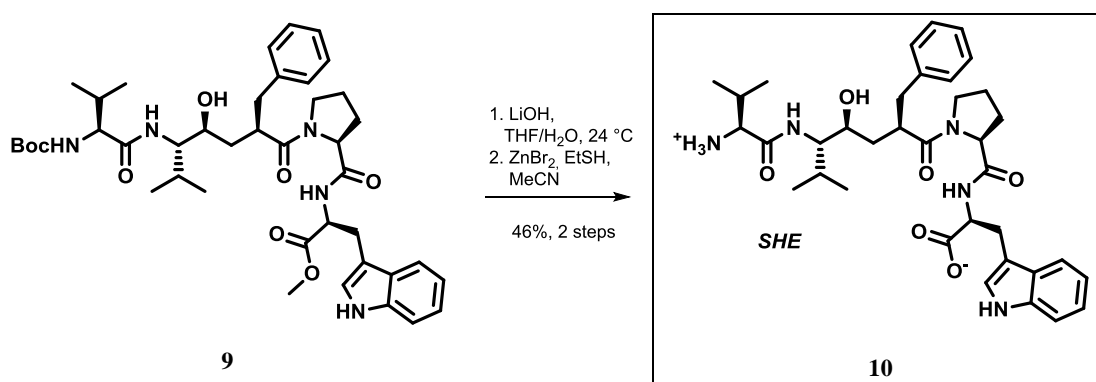


Figure 45 HPLC chromatograms of coupling products. **A**: reference mixture of L-Val and D-Val epimers of **9**; **B**: the L-Val epimer **9**, synthesized by coupling with HATU.

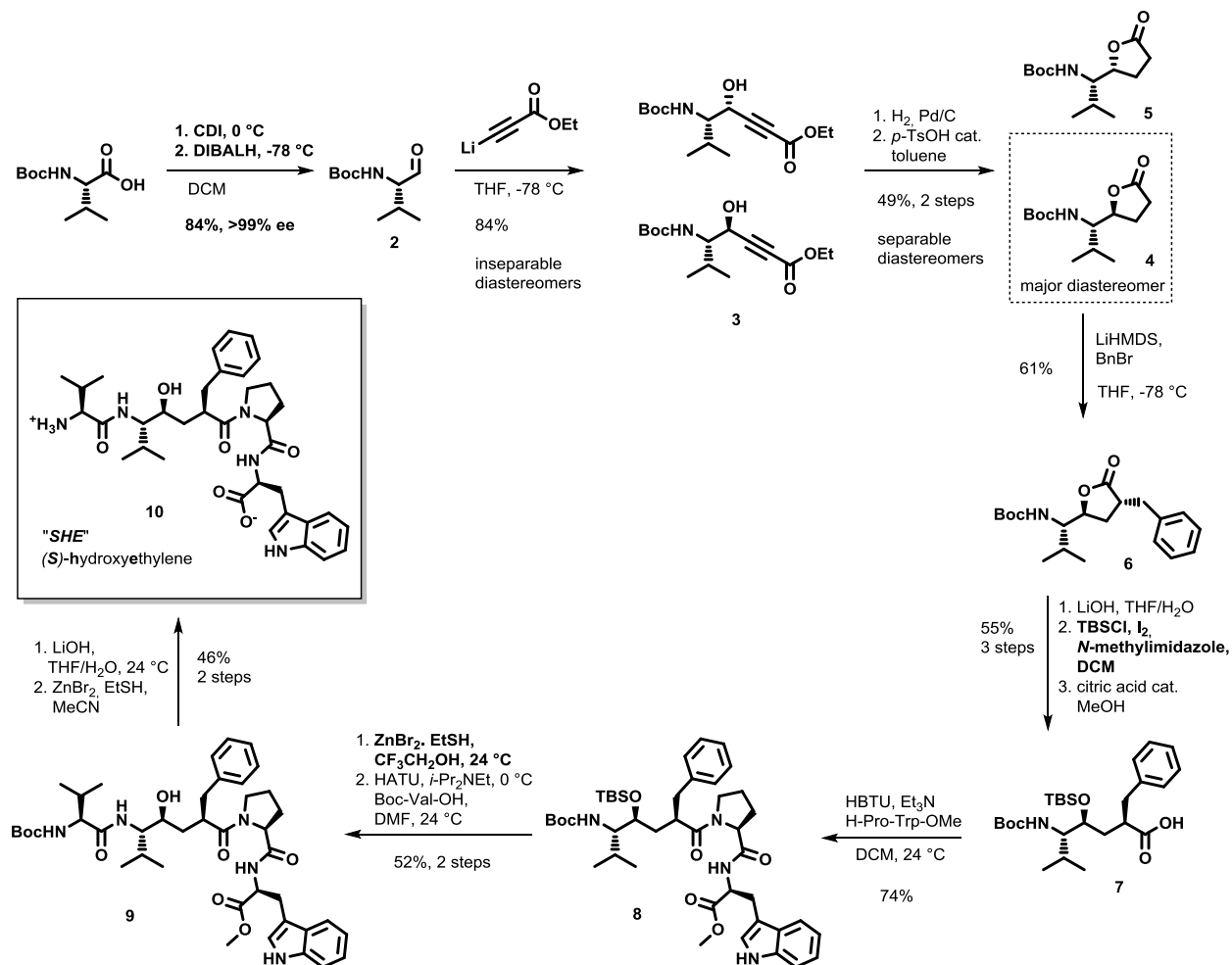
The target molecule **10** was easily obtained after saponification of the *C*-terminal methyl ester and *N*-Boc deprotection (Scheme 19). Since the (*S*)-hydroxyethylene transition state isostere is contained in **10**, we assigned an arbitrary abbreviation “*SHE*” to this final molecule.



Scheme 19 Methyl ester saponification and *N*-Boc deprotection, yielding the final compound **10**. Lower part presents an HPLC chromatogram with a clean peak of the isolated final product **10**, at 210 nm.

1.4.2.5 Summary of the Synthesis of *SHE*

SHE was synthesized in fourteen steps using Boc-protection compatible chemistry (Scheme 20). The chiral pool synthesis started from protected L-valine, from which diastereoselective formation of the two crucial stereogenic centers in the central pseudodipeptide fragment was controlled.

Scheme 20 Summary of the synthesis of *SHE*.

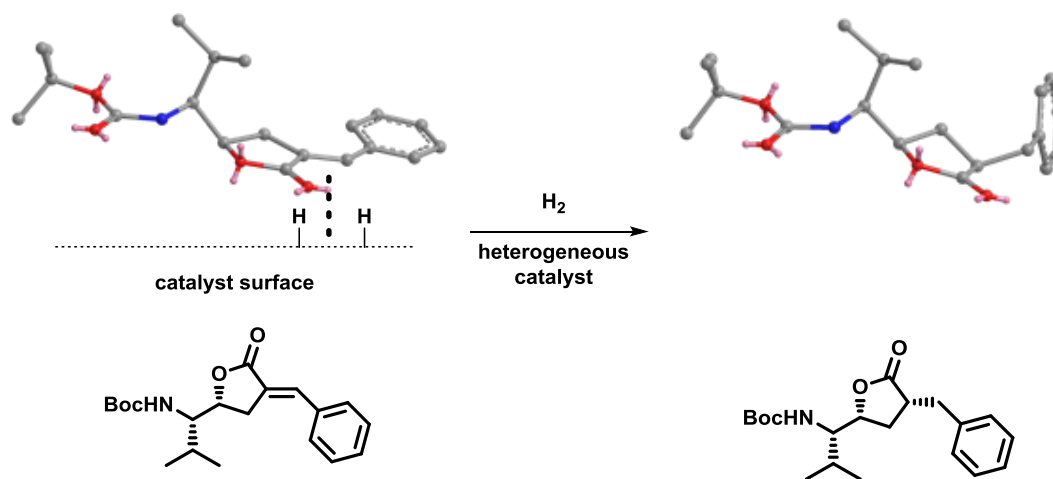
The poor stereoselectivity of addition of the lithiopropiolate to the aldehyde **2** provided also the lactone **5**, which is properly configured for use in the synthesis of the (*R*)-hydroxyethylene epimer. Diastereoselective enolate alkylation afforded lactone **6**, which was opened and protected to yield the stable pseudodipeptide acid **7**, setting the stage for peptide coupling with the Pro-Trp fragment. Careful development of simultaneous Boc and TBS

deprotections shortened the synthesis. Additional peptide coupling with Boc-valine provided the desired scaffold **9**. The target compound **10** was obtained via consecutive *C*-terminal methyl ester saponification and *N*-terminal Boc-deprotection.

1.4.3 Synthesis of (*R*)-Hydroxyethylene Pseudopeptide

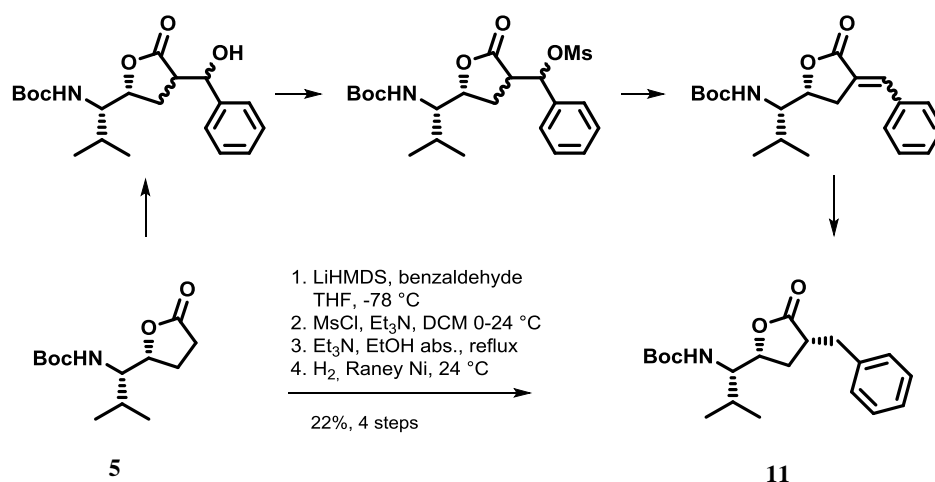
Lactone **5** was obtained from the sequence of transformation of the chiral α -amino aldehyde **2**, via lithiated propiolate addition, hydrogenation and lactonization and has its 4-carboxyl-attached stereogenic center (*R*)-configured. The low stereoselectivity of the lithiopropiolate addition to the aldehyde allowed us to utilize lactone **5** to obtain the (*R*)-hydroxyethylene target molecule.

If an enolate of the lactone **5** would have been alkylated in the equivalent manner as the enolate of lactone **4**, the undesired diastereomer would be the major product, in respect to the requirement for the peptide mimetics. There are fewer case studies where the lactone intermediate with this (*2R,4R,5S*) stereochemical pattern could be easily accessed in the synthesis of hydroxyethylene peptides.^[284,285] It is suggested to perform a relatively complex sequence of reactions: an aldol reaction, eliminative dehydration of four aldol diastereomers to cinammic-like derivatives, and then a heterogeneous hydrogenation would form the desired (*2R,4R,5S*)-diastereomer of the alkylated lactone. The desired stereoselectivity in heterogeneous hydrogenation is rationalized in the way that the eliminated intermediate with the double bond adsorbs onto the surface of the catalyst preferentially with the less hindered face (Scheme 21). According to Horiuti and Polanyi,^[286] the generally accepted mechanism of hydrogenation in heterogeneous conditions produces the *cis*-hydrogenated product, which in our case ultimately results in the configuration required to obtain the correct peptide-like topology in later steps.



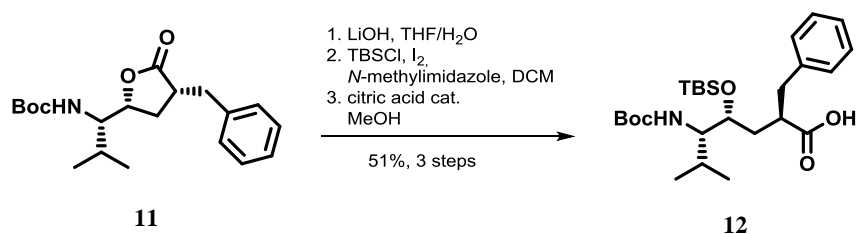
Scheme 21 The model of diastereoselective cis-hydrogenation. Perkin-Elmer Chem3D[®] software was used to acquire the force-field optimized 3D-models of molecules.

The lactone **5** was deprotonated with LiHMDS and reacted with freshly distilled benzaldehyde. The crude mixture of four aldol diastereomers was treated with methanesulfonyl chloride and trimethylamine in DCM to yield a complex mixture of MsO- and chloro-substituted analogues. The new crude mixture was successfully eliminated to the expected mixture of only two elimination product isomers. Triethylamine was used as a base and EtOH as a protic, carbocation-stabilizing solvent, because the elimination was expected to proceed via E1 mechanism. Initial attempts to hydrogenate these intermediates over palladium on active charcoal in different solvents and at elevated temperatures did not proceed at all. Finally, hydrogenation over Raney nickel afforded the desired alkylated lactone **11** (Scheme 22). The overall isolated yield after four consecutive steps was 22%. The absolute configuration was confirmed by observation of mutual NOE enhancements between NMR signals of H2 and H5 in the lactone ring.



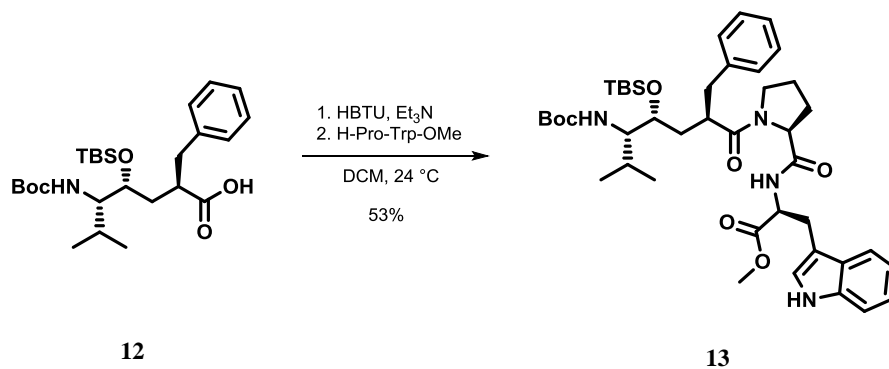
Scheme 22 A consecutive four-step sequence yielding stereoselectively alkylated γ -lactone **11**.

After the lactone **11** had been obtained, the rest of the synthesis proceeded in a similar way as the synthesis of *SHE*. Once again, the robust silylation method using TBSCl, *N*-methylimidazole and iodine was used to trap the 4-hydroxyacid derived from **11** into the TBS-protected acid **12** (Scheme 23).



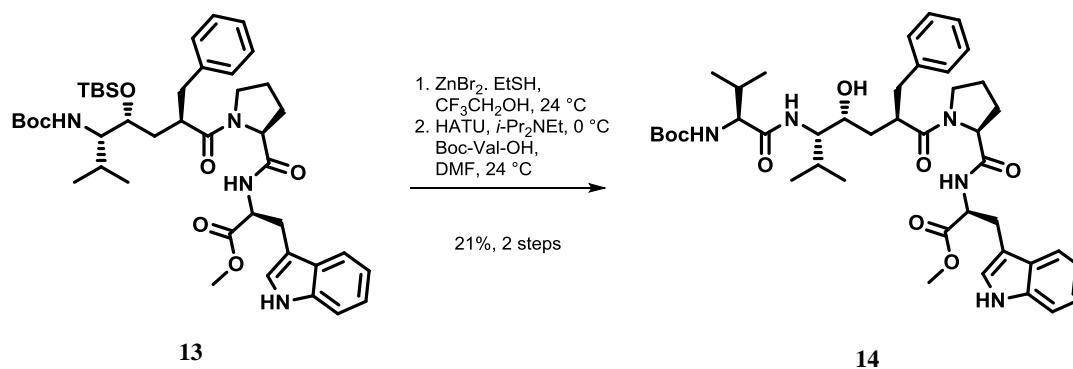
Scheme 23 Lactone opening and TBS protection.

Subsequently, the acid **12** was coupled with the Pro-Trp peptide fragment, providing pseudotetrapeptide **13** (Scheme 24).



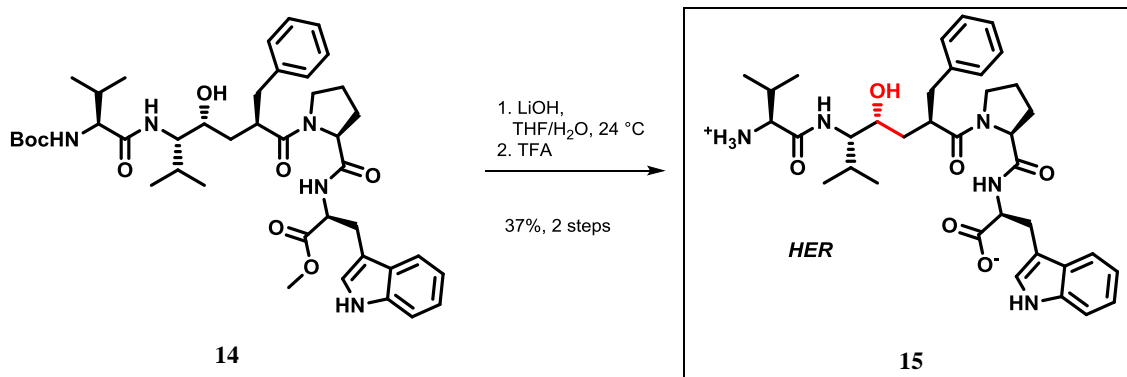
Scheme 24 Peptide coupling of the acid **12** with the dipeptide H-Pro-Trp-OMe, using HBTU as an activation reagent.

The method for simultaneous deprotection of TBS and Boc that was established in the synthesis of *SHE*, worked out in the equivalent way with pseudotetrapeptide **13**. The following peptide coupling was performed with Boc-valine and the pseudopentapeptide **14** was obtained (Scheme 25).



Scheme 25 Simultaneous *N*-Boc and TBS deprotection and subsequent coupling with Boc-valine.

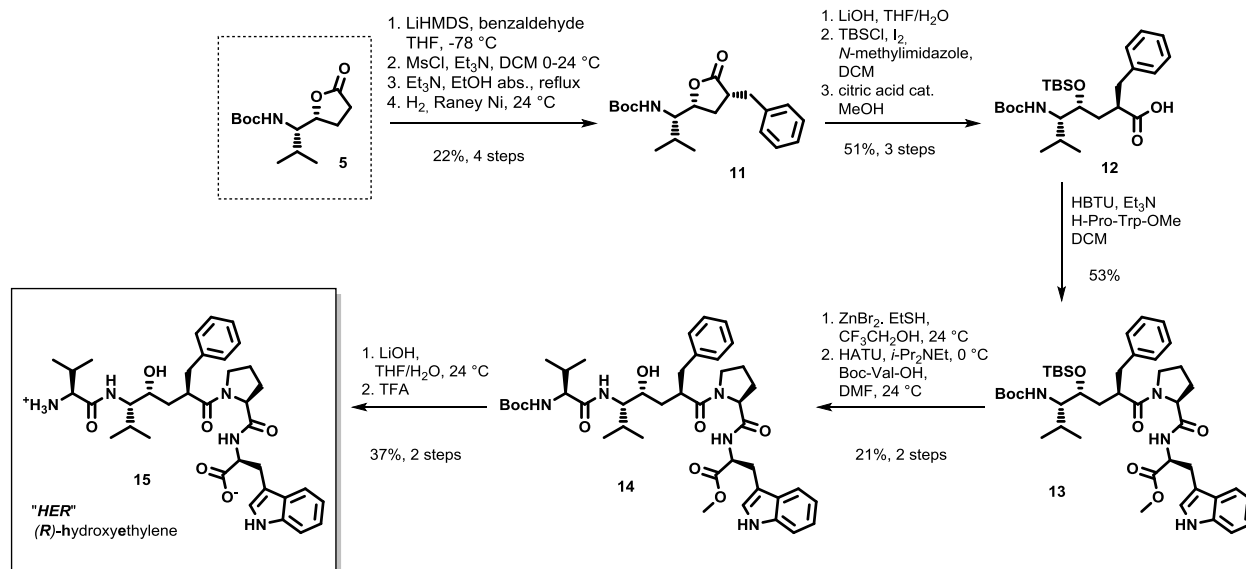
The final molecule **15** was produced in the last two steps via ester saponification and Boc-deprotection (Scheme 26). In a similar manner as it was done with *SHE*, hydroxyethylene with (*R*)-configuration was abbreviated “*HER*” for the target molecule **15**.



Scheme 26 Saponification and *N*-Boc deprotection yielding the final compound.

1.4.3.1 Summary of the Synthesis of *HER*

SHE was synthesized in a three step shorter sequence, taking into account that we produced *HER* performing a considerably more demanding stereoselective alkylation of the γ -lactone **5** (Scheme 27). Formation of the desired topology of the alkylated lactone **11** required an aldol reaction and subsequent handling of a mixture of four aldol diastereomers through mesylation, elimination and diastereoselective hydrogenation. From that point on, the synthetic pathway through lactone opening, and two peptide couplings afforded the final molecule.

Scheme 27 Summary of the synthesis of *SHE*.

1.4.4 Design and Synthesis of Smaller Pseudopeptide Analogues

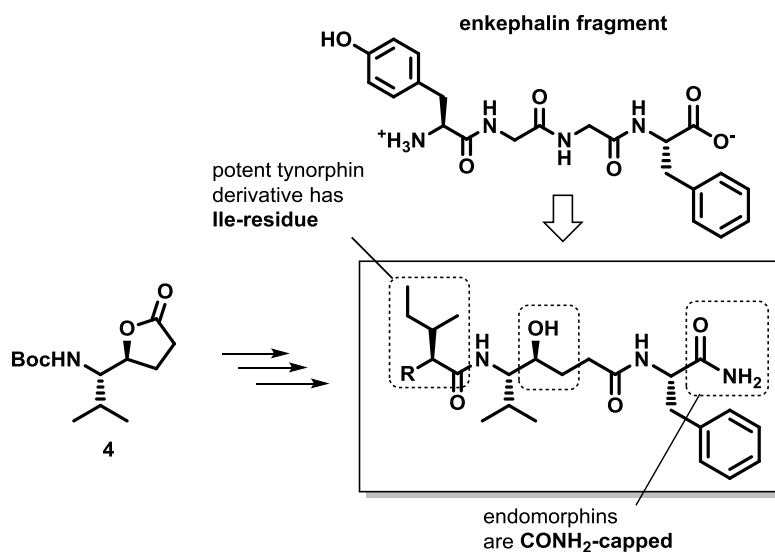
1.4.4.1 Short Hydroxyethylene Pseudopeptide Analogues

Tynorphin and its *N*-terminal mutant peptides have been characterized as potent substrate inhibitors of rat DPP3,^[19,20,116] having a higher binding affinity to the active site of rat DPP3 than the standard synthetic test substrate Arg-Arg-βNA. In 2007 Abramic *et al.* performed a study of the competitive substrate inhibition capacity of known endogenous substrates of human DPP3.^[63] It was found that endogenous opioid peptides endomorphin-1 and endomorphin-2, and the *N*-terminal tetrapeptide fragment of enkephalins can inhibit the degradation of the Arg-Arg-βNA substrate within the same *K_i* range as Leu-enkephalin does. Since endomorphins and the enkephalin fragment consist of only four amino acid residues, which is shorter than any other DPP3 substrate, it was thus indicated that shorter transition state mimetics could inhibit DPP3 (Table 8).

Peptide sequence (name)	K_i (μM)
Val-Val-Tyr-Pro-Trp-Thr-Gln (valorphin)	0.049 \pm 0.006
Leu-valorphin-Arg	3.41 \pm 0.49
Tyr-Pro-Trp-Phe-NH ₂ (endomorphin-1)	5.00 \pm 0.12
Tyr-Pro-Phe-Phe-NH ₂ (endomorphin-2)	2.49 \pm 0.64
Tyr-Pro-Phe-Val-Glu-Pro-Ile (human β -casomorphin)	0.56 \pm 0.28
Tyr-Gly-Gly-Phe-Leu (Leu-enkephalin)	3.65 \pm 0.60
Tyr-Ala-Gly-Phe-Leu (Ala ² -Leu-enkephalin)	0.375 \pm 0.20
Tyr-D-Ala-Gly-Phe-Leu (D-Ala ² -Leu-enkephalin)	27.00 \pm 2.61
Tyr(SO ₃ H)-Gly-Gly-Phe-Leu	43.40 \pm 11.50
Tyr-Gly-Gly-Phe-Leu-Arg-Arg-Ile (dynorphin A 1-8)	69.90 \pm 15.30
Tyr-Gly-Gly-Phe (enkephalin fragment)	4.00 \pm 0.30
Gly-Gly-Phe-Leu (enkephalin fragment)	23.50 \pm 1.30

Table 8 Competitive inhibition of various substrates of hDPP3 against degradation of a synthetic substrate Arg-Arg- β NA. Table taken from ref. 63.

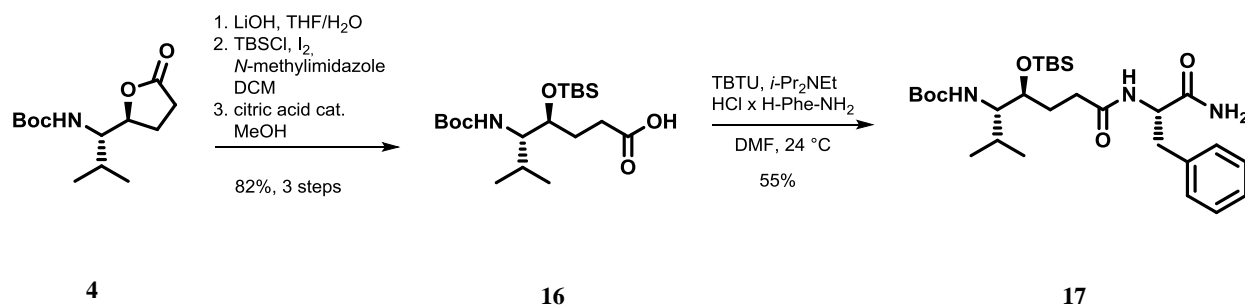
We were primarily interested in reducing the synthetic complexity of our initial inhibitor scaffold design, based on tynorphin. The synthetic protocols that would provide more potential inhibitors in shorter time are the prerequisite for efficient structure-activity probing in inhibitor design.^[168] Lactones **4** and **5**, which we synthesized as intermediates in the syntheses of **SHE** and **HER**, provided us with the opportunity to synthesize simpler hydroxyethylene derivatives resembling the shorter and structurally simpler enkephalin sequence. We proposed a new design based on four premises. Enkephalin fragment Tyr-Gly-Gly-Phe binds to hDPP3. Endomorphins I and II bind with a similar affinity and are amide-capped at their C-terminus. Chiba et al. found that the inhibition of tynorphin is significantly enhanced if an N-terminal isoleucine is introduced instead of valine.^[20] Enthalpic desolvation penalty upon binding of inhibitor to the enzyme could be reduced by introducing a hydroxyl function instead of N-terminal amine, which is ionized by protonation and thus strongly solvated in the aqueous environment (Scheme 28).



Scheme 28 The design of shorter hydroxyethylene derivatives.

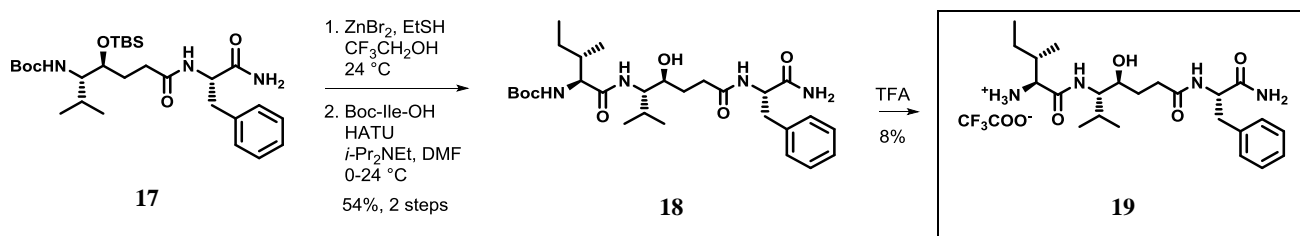
1.4.4.2 Synthesis of the Short Hydroxyethylene Analogues

A new central pseudodipeptide core was obtained from lactone **4**. **4** was easily opened by treatment with LiOH in THF/H₂O and the robust silylation method was employed again to furnish the product **16** in excellent yield after 2 steps (Scheme 29). Acid **16** was coupled with phenylalanine amide using coupling reagent TBTU and Hünig's base.



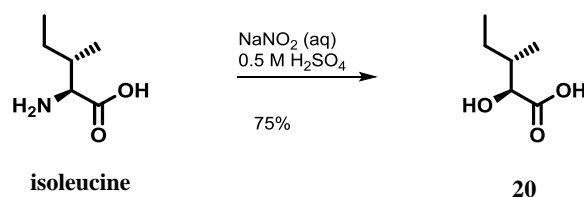
Scheme 29 Lactone opening and TBS protection yielding acid **17**.

The intermediate **17** was deprotected and coupled with Boc-isoleucine and subsequently Boc-deprotected to afford the final molecule **19** (Scheme 30).



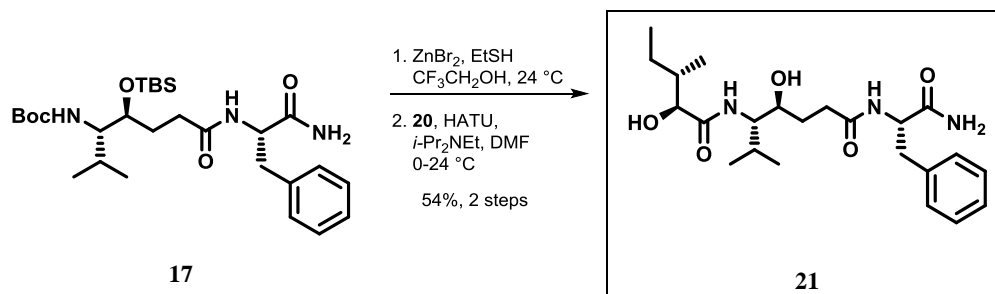
Scheme 30 Synthesis of the target molecule **19**.

In order to obtain a hydroxyl-terminal analogue of the molecule **19**, α -hydroxy leucine derivative **20** was obtained via well-known method involving amino acid diazotization,^[287–289] where the hydroxyacid retains the same stereoconfiguration as the original amino acid (Scheme 31).



Scheme 31 Preparation of α -hydroxy analogue of isoleucine (**20**).

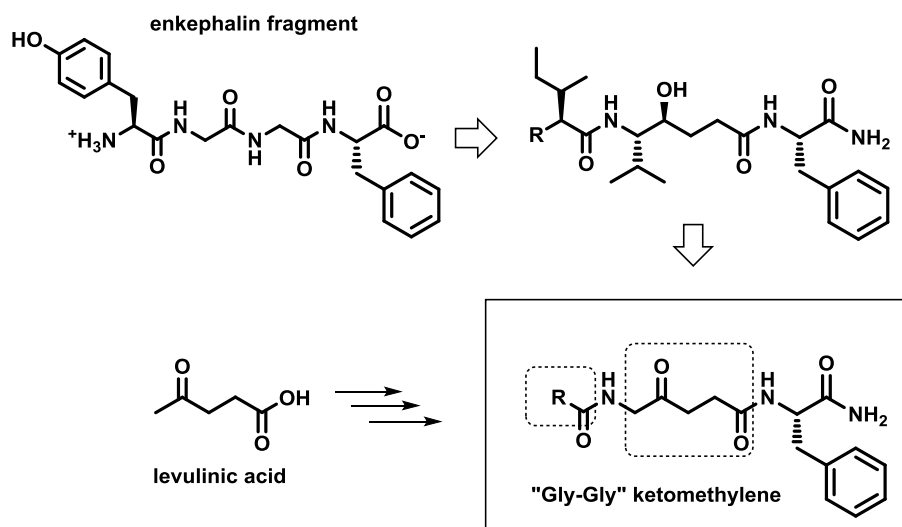
The final hydroxy-derivative **21** was synthesized also by dual deprotection and subsequent coupling using HATU (Scheme 32). In this case there was no necessity for additional Boc-deprotection, because, as noted already earlier in this work the hydroxyl function does not interfere with amide coupling.



Scheme 32 Simultaneous *N*-Boc- and TBS- deprotection and subsequent peptide coupling towards **21**.

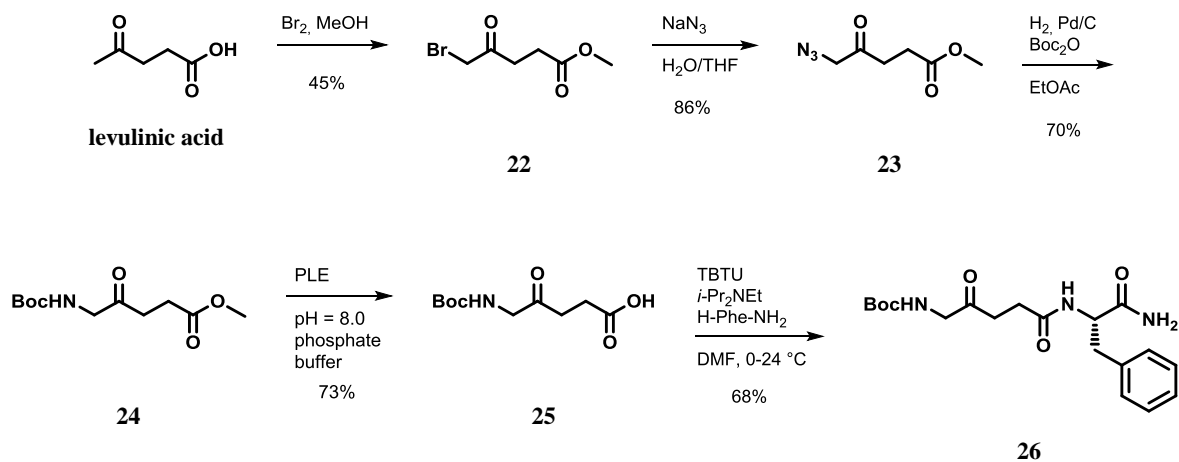
1.4.4.3 Short Ketomethylene Pseudopeptide Analogues

We have tried to simplify the inhibitor design even further, using ketomethylene as a peptide bond isostere. The easiest way to make the ketomethylene analogues of the truncated enkephalin was to use levulinate as a central core motif (Scheme 33).



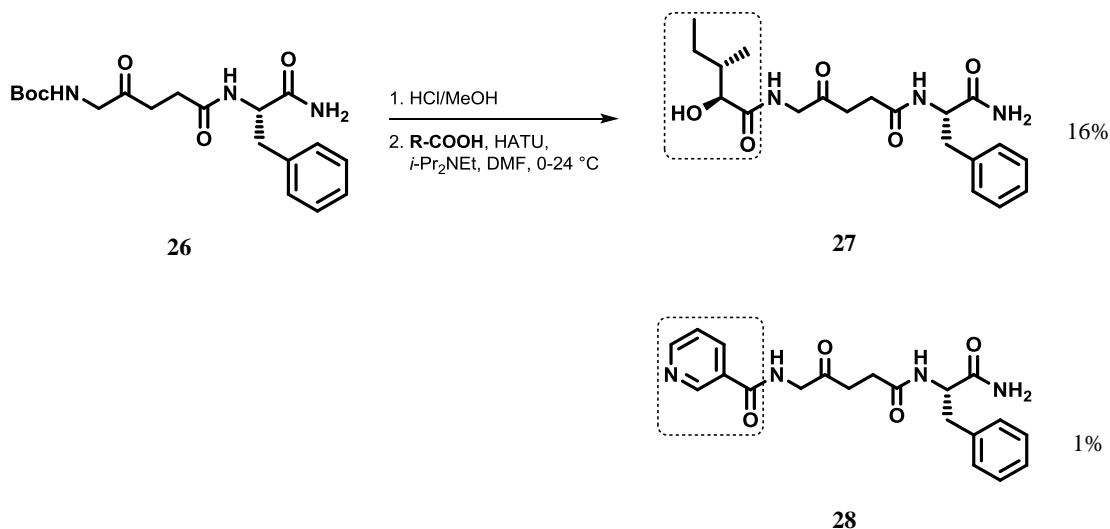
Scheme 33 The design of shorter ketomethylene derivatives.

A 5-aminolevulinic acid derivative was required for this endeavor. Unprotected 5-aminolevulinate is an important natural precursor, known to be unstable and immediately recruited in biosynthesis of heme and corrin.^[290,291] A protocol yielding the stable *N*-Boc-5-aminolevulinic acid was successfully employed for the synthesis of new peptidomimetics.^[292] *N*-Boc-5-aminolevulinic acid (**25**) was synthesized from levulinic acid by a sequence of ketone bromination, substitution with azide, hydrogenation in presence of Boc_2O , and enzymatic methyl ester cleavage with porcine liver esterase (Scheme 34). Protected aminolevulinic acid was extended to the ketomethylene pseudopeptide **26**.

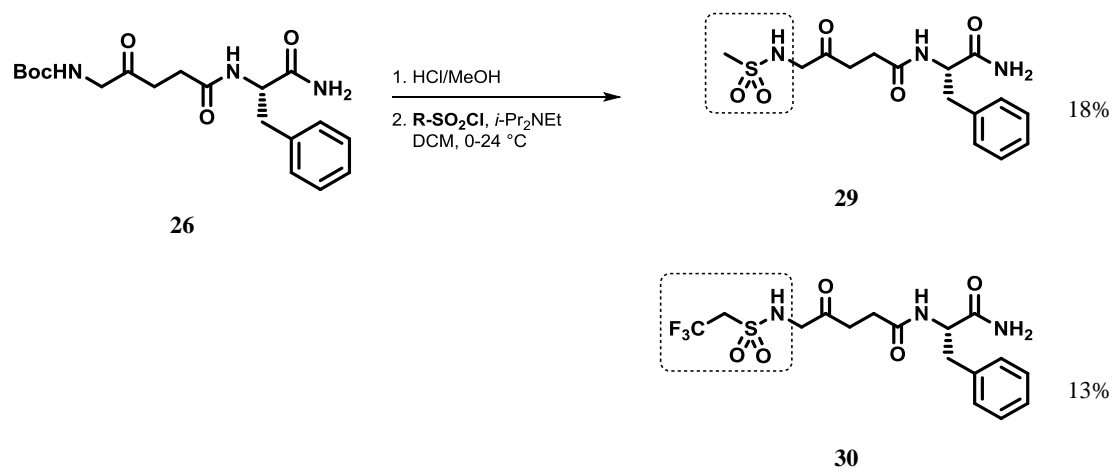


Scheme 34 Synthesis of *N*-Boc-5-aminolevulinic acid and extension to the ketomethylene peptide **26**.

Pseudopeptide **26** was used to synthesize four interesting peptidomimetic derivatives by Boc-deprotection with anhydrous methanolic HCl and peptide coupling (Scheme 35) or reacting the intermediate free amine with sulfonyl chlorides (Scheme 36).



Scheme 35 Synthesis of two peptide-coupled final ketomethylene compounds.



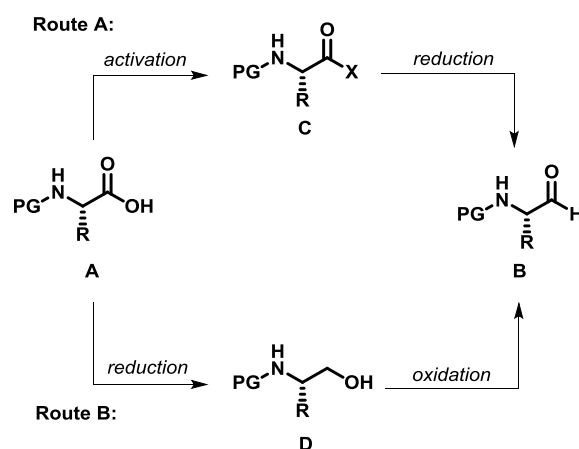
Scheme 36 Synthesis of two sulfonamide-coupled final ketomethylene compounds.

1.4.5 Development of CDI/DIBAL-H Method for the Synthesis of Chiral α -Amino Aldehydes from α -Amino Acids

In the case of the synthesis of *SHE* we have developed a new method for the preparation of chiral α -amino aldehydes. The results of this investigation have been published in *Organic and Biomolecular Chemistry*, from which the following paragraphs are taken.^[293]

1.4.5.1 Existing Methods for Synthesis of α -Amino Acids

Chiral *N*-protected α -amino aldehydes are very important building blocks across organic chemistry.^[294–296] They are used in a multitude of syntheses of biologically active molecules.^[297,298] Typically their synthesis starts from the chiral pool with readily accessible *N*-protected amino acids following two distinct routes (Scheme 37).^[299,300] In the first (Route A), the amino acid **A** is converted into an activated carboxylic acid derivative **C**, such as an ester^[301–308] or a Weinreb amide,^[309,310] and then directly reduced to the corresponding aldehyde **B**.



Scheme 37 Two distinct routes for the synthesis of α -amino aldehydes and conversion of amino acids to amino aldehydes using CDI/DIBAL-H.

The second (Route B) starts from the same *N*-protected amino acid **A**, which is first fully reduced to the corresponding amino alcohol **D** and selectively reoxidized to the desired α -amino aldehyde **B**.^[311–317] The major challenge for both routes is the intrinsic lability of the stereogenic centre of α -amino aldehydes, which is prone to epimerization, especially in the presence of an acid or a base.^[318,319]

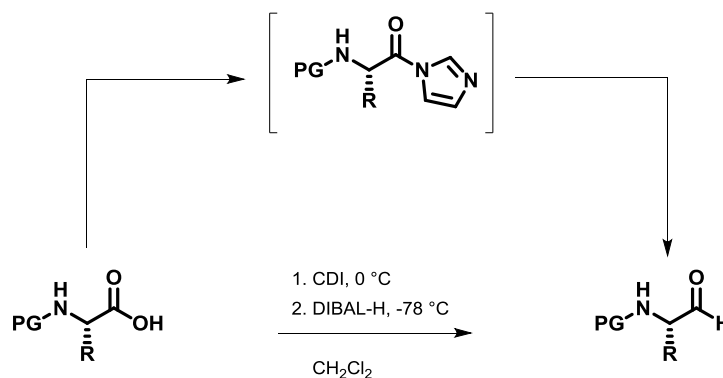
For the purpose of synthesis of *SHE*, as previously discussed, we required a scalable access to Boc-valinal. In our first attempt we synthesized the aldehyde following the procedure of Morwick by converting Boc-valine into the corresponding Weinreb amide using activation by Staab's reagent (CDI, 1,1'-carbonyldiimidazole).^[271] The Weinreb amide was isolated and converted to Boc-valinal by reduction with LiAlH_4 in 85% yield under complete retention of stereoconfiguration.

1.4.5.2 Development of CDI/DIBAL-H Method

While this two-step method delivered the desired product, we regarded the necessity to isolate the intermediate Weinreb-amide as a time-consuming nuisance, and reasoned that this step could be avoided if the intermediate acyl imidazolide^[320] would serve as a substrate for the DIBAL-H reaction. Stammer et al. have already reported in 1979 such a method,^[321] which despite its apparent attractiveness has seen little application,^[298,322] very likely because in the original paper optical rotation studies, which have been pursued for only one product in detail (Cbz-leucinal), indicated that this product was produced in only 60% ee. Despite this caveat we were encouraged by this literature precedence and can now report that through optimization of reaction parameters the one-pot production and reduction of acyl imidazolides provides an attractive rapid and efficient access to chiral α -amino aldehydes.

As a test substrate we chose Boc-valine to establish a suitable protocol for the CDI/DIBAL-H method. After considerable optimization in which we varied solvent, temperature, reaction time and workup conditions in comparison to the literature precedence of Stammer,^[321] we arrived at the following protocol in which a solution of *N*-protected amino acid in DCM was

treated with 1.1 eq of CDI at 0 °C for 60 min. Subsequently 2.1 eq of DIBAL-H were added dropwise to the resulting solution at -78 °C (Scheme 38).



Scheme 38 One-pot synthesis of α -amino aldehydes using CDI and DIBAL-H.

In the course of our studies we recognized that the outcome of this process depended on the quality of the used CDI and we recommend the use of CDI recrystallized from dry THF,^[272] which can be stored in nitrogen or argon atmosphere at 4 °C for at least 8 weeks. Special attention had to be paid for the workup of the DIBAL-H reduction reaction. In order to avoid basic conditions and prolonged workup, which could cause loss of chiral integrity of the resulting amino aldehyde,^[318,319] we have devised a quick method of quenching and aluminium complexation using a solution of tartaric acid instead of the commonly used Rochelle-salt solution.^[323–325] This method provided slightly acidic quenching conditions, and dramatically shortened the dissolution times of aluminium salts to less than 20 min even on multigram scale reactions compared to 2 h when using Rochelle-salt. We were pleased to see that by this extractive workup we could isolate Boc-valinal (**31**) already in pure form as judged by NMR and chiral GC, thereby avoiding purification via flash chromatography which causes racemization of these aldehydes according to our findings.

Entry	Product	Yield	ee	Entry	Product	Yield	ee		
1		31	84%	>99% ^a	8		38	87%	>98% ^a
2		32	87%	-	9		39	99%	>97% ^b
3		33	96%	>99% ^a	10		40	94%	>99% ^b
4		34	97%	>99% ^b	11		41	72% ^{d,e}	>99% ^b
5		35	92%	>99% ^a	12		42	52% ^{d,f}	-
6		36	91%	>99% ^{a,c}	13		43	88%	83% (72%) ^{a,g}
7		37	62% ^d	-					

Table 9 ^a Chiral-GC-FID based measurement; ^b diastereomeric excess; ^c Isolated by flash chromatography on silica due to lower purity of the crude material, to determine the abundance of the desired aldehyde; ^d Chiral HPLC-based measurement; ^e 3.35 eq DIBAL-H used; ^f 4.00 eq DIBAL-H used; ^g 83% ee obtained by adding 0.5 eq CuCl₂ during the activation step, and 72% ee when no additive was used under the same conditions.

With the optimized protocol in hands, a selection of proteinogenic amino acids with different *N*-protecting groups was converted to the corresponding aldehydes in excellent yields and high purity based on NMR and gas chromatography analysis (Table 9). The data on enantiomeric purity were determined by gas chromatography using prepared reference racemic samples, while for substrates which could not be separated via chiral GC optical rotations are reported. Boc-valine was converted to the corresponding aldehyde in 84% yield and >99% ee on a 10 gram-scale (Entry 1), as well as other Boc-protected amino acids (Entries 2-6) were obtained in excellent yields. An informative test substrate for this method was phenylalanine, known as the

most racemisation-prone proteinogenic amino acid in peptide synthesis.^[278,279,326–329] Boc-phenylalaninal (**33**) was produced with the CDI/DIBAL-H method in >99% ee as judged by chiral GC (Entry 3), and Cbz-phenylalaninal (**39**) with >97% ee measured by chiral HPLC after reduction of the isolated aldehyde with NaBH₄ (Entry 9).^[330] This result allows us to expect that our method can generally cover the conversion of proteinogenic amino acids to chiral amino aldehydes without racemization – even in the cases in which no suitable ee-determination method with chiral GC or HPLC is currently available. In order to compare our improved protocol with the original one by Stammer, we investigated the reduction of Cbz-leucine to Cbz-leucinal (**38**) (Entry 8) and could determine >98% ee via chiral GC (compared to the reported 60 % ee in their publication, which had been determined via optical rotation). This confirms that by our modifications the one-pot strategy of CDI-activation/DIBAL-H reduction could be developed into a feasible and useful method for the synthesis of *N*-protected α -amino aldehydes.

In terms of functional groups in the side chain, we could notice that this method reduces acyl imidazolide significantly faster than methyl ester, as exemplified for protected aspartate aldehyde **37** (Entry 7). Notably Fmoc-protection was orthogonal to the reaction conditions, although at least another equivalent of DIBAL-H had to be added to complete the conversion to the aldehydes **41** and **42** (Entries 11-12).

After having established the scope of this robust protocol for the conversion of proteinogenic amino acids, we wanted to check the limitations of our method and apply it to phenylglycine – a very challenging substrate, which racemizes very easily and for which only few stereoselective transformations are known.^[331] Myers et al. have successfully accessed Fmoc-phenylglycinal via oxidation of Fmoc-phenylglycinol with Dess-Martin-periodinane,^[332] while Wroblewski and Piotrowska demonstrated the same with Boc- and Bz-phenylglycine.^[333,334] When we tested our CDI/DIBAL-H method for Boc-Phg, we received the product in good 88% yield, but disappointing enantiopurity of 72% ee. We rationalized that the second equivalent of DIBAL-H is necessary to complete the conversion of the acyl imidazolide intermediate due to the presence of one equivalent of imidazole byproduct from the activation step. Thus imidazole deprotonated by the hydride reagent is thought to be a base contributing to racemization of the product. We hypothesized that by addition of complexing metal salts we could scavenge deprotonated imidazole. Copper(II) salts were found to produce complexes with imidazole in DCM (in 60 min vs >24 h in case of nickel salts) based on visual observation.^[335,336]

Consequently, we performed a series of experiments adding copper(II) chloride as a scavenging agent additive after CDI activation and prior to the addition of DIBAL-H. The addition of 0.5 eq CuCl_2 enhanced the ee of produced Boc-phenylglycinal (**43**) in each experiment, in contrast to parallel experiments with no additives (Table 10). Adding more than 0.5 eq of CuCl_2 did not further increase the enantiomeric purity.

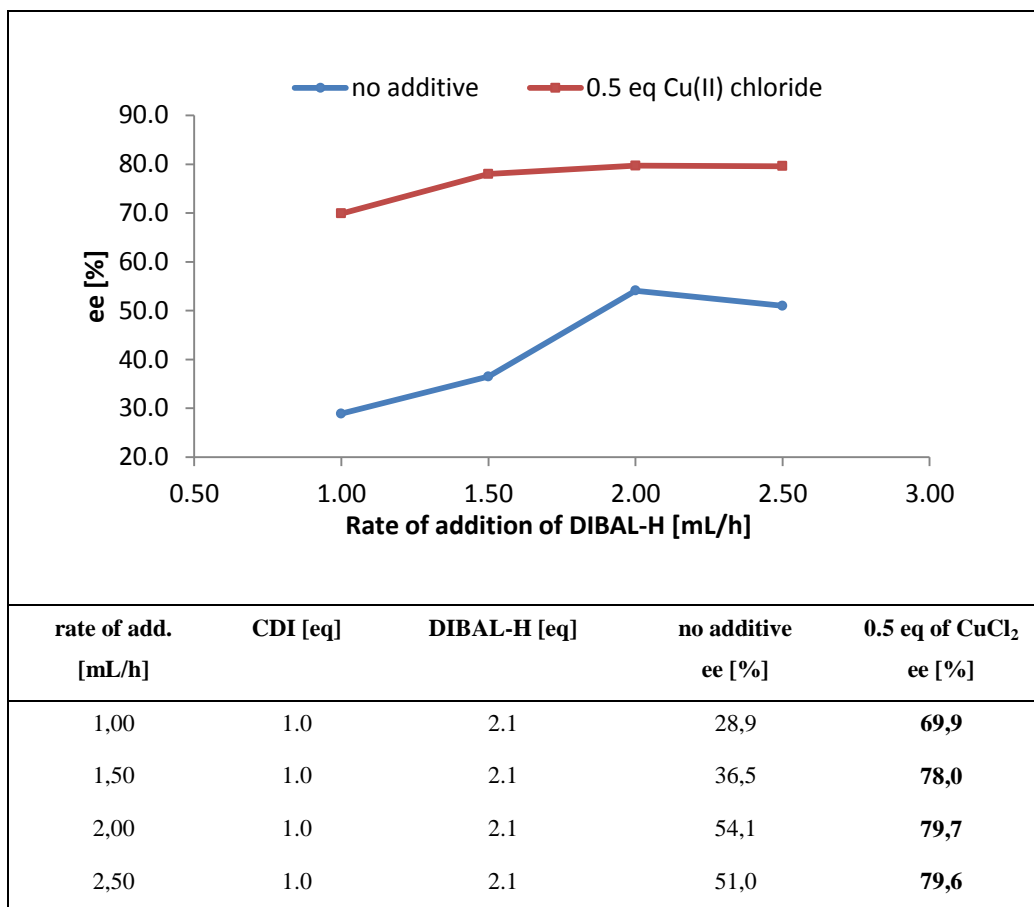


Table 10 Dependence of ee of Boc-phenylglycinal on the rate of addition of DIBALH. Each reaction instance was performed using 50 mg (0.20 mmol) Boc-L-Phg-OH, 32 mg (0.20 mmol, 1.0 eq) CDI and 0.42 mL (0.42 mmol, 2.1 eq) 1M DIBAL-H in 2.0 mL of absolute CH_2Cl_2 , according to the general procedure, with the altered rates of addition, regulated by settings on the syringe pump. A parallel instance was performed for each reaction, differing by having 13 mg (0.10 mmol, 0.5 eq) of CuCl_2 added after the activation step and stirred for 60 min more before the DIBAL-H reduction. Enantiopurity was determined by chiral GC-FID.

Temperature maintained during the reduction step affects both the resulting yield (Table 11) and ee (Table 12) of Boc-phenylglycinal.

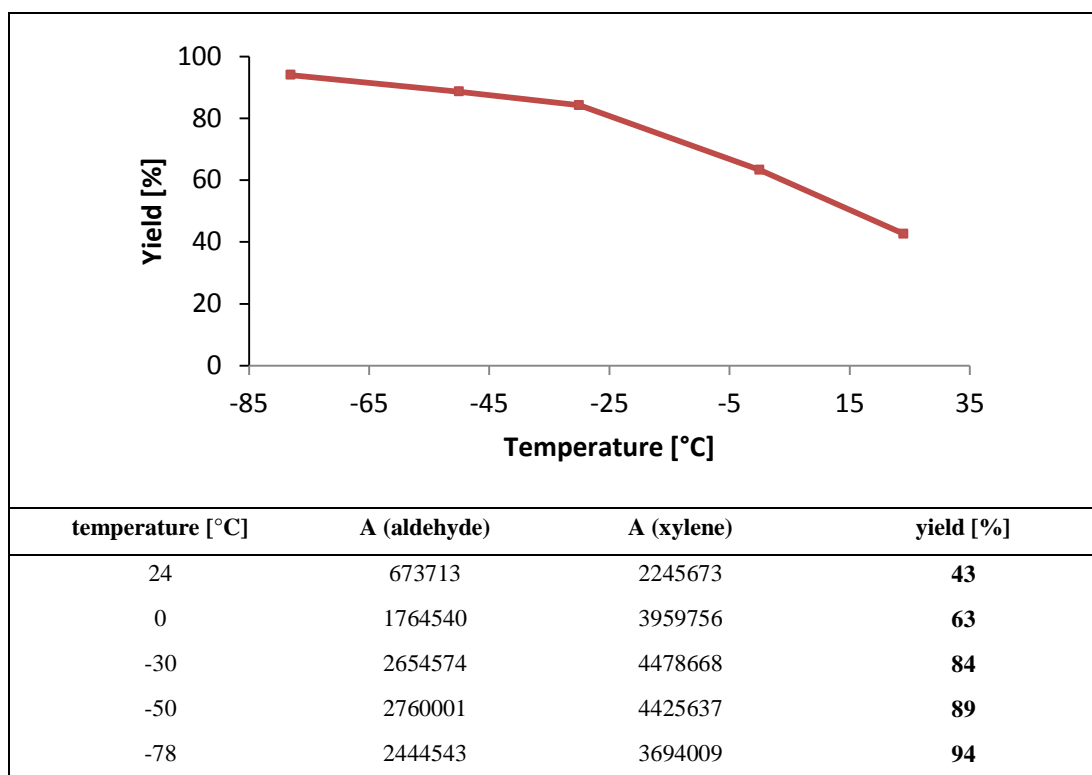


Table 11 Dependence of yield of Boc-phenylglycinal on the temperature during addition DIBAL-H. Each reaction instance was performed using a 2.0 mL aliquot of a stock solution of 270 mg (1.07 mmol) of Boc-L-Phg-OH and 135 μ L (1.07 mmol) of *p*-xylene (internal standard) in 10.8 mL of absolute CH_2Cl_2 , according to the general procedure with altered temperatures used during the reduction step (-78 $^\circ\text{C}$, -50 $^\circ\text{C}$, -30 $^\circ\text{C}$, 0 $^\circ\text{C}$ and RT respectively). For other temperatures relative yield was calculated using the determined isolated yield at -78 $^\circ\text{C}$ and the integrated GC-based peak areas (A), according to the following equation:

$$\text{Yield} = \frac{A(\text{aldehyde}) / A(\text{xylene})}{A(\text{aldehyde})_{-78^\circ\text{C}} / A(\text{xylene})_{-78^\circ\text{C}}} * \text{Yield}_{-78^\circ\text{C}}$$

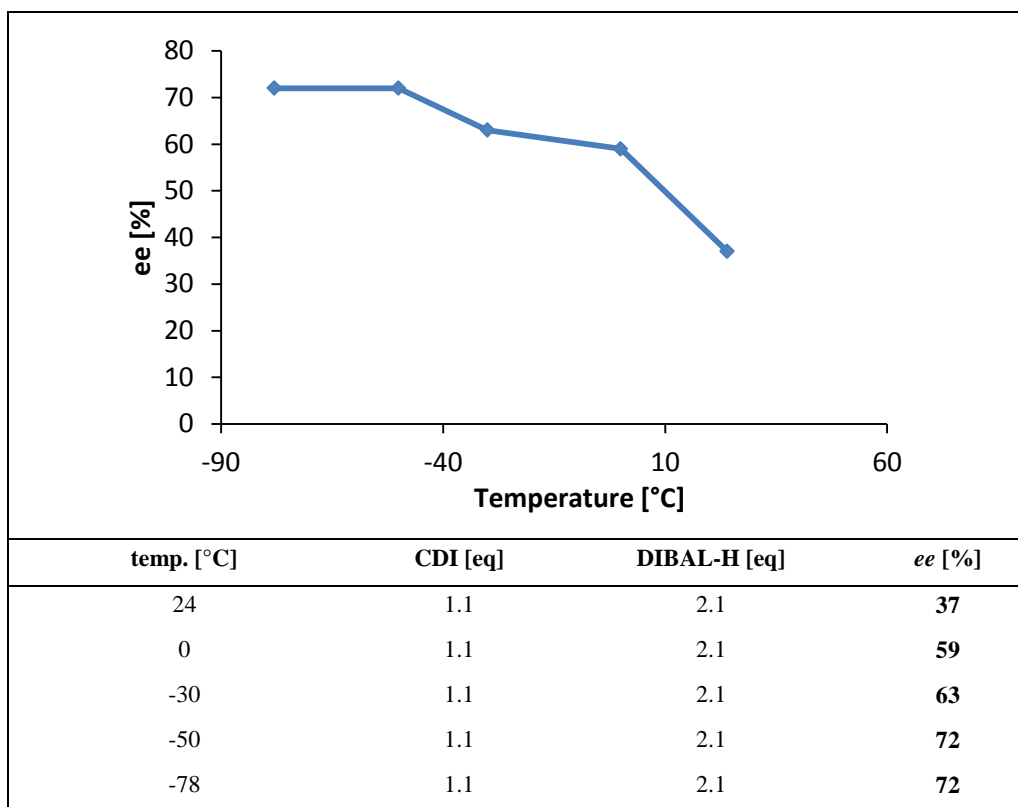


Table 12 Dependence of ee of Boc-phenylglycinal on the temperature during addition DIBAL-H. Each reaction instance was performed using 50 mg (0.20 mmol) Boc-L-Phg-OH, 36 mg (0.22 mmol, 1.1 eq) CDI and 0.42 mL (0.42 mmol, 2.1 eq) 1M DIBAL-H in 2.0 mL of absolute CH₂Cl₂, according to the general procedure with altered temperatures used during the reduction step (-78 °C, -50 °C, -30 °C, 0 °C and RT respectively). Enantiopurity was determined by chiral GC-FID.

We have developed an efficient one-pot method for the conversion of *N*-protected amino acids into chiral *N*-protected α -amino aldehydes by *in situ* activation with CDI followed by reduction with DIBAL-H. The advantages of this method compared to established two-step protocols are 1) its operational simplicity, 2) the use of inexpensive reagents, 3) the simple extractive workup and 4) its short overall processing time (typically less than 4 hours) to deliver the product in high purity. While the presented method is excellent for proteinogenic amino acids leading to good yields and preserved stereointegrity, it has its limitation in phenylglycine, where the corresponding aldehyde gets significantly racemized.

1.4.6 *In Vitro* Evaluation of the Proposed Peptidomimetic Inhibitors

1.4.6.1 Isothermal Microcalorimetry Assay

In ITC (isothermal calorimetry) measurements Bezerra *et al.* found that the ligand-hDPP3 binding process has an endothermic profile.^[106] Usually, the thermodynamics of peptide binding to a protein is dominated by formation of hydrogen bonds between the ligand and complementary ordered H-bond donors/acceptors of the binding site.^[337] Formation of polar interactions is accompanied by favorable enthalpic change. The strongly endothermic profile of ligand binding to hDPP3 indicated that the entropy term dominates the process in this case, which is a rare phenomenon among peptidases.^[338] Based on structural observation of a large collapse of two domains upon binding, expelling up to 30 ordered molecules of water, it was rationalized that these water molecules provide an “entropy pool” which greatly outcompetes the positive enthalpic term (Figure 46).

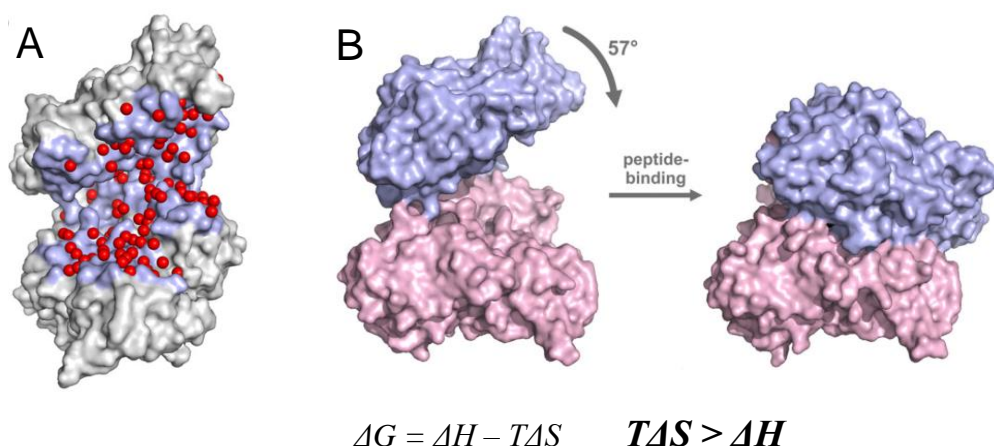


Figure 46 **A:** Ordered water molecules in the nonbound hDPP3. **B:** Large structural collapse upon ligand binding.^[17]

In order to investigate whether the hydroxyethylene transition state mimetics binds to hDPP3 and to compare the thermodynamic profile with the tynorphin binding event, hDPP3 was subjected to isothermal microcalorimetric titration with *SHE*. We were pleased to observe that *SHE* binds to hDPP3 displaying equivalent endothermic character (Figure 47). Moreover, *SHE*

was the first molecule subjected to an ITC assay with the active wild type hDPP3 enzyme. Calorimetric binding experiments and cocrystallization with tynorphin and other peptide substrate inhibitors (like IVYPW) were not feasible with the active enzyme, leading to the use of E451A inactive mutant instead (catalytic base Glu451 residue was mutated to Ala).^[106]

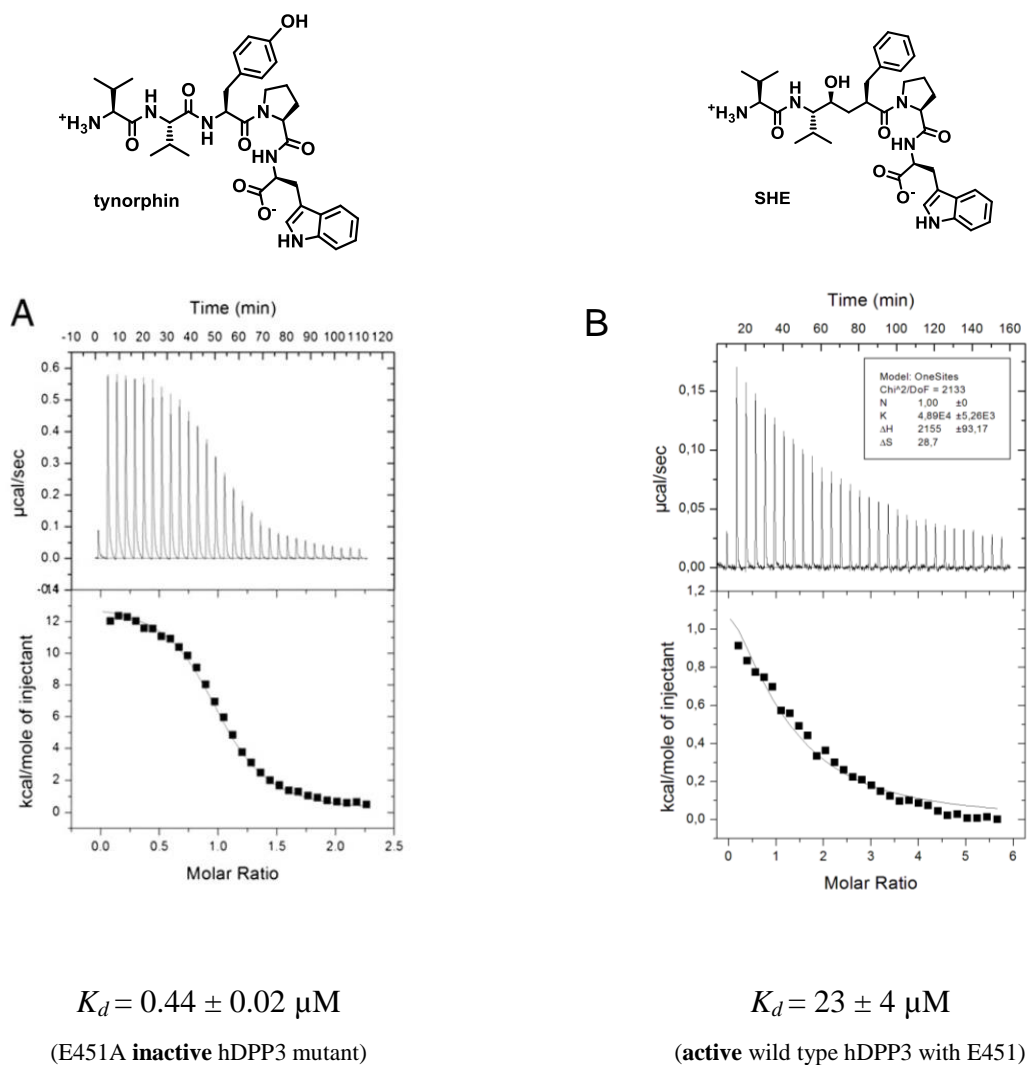


Figure 47 ITC thermograms at 298K. **A:** tynorphin binding to the mutant E451A hDPP3.^[17] **B:** SHE binding to the wild type hDPP3.

The calorimetric experiment demonstrated that *SHE* is recognized by the enzyme, and that it is resistant to the catalytic hydrolysis of the active enzyme, as expected. To confirm the full stability of *SHE* in presence of hDPP3, the mixture from the calorimetric cell recovered after 5 h, containing hDPP3 and *SHE* was analyzed by reverse phase HPLC-MS. The analysis resulted with a chromatogram displaying a clean, intact peak of *SHE* and its identity was confirmed by mass spectrometry (Figure 48).

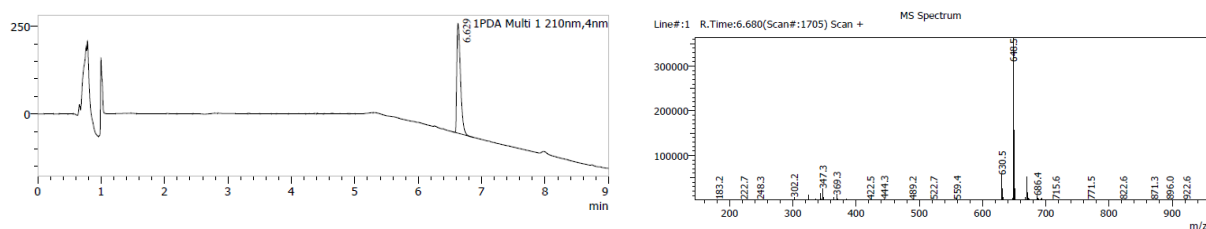


Figure 48 HPLC chromatogram (left) and ESI-MS spectrum of the peak of *SHE* (right), after titration of the active hDPP3.

1.4.6.2 Inhibition of hDPP3 with Hydroxyethylene Transition State Mimetics

Inhibition potencies of both *SHE* and *HER* were investigated via fluorescence-based competitive inhibition assay of degradation of the Arg-Arg- β -naphthylamide substrate. IVYPW peptide, which is the *N*-terminal mutant derivative of tynorphin and the most potent known substrate inhibitor of DPP3,^[20] was assayed along for comparison (Table 13). IC₅₀ values were calculated based on the resulting dose response curves. Both transition state mimetics inhibited hDPP3. *SHE* inhibited the enzyme with IC₅₀ = 98 μ M, and inhibition with *HER* resulted in IC₅₀ = 8.8 μ M, making it 11-fold more potent than *SHE*. Importantly, *HER* inhibits hDPP3 within an order of magnitude of the potency of IVYPW (IC₅₀ = 2.9 μ M). Difference in potency between *SHE* and *HER* is in line with the expectations proposed based on the structure based design, where structural motifs of both transition state mimetics were compared to the transition state of peptide cleavage. The (*S*)-hydroxyethylene was expected to bind to the zinc ion of the active site,

and the (*R*)-hydroxyethylene was expected to strengthen its enthalpic binding term by the additional hydrogen bond to His568.

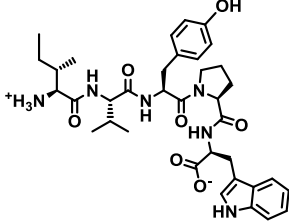
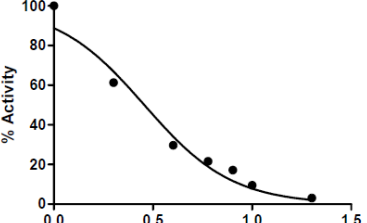
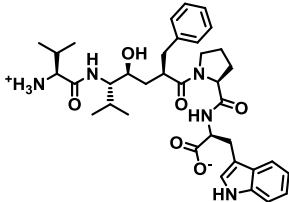
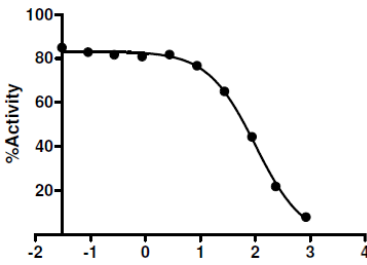
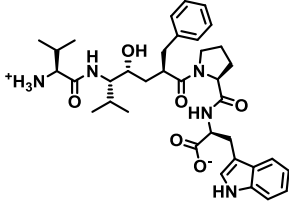
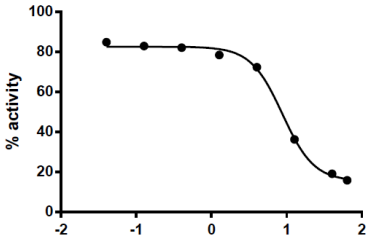
inhibitor	structure	dose-response curve	IC ₅₀ [μM]
IVYPW			2.9 ± 1.1
<i>SHE</i>			98 ± 7
<i>HER</i>			8.8 ± 1.1

Table 13 Fluorescence-based inhibition assays of degradation of Arg-Arg-βNA with hDPP3. Data calculated based on dependence of %activity vs. concentration of inhibitor. Fluorescence vs time was collected at 410 nm.

1.4.6.3 Inhibition of hDPP3 with Shorter Peptidomimetic Hydroxyethylene and Ketomethylene Transition State Mimetics

The fluorescence-based assay of degradation of the Arg-Arg-β-naphthylamide was used to determine the IC₅₀ inhibition values for shorter hydroxyethylene and ketomethylene tetrapeptide mimetics (Table 14). Most of the smaller inhibitors displayed dramatically lower inhibition. As the IC₅₀ values were >200 μM and reaching the limits of solubility the IC₅₀ values were computationally extrapolated from the weak inhibition profiles.

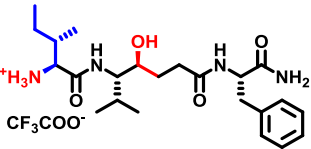
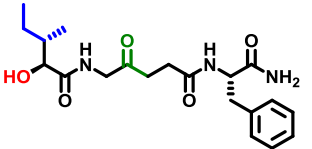
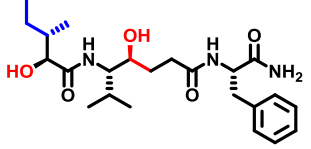
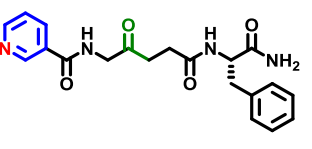
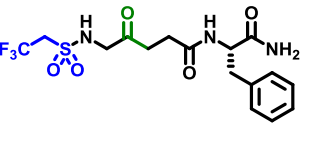
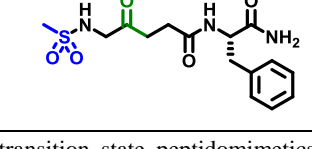
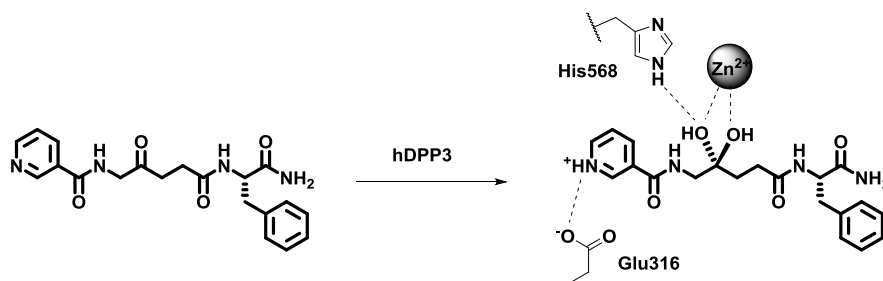
Hydroxyethylene mimetics	IC ₅₀ [μM]	Ketomethylene mimetics	IC ₅₀ [μM]
	19 2766		27 2290
	21 20542		28 388
			30 2511
			29 3567

Table 14 Extrapolated IC₅₀ values for inhibition of hDPP3 with shorter transition state peptidomimetics. GraphPad® software was used for calculations.

It appears that generally the ketomethylene transition state mimetics show stronger inhibition than the shorter hydroxyethylenes. With the examples **19** and **21**, which differ only in having or not having the peptide *N*-terminus, the results of the inhibition assay stresses the importance of having a charged *N*-terminus. This confirms the observed structural feature of the salt bridge to the negatively charged carboxylate residue of the Glu316 in the tynorphin-hDPP3 complex.^[17] Among the ketomethylene derivatives^[17] only ketomethylene **28** has an equivalent of *N*-terminus of peptides. Its pyridine nitrogen is very likely charged, having probably higher p*K_a* value than the typical p*K_a* ≈ 5 for pyridines^[339,340] which is enhanced in the closed binding pocket in the vicinity of Glu316. Moreover, the assayed ketomethylene molecules completely lack the substituent which would mimic the second amino acid residue, counting from the true peptide *N*-terminus (the P1 residue, according to the Schechter-Berger notation).^[187] Thus, the ketomethylene molecules do not fill the lipophilic S1' pocket observed in the structure, so they could have even better affinity over the shorter (*S*)-hydroxyethylene mimetics, if they had the P1' residue.

The ketomethylene inhibitor **28** shows almost an order of magnitude stronger inhibition than any of the shorter synthesized molecules. Like with the other ketomethylene molecules, its advantage over hydroxyethylenes is that its ketone carbonyl can be attacked by the nucleophilic water in the active site of hDPP3, in the manner equivalent to the nucleophilic attack during peptide bond hydrolysis. The product of such attack on ketomethylene is a noncleavable geminal diol. It is known that HIV-1 protease can stabilize such highly inhibiting ketomethylene diols in their active sites,^[341] whose cocrystal structure aligns very nicely with the cocrystallized tetrahedral intermediate of the peptide cleavage.^[246] This process would provide molecule **28** with two hydroxyl residues, spatially configured like those in both (*S*)-hydroxyethylene and (*R*)-hydroxyethylene simultaneously. Hence, we propose that the bound ketomethylene diol adopts features of both hydroxyethylene epimers at once, interacting with two coordinating bonds to the zinc ion, and one hydrogen bond to the His568 (Scheme 39). The strong ion-ion interaction of the pyridinium terminus of molecule **28** to the Glu316 rounds up the rationale of its exceptional inhibition potency among the shorter analogues.



Scheme 39 Binding of the ketomethylene inhibitor to hDPP3 via a tightly bound transition state mimicking geminal diol.

1.4.7 Structure of hDPP3 in Complex with the Hydroxyethylene Transition State Mimicking Inhibitors

1.4.7.1 X-ray Crystallographic Structure of hDPP3-*SHE* Complex

Considerable crystallization efforts were invested to get a crystallographic structural proof of the proposed interactions of the synthesized hydroxyethylene transition state mimetics with hDPP3. Pleasingly, a structure of hDPP3 in complex with *SHE* has been determined by Prashant Kumar (group of Prof. Karl Gruber, Institute of Molecular Biosciences, KFU Graz) at a resolution of 2.6 Å (Figure 49).

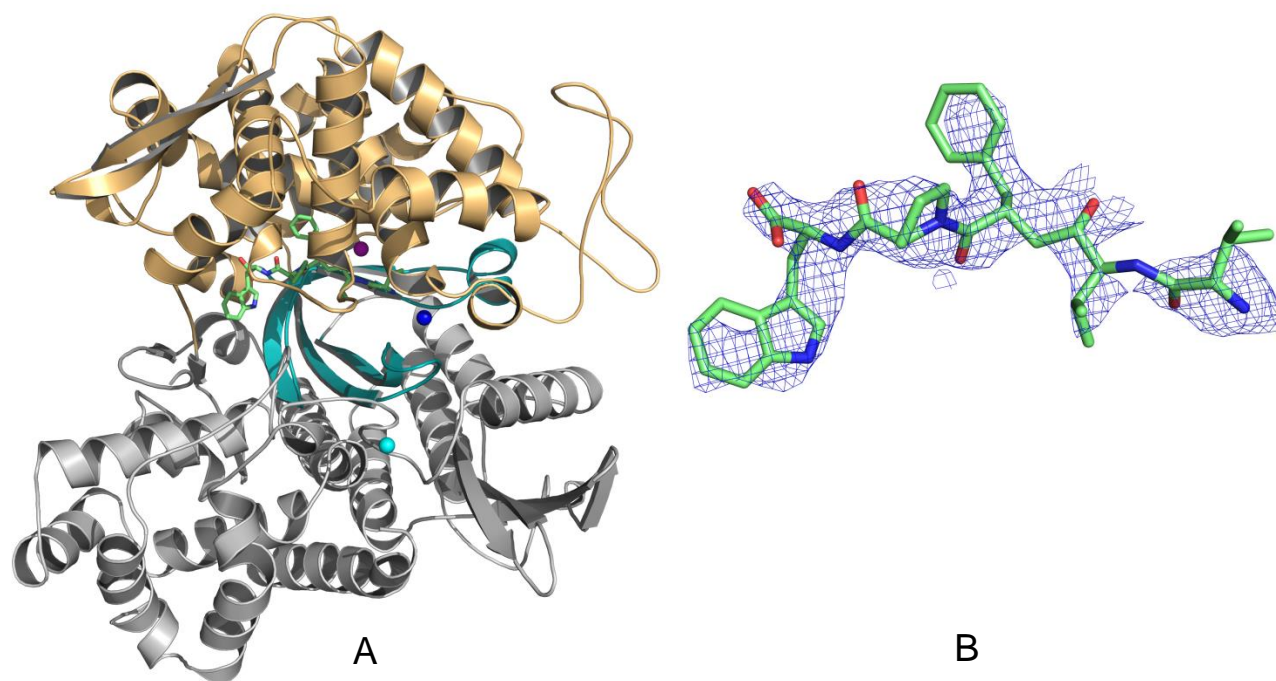


Figure 49 **A:** Human DPP3 in complex with (*S*)-hydroxyethylene transition state mimicking inhibitor (*SHE*). Structure solved with a resolution of 2.6 Å. **B:** Spatial electron density map of *SHE* ligand.

The determined cocrystal structure of the *SHE*-hDPP3 complex strongly resembles the structure of the tynorphin-hDPP3 complex.^[17] It consists of two predominantly α -helical domains (Figure 49A, ochre and grey), enclosing the *SHE* ligand in a clamshell fashion. In the binding site there is a β -barrel-like structure (Figure 49A, teal), where the electron density of *SHE* was found (Figure 49B). The ligand binds as a β -sheet extension (Figure 49A, green) to the β -barrel-like structure.

The binding mode of *SHE* can be almost perfectly aligned with the binding mode of tynorphin, the main differences being around the catalytic zinc-complex. The C-terminal part of the ligand is bound in the cation- π complex of indole substituent of *SHE* with Lys670 and Arg669 cationic residues of hDPP3. Arg669 participates also in the salt bridge interaction to the carboxylate group of *SHE*. The equivalence to the tynorphin-hDPP3 complex is also apparent at the N-terminus of *SHE*, which is also tightly bound by the same three hydrogen bonds (Glu316, Asn394, Asn391) and salt bridge to the Glu316.

In contrast to the binding mode of tynorphin, the hydroxyethylene in *SHE* does not make any interaction with the His568 residue, which most probably presents a significant penalty to the enthalpy of binding (Figure 50A and B). On the other hand, based on the initial rough model of binding of (*S*)-hydroxyethylene type of inhibitor (Figure 50C), the hydroxyl substituent complexes as expected to the zinc ion, which was confirmed by measurement of the bond length from the crystallographic data. The Zn–O bond was found to be 1.9 Å (Figure 50 D), which falls into the range of 1.9–2.4 Å for values typically observed for the length of Zn–O coordinating bonds in literature.^[342–346] Another interesting feature is a water molecule (Figure 50A and D) hydrogen-bound to the hydroxyethylene, which occupies the space where normally the carboxylate from Glu451 would be positioned within the active hDPP3 (Figure 50B).

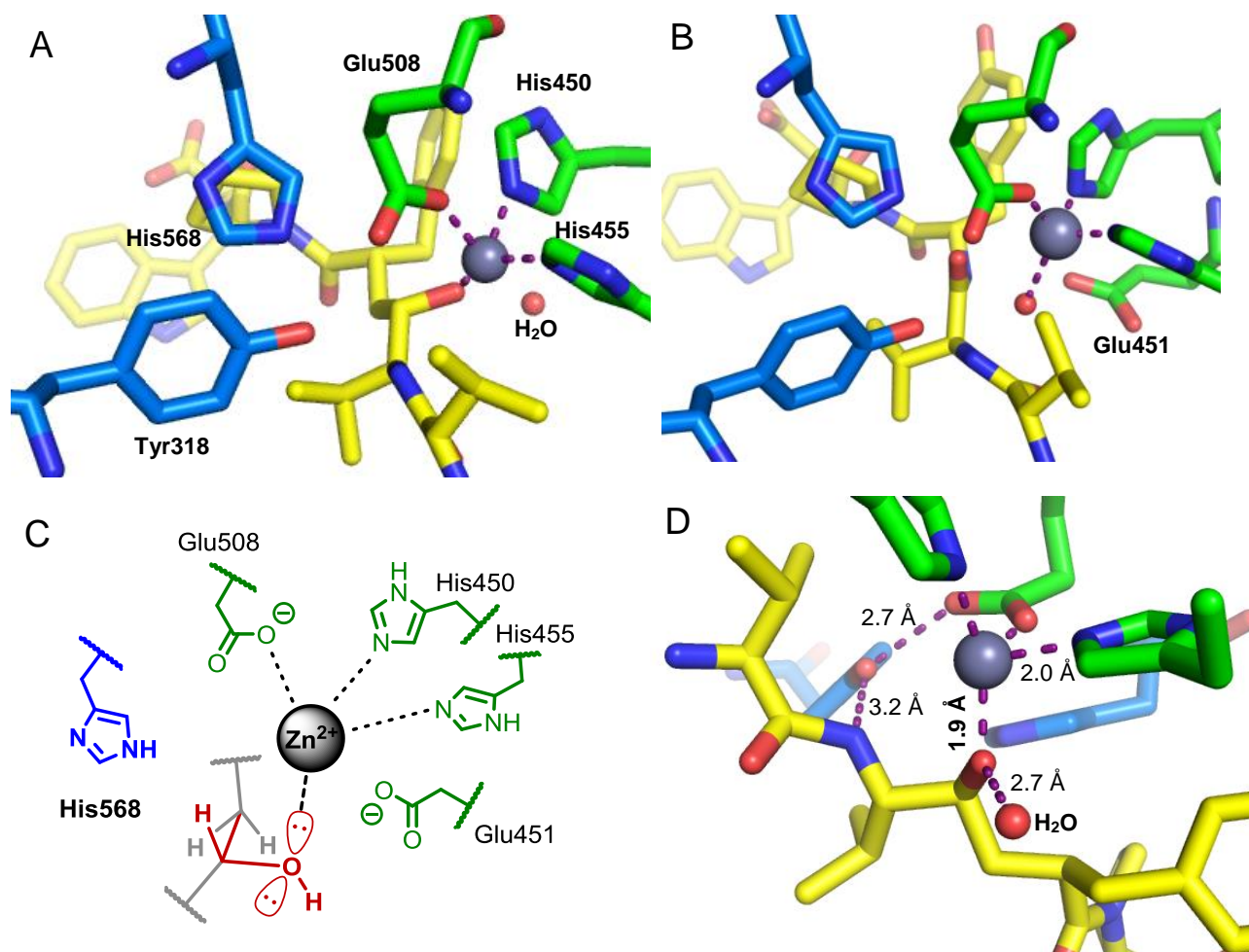


Figure 50 **A:** Binding mode of *SHE* in the binding site of the inactive E451A mutant of hDPP3. **B:** Binding mode of tynorphin in the binding site of the inactive E451A mutant of hDPP3.^[17] Glu451, Zn-ion and the water molecule, missing out from the tynorphin-hDPP3 structure, were computationally added and force field-optimized using MOLOC software.^[108] **C:** Initially proposed scheme of binding mode of *SHE* to the active of the wild type hDPP3, having the catalytic Glu451 residue. **D:** Measured hydrogen bonding and zinc coordinating interactions around the hydroxyethylene moiety in the *SHE*-hDPP3 complex.

Crystallographic structural findings show that the binding mode of *SHE* is in line with the initial model expectations. This provides confidence to propose a model for the experimentally determined stronger inhibition of hDPP3 with *HER*. For this purpose, computational molecular modelling tools were used.

1.4.7.2 Computer-assisted Molecular Modelling

Before the cocrystal structure of **SHE** in complex with hDPP3 was available, an attempt was made to get more insight into how hydroxyethylene transition state mimetics interact with hDPP3. The available cocrystal structure of tynorphin and hDPP3 was used to model the binding modes of the tynorphin derived molecules *in silico*.

The X-ray structure was loaded into MOLOC computer software.^[108] For both **SHE** and **HER** an instance was generated by editing the central amide bond of tynorphin, being the subject of enzymatic cleavage. The structures containing artificially introduced hydroxyethylene moieties were optimized by the MAB molecular force field and its energy minimization protocol. MAB force field is part of the MOLOC software, and it has been trained versus a test set of highly refined 1589 structures from the Cambridge Structural Database. When the optimization protocol is initiated, it searches for the local minimum of total energy, containing the following terms:

$$E = E_{HB} + E_{VB} + E_{tor} + E_{disp} + E_{BS} + E_{pyr} + E_{1,4}$$

The protocol takes into account simultaneously the energy terms of hydrogen bonds (E_{HB}), valence angle bending distortions (E_{VB}), bond torsion angle strain (E_{tor}), dispersion interactions from van der Waals contacts (E_{disp}), bond stretching (E_{BS}), distortion of pyramidalicity (E_{pyr}), and 1,4-interactions ($E_{1,4}$). Although it lacks a good model of Coulomb interactions and solvation, its output of force field minimized structure may indicate the relationship between certain aspects of molecular mechanics of the inhibitor with the experimentally measured inhibition data.

Since the original complex did not contain the catalytic zinc ion, it was incorporated together with the activated, complexed, nucleophilic water molecule. It was optimized to the local energy minimum using the MAB force field minimization. Subsequently, the energy minimized structures have been obtained for both **SHE** and **HER** (Figure 51). In the simulations, all of the residues of the enzyme were kept rigid, while the newly edited ligand was allowed to relax with the gradient of the force field. In the outcome, there were no significant changes in the

way that parts of the ligand interact with the enzyme, except that hydroxyethylene functions adjusted their positions to minimize the energy.

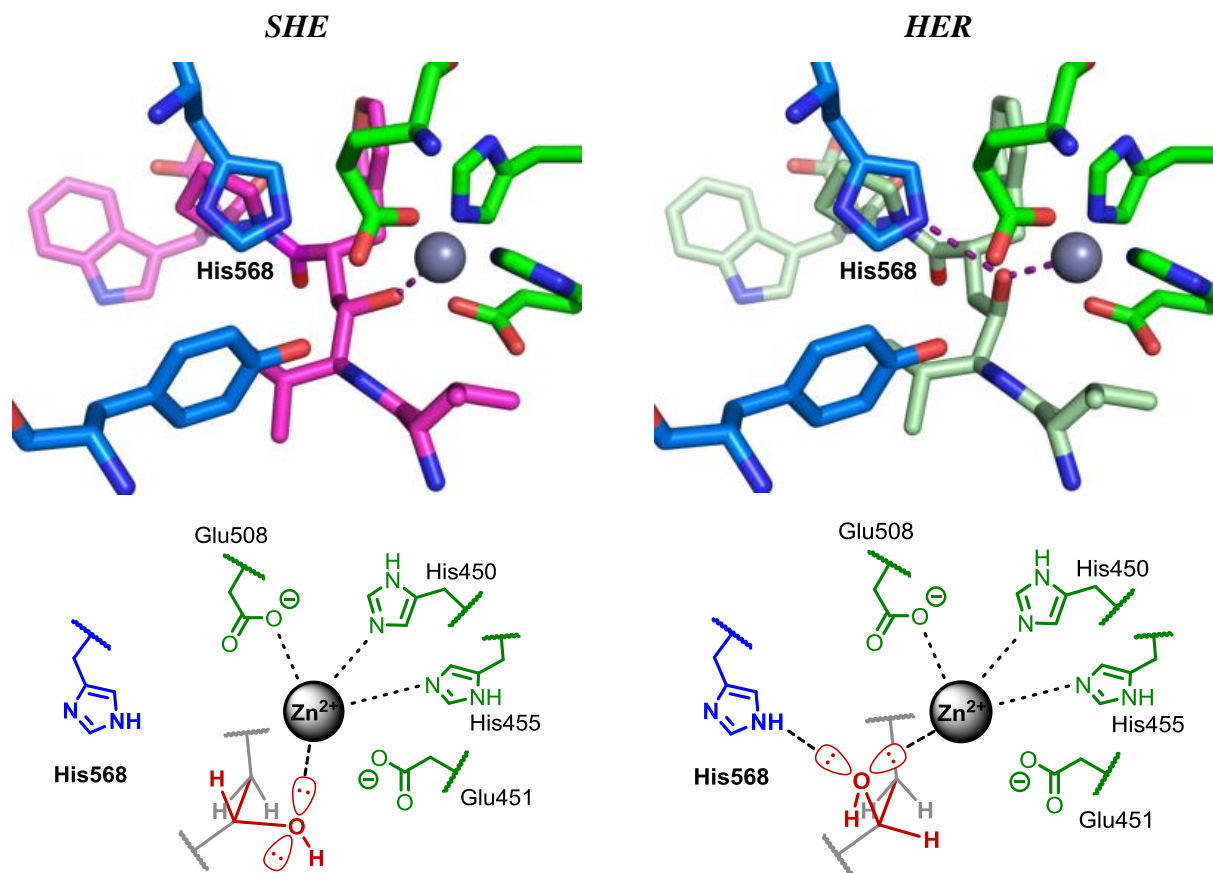


Figure 51 Binding modes of *SHE* and *HER* in the active site of hDPP3, as modelled via force field optimization in MOLOC.^[108]

SHE adopted a binding mode almost identical to the one observed in the subsequently obtained cocrystal structure of *SHE* with hDPP3. (*R*)-Hydroxyethylene occupied a different binding pose. The hydroxyl group of *HER* found an optimal position between the zinc ion and the His568 side chain. Measurements of interatomic distances (2.0 Å for Zn–O dative bond, in particular) in the resulting structures indicate that these complexes are in good agreement with the initial hypothesis. Successful prediction of the binding mode of *SHE* implicated by good alignment of the X-ray structure and the structure obtained by modelling *in silico* (Figure 52), puts credibility into the predicted structure of the *HER*-hDPP3 complex. Hence, formation of

both zinc-coordinating bond and the hydrogen bond to His568 are very likely to occur in the case of *HER*-hDPP3 complex.

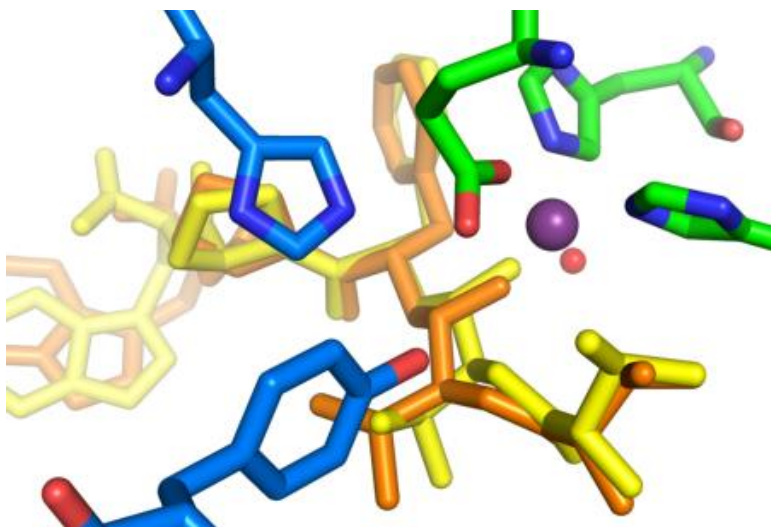


Figure 52 Structure of the *SHE*-hDPP3 complex. Alignment of cocrystal structure (yellow) and the structure obtained via modelling in MOLOC (orange).

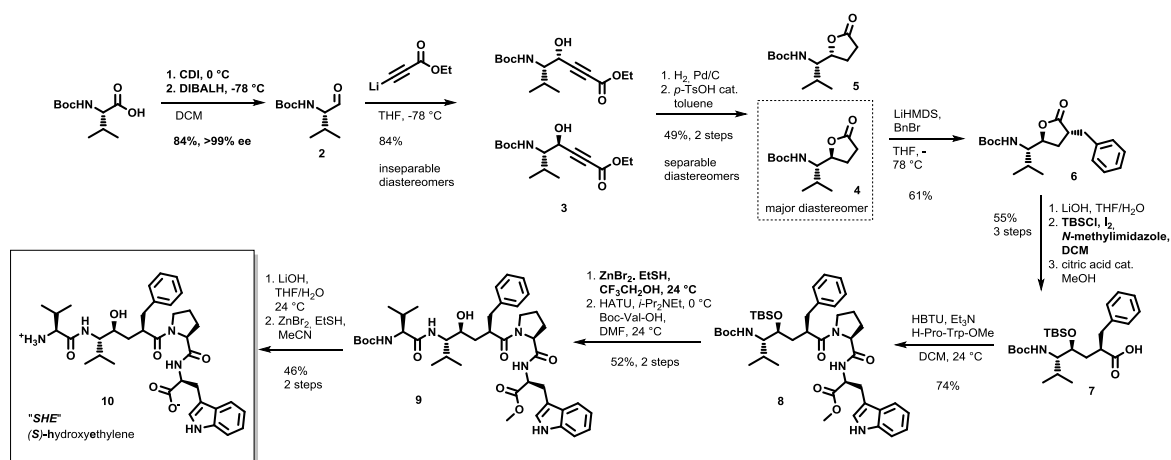
Both *SHE* and *HER* are basically linear isomers bearing the same functional groups. Accordingly, their solvation energies in aqueous buffer environments should be very similar. Since the formation of a hydrogen bond to the His568 side chain of hDPP3 is the major observable difference that *HER* boasts over *SHE*, it apparently enhances the enthalpic term of binding, which results in a stronger observed inhibition of the enzyme. The presented structural findings provide the following perspective: positioning of the hydroxyl group of *SHE* can be perceived as the mimetics of nucleophilic attack of the water molecule, and the positioning of the hydroxyl group of *HER* as a stabilized transition state oxyanion mimetics. For types of zinc metallopeptidases, which have the transition state stabilizing residue equivalent to the His568 in hDPP3, oxyanion mimetics present an efficient modification of a substrate into an inhibitor, simultaneously gaining two new tight interactions.

1.5 Summary

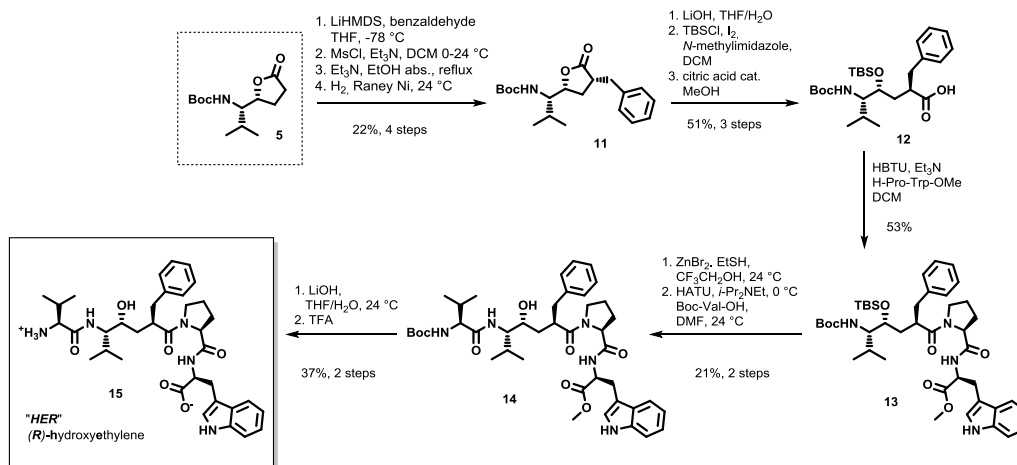
In one of the greatest historical efforts of in drug design hydroxyethylene-based HIV-1 protease targeting drugs have been developed, indicating that hydroxyethylene is a privileged molecular feature in protease inhibitor design. Presently, some of the most attractive drug targets among metalloproteases are matrix metalloproteases. All of the drug development efforts on these zinc endopeptidases have failed so far, one of the major reasons being lack of selectivity.^[347] A new type of metallopeptidase inhibitors would provide fresh starting grounds in contrast to the metal chelating inhibitors, whose chelation ability often proves to be very problematic in terms of selectivity over metalloprotein off-targets.

To the best of our knowledge, no hydroxyethylene transition state mimetic inhibitors have been previously reported as inhibitors of a metalloenzyme. Herein, we demonstrate the viability of hydroxyethylene transition state mimetics in the design of metallopeptidase inhibitors, and inspire confidence that the hydroxyethylene type inhibitors could be developed into metallopeptidase targeting drugs (e.g. neprilysin, matrix metalloproteases).

A stereodivergent approach towards both hydroxyethylene epimers was devised based on different existing methods for synthesis of central hydroxyethylene pseudodipeptide cores (Scheme 40 and Scheme 41). The molecular scaffold of tynorphin, a high affinity hDPP3 substrate, was translated into two epimers of hydroxyethylene transition state peptidomimetics **SHE** ((*S*)-hydroxyethylene) and **HER** ((*R*)-hydroxyethylene).



Scheme 40 Summary of the synthesis of **SHE**.



Scheme 41 Summary of the synthesis of *HER*.

Both *SHE* and *HER* inhibited hDPP3 in a standard fluorescence-based inhibition assay (Figure 53). In general, they achieve the binding affinity by molecular recognition of the residues originating from the template substrate tynorphin. The key inhibition-related properties of the transition state mimicking inhibitors of hDPP3 are found in the binding characteristics in the active site around the zinc ion. In order to get more insight about this, cocrystallization experiments have been performed. The cocrystal structure of the (*S*)-hydroxyethylene analogue in complex with hDPP3 has been determined (Figure 54).

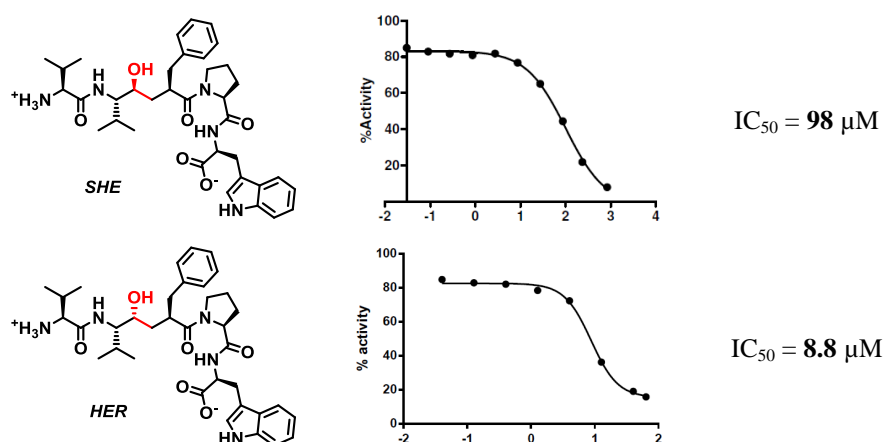


Figure 53 Inhibition potencies of *SHE* and *HER* in assays with hDPP3.

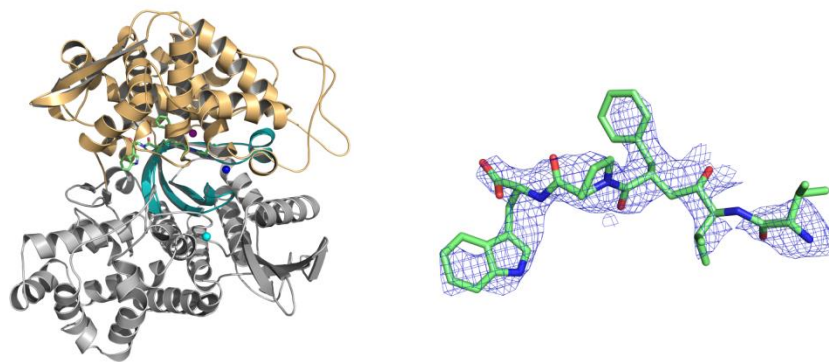


Figure 54 Cocystal structure of *SHE* in complex with hDPP3 (left) and the electron density of *SHE* extracted from the calculated crystallographic data.

Together with computational structural modeling and mechanistic considerations it gives a perspective that one of the hydroxyethylene epimers represents a *nucleophilic attack mimetics*, where the hydroxyl substituent is positioned in space of the active site where normally the nucleophilic water molecule is positioned, while the other represents an *oxyanion mimetics*, where hydroxyl substituent occupies space which would be occupied by the oxyanion generated in the event of peptide hydrolysis. In the case of hDPP3, oxyanion mimetics incorporated by *HER* proved to be more successful, enhancing inhibition potency by an order of magnitude (Figure 55).

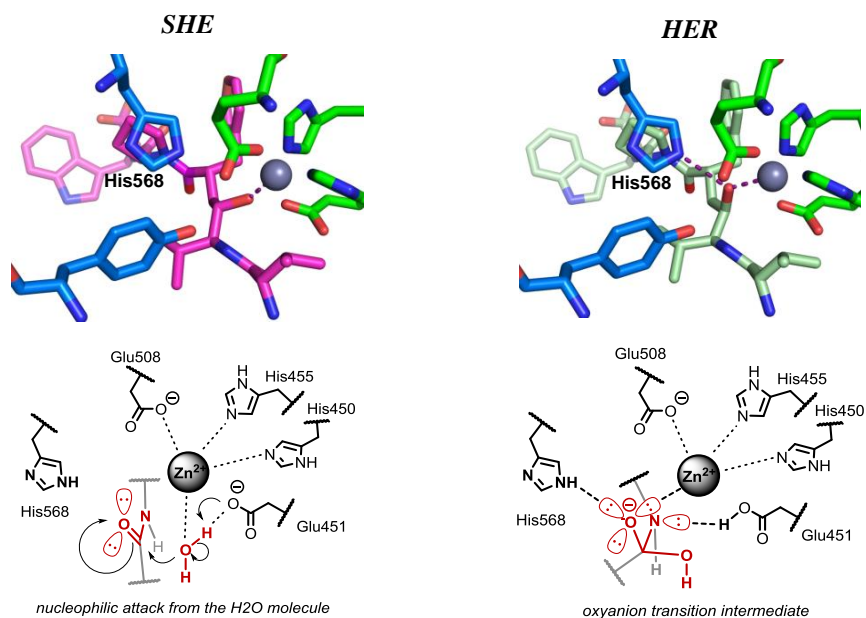


Figure 55 Binding modes of *SHE* and *HER* in the active site of hDPP3 compared to the corresponding stages in the mechanism of hydrolysis.

The advantage of the hydroxyethylene inhibitors is their fundamental property of resistance to the action of the enzyme, which cannot cleave the C–C bond introduced instead of the peptide bond. Furthermore, both hydroxyethylene epimers are binding zinc with only one coordinating bond in contrast to the chelating inhibitors still being developed for zinc metallopeptidases, which are predestined to lose selectivity to a certain degree by the sole fact that the chelation ability increases the affinity to the metal ions in other proteins and in solution. Rather than focusing on the tight binding to zinc, the advantage of a hydroxyethylene inhibitor is that a properly configured hydroxyethylene epimer can exploit additional interactions to the side chains of the enzyme. In the case of hDPP3, (*R*)-hydroxyethylene provides the advantage of simultaneous binding to zinc and the His568 side chain of the protein.

The exact role of hDPP3 *in vivo* remains elusive. Investigation on a murine model, including the DPP3 knock-out specimens, is an ongoing effort. Access to smaller and easily synthesized inhibitors would provide an invaluable tool for studying activity of DPP3 in organisms and could provide a foundation to DPP3 targeting drug design. The design of smaller inhibiting lead structures was investigated. Among shorter hydroxyethylene and ketomethylene peptidomimetics, a small-molecule ketomethylene inhibitor with $IC_{50} = 388 \mu\text{M}$ has been discovered. It presents a lead structure which is easy to synthesize, without stereoselective steps, with robust means for introduction of diversity (Figure 56).

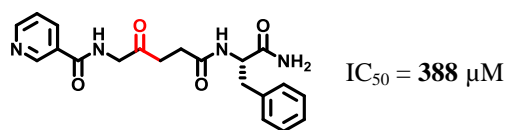
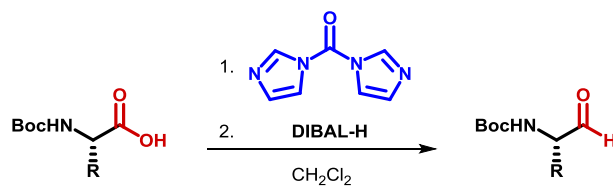


Figure 56 The small ketomethylene inhibitor

Additionally, in the wake of synthetic efforts, a new method for rapid and efficient synthesis of chiral α -amino aldehydes from α -amino acids have been established and used to obtain an important intermediate for the synthesis of inhibitors of hDPP3. The described one-pot sequence consisting of activation of *N*-protected proteinogenic amino acids by CDI and subsequent reduction by DIBAL-H successfully furnishes the corresponding amino aldehydes in excellent yields with completely preserved stereointegrity (Scheme 42).



Scheme 42 The rapid one-pot method for synthesis of α -amino aldehydes via CDI/DIBAL-H

1.6 Outlook

1.6.1 Lead Optimization

In order to produce efficient inhibitors of hDPP3 with special emphasis to the ultimately required bioavailability, considerable optimization of the most interesting lead structures from this work is necessary. It is suggested to use *HER* and the pyridine ketomethylene as the lead structures, based on their exceptional properties.

On the grounds of previously discussed structural aspects of ligand interactions to hDPP3, insights gained from hydroxyethylene epimers study and the structure-activity relationship data collected with the shorter analogues, there is a number of structural features that could lead to improvements in the size and potency of the transition state mimicking peptidomimetic inhibitors of hDPP3.

1.6.1.1 Structure-activity Relationship for Use in the Design of New Inhibitors

The binding pockets of hDPP3 can be dissected using the Schechter-Berger notation.^[187] The binding subsites are named with “S”, followed by a number indicating their position in respect to the site of the peptide bond cleavage (Figure 57).

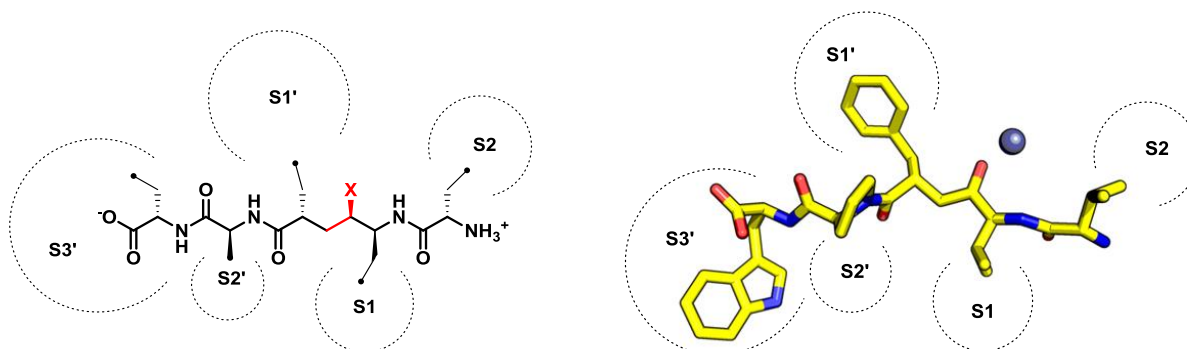


Figure 57 The subsites of the binding site in hDPP3, according to the Schechter-Berger notation.^[187]

The cocrystal structure of *SHE* in complex with hDPP3 was used to examine the subsites in detail. The ketomethylene inhibitor assay and the structural data firmly stress that the *N*-terminal positive charge is necessary to stabilize the closed structure. The Glu316 side chain is localized in the immediate vicinity of the *N*-terminus of the ligand. No residues that could be positively charged were found in its vicinity, so the ion-ion interaction stabilization has to come from the ligand, once the enzyme closes the site upon binding (Figure 58).

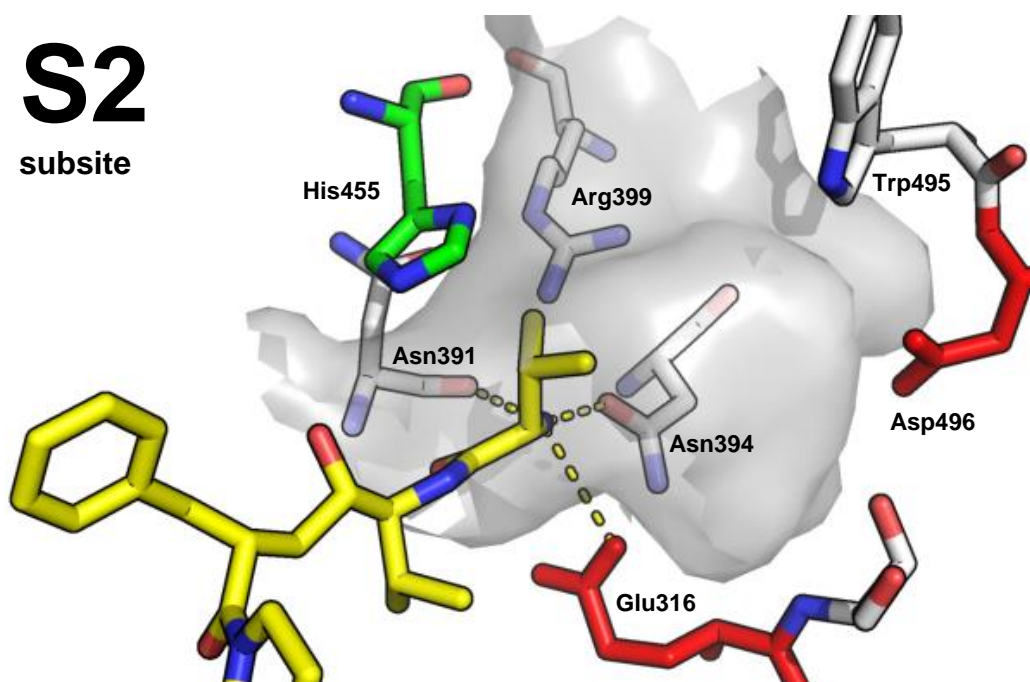


Figure 58 The S2 subsite of hDPP3. Emphasis is placed on the extent of van der Waals contact-free space in the cavity, and the tight interactions of the *N*-terminus. The negatively charged side chains are colored red. The figure has been created and rendered from the *SHE*-hDPP3 cocrystal structure in PyMOL software.

The affinity of enkephalins (having a tyrosine side chain occupying the S2) to hDPP3, structural features of the S2 subsite and the study of Chiba et al.^[20] shed more light onto the size and shape of the S2 subsite. This subsite can apparently fit somewhat bulkier lipophilic residues, like isoleucine, since the IVYPW peptide is a stronger binder than tynorphin (VVYPW) and *HER*. The Lewis-basic oxygen on the available side chains in the S2 site presents the opportunity to harness the power of halogen bonding by decorating the ligand residue with bromine or iodine.^[5,348–350] This could be particularly useful for modifications of the pyridine ring in the ketomethylene inhibitor **28**.

To simplify the long synthesis of transition state mimetic analogues of tynorphin, we have omitted the phenolic hydroxyl function from the aromatic residue that occupies the S1' subsite (Figure 59). Computational visualization of the exposed cavity in that site reveals a tunnel-shaped extension, capable of accommodating even a shorter alkyl chain. It would be interesting to see whether such modifications could cause significant enhancement in potency driven by the hydrophobic effect.^[7,351,352]

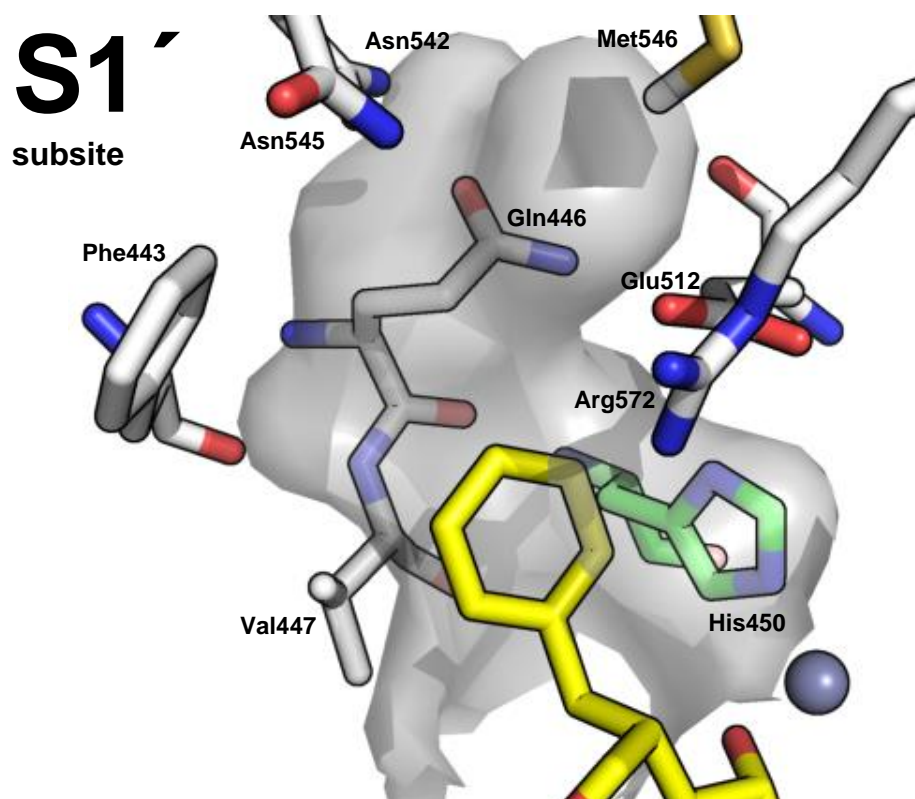


Figure 59 The S1' subsite of hDPP3. Emphasis is placed on the size of the free cavity (gray) that extends above the *para*-position of the phenyl residue of the ligand (yellow). The figure has been created in PyMOL software from the *SHE*-hDPP3 cocrystal structure.

Visualization of the S3' subsite cavity (around the C-terminal portion of the *SHE* ligand) showed that it actually presents a large, mostly unoccupied cavity together with the S2' subsite, which accommodates the proline ring portion of *SHE* (Figure 60). Besides the opportunity of exploiting the cation- π "pincer" facilitated by Lys670 and Arg669, the whole S3'/S2' cavity presents a relatively big and demanding space for structure-activity relationship exploration. Instead, it is recommended to focus on the S2' part of the subsite, trying to interact with Arg572 and other mainly lipophilic side chains.

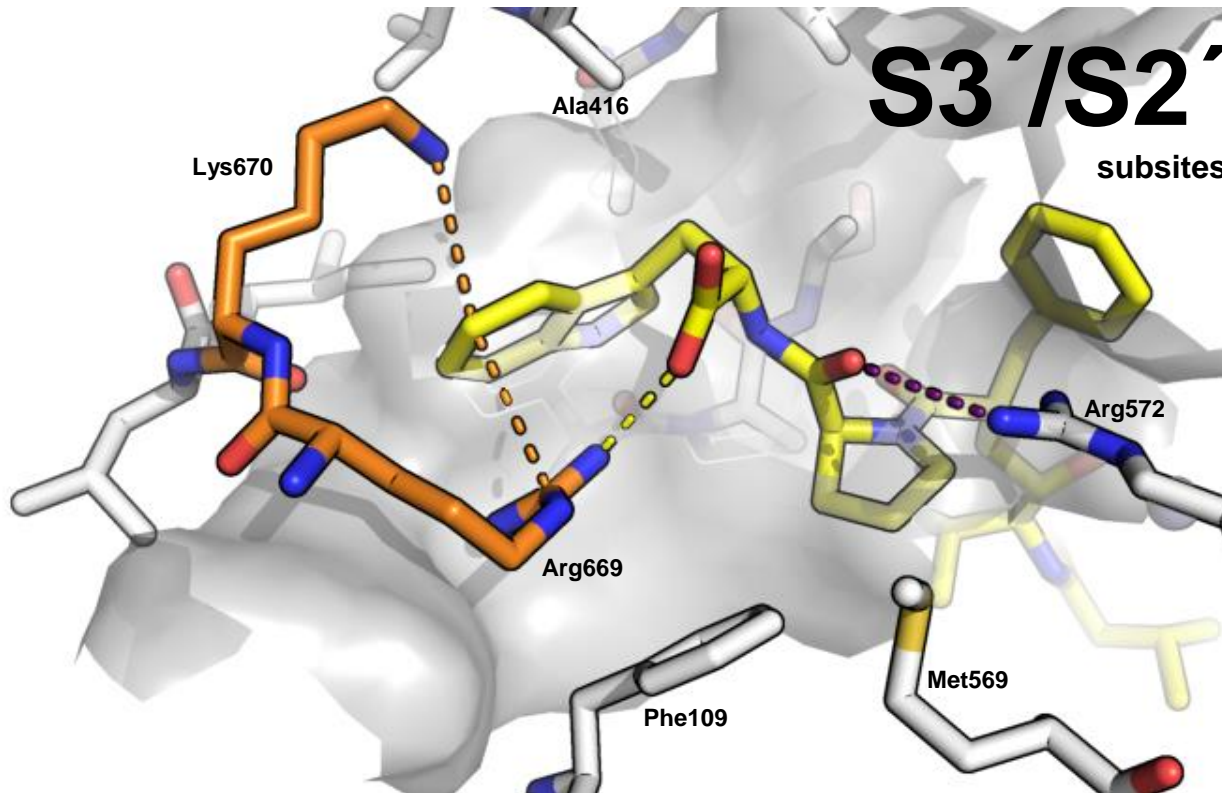


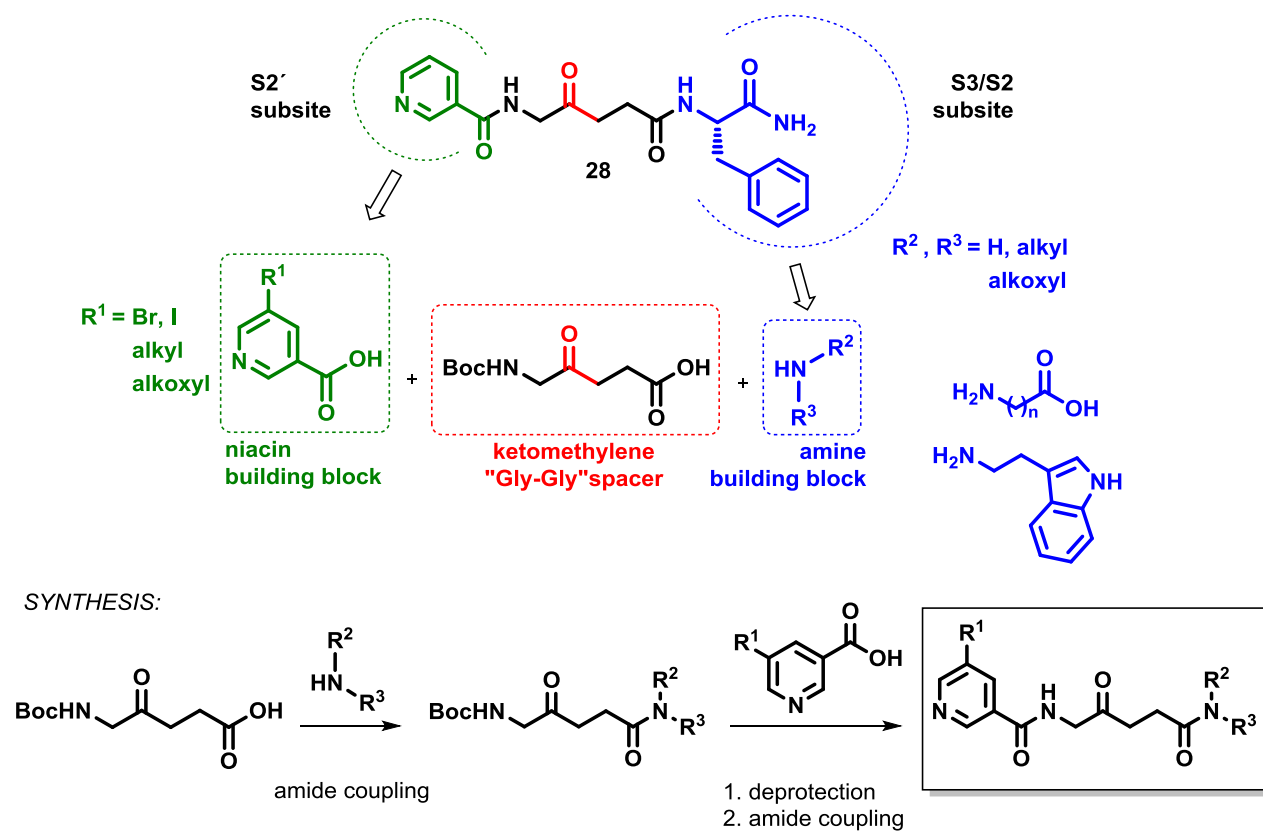
Figure 60 The S3'/S2' subsite of hDPP3. The cation- π interactions of the Lys-Arg “pincer” are represented as orange-dashed lines. The hydrogen bond and the salt bridge is represented with the yellow-dashed line. The violet-dashed line represents the close vicinity of the Arg572 and the carbonyl of the proline unit in the ligand. The figure has been created in PyMOL software from the *SHE*-hDPP3 cocrystal structure.

The S2' subsite contains also Arg572 which is positioned in the close vicinity of the carbonyl of proline in the ligand which represents a terminal carbonyl function of the shorter analogues. The measured distance between that carbonyl and the Arg572 is 4.3 Å. This distance very likely falls down to enable hydrogen bonding in the tetrapeptide mimetics, where the C-terminus is not restricted by the rigid proline ring and the interactions of the fifth amino acid residue with the Lys-Arg cation- π “pincer”. These insights suggest focusing on the development of tetrapeptide mimetics, exploring primarily the S2' part of this relatively big cavity.

1.6.1.2 Quick and Scalable Approaches for the Synthesis of Next Generation of hDPP3 Inhibitors

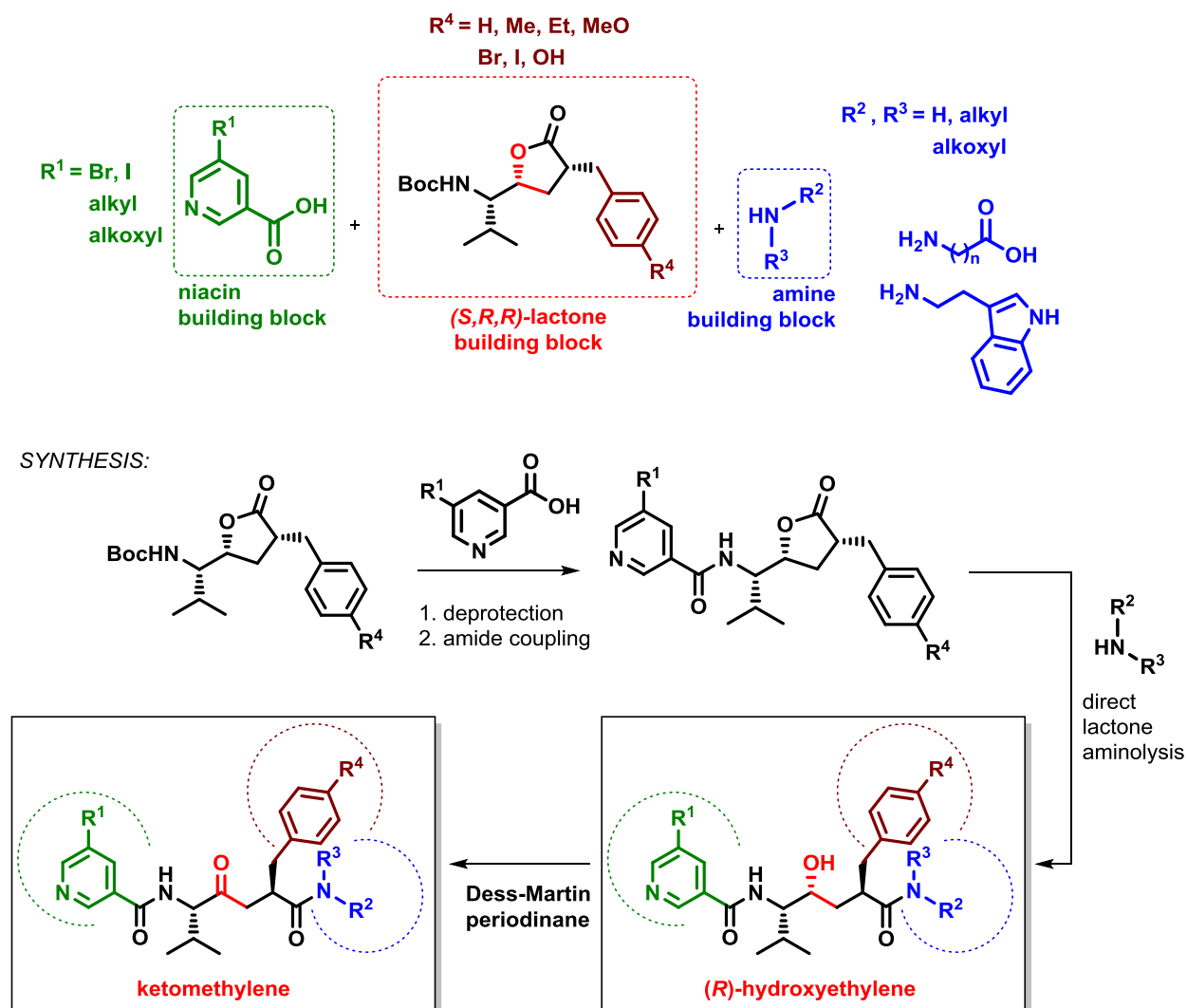
Based on the synthetic methodology utilized in this work, and considering the acquired structure-activity relationship informations, two approaches for the rapid synthesis of a new generation of inhibitors have been devised.

The first approach easily introduces modifications into the niacin-ketomethylene scaffold of **28** ($IC_{50} = 388 \mu M$), addressing the affinity to the S2 and S3'/S2' subsites. Access to the amino levulinate core of this inhibitor (the ketomethylene "Gly-Gly" spacer) has been established on a multigram scale. New modified niacins, and the enhancements in the C-terminal part can be installed in a facile coupling-deprotection-coupling three steps sequence using simple peptide coupling methods (Scheme 43). An advantage of this scaffold could be resistance to aminopeptidases, due to the noncanonical N-terminal amino acid (niacin and its derivatives). Aminopeptidases are known to rapidly degrade peptide substrate inhibitors of DPP3.^[19]



Scheme 43 The design of new niacin-ketomethylene inhibitors.

Putting an effort into filling the S1' subsite of hDPP3 may introduce a dramatic boost in activity for small-molecule inhibitors. A method has been devised for scalable stereoselective synthesis of alkylated γ -lactone, which has the required (*S,R,R*)-configuration for synthesis of the (*R*)-hydroxyethylene pseudodipeptide core.^[285] This method, in combination with a direct aminolysis of the γ -lactone with amines,^[353–356] presents an exceptional opportunity for rapid access of (*R*)-hydroxyethylene derivatives, which would address all of the three main subsites in the binding site of hDPP3, S2, S1' and S3'/S2' (Scheme 44). From the resulting target molecules the ketomethylene counterparts can be easily produced in a single step via application of the mild oxidant Dess-Martin periodinane. This method would successfully avoid the acid-promoted lactonization backbite and the potential epimerization of α -amino ketone in the ketomethylene scaffold, by the use of the mild Dess-Martin reagent.^[332,333]



Scheme 44 The design and synthetic plan for new niacin-hydroxyethylene and niacin-ketomethylene inhibitors.

1.6.2 Efficient Design of hDPP3 Inhibitors for *In Vivo* Studies

Investigations of *in vivo* activity and the potential druggability require primarily a special care to bioavailability and stability of the designed inhibitor. Typical structural and physical properties of molecules which satisfied such criteria in the history of drug development are constant subject of research towards better understanding of drug delivery. One of the most notable sets of descriptors of a good drug is Lipinski's "Rule of Five".^[357] In order to assess the drug-likeness of both our synthesized and proposed molecules, we have calculated the relevant properties (Table 15).

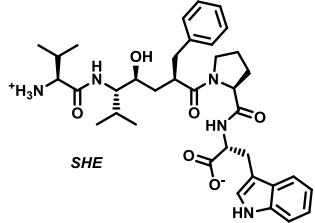
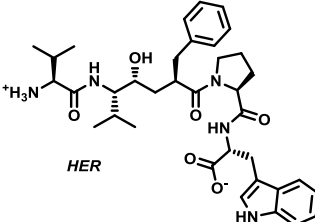
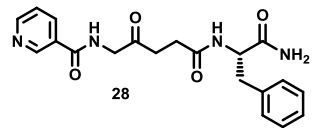
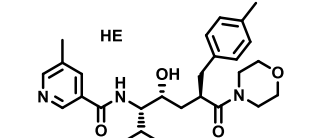
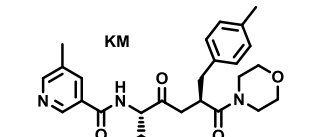
molecule	M _w	clogP (clogD at pH = 7.4)	D / A
 <p>SHE</p>	647.80	1.21 (1.86)	5 / 6
 <p>HER</p>	647.80	1.21 (1.86)	5 / 6
 <p>28</p>	382.42	-0.22 (-0.22)	3 / 5
 <p>HE</p>	467.61	3.08 (3.08)	2 / 5
 <p>KM</p>	465.59	3.49 (3.49)	1 / 5

Table 15 Properties of peptidomimetic molecules in respect to Lipinski's "Rule of Five". clogP and clogD values have been calculated using ChemAxon MarvinSketch[®] software. Failing properties are marked in red. M_w – molecular weight; clogP – calculated logarithm of the partitioning coefficient; clogD – calculated logarithm of the distribution coefficient; D/A – number of hydrogen bond donors /acceptors.

According to Lipinski's "Rule of Five", the molecular weight should be <500 , octanol/water partitioning coefficient $\text{clog}P < 5$, the compound should have less than five hydrogen bond donors and less than ten hydrogen bond acceptors. The distribution coefficient $\text{log}D$ presents a better measure for indication how available could a compound be on biological interfaces, especially with charged molecules like peptides. It was thus prudent to calculate that value alongside the $\text{clog}P$. Large molecules with many polar functional groups, like **SHE** and **HER**, are failing according to Lipinski's rule of five. Smaller analogue **28** and the simpler examples of the next generation molecules (**HE** and **KM**) seem to satisfy these criteria. According to known empirical clues in the drug development strategies, they are much more likely to be bioavailable.

However, this rule has not to be taken for granted. Newer models prove that they can be misleading, because there are examples of FDA approved drugs which fail one Lipinski property but satisfy sets of criteria determined by more precise quantitative mathematical models (e.g. Quantitative Estimate of Drug-Likeness, QED, introduced by Andrew L. Hopkins).^[358,359]

The molecules presented in this work are designed based on peptide scaffolds. The tynorphin discovery investigation of Yamamoto et al. alerts that such peptides are very vulnerable to degradation by aminopeptidases.^[19] It is reported that tynorphin is completely degraded in rat blood serum in 4 h, and the cleavage of the first peptide bond was found to be the quickest. This undesirable feature has been taken into account in the design of the new generation of hDPP3 inhibitors by introduction of the niacin unit in the *N*-terminal portion of the scaffold. Niacin is a noncanonical amino acid. It possesses a significant geometric deviation in the shape and relative positioning of the polar features in comparison to the canonical amino acids, which are well recognized by aminopeptidases.^[360-362] It is quite plausible to expect that the niacin-containing peptidomimetics will be resistant to action of aminopeptidases due to their evolution-conditioned substrate recognition of canonical amino acids.

1.7 Experimental Section

1.7.1 Organic Chemistry Experiments

All commercially available reagents and solvents were purchased from Sigma-Aldrich, Alfa Aesar, ABCR, Fisher Scientific, Acros Organics, Roth or VWR, and were used without further purification except otherwise stated. When it was required, non-dry solvents were distilled before use. If reactions were performed under inert conditions, e.g. exclusion of water, oxygen or both, all experiments were carried out using established Schlenk techniques. Herein solvents were dried and/or degassed with common methods and afterwards stored under inert gas atmosphere (argon or N₂) over molecular sieves. In some cases, when explicitly mentioned, dry solvents were received from the listed suppliers. DCM (EtOH stabilized) was distilled first over P₄O₁₀ to remove the stabilizer and then over CaH₂ under argon atmosphere and stored over 4 Å molecular sieves in an amber 1000 mL Schlenk bottle. THF was dried over Na under reflux and argon atmosphere until benzophenone indicated its dryness by turning into deep blue color. The dry THF was stored over 4 Å molecular sieves in an amber 1000 mL Schlenk bottle under argon atmosphere.

In general, when high vacuum was declared in experimental procedures, typically a vacuum of 10⁻²-10⁻³ mbar was applied. All reactions were stirred with Teflon-coated magnetic stirring bars. Molecular sieves (Sigma Aldrich, beads with 8-12 mesh) were activated in a round-bottom flask with a gas-inlet adapter by heating them carefully in a heating mantle for approximately 12 h under high vacuum until complete dryness was obtained. These activated molecular sieves were stored at room temperature under argon atmosphere.

Temperatures were measured externally if not otherwise stated. When working at a temperature of 0 °C, an ice-water bath served as the cooling medium. Reactions, which were carried out at -78 °C were cooled by keeping the reaction vessel immersed in a properly sized Dewar vessel containing acetone/dry ice.

Analytical thin layer chromatography (TLC) was carried out on Merck TLC silica gel 60 F254 aluminium sheets and spots were visualized by UV light ($\lambda = 254$ and/or 366 nm) or by staining with iodide, cerium ammonium molybdate (2.0 g Ce(SO₄)₂, 50.0 g (NH₄)₆Mo₇O₂₄ and 50

mL conc. H₂SO₄ in 400 mL water) (CAM) or potassium permanganate (0.3 g KMnO₄, 20 g K₂CO₃, 5 mL 5 % aqueous NaOH in 300 mL H₂O) followed by the development of the stains in the heat. Flash column chromatography was performed on silica gel 0.035-0.070 mm, 60 Å (Acros Organics). A 30 to 100 fold excess of silica gel was used with respect to the amount of dry crude product, depending on the separation problem. The dimensions of the column were selected in such a way that the required amount of silica gel formed a pad between 10 cm and 25 cm. The column was equilibrated first with the solvent or solvent mixture, and the crude product diluted with the eluent was applied onto the top of the silica pad. In case when the crude product was insoluble in the eluent, the sample was dissolved in an appropriate solvent (EtOAc or DCM), and the equal amount of diatomaceous earth was added, followed by removal of the solvent under reduced pressure and drying the sample in vacuo, which was then directly loaded onto the top of the silica pad. The mobile phase was forced through the column using a rubber bulb pump.

GC-MS analyses were carried out on an Agilent Technologies 7890A GC system equipped with a 5975C mass selective detector (inert MSD with Triple Axis Detector system, EI, 70 eV). Samples were injected by employing autosampler 7683B in a split mode 20/1 (inlet temperature: 280 °C; injection volume: 0.2 µL) and separated on an Agilent Technologies J&W GC HP-5MS capillary column (30 m x 0.2 mm x 0.25 µm) at a constant helium flow rate (He 5.0 Air Liquide, 1.085 mL/min, average velocity 41.6 cm/sec). A general gradient temperature method was used (initial temperature: 50 °C for 2 min, linear increase to 300 °C (40 °C/min), hold for 5 min, 1 min post-run at 300 °C, detecting range: 50.0-550.0 amu, solvent delay of 2.80 min).

GC-FID analyses for separation of enantiomers or diastereomers were carried out on an Agilent Technologies 6890N GC system equipped with a flame ionization detector (FID). Samples were injected by employing autosampler CTC Analytics CombiPAL in a split mode 5/1 (inlet temperature: 200 °C; injection volume: 1.0 µL) and separated on a Varian CP7503 CP-Chiralsil Dex CP capillary column (25.0 m x 320 µm x 0.25 µm) at a constant nitrogen flow rate (Nitrogen 5.0 Messer, 4.5 mL/min, average velocity 68 cm/sec). Two gradient temperature methods were used: “AMAL_GCPAL.M” (initial temperature: 80 °C for 5 min, linear increase to 150 °C (10 °C/min), hold for 18 min, 1 min post-run at 160 °C) and “AMAL_GCPAL_PHE_4.M” (initial temperature: 80 °C for 5 min, linear increase to 125 °C (10 °C/min), hold for 40 min, 1 min post-run at 160 °C).

Analytical HPLC-MS analyses were performed on an Agilent Technologies 1200 Series system (G1379 Degasser, G1312 Binary Pump, G1367C HiP ALS SL Autosampler, G1330B FC/ALS Thermostat, G1316B TCC SL column compartment, G1365C MWD SL multiple wavelength detector (deuterium lamp, 190-400 nm)) equipped with a single quadrupole LCMS detector “6120 LC/MS” using electrospray ionization source (ESI in positive and negative mode). The analyses were carried out on an Agilent Poroshell 120 SB-C18 (100 x 3.0 mm, 2.7 μm) column equipped with a Merck LiChroCART[®] 4-4 pre-column. A general solvent gradient method was used (0-2.00 min: MeCN:H₂O = 10:90 (v/v), 2.00-10.00 min: linear increase to MeCN:H₂O = 95:5 (v/v), 10.00-16.00 min: holding of MeCN:H₂O = 95:5 (v/v), oven temperature: 40 °C, solvent flow: 0.700 mL/min).

Analytical HPLC analyses for separation of enantiomers were performed on an Agilent Technologies 1100 Series system (G1322A Degasser, G1311 Quaternary Pump, G1313A ALS Autosampler, G1316A Column Compartment, G1365B MWD multiple wavelength detector (deuterium lamp, 190-400 nm)). The analyses were carried out on a Daicel Chemical Technologies Chiralpak[®] AD-H (250 x 4.6 mm, 5.0 μm) column. An isocratic method was used (0-30.00 min: heptane:2-propanol = 90:10 (v/v), oven temperature: 15 °C, solvent flow: 0.850 mL/min).

Reverse phase preparative HPLC purifications were run on a Thermo Scientific UltiMate 3000 system (Dionex UltiMate Pump 3000, Dionex UltiMate Autosampler, Dionex UltiMate Column Compartment, Dionex UltiMate Diode Array Detector and Dionex UltiMate Automated Fraction Collector). The separations were carried out on a Macherey-Nagel 125/21 Nucleodur[®] 100-5 C18ec (125 x 21 mm, 5.0 μm) column. Three methods were used: JKV_NucleodurC18_001HCOOH_10to85 (gradient program: 0-3.00 min: MeCN/0.01% HCOOH = 10:90 (v/v), 3.00-11.00 min: linear increase to MeCN/0.01% HCOOH = 85:15 (v/v), 11.00-13.00 min: MeCN/0.01% HCOOH = 85:15 (v/v); oven temperature: 24 °C; solvent flow: 15.0 mL/min), JKV_NucleodurC18_001CF₃COOH_10to85 (gradient program: 0-3.00 min: MeCN/0.01% CF₃COOH = 10:90 (v/v), 3.00-11.00 min: linear increase to MeCN/0.01% CF₃COOH = 85:15 (v/v), 11.00-16.00 min: MeCN/0.01% CF₃COOH = 85:15 (v/v); oven temperature: 24 °C; solvent flow: 15.0 mL/min) and JKV_NucleodurC18_001HCOOH_sulfonamides (gradient program: 0-3.00 min: MeCN/0.01% HCOOH = 10:90 (v/v), 3.00-6.00 min: linear increase to MeCN/0.01% HCOOH = 35:65 (v/v),

6.00-14.00 min: MeCN/0.01% HCOOH = 35:65 (v/v), 14.00-23.00 min: linear increase to MeCN/0.01% HCOOH = 90:10 (v/v); oven temperature: 24 °C; solvent flow: 13.0 mL/min).

¹H-, ¹³C-NMR spectra were recorded on a Bruker AVANCE III 300 spectrometer (¹H: 300.36 MHz; ¹³C: 75.53 MHz). Chemical shifts were referenced to the residual proton and carbon signal of the deuterated solvent, respectively (CDCl₃: δ = 7.26 ppm (¹H), 77.16 ppm (¹³C); methanol-d₄: δ = 3.31 ppm (¹H), 49.00 ppm (¹³C); DMSO-d₆: δ = 2.50 ppm (¹H), 39.52 ppm (¹³C)). Signal multiplicities are abbreviated as s (singlet), bs (broad singlet), d (doublet), dd (doublet of doublet), t (triplet), q (quadruplet), p (pentet) and m (multiplet). Deuterated solvents for nuclear resonance spectroscopy were purchased from Euriso-top[®].

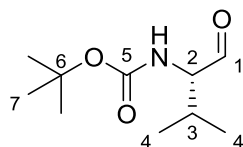
Optical rotations were measured in CH₂Cl₂, CHCl₃, EtOH and MeOH on a Perkin Elmer 341 polarimeter with a 10 cm cell. Concentration *c* given is in g/100 mL. Each optical rotation measurement was done five times and the mean value is reported.

Melting points were measured on a Mel-Temp[®] melting point apparatus (Electrothermal) with an integrated microscopical support in open capillary tubes and were not corrected. The temperature was measured with a mercury-in-glass thermometer.

High-resolution mass spectra obtained using ESI were recorded on a Thermo Scientific LTQ FT Ultra instrument. Samples were dissolved in HPLC-MS grade methanol and directly injected using a syringe pump with a flow of 3 μL/min. Capillary temperature was set to 270 °C and the sheath gas flow to 5 units. 10 spectra per sample were acquired in positive FT-mode with a resolution setting of 1000000. High-resolution mass spectra obtained using MALDI-TOF were recorded on a Micromass[®] MALDI micro MX[™] spectrometer. Dithranol (1,8-dihydroxy-9,10-dihydroanthracen-9-one) or α-cyano-4-hydroxycinnamic acid served as matrix. The stated values are m/z.

1.7.2 Synthesis of SHE

1.7.2.1 *tert*-Butyl *N*-[(2*S*)-3-methyl-1-oxobutan-2-yl]carbamate (**2**)^[363]

**2**

A 1000 mL two-neck round-bottom flask with a Schlenk adapter, a glass stopper and a magnetic stirring bar was heated, dried under vacuum and purged with N₂. Boc-L-Val-OH (10.864 g, 50.0 mmol, 1.0 eq) was added and dissolved in abs. dichloromethane (333 mL). The solution was cooled to 0 °C (ice bath) and 1,1'-carbonyldiimidazole (8.918 g, 55.0 mmol, 1.1 eq) was added. A gas bubbler was mounted instead of the glass stopper to allow pressure relief. After stirring for 60 min the gas bubbler was removed and the colorless reaction solution was cooled to -78 °C (CO₂/acetone bath) for 15 min. A septum was mounted instead of the glass stopper while maintaining a gentle counter flow of N₂. Subsequently, 1.0 M DIBAL-H solution in toluene (105 mL, 105 mmol, 2.1 eq) was added dropwise with a syringe through the septum throughout 110 min. The reaction mixture was stirred at -78 °C until TLC indicated quantitative conversion (45 min). The reaction mixture was quenched by the addition of EtOAc (335 mL). The acetone bath was removed, the gas bubbler was mounted, and 25% aqueous tartaric acid (222 mL) was added to the mixture under vigorous stirring. The mixture was warmed up by immersing the vessel into a water bath at RT and stirred vigorously for 15 min. The stirring was stopped and the layers were separated. The aqueous phase was extracted with EtOAc (333 mL) and the combined organic extracts were washed with 1 M HCl (222 mL), 0.8 M NaHCO₃ (222 mL) and brine (222 mL), dried over Na₂SO₄, filtered and concentrated under reduced pressure. The crude product was frozen in liquid nitrogen and was allowed to reach room temperature under high vacuum. The freeze-thaw procedure was repeated two times. Crude product (8.474 g, 42.10 mmol, 84 %) was furnished as a viscous colorless liquid, and used without further purification.

Yield: 8.474 g (42.10 mmol, 84 %), viscous colorless liquid.

$[\alpha]_D^{23} = +78.6^\circ$ ($c = 1.07$, CH_2Cl_2), lit. $[\alpha]_D^{20} = +82.1^\circ$ ($c = 1$, CH_2Cl_2).

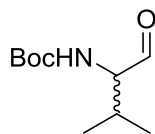
$R_f = 0.61$ (cyclohexane/ethyl acetate = 2:1 (v/v); staining: KMnO_4).

^1H NMR (300 MHz, CDCl_3) $\delta = 9.63$ (s, 1H, H-C1), 5.15-4.99 (m, 1H, NH), 4.33-4.15 (m, 1H, H-C2), 2.37-2.14 (m, 1H, H-C3), 1.44 (s, 9H, H-C7), 1.02 (d, $^3J = 6.9$ Hz, 3H, H-C4), 0.93 (d, $^3J = 7.0$ Hz, 3H, H-C4).

^{13}C NMR (75 MHz, CDCl_3) $\delta = 200.5$ (s, 1C, C1), 156.0 (s, 1C, C5), 80.1 (s, 1C, C6), 64.8 (s, 1C, C2), 29.2 (s, 1C, C3), 28.4 (s, 3C, C7), 19.2 (s, 1C, C4), 17.7 (s, 1C, C4).

GC-FID (CP-Chirasil Dex): $t_R((S)\text{-}2) = 9.0$ min, 100%; $t_R((R)\text{-}2) = 9.2$ min, no abundance detected; ee > 99%.

1.7.2.2 Racemic *tert*-butyl *N*-[(2*S*)-3-methyl-1-oxobutan-2-yl]carbamate (*rac*-2)



rac-2

A 10 mL Schlenk tube, a glass stopper and a magnetic stirring bar was heated, dried under vacuum and purged with N_2 . Boc-DL-Val-OH (43 mg, 0.20 mmol, 1.0 eq) was added and dissolved in abs. dichloromethane (1.3 mL). The solution was cooled to 0°C (ice bath) and 1,1'-carbonyldiimidazole (36 mg, 0.22 mmol, 1.1 eq) was added. A gas bubbler was mounted instead of the glass stopper to allow pressure relief. After stirring for 60 min the gas bubbler was removed and the colorless reaction solution was cooled to -78°C (CO_2 /acetone bath) for 15 min. A septum was mounted instead of the glass stopper while maintaining a gentle counter flow of N_2 . Subsequently, 1.0 M DIBAL-H solution in toluene (0.42 mL, 0.42 mmol, 2.1 eq) was added dropwise with a syringe through the septum throughout 10 min. The reaction mixture was stirred at -78°C until TLC indicated quantitative conversion (60 min). The reaction mixture was quenched by the addition of EtOAc (1.3 mL). The acetone bath was removed, the gas bubbler

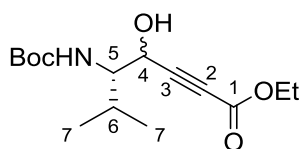
was mounted, and 25% aqueous tartaric acid solution (1.0 mL) was added to the mixture under vigorous stirring. The mixture was warmed up by immersing the vessel into a water bath at RT and stirred vigorously for 15 min. The stirring was stopped and the layers were separated. The aqueous phase was extracted with EtOAc (1.3 mL) and the combined organic extracts were washed with 1 M HCl (1.0 mL), 0.8 M NaHCO₃ (1.0 mL) and brine (1.0 mL), dried over Na₂SO₄, filtered and concentrated under reduced pressure. The crude product was frozen in liquid nitrogen and was allowed to reach room temperature under high vacuum. The freeze-thaw procedure was repeated two times. The crude product (33 mg, 0.16 mmol, 80 %) was furnished as a colorless liquid.

Yield: 33 mg (0.16 mmol, 80 %), colorless liquid.

R_f = 0.61 (cyclohexane/ethyl acetate = 2:1 (v/v); staining: KMnO₄).

GC-FID (CP-Chiralsil Dex CP): t_R ((*S*)-**2**) = 9.0 min; t_R ((*R*)-**2**) = 9.2 min.

1.7.2.3 Ethyl (5*S*)-5-[[(*tert*-butoxy)carbonyl]amino]-4-hydroxy-6-methylhept-2-ynoate (**3**)^[273]



3

In an oven dried and nitrogen-purged 500 mL Schlenk vessel equipped with a Teflon[®]-coated magnetic stirring bar, 1-pentyne (7.87 mL, 79.8 mmol, 2.10 eq) was dissolved in 125 mL absolute THF and cooled to 0 °C in an ice bath. To the stirred solution 2.50 M *n*-BuLi in hexanes (30.40 mL, 76.0 mmol, 2.00 eq) was added dropwise via syringe and septum within 3 min. The yellow reaction solution was stirred and cooled for 15 min to -78 °C in an acetone/dry ice bath and subsequently ethyl propiolate (7.70 mL, 76.00 mmol, 2.00 eq) was added dropwise via syringe and septum. The orange reaction solution was stirred at -78 °C for 15 min and then a freshly prepared solution of aldehyde **2** (7.648 g, 38.00 mmol, 1.00 eq) in absolute THF (65 mL)

was added dropwise within 10 min via a cannula by applying a gentle nitrogen overpressure from the donor vessel. The reaction was stirred at $-78\text{ }^{\circ}\text{C}$ until TLC indicated full conversion of the aldehyde (60 min). The orange reaction mixture was quenched by the dropwise addition of a solution of AcOH (10 mL) in THF (20 mL) and was brought to RT by immersion in a water bath and stirring for 15 min. The mixture was diluted with EtOAc (380 mL) and washed with 5% NaHCO_3 (2x100 mL) and brine (50 mL). The organic extract was concentrated under reduced pressure. Flash chromatography (SiO_2 , cyclohexane/EtOAc 7:1) afforded a viscous orange liquid (9.515 g, 31.78 mmol, 84%) as a mixture of two diastereomers.

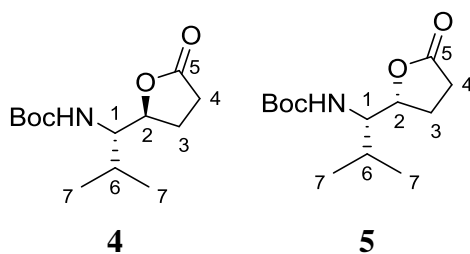
Yield: 9.515 g (31.78 mmol, 84%), viscous orange liquid.

$R_f = 0.30$ (cyclohexane/EtOAc 3:1 (v/v); staining: KMnO_4).

^1H NMR (300 MHz, CDCl_3 , mixture of 2 diastereomers, based on COSY and HSQC) $\delta = 4.91$ and 4.69 (d, $^3J = 8.6$ Hz, 1H, HNCO), 4.58 (br s and d, $^3J = 4.8$ Hz, 1H, H-C4), 4.28 – 4.14 (m, 2H, CH_2CH_3), 3.69 – 3.56 and 3.51 – 3.36 (m, 1H, H-C5), 2.20 – 2.01 and 1.88 – 1.73 (m, 1H, H-C6), 1.46 and 1.44 (s, 9H, $(\text{CH}_3)_3$), 1.34 – 1.25 (m, 3H, CH_2CH_3), 1.03 – 0.89 (m, 6H, H-C7).

^{13}C NMR (75 MHz, CDCl_3 , mixture of 2 diastereomers, based on COSY and HSQC) $\delta = 157.6$ and 157.1 (s, 1C, HNCO), 153.4 and 153.3 (s, 1C, C1), 86.2 and 84.8 (s, 1C, C3), 80.7 and 80.2 (s, 1C, $(\text{CH}_3)_3\text{C}$), 78.0 (s, 1C, C2), 64.9 and 64.0 (s, 1C, C4), 62.4 and 62.2 (s, 1C, CH_2CH_3), 61.4 and 60.8 (s, 1C, C5), 30.3 and 28.8 (s, 1C, C6), 28.4 (s, 3C, $(\text{CH}_3)_3$), 20.1 and 20.0 (s, 1C, C7), 19.2 and 18.5 (s, 1C, C7), 14.1 (CH_2CH_3).

1.7.2.4 *tert*-Butyl *N*-[(1*S*)-2-methyl-1-[(2*S*)-5-oxooxolan-2-yl]propyl]carbamate (**4**) and *tert*-butyl *N*-[(1*S*)-2-methyl-1-[(2*R*)-5-oxooxolan-2-yl]propyl]carbamate (**5**)^[273]



Hydrogenation: In a 250 mL round-bottom two-neck flask equipped with a Schlenk adapter, glass stopper and a Teflon[®]-coated magnetic stirring bar, **3** (9.400 g, 31.40 mmol, 1.00 eq) was dissolved in EtOAc (126 mL) and stirred at RT. The solution was degassed three times by alternate evacuation and filling with N₂ gas. 5% Pd/C (668 mg, 0.310 mmol, 0.01 eq) was added to the solution and a hydrogen balloon was mounted. The solution was purged three times by alternate evacuation and filling with H₂ gas. The black mixture was vigorously stirred in the H₂-atmosphere until complete consumption of starting material was indicated by TLC (20 h). The reaction flask was disconnected from the hydrogen balloon and purged with N₂. Under nitrogen atmosphere the content of the flask was transferred to the nitrogen-purged fritted Schlenk type funnel containing a 1.5 cm thick compressed bed of Celite. The product was eluted from the filter cake with EtOAc (3×13 mL). The Celite bed with the solid catalyst was washed with THF (5 mL) and water (5 mL), and stored under water in a container dedicated for catalyst waste. The product containing filtrate was concentrated under reduced pressure to furnish a yellow liquid residue.

Lactonization: In a 250 mL round-bottom flask equipped with a Teflon[®]-coated magnetic stirring bar, the yellow liquid residue was dissolved in toluene (126 mL) and *p*-TsOH×H₂O (60 mg, 0.31 mmol, 0.01 eq) was added. The pale yellow solution was stirred and heated at 50 °C (oil bath) for 2 h. The reaction solution was cooled to RT, washed with 5% NaHCO₃ (2×100 mL) and brine (100 mL), dried over Na₂SO₄ and concentrated under reduced pressure. Flash chromatography (SiO₂, cyclohexane/EtOAc 6:1 to 4:1) afforded two separated diastereomers: **4** (2.661 g, 10.34 mmol, 33%) as a viscous pale yellow liquid, and **5** (1.262 g, 4.904 mmol, 16%) as a pale yellow solid.

*Characterization of tert-butyl N-[(1S)-2-methyl-1-[(2S)-5-oxooxolan-2-yl]propyl]carbamate (**4**):*

Yield: 2.661 g (10.34 mmol, 33%, 2 steps), viscous pale yellow liquid.

$[\alpha]_D^{23} = -51.7^\circ$ (c = 0.56, CHCl₃).

R_f = 0.31 (cyclohexane/EtOAc 2:1 (v/v); staining: KMnO₄).

¹H NMR (300 MHz, CDCl₃, based on HSQC) δ = 4.76–4.64 (m, 1H, H–C2), 4.57 (d, ³J = 10.1 Hz, 1H, NH), 3.43 (m, 1H, H–C1), 2.50 (dd, ³J = 9.4 Hz, 7.4 Hz, 2H, H–C4), 2.28–1.98 (m, 2H, H–C3), 1.90–1.73 (m, 1H, H–C6), 1.42 (s, 9H, (CH₃)₃), 1.06–0.89 (m, 6H, H–C7).

^{13}C NMR (75 MHz, CDCl_3 , based on HSQC) δ = 177.5 (s, 1C, C5), 156.5 (s, 1C, HNCO), 80.0 (s, 1C, C2), 79.8 (s, 1C, Me_3C), 58.5 (s, 1C, C1), 31.5 (s, 1C, C6), 28.7 (s, 1C, C4), 28.4 (s, 3C, $(\text{CH}_3)_3$), 24.9 (s, 1C, C3), 19.8 (s, 1C, C7), 19.4 (s, 1C, C7).

Characterization of tert-butyl N-[(1S)-2-methyl-1-[(2R)-5-oxooxolan-2-yl]propyl]carbamate (5):

Yield: 1.262 g (4.904 mmol, 16%, 2 steps), pale yellow solid.

$[\alpha]_D^{23} = -7.6^\circ$ (c = 1.00, CHCl_3).

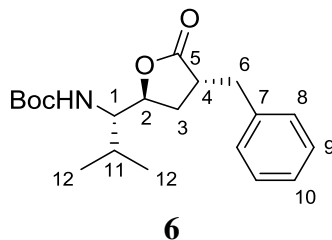
m.p. = 100–105 $^\circ\text{C}$.

$R_f = 0.24$ (cyclohexane/EtOAc 2:1 (v/v); staining: KMnO_4).

^1H NMR (300 MHz, CDCl_3 , based on HSQC) δ = 4.43 (d, $^3J = 9.5$ Hz, 1H, NH), 4.38–4.25 (m, 1H, H-C2), 3.74–3.51 (m, 1H, H-C1), 2.66–2.38 (m, 2H, H-C4), 2.36–1.94 (m, 3H, H-C3 and H-C6), 1.42 (s, 9H, $(\text{CH}_3)_3$), 1.06–0.75 (m, 6H, H-C7).

^{13}C NMR (75 MHz, CDCl_3 , based on HSQC) δ = 177.0 (s, 1C, C5), 156.2 (s, 1C, HNCO), 79.9 (s, 1C, Me_3C), 79.8 (s, 1C, C2), 57.8 (s, 1C, C1), 28.4 (s, 3C, $(\text{CH}_3)_3$), 28.3–27.9 (m, 2C, C4 and C6), 25.2 (s, 1C, C3), 19.9 (s, 1C, C7), 15.7 (s, 1C, C7).

1.7.2.5 *tert*-Butyl N-[(1S)-1-[(2S,4R)-4-benzyl-5-oxooxolan-2-yl]-2-methylpropyl]carbamate (6)^[273]



In an oven dried, argon purged 250 mL two-neck round-bottom flask, equipped with a dropping funnel, a gas valve adapter and a Teflon[®]-coated magnetic stirring bar, **4** (1.590 g, 6.228 mmol, 1.00 eq) was dissolved in THF (32.8 mL), stirred and cooled to -78 $^\circ\text{C}$ in an acetone/dry ice bath.

1.0 M LiHMDS solution in hexanes (12.8 mL, 12.8 mmol, 2.05 eq) was added dropwise within 5 min and the resulting solution was stirred for 30 min. A solution of benzyl bromide (741 μ L, 6.23 mmol, 1.00 eq) in THF (32.8 mL) was charged into the dropping funnel, added dropwise to the reaction mixture within 10 min and the resulting orange reaction solution was stirred at -78 $^{\circ}$ C, until TLC indicated full conversion (55 min). The reaction mixture was poured into a vigorously stirred 3 M NH_4Cl aqueous solution (65.6 mL). The layers were separated and the aqueous layer was extracted with EtOAc (2 \times 66 mL). The combined organic extracts were washed with 0.1 M HCl (33 mL), NaHCO_3 (33 mL), brine (11 mL), dried over Na_2SO_4 , and concentrated and dried under reduced pressure. Flash chromatography (SiO_2 , cyclohexane/EtOAc 8:1 to 5:1) furnished **6** (1.330 g, 3.828 mmol, 61%) as a colorless viscous liquid.

Yield: 1.330 g (3.828 mmol, 61%), colorless viscous liquid.

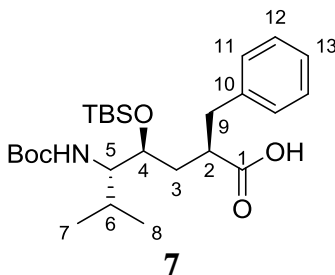
$[\alpha]_D^{23} = -13.0$ $^{\circ}$ ($c = 1.0$, CHCl_3); lit. $[\alpha]$ not disclosed.

$R_f = 0.60$ (cyclohexane/EtOAc 2:1 (v/v); staining: KMnO_4).

^1H NMR (300 MHz, CDCl_3) $\delta = 7.40$ – 7.11 (m, 5H, H–C8, H–C9 and H–C10), 4.55 (d, $^3J = 10.1$ Hz, 1H, NH), 4.48–4.38 (m, 1H, H–C2), 3.42–3.29 (m, 1H, H–C1), 3.14 (dd, $^2J = 13.5$ Hz, $^3J = 4.2$ Hz, 1H, H_a –C6), 3.05–2.90 (m, 1H, H–C4), 2.82 (dd, $^2J = 13.5$ Hz, $^3J = 8.9$ Hz, 1H, H_b –C6), 2.27–2.12 (m, 1H, H_a –C3), 2.11–1.96 (m, 1H, H_b –C3), 1.86–1.69 (m, 1H, H–C11), 1.42 (s, 9H, $(\text{CH}_3)_3$), 0.94 (d, $^3J = 6.7$ Hz, 6H, H–C12).

^{13}C NMR (75 MHz, CDCl_3) $\delta = 179.3$ (s, 1C, C5), 156.4 (s, 1C, HNCO), 138.1 (s, 1C, C7), 129.0 (s, 2C, H–C9), 128.8 (s, 2C, H–C8), 127.0 (s, 1C, H–C10), 79.8 (s, 1C, Me_3C), 78.2 (s, 1C, C2), 59.0 (s, 1C, C1), 41.4 (s, 1C, C4), 37.0 (s, 1C, C6), 31.06 (s, 1C, C3), 30.0 (s, 1C, C11), 28.4 (s, 3C, $(\text{CH}_3)_3$), 19.8 (s, 1C, C12), 19.3 (s, 1C, C12).

1.7.2.6 (2R,4S,5S)-2-Benzyl-5-[[*tert*-butoxy]carbonyl]amino]-4-[[*tert*-butyldimethylsilyl]oxy]-6-methylheptanoic acid (7**)^[273]**



Lactone opening: In a 25 mL round-bottom flask, equipped with a Teflon[®]-coated magnetic stirring bar, **6** (500 mg, 1.44 mmol, 1.00 eq) was dissolved in THF (5.3 mL) and stirred vigorously. A 1 M solution of LiOH×H₂O (329 mg, 7.84 mmol, 4.00 eq) in H₂O (7.8 mL) was added dropwise from a syringe within 3 min. TLC indicated full conversion after 70 min. Et₂O (7.8 mL) was added and the biphasic mixture was cooled down to 0 °C in an ice bath. Under vigorous stirring the aqueous phase was carefully adjusted to pH = 4 with 25% aqueous citric acid. The layers were separated and the aqueous layer was extracted with Et₂O (2×7.8 mL). The combined organic extracts were washed with H₂O (5.0 mL), dried over Na₂SO₄, and concentrated and dried under reduced pressure and temperatures <30 °C to furnish a white solid substance.

Silylation: In a nitrogen-purged 25 mL Schlenk tube equipped with a Teflon[®]-coated magnetic stirring bar, the isolated white solid and *N*-methylimidazole (941 μL, 11.8 mmol, 6.00 eq) were dissolved in absolute CH₂Cl₂ (7.8 mL) and stirred. The solution was cooled to 0 °C in an ice bath and iodine (2.990 g, 11.8 mmol, 6.00 eq) was added. After stirring for 15 min TBSCl (0.886 g, 5.88 mmol, 3.00 eq) was added in portions within 1 min and the cooling bath was removed. TLC indicated full conversion after 14 h. The dark red mixture was transferred into a separation funnel, diluted with Et₂O (25 mL) and treated with saturated aqueous Na₂S₂O₃ (7.8 mL). The organic phase was washed with 25% citric acid (7.8 mL) and brine, concentrated under reduced pressure and dried *in vacuo* to yield a yellow oil.

Silyl ester methanolysis: In a 10 mL round-bottom flask equipped with a Teflon[®]-coated magnetic stirring bar, the yellow oil was dissolved in MeOH (1.0 mL) and 25% citric acid (20 μL) was added. The mixture was stirred until TLC indicated full conversion (22 h). The mixture

was concentrated under reduced pressure and purified via flash chromatography (SiO₂, cyclohexane/EtOAc 4:1 to 2:1) to furnish **7** (383 mg, 0.798 mmol, 55% in 3 steps) as a colorless viscous liquid.

Yield: 383 mg (0.798 mmol, 55%, 3 steps), colorless viscous liquid.

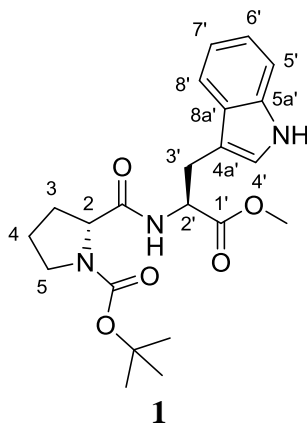
$[\alpha]_D^{23} = -17.2^\circ$ (c = 1.0, CHCl₃); lit. $[\alpha]$ not disclosed.

$R_f = 0.47$ (cyclohexane/EtOAc/AcOH 2:1:0.05 (v/v); staining: KMnO₄).

¹H NMR (300 MHz, CDCl₃, based on HSQC) $\delta = 7.36$ – 7.10 (m, 5H, H–C11, H–C12 and H–C13), 4.70 (d, ³ $J = 10.1$ Hz, 1H, NH), 3.89–3.78 (m, 1H, H–C4), 3.26–3.16 (m, 1H, H–C5), 3.11 (dd, ² $J = 13.5$ Hz, ³ $J = 7.3$ Hz, 1H, H_a–C9), 2.87–2.76 (m, 1H, H–C2), 2.71 (dd, ² $J = 13.5$ Hz, ³ $J = 6.1$ Hz, 1H, H_b–C9), 1.94–1.77 (m, 1H, H_a–C3), 1.72–1.54 (m, 2H, H_b–C3 and H–C6), 1.44 (s, 9H, (CH₃)₃CO), 0.92 (d, ³ $J = 6.6$ Hz, 3H, H–C7), 0.86 (s, 9H, (CH₃)₃CSi), 0.80 (d, ³ $J = 6.6$ Hz, 3H, H–C8), 0.04 (s, 3H, CH₃Si), 0.00 (s, 3H, CH₃Si).

¹³C NMR (75 MHz, CDCl₃, based on HSQC) $\delta = 177.0$ (s, 1C, C1), 157.7 (s, 1C, HNCO), 139.4 (s, 1C, C10), 129.1 (s, 2C, H–C12), 128.8 (s, 2C, H–C11), 126.7 (s, 1C, H–C13), 80.3 (s, 1C, Me₃C), 69.6 (s, 1C, C4), 58.8 (s, 1C, C5), 44.0 (s, 1C, C2), 38.1 (s, 1C, C9), 37.6 (s, 1C, C3), 29.6 (s, 1C, C6), 28.6 (s, 3C, (CH₃)₃CO), 26.0 (s, 3C, (CH₃)₃CSi), 20.0 (s, 1C, C7), 18.2 (s, 1C, C8), -3.7 (CH₃Si), -4.5 (CH₃Si).

1.7.2.7 *tert*-Butyl (2*S*)-2-[[*(2S)*-3-(1*H*-indol-3-yl)-1-methoxy-1-oxopropan-2-yl]carbamoyl]pyrrolidine-1-carboxylate (1**)^[364]**



A 250 mL three-neck round-bottom flask, equipped with a Schlenk adapter, a dropping funnel and a Teflon[®]-coated magnetic stirring bar, was purged with nitrogen. In the flask, Boc-Pro-OH (6.458 g, 30.00 mmol, 1.00 eq) was dissolved in DCM (50 mL), stirred and cooled to 0 °C in an ice bath. Diisopropylcarbodiimide (5.637 mL, 36.00 mmol, 1.20 eq) was added and the resulting mixture was stirred for 10 min. A solution of H-Trp-OMe×HCl (7.641 g, 30.00 mmol, 1.00 eq) and triethylamine (8.363 mL, 60.00 mmol, 2.00 eq) in DCM (50 mL) was added dropwise within 5 min. The reaction mixture was stirred for 2 h and then concentrated under reduced pressure. The residue was dissolved in EtOAc (250 mL) and washed with 1 M HCl (2×125 mL), 0.1 M NaOH (3×125 mL), H₂O (100 mL) and brine (50 mL). The organic phase was dried over Na₂SO₄ and stored in a sealed flask overnight at 4 °C. Subsequently, the solution was cooled to -20 °C for 30 min and filtered to remove a white precipitate. The filtrate was concentrated and dried *in vacuo* to furnish a white solid substance (7.560 g, 18.20 mmol, 61%).

Yield: 7.560 g (18.20 mmol, 61%), white solid.

m.p. = 97–100 °C; lit. m.p. not disclosed.

$[\alpha]_D^{23} = -33.1^\circ$ (c = 1.37, CHCl₃); lit. $[\alpha]$ not disclosed.

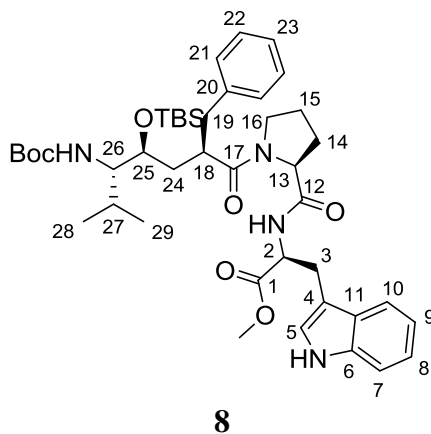
$R_f = 0.26$ (cyclohexane/EtOAc 1:1 (v/v); staining: KMnO₄).

^1H NMR (300 MHz, CDCl_3 , based on HSQC) δ = 8.37 (br s, 1H, indole NH), 7.52 (d, 3J = 7.7 Hz, 1H, H-C8'), 7.33 (d, 3J = 7.7 Hz, 1H, H-C5'), 7.23–6.89 (m, 3H, H-C5', H-C6' and H-C7'), 6.51 (br s, 1H, HNCO), 4.89 (br s, 1H, H-C2'), 4.34–4.09 (m, 1H, H-C2), 3.67 (s, 3H, CH_3O), 3.42–3.03 (m, 4H, H-C3' and H-C5), 2.31–1.52 (m, 4H, H-C3 and H-C4), 1.38 (s, 9H, $(\text{CH}_3)_3\text{CO}$).

^{13}C NMR (75 MHz, CDCl_3 , based on HSQC) δ = 172.2 (m, 2C, CONH and H-C1'), 154.8 (s, 1C, $\text{CO}_2t\text{-Bu}$), 136.3 (s, 1C, C5a'), 127.7 (s, 1C, C8a'), 122.8 (s, 1C, C4'), 122.3 (s, 1C, C6'), 119.7 (s, 1C, C7'), 118.5 (s, 1C, C8'), 111.4 (s, 1C, C5'), 110.1 (s, 1C, C4a'), 81.2–79.9 (m, 1C, Me_3C), 61.6–59.6 (s, 1C, C2), 53.7–52.5 (m, 1C, C2'), 52.4 (s, 1C, CH_3O), 47.0 (s, 1C, C5), 30.7 (br s, 1C, C3), 28.3 (s, 3C, $(\text{CH}_3)_3\text{CO}$), 27.9 (s, 1C, C3'), 25.1–22.9 (m, 1C, C4).

HPLC-ESI-MS (Agilent Poroshell120; method: fast_Poroshell120_001HCOOH_10to95): $t_R(\mathbf{1})$ = 5.41 min, 100%, $[\text{M} + \text{Na}]^+ = 438$, $[\text{M} + \text{K}]^+ = 454$.

1.7.2.8 Methyl (2S)-2-[[[(2S)-1-[(2R,4S,5S)-2-benzyl-5-[[*tert*-butoxy]carbonyl]amino]-4-[[*tert*-butyldimethylsilyl]oxy]-6-methylheptanoyl]pyrrolidin-2-yl]formamido]-3-(1*H*-indol-3-yl)propanoate (8)



In a 5 mL glass vial equipped with a Teflon[®]-coated magnetic stirring bar, **1** (200 mg, 0.481 mmol, 1.20 eq) was dissolved in TFA (1.10 mL). Ethanethiol (357 μL , 4.77 mmol, 1.19 eq) was

added and the solution was stirred for 60 min at RT. The volatiles were evaporated, the residue was dried in high vacuum to constant mass to yield deprotected H-Pro-Trp-OMe.

In a nitrogen-purged 10 mL Schlenk tube equipped with a Teflon[®]-coated magnetic stirring bar, **7** (189 mg, 0.400 mmol, 1.00 eq) and Hünig's base (69 μ L, 0.40 mmol, 1.0 eq) were dissolved in absolute DMF (1.60 mL). The solution was stirred, cooled to 0 °C in an ice bath and HBTU (180 mg, 0.47 mmol, 1.20 eq) was added. Immediately after 5 min of activation a solution of the freshly prepared H-Pro-Trp-OMe and Hünig's base (137 μ L, 0.793 mmol, 1.98 eq) in absolute DMF (1.00 mL) was added via syringe and septum. The ice bath was removed and the mixture was stirred for 120 min. Subsequently, brine (2.6 mL) and EtOAc (8.0 mL) were added and the mixture was stirred vigorously for 5 min. The layers were separated and the organic phase washed with brine (3 \times 2.6 mL), dried over Na₂SO₄, and concentrated under reduced pressure. After purification via flash chromatography (SiO₂, CH₂Cl₂/MeOH 80:1 to 20:1) **8** (231 mg, 0.297 mmol) was achieved as a white solid.

Yield: 231 mg (0.297 mmol, 74% from **7**), white solid.

m.p. = 76–79 °C.

$[\alpha]_D^{23} = -22^\circ$ (c = 0.2, CHCl₃).

R_f = 0.38 (CH₂Cl₂/MeOH 20:1 (v/v); staining: KMnO₄).

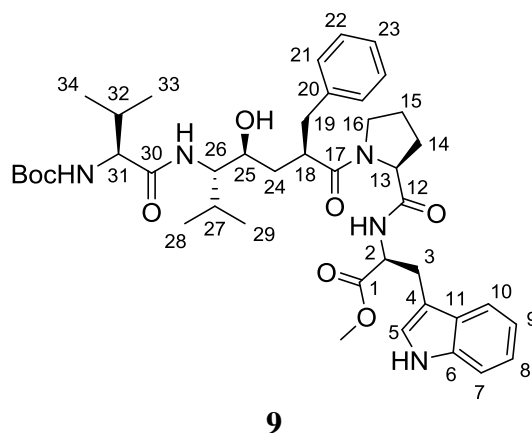
¹H NMR (300 MHz, CDCl₃, based on COSY and HSQC) δ = 8.42 (br s, 1H, indole NH), 7.49 (d, ³J = 7.6 Hz, 1H, H-C10), 7.35–6.98 (m, 10H, H-Ar and HNCO), 4.75–4.64 (m, 2H, HNCO₂ and H-C2), 4.57–4.54 (m, 1H, H-C13), 3.84 (dd, ³J = 9.3 Hz, 3.3 Hz, 1H, H-C25), 3.68 (s, 3H, CH₃O), 3.55–3.41 (m, 1H, H-C16), 3.31–3.20 (m, 2H, H-C3 and H-C26), 3.13 (dd, ²J = 14.6 Hz, ³J = 7.3 Hz, 1H, H-C26), 3.04–2.96 (m, 1H, H-C16), 2.86–2.83 (m, 1H, H-C18), 2.65 (dd, ²J = 13.4 Hz, ³J = 8.1 Hz, 1H, H-C19), 2.44 (dd, ²J = 13.4 Hz, ³J = 5.7 Hz, 1H, H-C19), 2.27–2.14 (m, 1H, H-C14), 1.87–1.55 (m, 6H, H₂-C15, H-C14, H₂-C24 and H-C27), 1.44 (s, 9H, (CH₃)₃C), 0.94 (d, ³J = 6.7 Hz, 3H, H-C28), 0.87 (s, 9H, (CH₃)₃CSi), 0.83 (d, ³J = 6.6 Hz, 3H, H-C29), 0.06 (s, 3H, CH₃Si), 0.02 (s, 3H, CH₃Si).

¹³C NMR (75 MHz, CDCl₃, based on COSY, HSQC and HMBC) δ = 174.9 (s, 1C, C=O), 172.5 (s, 1C, C=O), 171.1 (s, 1C, C=O), 156.7 (s, 1C, CO₂t-Bu), 139.5 (s, 1C, C20), 136.3 (s, 1C, C6),

129.0 (s, 2C, C22), 128.7 (s, 2C, C21), 127.6 (s, 1C, C11), 126.7 (s, 1C, C23), 123.7 (s, 1C, C5), 122.1 (s, 1C, C8), 119.5 (s, 1C, C9), 118.7 (s, 1C, C10), 111.3 (s, 1C, C7), 110.1 (s, 1C, C4), 79.1 (s, 1C, Me₃C), 69.4 (s, 1C, C25), 59.9 (s, 1C, C13), 58.5 (s, 1C, C26), 53.4 (s, 1C, C2), 52.3 (s, 1C, CH₃O), 47.1 (s, 1C, C16), 42.4 (s, 1C, C18), 38.2 (s, 1C, C19), 36.6 (s, 1C, 24), 30.2 (s, 1C, C27), 28.5 (s, 3C, (CH₃)₃CO), 27.7 (s, 1C, C3), 27.3 (s, 1C, C14), 26.0 (s, 3C, (CH₃)₃CSi), 24.8 (s, 1C, C15), 20.0 (s, 1C, C28), 19.8 (s, 1C, C29), 18.2 (s, 1C, (CH₃)₃CSi), -3.66 (CH₃Si), -4.61 (CH₃Si).

HRMS (ESI): m/z (%): 777.4620 (87%, [M + H]⁺, calcd for C₄₃H₆₅N₄O₇Si⁺: 777.4617), 799.4441 (100%, [M + Na]⁺, calcd for C₄₃H₆₄N₄NaO₇Si⁺: 799.4442), 815.4184 (100%, [M + K]⁺, calcd for C₄₃H₆₄KN₄O₇Si⁺: 815.4181).

1.7.2.9 Methyl (2S)-2-[[[(2S)-1-[(2R,4S,5S)-2-benzyl-5-[(2S)-2-[[tert-butoxy)carbonyl]amino]-3-methylbutanamido]-4-hydroxy-6-methylheptanoyl]pyrrolidin-2-yl]formamido]-3-(1H-indol-3-yl)propanoate (9)



Deprotection: In a 5 mL glass vial equipped with a Teflon[®]-coated magnetic stirring bar, **8** (132 mg, 0.170 mmol, 1.00 eq) was dissolved in 2,2,2-trifluoroethanol (1.7 mL). Ethanethiol (51 μL, 0.68 mmol, 4.0 eq) and ZnBr₂ were added, and the solution was stirred for 4 h at RT, accompanied with formation of a white precipitate. Subsequently, the reaction mixture was treated with 25% aqueous ammonia (0.80 mL). After EtOAc (5.1 mL) was added, the mixture was transferred into a 20 mL Erlenmeyer flask and stirred vigorously for 5 min. The layers were

separated, and the aqueous layer was extracted with EtOAc (2×3.4 mL). The combined organic extracts were dried over Na₂SO₄, concentrated under reduced pressure and the residue was dried in high vacuum to constant mass to yield the crude deprotected intermediate as a white amorphous solid (97 mg).

Coupling: In an oven-dried, nitrogen-purged 10 mL Schlenk tube, equipped with a Teflon[®]-coated magnetic stirring bar, Boc-Val-OH (44 mg, 0.20 mmol, 1.2 eq) and Hünig's base (30 μL, 0.17 mmol, 1.0 eq) were dissolved in absolute DMF (0.70 mL) and stirred at RT. A solution of HATU (78 mg, 0.20 mmol, 1.2 eq) in abs. DMF (0.70 mL) was added and the reaction solution was stirred for 1 min before a solution of the deprotected intermediate and Hünig's base (30 μL, 0.17 mmol, 1.0 eq) in abs. DMF (1.00 mL) was added. After TLC indicated full conversion of the intermediate (15 min), the reaction was quenched by addition of brine (1.0 mL) and extracted with EtOAc (3×3.6 mL). The combined organic extracts were washed with brine (3×1.0 mL), dried over Na₂SO₄, and concentrated under reduced pressure. Purification via flash chromatography (SiO₂, CH₂Cl₂/MeOH 50:1 to 20:1) furnished **9** (68 mg, 0.089 mmol) as a white solid.

Yield: 68 mg (0.089 mmol, 52%, 2 steps, from **8**), white solid.

m.p. = 90–93 °C.

$[\alpha]_D^{23} = -26.4^\circ$ (c = 0.23, CHCl₃).

R_f = 0.51 (CH₂Cl₂/MeOH 10:1 (v/v); staining: KMnO₄).

¹H NMR (300 MHz, CDCl₃, complex mixture of signals of 2 rotamers in 1.2:1 ratio, assigned based on COSY, HSQC, HMBC and EXSY) δ = 9.19 and 8.63 (br s, 1H, indole NH), 7.60–7.47 (m, 1H, H-C10), 7.46–6.97 (m, 7.5H, H-Ar and amide H from *cis*-rotamer's Trp), 6.54–6.31 (m, 1H, H-Ar), 6.12 (d, ³J = 7.3 Hz, 0.5H, amide H from *trans*-rotamer's Trp), 5.19–4.97 (m, 1H, carbamate H), 4.86–4.68 (m, 1H, H-C2), 4.58–4.27 (m and br s, 1.5H, H-C13 from one rotamer, and OH), 3.89–3.73 (m, 2H, H-C31 and H-C25), 3.76 and 3.68 (s, 3H, CH₃O), 3.56–2.38 (m, 8.5H, H₂-C3, H-C13 from one rotamer, H₂-C16, H-C18, H₂-C19, H-C26), 2.34–1.05 (m, 17H, H₂-C14, H₂-C15, H₂-C24, H-C27, H-C32 and (CH₃)₃C), 1.04–0.72 (m, 12H, H₃-C28, H₃-C29, H₃-C33 and H₃-C34).

^{13}C NMR (75 MHz, CDCl_3 , complex mixture of signals of 2 rotamers, assigned based on COSY, HSQC, HMBC and EXSY) δ = 176.2 and 175.2 (s, 1C, C17), 172.9, 172.5, 172.4, 172.2, 172.1 and 170.7 (s, 3C, 2 amide C=O and an ester C=O), 156.2–156.0 (m, 1C, carbamate C=O), 139.1 and 138.8 (s, 1C, C20), 136.5 and 136.4 (s, 1C, C6), 128.9 and 128.8 (s, 2C, C22), 128.6 (s, 2C, C21), 127.6 and 127.5 (s, 1C, C11), 126.7 and 126.6 (s, 1C, C23), 123.8 and 123.0 (s, 1C, C5), 122.4 and 122.1 (s, 1C, C8), 119.8 and 119.5 (s, 1C, C9), 118.5 and 118.1 (s, 1C, C10), 111.8 and 111.4 (s, 1C, C7), 109.7 and 109.5 (s, 1C, C4), 80.3–79.9 (m, 1C, Me_3C), 67.3 and 67.0 (s, 1C, C25), 61.1–60.6 (m, 1C, C31), 60.5 and 59.8 (s, 1C, C13), 60.0 and 59.7 (s, 1C, C26), 53.4 and 53.2 (s, 1C, C2), 52.8 and 52.4 (s, 1C, CH_3O), 47.5 and 46.4 (s, 1C, C16), 43.3 and 42.7 (s, 1C, C18), 40.0 and 37.8 (s, 1C, C19), 37.8 and 35.9 (s, 1C, 24), 31.3 and 27.5 (s, 1C, C14), 30.4, 30.1 and 29.8 (s, 2C, C27 and C32), 28.7–28.1 (m, 3C, $(\text{CH}_3)_3\text{CO}$), 27.6 and 26.9 (s, 1C, C3), 24.9 and 22.0 (s, 1C, C15), 20.2–20.0, 19.9–19.6, 19.3–19.2 and 18.0–17.7 (m, 4C, C33, C34, C28, C29).

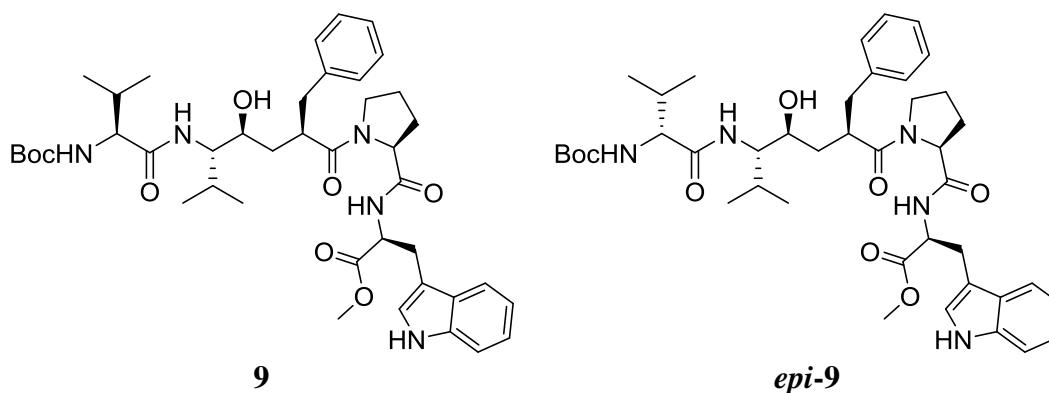
HPLC-ESI-MS (Agilent Poroshell120; method: SHE_Poroshell120_HCOOHMeCN_40_60_95): $t_R(\mathbf{9})$ = 7.62 min, 100%, $[\text{M} + \text{Na}]^+ = 785$, $[\text{M} + \text{K}]^+ = 801$; $t_R(\textit{epi-9})$ = 7.79 min, no abundance detected; de >99%, based on comparison to the HPLC-ESI-MS trace of reference epimer mixture (*vide infra*).

HRMS (ESI): m/z (%): 784.4257 (100%, $[\text{M} + \text{Na}]^+$, calcd for $\text{C}_{42}\text{H}_{59}\text{N}_5\text{NaO}_8^+$: 784.4261).

1.7.2.10 Reference epimer mixture microsynthesis:

Methyl (2*S*)-2-[[[(2*S*)-1-[(2*R*,4*S*,5*S*)-2-benzyl-5-[(2*S*)-2-[[(*tert*-butoxy)carbonyl]amino]-3-methylbutanamido]-4-hydroxy-6-methylheptanoyl]pyrrolidin-2-yl]formamido]-3-(1*H*-indol-3-yl)propanoate (**9**) and

Methyl (2*S*)-2-[[[(2*S*)-1-[(2*R*,4*S*,5*S*)-2-benzyl-5-[(2*R*)-2-[[(*tert*-butoxy)carbonyl]amino]-3-methylbutanamido]-4-hydroxy-6-methylheptanoyl]pyrrolidin-2-yl]formamido]-3-(1*H*-indol-3-yl)propanoate (*epi*-**9**)



According to the procedure for preparation of **9**, in a 1.5 mL glass vial, equipped with a small Teflon[®]-coated magnetic stirring bar, an aliquot (88 μ L, 1.2 eq) of a stock solution of Boc-DL-Val-OH (5.0 mg, 0.023 mmol) in absolute DMF (1.00 mL) was treated with an aliquot (7 μ L, 1.2 eq) of a stock solution of HATU (78 mg, 0.21 mmol) in absolute DMF (0.70 mL) using microliter-syringes. The mixture was stirred for 1 min and then immediately treated with an aliquot (10 μ L) of the solution of the crude deprotected intermediate in absolute DMF (97 mg in 1.00 mL, from the preparation of **9**). After 15 min, the reaction was quenched by the addition of water (200 μ L) and extracted with EtOAc (500 μ L). The organic layer was separated, and evaporated under reduced pressure. The residue was dissolved in 1000 μ L of MeCN and analyzed by TLC and HPLC-ESI-MS.

$R_f = 0.51$ (CH₂Cl₂/MeOH 10:1 (v/v); staining: KMnO₄).

(1.20 mL) and MeOH (200 μ L). Purification via preparative reverse phase HPLC (method: JKV_NucleodurC18_001HCOOH_10to85) afforded **10** (18 mg, 0.028 mmol, 46%, 2 steps) as a white solid.

Yield: 18 mg (0.028 mmol, 46%, 2 steps, from **9**), white solid.

m.p. = 151–155 $^{\circ}$ C

$[\alpha]_D^{23} = -24^{\circ}$ (c = 0.61, MeOH).

^1H NMR (300 MHz, methanol- d_4 / D_2O 5:1, complex mixture of signals of cabamate rotamers and intramolecular interaction stabilized conformers in equilibrium, assigned based on COSY and HSQC) $\delta = 7.69$ – 7.55 (m, 1H, H–C10), 7.41 – 6.89 (m, 9H, H–Ar), 4.65 – 4.37 (m, 1H, H–C2), 3.83 – 2.58 (m, 11H, H–C13, H–C31, H–C25, H_2 –C3, H_2 –C16, H–C18, H_2 –C19, H–C26), 2.36 – 2.18 (m, 1H, H–C32), 2.11 – 1.14 (m, 7H, H_2 –C14, H_2 –C15, H_2 –C24 and H–C27), 1.14 – 0.76 (m, 12H, H_3 –C28, H_3 –C29, H_3 –C33 and H_3 –C34).

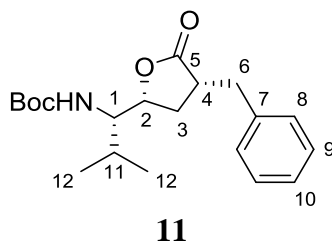
^{13}C NMR (75 MHz, methanol- d_4 / D_2O 5:1, complex mixture of signals of cabamate rotamers and intramolecular interaction conformers in equilibrium, assigned based on COSY and HSQC) $\delta = 177.2$, 176.4 , 173.6 and 169.2 (s, 4C, 3 amide C=O and an ester C=O), 140.0 (s, 1C, C20), 137.9 (s, 1C, C6), 130.4 – 126.7 (m, 6C, C11, C21, C22 and C23), 124.4 (s, 1C, C5), 122.4 (s, 1C, C8), 119.8 (s, 1C, C9), 119.6 (s, 1C, C10), 112.3 (s, 1C, C7), 68.6 (s, 1C, C25), 62.3 – 61.9 (m, 2C, C31 and C13), 47.5 (s, 1C, C16), 44.2 (s, 1C, C18), 42.8 (s), 41.4 (s, 1C, C19), 40.4 , 39.2 (s, 1C, C24), 37.4 (s, 1C, C2), 32.2 (s, 1C, C14), 31.6 (s, 1C, C32), 30.6 (s, 1C, C27), 28.6 (s, 1C, C3), 22.4 (s, 1C, C15), 20.8 – 17.5 (m, 4C, C33, C34, C28, C29).

HPLC-ESI-MS (Agilent Poroshell120; method: fast_Poroshell_001HCOOH_8mingradient.lc): $t_R(\mathbf{10}) = 5.54$ min, 100%, $[\text{M} + 1]^+ = 648$, $[\text{M} + \text{Na}]^+ = 670$.

HRMS (ESI): m/z (%): 648.3756 (100%, $[\text{M} + 1]^+$, calcd for $\text{C}_{36}\text{H}_{50}\text{N}_5\text{O}_6^+$: 648.3756), 670.3577 (100%, $[\text{M} + \text{Na}]^+$, calcd for $\text{C}_{36}\text{H}_{49}\text{N}_5\text{NaO}_6^+$: 670.3575).

1.7.3 Synthesis of *HER*

1.7.3.1 *tert*-Butyl *N*-[(1*S*)-1-[(2*R*,4*R*)-4-benzyl-5-oxooxolan-2-yl]-2-methylpropyl]carbamate (**11**)



Aldol reaction: In an oven dried, nitrogen purged 100 mL two-neck round-bottom flask, equipped with a dropping funnel, a gas valve adapter and a Teflon[®]-coated magnetic stirring bar, **5** (1.03 g, 4.00 mmol, 1.00 eq) was dissolved in absolute THF (29.9.8 mL), stirred and cooled to -78 °C in an acetone/dry ice bath. 1.0 M LiHMDS solution in hexanes (8.00 mL, 8.00 mmol, 2.00 eq) was added dropwise within 20 min and the resulting solution was stirred for 20 min. A solution of benzaldehyde (813 μL, 8.00 mmol, 2.00 eq) in THF (10.3 mL) was charged into the dropping funnel and added dropwise to the reaction mixture within 15 min. The resulting reaction solution was stirred at -78 °C until TLC indicated full conversion of lactone **5** (60 min). The reaction solution was poured into a vigorously stirred 3 M NH₄Cl aqueous solution (20 mL). The mixture was extracted with EtOAc (2×40 mL). The combined organic extracts were washed with 1 M HCl (20 mL), saturated aqueous NaHCO₃ (20 mL), brine (10 mL), dried over Na₂SO₄, and concentrated and dried under reduced pressure. Purification via flash chromatography (SiO₂, cyclohexane/EtOAc 4:1 to 2:1) furnished a mixture of 4 aldol diastereomers (528 mg, 1.75 mmol, 44%) as a pale yellow viscous liquid.

Mesylation: In an oven dried, nitrogen purged 20 mL Schlenk tube, equipped with a Teflon[®]-coated magnetic stirring bar, the mixture of aldol diastereomers (472 mg, 1.30 mmol, 1.00 eq) was dissolved in absolute CH₂Cl₂ (6.5 mL), stirred and cooled to 0 °C in an ice bath. Methanesulfonyl chloride (201 μL, 2.60 mmol, 2.00 eq) was added dropwise *via* syringe within 10 min and, subsequently, triethylamine (544 μL, 3.90 mmol, 3.00 eq) was added dropwise *via*

syringe within 2 min. The resulting solution was stirred overnight in the warming ice bath, reaching RT. Additional methanesulfonyl chloride (201 μL , 2.60 mmol, 2.00 eq) and triethylamine (544 μL , 3.90 mmol, 3.00 eq) were added and the reaction solution was stirred again overnight to complete the conversion. The reaction was quenched by the addition of ice-cold water (4.0 mL). The resulting biphasic mixture was extracted with EtOAc (2 \times 13 mL), the combined organic extracts were washed with brine (4.0 mL), dried over Na_2SO_4 , and concentrated under reduced pressure to afford a brown oily residue (571 mg), which was composed of a diastereomeric mixture of β' -chlorolactones and the desired elimination intermediates (based on HPLC-MS and NMR analysis of the crude mixture).

Elimination: In a 10 mL round-bottom flask, equipped with a reflux condenser and a Teflon[®]-coated magnetic stirring bar, the crude intermediate mixture was dissolved in EtOH (5.2 mL). Triethylamine (172 μL , 1.24 mmol, 0.95 eq) was added and the reaction mixture was heated overnight at 50 °C in an oil bath. After concentration *in vacuo*, the residue was partitioned between EtOAc (10 mL) and water (4.0 mL) and the aqueous layer extracted with EtOAc (5.0 mL). The combined organic layers were washed with brine (5 mL) and concentrated under reduced pressure to furnish a viscous oily residue containing only the desired elimination intermediate diastereomers (based on HPLC-MS and NMR analysis of the crude mixture).

Hydrogenation: In a 50 mL two-neck round-bottom flask, equipped with a gas valve adaptor and a mechanical stirring apparatus, the crude intermediate mixture was dissolved in THF (15.2 mL). A portion of aqueous slurry of Raney-Ni (1.0 mL) was pipetted into a test tube, the water was decanted and the mass of the tube was recorded. Wet Raney-Ni was suspended in THF (1.0 mL), transferred into the reaction flask and the mass of the tube was recorded again to determine the difference which corresponds to the mass of Raney-Ni (17 mg). The apparatus was first purged with nitrogen and then with hydrogen, and the reaction mixture was stirred vigorously at RT overnight, under hydrogen atmosphere. The reaction flask was disconnected from the hydrogen balloon and purged with N_2 . Under nitrogen atmosphere the content of the flask was transferred to the nitrogen-purged fritted Schlenk type funnel containing a 2 cm thick compressed bed of Celite[®]. The product was eluted from the filter cake with THF (3 \times 5 mL). The Celite[®] bed with the solid catalyst was washed with water (5 mL), and stored under water in a container dedicated for catalyst waste. The product-containing filtrate was evaporated under reduced pressure, and

the residue was purified via flash chromatography (SiO₂, cyclohexane/EtOAc 9:1 to 4:1) to furnish a white solid **11** (311 mg, 0.895 mmol, 30%, 4 steps).

Yield: 311 mg (0.895 mmol, 30%, in 4 steps from **5**), white solid.

m.p. = 83–86 °C.

$[\alpha]_D^{23} = -50.8^\circ$ (c = 0.7, CHCl₃).

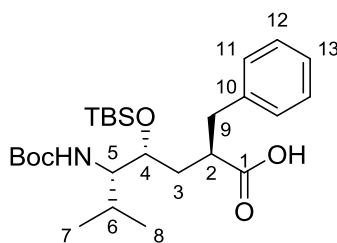
R_f = 0.42 (cyclohexane/EtOAc 2:1 (v/v); staining: KMnO₄).

¹H NMR (300 MHz, CDCl₃, based on COSY and HSQC) δ = 7.39–7.10 (m, 5H, H–C8, H–C9 and H–C10), 4.31 (d, ³J = 9.9 Hz, 1H, NH), 4.25–4.03 (m, 1H, H–C2), 3.75–3.54 (m, 1H, H–C1), 3.31 (dd, ²J = 13.5 Hz, ³J = 2.7 Hz, 1H, H_a–C6), 2.95–2.77 (m, 1H, H–C4), 2.77–2.60 (m, 1H, H_b–C6), 2.33–2.18 (m, 1H, H_a–C3), 2.15–1.98 (m, 1H, H–C11), 1.95–1.76 (m, 1H, H_b–C3), 1.43 (s, 9H, (CH₃)₃), 0.94 (d, ³J = 6.8 Hz, 3H, H–C12), 0.85 (d, ³J = 6.9 Hz, 3H, H–C12).

¹³C NMR (75 MHz, CDCl₃, based on COSY and HSQC) δ = 177.8 (s, 1C, C5), 156.1 (s, 1C, HNCO), 138.9 (s, 1C, C7), 129.0 (s, 2C, H–C9), 128.8 (s, 2C, H–C8), 126.8 (s, 1C, H–C10), 79.9 (s, 1C, Me₃C), 78.2 (s, 1C, C2), 58.3 (s, 1C, C1), 42.7 (s, 1C, C4), 36.5 (s, 1C, C6), 32.2 (s, 1C, C3), 28.6–28.3 (m, 4C, C11 and (CH₃)₃), 20.0 (s, 1C, C12), 16.0 (s, 1C, C12).

HRMS (ESI): m/z (%): 370.1987 (100%, [M + Na]⁺, calcd for C₂₀H₂₉NNaO₄⁺: 370.1989).

1.7.3.2 (2R,4R,5S)-2-Benzyl-5-[[*tert*-butoxy]carbonyl]amino]-4-[[*tert*-butyldimethylsilyl]oxy]-6-methylheptanoic acid (**12**)



12

Lactone opening: In a 10 mL round-bottom flask, equipped with a Teflon[®]-coated magnetic stirring bar, **11** (108 mg, 0.42 mmol, 1.00 eq) was dissolved in THF (1.4 mL) and stirred vigorously. A 1 M solution of LiOH×H₂O (70 mg, 1.7 mmol, 4.0 eq) in H₂O (2.1 mL) was added dropwise via syringe. After TLC indicated full conversion (90 min), Et₂O (4.0 mL) was added and the biphasic mixture was cooled down to 0 °C in an ice bath. Under vigorous stirring, the acidity of the aqueous phase was carefully adjusted to pH=4 with 25% aqueous citric acid. The layers were separated and the aqueous layer was extracted with Et₂O (2×3.0 mL). The combined organic extracts were washed with H₂O (3.0 mL) and brine (3.0 mL), dried over Na₂SO₄, and concentrated and dried under reduced pressure and temperatures <30 °C to furnish a white solid substance.

Silylation: In a nitrogen-purged 10 mL Schlenk tube, equipped with a Teflon[®]-coated magnetic stirring bar, the isolated white solid and *N*-methylimidazole (201 μL, 2.52 mmol, 6.00 eq) were dissolved in absolute CH₂Cl₂ (1.7 mL). The solution was cooled to 0 °C in an ice bath and iodine (640 mg, 2.52 mmol, 6.00 eq) was added. After stirring for 15 min, TBSCl (190 mg, 1.26 mmol, 3.00 eq) was added in portions within 1 min. The cooling bath was removed and the deep-red mixture stirred overnight. The dark red mixture was transferred into a separation funnel, diluted with Et₂O (4.0 mL) and washed with saturated aqueous Na₂S₂O₃ (3.0 mL). The organic phase was washed with 25% citric acid (3.0 mL) and brine (3.0 mL), concentrated under reduced pressure and dried *in vacuo* to yield a yellow oily residue.

Silyl ester methanolysis: In a 5 mL glass vial, equipped with a Teflon[®]-coated magnetic stirring bar, the yellow oil was dissolved in MeOH (1.1 mL) and 25% citric acid (32 μL) was added. The mixture was stirred until TLC indicated full conversion (6 h) of the least polar component observable. The mixture was concentrated under reduced pressure and purified via flash chromatography (SiO₂, CH₂Cl₂/MeOH/AcOH 100:1:0.5) to furnish **12** (102 mg, 0.213 mmol, 51% in 3 steps) as a colorless viscous oil.

Yield: 102 mg (0.213 mmol, 51%, in 3 steps from **11**), colorless viscous oil.

$[\alpha]_D^{23} = -5.5^\circ$ (c = 0.7, CHCl₃).

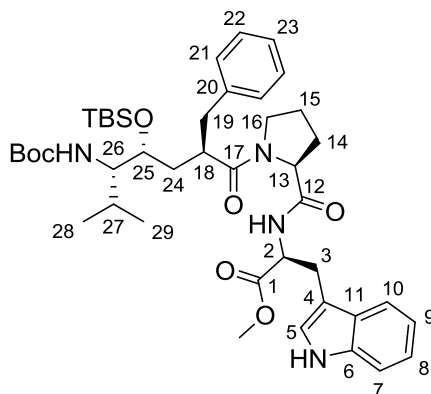
R_f = 0.14 (CH₂Cl₂/MeOH/AcOH 100:3:0.5 (v/v); staining: KMnO₄).

^1H NMR (300 MHz, CDCl_3 , mixture of 2 rotamers, based on COSY, HSQC and EXSY) δ = 7.37–7.11 (m, 5H, H–C11, H–C12 and H–C13), 6.17 and 4.61 (d, 3J = 9.9 Hz, 1H, NH), 3.86–3.66 (m, 1H, H–C4), 3.52–3.23 (m, 1H, H–C5), 3.12–2.93 (m, 1H, H_a –C9), 2.87–2.66 (m, 2H, H–C2 and H_b –C9), 2.00–1.76 (m, 1H, H_a –C3), 1.74–1.50 (m, 2H, H_b –C3 and H–C6), 1.43 (s, 9H, $(\text{CH}_3)_3\text{CO}$), 0.88 (s, 9H, $(\text{CH}_3)_3\text{CSi}$), 0.84–0.70 (m, H–C7 and H–C8), 0.15–0.01 (s, 6H, $(\text{CH}_3)_2\text{Si}$).

^{13}C NMR (75 MHz, CDCl_3 , mixture of 2 rotamers, citing major rotamer based on COSY, HSQC and EXSY) δ = 179.0 (s, 1C, C1), 156.2 (s, 1C, HNCO), 138.8 (s, 1C, C10), 129.1 (s, 2C, H–C12), 128.6 (s, 2C, H–C11), 126.7 (s, 1C, H–C13), 79.4 (s, 1C, Me_3C), 71.9 (s, 1C, C4), 58.0 (s, 1C, C5), 43.5 (s, 1C, C2), 38.6 (s, 1C, C9), 35.3 (s, 1C, C3), 28.6 (s, 3C, $(\text{CH}_3)_3\text{CO}$), 28.1 (s, 1C, C6), 26.0 (s, 3C, $(\text{CH}_3)_3\text{CSi}$), 20.9 (s, 1C, C7), 18.1 (s, 1C, C8), -4.3 (CH_3Si), -4.6 (CH_3Si).

HRMS (ESI): m/z (%): 502.2956 (100%, $[\text{M} + \text{Na}]^+$, calcd for $\text{C}_{26}\text{H}_{45}\text{NNaO}_5\text{Si}^+$: 502.2959).

1.7.3.3 Methyl (2R)-2-[[[(2S)-1-[(2R,4S,5S)-2-benzyl-5-[[*tert*-butoxy]carbonyl]amino]-4-[[*tert*-butyldimethylsilyl]oxy]-6-methylheptanoyl]pyrrolidin-2-yl]formamido]-3-(1*H*-indol-3-yl)propanoate (13)



13

In a 5 mL glass vial equipped with a Teflon[®]-coated magnetic stirring bar, **1** (110 mg, 0.260 mmol, 1.20 eq) was dissolved in TFA (508 μL), ethanethiol (165 μL , 2.20 mmol, 10 eq) was

added, and the solution was stirred for 60 min at RT. The volatiles were evaporated, the residue was dried in high vacuum to constant mass to yield a deprotected H-Pro-Trp-OMe.

In a nitrogen-purged 10 mL Schlenk tube equipped with a Teflon[®]-coated magnetic stirring bar, **12** (106 mg, 0.220 mmol, 1.00 eq) and Hünig's base (38 μ L, 0.22 mmol, 1.0 eq) were dissolved in absolute DMF (1.00 mL). The solution was stirred, cooled to 0 °C in an ice bath and HBTU (100 mg, 0.260 mmol, 1.20 eq) was added. Immediately after 5 min of activation a solution of the freshly prepared H-Pro-Trp-OMe and Hünig's base (77 μ L, 0.44 mmol, 2.0 eq) in absolute DMF (0.47 mL) was added via syringe and septum. The ice bath was removed and the mixture was stirred for 60 min. Subsequently, brine (2.0 mL) and EtOAc (6.0 mL) were added, and the mixture was stirred vigorously for 5 min. The layers were separated and the organic phase was washed with brine (3 \times 2.0 mL), dried over Na₂SO₄, and concentrated under reduced pressure. Purification via flash chromatography (SiO₂, CH₂Cl₂/MeOH 100:3) furnished **13** (91 mg, 0.12 mmol, 53%) as a white solid.

Yield: 91 mg (0.12 mmol, 53% from **12**), white solid.

m.p. = 55–58 °C

$[\alpha]_D^{23} = -3.0^\circ$ (c = 1.12, CHCl₃).

R_f = 0.36 (CH₂Cl₂/MeOH 10:1 (v/v); staining: KMnO₄).

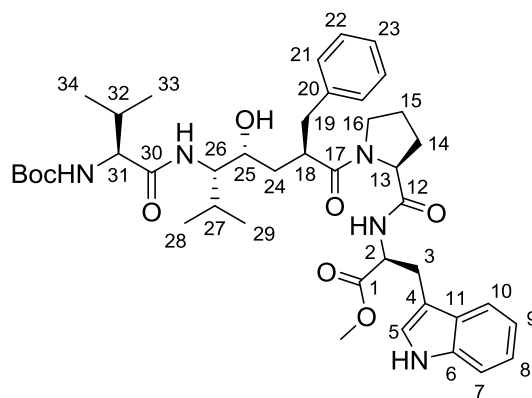
¹H NMR (300 MHz, CDCl₃, only *trans*-Pro rotamer observable, based on HSQC) δ = 8.15 (br s, 1H, indole NH), 7.53 (d, ³J = 7.0 Hz, 1H, H-C10), 7.34 (d, ³J = 6.1 Hz, 1H, amide NH), 7.30–6.90 (m, 9H, H-Ar), 4.82–4.71 (m, 1H, H-C2), 4.62–4.47 (m, 2H, H-C13 and carbamate NH), 3.75–3.58 (m, 4H, CH₃O and H-C25), 3.57–3.42 (m, 1H, H_a-C16), 3.40–3.15 (m, 3H, H₂-C3 and H-C26), 3.00–2.87 (m, 1H, H_b-C16), 2.80–2.67 (m, 1H, H-C18), 2.67–2.45 (m, 1H, H-C19), 2.29–2.14 (m, 1H, H_a-C14), 1.97–1.50 (m, 6H, H_a-C14, H₂-C15, H₂-C24 and H-C27), 1.40 (s, 9H, (CH₃)₃C), 0.99–0.71 (m, 15H, (CH₃)₃CSi, H₃-C28 and H₃-29), 0.11 (s, 3H, CH₃Si), 0.07 (s, 3H, CH₃Si).

¹³C APT NMR (75 MHz, CDCl₃, only *trans*-Pro rotamer observable, based on HSQC) δ = 175.0 (s, 1C, C=O), 172.5 (s, 1C, C=O), 171.2 (s, 1C, C=O), 156.0 (s, 1C, carbamate C=O), 139.2 (s, 1C, C20), 136.2 (s, 1C, C6), 129.0 (s, 2C, C22), 128.5 (s, 2C, C21), 127.8 (s, 1C, C11), 126.6 (s,

1C, C23), 123.5 (s, 1C, C5), 122.2 (s, 1C, C8), 119.6 (s, 1C, C9), 118.7 (s, 1C, C10), 111.3 (s, 1C, C7), 110.3 (s, 1C, C4), 79.0 (s, 1C, Me₃C), 72.2 (s, 1C, C25), 60.1 (s, 1C, C13), 57.7 (s, 1C, C26), 53.5 (s, 1C, C2), 52.4 (s, 1C, CH₃O), 47.3 (s, 1C, C16), 42.0 (s, 1C, C18), 39.0 (s, 1C, C19), 35.5 (s, 1C, 24), 28.5 (s, 3C, (CH₃)₃CO), 27.8 (s, 1C, C27), 27.6 (s, 1C, C3), 27.4 (s, 1C, C14), 26.0 (s, 3C, (CH₃)₃CSi), 24.9 (s, 1C, C15), 21.4 (s, 1C, C28), 18.4 (s, 1C, C29), 18.1 (s, 1C, (CH₃)₃CSi), -4.1 (CH₃Si), -4.7 (CH₃Si).

HRMS (ESI): m/z (%): 799.4442 (100%, [M + Na]⁺, calcd for C₄₃H₆₄N₄NaO₇Si⁺: 799.4442).

1.7.3.4 Methyl (2R)-2-[[[(2S)-1-[(2R,4S,5S)-2-benzyl-5-[(2S)-2-[[tert-butoxy)carbonyl]amino]-3-methylbutanamido]-4-hydroxy-6-methylheptanoyl]pyrrolidin-2-yl]formamido]-3-(1H-indol-3-yl)propanoate (14)



14

Deprotection: In a 5 mL glass vial equipped with a Teflon[®]-coated magnetic stirring bar, **13** (97 mg, 0.125 mmol, 1.00 eq) was dissolved in 2,2,2-trifluoroethanol (1.3 mL). Ethanethiol (37 μ L, 0.50 mmol, 4.0 eq) and ZnBr₂ (197 mg, 0.875 mmol, 7.00 eq) were added, and the solution was stirred for 7 h at RT, accompanied with formation of a white precipitate. Subsequently, the reaction mixture was treated with 25% aqueous ammonia (2.0 mL) to adjust to pH=11. After stirring for 10 min the mixture was extracted with EtOAc (2 \times 4.0 mL). The combined organic layers were washed with water (2.0 mL) and brine (2.0 mL), dried over Na₂SO₄, concentrated under reduced pressure and the residue was dried in high vacuum to constant mass to yield the crude deprotected intermediate as a white amorphous solid.

Coupling: In an oven-dried, nitrogen-purged 10 mL Schlenk tube, equipped with a Teflon[®]-coated magnetic stirring bar, Boc-Val-OH (33 mg, 0.15 mmol, 1.2 eq) and Hünig's base (22 μ L, 0.13 mmol, 1.0 eq) were dissolved in absolute DMF (0.35 mL), stirred and cooled to 0 °C in an ice bath. A solution of HATU (57 mg, 0.15 mmol, 1.2 eq) in abs. DMF (0.35 mL) was added and the reaction solution was stirred for 1 min before a solution of the deprotected intermediate and Hünig's base (22 μ L, 0.13 mmol, 1.0 eq) in abs. DMF (0.60 mL) was added. After TLC indicated full conversion of the intermediate (30 min), the reaction was quenched by addition of brine (1.3 mL) and extracted with EtOAc (3 \times 3.0 mL). The combined organic extracts were washed with brine (3 \times 1.5 mL), dried over Na₂SO₄, and concentrated under reduced pressure. Purification via flash chromatography (SiO₂, CH₂Cl₂/MeOH 50:1 to 20:1) furnished **14** (20 mg, 0.026 mmol) as a white solid.

Yield: 20 mg (0.026 mmol, 21%, 2 steps, from **13**), white solid.

m.p. = 87–89 °C.

$[\alpha]_D^{23} = -26.6^\circ$ (c = 0.52, CHCl₃).

R_f = 0.20 (CH₂Cl₂/MeOH 20:1 (v/v); staining: KMnO₄).

¹H NMR (300 MHz, CDCl₃, complex mixture of signals of 2 rotamers in 7:1 ratio; major rotamer assigned based on COSY, HSQC, and EXSY) δ = 9.02 (br s, 1H, indole NH), 7.50 (d, ³J = 7.6 Hz, 1H, H-C10), 7.42–6.89 (m, 10H, H-Ar and amide NH from Trp), 6.13 (d, ³J = 9.2 Hz, 1H, amide NH), 5.04 (d, ³J = 8.9 Hz, 1H, carbamate NH), 4.81–4.58 (m, 1H, H-C2), 3.93–3.87 (m, 1H, H-C31), 3.83–3.52 (m, 4H, CH₃O and H-C26), 3.50–3.15 (m, 3H, H₂-C3 and H-C13), 3.14–2.96 (m, 1H, H_a-C16), 2.91–2.73 (m, 1H, H_b-C16), 2.71–2.55 (m, 2H, H₂-C19), 2.55–2.40 (m, 1H, H-C18), 2.36–1.50 (m, 5H, H-C32, H-C27, H₂-C24, H_a-C14), 1.50–1.38 (m, 9H, (CH₃)₃C), 1.37–1.18 (m, 1H, H_a-C15), 1.12–0.75 (m, 14H, H₃-C33, H₃-C34, H_b-C14, H_b-C15, H₃-C28 and H₃-C29).

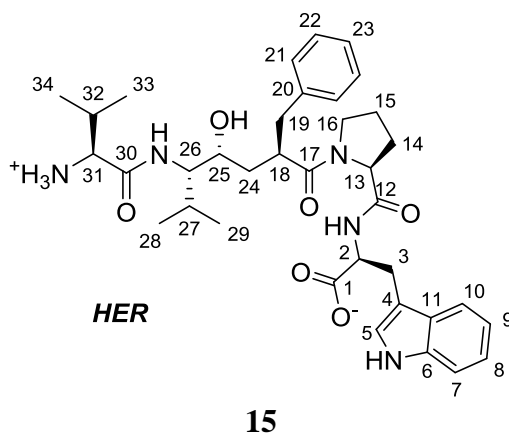
¹³C NMR (75 MHz, CDCl₃, complex mixture of signals of 2 rotamers in 7:1 ratio; major rotamer assigned based on COSY, HSQC, and EXSY) δ = 175.4 (s, 1C, C17), 172.8 (s, 1C, C=O), 172.7 (s, 1C, C=O), 172.3 (s, 1C, C=O), 156.2 (s, 1C, carbamate C=O), 138.8 (s, 1C, C20), 136.3 (s, 1C, C6), 129.2 (s, 2C, C22), 128.5 (s, 2C, C21), 127.6 (s, 1C, C11), 126.8 (s, 1C, C23), 123.4 (s, 1C, C5), 122.3 (s, 1C, C8), 119.9 (s, 1C, C9), 118.0 (s, 1C, C10), 111.8 (s, 1C, C7), 109.9 (s, 1C,

C4), 80.4 (s, 1C, Me₃C), 71.0 (s, 1C, C25), 60.8 (s, 1C, C31), 60.1 (s, 1C, C13), 59.3 (s, 1C, C26), 53.6 (s, 1C, C2), 52.6 (s, 1C, CH₃O), 46.2 (s, 1C, C16), 44.0 (s, 1C, C18), 39.9 (s, 1C, C19), 37.1 (s, 1C, 24), 31.0 (s, 1C, C14), 30.0 (s, 1C, C32), 28.5 (s, 3C, (CH₃)₃CO), 27.5 (s, 1C, C27), 26.2 (s, 1C, C3), 21.8 (s, 1C, C15), 20.6 (s, 1C, C28), 19.9 (s, 1C, C33), 18.2 (s, 1C, C34) and 16.8 (s, 1C, C29).

HPLC-ESI-MS (Agilent Poroshell120; method: fast_Poroshell120_001HCOOHMeCN): $t_R(\mathbf{14}) = 9.14$ min, 100%, $[M + Na]^+ = 785$, $[M + K]^+ = 801$.

HRMS (ESI): m/z (%): 784.4245 (100%, $[M + Na]^+$, calcd for C₄₂H₅₉N₅NaO₈⁺: 784.4256).

1.7.3.5 (2S)-2-{[(2S)-1-[(2R,4R,5S)-5-[(2S)-2-Azaniumyl-3-methylbutanamido]-2-benzyl-4-hydroxy-6-methylheptanoyl]pyrrolidin-2-yl]formamido}-3-(1H-indol-3-yl)propanoate (15)



Saponification: In a 5 mL glass vial equipped with a Teflon[®]-coated magnetic stirring bar, **14** (11 mg, 0.015 mmol, 1.0 eq) was dissolved in THF (0.20 mL). A solution of LiOH×H₂O (5 mg, 0.12 mmol, 8.0 eq) in H₂O (0.10 mL) was added and the mixture was stirred vigorously until TLC indicated full conversion (60 min). The acidity of the solution was adjusted to pH=3 with 1M

HCl. The resulting white colloidal mixture was extracted with EtOAc (3×1 mL). The combined organic extracts were merged, dried over Na₂SO₄, concentrated under reduced pressure and dried in high vacuum to constant mass to yield a saponified intermediate as an off-white powder (5 mg).

Boc-deprotection: In a 5 mL glass vial equipped with a Teflon[®]-coated magnetic stirring bar, the saponified intermediate (40 mg) was dissolved in trifluoroacetic acid (150 μL) and stirred for 5 min. The mixture was concentrated under reduced pressure and dried under high vacuum to constant mass. The residue was dissolved in water (600 μL), MeCN (200 μL) and DMSO (300 μL) and purified via preparative reverse phase HPLC (method: JKV_NucleodurC18_001HCOOH_10to85) to yield **15** (4.0 mg, 0.0062 mmol, 41%, 2 steps) as a white solid.

Yield: 4.0 mg (0.0062 mmol, 41%, 2 steps, from **14**), white solid.

m.p. = 123–126 °C.

$[\alpha]_D^{23} = -25^\circ$ (c = 0.13, MeOH).

¹H NMR (500 MHz, methanol-d₄, complex mixture of signals of 2 Pro-peptide rotamers in equilibrium, major rotamer assigned based on COSY and HSQC) δ = 8.53 (br s, 1H, indole NH), 7.73–6.88 (m, 10H, H-Ar), 4.66–4.56 (m, 1H, H-C2), 3.85–3.78 (m, 2H, H-C25 and H-C26), 3.70 (d, 1H, ³J = 4.9 Hz, H-C31), 3.52–3.36 (m, 2H, H-C13 and H_a-C3), 3.25–3.12 (m, 1H, H_b-C3), 3.11–3.01 (m, 1H, H_a-C16), 2.94–2.82 (m, 1H, H_b-C16), 2.81–2.70 (m, 2H, H-C18 and H_a-C19), 2.69–2.59 (m, 1H, H_b-C19), 2.35–2.10 (m, 2H, H-C32 and H-C27), 2.08–1.94 (m, 1H, H_a-C24), 1.68–1.58 (m, 1H, H_b-C24), 1.53–1.42 (m, 1H, H_a-C14), 1.24–0.68 (m, 15H, H_b-C14, H₂-C15, H₃-C33, H₃-C34, H₃-C28 and H₃-C29).

¹³C NMR (125 MHz, methanol-d₄, complex mixture of signals of 2 Pro-peptide rotamers in equilibrium, major rotamer assigned based on COSY and HSQC) δ = 177.8 (C=O), 173.1 (s, 1C, C=O), 170.7 (s, 1C, C=O), 169.6 (s, 1C, C=O), 140.3 (s, 1C, C20), 138.0 (s, 1C, C6), 130.1 (s, 2C, C22), 129.6 (s, 2C, C21), 127.9–127.2 (m, 2C, C23 and C11), 124.2 (s, 1C, C5), 122.3 (s, 1C, C8), 119.7 (s, 1C, C9), 119.5 (s, 1C, C10), 112.2 (s, 1C, C4), 112.1 (s, 1C, C7), 71.1 (s, 1C, C25), 62.3 (s, 1C, C13), 61.4 (s, 1C, C26), 60.5 (s, 1C, C31), 57.0 (s, 1C, C2), 47.3 (s, 1C, C16), 45.4 (s, 1C, C18), 40.5 (s, 1C, C19), 37.5 (s, 1C, C24), 31.9 (s, 1C, C32), 31.7 (s, 1C, C14), 29.3

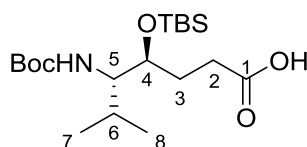
(s, 1C, C27), 28.5 (s, 1C, C3), 22.4 (s, 1C, C15), 21.1 (s, 1C, C28), 19.6 (s, 1C, C33), 18.4 (s, 1C, C29) and 17.5 (s, 1C, C34).

HPLC-ESI-MS (Agilent Poroshell120; method: fast_Poroshell_001HCOOH_8mingradient.lc):
 $t_R(\mathbf{15}) = 6.56$ min, 100%, $[M + 1]^+ = 648$, $[M + Na]^+ = 670$.

HRMS (ESI): m/z (%): 648.3752 (100%, $[M + 1]^+$, calcd for $C_{36}H_{50}N_5O_6^+$: 648.3756), 1295.7433 (91%, $[2M + 1]^+$, calcd for $C_{72}H_{99}N_{10}O_{12}^+$: 1295.7438).

1.7.4 Synthesis of Shorter Peptidomimetics

1.7.4.1 (4*S*,5*S*)-5-[[*tert*-Butoxy]carbonyl]amino}-4-[[*tert*-butyldimethylsilyl]oxy]-6-methylheptanoic acid (**16**)



16

Lactone opening: In a 50 mL round-bottom flask, equipped with a Teflon[®]-coated magnetic stirring bar, **4** (643 mg, 2.50 mmol, 1.00 eq) was dissolved in THF (8.3 mL) and stirred vigorously. A 1 M solution of LiOH×H₂O (420 mg, 10.0 mmol, 4.00 eq) in H₂O (12.5 mL) was added dropwise via syringe within 3 min. After 90 min full conversion was indicated by TLC. Et₂O (20.0 mL) was added and the biphasic mixture was cooled down to 0 °C in an ice bath. Under vigorous stirring, the acidity of the aqueous phase was carefully adjusted to pH=4 with 25% aqueous citric acid. The layers were separated and the aqueous layer was extracted with Et₂O (2×10.0 mL). The combined organic extracts were washed with H₂O (10.0 mL) and brine (10.0 mL), dried over Na₂SO₄, and concentrated and dried under reduced pressure and temperatures <30 °C to furnish a white solid substance.

Silylation: In a nitrogen-purged 25 mL Schlenk tube equipped with a Teflon[®]-coated magnetic stirring bar, the isolated white solid and *N*-methylimidazole (1196 μL, 15.0 mmol, 6.00 eq) were dissolved in absolute CH₂Cl₂ (10.0 mL). The stirred solution was cooled to 0 °C in an ice bath and iodine (3.807 g, 15.0 mmol, 6.00 eq) was added. After stirring for 15 min, TBSCl (1.130 g, 7.50 mmol, 3.00 eq) was added in portions within 1 min and the cooling bath was removed. After 14 h full conversion was indicated by TLC. The dark red mixture was transferred into a separation funnel, diluted with Et₂O (20 mL) and washed with saturated aqueous Na₂S₂O₃ (28 mL). The organic phase was washed with 25% citric acid (10 mL) and brine (10 mL), concentrated under reduced pressure and dried *in vacuo* to yield a yellow oil.

Silyl ester methanolysis: In a 50 mL round-bottom flask equipped with a Teflon[®]-coated magnetic stirring bar, the yellow oil was dissolved in MeOH (6.3 mL) and 25% citric acid (196 μ L) was added. The mixture was stirred until TLC indicated full conversion of the least polar compound (4 h). The mixture was concentrated under reduced pressure and purified via flash chromatography (SiO₂, cyclohexane/EtOAc 4:1 to 2:1) to furnish **16** (801 mg, 2.06 mmol, 82% in 3 steps) as a pale yellow oil.

Yield: 801 mg (2.06 mmol, 82% in 3 steps); pale yellow oil.

$[\alpha]_D^{23} = -8.2^\circ$ (c = 2.5, CHCl₃).

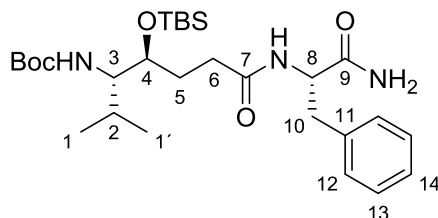
$R_f = 0.43$ (cyclohexane/EtOAc/AcOH 2:1:0.05 (v/v); staining: KMnO₄).

¹H NMR (300 MHz, CDCl₃, mixture of two rotamers, based on COSY, HSQC and EXSY) $\delta = 8.72$ (br s, 1H, COOH), 5.04 and 4.68 (d, ³J = 10.1 Hz, 1H, NH), 3.96–3.78 (m, 1H, H–C4), 3.26–2.99 (m, 1H, H–C5), 1.88–1.60 (m, 1H, H₂–C3, and H–C6), 1.72–1.54 (m, 2H, H_b–C3 and H–C6), 1.50–1.39 (m, 9H, (CH₃)₃CO), 1.01–0.78 (m, 15H, H₃–C7, H₃–C8 and (CH₃)₃CSi), 0.12–0.02 (m, 6H, 2 \times CH₃Si).

¹³C NMR (75 MHz, CDCl₃, mixture of two rotamers, based on COSY, HSQC and EXSY) $\delta = 178.6$ (s, 1C, C1), 156.9 and 156.6 (s, 1C, HNCO), 80.2 and 79.3 (s, 1C, Me₃C), 70.7 and 70.6 (s, 1C, C4), 59.9 and 58.4 (s, 1C, C5), 30.3–29.3 (m, 3C, C2, C3 and C6), 28.6 (s, 3C, (CH₃)₃CO), 26.3–25.8 (m, 3C, (CH₃)₃CSi), 20.2 and 20.0 (s, 1C, C7), 19.7 (s, 1C, C8), 18.2 (s, 1C, (CH₃)₃CSi), -3.8 and -3.9 (CH₃Si), -4.61 (CH₃Si).

HRMS (ESI): m/z (%): 390.2665 (100%, [M + 1]⁺, calcd for C₁₉H₄₀NO₅Si⁺: 390.2670), 412.2490 (11%, [M + Na]⁺, calcd for C₁₉H₃₉NNaO₅Si⁺: 412.2490), 428.2227 (11%, [M + K]⁺, calcd for C₁₉H₃₉KNO₅Si⁺: 428.2229).

1.7.4.2 *tert*-Butyl *N*-[(3*S*,4*S*)-4-[(*tert*-butyldimethylsilyloxy)]-6-[[*(1S)*-1-carbamoyl-2-phenylethyl]carbamoyl]-2-methylhexan-3-yl]carbamate (17**)**



17

In a 50 mL nitrogen-purged Schlenk tube, equipped with a Teflon[®]-coated magnetic stirring bar, **16** (760 mg, 1.95 mmol, 1.00 eq) was dissolved in absolute DMF (13.0 mL) and stirred. Hünig's base (1.36 mL, 7.80 mmol, 4.00 eq) and TBTU (939 mg, 2.93 mmol, 1.50 eq) were added to the solution. After 30 min HCl×H-Phe-NH₂ was added, and the mixture was stirred for another 30 min. The reaction was quenched by addition of brine (13 mL), and extracted with EtOAc (40 mL). The organic layer was washed with brine (2×13 mL), 1 M HCl (13 mL), brine (13 mL) again, dried over Na₂SO₄, and concentrated and dried under reduced pressure. Purification via flash chromatography (SiO₂, cyclohexane/EtOAc 1:1) afforded **17** (577 mg, 1.08 mmol, 55%) as a white solid.

Yield: 577 mg (1.08 mmol, 55%), white solid.

m.p. = 66–69 °C.

$[\alpha]_D^{23} = -12.9^\circ$ (c = 1.95, CHCl₃).

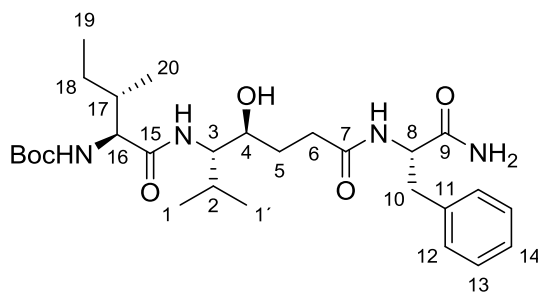
$R_f = 0.29$ (cyclohexane/EtOAc 1:2 (v/v); staining: KMnO₄).

¹H NMR (300 MHz, CDCl₃, based on HSQC) $\delta = 7.41$ – 7.17 (m, 5H, H–Ar), 6.88 (d, ³*J* = 7.9 Hz, 1H, C8–NH), 6.11 (m, 2H, C9–NH₂), 4.82–4.62 (m, 2H, C3–NH and H–C8), 3.94–3.79 (m, 1H, H–C4), 3.29–2.94 (m, 3H, H–C3 and H₂–C10), 2.44–2.05 (m, 2H, H₂–C6), 1.97–1.55 (m, 3H, H₂–C5 and H–C2), 1.47 (s, 9H, (CH₃)₃CO), 1.03–0.80 (m, 15H, H₃–C1, H₃–C1' and (CH₃)₃CSi), 0.18–0.02 (m, 6H, 2×CH₃Si).

^{13}C NMR (75 MHz, CDCl_3 , based on HSQC) δ = 173.4 (s, 1C, C=O), 172.8 (s, 1C, C=O), 156.7 (s, 1C, carbamate C=O), 137.0 (s, 1C, C11), 129.4 (s, 2C, C13), 128.7 (s, 2C, C12), 127.0 (s, 1C, C14), 79.2 (s, 1C, Me_3C), 70.7 (s, 1C, C4), 58.1 (s, 1C, C3), 54.2 (s, 1C, C8), 38.2 (s, 1C, C10), 32.0 (s, 1C, C6), 30.4 (s, 1C, C5), 30.1 (s, 1C, C2), 28.6 (s, 3C, $(\text{CH}_3)_3\text{CO}$), 26.0 (s, 3C, $(\text{CH}_3)_3\text{CSi}$), 19.9 (s, 1C, C1), 19.8 (s, 1C, C1'), 18.2 (s, 1C, $(\text{CH}_3)_3\text{CSi}$), -3.7 (CH_3Si), -4.7 (CH_3Si).

HRMS (ESI): m/z (%): 536.3515 (38%, $[\text{M} + 1]^+$, calcd for $\text{C}_{28}\text{H}_{50}\text{N}_3\text{O}_5\text{Si}^+$: 536.3514), 558.3331 (65%, $[\text{M} + \text{Na}]^+$, calcd for $\text{C}_{28}\text{H}_{49}\text{N}_3\text{NaO}_5\text{Si}^+$: 558.3334), 574.3075 (15%, $[\text{M} + \text{K}]^+$, calcd for $\text{C}_{28}\text{H}_{49}\text{KN}_3\text{O}_5\text{Si}^+$: 574.3073).

1.7.4.3 *tert*-Butyl ((2*S*,3*S*)-1-(((3*S*,4*S*)-7-(((*S*)-1-amino-1-oxo-3-phenylpropan-2-yl)amino)-4-hydroxy-2-methyl-7-oxoheptan-3-yl)amino)-3-methyl-1-oxopentan-2-yl)carbamate (18**)**



18

Deprotection: In a 10 mL round-bottom flask, equipped with a Teflon[®]-coated magnetic stirring bar, **17** (198 mg, 0.373 mmol, 1.00 eq) was dissolved in 2,2,2-trifluoroethanol (7.5 mL). ZnBr_2 (583 mg, 2.59 mmol, 7.00 eq) and EtSH (194 μL , 2.59 mmol, 7.00 eq) were added to the solution and the mixture was stirred vigorously for 5 h. The reaction was quenched by addition of 25% aqueous ammonia (15 mL), and extracted with EtOAc (2 \times 30 mL). The combined organic extracts were washed with brine (20 mL), dried over Na_2SO_4 , concentrated under reduced pressure, and

dried under high vacuum to constant mass to yield the deprotected intermediate as a white amorphous solid.

Coupling: In a 10 mL nitrogen-purged Schlenk tube, equipped with a Teflon[®]-coated magnetic stirring bar, Boc-Ile-OH (95 mg, 0.41 mmol, 1.1 eq) and the deprotected intermediate were dissolved in absolute DMF (3.74 mL). Hünig's base (195 μ L, 1.12 mmol, 3.00 eq) was added and the solution was cooled to 0 °C in an ice bath. Subsequently, HATU (156 mg, 0.41 mmol, 1.1 eq) was added and the mixture was stirred for 30 min. The reaction solution was quenched by addition of brine (3.0 mL) and extracted with EtOAc (15 mL). The organic layer was washed with brine (3 \times 4.0 mL), dried over Na₂SO₄, concentrated *in vacuo*, adsorbed via evaporation under reduced pressure onto Celite (1.3 g), and purified via flash chromatography to furnish **18** (106 mg, 0.189 mmol, 54% in 2 steps) as a white solid.

Yield: 106 mg (0.189 mmol, 54% in 2 steps), white solid.

m.p. = 199–201 °C.

$[\alpha]_D^{23} = +5.2^\circ$ (c = 0.20, MeOH).

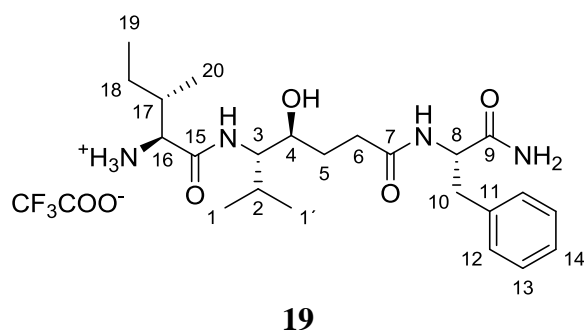
$R_f = 0.27$ (CH₂Cl₂/MeOH 10:1 (v/v); staining: KMnO₄).

¹H NMR (300 MHz, DMSO-d₆, based on HSQC) $\delta = 7.89$ (d, ³*J* = 8.5 Hz, 1H, C8–NH), 7.36 (s, 1H, C9–NH), 7.30–7.12 (m, 5H, H–Ar), 7.08 (d, ³*J* = 9.6 Hz, 1H, C3–NH), 7.01 (s, 1H, C9–NH), 6.85 (d, ³*J* = 8.7 Hz, 1H, C16–NH), 4.59 (d, ³*J* = 5.6 Hz, 1H, C4–OH), 4.47–4.31 (m, 1H, H–C8), 3.82–3.69 (m, 1H, H–C16), 3.61–3.46 (m, 1H, H–C4), 3.39–3.21 (m, 1H, H–C3), 2.97 (dd, ²*J* = 13.6 Hz, ³*J* = 4.6 Hz, 1H, H_a–C10), 2.74 (dd, ²*J* = 13.6 Hz, ³*J* = 9.6 Hz, 1H, H_b–C10), 2.17–1.96 (m, 2H, H₂–C6), 1.85–1.62 (m, 2H, H–C17 and H–C2), 1.53–0.98 (m, 13H, H₂–C5, (CH₃)₃CO and H₂–C18), 0.96–0.67 (m, 12H, H₃–C1, H₃–C1' H₃–C20 and H₃–C19).

¹³C NMR (75 MHz, DMSO-d₆, based on HSQC) $\delta = 173.2$ (s, 1C, C=O), 172.1 (s, 1C, C=O), 171.4 (s, 1C, C=O), 155.4 (s, 1C, carbamate C=O), 138.1 (s, 1C, C11), 129.1 (s, 2C, C13), 128.0 (s, 2C, C12), 126.1 (s, 1C, C14), 68.7 (s, 1C, C4), 59.4 (s, 1C, C16), 57.5 (s, 1C, C3), 53.7 (s, 1C, C8), 37.6 (s, 1C, C10), 35.6 (s, 1C, C17), 31.9 (s, 1C, C6), 30.2 (s, 1C, C5), 29.4 (s, 1C, C2), 28.2 (s, 3C, (CH₃)₃CO), 24.3 (s, 1C, C18), 19.9 (s, 1C, C1), 19.5 (s, 1C, C1'), 15.6 (s, 1C, C20), 10.8 (s, 1C, C19).

HRMS (ESI): m/z (%): 557.3306 (100%, $[M + 1]^+$, calcd for $C_{28}H_{46}N_4NaO_6^+$: 557.3310).

1.7.4.4 (2*S*,3*S*)-1-(((3*S*,4*S*)-7-(((*S*)-1-Amino-1-oxo-3-phenylpropan-2-yl)amino)-4-hydroxy-2-methyl-7-oxoheptan-3-yl)amino)-3-methyl-1-oxopentan-2-aminium 2,2,2-trifluoroacetate (19**)**



In a 5 mL glass vial, equipped with a Teflon[®]-coated magnetic stirring bar, **18** (53 mg, 0.10 mmol, 1.0 eq) was dissolved in trifluoroacetic acid (1.0 mL) and stirred for 30 min. The solution was concentrated under reduced pressure, and dried at high vacuum to constant mass. The residue was dissolved in water (600 μ L), acetonitrile (200 μ L) and DMSO (300 μ L), and purified via preparative reverse phase HPLC (method: JKV_NucleodurC18_001CF3COOH_10to85) to yield **19** (4.3 mg, 7.8 μ mol, 8%) as a white solid.

Yield: 4.3 mg (7.8 μ mol, 8%), white solid.

m.p. = 93–95 °C.

$[\alpha]_D^{23} = +4.0$ ($c = 0.25$, MeOH).

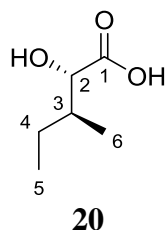
¹H NMR (300 MHz, methanol-d₄, based on HSQC) $\delta = 7.34$ – 7.12 (m, 5H, H–Ar), 4.60 (dd, ³ $J = 8.8$ Hz, 5.7 Hz, 1H, H–C8), 3.84 (d, ³ $J = 4.0$ Hz, 1H, H–C16), 3.80–3.69 (m, 1H, H–C4), 3.48 (d, ³ $J = 9.0$ Hz, 1H, H–C3), 3.13 (dd, ² $J = 13.9$ Hz, ³ $J = 5.7$ Hz, 1H, H_a–C10), 2.87 (dd, ² $J = 13.9$ Hz, ³ $J = 8.9$ Hz, 1H, H_b–C10), 2.40–2.15 (m, 2H, H₂–C6), 2.05–1.80 (m, 2H, H–C17 and H–C2),

1.70–1.42 (m, 3H, H₂–C5 and H_a–C18), 1.26–1.11 (m, 1H, H_b–C18), 1.07 (d, ³J = 4.0 Hz, 3H, H₃–C20), 1.03–0.87 (m, 9H, H₃–C1, H₃–C1' and H₃–C19).

¹³C NMR (75 MHz, methanol-d₄, based on HSQC) δ = 176.2 (s, 1C, C=O), 175.5 (s, 1C, C=O), 169.7 (s, 1C, C=O), 138.6 (s, 1C, C11), 130.3 (s, 2C, C13), 129.4 (s, 2C, C12), 127.8 (s, 1C, C14), 70.5 (s, 1C, C4), 60.81 (s, 1C, C3), 59.5 (s, 1C, C16), 55.7 (s, 1C, C8), 39.1 (s, 1C, C10), 38.4 (s, 1C, C17), 33.4 (s, 1C, C6), 31.9 (s, 1C, C5), 30.7 (s, 1C, C2), 24.7 (s, 1C, C18), 20.2 (s, 1C, C1), 19.9 (s, 1C, C1'), 15.6 (s, 1C, C20), 11.9 (s, 1C, C19).

HRMS (ESI): m/z (%): 435.2962 (77%, [M + 1]⁺, calcd for C₂₃H₃₉N₄O₄⁺: 435.2966), 869.5849 (100%, [2M + 1]⁺, calcd for C₄₆H₇₇N₈O₈⁺: 869.5859).

1.7.4.5 (2*S*,3*S*)-2-Hydroxy-3-methylpentanoic acid (**20**)^[287]



In a 250 mL round-bottom flask, equipped with a dropping funnel and a Teflon[®]-coated magnetic stirring bar, (*S*)-isoleucine (2.624 g, 20.00 mmol, 1.0 eq) was dissolved in 0.5 M sulfuric acid (80.0 mL) and cooled to 0 °C. A solution of NaNO₂ (5.52 g, 80.0 mmol, 4.00 eq) in H₂O (18.00 mL) was added slowly dropwise over 90 min, stirred for 2 h at 0 °C, and left spontaneously warming up to RT over 5 h. The reaction mixture was extracted with Et₂O (2×80 mL). The combined organic extracts were washed with brine (2×50 mL), dried over Na₂SO₄, concentrated under reduced pressure, and dried under high vacuum to constant mass to yield **20** (1.980 g, 14.98 mmol, 75%) as a colorless viscous liquid.

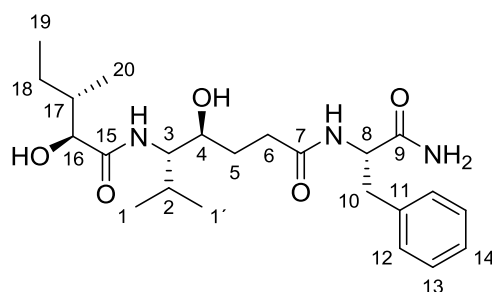
Yield: 1.980 g (14.98 mmol, 75%), colorless viscous liquid.

$[\alpha]_D^{23} = +19.7^\circ$ ($c = 0.92$, CHCl_3); lit. $[\alpha]_D^{24} = +20.8^\circ$ ($c = 1.02$, CHCl_3).

^1H NMR (300 MHz, CHCl_3) $\delta = 6.98$ (br s, 1H, COOH), 4.19 (d, $^3J = 3.6$ Hz, 1H, H-C2), 1.99–1.79 (m, 1H, H-C3), 1.53–1.17 (m, 2H, H₂-C4), 1.02 (d, $^3J = 6.9$ Hz, 3H, H₃-C6), 0.92 (t, $^3J = 7.4$ Hz, 3H, H₃-C5).

^{13}C APT NMR (75 MHz, CHCl_3) $\delta = 179.5$ (s, 1C, C1), 74.8 (s, 1C, C2), 39.0 (s, 1C, C3), 23.8 (s, 1C, C4), 15.5 (s, 1C, C6), 11.8 (s, 1C, C5).

1.7.4.6 (4*S*,5*S*)-*N*-((*S*)-1-Amino-1-oxo-3-phenylpropan-2-yl)-4-hydroxy-5-((2*S*,3*S*)-2-hydroxy-3-methylpentanamido)-6-methylheptanamide (**21**)



21

Deprotection: In a 10 mL round-bottom flask, equipped with a Teflon[®]-coated magnetic stirring bar, **17** (198 mg, 0.373 mmol, 1.00 eq) was dissolved in 2,2,2-trifluoroethanol (7.5 mL). ZnBr_2 (583 mg, 2.59 mmol, 7.00 eq) and EtSH (194 μL , 2.59 mmol, 7.00 eq) were added and the mixture was stirred vigorously for 5 h. The reaction was quenched by addition of 25% aqueous ammonia (15 mL) and extracted with EtOAc (2 \times 30 mL). The combined organic extracts were merged, washed with brine (20 mL), dried over Na_2SO_4 , concentrated under reduced pressure, and dried under high vacuum to constant mass, to yield the deprotected intermediate as a white amorphous solid.

Coupling: In a 10 mL nitrogen-purged Schlenk tube, equipped with a Teflon[®]-coated magnetic stirring bar, **20** (54 mg, 0.41 mmol, 1.1 eq) and the deprotected intermediate were dissolved in

absolute DMF (3.74 mL). Hünig's base (195 μL , 1.12 mmol, 3.00 eq) was added and the solution was cooled to 0 $^{\circ}\text{C}$ in an ice bath. Subsequently, HATU (156 mg, 0.41 mmol, 1.1 eq) was added and the mixture was stirred for 30 min. The reaction solution was quenched by addition of brine (3.0 mL) and extracted with EtOAc (15 mL). The organic layer was washed with brine (3 \times 4.0 mL), dried over Na_2SO_4 , concentrated *in vacuo*, adsorbed via evaporation under reduced pressure onto Celite (1.4 g), and purified via flash chromatography to furnish **21** (93 mg, 0.214 mmol, 58% in 2 steps) as a white solid.

Yield: 106 mg (0.189 mmol, 54% in 2 steps), white solid.

m.p. = 66–70 $^{\circ}\text{C}$

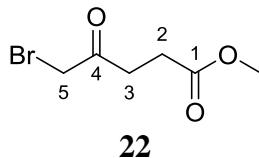
$[\alpha]_D^{23} = -22.9^{\circ}$ (c = 1.57, MeOH).

$R_f = 0.26$ ($\text{CH}_2\text{Cl}_2/\text{MeOH}$ 10:1 (v/v); staining: KMnO_4).

^1H NMR (300 MHz, methanol- d_4 , based on COSY and HSQC) $\delta = 7.37\text{--}7.11$ (m, 5H, H-Ar), 4.60 (dd, $^3J = 9.1$ Hz, 5.5 Hz, 1H, H-C8), 3.95 (d, $^3J = 3.4$ Hz, 1H, H-C16), 3.80–3.68 (m, 1H, H-C4), 3.45 (d, $^3J = 8.6$ Hz, 1H, H-C3), 3.15 (dd, $^2J = 13.9$ Hz, $^3J = 5.4$ Hz, 1H, $\text{H}_a\text{-C10}$), 2.86 (dd, $^2J = 13.9$ Hz, $^3J = 9.3$ Hz, 1H, $\text{H}_b\text{-C10}$), 2.35–2.15 (m, 2H, $\text{H}_2\text{-C6}$), 1.85–1.75 (m, 2H, H-C17 and H-C2), 1.71–1.35 (m, 3H, $\text{H}_2\text{-C5}$ and $\text{H}_a\text{-C18}$), 1.33–1.10 (m, 1H, $\text{H}_b\text{-C18}$), 1.07–0.81 (m, 12H, $\text{H}_3\text{-C1}$, $\text{H}_3\text{-C1}'$, $\text{H}_3\text{-C20}$ and $\text{H}_3\text{-C19}$).

^{13}C NMR (75 MHz, methanol- d_4 , based on COSY and HSQC) $\delta = 176.7$ (s, 1C, C=O), 176.3 (s, 1C, C=O), 175.8 (s, 1C, C=O), 138.6 (s, 1C, C11), 130.2 (s, 2C, C13), 129.4 (s, 2C, C12), 127.7 (s, 1C, C14), 77.2 (s, 1C, C16), 70.8 (s, 1C, C4), 59.5 (s, 1C, C8), 55.7 (s, 1C, C3), 39.7 (s, 1C, C17), 39.0 (s, 1C, C10), 33.4 (s, 1C, C6), 31.7 (s, 1C, C5), 30.9 (s, 1C, C2), 24.5 (s, 1C, C18), 20.3 (s, 1C, C1), 20.1 (s, 1C, C1'), 16.1 (s, 1C, C20), 12.2 (s, 1C, C19).

HRMS (ESI): m/z (%): 458.2628 (96%, $[\text{M} + \text{Na}]^+$, calcd for $\text{C}_{23}\text{H}_{37}\text{N}_3\text{NaO}_5^+$: 458.2625).

1.7.4.7 Methyl 5-bromo-4-oxopentanoate (22)^[292]

In a 1 L round-bottom flask, equipped with a dropping funnel, and a Teflon[®]-coated magnetic stirring bar, levulinic acid (46.448 mg, 400.00 mmol, 1.00 eq) was dissolved in MeOH (400 mL). The flask was covered with an aluminium foil to exclude light and the solution was stirred and cooled to 0 °C in an ice bath. Br₂ (20.55 mL, 400 mmol, 1.00 eq) was added dropwise over 1 h. The resulting brown solution turned colorless 60 min after completed addition. The solution was stirred overnight and left to spontaneously warm up to RT. Subsequently, the reaction flask was equipped with a distillation apparatus and the solvent containing HBr byproduct was distilled into a 1 L receiving round-bottom flask. The residue was dissolved in EtOAc (400 mL), washed with 5% NaHCO₃ (2×200 mL) and brine (200 mL), dried over Na₂SO₄, and concentrated under reduced pressure. Fractional distillation afforded **22** (37.541 g, 179.59 mmol, 45 %) as a yellow liquid.

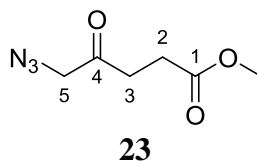
Yield: 37.541 g (179.59 mmol, 45 %), yellow liquid.

b.p. = 75 °C, 0.34 mbar; lit. 80 °C, 0.045 mbar.^[292]

R_f = 0.58 (cyclohexane/EtOAc 1:1 (v/v); staining: KMnO₄).

¹H NMR (300 MHz, CHCl₃) δ = 3.95 (s, 2H, H₂-C5), 3.66 (m, 3H, CH₃), 2.94 (t, ³J = 6.4 Hz, 2H, H₂-C3), 2.64 (t, ³J = 6.4 Hz, 2H, H₂-C2).

¹³C NMR (75 MHz, CHCl₃) δ = 200.7 (s, 1C, C4), 172.9 (s, 1C, C1), 52.1 (s, 1C, CH₃), 34.5 (s, 1C, C5), 34.2 (s, 1C, C3), 28.2 (s, 1C, C2).

1.7.4.8 Methyl 5-azido-4-oxopentanoate (23)^[292]

In a 250 mL round-bottom flask, equipped with a dropping funnel, and a Teflon[®]-coated magnetic stirring bar, sodium azide (7.801 g, 120.0 mmol, 2.00 eq) was dissolved in water (30.0 mL), stirred and cooled to 0 °C in an ice bath. A solution of **22** (12.542 g, 60.000 mmol, 1.00 eq) in THF (30.0 mL) was slowly added dropwise, and the biphasic mixture was vigorously stirred at 0 °C for 60 min after completion of addition. Subsequently, the layers were separated. The aqueous layer was extracted with EtOAc (2×85 mL). The combined organic layers were washed with water (2×85 mL) and brine (40 mL), dried over Na₂SO₄, concentrated under reduced pressure, and dried in high vacuum to yield **23** (8.883 g, 51.90 mmol, 86%) as a yellow viscous liquid.

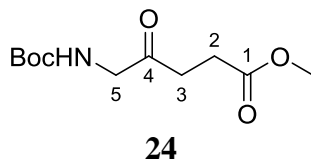
Yield: 8.883 g (51.90 mmol, 86%), viscous yellow liquid.

R_f = 0.36 (cyclohexane/EtOAc 2:1 (v/v); staining: KMnO₄).

¹H NMR (300 MHz, CHCl₃) δ = 4.02 (s, 2H, H₂-C5), 3.67 (s, 3H, CH₃), 2.76–2.61 (m, 4H, H₂-C3 and H₂-C2).

¹³C APT NMR (75 MHz, CHCl₃) δ = 203.1 (s, 1C, C4), 172.9 (s, 1C, C1), 57.7 (s, 1C, C5), 52.1 (s, 1C, CH₃), 34.6 (s, 1C, C3), 27.7 (s, 1C, C2).

1.7.4.9 Methyl 5-((*tert*-butoxycarbonyl)amino)-4-oxopentanoate (**24**)^[292]



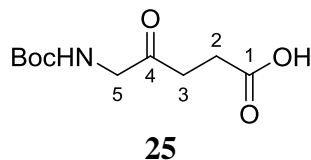
In a 250 mL two-neck round-bottom flask, equipped with a gas valve adapter, a Teflon[®]-coated magnetic stirring bar and a hydrogen balloon, **23** (8.883 g, 51.90 mmol, 1.00 eq) and Boc₂O (11.440 g, 52.42 mmol, 1.01 eq) were dissolved in EtOAc (104 mL). The solution was stirred and purged three times with nitrogen. 5% Pd/C (1.657 g, 0.779 mmol, 0.015 eq) was added, the mixture was purged with hydrogen three times, and left stirring vigorously under hydrogen atmosphere for 48 h. The reaction flask was disconnected from the hydrogen balloon and purged with N₂. Under nitrogen atmosphere the content of the flask was transferred to a nitrogen-purged fritted Schlenk type funnel containing a 2 cm thick compressed bed of Celite[®]. The product was eluted from the filter cake with EtOAc (2×50 mL). The Celite[®] bed with the solid catalyst was washed with THF (5 mL) and water (5 mL), and stored under water in a container dedicated for catalyst waste. The product-containing filtrate was concentrated under reduced pressure and dried *in vacuo*. Purification via flash chromatography (SiO₂, cyclohexane/EtOAc 2:1) afforded **24** (8.920 g, 36.37 mmol, 70%) as a yellow liquid.

Yield: 8.920 g (36.37 mmol, 70%), yellow liquid.

R_f = 0.18 (cyclohexane/EtOAc 2:1 (v/v); staining: KMnO₄).

¹H NMR (300 MHz, CHCl₃) δ = 5.21 (br s, 1H, carbamate H), 4.05 (d, ³J = 3.9 Hz, 2H, H₂-C5), 3.66 (s, 3H, CH₃O₂C), 2.78–2.55 (m, 4H, H₂-C3 and H₂-C2), 1.42 (s, 9H, (CH₃)₃C).

¹³C NMR (75 MHz, CHCl₃) δ = 204.4 (s, 1C, C4), 173.0 (s, 1C, C1), 155.8 (s, 1C, carbamate C=O), 80.0 (Me₃C), 52.0 (s, 1C, ester CH₃), 50.4 (s, 1C, C5), 34.5 (s, 1C, C3), 28.4 (s, 3C, (CH₃)₃C), 27.7 (s, 1C, C2).

1.7.4.10 5-((*tert*-Butoxycarbonyl)amino)-4-oxopentanoic acid (25**)^[292]**

In a 500 mL round-bottom flask, equipped with a Teflon[®]-coated magnetic stirring bar, **24** (7.010 g, 28.50 mmol, 1.00 eq) was added into a 0.1 M sodium phosphate buffer of pH = 8.0 (143 mL). The reaction mixture was stirred at 600 rpm and RT, and porcine liver esterase (0.114 g, 15.0 unit/mg) was added. After each 24 h, the mixture was adjusted to pH=8.0 with 5 M NaOH. After 7 d, full conversion was indicated by TLC. The reaction mixture was extracted with EtOAc (3×60 mL) and these organic extracts were discarded. The aqueous layer was acidified to pH=2 with 20% HCl and extracted with EtOAc (4×150 mL). The combined organic extracts were washed with water (150 mL) and brine (150 mL), dried over Na₂SO₄, concentrated under reduced pressure, and dried *in vacuo*. The residue was triturated with Et₂O (150 mL) and subsequently collected by filtration and dried *in vacuo* to afford **25** (4.803 g, 20.77 mmol, 73%) as a white solid.

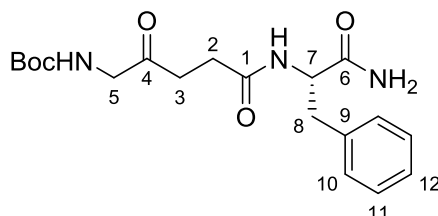
Yield: 4.803 g (20.77 mmol, 73%), white solid.

R_f = 0.31 (cyclohexane/EtOAc/AcOH 1:3:0.01 (v/v); staining: KMnO₄).

¹H NMR (300 MHz, CHCl₃) δ = 9.14 (br s, 1H, COOH), 6.09 and 5.28 (br s, 1H, carbamate H), 4.15–3.87 (m, 2H, H₂-C5), 2.84–2.56 (m, 4H, H₂-C3 and H₂-C2), 1.43 (s, 9H, (CH₃)₃C).

¹³C APT NMR (75 MHz, CHCl₃) δ = 204.4 (s, 1C, C4), 177.4 (s, 1C, C1), 156.0 (s, 1C, carbamate C=O), 80.2 (Me₃C), 50.4 (s, 1C, C5), 34.3 (s, 1C, C3), 28.4 (s, 3C, (CH₃)₃C), 27.7 (s, 1C, C2).

1.7.4.11 *tert*-Butyl *N*-(4-[[*(1S)*-1-carbamoyl-2-phenylethyl]carbamoyl]-2-oxobutyl)carbamate (26**)**



26

In a 50 mL nitrogen-purged Schlenk tube, equipped with a Teflon[®]-coated magnetic stirring bar, **25** (463 mg, 2.00 mmol, 1.00 eq) and HCl×H-Phe-NH₂ (803 mg, 4.00 mmol, 2.00 eq) were dissolved in absolute DMF (13.3 mL). The solution was cooled to 0 °C in an ice bath, and Hünig's base (1.397 mL, 8.00 mmol, 4.00 eq) and TBTU (939 mg, 2.93 mmol, 1.50 eq) were added in immediate succession. The cooling bath was removed and the mixture was stirred for 50 min at RT. The reaction was quenched by addition of brine (13 mL), and extracted with EtOAc (40 mL). The organic layer was washed with brine (2×13 mL), 1 M HCl (13 mL), brine (13 mL), dried over Na₂SO₄, and concentrated and dried under reduced pressure. Purification via flash chromatography (SiO₂, CH₂Cl₂/MeOH 20:1 to 15:1) afforded **26** (510 mg, 1.35 mmol, 68%) as a white solid.

Yield: 510 mg (1.35 mmol, 68%), white solid.

m.p. = 140–141 °C.

$[\alpha]_D^{23} = -2.3^\circ$ (c = 1.15, DMSO).

$R_f = 0.35$ (CH₂Cl₂/MeOH 10:1 (v/v); staining: KMnO₄).

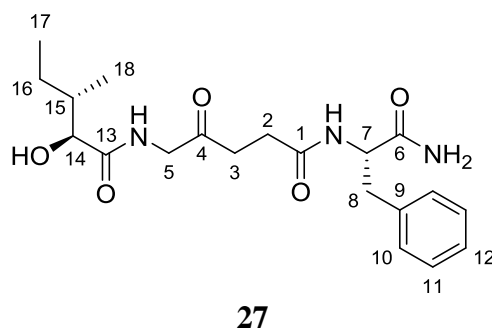
¹H NMR (300 MHz, DMSO-d₆, based on COSY and HSQC) $\delta = 8.06$ (d, ³J = 8.4 Hz, 1H, C7–NH), 7.36 (s, 1H, C6–NHH), 7.32–7.12 (m, 5H, H–Ar), 7.11–6.94 (m, 2H, C6–NHH and C5–NH), 4.48–4.30 (m, 1H, H–C7), 3.72 (d, ³J = 5.7 Hz, 2H, H–C5), 3.00 (dd, ²J = 13.6 Hz, ³J = 4.3

Hz, 1H, H_a-C8), 2.73 (dd, ²J = 13.6 Hz, ³J = 9.9 Hz, 1H, H_b-C8), 2.56–2.47 (m, 2H, H₂-C3), 2.41–2.14 (m, 2H, H₂-C2), 1.37 (s, 9H, (CH₃)₃CO).

¹³C NMR (75 MHz, DMSO-d₆, based on COSY and HSQC) δ = 206.6 (s, 1C, C4), 173.1 (s, 1C, C=O), 170.9 (s, 1C, C=O), 155.7 (s, 1C, carbamate C=O), 138.2 (s, 1C, C9), 129.1 (s, 2C, C11), 128.0 (s, 2C, C10), 126.2 (s, 1C, C12), 78.1 (s, 1C, Me₃C), 53.8 (s, 1C, C7), 49.5 (s, 1C, C5), 37.6 (s, 1C, C8), 34.2 (s, 1C, C3), 28.7 (s, 1C, C2), 28.2 (s, 3C, (CH₃)₃CO).

HRMS (ESI): m/z (%): 400.1848 (24%, [M + Na]⁺, calcd for C₁₉H₂₇N₃NaO₅⁺: 400.1843), 777.3802 (100%, [2M + Na]⁺, calcd for C₃₈H₅₄N₆NaO₁₀⁺: 777.3794).

1.7.4.12 (2*S*,3*S*)-*N*-(4-[[*(1S)*-1-Carbamoyl-2-phenylethyl]carbamoyl]-2-oxobutyl)-2-hydroxy-3-methylpentanamide (**27**)



Preparation of a solution of anhydrous HCl in MeOH: In a 10 mL nitrogen-purged Schlenk tube, equipped with a Teflon[®]-coated magnetic stirring bar, 1.0 mL of absolute MeOH was cooled to 0 °C in an ice bath. AcCl (440 μL, 6.16 mmol) was added dropwise via syringe, and the solution was stirred for 4 h at 0 °C before further use.

Deprotection: In a 5 mL glass vial, equipped with a Teflon[®]-coated magnetic stirring bar, **26** (38 mg, 0.10 mmol, 1.00 eq) was dissolved in EtOAc (200 μL). To the stirred solution the freshly prepared anhydrous solution of HCl in MeOH (70 μL) was added and the reaction mixture was stirred for 10 min, when the full conversion was indicated by TLC. The solution was

concentrated under reduced pressure and dried under high vacuum to constant mass yielding the deprotected intermediate as a white solid.

Coupling: In a 10 mL nitrogen-purged Schlenk tube, equipped with a Teflon[®]-coated magnetic stirring bar, **20** (14 mg, 0.11 mmol, 1.1 eq) and the deprotected intermediate were dissolved in absolute DMF (0.99 mL). Hünig's base (52 μ L, 0.30 mmol, 3.0 eq) was added and the solution was cooled to 0 °C in an ice bath. Subsequently, HATU (156 mg, 0.41 mmol, 1.1 eq) was added, the cooling bath removed, and the mixture was stirred for 60 min at RT. The reaction solution was quenched by addition of brine (1.0 mL) and extracted with EtOAc (4 mL). The organic layer was washed with brine (3 \times 1.0 mL), concentrated and dried under reduced pressure. The residue was dissolved in DMSO (200 μ L), diluted with acetonitrile (400 μ L) and water (600 μ L), and purified via reversed phase preparative HPLC (method: JKV_NucleodurC18_001HCOOH_sulfonamides) to furnish **27** (6.2 mg, 0.016 mmol, 16% in 2 steps) as a white solid.

Yield: 6.2 mg (0.016 mmol, 16% in 2 steps), white solid.

m.p. = 123–126 °C.

$[\alpha]_D^{23} = -17.7^\circ$ (c = 0.27, DMSO).

$R_f = 0.21$ (CH₂Cl₂/MeOH 10:1 (v/v); staining: KMnO₄).

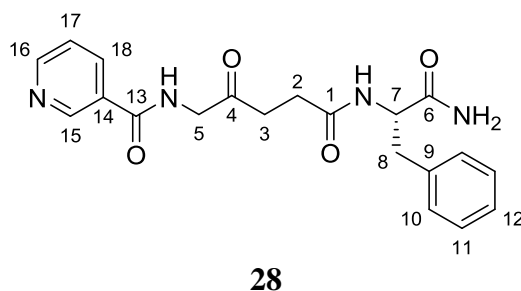
¹H NMR (300 MHz, DMSO-d₆, based on COSY and HSQC) $\delta = 8.06$ (d, ³J = 8.3 Hz, 1H, C7–NH), 7.89 (t, ³J = 5.3 Hz, 1H, C5–NH), 7.36 (s, 1H, C6–NHH), 7.32–7.09 (m, 5H, H–Ar), 7.05 (s, 1H, C6–NHH), 5.50 (br s, 1H, OH), 4.48–4.30 (m, 1H, H–C7), 3.91 (d, ³J = 5.3 Hz, 1H, H–C5), 3.76 (br s, 1H, H–C14), 2.99 (dd, ³J = 13.4 Hz, 4.4 Hz 1H, H_a–C8), 2.73 (dd, ³J = 13.4 Hz, 9.8 Hz 1H, H_b–C8), 2.60–2.50 (m, 2H, H₂–C3), 2.42–2.15 (m, 2H, H₂–C2), 1.80–1.60 (m, 1H, H–C15), 1.45–1.27 (m, 1H, H_a–C16), 1.19–1.01 (m, 1H, H_b–C16), 0.88 (d, ³J = 6.8 Hz, 3H, H–C17), 0.80 (t, ³J = 7.4 Hz, 3H, H–C17).

¹³C NMR (75 MHz, DMSO-d₆, based on COSY and HSQC) $\delta = 205.8$ (s, 1C, C4), 173.5 (s, 1C, C=O), 173.1 (s, 1C, C=O), 170.9 (s, 1C, C=O), 138.2 (s, 1C, C9), 129.1 (s, 2C, C11), 128.0 (s, 2C, C10), 126.2 (s, 1C, C12), 75.0 (s, 1C, C14), 53.8 (s, 1C, C7), 48.1 (s, 1C, C5), 38.1 (s, 1C,

C15), 37.6 (s, 1C, C8), 34.5 (s, 1C, C3), 28.7 (s, 1C, C2), 23.1 (s, 1C, C16), 15.6 (s, 1C, C18), 11.8 (s, 1C, 17).

HRMS (ESI): m/z (%): 392.2184 (14%, $[M + 1]^+$, calcd for $C_{20}H_{30}N_3O_5^+$: 392.2180), 414.2002 (50%, $[M + Na]^+$, calcd for $C_{20}H_{29}N_3NaO_5^+$: 414.1999).

1.7.4.13 *N*-[(1*S*)-1-Carbamoyl-2-phenylethyl]-4-oxo-5-(pyridin-3-ylformamido)pentanamide (28)



Preparation of a solution of anhydrous HCl in MeOH: In a 10 mL nitrogen-purged Schlenk tube, equipped with a Teflon[®]-coated magnetic stirring bar, 1.0 mL of absolute MeOH was cooled to 0 °C in an ice bath. AcCl (440 μ L, 6.16 mmol) was added dropwise via syringe, and the solution was stirred for 4 h at 0 °C before further use.

Deprotection: In a 5 mL glass vial, equipped with a Teflon[®]-coated magnetic stirring bar, **26** (38 mg, 0.10 mmol, 1.00 eq) was dissolved in EtOAc (200 μ L). The anhydrous solution of HCl in MeOH (70 μ L) was added and the reaction solution was stirred for 10 min, when full conversion was indicated by TLC. The solution was concentrated under reduced pressure and dried under high vacuum to constant mass yielding the deprotected intermediate as a white solid.

Coupling: In a 10 mL nitrogen-purged Schlenk tube, equipped with a Teflon[®]-coated magnetic stirring bar, nicotinic acid (13 mg, 0.11 mmol, 1.1 eq) and the deprotected intermediate were dissolved in absolute DMF (0.99 mL). Hünig's base (69 μ L, 0.40 mmol, 4.0 eq) was added and the solution was cooled to 0 °C in an ice bath. Subsequently, HATU (41 mg, 0.11 mmol, 1.1 eq)

was added, the cooling bath removed, and the mixture was stirred for 60 min at RT. The reaction solution was quenched by addition of brine (1.0 mL) and extracted with EtOAc (4 mL). The organic layer was washed with brine (3×1.0 mL), concentrated and dried under reduced pressure. The residue was dissolved in DMSO (200 μ L), diluted with acetonitrile (400 μ L) and water (600 μ L), and purified via reverse phase preparative HPLC (method: JKV_NucleodurC18_001HCOOH_sulfonamides) to furnish **28** (1.5 mg, 0.039 mmol, 4% in 2 steps) as a white solid.

Yield: 1.5 mg (0.039 mmol, 4% in 2 steps), white solid.

m.p. = 148 °C, decomposition.

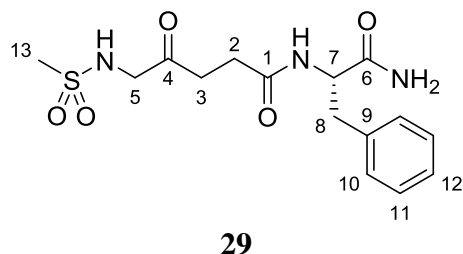
$[\alpha]_D^{23} = -2.0^\circ$ (c = 0.15, DMSO).

$R_f = 0.32$ (CH₂Cl₂/MeOH 10:1 (v/v); staining: KMnO₄).

¹H NMR (500 MHz, DMSO-d₆, based on COSY and HSQC) $\delta = 9.02$ (s, 1H, H-C15), 8.98 (t, ³J = 5.6 Hz, 1H, C5-NH), 8.72 (d, ³J = 4.8 Hz, 1H, H-C16), 8.20 (d, ³J = 8.0 Hz, 1H, H-C18), 8.05 (d, ³J = 8.5 Hz, 1H, C7-NH), 7.52 (dd, ³J = 8.0, 4.8 Hz, 1H, H-C17), 7.37 (s, 1H, C6-NHH), 7.28–7.12 (m, 5H, phenyl H-Ar), 7.02 (s, 1H, C6-NHH), 4.43–4.35 (m, 1H, H-C7), 4.11 (d, ³J = 5.7 Hz, 2H, H₂-C5), 3.00 (dd, ²J = 13.8 Hz, ³J = 4.8 Hz, 1H, H_a-C8), 2.74 (dd, ²J = 13.8 Hz, ³J = 9.6 Hz, 1H, H_b-C8), 2.66–2.56 (m, 2H, H₂-C3), 2.38 (dt, ²J = 15.7 Hz, ³J = 7.1 Hz, 1H, H_a-C2), 2.28 (dt, ²J = 15.7 Hz, ³J = 7.1 Hz, 1H, H_b-C2).

¹³C NMR (125 MHz, DMSO-d₆, based on COSY and HSQC) $\delta = 205.6$ (s, 1C, C4), 173.1 (s, 1C, C=O), 170.9 (s, 1C, C=O), 165.0 (s, 1C, C13), 152.1 (s, 1C, C15), 148.4 (s, 1C, C16), 138.2 (s, 1C, C9), 135.0 (s, 1C, C18), 129.3 (s, 1C, C14), 129.1 (s, 2C, C11), 128.0 (s, 2C, C10), 126.1 (s, 1C, C12), 123.5 (s, 1C, C17), 53.8 (s, 1C, C7), 48.8 (s, 1C, C5), 40.4–39.5 (1C, C8, indicated in HSQC and overlapped by the solvent signal in ¹H spectrum), 34.5 (s, 1C, C3), 28.8 (s, 1C, C2).

HRMS (ESI): m/z (%): 383.1722 (5%, [M + 1]⁺, calcd for C₂₀H₂₃N₄O₄⁺: 383.1714), 405.1534 (42%, [M + Na]⁺, calcd for C₂₀H₂₂N₄NaO₄⁺: 405.1533).

**1.7.4.14 N-[(1S)-1-Carbamoyl-2-phenylethyl]-5-methanesulfonamido-4-oxopentanamide
(29)**

Preparation of a solution of anhydrous HCl in MeOH: In a 10 mL nitrogen-purged Schlenk tube, equipped with a Teflon[®]-coated magnetic stirring bar, 1.0 mL of absolute MeOH was cooled to 0 °C in an ice bath. AcCl (440 µL, 6.16 mmol) was added dropwise via syringe, and the solution was stirred for 4 h at 0 °C before further use.

Deprotection: In a 5 mL glass vial, equipped with a Teflon[®]-coated magnetic stirring bar, **26** (38 mg, 0.10 mmol, 1.00 eq) was dissolved in EtOAc (200 µL). The anhydrous solution of HCl in MeOH (70 µL) was added and the reaction solution was stirred for 10 min, when full conversion was indicated by TLC. The solution was concentrated under reduced pressure and dried under high vacuum to constant mass yielding the deprotected intermediate as a white solid.

Sulfonamide preparation: In a 5 mL glass vial, equipped with a Teflon[®]-coated magnetic stirring bar, the deprotected intermediate was suspended in absolute CH₂Cl₂ (0.99 mL). The mixture was cooled to 0 °C in an ice bath and Hünig's base (34 µL, 0.20 mmol, 2.0 eq) was added. Subsequently, an aliquot (500 µL, 0.10 mmol, 1.0 eq) of a stock solution of methanesulfonyl chloride (30 µL, 0.40 mmol) in abs. CH₂Cl₂ (2.00 mL) was added dropwise via syringe. The cooling bath was removed and the mixture was stirred for 30 min at RT. The reaction solution was concentrated and dried under reduced pressure. The residue was dissolved in DMSO (200 µL), diluted with acetonitrile (400 µL) and water (600 µL), and purified via reversed phase preparative HPLC (method: JKV_NucleodurC18_001HCOOH_sulfonamides) to furnish **29** (6.3 mg, 0.018 mmol, 18% in 2 steps) as a white solid.

Yield: 6.3 mg (0.018 mmol, 18% in 2 steps), white solid.

m.p. = 190–191 °C.

$[\alpha]_D^{23} = -11.2^\circ$ (c = 0.32, DMSO).

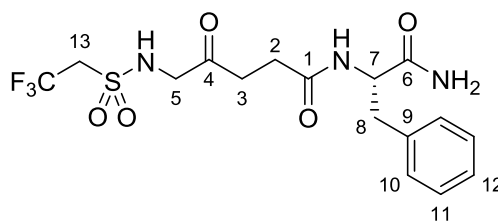
$R_f = 0.24$ (CH₂Cl₂/MeOH 10:1 (v/v); staining: KMnO₄).

¹H NMR (500 MHz, DMSO-d₆, based on COSY and HSQC) $\delta = 8.05$ (d, ³J = 8.4 Hz, 1H, C7–NH), 7.35 (s, 1H, C6–NH), 7.32–7.15 (m, 6H, H–Ar and SO₂NH), 7.02 (s, 1H, C6–NH), 4.44–4.34 (m, 1H, H–C7), 3.90 (d, ³J = 4.6 Hz, 2H, H₂–C5), 3.00 (dd, ²J = 13.7 Hz, ³J = 4.8 Hz, 1H, H_a–C8), 2.87 (s, 3H, H₃–C13), 2.74 (dd, ²J = 13.7 Hz, ³J = 9.5 Hz, 1H, H_b–C8), 2.55 (t, ³J = 6.9 Hz, 2H, H₂–C3), 2.42–2.34 (m, 1H, H_a–C2), 2.32–2.23 (m, 1H, H_b–C2).

¹³C NMR (125 MHz, DMSO-d₆, based on COSY and HSQC) $\delta = 205.6$ (s, 1C, C4), 173.1 (s, 1C, C=O), 170.9 (s, 1C, C=O), 138.1 (s, 1C, C9), 129.1 (s, 2C, C11), 128.0 (s, 2C, C10), 126.2 (s, 1C, C12), 53.8 (s, 1C, C7), 51.4 (s, 1C, C5), 40.2 (1C, C13, visible in HSQC and overlapped by the solvent signal in ¹H spectrum), 37.6 (s, 1C, C8), 34.2 (s, 1C, C3), 28.8 (s, 1C, C2).

HRMS (ESI): m/z (%): 378.1095 (13%, [M + Na]⁺, calcd for C₁₅H₂₁N₃NaO₅S⁺: 378.1094), 733.2302 (100%, [2M + Na]⁺, calcd for C₃₀H₄₂N₆NaO₁₀S₂⁺: 733.2296).

1.7.4.15 *N*-[(1*S*)-1-Carbamoyl-2-phenylethyl]-4-oxo-5-(2,2,2-trifluoroethanesulfonamido)pentanamide (30)



30

Preparation of a solution of anhydrous HCl in MeOH: In a 10 mL nitrogen-purged Schlenk tube, equipped with a Teflon[®]-coated magnetic stirring bar, 1.0 mL of absolute MeOH was cooled to 0

°C in an ice bath. AcCl (440 μ L, 6.16 mmol) was added dropwise via syringe, and the solution was stirred for 4 h at 0 °C before further use.

Deprotection: In a 5 mL glass vial, equipped with a Teflon[®]-coated magnetic stirring bar, **26** (38 mg, 0.10 mmol, 1.00 eq) was dissolved in EtOAc (200 μ L). The anhydrous solution of HCl in MeOH (70 μ L) was added and the solution was stirred for 10 min, when full conversion was indicated by TLC. The solution was concentrated under reduced pressure and dried under high vacuum to constant mass yielding the deprotected intermediate as a white solid.

Sulfonamide preparation: In a 5 mL glass vial, equipped with a Teflon[®]-coated magnetic stirring bar, the deprotected intermediate was suspended in absolute CH₂Cl₂ (0.99 mL). The mixture was cooled to 0 °C in an ice bath and Hünig's base (34 μ L, 0.20 mmol, 2.0 eq) was added. Subsequently, an aliquot (500 μ L, 0.10 mmol, 1.0 eq) of a stock solution of 2,2,2-trifluoromethanesulfonyl chloride (44 μ L, 0.40 mmol) in abs. CH₂Cl₂ (2.00 mL) was added dropwise via syringe. The cooling bath was removed, and the mixture was stirred for 30 min at RT. The reaction solution was concentrated and dried under reduced pressure. The residue was dissolved in DMSO (200 μ L), diluted with acetonitrile (400 μ L)/water (600 μ L), and purified via reversed phase preparative HPLC (method: JKV_NucleodurC18_001HCOOH_sulfonamides) to furnish **30** (5.5 mg, 0.013 mmol, 13% in 2 steps) as a white solid.

Yield: 6.3 mg (0.018 mmol, 18% in 2 steps), white solid.

m.p. = 180–182 °C.

$[\alpha]_D^{23} = -6.8^\circ$ (c = 0.28, DMSO).

$R_f = 0.27$ (CH₂Cl₂/MeOH 10:1 (v/v); staining: KMnO₄).

¹H NMR (500 MHz, DMSO-d₆, based on COSY and HSQC) $\delta = 8.19$ – 7.96 (m, 2H, SO₂NH and C7–NH), 7.38 (s, 1H, C6–NHH), 7.33–7.12 (m, 5H, H–Ar), 7.04 (s, 1H, C6–NHH), 4.47–4.25 (m, 3H, H–C7 and H₂–C13), 3.97 (br s, 2H, H₂–C5), 2.99 (dd, ²J = 13.8 Hz, ³J = 4.6 Hz, 1H, H_a–C8), 2.73 (dd, ²J = 13.8 Hz, ³J = 9.6 Hz, 1H, H_b–C8), 2.60–2.50 (m, 2H, H₂–C3), 2.42–2.20 (m, 2H, H₂–C2).

^{13}C NMR (125 MHz, DMSO- d_6 , based on COSY and HSQC) δ = 205.2 (s, 1C, C4), 173.1 (s, 1C, C=O), 170.9 (s, 1C, C=O), 138.1 (s, 1C, C9), 129.1 (s, 2C, C11), 128.0 (s, 2C, C10), 126.2 (s, 1C, C12), 53.8 (s, 1C, C7), 51.1 (s, 1C, C5), 37.6 (s, 1C, C8), 34.2 (s, 1C, C3), 28.8 (s, 1C, C2).

^{19}F NMR (470 MHz, DMSO- d_6) δ = -60.92 (CF_3).

HRMS (ESI): m/z (%): 446.0969 (11%, $[\text{M} + \text{Na}]^+$, calcd for $\text{C}_{16}\text{H}_{20}\text{F}_3\text{N}_3\text{NaO}_5\text{S}^+$: 446.0968), 869.2046 (100%, $[2\text{M} + \text{Na}]^+$, calcd for $\text{C}_{32}\text{H}_{40}\text{F}_6\text{N}_6\text{NaO}_{10}\text{S}_2^+$: 869.2044).

1.7.5 Synthesis of Chiral *N*-protected α -Amino Aldehydes via CDI/DIBAL-H Method

1.7.5.1 Purification of CDI (1,1'-carbonyldiimidazole)^[272]

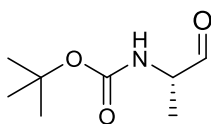
According to the procedure published by H. A. Staab and K. Wendel^[272] an oven dried 250 mL two-neck round-bottom flask with a Schlenk adapter, a reflux condenser, a gas bubbler and a magnetic stirring bar, were purged with N₂. In this flask 25.0 g (154 mmol) CDI were suspended in 40 mL abs. THF and stirred. The mixture was heated to reflux in an oil bath and 20 mL abs. THF were added to facilitate full dissolution. Stirring was stopped and the pale yellow solution was allowed to cool down to RT for 60 min. Crystallization was completed by cooling in an ice bath for 30 min. Subsequently, under nitrogen counter flow, the reflux condenser was removed and a fritted Schlenk funnel was mounted together with an additional receiving 250 mL two-neck round-bottom flask at the opposite end of the frit. White crystals were collected by filtration under inert atmosphere, washed with 15 mL of ice-cold abs. THF and dried *in vacuo*. 19.9 g (123 mmol, 80%) white crystalline solid were recovered and stored in a Schlenk flask under nitrogen atmosphere.

1.7.5.2 General procedure for one-pot conversion of *N*-protected α -amino acids to *N*-protected α -amino aldehydes

A 1000 mL two-neck round-bottom flask with a Schlenk adapter, a glass stopper and a magnetic stirring bar was heated, dried under vacuum and purged with N₂. 50.0 mmol (1.0 eq) protected amino acid were added and dissolved in 333 mL abs. DCM. The solution was cooled to 0 °C (ice bath) and 8.918 g (55.0 mmol, 1.1 eq) 1,1'-carbonyldiimidazole (CDI) were added. A gas bubbler was mounted instead of the glass stopper to allow pressure relief. After stirring for 60 min the gas bubbler was removed and the colorless reaction solution was cooled to -78 °C (CO₂/acetone bath) for 15 min. A septum was mounted instead of the glass stopper while maintaining a gentle

counter flow of N₂. Subsequently, 105 mL (105 mmol, 2.1 eq) DIBAL-H solution (1.0 M in toluene) were added dropwise with a syringe through the septum over 110 min. The reaction mixture was stirred at -78 °C until TLC indicated quantitative conversion (30–60 min). The reaction mixture was quenched by the addition of 335 mL EtOAc. The cooling bath was removed and a gas bubbler was mounted. Immediately, 222 mL tartaric acid solution (25 % in H₂O) were added dropwise to the mixture via a dropping funnel, under vigorous stirring. The mixture was warmed up by immersing the vessel into a water bath at RT and stirred vigorously for 15 min. The stirring was stopped and the layers were separated. The aqueous phase was extracted with EtOAc (1 x 333 mL) and the combined organic extracts were washed with 1 M HCl (1 x 222 mL), 0.8 M NaHCO₃ (1 x 222 mL) and brine (1 x 222 mL), dried over Na₂SO₄, filtered and concentrated under reduced pressure. The crude product was frozen in liquid nitrogen and was allowed to reach RT under high vacuum. The freeze-thaw procedure was repeated two times. The crude product was used without further purification.

1.7.5.3 *tert*-Butyl (*S*)-(1-oxopropan-2-yl)carbamate (**32**)^[311,365]



32

This compound was synthesized according to the general procedure using 9.460 g (50.0 mmol, 1.0 eq) Boc-L-Ala-OH. The colorless solution was treated with 8.918 g (55.0 mmol, 1.1 eq) CDI at 0 °C for 60 min, and subsequently, dropwise with 105 mL (105 mmol, 2.1 eq) DIBAL-H. The mixture was stirred for 45 min at -78 °C until TLC indicated full conversion. Extractive workup and drying provided 7.510 g (43.40 mmol, 87 %) of a white solid.

Yield: 7.510 g (43.40 mmol, 87 %), white solid.

m.p. = 81–84 °C, lit. 90–92 °C^[311] and 70 °C.^[365]

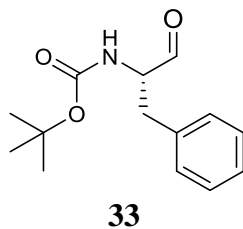
$[\alpha]_D^{23} = -39.0^\circ$ ($c = 1.0$, MeOH), lit. $[\alpha]_D^{20} = -40.9^\circ$ ($c = 1$, MeOH)³ and $[\alpha]_D^{\text{undisclosed}} = -39.1^\circ$ ($c = 0.69$, MeOH).^[365]

$R_f = 0.38$ (cyclohexane/ethyl acetate = 2:1 (v/v); staining: KMnO_4).

$^1\text{H NMR}$ (300 MHz, CDCl_3) $\delta = 9.55$ (s, 1H, CHO), 5.11-4.99 (m, 1H, NH), 4.30-4.12 (m, 1H, CHCHO), 1.44 (s, 9H, $(\text{CH}_3)_3\text{CO}$), 1.32 (d, $^3J = 7.4$ Hz, 3H, CHCH_3).

$^{13}\text{C NMR}$ (75 MHz, CDCl_3) $\delta = 199.9$ (s, 1C, CHO), 155.4 (s, 1C, C=O), 80.2 (s, 1C, Me_3C), 55.7 (s, 1C), 28.4 (s, 3C), 15.0 (s, 1C).

1.7.5.4 *tert*-Butyl (*S*)-(1-oxo-3-phenylpropan-2-yl)carbamate (**33**)^[366]



This compound was synthesized according to the general procedure using 53 mg (0.20 mmol, 1.0 eq) Boc-L-Phe-OH. The colorless solution was treated with 36 mg (0.22 mmol, 1.1 eq) CDI at 0 °C for 60 min, and subsequently, dropwise with 0.42 mL (0.42 mmol, 2.1 eq) DIBAL-H. The mixture was stirred for 60 min at -78 °C until TLC indicated full conversion. Extractive workup and drying provided 48 mg (0.19 mmol, 96 %) of a white solid.

Yield: 48 mg (0.19 mmol, 96 %), white solid.

m.p. = 80–84 °C, lit. 82 °C.^[366]

$[\alpha]_D^{23} = +39.3^\circ$ ($c = 1.02$, CH_2Cl_2), $[\alpha]_D^{\text{undisclosed}} = +41.6^\circ$ ($c = 1.1$, CH_2Cl_2).^[366]

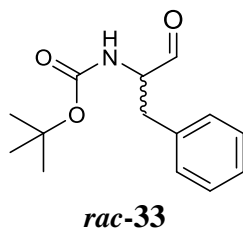
$R_f = 0.26$ (cyclohexane/ethyl acetate = 4:1 (v/v); staining: KMnO_4).

^1H NMR (300 MHz, CDCl_3) δ = 9.62 (s, 1H, CHO), 7.40–7.06 (m, 5H, Ar-H), 5.15–4.97 (m, 1H, NH), 4.50–4.32 (m, 1H, CHCHO), 3.22–2.98 (m, 2H, CH_2), 1.42 (s, 9H, $(\text{CH}_3)_3\text{CO}$).

^{13}C NMR (75 MHz, CDCl_3) δ = 199.5 (s, 1C, CHO), missing carbamate signal (155 ppm), 135.9 (s, 1C, C_q), 129.5 (s, 2C), 128.9 (s, 2C), 127.2 (s, 1C), 80.4 (s, 1C, Me_3C), 60.8 (s, 1C), 35.6 (s, 1C), 28.4 (s, 3C).

GC-FID (CP-Chiralsil Dex): t_R ((*S*)-**33**) = 38.2 min, 99.51%; t_R ((*R*)-**33**) = 38.2 min, 0.49%; ee > 99%.

1.7.5.5 Racemic *tert*-butyl (1-oxo-3-phenylpropan-2-yl)carbamate (*rac*-**33**)

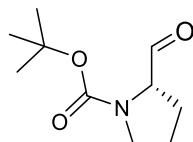


This compound was synthesized according to the general procedure using 53 mg (0.20 mmol, 1.0 eq) Boc-DL-Phe-OH. The colorless solution was treated with 36 mg (0.22 mmol, 1.1 eq) CDI at 0 °C for 60 min, and subsequently, dropwise with 0.42 mL (0.42 mmol, 2.1 eq) DIBAL-H. The mixture was stirred for 30 min at -78 °C until TLC indicated full conversion. Extractive workup and drying provided 46 mg (0.18 mmol, 90 %) of a white amorphous paste.

Yield: 48 mg (0.19 mmol, 96 %), white amorphous paste.

R_f = 0.26 (cyclohexane/ethyl acetate = 4:1 (v/v); staining: KMnO_4).

GC-FID (CP-Chiralsil Dex): t_R ((*S*)-**33**) = 38.3 min; t_R ((*R*)-**33**) = 39.5 min.

1.7.5.6 *tert*-Butyl (*S*)-2-formylpyrrolidine-1-carboxylate (34**)^[367]****34**

This compound was synthesized according to the general procedure using 86 mg (0.40 mmol, 1.0 eq) Boc-L-Pro-OH. The colorless solution was treated with 71 mg (0.44 mmol, 1.1 eq) CDI at 0 °C for 60 min, and subsequently, dropwise with 0.84 mL (0.84 mmol, 2.1 eq) DIBAL-H. The mixture was stirred for 60 min at -78 °C until TLC indicated full conversion. Extractive workup and drying provided 77 mg (0.39 mmol, 97 %) of a viscous colorless liquid.

Yield: 77 mg (0.39 mmol, 97 %), colorless liquid.

$[\alpha]_D^{23} = -97.9^\circ$ ($c = 1.02$, CHCl_3), lit. $[\alpha]_D^{24} = -96.1^\circ$ ($c = 0.6$, CHCl_3).^[367]

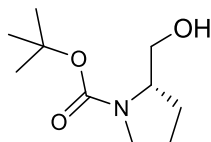
$R_f = 0.20$ (cyclohexane/ethyl acetate = 4:1 (v/v); staining: KMnO_4).

$^1\text{H NMR}$ (300 MHz, CDCl_3 , mixture of two rotamers) $\delta = 9.54$ and 9.44 (s, 1H, CHO), 4.24–4.15 and 4.10–3.99 (m, 1H, CHCHO), 3.62–3.38 (m, 2H, NCH_2), 2.21–1.73 (m, 4H, $\text{CH}_2\text{CH}_2\text{CH}$), 1.46 and 1.41 (s, 9H, $(\text{CH}_3)_3\text{CO}$).

$^{13}\text{C NMR}$ (75 MHz, CDCl_3) $\delta = 200.7$ and 200.5 (s, 1C, CHO), 155.0 and 154.1 (s, 1C, C=O), 80.8 and 80.3 (s, 1C, Me_3C), 65.1 and 65.0 (s, 1C), 47.0 and 46.9 (s, 1C), 28.5 and 28.4 (s, 3C), 28.1 and 26.8 (s, 1C), 24.7 and 24.1 (s, 1C).

Enantiomeric excess was determined indirectly by conversion of freshly isolated material into alcohol **44**.

1.7.5.7 *tert*-Butyl (2*S*)-2-(hydroxymethyl)pyrrolidine-1-carboxylate (**44**)^[368]

**44**

In a 5 mL glass vial equipped with a Teflon[®]-coated magnetic stirring bar 59 mg (0.27 mmol, 1.0 eq) freshly prepared compound **34** were dissolved in 4.0 mL MeOH, stirred and cooled to 0 °C in an ice bath. 17 mg (0.44 mmol, 1.1 eq) NaBH₄ were added to the colorless solution at 0 °C, the vial was covered with aluminium foil instead of a stopper to facilitate pressure relief. The mixture was stirred vigorously for 20 min at 0 °C, when TLC indicated full conversion. The reaction was quenched by the addition of 200 µL acetone and stirred for 5 min at RT. The solvents were removed under reduced pressure and the residue was partitioned between 3.0 mL EtOAc and 1.0 mL NaHCO₃ (sat). The organic phase was concentrated under reduced pressure and purified via flash chromatography (SiO₂, cyclohexane/EtOAc 2:1) to yield 50 mg (0.25 mmol, 93%) of a white solid.

Yield: 50 mg (0.25 mmol, 93%, 2 steps), white solid.

m.p. = 57–60 °C, lit. 58–59 °C.^[368]

$[\alpha]_D^{23} = -55.7^\circ$ (c = 0.83, CHCl₃), lit. $[\alpha]_D^{26} = -52.7^\circ$ (c = 1.05, CHCl₃).^[368]

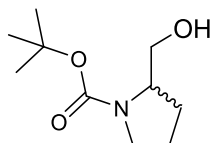
$R_f = 0.42$ (cyclohexane/ethyl acetate = 1:1 (v/v); staining: KMnO₄).

¹H NMR (300 MHz, CDCl₃) $\delta = 4.75$ (br s, 1H, OH), 4.01–3.81 (m, 1H, CH₂CHN), 3.68–3.49 (m, 2H, CH₂O), 3.49–3.36 (m, 1H, NCHH), 3.35–3.21 (m, 1H, NCHH), 2.07–1.49 (m, 4H, NCH₂CH₂CH₂), 1.45 (s, 9H, ((CH₃)₃C)).

¹³C NMR (75 MHz, CDCl₃) $\delta = 157.3$ (s, 1C, C=O), 80.3 (s, 1C, (CH₃)₃C), 67.8 (s, 1C), 60.3 (s, 1C), 47.7 (s, 1C), 28.8 (s, 1C), 28.6 (s, 3C), 24.4 (s, 1C).

HPLC (Daicel Chemical Technologies Chiralpak[®] AD-H): t_R ((*R*)-**44**) = 7.2 min, no abundance detected; t_R ((*S*)-**44**) = 8.4 min, 100%; ee >99%.

1.7.5.8 Racemic *tert*-butyl 2-(hydroxymethyl)pyrrolidine-1-carboxylate (**rac-44**)



rac-44

The aldehyde intermediate was synthesized according to the general procedure using 86 mg (0.400 mmol, 1.0 eq) Boc-DL-Pro-OH. The colorless solution was treated with 71 mg (0.440 mmol, 1.1 eq) CDI at 0 °C for 60 min, and subsequently, dropwise with 0.84 mL (0.84 mmol, 2.1 eq) 1 M DIBAL-H. The mixture was stirred for 60 min at -78 °C until TLC indicated full conversion. Extractive workup and drying provided 57 mg (0.29 mmol, 72%) of **rac-34** as a colorless oil.

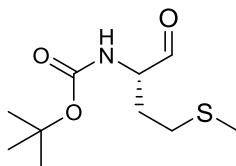
In a 5 mL glass vial equipped with a Teflon-coated magnetic stirring bar 57 mg (0.29 mmol, 1.0 eq) freshly prepared **rac-34** were dissolved in 4.0 mL MeOH, stirred and cooled to 0 °C in an ice bath. 17 mg (0.44 mmol, 1.1 eq) NaBH₄ were added to the colorless solution at 0 °C, the vial was covered with aluminium foil instead of a stopper to facilitate pressure relief. The mixture was stirred vigorously for 20 min at 0 °C, when TLC indicated full conversion. The reaction was quenched by the addition of 200 μL acetone and stirred for 5 min at RT. Solvents were removed under reduced pressure and the residue was partitioned between 3.0 mL EtOAc and 1.0 mL NaHCO₃ (sat). The organic extract was concentrated under reduced pressure and purified via flash chromatography (SiO₂, cyclohexane/EtOAc 2:1) to yield 43 mg (0.21 mmol, 53%, 2 steps) of a colorless oil.

Yield: 43 mg (0.21 mmol, 53%, 2 steps), colorless oil.

R_f = 0.42 (cyclohexane/ethyl acetate = 1:1 (v/v); staining: KMnO₄).

HPLC (Daicel Chemical Technologies Chiralpak[®] AD-H): t_R ((*R*)-**44**) = 7.2 min; t_R ((*S*)-**44**) = 8.4 min.

1.7.5.9 *tert*-Butyl (*S*)-(4-(methylthio)-1-oxobutan-2-yl)carbamate (**35**)^[369]



35

This compound was synthesized according to the general procedure using 100 mg (0.400 mmol, 1.0 eq) Boc-L-Met-OH. The colorless solution was treated with 71 mg (0.44 mmol, 1.1 eq) CDI at 0 °C for 60 min, and subsequently, dropwise with 0.84 mL (0.84 mmol, 2.1 eq) 1 M DIBAL-H. The mixture was stirred for 60 min at -78 °C until TLC indicated full conversion. Extractive workup and drying provided 86 mg (0.37 mmol, 96 %) of colorless oil.

Yield: 86 mg (0.37 mmol, 92 %), colorless oil.

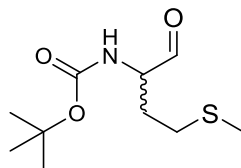
$[\alpha]_D^{23} = +27.0^\circ$ ($c = 1.74$, CH_2Cl_2), lit. $[\alpha]_D^{20} = +27.8^\circ$ ($c = 1$, CH_2Cl_2).^[369]

$R_f = 0.26$ (cyclohexane/ethyl acetate = 4:1 (v/v); staining: KMnO_4).

¹H NMR (300 MHz, CDCl_3) $\delta = 9.63$ (s, 1H, CHO), 5.29–5.13 (m, 1H, NH), 4.37–4.22 (m, 1H, CHCHO), 2.62–2.46 (m, 2H, SCH₂), 2.31–2.13 (m, 1H, NCHCH), 2.07 (s, 3H), 2.00–1.84 (m, 1H, NCHCH) 1.44 (s, 9H, (CH₃)₃CO).

¹³C NMR (75 MHz, CDCl_3) $\delta = 199.2$ (s, 1C, CHO), 155.7 (s, 1C, C=O), 80.4 (s, 1C, Me₃C), 59.2 (s, 1C), 30.0 (s, 1C), 28.9 (s, 1C), 28.4 (s, 3C), 15.5 (s, 1C).

GC-FID (CP-Chiralsil Dex): t_R ((*S*)-**35**) = 14.2 min, 100%; t_R ((*R*)-**35**) = 14.4 min, no abundance detected; ee >99%.

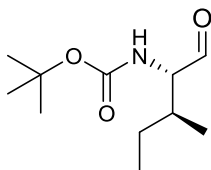
1.7.5.10 Racemic *tert*-butyl (4-(methylthio)-1-oxobutan-2-yl)carbamate (rac-35)**rac-35**

This compound was synthesized by mixing 50 mg (0.20 mmol, 0.5 eq) Boc-L-Met-OH and 50 mg (0.20 mmol, 0.5 eq) Boc-D-Met-OH, and converting the mixture according to the general procedure. The colorless solution was treated with 71 mg (0.44 mmol, 1.1 eq) CDI at 0 °C for 60 min, and subsequently, dropwise with 0.84 mL (0.84 mmol, 2.1 eq) DIBAL-H. The mixture was stirred for 30 min at -78 °C until TLC indicated full conversion. Extractive workup and drying provided 89 mg (0.38 mmol, 95 %) of a colorless oil.

Yield: 89 mg (0.38 mmol, 95 %), colorless oil.

$R_f = 0.26$ (cyclohexane/ethyl acetate = 4:1 (v/v); staining: KMnO_4).

GC-FID (CP-Chiralsil Dex): t_R ((*S*)-**35**) = 14.2 min; t_R ((*R*)-**35**) = 14.4 min.

1.7.5.11 *tert*-Butyl ((2*S*,3*S*)-3-methyl-1-oxopentan-2-yl)carbamate (36**)^[366]****36**

This compound was synthesized according to the general procedure using 185 mg (0.800 mmol, 1.0 eq) Boc-L-Ile-OH. The colorless solution was treated with 143 mg (0.880 mmol, 1.1 eq) CDI

at 0 °C for 60 min, and subsequently, dropwise with 1.68 mL (1.68 mmol, 2.1 eq) 1 M DIBAL-H. The mixture was stirred for 60 min at -78 °C until TLC indicated full conversion. Extractive workup and drying provided 156 mg (0.725 mmol, 91 %) of a colorless turbid oil.

Yield: 156 mg (0.725 mmol, 91 %), colorless turbid oil.

$[\alpha]_D^{23} = +87.1^\circ$ (c = 0.93, CH₂Cl₂), lit. $[\alpha]_D^{undisclosed} = +85.0^\circ$.^[366]

$R_f = 0.39$ (cyclohexane/ethyl acetate = 4:1 (v/v); staining: KMnO₄).

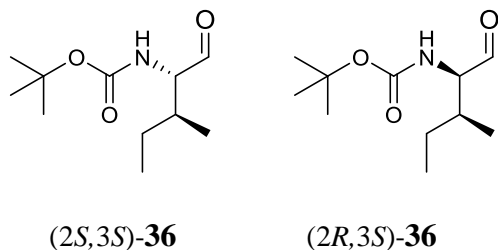
¹H NMR (300 MHz, CDCl₃) $\delta = 9.64$ (s, 1H, CHO), 5.23–4.97 (m, 1H, NH), 4.36–4.11 (m, 1H, CHCHO), 2.08–1.86 (m, 1H), 1.55–1.33 (m, 10H, (CH₃)₃CO and CH₃CHH), 1.32–1.12 (m, 1H, CH₃CHH), 1.03–0.79 (m, 6H, 2CH₃).

¹³C APT NMR (75 MHz, CDCl₃) $\delta = 200.8$ (s, 1C, CHO), 155.9 (s, 1C, C=O), 80.0 (s, 1C, Me₃C), 64.3 (s, 1C), 36.5 (s, 1C), 28.4 (s, 3C), 25.4 (s, 1C), 15.8 (s, 1C), 12.00 (s, 1C).

GC-EI-MS: t_R ((2*S*,3*S*)-**36**) = 6.09 min; $m/z = 57$ (100%), 69 (9%), 86 (47%), 112 (3%), 130 (29%), 142 (2%), 186 (2%).

GC-FID (CP-Chiralsil Dex): t_R ((2*R*,3*S*)-**36**) = 10.0 min, 0.46%; t_R ((2*S*,3*S*)-**36**) = 10.1 min, 99.54%; de = >99%.

1.7.5.12 Partial epimerization of *tert*-butyl ((2*S*,3*S*)-3-methyl-1-oxopentan-2-yl)carbamate ((2*S*,3*S*)-**36**) to *tert*-butyl ((2*R*,3*S*)-3-methyl-1-oxopentan-2-yl)carbamate ((2*R*,3*S*)-**36**)



In a 10 mL Schlenk tube 50 mg (0.23 mmol) crude freshly prepared **36** were dissolved in 2.0 mL cyclohexane/EtOAc 4:1. The solution was vigorously stirred with a Teflon-coated magnetic stirring bar and 1.0 g of silica was added. The mixture was immediately purged by three cycles of alternate evacuation to the point of gentle boiling and filling with nitrogen atmosphere. The colorless gel-like mixture was stirred for 45 h at RT. Subsequently, the mixture was concentrated and dried under reduced pressure. Filtration through a short pad of silica (SiO₂, cyclohexane/EtOAc 6:1) provided 47 mg (0.22 mmol, 96%) of a colorless oil.

Yield: 47 mg (0.22 mmol, 96%), colorless oil.

$[\alpha]_D^{23} = +26.1^\circ$ (c = 1.40, CHCl₃).

$R_f = 0.39$ (cyclohexane/ethyl acetate = 4:1 (v/v); staining: KMnO₄).

¹H NMR (300 MHz, CDCl₃, (2*R*,3*S*)-epimer, based on HSQC) $\delta = 9.60$ (s, 1H, CHO), 5.10–4.92 (m, 1H, NH), 4.41–4.31 (m, 1H, CHCHO), 2.10–1.86 (m, 1H), 1.55–1.36 (m, 10H, (CH₃)₃CO and CH₃CHH), 1.34–1.14 (m, 1H, CH₃CHH), 1.00–0.79 (m, 6H, 2CH₃).

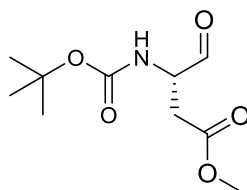
¹³C NMR (75 MHz, CDCl₃, (2*R*,3*S*)-epimer, based on HSQC) $\delta = 200.8$ (s, 1C, CHO), 156.0 (s, 1C, C=O), 80.1 (s, 1C, Me₃C), 63.3 (s, 1C), 35.3 (s, 1C), 28.4 (s, 3C), 26.4 (s, 1C), 14.6 (s, 1C), 12.00 (s, 1C).

GC-EI-MS:

t_R ((2*R*,3*S*)-**36**) = 6.04 min, 26.5%, $m/z = 57$ (100%), 69 (10%), 86 (56%), 112 (4%), 130 (36%), 142 (3%), 186 (4%);

t_R ((2*S*,3*S*)-**36**) = 6.08 min, 73.5%; $m/z = 57$ (100%), 69 (10%), 86 (57%), 112 (3%), 130 (36%), 142 (3%), 186 (4%).

GC-FID (CP-Chiralsil Dex): t_R ((2*R*,3*S*)-**36**) = 10.0 min, 31.58%; t_R ((2*S*,3*S*)-**36**) = 10.1 min, 68.42%.

1.7.5.13 Methyl (S)-3-((tert-butoxycarbonyl)amino)-4-oxobutanoate (37)^[369]**37**

This compound was synthesized according to the general procedure using 356 mg (1.44 mmol, 1.0 eq) Boc-L-Asp(OMe)-OH. The colorless solution was treated with 257 mg (1.58 mmol, 1.1 eq) CDI at 0 °C for 60 min, and subsequently, dropwise with 3.02 mL (3.02 mmol, 2.1 eq) 1 M DIBAL-H. The mixture was stirred for 60 min at -78 °C until TLC indicated full conversion. Extractive workup and drying provided 295 mg of a colorless turbid oil. Purification via flash chromatography (SiO₂, cyclohexane/EtOAc 4:1) furnished 206 mg (0.893 mmol, 62 %) of the desired aldehyde as a colorless oil.

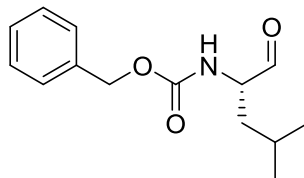
Yield: 206 mg (0.893 mmol, 62 %), colorless oil.

$[\alpha]_D^{23} = -16.9^\circ$ (c = 0.92, CHCl₃).

$R_f = 0.28$ (cyclohexane/ethyl acetate = 2:1 (v/v); staining: KMnO₄).

¹H NMR (300 MHz, CDCl₃) $\delta = 9.64$ (s, 1H, CHO), 5.72–5.52 (m, 1H, NH), 4.44–4.25 (m, 1H, CHCHO), 3.69 (s, 3H), 3.08–2.91 (m, 1H, COCHH), 2.90–2.74 (m, 1H, COCHH), 1.45 (s, 9H, (CH₃)₃CO).

¹³C NMR (75 MHz, CDCl₃) $\delta = 199.3$ (s, 1C, CHO), 171.8 (s, 1C, C=O), 155.6 (s, 1C, C=O), 80.7 (s, 1C, Me₃C), 56.1 (s, 1C), 52.3 (s, 1C), 34.5 (s, 1C), 28.4 (s, 3C).

1.7.5.14 Benzyl (*S*)-(4-methyl-1-oxopentan-2-yl)carbamate (**38**)^[321]**38**

This compound was synthesized according to the general procedure using 212 mg (0.800 mmol, 1.0 eq) Boc-L-Leu-OH. The colorless solution was treated with 143 mg (0.880 mmol, 1.1 eq) CDI at 0 °C for 60 min, and subsequently, dropwise with 1.68 mL (1.68 mmol, 2.1 eq) 1 M DIBAL-H. The mixture was stirred for 60 min at -78 °C until TLC indicated full conversion. Extractive workup and drying provided 174 mg (0.698 mmol, 87 %) of a colorless oil.

Yield: 174 mg (0.698 mmol, 87 %), colorless oil.

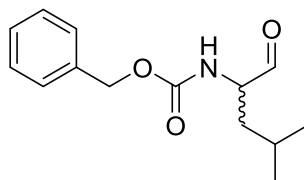
$[\alpha]_D^{23} = -41.7^\circ$ (c = 1.60, MeOH), $[\alpha]_D^{25} = -22.8^\circ$ (c = 0.74, MeOH).^[321]

$R_f = 0.58$ (cyclohexane/ethyl acetate = 1:1 (v/v); staining: KMnO_4).

$^1\text{H NMR}$ (300 MHz, CDCl_3 , based on HSQC) $\delta = 9.59$ (s, 1H, CHO), 7.47–7.20 (m, 5H, Ar-H), 5.30–5.16 (m, 1H, NH), 5.12 (s, 2H), 4.41–4.25 (m, 1H, CHCHO), 1.87–1.53 (m, 2H, $(\text{CH}_3)_2\text{CH}$ and NCHCHH), 1.51–1.30 (m, 1H, NCHCHH), 1.05–0.77 (m, 6H, 2 CH_3).

$^{13}\text{C NMR}$ (75 MHz, CDCl_3) $\delta = 199.8$ (s, 1C, CHO), 156.3 (s, 1C, C=O), 136.3 (s, 1C, C_q), 128.7 (s, 2C), 128.4 (s, 1C), 128.2 (s, 2C), 67.3 (s, 1C), 59.0 (s, 1C), 38.3 (s, 1C), 24.8 (s, 1C), 23.2 (s, 1C), 22.0 (s, 1C).

GC-FID (CP-Chiralsil Dex): t_R (*(S)*-**38**) = 24.5 min, 99.24%; t_R (*(R)*-**38**) = 25.0 min, 0.76%; ee >98%.

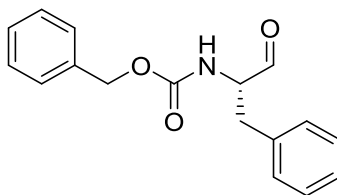
1.7.5.15 Racemic benzyl (4-methyl-1-oxopentan-2-yl)carbamate (rac-38)**rac-38**

This compound was synthesized according to the general procedure using 53 mg (0.20 mmol, 1.0 eq) Cbz-DL-Leu-OH. The colorless solution was treated with 36 mg (0.22 mmol, 1.1 eq) CDI at 0 °C for 60 min, and subsequently, dropwise with 0.42 mL (0.42 mmol, 2.1 eq) 1 M DIBAL-H. The mixture was stirred for 60 min at -78 °C until TLC indicated full conversion. Extractive workup and drying provided 43 mg (0.17 mmol, 85 %) of a colorless oil.

Yield: 43 mg (0.17 mmol, 85 %), colorless oil.

R_f = 0.58 (cyclohexane/ethyl acetate = 1:1 (v/v); staining: KMnO_4).

GC-FID (CP-Chiralsil Dex): t_R ((*S*)-**38**) = 24.5 min, t_R ((*R*)-**38**) = 25.0 min.

1.7.5.16 Benzyl (*S*)-(1-oxo-3-phenylpropan-2-yl)carbamate (39**)^[311]****39**

This compound was synthesized according to the general procedure using 239 mg (0.800 mmol, 1.0 eq) Cbz-L-Phe-OH. The colorless solution was treated with 143 mg (0.880 mmol, 1.1 eq) CDI at 0 °C for 60 min, and subsequently, dropwise with 1.68 mL (1.68 mmol, 2.1 eq) of 1 M

DIBAL-H. The mixture was stirred for 60 min at $-78\text{ }^{\circ}\text{C}$ until TLC indicated full conversion. Extractive workup and drying provided 225 mg (0.794 mmol, 99 %) of a white solid.

Yield: 225 mg (0.794 mmol, 99 %), white solid.

m.p. = $76\text{--}79\text{ }^{\circ}\text{C}$, lit. $77\text{--}79\text{ }^{\circ}\text{C}$.^[311]

$[\alpha]_D^{23} = +43.7\text{ }^{\circ}$ ($c = 0.56$, CH_2Cl_2), lit. $[\alpha]_D^{20} = +44.5\text{ }^{\circ}$ ($c = 1$, CH_2Cl_2).^[311]

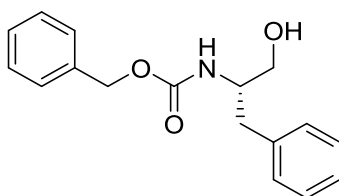
$R_f = 0.15$ (cyclohexane/ethyl acetate = 4:1 (v/v); staining: KMnO_4).

^1H NMR (300 MHz, CDCl_3) $\delta = 9.63$ (s, 1H, CHO), 7.44–7.02 (m, 10H, Ar-H), 5.39–5.22 (m, 1H, NH), 5.11 (s, 2H, CH_2O), 4.59–4.43 (m, 1H, CHCHO), 3.13 (d, $^3J = 6.3$ Hz, 2H, CH_2).

^{13}C APT NMR (75 MHz, CDCl_3) $\delta = 199.0$ (s, 1C, CHO), 156.0 (s, 1C, C=O), 136.2 (s, 1C, C_q), 135.5 (s, 1C, C_q), 129.4 (s, 2C), 129.0 (s, 2C), 128.7 (s, 1C), 128.4 (s, 1C), 128.3 (s, 2C), 127.3 (s, 1C), 67.3 (s, 1C), 61.2 (s, 1C), 35.5 (s, 1C).

Enantiomeric excess was determined indirectly by conversion of freshly isolated material into alcohol **45**.

1.7.5.17 Benzyl (S)-(1-hydroxy-3-phenylpropan-2-yl)carbamate (**45**)^[370,371]



45

In a 5 mL glass vial equipped with a Teflon[®]-coated magnetic stirring bar 42 mg (0.15 mmol, 1.0 eq) freshly prepared compound **39** were dissolved in 1.5 mL MeOH, stirred and cooled to $0\text{ }^{\circ}\text{C}$ in an ice bath. 27 mg (0.17 mmol, 1.1 eq) NaBH_4 were added to the colorless solution at $0\text{ }^{\circ}\text{C}$. The vial was covered with aluminium foil instead of a stopper to facilitate pressure relief. The mixture

was stirred vigorously for 20 min at 0 °C, when TLC indicated full conversion. The reaction was quenched by the addition of 200 μ L acetone and stirred for 5 min at RT. The solvents were removed under reduced pressure and the residue was partitioned between 3.0 mL EtOAc and 1.0 mL NaHCO₃ (sat). The organic phase was concentrated under reduced pressure and purified via flash chromatography (SiO₂, cyclohexane/EtOAc 2:1) to yield 38 mg (0.13 mmol, 86%) of a white solid.

Yield: 38 mg (0.13 mmol, 86%), white solid.

m.p. = 88–90 °C, lit. 90–91 °C. [371]

$[\alpha]_D^{23} = -23.2^\circ$ (c = 0.69, CHCl₃), lit. $[\alpha]_D^{19} = -28.5^\circ$ (c = 1.0, CHCl₃). [370]

$R_f = 0.37$ (cyclohexane/ethyl acetate = 1:1 (v/v); staining: KMnO₄).

¹H NMR (300 MHz, CDCl₃) $\delta = 7.42$ – 7.09 (m, 10H, Ar-H), 5.06 (s, 2H, CH₂OCO), 5.06–4.88 (m, 1H, NH), 4.02–3.84 (m, 1H, CHCH₂O), 3.67 (dd, ²J = 10.5 Hz, ³J = 2.7 Hz, 2H, NCHCHH), 3.56 (dd, ²J = 10.5 Hz, ³J = 4.4 Hz, 2H, NCHCHH), 2.85 (d, ³J = 7.0 Hz, 2H, CH₂OH), 2.08 (s, 1H, OH).

¹³C NMR (75 MHz, CDCl₃) $\delta = 156.6$ (s, 1C, C=O), 137.7 (s, 1C, C_q), 136.5 (s, 1C, C_q), 129.4 (s, 2C), 128.8 (s, 2C), 128.7 (s, 2C), 128.3 (s, 1C), 128.2 (s, 2C), 126.8 (s, 1C), 67.0 (s, 1C), 64.1 (s, 1C), 54.3 (s, 1C), 37.5 (s, 1C).

HPLC (Daicel Chemical Technologies Chiralpak[®] AD-H): t_R ((S)-**45**) = 17.2 min, 98.56%; t_R ((R)-**45**) = 21.0 min, 1.44%; ee > 97%.

1.7.5.18 Racemic benzyl (1-hydroxy-3-phenylpropan-2-yl)carbamate (*rac*-45)***rac*-45**

The aldehyde intermediate was synthesized according to the general procedure using 60 mg (0.200 mmol, 1.0 eq) Cbz-DL-Phe-OH. The colorless solution was treated with 36 mg (0.220 mmol, 1.1 eq) CDI at 0 °C for 60 min, and subsequently, dropwise with 0.42 mL (0.42 mmol, 2.1 eq) 1 M DIBAL-H. The mixture was stirred for 60 min at -78 °C until TLC indicated full conversion. Extractive workup and drying provided 53 mg (0.19 mmol, 94%) of ***rac*-39** as a colorless oil.

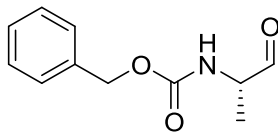
In a 5 mL glass vial equipped with a Teflon-coated magnetic stirring bar 42 mg (0.15 mmol, 1.0 eq) freshly prepared ***rac*-39** were dissolved in 1.5 mL MeOH, stirred and cooled to 0 °C in an ice bath. 27 mg (0.17 mmol, 1.1 eq) NaBH₄ were added to the colorless solution at 0 °C, the vial was covered with aluminium foil instead of a stopper to facilitate pressure relief. The mixture was stirred vigorously for 20 min at 0 °C, when TLC indicated full conversion. The reaction was quenched by the addition of 200 µL acetone and stirred for 5 min at RT. Solvents were removed under reduced pressure and the residue was partitioned between 3.0 mL EtOAc and 1.0 mL NaHCO₃ (sat). The organic extract was concentrated under reduced pressure and purified via flash chromatography (SiO₂, cyclohexane/EtOAc 2:1) to yield 37 mg (0.13 mmol, 81%, 2 steps) of a white solid.

Yield: 37 mg (0.13 mmol, 81%, 2 steps), white solid.

m.p. = 86–89 °C.

R_f = 0.37 (cyclohexane/ethyl acetate = 1:1 (v/v); staining: KMnO₄).

HPLC (Daicel Chemical Technologies Chiralpak[®] AD-H): t_R ((*S*)-**45**) = 17.3 min; t_R ((*R*)-**45**) = 22.0 min.

1.7.5.19 Benzyl (S)-(1-oxopropan-2-yl)carbamate (40)^[372]**40**

This compound was synthesized according to the general procedure using 179 mg (0.800 mmol, 1.0 eq) Cbz-L-Ala-OH. The colorless solution was treated with 143 mg (0.880 mmol, 1.1 eq) CDI at 0 °C for 60 min, and subsequently 1.68 mL (1.68 mmol, 2.1 eq) 1 M DIBAL-H were added dropwise. The mixture was stirred for 60 min at -78 °C until TLC indicated full conversion. Extractive workup and drying provided 156 mg (0.753 mmol, 94 %) of colorless oil.

Yield: 156 mg (0.753 mmol, 94 %), colorless oil.

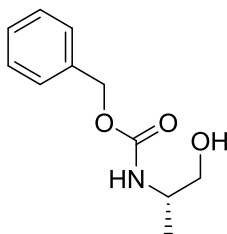
$[\alpha]_D^{23} = +10.4^\circ$ (c = 1.17, CH₂Cl₂), lit. $[\alpha]_D^{23} = +9.9^\circ$ (c = 0.75, CH₂Cl₂).^[372]

$R_f = 0.12$ (cyclohexane/ethyl acetate = 4:1 (v/v); staining: KMnO₄).

¹H NMR (300 MHz, CDCl₃) $\delta = 9.54$ (s, 1H, CHO), 7.43–7.21 (m, 5H, Ar-H), 5.59–5.39 (m, 1H, NH), 5.11 (s, 2H, CH₂O), 4.38–4.20 (m, 1H, CHCHO), 1.42–1.24 (m, 3H, CH₃).

¹³C APT NMR (75 MHz, CDCl₃) $\delta = 199.2$ (s, 1C, CHO), 156.0 (s, 1C, C=O), 136.2 (s, 1C, C_q), 128.7 (s, 2C), 128.4 (s, 1C), 128.2 (s, 2C), 67.2 (s, 1C), 56.0 (s, 1C), 14.9 (s, 1C).

Enantiomeric excess was determined indirectly by conversion of freshly isolated material into alcohol **46**.

1.7.5.20 Benzyl *N*-[(2*S*)-1-hydroxypropan-2-yl]carbamate (**46**)^[373]**46**

In a 5 mL glass vial equipped with a Teflon[®]-coated magnetic stirring bar 81 mg (0.39 mmol, 1.0 eq) freshly prepared compound **40** were dissolved in 4.0 mL MeOH, stirred and cooled to 0 °C in an ice bath. 17 mg (0.44 mmol, 1.1 eq) NaBH₄ were added to the colorless solution at 0 °C. The vial was covered with aluminium foil instead of a stopper to facilitate pressure relief. The mixture was stirred vigorously for 20 min at 0 °C, when TLC indicated full conversion. The reaction was quenched by the addition of 200 µL acetone and stirred for 5 min at RT. The solvents were removed under reduced pressure and the residue was partitioned between 3.0 mL EtOAc and 1.0 mL NaHCO₃ (sat). The organic phase was concentrated under reduced pressure and purified via flash chromatography (SiO₂, cyclohexane/EtOAc 2:1) to yield 75 mg (0.36 mmol, 92%) of a colorless oil.

Yield: 50 mg (0.25 mmol, 92%), colorless oil.

$[\alpha]_D^{23} = -10.7^\circ$ ($c = 0.55$, CHCl₃), lit. $[\alpha]_D^{22} = -6.53^\circ$ ($c = 0.95$, CHCl₃).^[373]

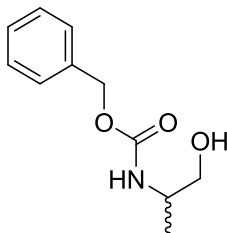
$R_f = 0.30$ (cyclohexane/ethyl acetate = 1:1 (v/v); staining: KMnO₄).

¹H NMR (300 MHz, CDCl₃, based on HSQC) $\delta = 7.44$ – 7.21 (m, 5H, Ar-*H*), 5.09 (s, 2H, CH₂OCO), 5.03–4.89 (m, 1H, NH), 3.91–3.75 (m, 1H, CHCH₂O), 3.65 (dd, ² $J = 10.7$ Hz, ³ $J = 2.8$ Hz, 2H, NCHCHH), 3.51 (dd, ² $J = 10.7$ Hz, ³ $J = 5.7$ Hz, 2H, NCHCHH), 2.57 (s, 1H, OH), 1.16 (d, ³ $J = 6.8$ Hz, 3H, CH₃).

¹³C NMR (75 MHz, CDCl₃, based on HSQC) $\delta = 156.7$ (s, 1C, C=O), 136.5 (s, 1C, C_q), 128.7 (s, 2C), 128.3 (s, 1C), 128.2 (s, 2C), 67.0 (s, 2C, CH₂CO₂ and CH₂OH), 49.1 (s, 1C), 17.4 (s, 1C).

HPLC (Daicel Chemical Technologies Chiralpak[®] AD-H): t_R ((*S*)-**46**) = 12.3 min, 100%; t_R ((*R*)-**46**) = 15.6 min, no abundance detected; ee >99%.

1.7.5.21 Racemic benzyl *N*-[1-hydroxypropan-2-yl]carbamate (**rac-46**)



rac-46

The aldehyde intermediate was synthesized according to the general procedure using 45 mg (0.20 mmol, 1.0 eq) Cbz-DL-Ala-OH. The colorless solution was treated with 36 mg (0.22 mmol, 1.1 eq) CDI at 0 °C for 60 min, and subsequently 0.42 mL (0.42 mmol, 2.1 eq) 1 M DIBAL-H were added dropwise. The mixture was stirred for 60 min at -78 °C until TLC indicated full conversion. Extractive workup and drying provided 29 mg (0.14 mmol, 70%) of **rac-40** as a colorless oil.

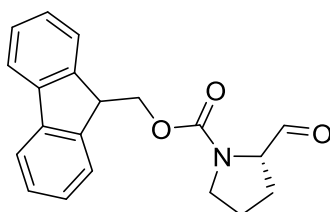
In a 5 mL glass vial equipped with a Teflon-coated magnetic stirring bar 29 mg (0.14 mmol, 1.0 eq) freshly prepared **rac-40** were dissolved in 2.0 mL MeOH, stirred and cooled to 0 °C in an ice bath. 8 mg (0.2 mmol, 1.1 eq) NaBH₄ were added to the colorless solution at 0 °C. The vial was covered with aluminium foil instead of a stopper to facilitate pressure relief. The mixture was stirred vigorously for 20 min at 0 °C, when TLC indicated full conversion. The reaction was quenched by the addition of 200 μL acetone and stirred for 5 min at RT. Solvents were removed under reduced pressure and the residue was partitioned between 3.0 mL EtOAc and 1.0 mL NaHCO₃ (sat). The organic extract was concentrated under reduced pressure and purified via flash chromatography (SiO₂, cyclohexane/EtOAc 2:1) to yield 19 mg (0.091 mmol, 45%, 2 steps) of a colorless oil.

Yield: 19 mg (0.091 mmol, 45%, 2 steps), colorless oil.

$R_f = 0.30$ (cyclohexane/ethyl acetate = 1:1 (v/v); staining: KMnO_4).

HPLC (Daicel Chemical Technologies Chiralpak[®] AD-H): t_R ((*S*)-**46**) = 12.3 min; t_R ((*R*)-**46**) = 15.6 min.

1.7.5.22 (*9H*-Fluoren-9-yl)methyl (*S*)-2-formylpyrrolidine-1-carboxylate (**41**)^[374]



41

This compound was synthesized according to the general procedure using 270 mg (0.800 mmol, 1.0 eq) Fmoc-L-Pro-OH. The colorless solution was treated with 143 mg (0.880 mmol, 1.1 eq) CDI at 0 °C for 60 min, and subsequently 2.68 mL (2.68 mmol, 3.1 eq) 1 M DIBAL-H were added dropwise. The mixture was stirred for 60 min at -78 °C until TLC indicated full conversion. Extractive workup and drying provided 272 mg of white amorphous gel. Purification via flash chromatography¹ (SiO_2 , cyclohexane/EtOAc 4:1) provided 184 mg (0.573 mmol, 72 %) of the desired aldehyde as a colorless oil.

Yield: 184 mg (0.573 mmol, 72 %), colorless oil.

$[\alpha]_D^{23} = -62.7^\circ$ (c = 3.60, CHCl_3).

$R_f = 0.25$ (cyclohexane/ethyl acetate = 2:1 (v/v); staining: KMnO_4).

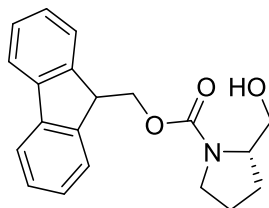
¹ Flash chromatography was performed due to some impurities to determine the exact yield of the desired aldehyde. Due to propensity for racemization on silica (demonstrated in epimerization experiment for (**2R,3S**)-**36**), for further synthetic use we recommend the usage of nonchromatographed material, as demonstrated in the examples **47** and *rac*-**47**.

^1H NMR (300 MHz, CDCl_3 , mixture of two conformers, based on HSQC) δ = 9.58 and 9.25 (s, 1H, CHO), 7.88–7.20 (m, 8H, Ar-H), 4.65–4.37 (m, 2H, CH_2O), 4.37–3.39 (m, 2H, CHCHO and CHCH_2O), 3.66–3.38 (m, 2H, NCH_2), 2.20–1.69 (m, 4H, $\text{NCH}_2(\text{CH}_2)_2$).

^{13}C NMR (75 MHz, CDCl_3 , based on HSQC) δ = 200.0 and 199.8 (s, 1C, CHO), 155.4 and 154.6 (s, 1C, C=O), 143.9 and 143.8 (s, 2C, C_q), 141.4 (s, 2C, C_q), 127.8 (s, 2C), 127.1 (s, 2C), 125.2 and 124.9 (s, 2C), 120.0 (s, 2C), 67.6 and 67.3 (s, 1C), 65.3 and 64.8 (s, 1C), 47.3 (s, 1C), 46.7 (s, 1C), 27.8 and 26.6 (s, 1C), 24.6 and 23.6 (s, 1C).

Enantiomeric excess was determined indirectly by conversion of crude, freshly isolated material, not subjected to flash chromatography, into alcohol **47**.

1.7.5.23 9H-Fluoren-9-ylmethyl (2S)-2-(hydroxymethyl)pyrrolidine-1-carboxylate (**47**)^[375]



47

In a 5 mL glass vial equipped with a Teflon[®]-coated magnetic stirring bar 103 mg (0.320 mmol, 1.0 eq) freshly prepared, nonchromatographed compound **41** were dissolved in 4.0 mL MeOH, stirred and cooled to 0 °C in an ice bath. 17 mg (0.44 mmol, 1.4 eq) NaBH_4 were added to the colorless solution at 0 °C, the vial was covered with aluminium foil instead of a stopper to facilitate pressure relief. The mixture was stirred vigorously for 20 min at 0 °C, when TLC indicated full conversion. The reaction was quenched by the addition of 200 μL acetone and stirred for 5 min at RT. The solvents were removed under reduced pressure and the residue was partitioned between 3.0 mL EtOAc and 1.0 mL NaHCO_3 (satd). The organic phase was concentrated under reduced pressure and purified via flash chromatography (SiO_2 , cyclohexane/EtOAc 2:1) to yield 85 mg (0.26 mmol, 81%) of a white solid.

Yield: 85 mg (0.26 mmol, 81%), white solid.

m.p. = 89 °C, lit. 89–90 °C.^[375]

$[\alpha]_D^{23} = -29.2^\circ$ (c = 0.42, CHCl₃), lit. $[\alpha]_D^{24} = -30.3^\circ$ (c = 1.02, CHCl₃).^[375]

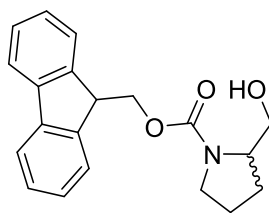
$R_f = 0.40$ (cyclohexane/ethyl acetate = 1:1 (v/v); staining: KMnO₄).

¹H NMR (300 MHz, CDCl₃, based on HSQC) $\delta = 7.78$ (d, ³J = 7.3 Hz, 2H, Ar-H), 7.61 (d, ³J = 7.3 Hz, 2H, Ar-H), 7.42 (t, ³J = 7.3 Hz, 2H, Ar-H), 7.33 (t, ³J = 7.3 Hz, 2H, Ar-H), 4.45 (br s, 2H, CH₂OCO), 4.25 (t, ³J = 6.5 Hz, 1H, benzylic CH), 4.10–3.87 (m, 1H, NCHCH₂O), 3.78–2.99 (m, 5H, CH₂OH and NCH₂CH₂), 2.14–1.53 (m, 4H, NCH₂CH₂CH₂).

¹³C NMR (75 MHz, CDCl₃, based on HSQC) $\delta = 157.3$ (s, 1C, C=O), 144.1 (s, 1C, C_q), 141.5 (s, 1C, C_q), 127.8 (s, 2C), 127.2 (s, 2C), 125.1 (s, 2C), 120.1 (s, 2C), 67.6 (s, 1C, CH₂CO₂), 67.1 (s, 1C, CH₂OH), 60.9 (s, 1C), 47.5 (s, 1C), 47.4 (s, 1C), 28.7 (s, 1C), 24.2 (s, 1C).

HPLC (Daicel Chemical Technologies Chiralpak[®] AD-H): t_R ((S)-**47**) = 20.5 min, 100%; t_R ((R)-**47**) = 24.3 min, no abundance detected; ee >99%.

1.7.5.24 Racemic 9H-fluoren-9-ylmethyl (2S)-2-(hydroxymethyl)pyrrolidine-1-carboxylate (rac-47)



rac-47

This compound was synthesized by mixing 68 mg (0.20 mmol, 0.5 eq) Fmoc-L-Pro-OH and 68 mg (0.20 mmol, 0.5 eq) Fmoc-D-Pro-OH, and converting the mixture according to the general procedure. The colorless solution was treated with 71 mg (0.44 mmol, 1.1 eq) CDI at 0 °C for 60

min, and subsequently 0.84 mL (0.84 mmol, 2.1 eq) 1 M DIBAL-H were added dropwise. The mixture was stirred for 60 min at -78 °C until TLC indicated full conversion. Extractive workup and drying provided 29 mg (0.14 mmol, 70%) of **rac-41** as a colorless oil.

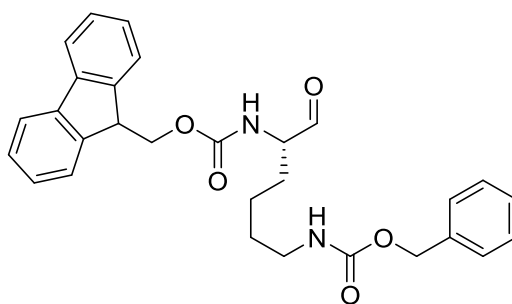
In a 5 mL glass vial equipped with a Teflon-coated magnetic stirring bar 111 mg (0.345 mmol, 1.0 eq) freshly prepared **rac-41** were dissolved in 4.0 mL MeOH, stirred and cooled to 0 °C in an ice bath. 17 mg (0.44 mmol, 1.1 eq) NaBH₄ were added to the colorless solution at 0 °C. The vial was covered with aluminium foil instead of a stopper to facilitate pressure relief. The mixture was stirred vigorously for 20 min at 0 °C, when TLC indicated full conversion. The reaction was quenched by the addition of 200 µL acetone and stirred for 5 min at RT. Solvents were removed under reduced pressure and the residue was partitioned between 3.0 mL EtOAc and 1.0 mL NaHCO₃ (satd). The organic extract was concentrated under reduced pressure and purified via flash chromatography (SiO₂, cyclohexane/EtOAc 2:1) to yield 68 mg (0.21 mmol, 53%, 2 steps) of a colorless oil.

Yield: 68 mg (0.21 mmol, 53%, 2 steps), colorless oil.

R_f = 0.40 (cyclohexane/ethyl acetate = 1:1 (v/v); staining: KMnO₄).

HPLC (Daicel Chemical Technologies Chiralpak[®] AD-H): t_R ((*S*)-**47**) = 20.5 min; t_R ((*R*)-**47**) = 24.3 min.

1.7.5.25 (9*H*-Fluoren-9-yl)methyl benzyl (6-oxohexane-1,5-diyl)(*S*)-dicarbamate (**42**)^[376]



42

This compound was synthesized according to the general procedure using 402 mg (0.800 mmol, 1.0 eq) Fmoc-L-Lys(Cbz)-OH. The white colloidal solution was treated with 143 mg (0.880 mmol, 1.1 eq) CDI at 0 °C for 60 min, which resulted in complete dissolution. Subsequently, the reaction solution was treated dropwise with 3.20 mL (3.20 mmol, 4.0 eq) 1 M DIBAL-H. The mixture was stirred for 60 min at -78 °C until TLC indicated full conversion. Extractive workup and drying provided 391 mg of a turbid gel. Purification via flash chromatography^{II} (SiO₂, cyclohexane/EtOAc 4:1) furnished 201 mg (0.413 mmol, 52 %) of the desired aldehyde as a viscous colorless oil.

Yield: 201 mg (0.413 mmol, 52 %), viscous colorless oil.

$[\alpha]_D^{23} = +10.7^\circ$ (c = 5.30, CHCl₃).

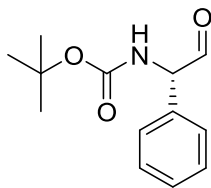
$R_f = 0.44$ (cyclohexane/ethyl acetate = 1:1 (v/v); staining: KMnO₄).

¹H NMR (300 MHz, CDCl₃) δ = 9.48 (s, 1H, CHO), 7.71 (d, ³J = 7.4 Hz, 2H, Ar-H), 7.56 (d, ³J = 7.0 Hz, 2H, Ar-H), 7.40–7.19 (m, 9H, Ar-H), 5.65–5.46 (m, 1H, FmocNH), 5.04 (s, 2H, PhCH₂O), 4.99–4.82 (m, 1H, CbzNH), 4.39 (d, ³J = 4.7 Hz, 2H, CHCH₂O), 4.27–4.07 (m, 2H, NCH and CHCH₂O), 3.24–2.96 (m, 2H, NCH₂), 1.94–1.19 (m, 6H, NCH₂(CH₂)₃).

¹³C NMR (75 MHz, CDCl₃) δ = 199.5 (s, 1C, CHO), 156.7 (s, 1C, C=O), 156.3 (s, 1C, C=O), 143.8 (s, 2C, C_q), 141.4 (s, 2C, C_q), 136.6 (s, 1C, C_q), 128.6 (s, 2C), 128.2 (s, 1C), 128.1 (s, 2C), 127.8 (s, 2C), 127.1 (s, 2C), 125.1 (s, 2C), 67.0 (s, 1C), 66.7 (s, 1C), 60.0 (s, 1C), 47.2 (s, 1C), 40.4 (s, 1C), 29.6 (s, 1C), 28.5 (s, 1C), 22.1 (s, 1C).

HRMS (MALDI-TOF): Calcd. for C₂₉H₃₀N₂O₅Na [M+Na]⁺: 509.2052; found: 509.2055.

^{II} Flash chromatography was performed due to some impurities to determine the exact yield of the desired aldehyde. Due to propensity for racemization on silica (demonstrated in epimerization experiment for **(2R,3S)-36**), for further synthetic use we recommend the usage of nonchromatographed material, as demonstrated in the examples **47** and *rac-47*.

1.7.5.26 *tert*-Butyl (*S*)-(2-oxo-1-phenylethyl)carbamate (43**)**^[333]**43**

This compound was synthesized via a modified procedure using 100 mg (0.400 mmol, 1.0 eq) Boc-L-Phg-OH. The colorless solution was treated with 72 mg (0.44 mmol, 1.2 eq) CDI at 0 °C. After 30 min of stirring 27 mg (0.20 mmol, 0.5 eq) CuCl₂ were added and the mixture was stirred at RT for 60 min. Subsequently, 0.84 mL (0.84 mmol, 2.1 eq) 1 M DIBAL-H were added dropwise at the rate of 2.0 mL/min via a syringe pump. The mixture was stirred for 30 min at -78 °C until TLC indicated full conversion. Extractive workup and drying provided 82 mg (0.35 mmol, 88 %) of a pale yellow oil.

Yield: 82 mg (0.35 mmol, 88 %), pale yellow oil.

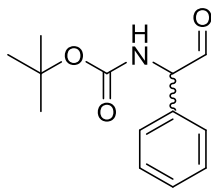
$[\alpha]_D^{23} = +213^\circ$ (c = 1.98, CH₂Cl₂), lit. $[\alpha]_D^{20} = +272^\circ$ (c = 0.9, CH₂Cl₂).^[333]

$R_f = 0.27$ (cyclohexane/ethyl acetate = 4:1 (v/v); staining: KMnO₄).

¹H NMR (300 MHz, CDCl₃) $\delta = 9.53$ (s, 1H, CHO), 7.53–7.16 (m, 5H, Ar-H), 5.88–5.67 (m, 1H, NH), 5.42–5.19 (m, 1H, CHCHO), 1.42 (s, 9H, (CH₃)₃CO).

¹³C NMR (75 MHz, CDCl₃) $\delta = 195.2$ (s, 1C, CHO), 155.1 (s, 1C, C=O), 132.9 (s, 1C, C_q), 129.5 (s, 2C), 128.9 (s, 1C), 127.9 (s, 2C), 80.4 (s, 1C, Me₃C), 65.0 (s, 1C), 28.4 (s, 3C).

GC-FID (CP-Chiralsil Dex): t_R ((*S*)-**43**) = 14.1 min, 91.51%; t_R ((*R*)-**43**) = 14.6 min, 8.49%; ee = 83%.

1.7.5.27 Racemic *tert*-butyl (2-oxo-1-phenylethyl)carbamate (*rac*-43)***rac*-43**

This compound was synthesized according to the general procedure using 75 mg (0.30 mmol, 1.0 eq) Boc-DL-Phg-OH. The colorless solution was treated with 54 mg (0.33 mmol, 1.1 eq) CDI at 0 °C for 60 min, and subsequently 0.63 mL (0.63 mmol, 2.1 eq) of 1 M DIBAL-H were added dropwise. The mixture was stirred for 60 min at -78 °C until TLC indicated full conversion. Extractive workup and drying provided 58 mg (0.25 mmol, 83 %) of a pale yellow oil.

Yield: 58 mg (0.25 mmol, 83 %), pale yellow oil.

$R_f = 0.27$ (cyclohexane/ethyl acetate = 4:1 (v/v); staining: KMnO_4).

GC-FID (CP-Chiralsil Dex): t_R (*(S)*-43) = 14.2 min; t_R (*(R)*-43) = 14.6 min.

1.7.6 Biological Assays

1.7.6.1 Isothermal Microcalorimetry

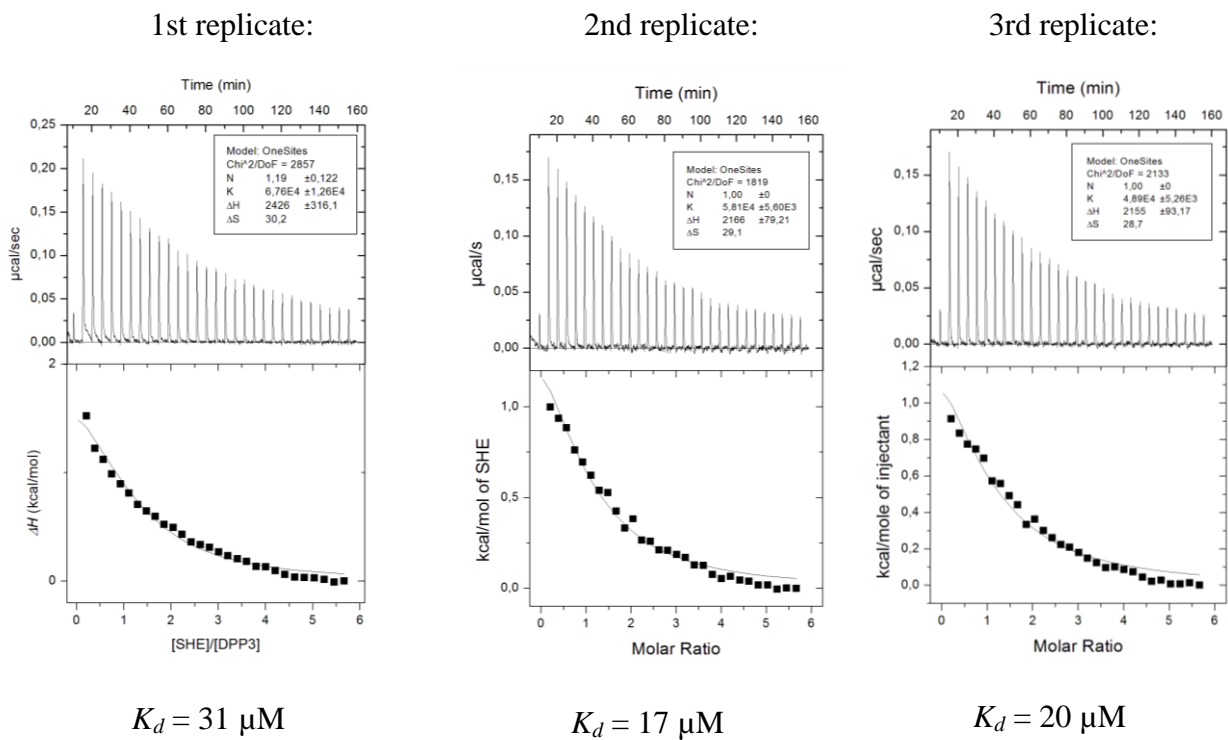
The wild type recombinant hDPP3 expressed in *E. coli* was used for the microcalorimetric analysis. The titrations were performed in a buffer with pH=8.0 containing 50 mM Tris-HCl and 100 mM NaCl. Both the purified enzyme and ligand were dissolved in exactly the same buffer, and all solutions were degassed immediately before the measurements. The measurements were performed on VP-ITC microcalorimeter (MicroCal, Northampton, MA, USA).

In each measurement run the temperature was equilibrated at 298 K. A 500 μM solution of ligand in the syringe was titrated into a 20 μM solution of hDPP3 in the measurement cell. In a typical experiment, under constant stirring at 270 rpm, a total of one aliquot of 2 μL and 29 aliquots of 10 μL of the ligand solution were injected at a rate of 0.5 $\mu\text{L/s}$ into 1.421 mL of the enzyme solution. Every injection was carried out over a period of 20 s with a spacing of 300 s between the injections. The heats of binding were determined by integration of the observed peaks. The heat values were plotted against the ratio of peptide vs. protein concentration in the cell to generate the binding isotherm. Nonlinear least-squares fitting using Origin® version 7.0 (MicroCal®) was used to obtain association constants (K_a), heats of binding (ΔH) and stoichiometries. Dissociation constant (K_d) values were calculated according to the simple reciprocal equation:

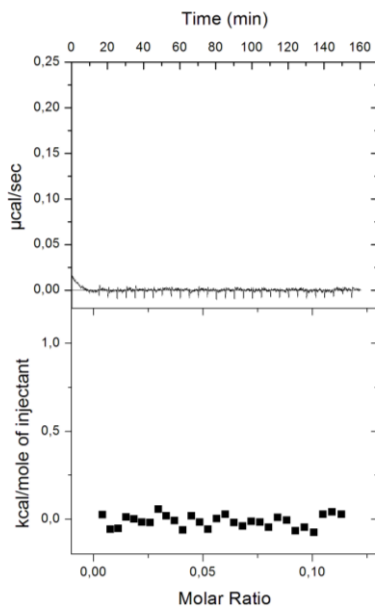
$$K_d = \frac{1}{K_a}$$

1.7.6.1.1 Binding of SHE to hDPP3

hDPP3 was titrated with *SHE* in three separate measurement runs performed as described above (Figure 61).



Control (SHE → buffer)



$K_d = 23 \pm 4 \mu\text{M}$

Figure 61 ITC thermograms of titrations of hDPP3 with *SHE*. Three replicates were performed and one control run without the enzyme. The calculated mean value of dissociation constant of *SHE*-hDPP3 complex is printed in bold.

1.7.6.2 Fluorescence-based Inhibition Assays

Fluorescence based inhibition assays were performed at the Institute of Biochemistry, TU Graz, by PhD student researcher Shaline Jha under the supervision of Prof. Peter Macheroux.

The inhibition of the recombinant wild type hDPP3 by inhibitors produced in this work was investigated via fluorescence measurements. The fluorescence was produced by liberation of 2-naphthylamine (excitation, 332 nm; emission, 420 nm) at 37°C in a mixture containing 25 µl of 200µM Arg-Arg-2-naphthylamide as substrate in 50 mM Tris-HCl buffer, pH 8.0, 0.05-0.1 µM of enzyme in a total reaction mixture of 235 µl. Measurements for at least eight inhibitor concentrations have been performed in a well plate (White, Tissue Culture treated Krystal 2000 96-well plate from Porvair sciences, Norfolk, UK) for each inhibitor. The activity assay was performed by continuous measurement of fluorescence of 2-naphthylamide for 30 min (Fluorescent plate reader from Molecular Devices, Sunnyvale CA, USA). For inhibition assay, the inhibitors were added to the mixture without the substrate and incubated for 10 min at room temperature. The reaction was started by the addition of the substrate.

The concentration of an inhibitor that gave 50% inhibition (IC₅₀) was determined through series of assays with a fixed substrate concentration and varied inhibitor concentrations. 5% DMSO was used in the control assay. Percentage of activity in the presence of increasing concentrations of inhibitor was calculated:

$$\% \text{ activity} = 100 \times (\Delta\text{fluorescence} / \Delta\text{fluorescence of control})$$

For each inhibitor percentage of activity (y-axis) against concentration (logarithmic scale, x-axis) of inhibitor was plotted. Percent activity vs. log of concentration was fitted to a sigmoidal dose-response curve using the four parameter logistic equation entitled “log(inhibitor) vs. response -- Variable slope” in GraphPad Prism®. Based on the fitted curves the software calculated the IC₅₀ values presented in Table 13 and Table 14.

1.7.6.3 X-ray Structure Determination

The extensive enzyme engineering and crystallization experiments in order to obtain new X-ray structures of hDPP3 and the cocrystal structure of *SHE* and hDPP3, were performed by Prashant Kumar at the Institute of Molecular Biosciences, University of Graz, under supervision of Prof. Karl Gruber.

2

Synthesis of New Triazine Nitrile Inhibitors of Rhodesain and hCatL for Probing of Amide- π Stacking Interactions

2.1 Introduction

New scientific reports of theoretical and experimental investigations on less characterized noncovalent interactions across chemical and biological supramolecular systems^[349,350,377–383] are important factors for speeding up rational development of suitable enzyme inhibitors,^[348,384,385] catalysts^[386,387] and novel functional materials.^[388,389]

A newly proposed specific type of a π -interaction is found between amide bond π -system and aromatic systems. The research on characterization of this type of interaction has recently started and it has already produced valuable theoretical and experimental information.^[377,383,384] Due to the high abundance of peptide bonds in proteins and their binding sites, better understanding of this interaction could greatly enhance the efficiency in the design of enzyme inhibitors and receptor agonists.

2.2 State of the Art

2.2.1 Noncovalent Interactions in Molecular Recognition

Highly specific and spatially organized interactions of two or more molecules through noncovalent bonding are referred to as molecular recognition.^[5,6,128] Most familiar among those is hydrogen bonding, the phenomenon that makes water liquid in standard conditions, and is regarded as the culprit for its higher density when it solidifies.^[390–392] Metal coordination is of natural importance in protein complexes, in catalytic applications used by nature and humans.^[393–395] Van der Waals interactions, as various dipolar interactions between permanent dipoles and induced dipoles, are critical to ligand binding. They were recently directly measured for the first time.^[396] Orthogonal interactions of dipoles, of C–X···C=O type, have been identified and quantified.^[397,398] Hydrophobic effect, in tight relation to the precise role of solvent molecules, can play a dominant indirect role in driving molecular recognition in solution.^[351,399,400]

Cooperativity between these interactions and molecular complementarity, are characteristics of fine examples of tightly binding molecules in nature, science and technology.^[401] In particular, halogen bonding and amide- π stacking are subject of vigorous state of the art research.^[349,350,377,402,403]

2.2.1.1 Amide- π Stacking

π -Stacking interactions are used in drug design. These interactions are mostly investigated in purely aromatic systems. Stacking parameters of different aromatic partners have been studied in theory and experiments.^[404–406] While eclipsed stacking geometry is hardly observed in protein structures, QM calculations predict favorable association energy of -2.7 kcal/mol for the parallel-displaced configuration of benzene dimer in the gas phase, in contrast to 1.0 kcal/mol for the eclipsed configuration.^[407] Significant energy differences have been found in pyridine dimer systems, emphasizing important influence of dipole alignment.^[408]

Stacking interactions of other π -systems, like amides, are less known. Amide functionalities in proteins are especially interesting. They are highly abundant in proteins, and that makes them attractive in inhibitor design. Moreover, in the secondary structures, α -helices and β -sheets, peptide bonds are more rigid and their π -surfaces are exposed for ligand binding.

Relatively strong dipole moment of amide bonds, e.g. *N*-methylacetamide, suggests that stacking to amide bonds could be well enhanced by proper alignment with a polar stacking moiety.^[409] There are examples of protein-inhibitor complexes where stacking to backbone amides is found: the selectivity pocket in phosphodiesterase 10a,^[410] S1 pocket in factor Xa,^[384] and S3 pocket in human Cathepsin L.^[348] Interestingly, two isomeric oxazole inhibitors of factor Xa have been identified, one of them being 11-fold more potent. Cocystal structures of both inhibitors with the enzyme reveal that the higher potency can be attributed to the antiparallel alignment of the oxazole dipole moment in respect to the adjacent stacking backbone peptide bond of Cys191–Gln192 (Figure 62).

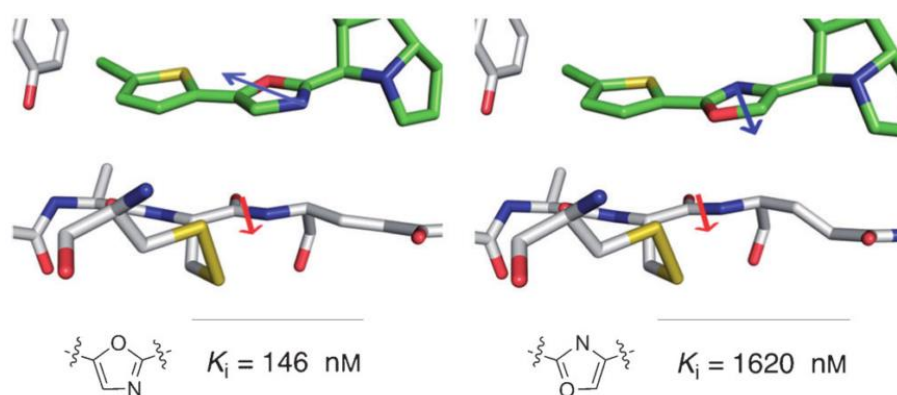


Figure 62 Binding modes of two oxazole inhibitors of factor Xa. (1.29 Å resolution, PDB: 2Y5G, and 1.33 Å resolution, PDB: 2Y5H). Color code: C_{enzyme} light grey, C_{ligand} green, O red, N blue, S yellow.^[384]

Stacking of aromatic heterocycles to an amide bond was investigated in a computational study using *ab initio* calculations in spin component scaled MP2 level of theory.^[377] Parallel-displaced stacking of pyridine to *N*-methylacetamide was used as a model system. Preference for antiparallel arrangement between the dipole moments was determined (-2.5 kcal/mol) over the parallel arrangement (-0.9 kcal/mol, Figure 63).

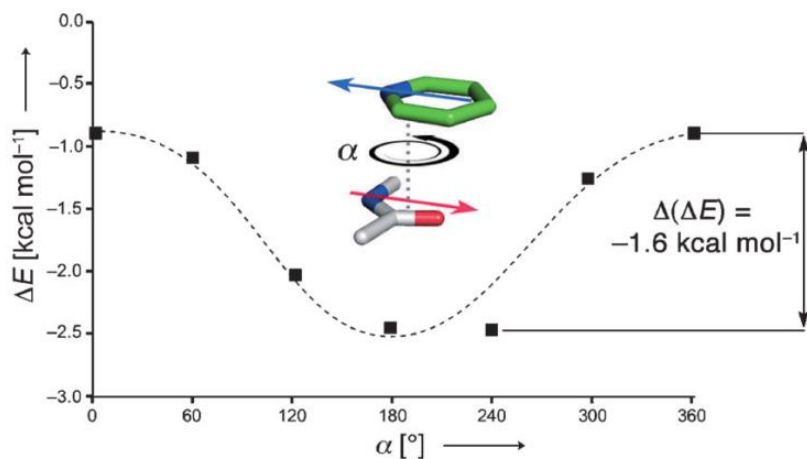


Figure 63 Rotational scan in stacking of pyridine and *N*-methylacetamide.^[377]

A library of aromatic heterocycles with significant variation of dipole moments was also investigated in terms of parallel-displaced stacking to *N*-methylacetamide. Median moment in the optimized structures was 161° , that is, they were almost antiparallel. It was observed that there is a linear trend of stronger interaction energy with increasing dipole moment strength, with a correlation coefficient of $R^2 = 0.84$ (Figure 64). Selection of three arenes with zero dipole moment displayed a favorable effect of lower electron density on the efficiency of stacking.

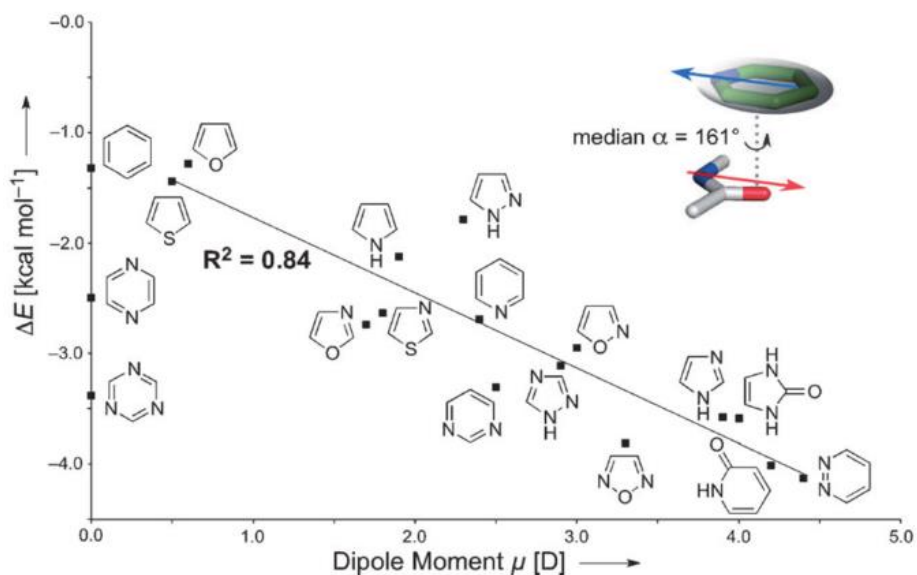


Figure 64 Linear trend of energy vs dipole moment of various heteroaromatics stacking onto *N*-methylacetamide.^[377]

In this work, as a part of much broader study (Maude Giroud, ETH Zürich), a selection of novel inhibitors of cysteine proteases have been synthesized, and the effects of amide- π stacking on their potencies was investigated.

2.2.2 Inhibitors for Targeting African Sleeping Sickness

2.2.2.1 African Sleeping Sickness

African Sleeping Sickness (human African trypanosomiasis), along with malaria, is one of the major diseases troubling the developing countries. It is caused by a parasite *Trypanosoma brucei*.^[411] The disease outbreak was moderately controlled in the middle of 20th century, but in recent years its incidence is on a rise. The disease has been considered invariably fatal without anti-parasitic treatment. This was found not to be correct, because numerous healthy carriers have been diagnosed to have it, years after they have been infected, mostly upon migration from Africa to Europe.^[412–414] Since there are great variations in severity and speed of progression, there is high potential for big scale outbreaks. There is a great need for development of the anti-trypanosomal drugs, and a strategy to avoid drug resistance development.

Protease-based drug development can be excessively challenging, because proteolytic pathways often involve closely related enzymes. A number of essential cysteine proteases have been implicated in pathogenesis of human African trypanosomiasis.^[415]

2.2.2.2 Cysteine Proteases Targeted in African Sleeping Sickness

Two of these have papain-like fold and are expressed by bloodstream *Trypanosoma brucei rhodesiense*: human Cathepsin B-type cysteine protease TbCatB, and human Cathepsin L-like enzyme named rhodesain.^[416–418] It was found that they are essential for host protein degradation.

In cell culture and animal models it was demonstrated that cysteine protease inhibitors kill these parasites.^[419]

In this work, the focus is given to inhibition of rhodesain and selectivity over human Cathepsin L. First X-ray based structures of rhodesain have been determined in 2009 and 2010, and enabled structure-based design of inhibitors.^[241,420] The structure features classical papain fold consisting of two domains, having highly conserved peptide sequences around the narrow groove on the interface between the two domains, facilitating the catalytic dyad, Cys25 and His162 (Figure 65A). The active site also consists of S1, S2 and S3 subsites, of which strongly hydrophobic S2 site is considered to be crucial for substrate specificity in papain-like proteases.^[421] S3 subsite is particularly interesting, because it features a flat part in the protein backbone, Gly65–Gly66, with two unhindered peptide bonds, lying in the same plane (Figure 65B).

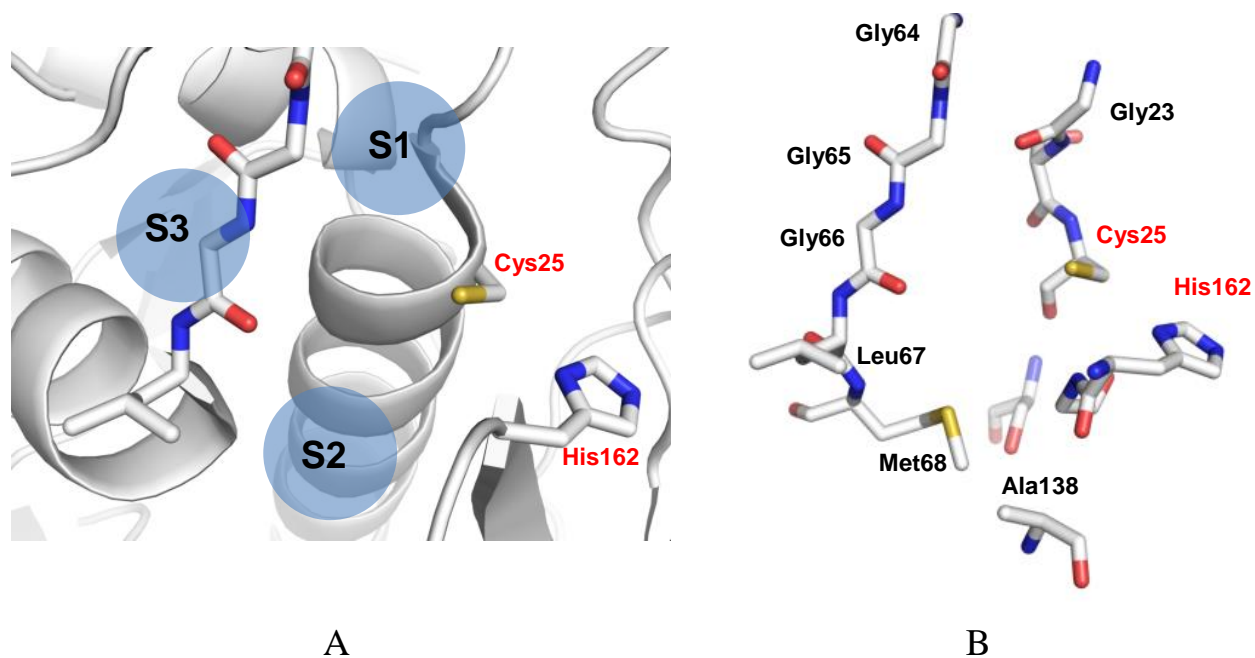


Figure 65 **A:** Subsites of the active site of rhodesain (1.16 Å resolution PDB: 2P86).^[422] **B:** Residues of the active site. Color code: C_{enzyme} light grey, O red, N blue, S yellow.

The known enzyme structures, together with previously identified triazine nitrile inhibitor scaffold, provided the opportunity for structure-based design of new inhibitors.^[234–236,423]

2.2.3 Chemistry of Selected Heterocycles

Previous computer-aided efforts guided the development of rhodesain and falcipain-2 inhibitors.^[423] Triazine scaffold have been identified as an ideal core used to carry the residues that address the binding subsites in rhodesain, and nitrile function was used as an electrophile to provide means of reversible covalent attachment to the active cysteine residue of the cysteine protease, via a thioimidate bond (Figure 66). However, this type of inhibitor displayed low target selectivity and moderate cytotoxicity. It was shown that the off-target activity comes from the higher electrophilicity of electron-deficient triazine.^[236] They were further optimized in a structure-based study for optimization of rhodesain inhibitors.^[234] For the purpose of this study, toxicity was not relevant, so therefore we chose to continue working on this series.

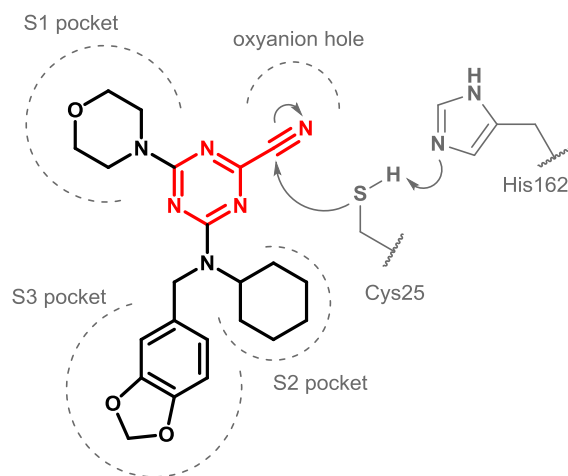


Figure 66 Scaffold of the triazine nitrile inhibitor of rhodesain and thioimidate bond formation mechanism.^[234]

2.2.3.1 Triazines

Triazines are three nitrogen atom containing, six-membered heteroaromatics, and a subgroup of azines (Figure 67). In comparison to pyridines and diazines, inductive effects of additional nitrogen atoms in the aromatic rings, lead to greater electrophilicity. Simple

electrophilic substitutions like bromination of 1,3,5-triazine do not occur. Bromination on them is considered a nucleophilic addition of bromide to an N^+-Br triazinium salt.^[424]

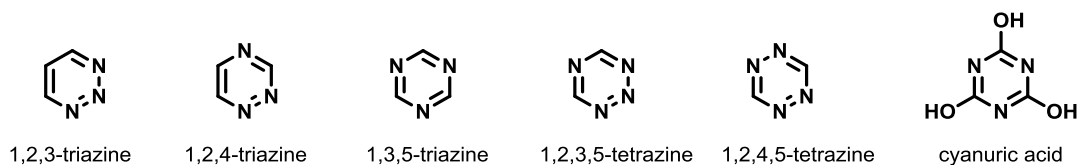
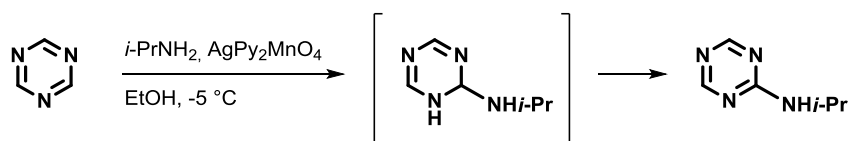


Figure 67 Structural formulas of selected azines.

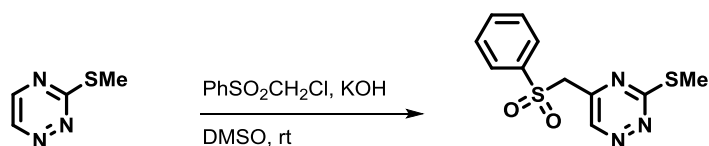
Derivatives of 1,3,5-triazines are some of the oldest known heterocycles and they are industrially available in bulk quantities. K. F. Scheele has synthesized cyanuric acid in 1776, by pyrolysis of uric acid. Properties of triazines vary, e.g. 1,2,3-triazine is thermally stable up to 200 °C, while 1,3,5-triazine decomposes only at 600 °C to its formal monomer, hydrogen cyanide.

Electrophilic reactivity of triazines is further illustrated in examples where ammonia or amines add to them in much milder conditions than, e.g. in a Chichibabin reaction to pyridine. Resulting alkylamino derivatives are finally obtained by oxidative trapping with permanganates (Scheme 45).^[425]

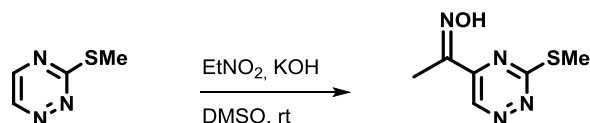


Scheme 45 Oxidative amination of 1,3,5-triazine.

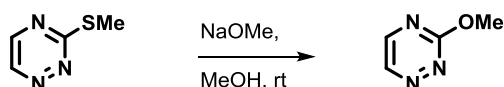
1,2,4-Triazines that bear a 3-methylthio substituent, are easily substituted in at C-5 position (Scheme 46).^[426] Similarly, nitroalkanes engage in a nucleophilic acylation in the same position (Scheme 47).^[427] Interestingly, the 3-methylthio substituent in 1,2,4-triazines can be substituted with methoxide (Scheme 48).^[428]



Scheme 46 Substitution of 1,2,4-triazine in C-5 position.

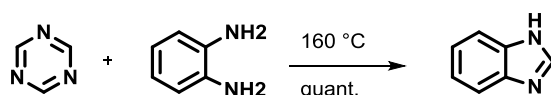


Scheme 47 Substitution of 1,2,4-triazine in C-5 position by reaction with a nitroalkane.



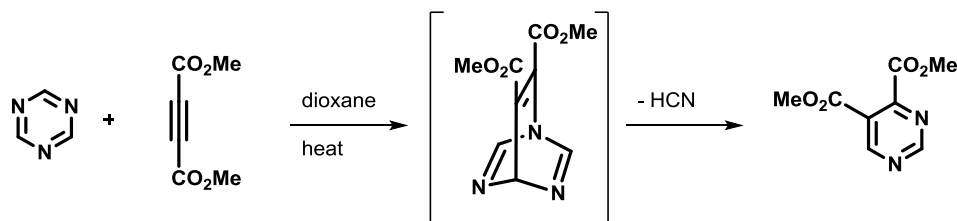
Scheme 48 Substitution of a methylthio substituent by methoxide in 1,2,4-triazine.

1,3,5-Triazine can be thought of as an equivalent of formate or formamide, because of its susceptibility to nucleophilic attack. This is very useful for synthesis of heterocycles like imidazoles and triazoles (Scheme 49).^[429,430]



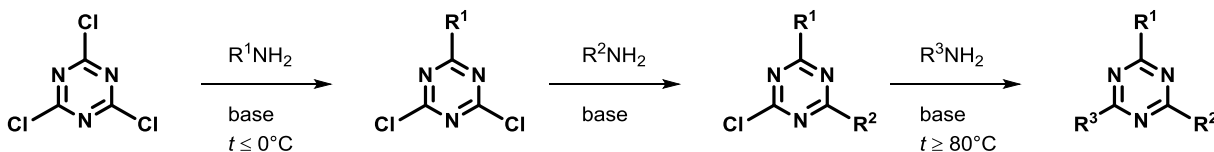
Scheme 49 Synthesis of benzimidazole using 1,3,5-triazine.

One of the most useful reactions of tetrazines and triazines is the inverse-electron demand Diels-Alder reaction with acetylenes (Scheme 50). Pyridines or diazines are resulting products after elimination of hydrogen cyanide or nitrogen.^[431]



Scheme 50 Inverse demand Diels-Alder reaction of 1,3,5-triazine and alkyne, and subsequent eliminative aromatization.

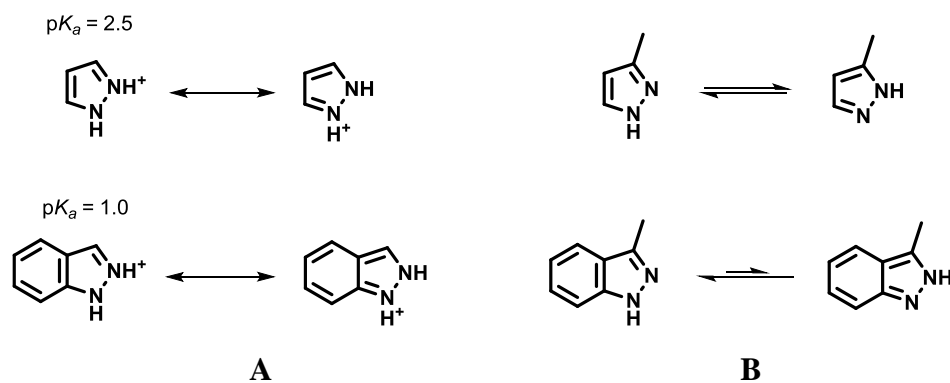
1,3,5-Triazines are specifically interesting because numerous analogs can be generated relatively easily. For this reason, they are quite often used in medicinal chemistry.^[432,433] They are usually synthesized by treating cyanuric chloride with equimolar amounts of nucleophiles, in a sequential manner, to achieve the desired substitution pattern.^[234,434,435] This strategy usually yields big amounts of analogues relatively quickly, so it is excellent for highly productive parallel synthesis (Scheme 51).



Scheme 51 Sequence leading to fully substituted 1,3,5-triazines, starting from cyanuric chloride.

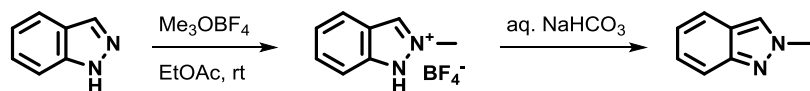
2.2.3.2 Indazoles

Indazoles are somewhat related to their parent monocycles pyrazoles. Annelated benzene ring makes it a weaker base, which is in agreement with the fact that generally bicyclic systems are weaker bases than their corresponding monocycles (Scheme 52A). While pyrazoles are normally mixtures of rapidly switching tautomers, indazole's *2H*-tautomer is undetectable (Scheme 52B). *2H*-indazoles are only stabilized when 2-substituted.

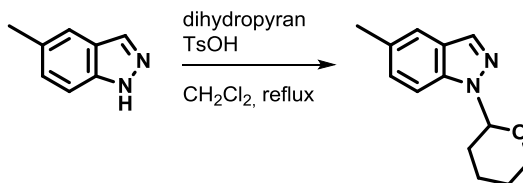


Scheme 52 Comparison of acidity and tautomerism in pyrazoles and indazoles.

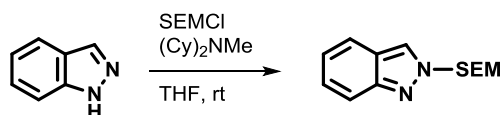
Regioselective *N*-alkylation of indazoles is difficult to achieve. It preferentially occurs on the N-2 position, yielding substituted 2*H*-indazoles, but there are rare examples of exclusive regioselectivity (Scheme 53).^[436] On the other hand, in reflux with dihydropyran and an acid, N-1 tetrahydropyranyl protected derivative is produced (Scheme 54).^[437] N-2 protection of indazoles can be selectively achieved using silyl chlorides and a hindered base (Scheme 55).^[438]



Scheme 53 Regioselective alkylation of indazole with trimethyloxonium tetrafluoroborate

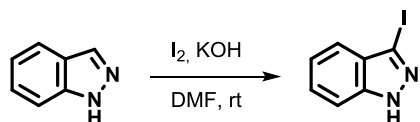


Scheme 54 Alkylation of indazole with dihydropyran.

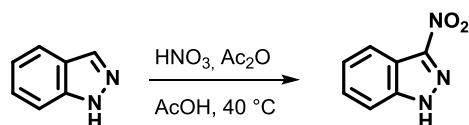


Scheme 55 Regioselective protection of indazole using a hindered base.

Direct C-substitution on indazoles can only be achieved in 3-position. 3-iodoindazole is obtained in presence of a base, and it is said to proceed via iodination of indazolyl anion (Scheme 56).^[439] 3-Nitration is also readily achieved (Scheme 57).^[440]

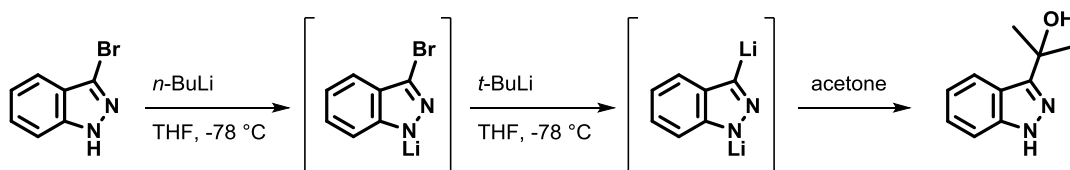


Scheme 56 3-Iodination of indazole.



Scheme 57 3-Nitration of indazole.

Indazole can be metallated in 3-position, either by metal-halogen exchange (Scheme 58),^[441] or direct lithiation, and subsequently functionalized with various electrophiles (Scheme 59).^[442]

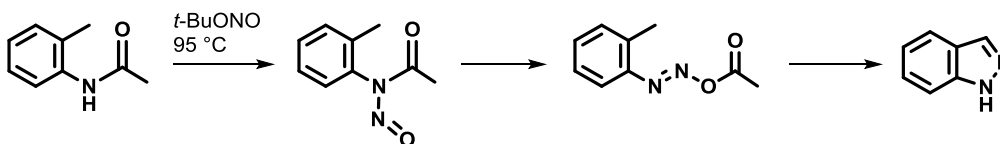


Scheme 58 Lithiation of 3-bromoindazole and reaction with acetone.

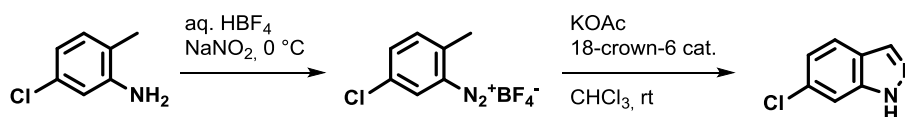


Scheme 59 Lithiation of 2-((2-(trimethylsilyl)ethoxy)methyl)-2H-indazole and reaction with phenyl isocyanate.

Best approaches to synthesis of indazoles with the desired substitution pattern are through its ring formation. Classical approaches involve various modifications of Jacobson's synthesis of indazoles via nitrosations and diazotisations of anilines (Scheme 60).^[443–446] Jacobson type indazole synthesis modification by Bartsch and Rault is particularly general for obtaining both electron rich and electron deficient indazoles (Scheme 61).^[447,448]

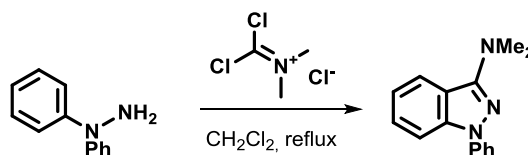


Scheme 60 Jacobson's synthesis of indazoles from *N*-acyl-*ortho*-toluidines.



Scheme 61 General, diazonium tetrafluoroborate based synthetic method for formation of indazoles.

Less frequent methods proceed through electrophilic cyclizations of phenylhydrazines (Scheme 62),^[449] and benzyne trapping with lithium trimethylsilyldiazomethane (Scheme 63).^[450]



Scheme 62 Electrophilic cyclization via a phenylhydrazone.



Scheme 63 Synthesis of indazole via benzyne trapping.

2.3 Aims of Work

In terms of medicinal chemistry, rhodesain has attracted attention as a target for fighting parasites causing African Sleeping Sickness. Potent and selective inhibitors of Rhodesain have already been designed via a structure-based approach.^[234,422]

Within obtained X-ray-based structure of human Cathepsin L complex with a potent triazine nitrile-based covalent inhibitor, a particularly interesting contact was observed between an aromatic substituent of the inhibitor to a Gly67-Gly68 subsequence, also addressed as S3 subsite, in the binding site of the enzyme (Figure 68).^[234] The Gly-Gly subsite, as well as the most of the binding site surface, appears to be exposed to the solvent environment. Since glycines do not introduce significant steric hindrance due to a lack of amino acid side chain, this binding subsite has been seen as a good scenario for probing of the amide- π stacking interaction.^[5,377,403]

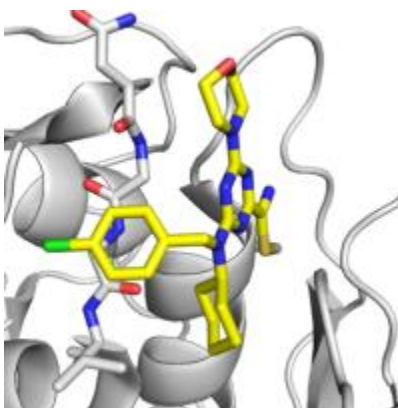


Figure 68 Crystal structure of human Cathepsin L (2.8 Å resolution, PDB: 4AXM)^[234] with a covalently bound triazine nitrile inhibitor. Color code: C_{enzyme} light grey, C_{ligand} yellow, O red, N blue, S dark yellow, Cl green.

In pursuit of conclusions on structure-activity relationships in enzyme inhibition, one of the most important research goals is to get access to a high number of rationally designed molecules and subject them to inhibition assays with the enzyme. In this project we wanted to characterize effects of tuning an amide- π interaction on affinity of a known class of inhibitors of

rhodesain and human Cathepsin L. Major objective that would lead to the results is synthesis of a number of analogues of the triazine nitrile inhibitor, with variations in stereoelectronic properties of its aromatic residue that is directed into the S3 subsite of rhodesain (Figure 69).

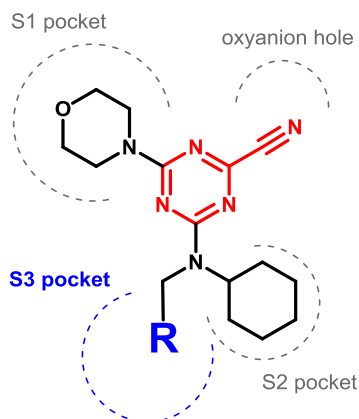


Figure 69 The triazine nitrile inhibitor scaffold with emphasis on the residue that stacks to peptide bonds (blue).

The simplified hypothesis is proposed: upon introduction of S3 pocket residues with ideal dipole alignments with the Gly-Gly motif, the overall inhibitor potency should be enhanced, while the rest of the molecule remains unchanged.

The objective was to synthesize as many analogues as possible of the triazine nitrile inhibitor, with the heteroaromatic residue that stacks onto the amide bonds as an only variable substituent.

Trends in quantitative values of inhibition potency would provide insight in how do changes in the varied heteroaromatic residue, e.g. electron abundance, dipole moment and the orientation of the dipole moment, affect the magnitude of amide- π stacking, and how important is to consider this type of nonbonding interaction in the inhibitor design.

2.4 Synthesis of Triazine Nitrile Inhibitors

2.4.1 Structure and Synthesis of the Triazine Nitrile Scaffold

A lead inhibitor scaffold, the morpholino- and cyclopentylamino-substituted triazine nitrile, was selected from previous studies.^[234] It gives potencies of 3–55 nM. A fixed secondary modification was introduced into it, in order to achieve lower potencies in nanomolar range (200 nM), due to quantitative precision limitations of a typical inhibition assay. Higher inhibition constant range obtained from *in vitro* inhibition assays would provide more fidelity to the differences in the inhibitor analogues' potencies. Overall inhibitor scaffold potency was downgraded by introducing a cyclopentyl residue instead of cyclohexyl, which binds a lipophilic pocket, referred to as S2 (Figure 70).

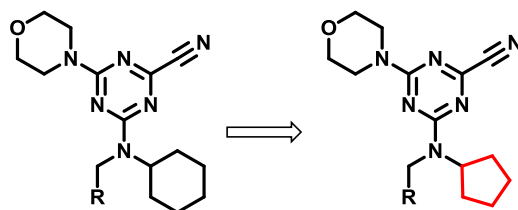
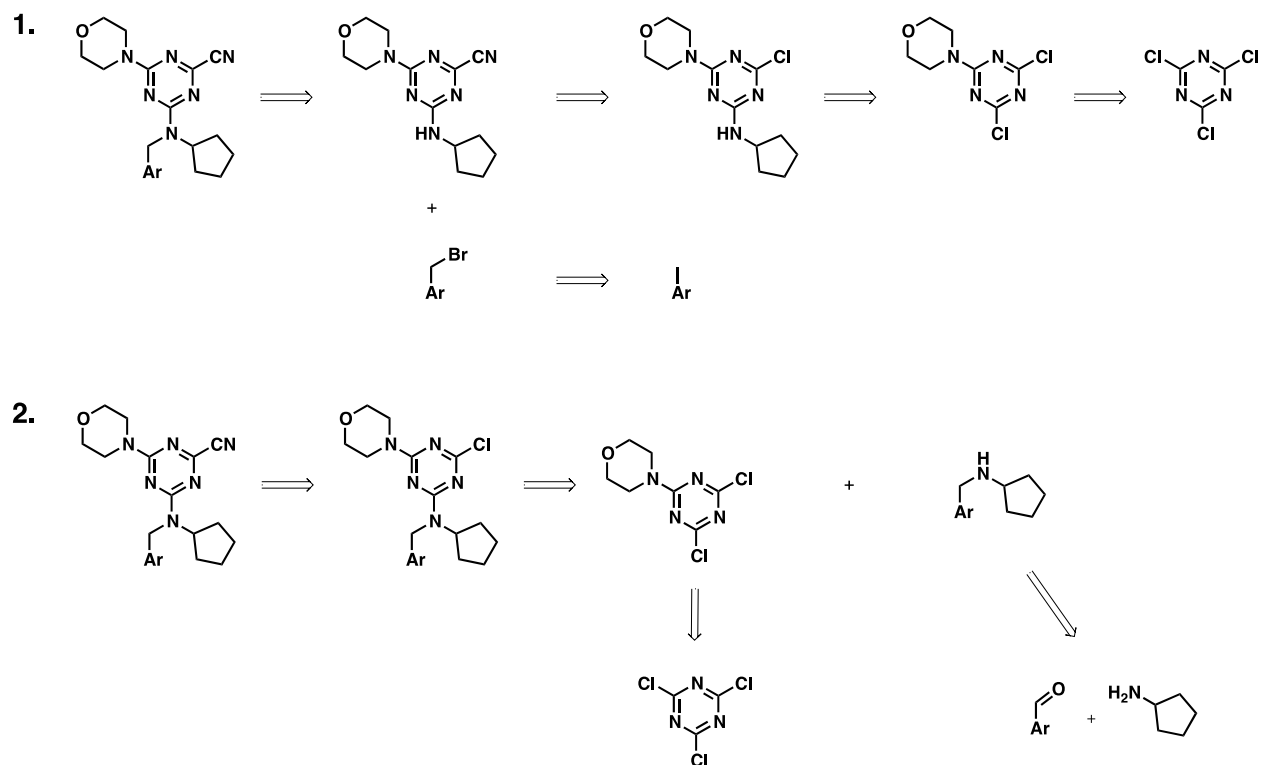


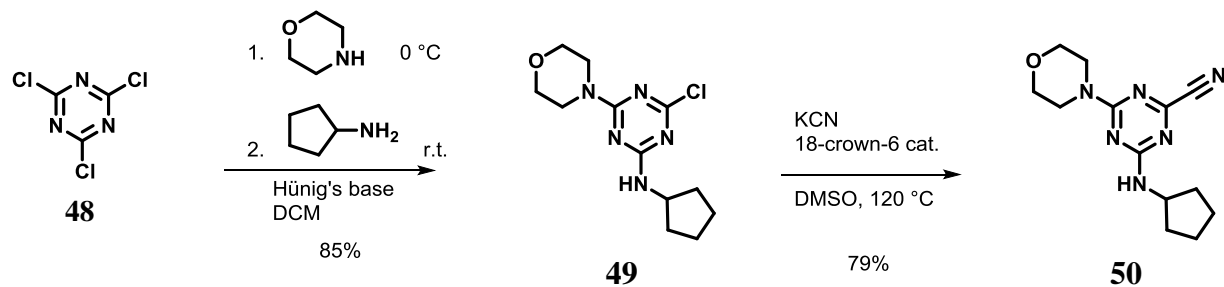
Figure 70 The fixed lipophilic vector in the inhibitor design, changed from cyclohexyl to cyclopentyl.

There are two different approaches to synthesize such type of molecules. Retrosynthetic disconnection analyses are based on previous work on this class of inhibitors.^[234,236,423] We have focused on two different approaches (Scheme 64). The first approach involves sequential nucleophilic aromatic substitution of cyanuric chloride as a starting compound. The resulting triazine nitrile, functionalized also with morpholine and cyclopentylamine, is a subject to deprotonation to the corresponding amide, and alkylation with various benzylic bromides (Scheme 64.1). The second approach also involves a sequential substitution of cyanuric chloride, but, instead of using cyclopentylamine as one of the nucleophiles, a disubstituted amine is first synthesized, by a reductive amination of aryl aldehyde with cyclopentylamine (Scheme 64.2).



Scheme 64 Retrosynthetic analysis depicting two different approaches in synthesis of the desired scaffold.

Preparation of key intermediate for the benzylic bromide-based approach is depicted on Scheme 65. Cyanuric chloride (**48**) was treated with morpholine at 0 °C and then with cyclopentylamine at room temperature, both in presence of Hünig's base. Intermediate **49** was isolated and then refluxed in DMSO with potassium cyanide and a catalytic amount of 18-crown-6 to enhance cyanide's nucleophilicity and yield **50**.



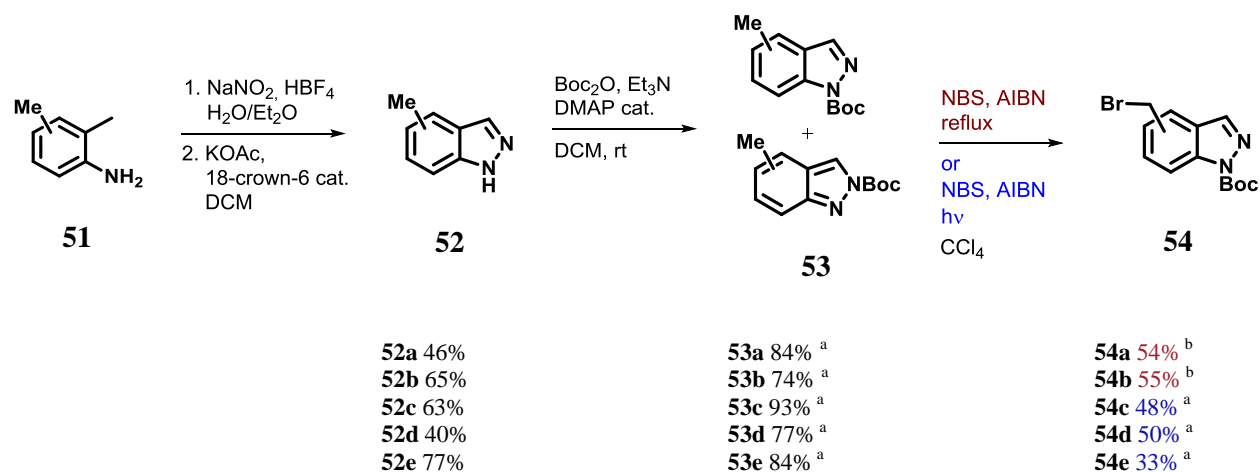
Scheme 65 Synthesis of the triazine nitrile intermediate **50**.

Interestingly, it was noticed that monochloro substituted triazine **49** is so much less electrophilic than cyanuric chloride, that it withstands recrystallization from a boiling water/isopropanol mixture. Similarly, even 2-(dialkylamino)-4,6-dichloro triazines have remarkable stability in hot water.^[451]

2.4.2 Synthesis of Indazole Series of Target Compounds

2.4.2.1 Bromomethyl Indazoles

Bromomethyl indazoles, as well as some of their non-brominated counterparts, are not commercially available, so they needed to be synthesized during the course of this project (Scheme 66). Among the variety of well known methods for formation of indazoles, a variant of a method that involves diazotization of dimethylanilines **51** and base induced cyclization was used to obtain all *C*-methyl substituted *1H*-indazoles **52**. Due to the need of selective deprotonation in the later stages of synthesis, methyl indazoles were *N*-Boc-protected, yielding mixtures of two regioisomers of derivatives **53**.



Scheme 66 Synthesis of *N*-Boc-protected bromomethyl indazoles from dimethyl anilines; ^a mixture of two *N*-Boc regioisomers; ^b single *N*-Boc regioisomer isolated.

Derivatives **54a** and **54b** (Figure 71) were obtained by refluxing corresponding protected methyl indazoles **53** in CCl_4 with *N*-bromosuccinimide and catalytic amount of AIBN. Under these thermal conditions, Boc-protecting groups have rearranged from *2H*-indazole regioisomers to corresponding *1H*-regioisomers. Attempts of radical bromination in reflux conditions with the other derivatives were unsuccessful, leading to complex mixtures of undesired byproducts. To brominate **53c-e** in the benzylic positions, we have turned to a UV-induced radical bromination at room temperatures, which afforded bromomethyl indazoles **54c-e**, though still as mixtures of two *N*-Boc-regioisomers, formed in the preceding step.

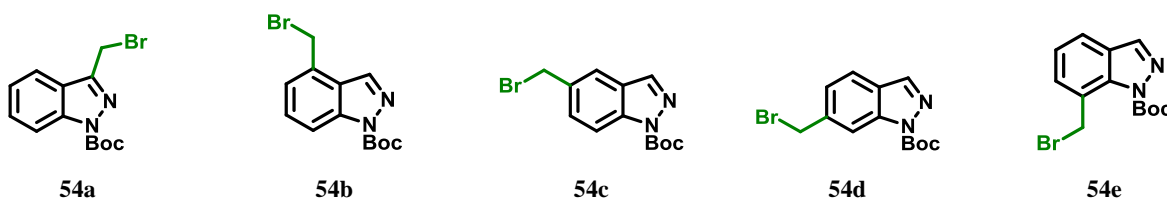
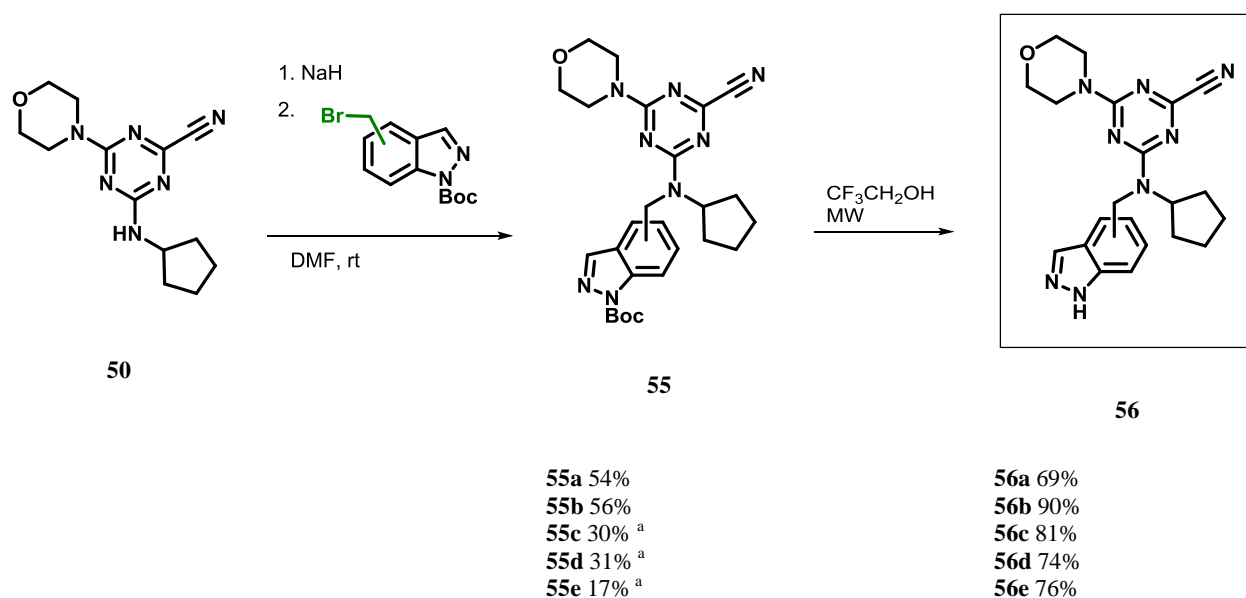


Figure 71 Synthesized *N*-Boc-protected bromomethyl indazoles.

2.4.2.2 Completion of the Indazole Series

Triazine nitrile intermediate **50** was deprotonated with sodium hydride in anhydrous DMF and then treated with bromomethyl indazoles **54** to yield *N*-protected derivatives **55**. Microwave irradiation in 2,2,2-trifluoroethanol facilitated removal of Boc-protecting groups, and thus furnished the desired indazole substituted triazine nitriles **56** (Scheme 67). The first approach to the desired triazine nitrile target molecules, using a straightforward, parallel methodology in six synthetic steps, successfully afforded series of five indazole derivatives **56a-e** (Figure 72).



Scheme 67 *N*-Alkylation and deprotection sequence for completion of indazole series of derivatives; ^a mixture of two *N*-Boc regioisomers.

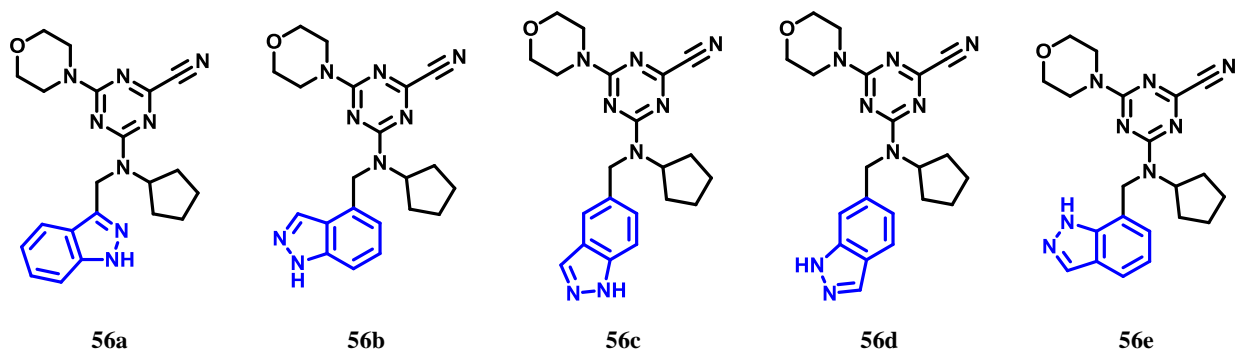


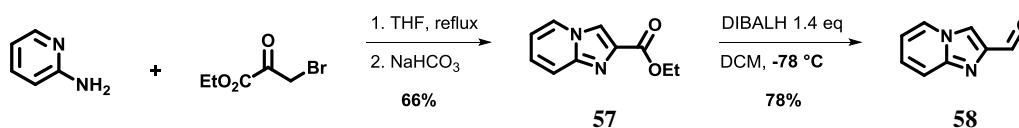
Figure 72 Completed desired indazole-substituted triazine nitrile compounds.

2.4.3 Synthesis of an Imidazopyridine Derivative

As a complement to the series of indazole derivatives, it was of interest to obtain a molecule that would have a bicyclic aromatic residue with different electronic properties, e.g. stronger dipole moment, different orientation in respect to its aryl-CH₂ bond. One of such derivatives which is usually easily accessible is imidazo[1,2-a]pyridine, substituted at position 4. It was rationalized that it could be prepared through the reductive amination approach, due to the fact that preparations of the corresponding required imidazo[1,2-a]pyridine-2-carbaldehyde are known.^[452,453]

2.4.3.1 The Imidazopyridine Aldehyde

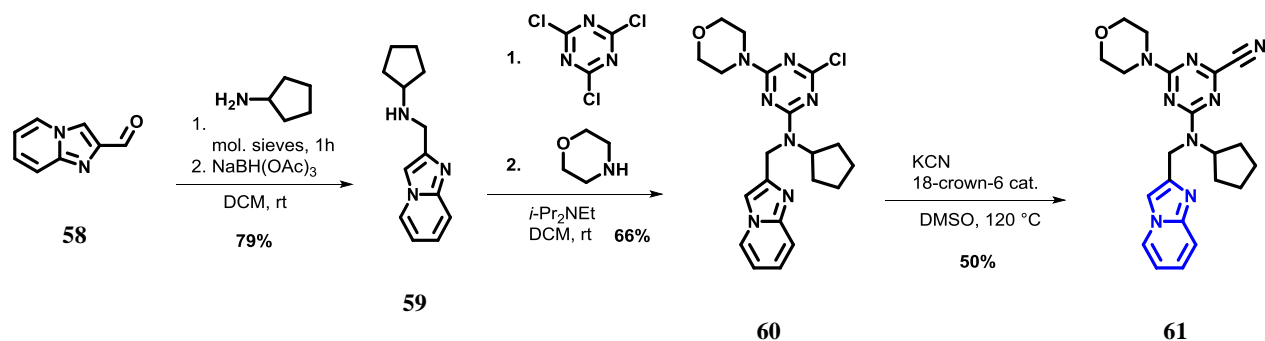
Preparation of this heterocycle is facile, through condensation of a bromopyruvate ester with 2-aminopyridine (Scheme 68). The allylic or heteroaromatic esters like **57** are usually reduced with LiAlH₄ to alcohol and then reoxidized to aldehyde with MnO₂.^[452] We have attempted a low temperature controlled reduction of **57** with DIBAL-H instead, which successfully directly yielded 78% of the desired aldehyde **58**.



Scheme 68 Synthesis of aldehyde **58**.

2.4.3.2 Completion of the Imidazopyridine Derivative

Aldehyde **58** was subjected to reductive amination with cyclopentylamine in the presence of molecular sieves for condensation to an imine (Scheme 69).



Scheme 69 Completion of synthesis of the triazine nitrile **61**.

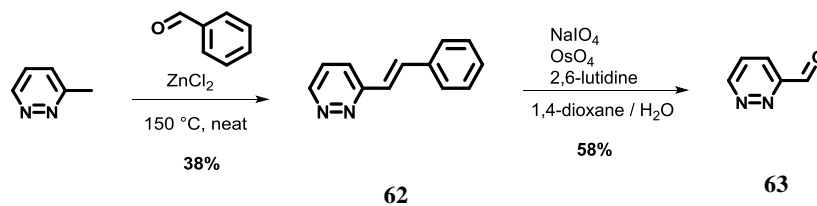
The resulting product amine **59** was used in substitution of cyanuric chloride, where an intermediate was immediately treated with morpholine in the same pot to furnish the triazine chloride **60**. The desired triazine nitrile target **61** was obtained after reaction with potassium cyanide in DMSO, at 120 °C.

2.4.4 Synthesis of a Pyridazine Derivative

It was envisioned that a pyridazine analogue of triazine nitrile inhibitors could be accessed via approach that utilizes reductive amination. The first task was to obtain the corresponding aldehyde.

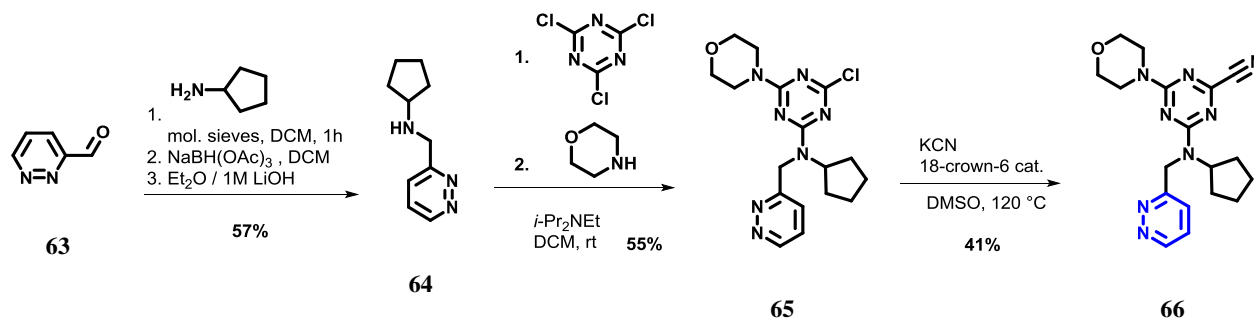
2.4.4.1 The Pyridazine Aldehyde

3-Methylpyridazine was neatly condensed with benzaldehyde, using stoichiometric amount of ZnCl₂ at 150 °C (Scheme 70). Resulting stilbene type pyridazine **62** was subjected to Lemieux-Johnson oxidation to afford the aldehyde **63**.

Scheme 70 Synthesis of aldehyde **63**.

2.4.4.2 Completion of the Pyridazine Derivative

With the aldehyde **63** in hands, the reductive amination with cyclopentylamine produced the disubstituted amine **64** (Scheme 71). Sequential nucleophilic aromatic substitution starting with cyanuric chloride provided intermediate **65** and, ultimately, the desired pyridazine substituted final compound **66**.

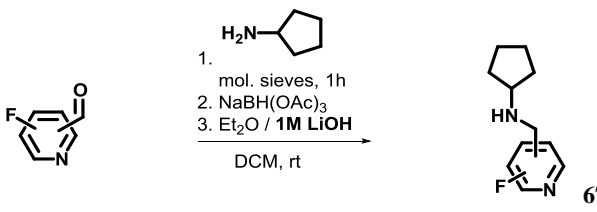
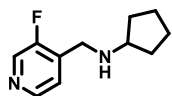
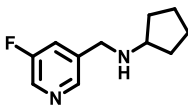
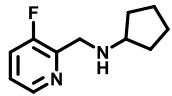
Scheme 71 Completion of synthesis of the triazine nitrile **66**.

2.4.5 Synthesis of Fluoropyridine Derivatives

2.4.5.1 Reductive Amination Towards Fluoropyridine Amines

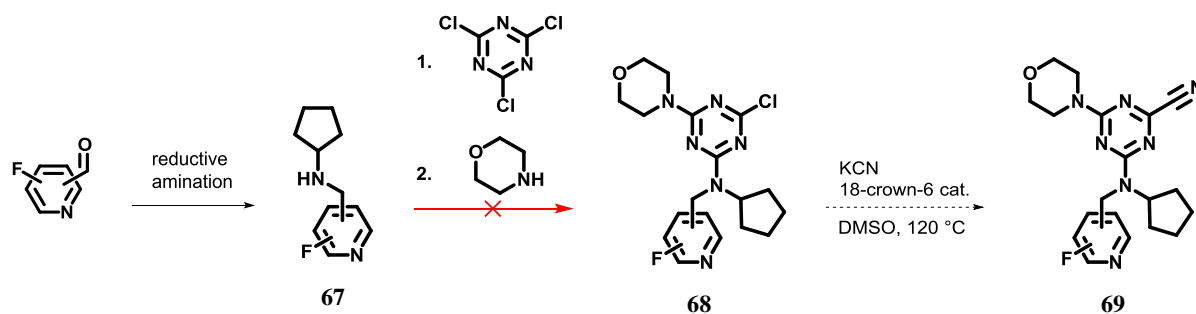
A selection of fluoropyridine aldehydes is commercially available. Due to possible problems with undesired electrophilicity of 2-fluoropyridines which could make them incompatible with our synthetic strategies, and since 3-fluoropyridine aldehydes are commercially available, we have decided to pursue synthesis of 3-fluoropyridine-substituted triazine nitrile targets via reductive amination strategy. Three fluoropyridines were converted successfully to disubstituted amines **67a-c** (Table 16).

Table 16 Reductive amination of fluoropyridine aldehydes with cyclopentylamine.

compound	struct. formula	isolated yield (%)
		
67a		48%
67b		72%
67c		68%

2.4.5.2 Methodology Adaptation for Selective Triazine Substitution

It was envisioned to obtain the final compounds in the analogous way to the synthesis of target compound **61**. Initial attempts of selective reaction of fluoropyridine amines **67** with cyanuric chloride failed (Scheme 72).



Scheme 72 Initial approach to synthesis of fluoropyridine substituted target molecules.

When each of the fluoropyridine amines **67** was reacted to cyanuric chloride at low temperatures in dichloromethane, the mixtures turned dark brown, containing dark brown precipitates. The analyses indicated formations of complex mixtures of products in each case. First probable cause for this lack of selectivity is high electrophilicity of cyanuric chloride, confronted with two nucleophilic nitrogens in the fluoropyridine amine molecule, one on pyridine being less sterically crowded, and thus more kinetically available to react (Figure 73A). In favor to this explanation is formation of strongly colored precipitates in the aforementioned reactions, and reported facile formation of pyridinium triazine betaines, which are sometimes also patented as dyes.^[454–459] Also, Mayr and Brotzel have demonstrated that in CH_2Cl_2 pyridines have nucleophilicities comparable to phosphanes.^[460]

It is known that chlorotriazines are becoming significantly less electrophilic after substitution of each sequential chlorine.^[451] Thus, first substitution on cyanuric chloride is usually performed at temperatures lower or equal to $0\text{ }^\circ\text{C}$, while the second chloride substitution requires $25\text{--}45\text{ }^\circ\text{C}$, and ultimately the third one needs to be heated at more than $80\text{ }^\circ\text{C}$ with good nucleophiles like amines, thiolates or cyanides.^[451,461,462]

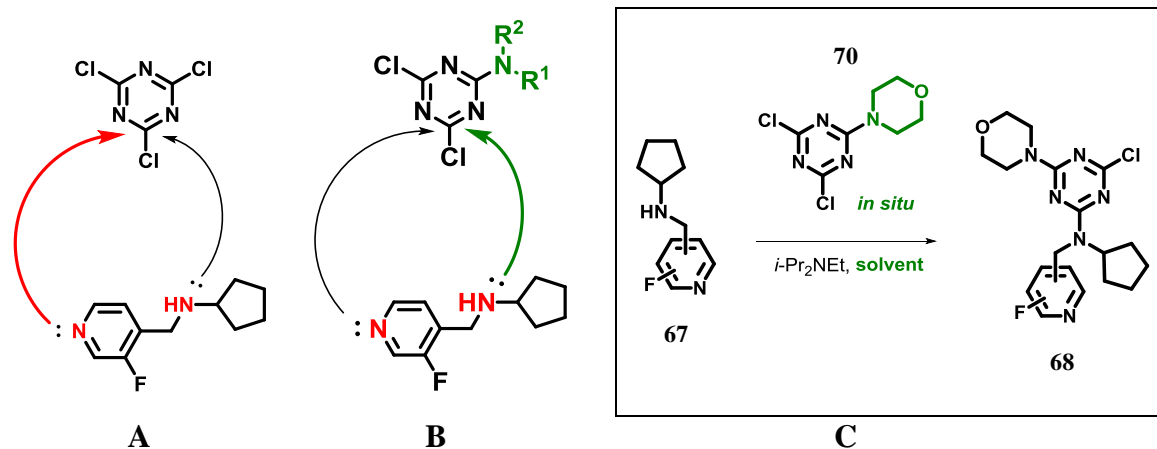


Figure 73 Competing nucleophilicities of unhindered pyridine nitrogen and hindered secondary amine, to cyanuric chloride (A) and less reactive 1-(*N,N*-dialkyl)amino-3,5-dichloro-triazine (B). C: Proposal of improved synthesis of intermediates **68**.

Treating cyanuric chloride first with morpholine would provide a much less electrophilic dichloro triazine **70**, which would presumably be much less kinetically reactive to more exposed pyridine nitrogen of the nucleophile **67**. Also, careful choice of the solvent could enhance the selectivity further (Figure 73B and C). In the initial failed experiment we have used exactly two equivalents of Hünig's base to scavenge two equivalents of HCl that get released during the proposed conversion. Since it is difficult to predict the difference between basicities of Hünig's base and the dialkylamine site of **67**, it was simply rationalized that higher excess of the sterically hindered base will cause lower extent of protonation and loss of nucleophilicity of **67**. Consequently, we set out to change several factors in our procedure for substitution of cyanuric chloride in a test experiment (Table 17).

It was found that in the first step, regardless of solvent, cyanuric chloride cleanly reacts with morpholine to produce intermediate **70**. On the other hand, the second step, when performed in methylene chloride and in tetrahydrofuran, produces significant amount of undesired byproducts, while in acetonitrile it produces only the desired **68a** at the fastest rate compared to other instances. The newly found optimal conditions were used for completion of synthesis of the fluoropyridine functionalized inhibitors.

Table 17 Investigation of effect of a selection of solvents on reaction rate and selectivity.

1. 1.0 eq, -20 °C, 30 min

2. 1.0 eq, RT, 60 min

$i\text{-Pr}_2\text{NEt}$, 4.0 eq
solvent

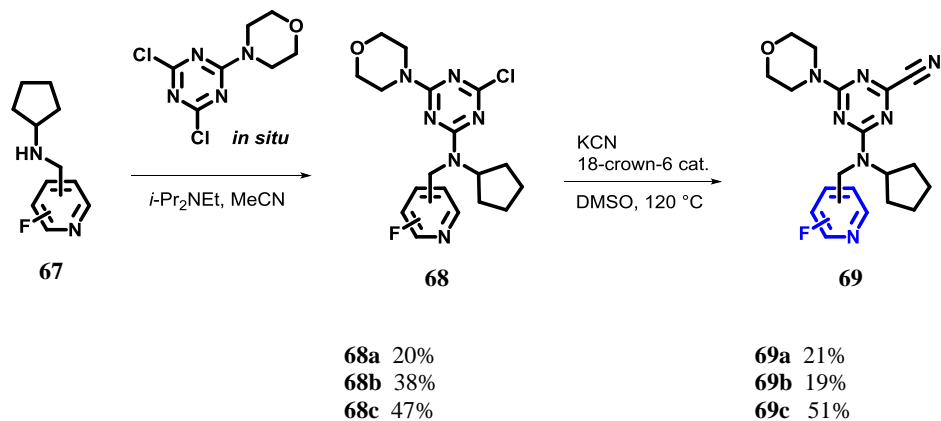
68a + **70** + unidentified byproducts

solvent	68a (A%, 254nm) ^a	70 (A%, 254nm)	byproducts (A%, 254nm)
CH ₂ Cl ₂	12	79	9 ^b
toluene	19	81	-
THF	18	77	5
MeCN	22	78	-
CH ₂ Cl ₂ / EtOH 9:1	7	93	-
DMF	3	97	-

Reaction conditions: In each instance, in a given anhydrous solvent, at -20 °C, cyanuric chloride was treated with 1.0 eq morpholine for 30 min, and then with 1.0 eq **67a** at room temperature for 60 min. ^aThe values are peak area percentages from HPLC chromatograms recorded by UV detection at 254 nm. ^b Prolonged reaction time (>60 min) in CH₂Cl₂ leads to further increase of amount of byproducts.

2.4.5.3 Completion of Fluoropyridine Derivatives

The series of three fluoropyridine inhibitors was completed by parallel synthesis starting by treatment of amines **67** with the *in situ* preformed morpholino-dichloro-triazine, in acetonitrile. Successfully obtained triazine chlorides **68** were converted to the desired targets **69** by the substitution with cyanide (Scheme 73).

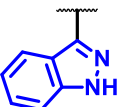
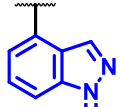
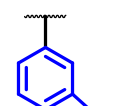
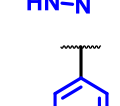
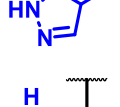


Scheme 73 Completion of synthesis of the desired fluoropyridine-substituted triazine nitrile derivatives.

2.5 Results and Discussion

2.5.1 Inhibition Assays with Rhodesain and hCatL

All of the final synthesized compounds were subjected to fluorescence based inhibition assays with both rhodesain and hCatL cysteine proteases.^[463] Constants of inhibition have been determined (Table 18). In inhibition of rhodesain, K_i values for indazole derivatives (**56a–e**) are in range from 147–247 nM, presenting no significant differences between each other. Fluoropyridine derivatives (**69a–c**) display somewhat lower K_i values in range 103–155 nM. The best inhibitor in both cases seems to be imidazo[1,2-a]pyridine derivative **61**. Interestingly, one can observe that most of the inhibitors have lower potency when assayed with hCatL, except the imidazopyridine **61** and 5-indazolyl derivative **56c**, which show higher potency to hCatL.

	<i>clogD</i>	rhodesain K_i [nM]	hCatL K_i [nM]
56a 	4.28	247	549
56b 	4.12	147	195
56c 	4.12	186	72
56d 	4.12	170	266
56e 	4.12	214	216

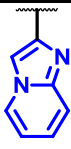
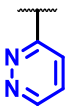
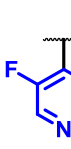
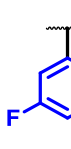
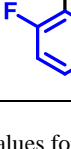
	<i>clogD</i>	rhodesain K_i [nM]	hCatL K_i [nM]
61 	3.84	96	35
66 	2.51	n/a (unstable)	n/a (unstable)
69a 	3.63	139	276
69b 	3.63	103	270
69c 	3.79	155	383

Table 18 Measured constants of inhibition and calculated *clogD* values for all final triazine nitrile inhibitors in this work.

Unfortunately, pyridazine compound **66** was found unstable in the assay conditions, making its K_i value impossible to determine.

Possible reasons for such observations in inhibition potencies, that is, the structure-activity relationship, have to be discussed in terms of structural features of binding interactions. Computational methods have been used to model and propose binding modes of inhibitors in this work, based on the determined X-ray structures of rhodesain (1.16 Å resolution, PDB: 2P86) and hCatL-inhibitor complex (2.8 Å resolution, PDB: 4AXM).^[234]

2.5.2 Computer Assisted Molecular Modelling

Molecular modelling study was performed to propose binding modes. The x-ray crystallography determined structure of complex of triazine nitrile inhibitor was loaded into MOLOC computer software.^[108] For each compound presented in this study, an instance was generated by editing the S3 pocket binding aromatic residue, and the structures were optimized by the MAB molecular force field energy minimization protocol. MAB force field is part of the MOLOC software, and it is trained versus a test set of highly refined 1589 structures from Cambridge Structural Database. When the optimization protocol is initiated, it searches for the local minimum of total energy, containing the following terms:

$$E = E_{HB} + E_{VB} + E_{tor} + E_{disp} + E_{BS} + E_{pyr} + E_{1,4} \quad \text{Eq. 1}$$

Simultaneously, the protocol takes into account energy terms of hydrogen bonds (E_{HB}), valence angle bending distortions (E_{VB}), bond torsion angle strain (E_{tor}), dispersion interactions from van der Waals contacts (E_{disp}), bond stretching (E_{BS}), distortion of pyramidality (E_{pyr}), and 1,4-interactions ($E_{1,4}$). Although it lacks a good model of Coulomb interactions and solvation, its output of force field minimized structure may indicate relationship of certain aspects of molecular mechanics of the inhibitor with the experimentally measured inhibition data.

In contrast to the symmetrical phenyl residues in triazine nitrile inhibitors from the previously published studies, the aromatic residues discussed in this work do not have the same axial symmetry. The consequence of this was observation that, upon force field optimization, depending on random preorientation, they can adopt two different stacking modes onto enzyme's S3 subsite peptide bonds (Figure 74). Since output of MAB force field optimization doesn't

indicate excessive, destabilizing steric energies in either of the binding modes for each of these molecules, it is rational to assume that they can both be adopted in reality. Equilibrium between those two poses is proposed. Naturally, the more energetically favored one should be more abundant.

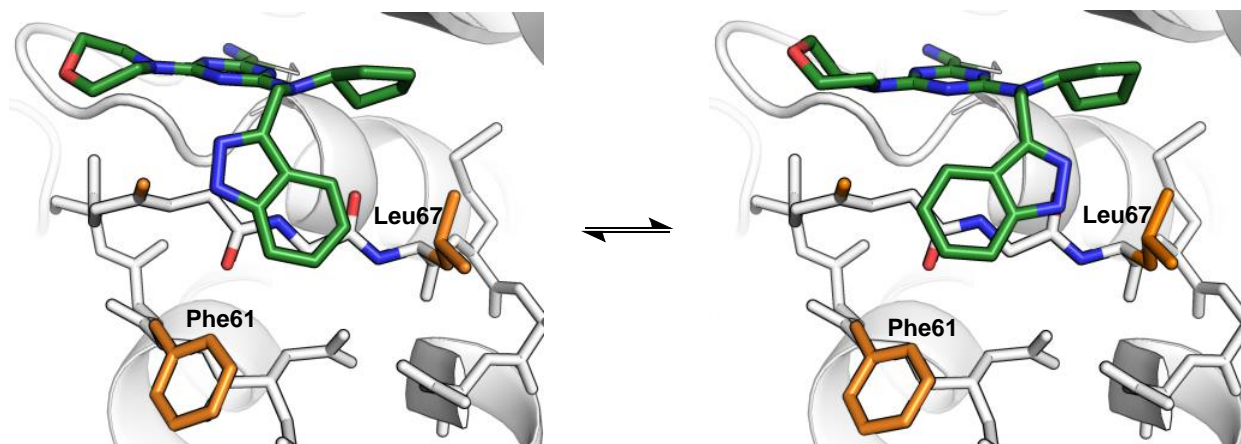


Figure 74 Two possible stacking modes of the inhibitor **56a** bound to rhodesain (1.16 Å resolution, PDB: 2P86),^[422] obtained by force field optimized modelling in MOLOC. Amide bonds stacked below the heteroaromatic residue are emphasized by standard peptide color-coding. Color code: C_{enzyme} white, C_{ligand} green, O red, N blue, and residues in vdW contact with the heteroarene are colored orange.

A force field optimization run has been performed for each inhibitor with both rhodesain and hCatL separately, at least in duplicates for both possible stacking modes. All optimization runs were setup with the inhibitor free to move, and all of the coordinates of atoms in the protein fixed, except for the peptide side chains which are in the range of van der Waals contact with the aromatic stacking substituent of the inhibitor.

The proposed equilibrium between stacking modes should shift in favor of energetically lower mode. MAB molecular force field predicts steric interactions very well, but it lacks Coulomb interaction contribution and a good solvation model. Since this scenario is set on the surface of the protein, which contains mostly polar and ionic residues, and thus also has a net surface electric field, it is very important to consider Coulomb interactions to determine the more adopted binding conformation of the inhibitor.

These observations call for consideration of additional factors. In the overlay ensemble of binding modes of all inhibitors in both rhodesain and hCatL, one can correlate the seemingly worst inhibition values with the highest declination of angle of axis that connects the benzylic carbon and adjacent nitrogen atom (attached to the triazine in the inhibitor), from the ideal angle

(Figure 75C). The highest lateral strain of the binding modes of **56a** (depicted in red) is best represented in the deviation of the “benzylamine axis” in respect to the centered best inhibitor, imidazo[1,2-*a*]pyridine **61** (blue), which seems to be ideally positioned. Higher strain imposed by efficiency of stacking could be one of the reasons of lower potency of 3-indazolyl derivative **56a**, which is not that significant in rhodesain ($K_i = 247$ nM) as it is in hCatL ($K_i = 549$ nM). In contrast to this, there is a significant enhancement in potency of **61** in hCatL ($K_i = 35$ nM) versus one that it manifests in rhodesain ($K_i = 96$ nM).

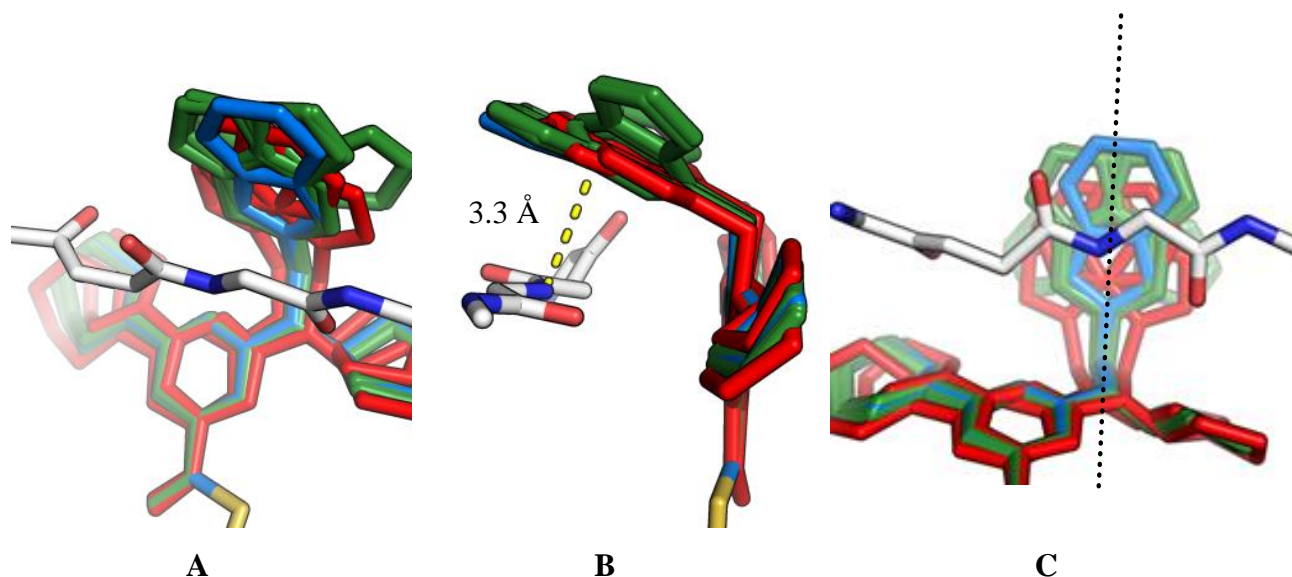


Figure 75 Ensemble of both possible modelled binding modes of each of inhibitors **56a–e** and **61** in rhodesain (1.16 Å resolution PDB: 2P86),^[422] depicted in three different perspectives (A, B and C). Red: E and W binding mode of **56a**; light blue: E and W binding mode of **61**; green: E and W binding modes of **56b–e**. Stacking amide bonds are represented in light grey with color coded carbonyl oxygen (red) and nitrogen atoms (dark blue).

The preceding investigation on amide- π stacking in a theoretical model between pyridine and *N*-methylacetamide, in different mutual orientations presented a calculated value of 3.4 Å as an optimal value in terms of distance of stacking planes.^[377] Our force field optimization finding of 3.3 Å of stacking distance is in a good agreement with the theoretical investigation (Figure 75B). The calculations also found antiparallel stacked configuration as the most favored one. This also supports a reported finding that antiparallel orientation of an oxazole dipole of an inhibitor of factor Xa, increases affinity 11-fold, in contrast to its isomer with the opposite oxazole dipole orientation.^[384]

In the case of heteroarene stacking in rhodesain and hCatL, this scenario is additionally complicated by having the heteroarene stacked onto **two** adjacent amide bonds of Gly-Gly, with

their dipole moments in **antiparallel** orientation. Moreover, this subsite is almost completely exposed to the solvent environment.

Two practical physical considerations are represented by basic electrostatic equations related to electric dipoles:

$$U = E * p * \cos \theta = -\vec{p} \cdot \vec{E} \quad \text{Eq. 2}$$

$$\tau = E * p * \sin \theta = \vec{p} \times \vec{E} \quad \text{Eq. 3}$$

where U is the potential energy of a dipole in an electric field, which depends on the magnitudes of the electric field E , the dipole moment p , and cosine of the angle θ between orientation of the dipole in respect to the vector of the electric field. Cosine relationship ensures that energy is lower if the dipole moment is aligned more parallel to the electric field. τ is a torque causing the force F which the electric field exerts onto the dipole, trying to rotate it into orientation parallel to the electric field (Figure 76). Product $\sin\theta * p$ represents the vector component of the dipole moment, orthogonal to the electric field, hence the closer angle to 90° , the higher the torque will be.

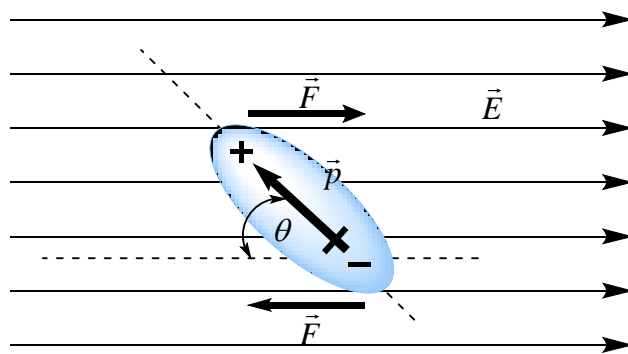


Figure 76 Dipole moment p in the electric field E

Based on these notions, it is viable to consider the local Coulomb contribution to the enthalpy of inhibitor binding, as the energy of the local dipole moments in the protein surface electric field. Hence, stabilization of stacking depends on how much do local vectors of dipoles of the heteroarene and the two peptide bonds cancel out each other.

To take into account how do local dipoles interact, isolated dipoles of all heteroaromatic residues and amide bonds have been computed using *ab initio* method MP2 with 3-21G basis set

(Table 19). Dipole moments were calculated for the discussed heterocycles, both without and with the benzylic carbon attached. It is apparent that benzylic substitution introduces significant perturbation in the charge distribution in each heterocycle, depending on the position of substitution, which is in line with the studies that suggest that small dipole moment contribution in toluene makes it a better model for π - π stacking interactions in proteins instead of benzene.^[464,465] For example, unsubstituted indazole has a calculated dipole moment of 2.16 D, while methyl substituted indazoles have it in range from 1.84–2.42 D. Similar effect is observed with imidazo[1,2-a]pyridines and 3-fluoropyridines. Unsubstituted imidazo[1,2-a]pyridine has a very strong dipole moment of 4.06 D, while methyl substituted has considerably lower 3.63 D, but still comparable to calculated 3.8 D for imidazole which was used as one of the stronger examples in the theoretical amide- π stacking study.^[377] In fluoropyridine derivatives, different methyl substitution patterns cause dipole moments to vary from 1.87–2.78 D. Dipole moment of an amide bond is exemplified on *N*-methylacetamide.

Table 19 Dipole moments of the discussed heteroaromatic residues, calculated via MP2/3-21G *ab initio* method.

structure	μ [D]						
	2.16		1.84		3.63		2.66
	4.06		1.96		2.78		
	3.92		2.29		1.87		
			2.51				
			2.42				

When it comes to comparison of each inhibitor in rhodesain and hCatL, significant enhancements in K_i values are observed for **9c** and **14** in hCatL. These differences can be explained via identification of contributing nonbonding interactions. The single important difference between binding sites of rhodesain and hCatL is that hCatL has a charged glutamate residue, instead of a neutral phenylalanine which replaces it in rhodesain (Figure 77 B and C). The negative charge of the Glu63 side chain in hCatL is in the immediate vicinity of the S3 subsite, and makes a significant perturbation of the local surface electric field. This change affects the energy of any dipoles next to it.

Two factors improve the potency of inhibitor **9c** in hCatL. The obvious one is the ideal mutual positioning of inhibitor's indazole and the glutamate residue of the enzyme, to engage in hydrogen bonding (Figure 77). It is apparent that this hydrogen bonding can happen only in the stacking mode in which the N–H hydrogen bond donor of indazole is properly positioned in the vicinity of Glu63 (Figure 77B). It is thus plausible to presume that this inhibitor is bound almost exclusively in that stacking mode in hCatL. One may notice that the dipole moments of the heterocycle and the peptide bonds below are oriented orthogonally to each other in this case, and that the dipole moment of the heterocycle is orthogonal to the electric field of the Glu63 side chain. This raises the energy of this stacking mode in respect to the electric field of the negative charge on Glu63, but in this case, given the experimentally observed enhancement, hydrogen bonding energy overwhelms ion-dipole repulsive torque.

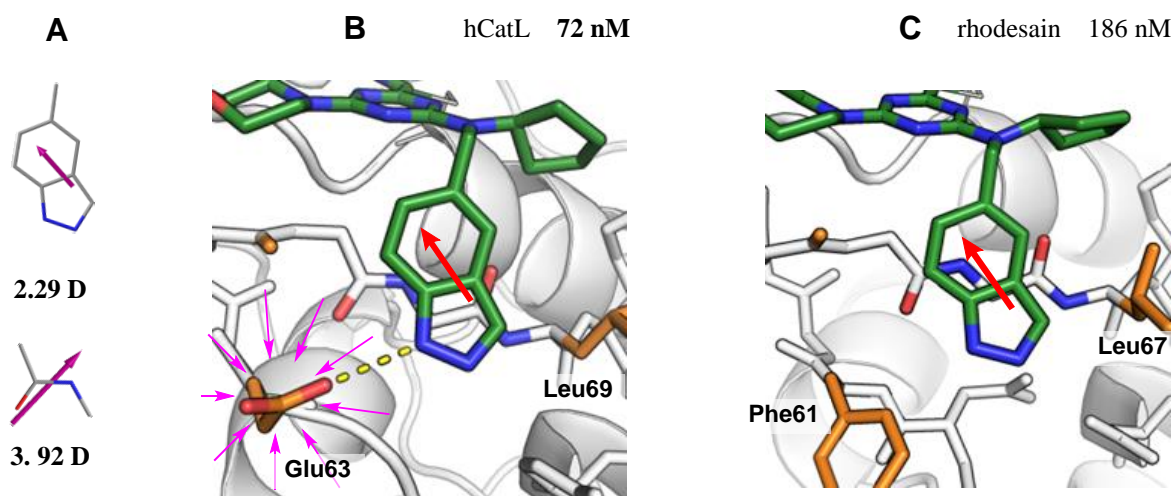


Figure 77 Dipole moments of the stacking residue of **56c** and one of the amide bonds (A), and modelled stacking modes of **56c** in hCatL (2.8 Å resolution PDB: 4AXM,^[234] B) and in rhodesain (1.16 Å resolution PDB: 2P86, C).^[422] Color code: C_{ligand} green, C_{protein} light grey, O red, N blue. Residues in vdW contact to the heteroarene are colored orange. Red arrows represent the dipole moments of the heterocycles. Pink arrows represent the electric field of Glu63.

Inhibitor **14** has already been presented as having the ideal “benzylamine axis” angle, after the force field optimization. It has the strongest enhancement in inhibition, down to $K_i = 35$ nM. In agreement with the theoretical study on stacking of heteroaromatics to amide bond, having the strongest dipole moment in this series of inhibitors, in an antiparallel alignment in respect to one of the protein backbone amide bonds, it is the best inhibitor in rhodesain. Also, it is even more potent inhibitor of hCatL. In hCatL, in its optimal stacking mode, its strong dipole moment is parallel to the electric field of the close Glu63 residue in the S3 subsite of hCatL (Figure 78). Additionally, the positive pole of the heteroaromatic residue is in a direct van der Waals contact with the carboxylate of Glu63, making it a strong, attractive ion-dipole interaction, fixing the inhibitor in an ideal stacking and binding pose.

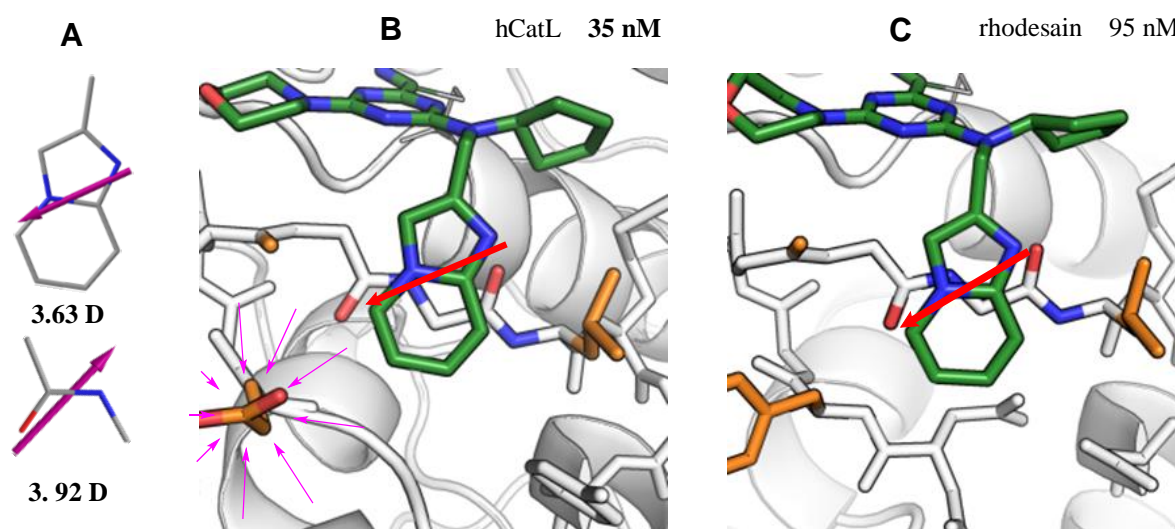


Figure 78 Dipole moments of the stacking residue of **61** and its antiparallel stacking amide bond (A), and stacking modes of **61** in hCatL (2.8 Å resolution PDB: 4AXM,^[234] B) and in rhodesain (1.16 Å resolution PDB: 2P86,^[422] C). Color code: C_{ligand} green, C_{protein} light grey, O red, N blue. Residues in vdW contact to the heteroarene are colored orange. Red arrows represent the dipole moments of the heterocycles. Pink arrows represent the electric field of Glu63. Red arrows represent the dipole moment of the heterocycle. Thin pink arrows represent the electric field of Glu63.

2.6 Summary and Outlook

Ten final compounds of the triazine nitrile type have been synthesized according to two different approaches. The series of five different indazole derivatives were obtained via alkylation with the in-house prepared indazole building blocks containing benzylic bromide function. On the other hand, three different fluoropyridine derivatives were obtained through the approach utilizing reductive amination in the early stage. A method for chemoselective reaction of pyridine amines was developed to enable successful synthesis of the final fluoropyridine triazine nitriles.

The final compounds have been assayed in the inhibition experiments with both rhodesain and human Cathepsin L, and their inhibition potencies have been acquired. While most of the inhibitors produced in this work have K_i values in the range 103–383 nM, one of the inhibitors was particularly more potent with both enzymes. The imidazo[1,2-a]pyridine derivative displays $K_i = 96$ nM in rhodesain and enhancement to $K_i = 35$ nM in hCatL. Significant enhancement of K_i in hCatL was observed for 5-indazolyl derivative. Based on molecular modeling this can be attributed to hydrogen bonding of indazole's N–H to the carboxylate oxygen in Glu63 in hCatL.

Binding mode of the imidazo[1,2-a]pyridine derivative has also been modelled in rhodesain and hCatL. Since this work is a smaller part of much bigger investigation in context of amide- π stacking interaction in biomolecular systems, we turned our attention to the previously proposed important factors in amide- π stacking.^[377] Since the theory advocates that the stacking is more efficient when the aromatic residue and the amide bond stack their dipole moments in the antiparallel configuration, we have calculated the dipole moments of all of the discussed stacking residues. Significantly better affinity of the imidazo[1,2-a]pyridine derivative can be attributed to the fact that this heterocycle has a much bigger dipole moment than the rest (3.63 D). Hence, it can nicely stack to almost completely “cancel out” one of the dipole moments (3.92 D) of the two amide bonds that it stacks to in an antiparallel fashion.

This study indicates that certain enhancements in binding can be explained in terms of interplay of local electrostatics and amide- π stacking. However, to get reliable information on the effects of amide- π stacking on inhibition potency, trends will be established based on broader selection of compounds (Maude Giroud, ETH Zürich) that surpass the scope of this work.

2.7 Experimental Section

2.7.1 General procedures

2.7.1.1 General Procedure A (methyldiazoles):

A solution of aniline (1.0 eq) in Et₂O was cooled down in an ice bath, maintained at 0–5 °C and was treated with 54% HBF₄ (2.5 eq) in Et₂O. After 15 min of stirring at 0–5 °C, the mixture was treated dropwise over 30 min with 0.216 g/mL NaNO₂ aqueous solution (1.0 eq). After 60 min at 0–5 °C, additional portion of the solution of NaNO₂ (0.5 eq) was added, and the mixture was stirred for an additional 60 min. A white solid precipitate was subsequently filtered off, washed three times with diethyl ether, charged into a new round-bottom flask, purged with N₂ and dried *in vacuo*. The white solid was then stirred in CH₂Cl₂ with 18-crown-6 (0.05 eq) and maintained at 0–5 °C with an ice bath. KOAc (2.0 eq) was added in portions over 1 min. The reaction mixture was stirred for 5 h and had spontaneously warmed up to 24 °C. The solids were then filtered off, washed with three portions of CH₂Cl₂. The combined filtrates were evaporated and purified by MPLC.

2.7.1.2 General Procedure B (*N*-Boc-methyldiazoles):

A solution of indazole (1.0 eq) in CH₂Cl₂ was treated with Et₃N (3.0 eq), DMAP (0.10 eq) and Boc₂O (1.1 eq) at 24 °C. Upon indication of the completion of the reaction by TLC, the reaction solution was concentrated under reduced pressure, and purified by MPLC.

2.7.1.3 General Procedure C (*N*-Boc-bromomethyldiazoles):

A solution of protected indazole (1.0 eq) in CCl₄ was treated with NBS (1.4 eq) and AIBN (0.05 eq) at 80 °C until TLC indicated maximum conversion. The reaction mixture was cooled down

and the solids were filtered off and washed with CCl_4 . The filtrate was evaporated, and purified by MPLC.

2.7.1.4 General Procedure D (*N*-Boc-bromomethylindazoles):

A solution of protected indazole (1.0 eq) in CCl_4 was treated with NBS (1.15 eq) and AIBN (0.05 eq). The suspension was stirred and irradiated in a photoreactor equipped with the 12", 8 W UVC lamps emitting with the maximum at 254 nm, until TLC indicated maximum conversion. The solids were filtered off and washed with CCl_4 . The filtrate was evaporated and purified by MPLC.

2.7.1.5 General Procedure E (protected indazole triazine nitriles):

A solution of 4-(cyclopentylamino)-6-(4-morpholinyl)-1,3,5-triazine-2-carbonitrile (1.0 eq) in dry DMF was treated with NaH (2.0 eq) at 0 °C, and stirred for 60 min. The resulting suspension was treated with a solution of protected bromoindazole (1.10 eq) in dry DMF and was left stirring and spontaneously warming up to 24 °C for 3 h. The reaction mixture was quenched with brine and extracted with EtOAc. Organic extract was washed two times with brine, dried over anhydrous Na_2SO_4 , evaporated and purified by MPLC.

2.7.1.6 General Procedure F (indazole triazine nitriles):

A solution of protected triazine nitrile in 2,2,2-trifluoroethanol was heated and stirred at 100 °C for 3 h. The solution was evaporated and purified by MPLC.

2.7.1.7 General Procedure G (fluoropyridinyl(cyclopentyl)amine):

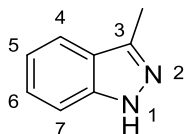
A solution of aldehyde (1.0 eq) and cyclopentylamine (1.0 eq) in CH_2Cl_2 was stirred over 4 Å molecular sieves at 24 °C for 60 min. $\text{NaBH}(\text{OAc})_3$ (2.0 eq) was added, and the mixture was stirred overnight. The mixture was quenched with 1M KOH, partitioned with EtOAc and decanted off from molecular sieves sediment. The aqueous layer was extracted two times with EtOAc. The merged organic extracts were washed with brine, dried over anhydrous Na_2SO_4 , and evaporated. The residue was purified by MPLC.

2.7.1.8 General Procedure H (fluoropyridinyl triazine chlorides):

A solution of cyanuric chloride (1.0 eq) in anhydrous MeCN was treated dropwise with a solution of *i*Pr₂NEt (4.0 eq) and morpholine (1.0 eq) in anhydrous MeCN at -20 °C and was stirred for 30 min at the same temperature. The mixture was subsequently treated dropwise with a solution of a secondary amine (1.0 eq) in anhydrous MeCN and left stirring overnight at 24°C. The mixture was evaporated and the residue was purified by MPLC.

2.7.2 Synthesized compounds

2.7.2.1 3-Methyl-1*H*-indazole (52a).^[466]



52a

A solution of 2-ethylaniline (3.12 g, 25.0 mmol) in Et₂O (3.0 mL) was treated with 54% HBF₄ in Et₂O (8.61 mL, 62.5 mmol), 0.216 g/mL NaNO₂ aqueous solution (12.1 mL, 37.9 mmol) 18-crown-6 (335 mg, 1.25 mmol) and KOAc (4.96 g, 50.0 mmol), according to GP-A. MPLC (SiO₂; cyclohexane/EtOAc 9:1 to 1:1) gave **52a** (1.510 g, 11.4 mmol, 46%) as an off-white solid.

$R_f = 0.44$ (SiO₂; cyclohexane/EtOAc 1:1);

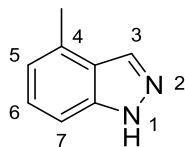
m.p. 111–113 °C (^[466]: 113 °C);

¹H NMR (400 MHz, CDCl₃): $\delta = 2.67$ (s, 3 H; CH₃), 7.16 (dd, $J = 8.1, 6.8$ Hz, 1 H; H–C(5)), 7.38 (dd, $J = 8.4, 6.8$ Hz, 1 H; H–C(6)), 7.46 (d, $J = 8.4$ Hz, 1 H; H–C(5)), 7.70 (d, $J = 8.1$ Hz, 1 H, H–C(7)), 11.14 ppm (br s, 1 H; H–N);

¹³C NMR (100 MHz, CDCl₃): $\delta = 12.12$ (CH₃), 109.92 (arom. C), 120.20 (arom. C), 120.31 (arom. C), 122.80 (arom. C), 126.79 (arom. C), 141.25 (arom. C), 143.22 ppm (arom. C);

IR (ATR): $\tilde{\nu} = 3063$ (very w), 2922 (very w), 1963 (very w), 1916 (very w), 1882 (very w), 1829 (very w), 1788 (very w), 1743 (very w), 1695 (very w), 1615 (w), 1498 (w), 1441 (w), 1387 (very w), 1366 (very w), 1334 (w), 1271 (very w), 1253 (w), 1156 (very w), 1137 (very w), 1115 (very w), 1071 (w), 1006 (very w), 984 (w), 940 (very w), 898 (very w), 746 (m), 678 cm⁻¹ (m);

HR-ESI-MS: m/z (%): 566.9301 (46.0), 566.4281 (73.5), 453.8461 (50.7), 453.3442 (85.2), 282.2793 (26.7), 133.0762 (24.9, $[M + H]^+$, calcd for C₈H₉N₂⁺: 133.0760).

2.7.2.2 4-Methyl-1*H*-indazole (**52b**).^[447]**52b**

A solution of 2,3-dimethylaniline (1.33 g, 10.7 mmol) in Et₂O (1.3 mL) was treated with 54% HBF₄ (3.71 mL, 26.9 mmol) in Et₂O, a 0.216 g/mL NaNO₂ aqueous solution (5.2 mL, 16.3 mmol), and the isolated solid was treated with 18-crown-6 (143 mg, 0.54 mmol) and KOAc (2.13 g, 21.5 mmol) in CH₂Cl₂ (28 mL), according to GP-A. MPLC (SiO₂; cyclohexane/EtOAc 100:1 to 1:1) gave **52b** (0.921 g, 6.97 mmol, 65%) as a pale orange solid.

$R_f = 0.21$ (SiO₂; cyclohexane/EtOAc 4:1);

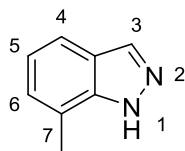
m.p. 113–114 °C (^[447]: 112–113 °C);

¹H NMR (400 MHz, CDCl₃): $\delta = 2.64$ (s, 3 H; CH₃), 6.95 (d, $J = 6.7$ Hz, 1 H; H–C(5)), 7.29 (dd, $J = 8.3, 6.7$ Hz, 1 H; H–C(6)), 7.34 (d, $J = 8.3$ Hz, 1 H; H–C(7)), 8.15 (s, 1 H; H–C(3)), 10.98 ppm (br s, 1 H; H–N);

¹³C NMR (100 MHz, CDCl₃): $\delta = 18.85$ (CH₃), 107.31 (arom. C), 120.98 (arom. C), 123.84 (arom. C), 127.06 (arom. C), 131.47 (arom. C), 133.72 (arom. C) and 140.15 ppm (arom. C);

IR (ATR): $\tilde{\nu} = 3164$ (very w), 3113 (very w), 3063 (very w), 2965 (very w), 2915 (very w), 2859 (very w), 1920 (very w), 1834 (very w), 1745 (very w), 1703 (very w), 1652 (very w), 1617 (w), 1591 (w), 1521 (very w), 1481 (w), 1450 (very w), 1391 (w), 1363 (w), 1300 (very w), 1246 (very w), 1204 (w), 1154 (w), 1075 (very w), 1052 (very w), 1033 (very w), 947 (w), 874 (very w), 850 (w), 779 (w), 731 (m), 669 (w), 608 cm⁻¹ (very w);

HR-MALDI-MS: m/z (%): 391.2843 (37.3), 265.1448 (32.1, [2*M* + H]⁺, calcd for C₁₆H₁₇N₄⁺: 265.1448), 133.0760 (16.3, [*M* + H]⁺, calcd for C₈H₉N₂⁺: 133.0760).

2.7.2.3 7-Methyl-1*H*-indazole (52e).^[446]**52e**

A solution of 2,6-dimethylaniline (1.33 g, 10.7 mmol) in Et₂O (1.3 mL) was treated with 54% HBF₄ (3.71 mL, 26.9 mmol) in Et₂O, a 0.216 g/mL NaNO₂ aqueous solution (5.2 mL, 16.3 mmol). and the isolated solid was treated with 18-crown-6 (143 mg, 0.54 mmol) and KOAc (2.13 g, 21.5 mmol) in CH₂Cl₂ (28 mL), according to GP-A. MPLC (SiO₂; cyclohexane/EtOAc 100:1 to 1:1) gave **52e** (1.10 g, 8.32 mmol, 77%) as an orange solid.

*R*_f = 0.21 (SiO₂; cyclohexane/EtOAc 4:1);

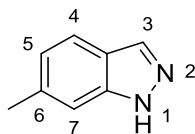
m.p. 134–137 °C (^[446]: 138 °C);

¹H NMR (400 MHz, CDCl₃): δ = 2.63 (s, 3 H; CH₃), 7.11 (dd, *J* = 7.9, 7.0 Hz, 1 H; H–C(5)), 7.18 (d, *J* = 7.0 Hz, 1 H; H–C(6)), 7.63 (d, *J* = 7.9 Hz, 1 H; H–C(4)), 8.16 (s, 1 H; H–C(3)) and 11.64 ppm (br s, 1 H; H–N);

¹³C NMR (100 MHz, CDCl₃): δ = 17.20 (arom. C), 118.43 (arom. C), 120.01 (arom. C), 121.42 (arom. C), 122.93 (arom. C), 126.85 (arom. C), 135.19 (arom. C), 140.57 ppm (arom. C);

IR (ATR): $\tilde{\nu}$ = 3141 (w), 3070 (w), 2910 (w), 2765 (very w), 1917 (very w), 1856 (very w), 1795 (very w), 1698 (very w), 1615 (w), 1600 (very w), 1511 (w), 1442 (w), 1381 (very w), 1347 (w), 1318 (very w), 1254 (very w), 1208 (w), 1166 (very w), 1070 (w), 1050 (w), 952 (m), 903 (very w), 848 (m), 772 (w), 738 (m), 666 (w), 616 cm⁻¹ (very w);

HR-MALDI-MS: *m/z* (%): 391.2843 (38.1), 272.1030 (30.0), 133.0760 (28.9, [*M* + H]⁺, calcd for C₈H₉N₂⁺: 133.0760).

2.7.2.4 6-Methyl-1*H*-indazole (52d).^[467]**52d**

A solution of 2,5-dimethylaniline (3.12 g, 25.0 mmol) in Et₂O (3.0 mL) was treated with 54% HBF₄ (8.61 mL, 62.5 mmol) in Et₂O, a 0.216 g/mL NaNO₂ aqueous solution (12.1 mL, 37.8 mmol), and the isolated solid was treated with 18-crown-6 (335 mg, 1.25 mmol) and KOAc (4.96 g, 50.0 mmol) in CH₂Cl₂ (28 mL), according to GP-A. MPLC (SiO₂; cyclohexane/EtOAc 4:1 to 2:1) gave **52d** (1.31 g, 9.93 mmol, 40%) as a pale orange solid.

*R*_f = 0.53 (SiO₂; cyclohexane/EtOAc 1:1);

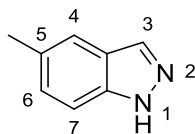
m.p. 174–176 °C (^[467]: 177–178 °C);

¹H NMR (400 MHz, CDCl₃): δ = 2.49 (s, 3 H; CH₃), 7.01 (d, *J* = 8.3 Hz, 1 H; H–C(5)), 7.28 (s, 1 H; H–C(7)), 7.64 (d, *J* = 8.3 Hz, 1 H; H–C(4)), 8.04 (s, 1 H; H–C(3)), 10.27 ppm (br s, 1 H; H–N);

¹³C NMR (100 MHz, CDCl₃): δ = 22.09 (CH₃), 109.25 (arom. C), 120.53 (arom. C), 121.53 (arom. C), 123.43 (arom. C), 134.85 (arom. C), 137.30 (arom. C), 140.85 ppm (arom. C);

IR (ATR): $\tilde{\nu}$ = 3177 (w), 3086 (w), 3013 (very w), 2945 (very w), 2918 (very w), 2863 (very w), 2800 (very w), 2718 (very w), 1902 (very w), 1626 (w), 1514 (very w), 1469 (very w), 1439 (w), 1355 (w), 1276 (very w), 1248 (very w), 1188 (very w), 1141 (very w), 1069 (w), 1033 (very w), 947 (w), 881 (very w), 844 (w), 801 (w), 772 (very w), 740 (w), 609 cm⁻¹ (very w);

HR-ESI-MS: *m/z* (%): 566.9296 (36.2), 566.4277 (53.1), 453.8455 (33.5), 453.3438 (66.1), 430.9139 (22.3), 265.1447 (28.8, [2*M* + H]⁺, calcd for C₁₆H₁₇N₄⁺: 265.1448).

2.7.2.5 5-Methyl-1*H*-indazole (52c).^[447]**52c**

A solution of 2,4-dimethylaniline (3.12 g, 25.0 mmol) in Et₂O (3.0 mL) was treated with 54% HBF₄ (8.61 mL, 62.5 mmol) in Et₂O, a 0.216 g/mL NaNO₂ aqueous solution (12.1 mL, 37.8 mmol), and the isolated solid was treated with 18-crown-6 (335 mg, 1.25 mmol) and KOAc (4.96 g, 50.0 mmol) in CH₂Cl₂ (28 mL), according to GP-A. MPLC (SiO₂; toluene/EtOAc 4:1 to 2:1) gave **52c** (0.916 g, 6.93 mmol, 28%) as an off-white solid.

*R*_f = 0.47 (SiO₂; cyclohexane/EtOAc 1:1);

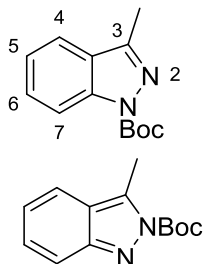
m.p. 110–113 °C (^[447]: 111 °C);

¹H NMR (400 MHz, CDCl₃): δ = 2.46 (s, 3 H; CH₃), 7.23 (d, *J* = 8.5 Hz, 1 H; H–C(6)), 7.39 (d, *J* = 8.5 Hz, 1 H; H–C(7)), 7.53 (s, 1 H; H–C(4)), 7.99 (s, 1 H; H–C(3)), 9.93 ppm (br s, 1 H; H–N);

¹³C NMR (100 MHz, CDCl₃): δ = 21.46 (CH₃), 109.38 (arom. C), 120.02 (arom. C), 123.80 (arom. C), 129.10 (arom. C), 130.60 (arom. C), 134.67 (arom. C), 138.85 ppm (arom. C);

IR (ATR): $\tilde{\nu}$ = 3178 (w), 3151 (w), 3055 (very w), 2923 (w), 2858 (very w), 2750 (very w), 1900 (very w), 1761 (very w), 1691 (very w), 1632 (very w), 1586 (very w), 1510 (w), 1478 (very w), 1455 (very w), 1434 (very w), 1388 (very w), 1344 (w), 1303 (very w), 1282 (very w), 1251 (very w), 1215 (very w), 1183 (very w), 1144 (w), 1074 (w), 1042 (very w), 1003 (very w), 952 (m), 884 (w), 842 (w), 805 (m), 765 (w), 738 (m), 613 cm⁻¹ (w);

HR-ESI-MS: *m/z* (%): 566.9301 (27.4), 566.4277 (42.9), 464.3354 (24.2), 453.8457 (35.6), 453.3440 (61.4), 271.0845 (27.4), 255.1106 (100.0), 133.0761 (38.7, [*M* + H]⁺, calcd for C₈H₉N₂⁺: 133.0760).

2.7.2.6 2-Methyl-2-propanyl 3-methyl-1*H*-indazole-1-carboxylate/2-Methyl-2-propanyl 3-methyl-2*H*-indazole-2-carboxylate (**53a**).^[448]**53a**

A solution of 3-methylindazole (0.601 g, 4.50 mmol) in CH_2Cl_2 (13.6 mL) was treated with Et_3N (1.90 mL, 13.5 mmol), DMAP (56 mg, 0.45 mmol) and Boc_2O (1.10 g, 4.95 mmol) at 24 °C, according to the GP-B. MPLC (SiO_2 ; cyclohexane/EtOAc 100:1 to 10:3) gave an inseparable mixture of two regioisomers **53a** (0.873 g, 3.76 mmol, 84%) in ratio of 9.6:1.0 as an orange oil.

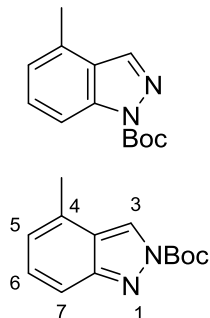
$R_f = 0.38$ (SiO_2 ; cyclohexane/EtOAc 4:1);

^1H NMR (400 MHz, CDCl_3 ; major regioisomer): $\delta = 1.72$ (s, 9 H; $(\text{CH}_3)_3$), 2.59 (s, 3 H; CH_3), 7.29 (dd, $J = 8.1, 7.2$ Hz, 1 H; H-C(5)), 7.50 (dd, $J = 8.4, 7.2$ Hz, 1 H; H-C(6)), 7.64 (d, $J = 8.1$ Hz, 1 H; H-C(4)), 8.10 ppm (d, $J = 8.4$ Hz, 1 H; H-C(7));

^{13}C NMR (100 MHz, CDCl_3 ; major regioisomer): $\delta = 12.44$ (CH_3), 28.33 (3 C; $(\text{CH}_3)_3$), 84.59 ($\text{C}(\text{Me})_3$), 114.77 (arom. C), 120.39 (arom. C), 123.29 (arom. C), 126.08 (arom. C), 128.90 (arom. C), 140.30 (arom. C), 148.65 (arom. C), 149.45 ppm (NCO_2);

IR (ATR): $\tilde{\nu} = 2980$ (w), 2929 (w), 1752 (m), 1726 (m), 1609 (very w), 1588 (very w), 1527 (w), 1476 (w), 1444 (w), 1400 (m), 1368 (m), 1354 (w), 1334 (w), 1291 (w), 1244 (m), 1150 (m), 1078 (m), 1039 (very w), 1021 (w), 998 (very w), 969 (very w), 942 (very w), 903 (very w), 849 (w), 842 (w), 747 (m), 627 cm^{-1} (w).

HR-ESI-MS: m/z (%): 577.4196 (25.4), 566.9300 (33.6), 566.4285 (51.8), 464.3352 (36.9), 453.8459 (45.5), 453.3441 (75.6), 255.1104 (31.2, $[M + \text{Na}]^+$, calcd for $\text{C}_{13}\text{H}_{16}\text{N}_2\text{NaO}_2^+$: 255.1109).

2.7.2.7 2-Methyl-2-propanyl 4-methyl-1*H*-indazole-1-carboxylate/2-Methyl-2-propanyl 4-methyl-2*H*-indazole-2-carboxylate (**53b**).^[468]**53b**

A solution of 4-methylindazole (0.801 g, 6.00 mmol) in CH₂Cl₂ (18 mL) was treated with Et₃N (2.53 mL, 18.0 mmol), DMAP (75 mg, 0.60 mmol) and Boc₂O (1.47 g, 6.60 mmol) at 24 °C, according to the GP-B. MPLC (SiO₂; cyclohexane/EtOAc 100:1 to 4:1) gave an inseparable mixture of two regioisomers **53b** (1.03 g, 4.43 mmol, 74%) in ratio of 1.1:1.0 as an orange oil.

$R_f = 0.34$ (SiO₂; cyclohexane/EtOAc 4:1);

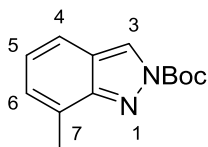
¹H NMR (400 MHz, CDCl₃; major regioisomer): $\delta = 1.72$ (s, 9 H; (CH₃)₃), 2.50 (s, 3 H; CH₃), 6.82 (d, $J = 6.6$ Hz, 1 H; H-C(5)), 7.20 (dd, $J = 8.9, 6.6$ Hz, 1 H; H-C(6)), 7.54 (d, $J = 8.9$ Hz, 1 H; H-C(7)), 8.59 ppm (s, 1 H; H-C(3));

¹³C NMR (100 MHz, CDCl₃; major regioisomer): $\delta = 19.08$ (CH₃), 28.05 (3 C; (CH₃)₃), 86.65 (C(Me)₃), 116.63 (arom. C), 122.83 (arom. C), 123.59 (arom. C), 129.44 (arom. C), 131.36 (arom. C), 138.45 (C(3)), 139.77 (arom. C), 148.49 ppm (NCO₂);

IR (ATR): $\tilde{\nu} = 3145$ (very w), 2981 (w), 2935 (very w), 2863 (very w), 1775 (w), 1751 (m), 1726 (m), 1643 (very w), 1529 (w), 1516 (very w), 1471 (w), 1431 (w), 1388 (m), 1368 (s), 1334 (w), 1285 (m), 1275 (m), 1248 (m), 1227 (w), 1147 (s), 1135 (s), 1107 (w), 1029 (m), 968 (m), 938 (very w), 845 (m), 802 (m), 767 (m), 756 (w), 740 (w), 697 (very w), 670 (very w), 627 (w), 610 cm⁻¹ (very w).

HR-ESI-MS: m/z (%): 566.9295 (23.4), 566.4285 (34.9), 464.3351 (26.2), 453.8459 (34.7), 453.3442 (62.4), 271.0844 (23.8), 255.1104 (100.0, $[M + Na]^+$, calcd for $C_{13}H_{16}N_2NaO_2^+$: 255.1109), 133.0756 (34.5, $[M - Boc + H]^+$, calcd for $C_8H_9N_2^+$: 133.0760).

2.7.2.8 2-Methyl-2-propanyl 7-methyl-2*H*-indazole-2-carboxylate (**53e**).



53e

A solution of 7-methylindazole (0.934 g, 7.00 mmol) in CH_2Cl_2 (21 mL) was treated with Et_3N (2.95 mL, 21.0 mmol), DMAP (87 mg, 0.70 mmol) and Boc_2O (1.72 g, 7.70 mmol) at 24 °C, according to the GP-B. MPLC (SiO_2 ; cyclohexane/ $EtOAc$ 100:1 to 4:1) gave a single regioisomer **53e** (1.36 g, 5.86 mmol, 84%) as an orange oil.

R_f = 0.41 (SiO_2 ; cyclohexane/ $EtOAc$ 4:1);

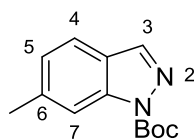
1H NMR (400 MHz, $CDCl_3$): δ = 1.70 (s, 9 H; $(CH_3)_3$), 2.63 (s, 3 H; CH_3), 6.98 (dd, J = 8.5, 6.6 Hz, 1 H; H-C(5)), 7.05 (d, J = 6.6 Hz, 1 H; H-C(6)), 7.43 (d, J = 8.5 Hz, 1 H; H-C(4)), 8.54 ppm (s, 1 H; H-C(3));

^{13}C NMR (100 MHz, $CDCl_3$): δ = 17.16 (CH_3), 28.02 (3 C; $(CH_3)_3$), 86.49 ($C(Me)_3$), 118.55 (arom. C), 121.91 (arom. C), 124.48 (2C, arom. C), 127. (arom. C), 129.38 (arom. C), 148.28 (NCO_2), 151.64 ppm (arom. C);

IR (ATR): $\tilde{\nu}$ = 3140 (very w), 2981 (w), 2935 (very w), 1775 (m), 1749 (s), 1630 (w), 1556 (w), 1542 (w), 1467 (w), 1437 (w), 1396 (w), 1366 (w), 1352 (s), 1335 (w), 1275 (s), 1251 (s) 1225 (s), 1142 (s), 1117 (w), 1077 (w), 1049 (very w), 1035 (very w), 1021 (m), 970 (m), 874 (w), 843 (m), 803 (w), 770 (w), 751 (s), 690 (very w), 669 (very w), 634 (very w), 610 cm^{-1} (very w).

HR-ESI-MS: m/z (%): 566.9297 (40.8), 566.4282 (63.7), 464.3350 (20.0), 453.8444 (44.5), 453.3438 (79.8), 282.2790 (56.2), 271.0845 (22.6), 255.1105 (67.7, $[M + Na]^+$, calcd for $C_{13}H_{16}N_2NaO_2^+$: 255.1109), 133.0758 (100.0, $[M - Boc + H]^+$, calcd for $C_8H_9N_2^+$: 133.0760).

2.7.2.9 2-Methyl-2-propanyl 6-methyl-1*H*-indazole-1-carboxylate (**53d**).



53d

A solution of 6-methyl-(1*H*)-indazole (0.601 g, 4.50 mmol) in CH_2Cl_2 (13.6 mL) was treated with Et_3N (1.90 mL, 13.5 mmol), DMAP (56 mg, 0.45 mmol) and Boc_2O (1.10 g, 4.95 mmol) at 24 °C, according to the GP-B. MPLC (SiO_2 ; cyclohexane/ $EtOAc$ 100:1 to 3:2) gave **53d** (0.807 g, 3.47 mmol, 77%) as an orange oil.

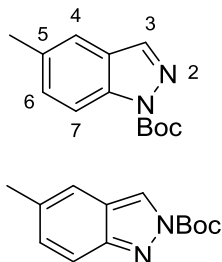
R_f = 0.35 (SiO_2 ; cyclohexane/ $EtOAc$ 4:1);

1H NMR (400 MHz, $CDCl_3$): δ = 1.72 (s, 9 H; $(CH_3)_3$), 2.51 (s, 3 H; CH_3), 7.13 (d, J = 8.2 Hz, 1 H; H-C(5)), 7.59 (d, J = 8.2 Hz, 1 H; H-C(4)), 8.02 (s, 1 H; H-C(7)), 8.09 ppm (s, 1 H; H-C(3));

^{13}C NMR (100 MHz, $CDCl_3$; based on HSQC): δ = 22.32 (CH_3), 28.33 (3 C; $(CH_3)_3$), 84.82 ($C(Me)_3$), 114.57 (C(7)), 120.69 (C(4)), 124.04 (arom. C), 125.68 (C(5)), 139.60 (C(3)), 139.73 (arom. C), 140.46 (arom. C), 149.61 (NCO_2);

IR (ATR): $\tilde{\nu}$ = 2980 (w), 2927 (very w), 1755 (m), 1733 (s), 1621 (w), 1484 (w), 1456 (w), 1410 (m), 1381 (s), 1368 (s), 1339 (m), 1297 (m), 1280 (m), 1251 (m), 1196 (w), 1148 (s), 1122 (m), 1040 (w), 1028 (m), 995 (w), 969 (w), 935 (m), 862 (w), 847 (m), 800 (m), 764 (m), 747 (w), 736 (w), 619 cm^{-1} (m).

HR-ESI-MS: m/z (%): 566.4280 (27.6), 453.3440 (79.8), 271.0843 (23.8), 255.1101 (100.0, $[M + Na]^+$, calcd for $C_{13}H_{16}N_2NaO_2^+$: 255.1109), 133.0759 (30.0, $[M - Boc + H]^+$, calcd for $C_8H_9N_2^+$: 133.0760).

2.7.2.10 2-Methyl-2-propanyl 5-methyl-1*H*-indazole-1-carboxylate/2-Methyl-2-propanyl 5-methyl-2*H*-indazole-2-carboxylate (**53c**).**53c**

A solution of 5-methyl-(1*H*)-indazole (0.601 g, 4.50 mmol) in CH₂Cl₂ (13.6 mL) was treated with Et₃N (1.90 mL, 13.5 mmol), DMAP (56 mg, 0.45 mmol) and Boc₂O (1.10 g, 4.95 mmol), according to the GP-B. MPLC (SiO₂; cyclohexane/EtOAc 100:1 to 7:3) gave an inseparable mixture of two regioisomers **53c** (0.970 g, 4.18 mmol, 93%) in ratio of 1.02:1.00 as an orange oil.

R_f = 0.35 (SiO₂; cyclohexane/EtOAc 4:1);

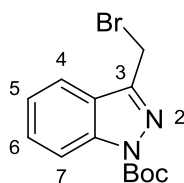
¹H NMR (400 MHz, CDCl₃; major regioisomer): δ = 1.72 (s, 9 H; (CH₃)₃), 2.46 (s, 3 H; CH₃), 7.35 (d, J = 8.7 Hz, 1 H; H-C(6)), 7.49 (s, 1 H; H-C(4)), 8.05 (d, J = 8.7 Hz, 1 H; H-C(7)), 8.08 ppm (s, 1 H; H-C(3));

¹³C NMR (100 MHz, CDCl₃; major regioisomer, based on HSQC): δ = 21.32 (CH₃), 28.05 (3 C, (CH₃)₃), 84.77 (C(Me)₃), 114.28 (C(7)), 120.49 (C(4)), 126.33 (arom. C), 130.79 (C(6)), 133.44 (arom. C), 138.30 (arom. C), 139.35 (C(3)), 149.40 (NCO₂);

IR (ATR): $\tilde{\nu}$ = 3140 (very w), 2981 (w), 2934 (very w), 2863 (very w), 1775 (w), 1752 (s), 1734 (m), 1642 (very w), 1529 (w), 1516 (w), 1471 (w), 1455 (w), 1431 (w), 1388 (m), 1368 (s), 1333 (w), 1285 (m), 1275 (m), 1248 (s), 1227 (m), 1213 (w), 1147 (s), 1133 (s), 1107 (m), 1029 (s), 968 (s), 940 (very w), 883 (very w), 858 (w), 845 (m), 801 (s), 767 (m), 757 (w), 740 (w), 699 (very w), 627 (w), 611 cm⁻¹ (very w).

HR-ESI-MS: m/z (%): 566.9301 (27.4), 566.4277 (42.9), 453.8457 (35.6), 453.3440 (61.4), 271.0845 (27.4), 255.1106 (100.0, $[M + Na]^+$, calcd for $C_{13}H_{16}N_2NaO_2^+$: 255.1109), 133.0761 (38.7, $[M - Boc + H]^+$, calcd for $C_8H_9N_2^+$: 133.0760).

2.7.2.11 2-Methyl-2-propanyl 3-(bromomethyl)-1*H*-indazole-1-carboxylate (**54a**).^[448]



54a

A solution of regioisomers **53a** (117 mg, 0.50 mmol) in CCl_4 (2.5 mL) was treated with NBS (126 mg, 0.70 mmol) and AIBN (4 mg, 0.03 mmol), according to the GP-C. MPLC (SiO_2 ; cyclohexane/EtOAc 100:1 to 4:1) gave a single regioisomer **54a** (84 mg, 0.27 mmol, 54%) as a pale yellow oil.

R_f = 0.66 (SiO_2 ; cyclohexane/EtOAc 4:1);

1H NMR (300 MHz, $CDCl_3$): δ = 1.73 (s, 9 H; $C(CH_3)_3$), 4.79 (s, 2 H; CH_2), 7.37 (dd, J = 8.0, 7.1 Hz, 1 H; H-C(5)), 7.55 (dd, J = 8.5, 7.1 Hz, 1 H; H-C(6)), 7.85 (d, J = 8.0 Hz, 1 H; H-C(4)), 8.13 ppm (d, J = 8.5 Hz, 1 H; H-C(7));

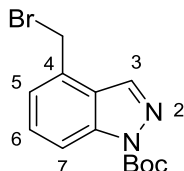
^{13}C NMR (75 MHz, $CDCl_3$): δ = 23.00 (CH_2), 28.27 (3 C; $(CH_3)_3$), 85.42 ($C(Me)_3$), 114.98 (arom. C), 120.77 (arom. C), 123.88 (arom. C), 124.14 (arom. C), 129.37 (arom. C), 140.80 (arom. C), 147.29 (arom. C); 149.01 ppm (NCO_2);

IR (ATR): $\tilde{\nu}$ = 2979 (w), 2936 (very w), 1734 (s), 1612 (w), 1513 (w), 1475 (very w), 1431 (w), 1392 (m), 1365 (s), 1333 (m), 1297 (m), 1246 (m), 1217 (w), 1151 (s), 1078 (s), 1013 (w), 910 (very w), 843 (m), 749 (s), 630 (very w), 609 cm^{-1} (very w).

HR-ESI-MS: m/z (%): 335.0187 (40.5, $[M + Na]^+$, calcd for $C_{13}H_{15}^{81}BrN_2NaO_2^+$: 335.0194), 333.0206 (38.4, $[M + Na]^+$, calcd for $C_{13}H_{15}^{79}BrN_2NaO_2^+$: 333.0215), 256.9745 (100.0, $[M - t-Bu$

+ H]⁺, calcd for C₉H₈⁸¹BrN₂⁺: 256.9743), 254.9766 (99.1, [M - *t*-Bu + H]⁺, calcd for C₉H₈⁷⁹BrN₂⁺: 254.9764).

2.7.2.12 2-Methyl-2-propanyl 4-(bromomethyl)-1*H*-indazole-1-carboxylate (**54b**).^[468]



54b

A solution of regioisomers **53b** (117 mg, 0.50 mmol) in CCl₄ (2.5 mL) was treated with NBS (126 mg, 0.70 mmol) and AIBN (4 mg, 0.03 mmol), according to the GP-C. MPLC (SiO₂; cyclohexane/EtOAc 100:1 to 4:1) gave a single regioisomer **54b** (86 mg, 0.28 mmol, 55%) as an off-white solid.

*R*_f = 0.58 (SiO₂; cyclohexane/EtOAc 4:1);

m.p. 93–95 °C;

¹H NMR (300 MHz, CDCl₃): δ = 1.72 (s, 9 H; (CH₃)₃), 4.77 (s, 2 H; CH₂), 7.29 (d, *J* = 7.3 Hz, 1 H; H-C(5)), 7.46 (dd, *J* = 8.5, 7.3 Hz, 1 H; H-C(6)), 8.16 (d, *J* = 8.5 Hz, 1 H; H-C(7)), 8.35 ppm (s, 1 H; H-C(3));

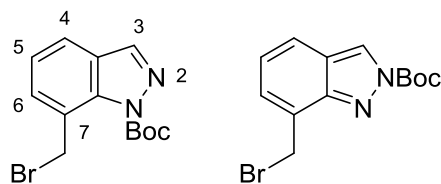
¹³C NMR (75 MHz, CDCl₃): δ = 28.27 (3 C; (CH₃)₃), 29.75 (CH₂), 85.31 (C(CH₃)₃), 115.28 (arom. C), 124.12 (arom. C), 124.83 (arom. C), 129.02 (arom. C), 130.99 (arom. C), 137.74 (arom. C), 140.30 (arom. C), 149.15 ppm (NCO₂);

IR (ATR): $\tilde{\nu}$ = 3086 (w), 3022 (very w), 2983 (w), 2938 (very w), 1737 (s), 1606 (w), 1505 (very w), 1464 (w), 1418 (m), 1365 (s), 1352 (s), 1278 (m), 1259 (m), 1215 (very w), 1202 (m), 1143 (s), 1070 (s), 974 (s), 928 (very w), 892 (w), 866 (very w), 842 (m), 797 (m), 769 (m), 748 (m), 682 (m), 647 (m), 621 cm⁻¹ (m);

HR-ESI-MS: m/z (%): 335.0182 (21.8, $[M + Na]^+$, calcd for $C_{13}H_{15}^{81}BrN_2NaO_2^+$: 335.0194), 333.0203 (23.2, $[M + Na]^+$, calcd for $C_{13}H_{15}^{79}BrN_2NaO_2^+$: 333.0215), 256.9736 (98.7, $[M - tBu + H]^+$, calcd for $C_9H_8^{81}BrN_2^+$: 256.9743), 254.9757 (100.0, $[M - tBu + H]^+$, calcd for $C_9H_8^{79}BrN_2^+$: 254.9764).

2.7.2.13 2-Methyl-2-propanyl 7-(bromomethyl)-1*H*-indazole-1-carboxylate/

2-Methyl-2-propanyl 7-(bromomethyl)-2*H*-indazole-2-carboxylate (**54e**).



54e

A solution of **53e** (100 mg, 0.43 mmol) in CCl_4 (3.0 mL) was treated with NBS (88 mg, 0.49 mmol) and AIBN (4 mg, 0.02 mmol), according to the GP-D. MPLC (SiO_2 ; cyclohexane/EtOAc 100:1 to 4:1) gave an inseparable mixture of two regioisomers **54e** (43 mg, 0.14 mmol, 33%) in ratio of 1.3:1.0 as a colorless oil.

R_f = 0.43 (SiO_2 ; cyclohexane/EtOAc 4:1);

1H NMR (400 MHz, $CDCl_3$; major regioisomer): δ = 1.74 (s, 9 H; $(CH_3)_3$), 5.23 (s, 2 H; CH_2), 7.27 (dd, J = 7.8, 7.4 Hz, 1H; H-C(5)), 7.49 (d, J = 7.4 Hz, 1H; H-C(6)), 7.72 (d, J = 7.8 Hz, 1H; H-C(4)), 8.19 ppm (s, 1H; H-C(3));

^{13}C NMR (100 MHz, $CDCl_3$; major regioisomer, based on HSQC): δ = 22.80 (3 C; $(CH_3)_3$), 34.57 (CH_2), 85.36 ($C(CH_3)_3$), 122.21 (C(4)), 124.02 (C(5)), 124.30 (arom. C), 127.86 (arom. C), 131.43 (C(6)), 137.50 (arom. C), 139.32 (C(3)), 149.60 (NCO_2);

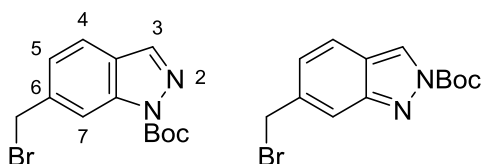
IR (ATR): $\tilde{\nu}$ = 2981 (w), 2927 (very w), 1777 (w), 1742 (s), 1629 (very w), 1605 (very w), 1555 (very w), 1537 (very w), 1517 (very w), 1458 (m), 1397 (w), 1360 (s), 1277 (m), 1245 (m), 1212

(w), 1140 (s), 1071 (very w), 1044 (m), 1013 (m), 972 (m), 910 (very w), 880 (m), 846 (m), 791 (very w), 765 (w), 745 (m), 700 (very w), 675 (w), 634 cm⁻¹ (w);

HR-ESI-MS: *m/z* (%): 419.9538 (29.3), 335.0194 (26.9, [*M* + Na]⁺, calcd for C₁₃H₁₅⁸¹BrN₂NaO₂⁺: 335.0194), 333.0212 (26.2, [*M* + Na]⁺, calcd for C₁₃H₁₅⁷⁹BrN₂NaO₂⁺: 333.0215), 256.9753 (23.0, [*M* - *t*-Bu + H]⁺, calcd for C₉H₈⁸¹BrN₂⁺: 256.9743), 254.9773 (20.2, [*M* - *t*-Bu + H]⁺, calcd for C₉H₈⁷⁹BrN₂⁺: 254.9764), 131.0633 (48.7).

2.7.2.14 2-Methyl-2-propanyl 6-(bromomethyl)-1*H*-indazole-1-carboxylate/

2-Methyl-2-propanyl 6-(bromomethyl)-2*H*-indazole-2-carboxylate (**54d**).^[469]



54d

A solution of **53d** (141 mg, 0.60 mmol) in CCl₄ (4.0 mL) was treated with NBS (124 mg, 0.69 mmol) and AIBN (5 mg, 0.03 mmol), according to the GP-D. MPLC (SiO₂; cyclohexane/EtOAc 100:1 to 4:1) gave an inseparable mixture of two regioisomers **54d** (94 mg, 0.30 mmol, 50%) in ratio of 5.1:1.0 as a colorless oil.

R_f = 0.43 (SiO₂; cyclohexane/EtOAc 4:1);

¹H NMR (400 MHz, CDCl₃; major regioisomer): δ = 1.71 (s, 9 H; (CH₃)₃), 4.62 (s, 2 H; CH₂), 7.34 (d, *J* = 8.3 Hz, 1 H; H-C(5)), 7.68 (d, *J* = 8.3 Hz, 1 H; H-C(4)), 8.13 (s, 1 H; H-C(3)), 8.25 ppm (s, 1 H; H-C(7));

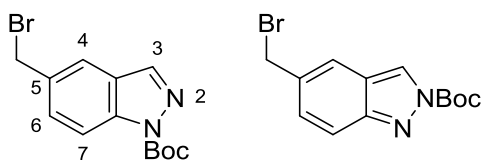
¹³C NMR (100 MHz, CDCl₃; major regioisomer, based on HSQC): δ = 28.23 (3 C; (CH₃)₃), 33.54 (CH₂), 85.25 (C(CH₃)₃), 115.07 (C(7)), 121.58 (C(4)), 125.07 (C(5)), 125.66 (arom. C), 138.92 (arom. C), 139.30 (C(3)), 139.89 (arom. C), 149.17 ppm (NCO₂);

IR (ATR): $\tilde{\nu}$ = 2980 (w), 2931 (very w), 2240 (very w), 1754 (m), 1735 (s), 1619 (w), 1481 (w), 1456 (very w), 1412 (m), 1369 (s), 1348 (m), 1286 (m), 1253 (m), 1215 (w), 1197 (w), 1148 (s), 1124 (m), 1030 (m), 979 (w), 943 (m), 909 (w), 870 (w), 845 (m), 816 (w), 804 (w), 765 (m), 731 (m), 663 (m), 620 cm^{-1} (w);

HR-ESI-MS: m/z (%): 256.9742 (95.4, $[M - t\text{-Bu} + \text{H}]^+$, calcd for $\text{C}_9\text{H}_8^{81}\text{BrN}_2^+$: 256.9743), 254.9763 (100.0, $[M - t\text{-Bu} + \text{H}]^+$, calcd for $\text{C}_9\text{H}_8^{79}\text{BrN}_2^+$: 254.9764).

2.7.2.15 2-Methyl-2-propanyl 5-(bromomethyl)-1*H*-indazole-1-carboxylate/

2-Methyl-2-propanyl 5-(bromomethyl)-2*H*-indazole-2-carboxylate (**54c**).



54c

A solution of regioisomers **53c** (141 mg, 0.60 mmol) in CCl_4 (4.0 mL) was treated with NBS (124 mg, 0.69 mmol) and AIBN (5 mg, 0.03 mmol), according to the GP-D. MPLC (SiO_2 ; cyclohexane/EtOAc 100:1 to 4:1) gave an inseparable mixture of two regioisomers **54c** (90 mg, 0.29 mmol, 48%) in ratio of 2.1:1.0 as a colorless oil.

R_f = 0.43 (SiO_2 ; cyclohexane/EtOAc 4:1);

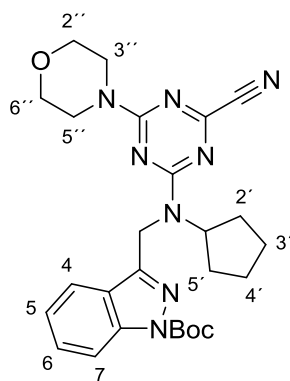
^1H NMR (400 MHz, CDCl_3 ; major regioisomer): δ = 1.70 (s, 9 H; $(\text{CH}_3)_3$), 4.60 (s, 2 H; CH_2), 7.55 (dd, J = 8.6, 1.7 Hz, 1 H; H-C(6)), 7.72 (s, 1 H; H-C(4)), 8.12–8.17 ppm (m, 2 H; H-C(7) and H-C(3));

^{13}C NMR (100 MHz, CDCl_3 ; major regioisomer, based on HSQC): δ = 28.21 (3 C, $(\text{CH}_3)_3$), 33.37 (CH_2), 85.23 ($\text{C}(\text{Me})_3$), 115.19 (C(7)), 121.38 (C(4)), 126.07 (arom. C), 130.50 (C(6)), 133.51 (arom. C), 139.41 (C(3)), 139.43 (arom. C), 149.04 ppm (NCO_2);

IR (ATR): $\tilde{\nu}$ = 3138 (very w), 2979 (w), 2934 (very w), 2241 (very w), 1752 (s), 1622 (w), 1515 (w), 1475 (w), 1434 (w), 1373 (s), 1342 (m), 1289 (m), 1249 (m), 1220 (m), 1144 (s), 1031 (m), 972 (w), 905 (w), 870 (w), 846 (m), 815 (m), 763 (m), 732 (m), 656 (w), 611 cm^{-1} (w);

HR-ESI-MS: m/z (%): 335.0188 (36.5, $[M + \text{Na}]^+$, calcd for $\text{C}_{13}\text{H}_{15}^{81}\text{BrN}_2\text{NaO}_2^+$: 335.0194), 333.0208 (31.5, $[M + \text{Na}]^+$, calcd for $\text{C}_{13}\text{H}_{15}^{79}\text{BrN}_2\text{NaO}_2^+$: 333.0215), 256.9744 (100.0, $[M - t\text{Bu} + \text{H}]^+$, calcd for $\text{C}_9\text{H}_8^{81}\text{BrN}_2^+$: 256.9743), 254.9764 (96.6, $[M - t\text{Bu} + \text{H}]^+$, calcd for $\text{C}_9\text{H}_8^{79}\text{BrN}_2^+$: 254.9764).

2.7.2.16 2-Methyl-2-propanyl-3-([4-cyano-6-(4-morpholinyl)-1,3,5-triazin-2-yl](cyclopentyl)amino)methyl)-1H-indazole-1-carboxylate (55a).



55a

A solution of 4-(cyclopentylamino)-6-(4-morpholinyl)-1,3,5-triazine-2-carbonitrile (48 mg, 0.17 mmol) in DMF (1.2 mL) was treated with NaH (14 mg, 0.34 mmol) and with a solution of **54a** (59 mg, 0.19 mmol) in DMF (0.50 mL), according to GP-E. MPLC (SiO_2 ; cyclohexane/EtOAc 100:1 to 4:1) gave **55a** (33 mg, 0.065 mmol, 38%) as a white solid.

R_f = 0.30 (SiO_2 ; cyclohexane/EtOAc 4:1);

m.p. 82–85 °C;

^1H NMR (400 MHz, CDCl_3): δ = 1.46–1.96 (m, 17 H; (H–C(2', 3', 4', 5')), (CH_3)₃), 3.33–3.88 (br m, 8 H; (H–C(2'', 3'', 5'', 6''))), 4.61–5.03 (m, 1 H; H–C(1')), 5.04 and 5.18 (2 s, 2 H; CH_2N),

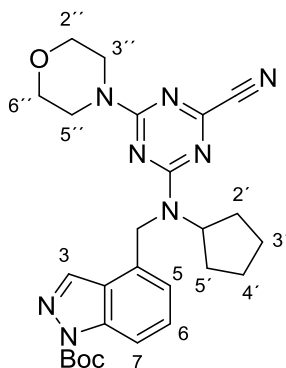
7.17–7.32 (m, 1 H; H–C(5)), 7.45–7.56 (m, 1 H; H–C(6)), 7.68–7.74 (m, 1 H; H–C(4)), 8.03–8.11 ppm (m, 1 H; H–C(7));

^{13}C NMR (100 MHz, CDCl_3): $\delta = 23.82$ and 24.01 (2 C; C(3',4')), 28.35 (3 C; $(\text{CH}_3)_3$), 28.57 and 29.30 (2 C; C(2',5')), 41.64 and 41.87 (CH_2N), 43.59 and 44.02 (2 C; C(2'',6'')), 57.99 and 58.59 (C(1')), 66.38 and 66.74 (2 C; C(3'',5'')), 84.94 and 85.10 ($\text{C}(\text{CH}_3)_3$), 114.67 and 114.89 (C(7)), 115.56 and 115.71 (CN), 120.68 and 121.39 (arom C.), 123.58 and 123.69 (arom. C), 124.55 and 124.86 (arom. C), 129.01 (arom. C), 140.51 (arom. C), 148.92 and 149.14 (NCO_2), 151.77 and 152.02 (CCN), 163.32 and 163.67 (CN_3), 164.40 and 164.63 ppm (CN_3);

IR (ATR): $\tilde{\nu} = 2960$ (w), 2854 (w), 1754 (m), 1732 (m), 1558 (s), 1490 (s), 1493 (m), 1367 (m), 1340 (w), 1303 (w), 1242 (m), 1152 (m), 1115 (w), 1074 (m), 1003 (w), 972 (very w), 956 (very w), 863 (w), 843 (w), 806 (w), 750 cm^{-1} (m);

HR-ESI-MS: m/z (%): 505.2679 (11.8, $[M + \text{H}]^+$, calcd for $\text{C}_{26}\text{H}_{33}\text{N}_8\text{O}_3^+$: 505.2670), 449.2045 (51.7, $[M - t\text{-Bu} + \text{H}]^+$, calcd for $\text{C}_{22}\text{H}_{25}\text{N}_8\text{O}_3^+$: 449.2044), 406.2174 (28.9, $[M - \text{Boc} + \text{H} + 1$ (^{13}C isotope nat. abundance)] $^+$, calcd for $\text{C}_{21}\text{H}_{25}\text{N}_8\text{O}^+$: 406.2179), 405.2147 (100.0, $[M - \text{Boc} + \text{H}]^+$, calcd for $\text{C}_{21}\text{H}_{25}\text{N}_8\text{O}^+$: 405.2146), 287.1609 (31.4, $[\text{C}_{14}\text{H}_{19}\text{N}_6\text{O}]^+$, calcd for $\text{C}_{14}\text{H}_{19}\text{N}_6\text{O}^+$: 287.1620).

2.7.2.17 2-Methyl-2-propanyl-4-([4-cyano-6-(4-morpholinyl)-1,3,5-triazin-2-yl](cyclopentyl)amino)methyl)-1H-indazole-1-carboxylate (55b).



55b

A solution of 4-(cyclopentylamino)-6-(4-morpholinyl)-1,3,5-triazine-2-carbonitrile (57 mg, 0.20 mmol) in DMF (1.4 mL) was treated with NaH (16 mg, 0.40 mmol) and with a solution of **54b** (69 mg, 0.22 mmol) in DMF (0.50 mL), according to GP-E. MPLC (SiO₂; cyclohexane/EtOAc 100:1 to 4:1) gave **55b** (34 mg, 0.067 mmol, 40%) as a white solid.

$R_f = 0.15$ (SiO₂; cyclohexane/EtOAc 4:1);

m.p. 114–117 °C;

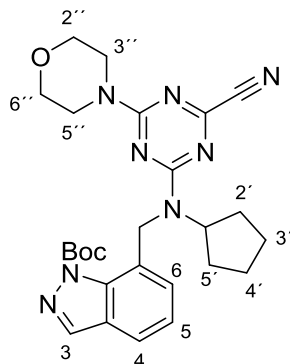
¹H NMR (400 MHz, CDCl₃): $\delta = 1.44$ – 1.96 (m, 17 H; (H–C(2', 3', 4', 5')), (CH₃)₃), 3.17–3.88 (br m, 8 H; (H–C(2'', 3'', 5'', 6'')), 4.75–5.16 (m, 3 H; H–C(1'), CH₂N), 6.99–7.05 (m, 1 H; H–C(5)), 7.40–7.47 (m, 1 H; H–C(6)), 8.03–8.11 (m, 1 H; H–C(7)), 8.13–8.23 ppm (m, 1 H; H–C(3));

¹³C NMR (100 MHz, CDCl₃): $\delta = 23.75$ and 23.90 (2 C; C(3',4')), 28.29 (3 C; (CH₃)₃), 28.99 and 29.43 (2 C; C(2',5')), 43.34 and 44.00 (2 C; C(2'',6'')), 44.61 and 45.03 (CH₂N), 57.42 and 57.83 (C(1')), 66.19 and 66.66 (2 C; C(3'',5'')), 85.08 and 85.29 (C(CH₃)₃), 113.15 and 113.41 (arom. C), 115.49 and 115.68 (CN), 120.72 and 121.25 (arom. C.), 123.65 and 123.77 (arom. C), 129.04 and 129.15 (arom. C), 132.48 and 132.65 (arom. C), 137.31 and 137.53 (arom. C), 140.00 and 140.12 (arom. C), 149.23 (NCO₂), 151.99 (CCN), 163.38 and 163.69 (CN₃), 164.55 and 164.84 ppm (CN₃);

IR (ATR): $\tilde{\nu} = 2961$ (w), 2859 (w), 1736 (m), 1558 (s), 1489 (m), 1446 (w), 1417 (w), 1356 (very w), 1283 (w), 1248 (w), 1198 (very w), 1149 (m), 1114 (w), 1068 (w), 1019 (very w), 1002 (very w), 975 (w), 847 (w), 806 (w), 782 (very w), 764 (very w), 670 (very w), 624 cm⁻¹ (very w);

HR-ESI-MS: m/z (%): 505.2667 (19.1, [M + H]⁺, calcd for C₂₆H₃₃N₈O₃⁺: 505.2670), 449.2041 (52.0, [M – *t*-Bu + H]⁺, calcd for C₂₂H₂₅N₈O₃⁺: 449.2044), 406.2170 (24.9, [M – Boc + H + 1 (¹³C isotope nat. abundance)]⁺, calcd for C₂₁H₂₅N₈O⁺: 406.2179), 405.2142 (100.0, [M – Boc + H]⁺, calcd for C₂₁H₂₅N₈O⁺: 405.2146).

2.7.2.18 2-Methyl-2-propanyl 7-([4-cyano-6-(4-morpholinyl)-1,3,5-triazin-2-yl](cyclopentyl)amino)methyl)-1*H*-indazole-1-carboxylate (55e**).**



55e

A solution of 4-(cyclopentylamino)-6-(4-morpholinyl)-1,3,5-triazine-2-carbonitrile (68 mg, 0.24 mmol) in DMF (1.5 mL) was treated with NaH (19 mg, 0.48 mmol) and with a solution of **54e** (98 mg, 0.31 mmol) in DMF (0.90 mL) according to GP-E. MPLC (SiO₂; cyclohexane/EtOAc 100:1 to 4:1) gave **55e** (20 mg, 0.040 mmol, 17%) as a colorless oil.

$R_f = 0.17$ (SiO₂; cyclohexane/EtOAc 4:1);

¹H NMR (400 MHz, CDCl₃): $\delta = 1.43$ – 2.00 (m, 17 H; (H–C(2', 3', 4', 5')), (CH₃)₃), 3.04 – 3.92 (br m, 8 H; (H–C(2'', 3'', 5'', 6'')), 4.83 – 5.28 (m, 3 H; H–C(1'), CH₂N), 7.05 – 7.25 (m, 2 H; H–C(5, 6)), 7.43 and 7.60 (m, 1 H; H–C(4)), 8.19 ppm (s, 1 H; H–C(3));

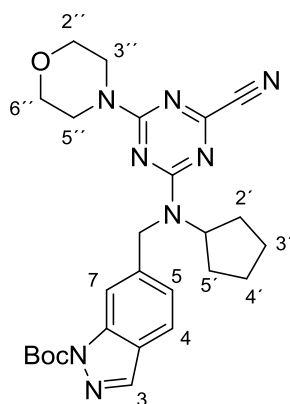
¹³C NMR (100 MHz, CDCl₃, based on HSQC): $\delta = 23.79$ and 23.84 (2 C; C(3',4')), 28.19 (3 C; (CH₃)₃), 29.17 and 29.48 (2 C; C(2',5')), 43.18 and 43.96 (2 C; C(2'',6'')), 45.67 and 46.01 (CH₂N), 57.22 and 57.47 (C(1')), 66.22 and 66.69 (2 C; C(3'',5'')), 85.05 and 85.19 (C(CH₃)₃), 115.64 and 115.80 (CN), 119.56 and 119.86 (C(4)), 124.10 and 124.41 (arom. C), 124.84 and 124.91 (arom. C), 126.92 and 127.04 (arom. C), 127.13 and 127.39 (arom. C), 137.69 and 137.90 (arom. C), 140.05 and 140.20 (C(3)), 150.12 and 150.20 (NCO₂), 151.89 and 152.16 (CCN), 163.35 and 163.72 (CN₃), 164.41 and 165.03 ppm (CN₃);

IR (ATR): $\tilde{\nu} = 2961$ (w), 2863 (w), 1740 (m), 1557 (s), 1488 (s), 1445 (w), 1370 (w), 1343 (w), 1306 (w), 1238 (m), 1204 (w), 1150 (m), 1114 (w), 1069 (very w), 1030 (w), 1004 (w), 973 (very

w), 909 (w), 847 (w), 806 (w), 768 (very w), 728 (m), 664 (very w), 647 (very w), 622 cm^{-1} (very w);

HR-ESI-MS: m/z (%): 505.2668 (8.9, $[M + H]^+$, calcd for $\text{C}_{26}\text{H}_{33}\text{N}_8\text{O}_3^+$: 505.2670), 406.2171 (32.4, $[M - \text{Boc} + H + 1$ (^{13}C isotope nat. abundance)] $^+$, calcd for $\text{C}_{21}\text{H}_{25}\text{N}_8\text{O}^+$: 406.2179), 405.2147 (100.0, $[M - \text{Boc} + H]^+$, calcd for $\text{C}_{21}\text{H}_{25}\text{N}_8\text{O}^+$: 405.2146).

2.7.2.19 2-Methyl-2-propanyl 6-([4-cyano-6-(4-morpholinyl)-1,3,5-triazin-2-yl](cyclopentyl)amino)methyl)-1H-indazole-1-carboxylate (55d).



55d

A solution of 4-(cyclopentylamino)-6-(4-morpholinyl)-1,3,5-triazine-2-carbonitrile (54 mg, 0.19 mmol) in DMF (1.0 mL) was treated with NaH (11 mg, 0.29 mmol) and with a solution of **54d** (90 mg, 0.29 mmol) in DMF (0.90 mL) according to the GP-E. MPLC (SiO_2 ; cyclohexane/EtOAc 100:1 to 4:1) gave **55d** (30 mg, 0.059 mmol, 31%) as a colorless oil.

$R_f = 0.49$ (SiO_2 ; cyclohexane/EtOAc 1:1);

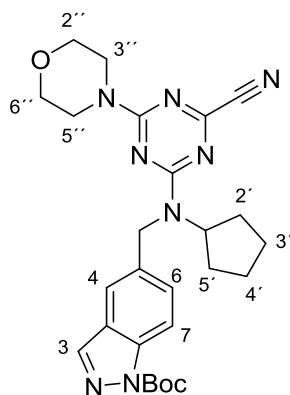
^1H NMR (400 MHz, CDCl_3): $\delta = 1.44\text{--}1.99$ (m, 17 H; (H-C(2', 3', 4', 5'), $(\text{CH}_3)_3$), 3.36–3.88 (br m, 8 H; (H-C(2'', 3'', 5'', 6'')), 4.77–5.15 (m, 3 H; H-C(1'), CH_2N), 7.11–7.16 (m, 1 H; H-C(5)), 7.61–7.67 (m, 1 H; H-C(4)), 7.95–8.04 (m, 1 H; H-C(7)), 8.11–8.14 ppm (m, 1 H; H-C(3));

^{13}C NMR (100 MHz, CDCl_3 , based on HSQC): $\delta = 23.71$ and 23.80 (2 C; C(3',4')), 28.29 (3 C; $(\text{CH}_3)_3$), 29.14 and 29.52 (2 C; C(2',5')), 43.53 and 44.03 (2 C; C(2'',6'')), 47.27 and 47.50 (CH_2N), 57.52 and 57.83 (C(1')), 66.36 and 66.72 (2 C; C(3'',5'')), 84.87 and 85.07 (C(CH_3)₃), 112.23 and 112.28 (C(7)), 115.60 and 115.73 (CN), 121.11 and 121.16 (C(4)), 122.36 and 122.69 (C(5)), 125.06 and 125.21 (arom. C), 139.46 and 139.51 (C(3)), 140.16 (arom. C), 140.60 and 140.68 (arom. C), 149.34 (NCO_2), 151.94 and 152.08 (CCN), 163.49 and 163.69 (CN_3), 164.66 and 164.90 ppm (CN_3);

IR (ATR): $\tilde{\nu} = 2960$ (w), 2859 (w), 1756 (m), 1734 (m), 1620 (very w), 1557 (s), 1487 (s), 1445 (w), 1414 (w), 1369 (m), 1336 (w), 1290 (w), 1238 (m), 1196 (w), 1149 (m), 1117 (w), 1069 (very w), 1030 (w), 1002 (w), 974 (very w), 941 (w), 864 (w), 848 (w), 805 (w), 765 (w), 736 (w), 621 cm^{-1} (w);

HR-ESI-MS: m/z (%): 506.2694 (23.7, $[M + H + 1$ (^{13}C isotope nat. abundance)] $^+$, calcd for $\text{C}_{21}\text{H}_{25}\text{N}_8\text{O}^+$: 506.2704), 505.2665 (83.1, $[M + H]^+$, calcd for $\text{C}_{26}\text{H}_{33}\text{N}_8\text{O}_3^+$: 505.2670), 406.2168 (27.1, $[M - \text{Boc} + H + 1$ (^{13}C isotope nat. abundance)] $^+$, calcd for $\text{C}_{21}\text{H}_{25}\text{N}_8\text{O}^+$: 406.2179), 405.2140 (100.0, $[M - \text{Boc} + H]^+$, calcd for $\text{C}_{21}\text{H}_{25}\text{N}_8\text{O}^+$: 405.2146).

2.7.2.20 2-Methyl-2-propanyl 5-({[4-cyano-6-(4-morpholinyl)-1,3,5-triazin-2-yl](cyclopentyl)amino}methyl)-1H-indazole-1-carboxylate (55c).



55c

A solution of 4-(cyclopentylamino)-6-(4-morpholinyl)-1,3,5-triazine-2-carbonitrile (54 mg, 0.19 mmol) in DMF (1.0 mL) was treated with NaH (11 mg, 0.29 mmol) and with a solution of **54c** (90 mg, 0.29 mmol) in DMF (0.90 mL) according to GP-E. MPLC (SiO₂; cyclohexane/EtOAc 100:1 to 4:1) gave **55c** (29 mg, 0.057 mmol, 30%) as a colorless oil.

$R_f = 0.57$ (SiO₂; cyclohexane/EtOAc 1:1);

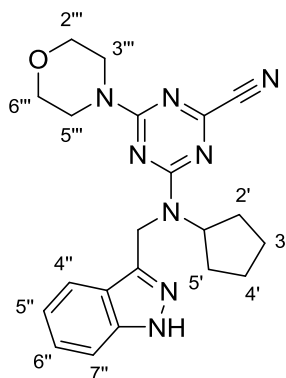
¹H NMR (400 MHz, CDCl₃): $\delta = 1.46$ – 1.96 (m, 17 H; (H–C(2', 3', 4', 5'), (CH₃)₃), 3.35–3.89 (br m, 8 H; (H–C(2'', 3'', 5'', 6'')), 4.73–5.13 (m, 3 H; H–C(1'), CH₂N), 7.33–7.39 (m, 1 H; H–C(6)), 7.44–7.50 (m, 1 H; H–C(4)), 8.07–8.14 ppm (m, 2 H; H–C(3, 7));

¹³C NMR (100 MHz, CDCl₃, based on HSQC): $\delta = 23.72$ and 23.82 (2 C; C(3',4')), 28.32 (3 C; (CH₃)₃), 29.13 and 29.48 (2 C; C(2',5')), 43.45 and 44.02 (2 C; C(2'',6'')), 46.63 and 46.92 (CH₂N), 57.46 and 57.83 (C(1')), 66.36 and 66.73 (2 C; C(3'',5'')), 85.01 and 85.11 (C(CH₃)₃), 114.67 and 114.73 (C(7)), 115.56 and 115.76 (CN), 118.09 and 118.69 (C(4)), 126.19 and 126.22 (arom. C), 127.66 and 128.12 (C(6)), 134.58 and 134.76 (arom. C), 139.03 and 139.10 (C(3)), 139.37 and 139.49 (arom. C), 149.28 (NCO₂), 151.98 and 152.08 (CCN), 163.54 and 163.70 (CN₃), 164.64 and 164.85 ppm (CN₃);

IR (ATR): $\tilde{\nu} = 2960$ (w), 2863 (w), 1757 (m), 1735 (m), 1557 (s), 1488 (s), 1443 (w), 1384 (w), 1357 (m), 1293 (w), 1238 (m), 1209 (w), 1149 (w), 1115 (m), 1069 (very w), 1029 (w), 1002 (w), 974 (very w), 913 (very w), 848 (w), 804 (w), 762 (w), 732 (w), 623 cm⁻¹ (very w);

HR-ESI-MS: m/z (%): 506.2691 (28.9, [$M + H + 1$ (¹³C isotope nat. abundance)]⁺, calcd for C₂₁H₂₅N₈O⁺: 506.2704), 505.2661 (100.0, [$M + H$]⁺, calcd for C₂₆H₃₃N₈O₃⁺: 505.2670), 405.2134 (60.4, [$M - \text{Boc} + H$]⁺, calcd for C₂₁H₂₅N₈O⁺: 405.2146).

2.7.2.21 4-[Cyclopentyl(1*H*-indazol-3-ylmethyl)amino]-6-(4-morpholinyl)-1,3,5-triazine-2-carbonitrile (56a).



56a

A solution of **55a** (28 mg, 0.054 mmol) in 2,2,2-trifluoroethanol (0.27 mL) was stirred at 100 °C for 3 h according to GP-F. MPLC (SiO₂; cyclohexane/EtOAc 100:1 to 4:1) gave **56a** (15 mg, 0.037 mmol, 67%) as a white solid.

$R_f = 0.45$ (SiO₂; cyclohexane/EtOAc 1:1);

m.p. 117–120 °C;

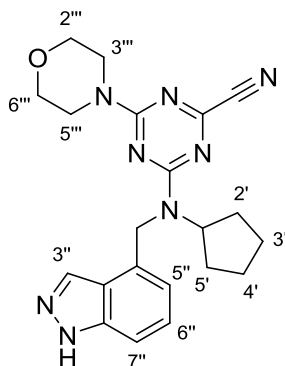
¹H NMR (400 MHz, CDCl₃): $\delta = 1.44$ – 1.98 (m, 8 H; H–C(2', 3', 4', 5')), 3.21–3.98 (br m, 8 H; (H–C(2''', 3''', 5''', 6''')), 4.62–5.25 (m, 3 H; H–C(1'), CH₂N), 7.06–7.20 (m, 1 H; H–C(5'')), 7.34–7.41 (m, 1 H; H–C(6'')), 7.41–7.47 (m, 1 H; H–C(4'')), 7.62 and 7.78 (d, $J = 8.2$ Hz, 1 H; H–C(7'')), 9.97 ppm (br s, 1 H; H–N);

¹³C NMR (100 MHz, CDCl₃): $\delta = 23.81$ and 24.08 (2 C; C(3',4')), 28.76 and 29.40 (2 C; C(2',5')), 41.05 and 41.11 (CH₂N), 43.54 and 44.03 (2 C; C(3''',5''')), 57.67 and 58.20 (C(1')), 66.36 and 66.78 (2 C; C(2''',6''')), 109.78 and 110.01 (C(7'')), 115.68 and 115.80 (CN), 120.19–121.10 (2 C, arom. C), 121.45 and 121.65 (arom. C), 127.11 (arom. C), 141.29 and 141.37 (arom. C), 144.06 and 144.19 (arom. C), 151.84 and 152.98 (CCN), 163.40 and 163.70 (CN₃), 164.33 and 164.38 ppm (CN₃);

IR (ATR): $\tilde{\nu}$ = 2956 (w), 2863 (w), 1557 (s), 1486 (s), 1442 (m), 1357 (w), 1306 (w), 1239 (m), 1202 (very w), 1158 (very w), 1112 (w), 1064 (w), 1000 (w), 969 (very w), 909 (very w), 863 (w), 804 (w), 743 cm^{-1} (m);

HR-ESI-MS: m/z (%): 427.1966 (23.7, $[M + \text{Na}]^+$, calcd for $\text{C}_{21}\text{H}_{25}\text{N}_8\text{O}^+$: 427.1971), 405.2146 (29.6, $[M + \text{H}]^+$, calcd for $\text{C}_{21}\text{H}_{25}\text{N}_8\text{O}^+$: 405.2146), 275.1614 (100.0, $[M - (\text{indazol-3-ylmethylene}) + \text{H}]^+$, calcd for $\text{C}_{13}\text{H}_{19}\text{N}_6\text{O}^+$: 275.1615).

2.7.2.22 4-[Cyclopentyl(1*H*-indazol-4-ylmethyl)amino]-6-(4-morpholinyl)-1,3,5-triazine-2-carbonitrile (**56b**).



56b

A solution of **55b** (34 mg, 0.066 mmol) in 2,2,2-trifluoroethanol (0.33 mL) was stirred at 100 °C for 3 h according to GP-F. MPLC (SiO_2 ; cyclohexane/EtOAc 100:1 to 4:1) gave **56b** (24 mg, 0.059 mmol, 90%) as a white solid.

R_f = 0.43 (SiO_2 ; cyclohexane/EtOAc 1:1);

m.p. 116–119 °C;

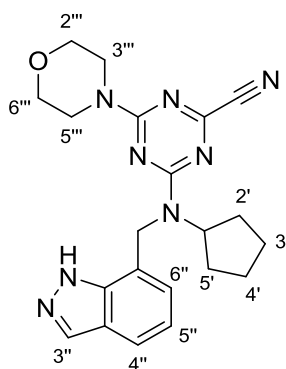
^1H NMR (400 MHz, CDCl_3): δ = 1.43–2.02 (m, 8 H; H–C(2', 3', 4', 5')), 3.05–3.96 (br m, 8 H; (H–C(2''', 3''', 5''', 6''')), 4.70–5.27 (m, 3 H; H–C(1'), CH_2N), 6.83–6.90 (m, 1 H; H–C(5'')), 7.26–7.33 (m, 1 H; H–C(6'')), 7.34–7.43 (m, 1 H; H–C(7'')), 8.04–8.16 (m, 1 H; H–C(3'')), 10.45 ppm (br s, 1 H; H–N);

^{13}C NMR (100 MHz, CDCl_3): δ = 23.83 and 23.98 (2 C; C(3',4')), 29.01 and 29.48 (2 C; C(2',5')), 43.35 and 44.00 (2 C; C(3''',5''')), 44.85 and 45.31 (CH_2N), 57.40 and 57.87 (C(1')), 66.23 and 66.69 (2 C; C(2'',6'')), 108.23 and 108.52 (arom. C), 115.62 and 115.78 (CN), 117.83 and 118.29 (arom. C), 121.32 (arom. C.), 126.97 and 127.11 (arom. C), 132.02 and 132.09 (arom. C), 132.93 and 133.12 (arom. C), 140.28 and 140.38 (C(3'')), 151.95 and 152.05 (CCN), 163.38 and 163.73 (CN_3), 164.49 and 164.87 ppm (CN_3);

IR (ATR): $\tilde{\nu}$ = 2957 (w), 2854 (w), 1558 (s), 1487 (s), 1443 (w), 1419 (w), 1355 (w), 1305 (w), 1243 (w), 1202 (w), 1155 (very w), 1112 (w), 1067 (very w), 999 (w), 942 (w), 860 (w), 804 (w), 777 (w), 730 (w), 661 cm^{-1} (very w);

HR-ESI-MS: m/z (%): 406.2168 (23.3, [$M + H + 1$ (^{13}C isotope nat. abundance)] $^+$, calcd for $\text{C}_{21}\text{H}_{25}\text{N}_8\text{O}^+$: 406.2179), 405.2145 (94.2, [$M + H$] $^+$, calcd for $\text{C}_{21}\text{H}_{25}\text{N}_8\text{O}^+$: 405.2146).

2.7.2.23 4-[Cyclopentyl(1*H*-indazol-7-ylmethyl)amino]-6-(4-morpholinyl)-1,3,5-triazine-2-carbonitrile (**56e**).



56e

A solution of **55e** (20 mg, 0.040 mmol) in 2,2,2-trifluoroethanol (0.20 mL) was stirred at 100 °C for 3 h according to GP-F. MPLC (SiO_2 ; cyclohexane/EtOAc 100:1 to 4:1) gave **56e** (15 mg, 0.037 mmol, 93%) as a white solid.

R_f = 0.43 (SiO_2 ; cyclohexane/EtOAc 1:1);

m.p. 115–119 °C;

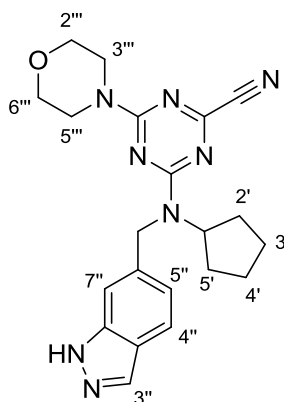
^1H NMR (400 MHz, CDCl_3): δ = 1.39–1.89 (m, 8 H; H–C(2', 3', 4', 5')), 3.38–3.99 (br m, 8 H; H–C(2'', 3'', 5'', 6'')), 4.42–5.23 (m, 3 H; H–C(1'), CH_2N), 7.11 (dd, J = 8.0, 7.2 Hz, 1 H; arom. H), 7.23–7.26 (m, 1 H; arom. H), 7.70 (d, J = 8.0 Hz, 1 H; arom. H), 8.07 ppm (s, 1 H; H–C(3'')), 10.99 ppm (br s, 1 H; H–N) ;

^{13}C NMR (100 MHz, CDCl_3): δ = 23.84 (2 C; C(3',4')), 28.25 and 29.05 (2 C; C(2',5')), 43.66 and 44.18 (2 C; C(3'',5'')), 45.89 and 46.32 (CH_2N), 58.73 and 59.08 (C(1')), 66.29 and 66.70 (2 C; C(2'',6'')), 115.38 and 115.50 (CN), 119.99–121.39 (3 C, arom. C), 123.55 (arom. C), 126.17 and 126.48 (arom. C), 135.13 (arom. C), 138.85 and 139.01 (C(3'')), 152.01 (CCN), 163.35 and 163.55 (CN_3), 164.20 and 164.49 ppm (CN_3);

IR (ATR): $\tilde{\nu}$ = 2957 (w), 2861 (w), 1556 (s), 1486 (s), 1441 (m), 1359 (w), 1305 (w), 1239 (m), 1203 (w), 1113 (w), 1067 (w), 1000 (w), 943 (w), 845 (m), 804 (w), 745 cm^{-1} (w);

HR-ESI-MS: m/z (%): 427.1964 (25.8, $[M + \text{Na}]^+$, calcd for $\text{C}_{21}\text{H}_{25}\text{N}_8\text{O}^+$: 427.1971), 405.2145 (81.4, $[M + \text{H}]^+$, calcd for $\text{C}_{21}\text{H}_{25}\text{N}_8\text{O}^+$: 405.2146).

2.7.2.24 4-[Cyclopentyl(1*H*-indazol-6-ylmethyl)amino]-6-(4-morpholinyl)-1,3,5-triazine-2-carbonitrile (56d).



56d

A solution of **55d** (30 mg, 0.059 mmol) in 2,2,2-trifluoroethanol (0.30 mL) was stirred at 100 °C for 3 h according to GP-F. MPLC (SiO₂; cyclohexane/EtOAc 100:1 to 4:1) gave **56d** (20 mg, 0.049 mmol, 84%) as a white solid.

$R_f = 0.44$ (SiO₂; cyclohexane/EtOAc 1:1);

m.p. 118–123 °C;

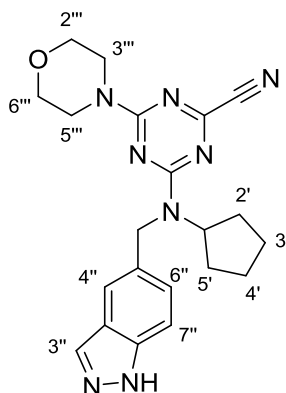
¹H NMR (400 MHz, CDCl₃): $\delta = 1.42$ – 1.98 (m, 8 H; H–C(2', 3', 4', 5')), 3.26 – 3.93 (br m, 8 H; H–C(2''', 3''', 5''', 6''')), 4.72 – 5.18 (m, 3 H; H–C(1'), CH₂N), 7.01 (d, $J = 8.4$ Hz, 1 H; arom. H), 7.23 (s, 1 H; H–C(7'')), 7.68 (d, $J = 8.4$ Hz, 1 H; arom. H), 8.04 (s, 1 H; H–C(3'')), 10.39 ppm (br s, 1 H; H–N);

¹³C NMR (100 MHz, CDCl₃): $\delta = 23.75$ and 23.86 (2 C; C(3',4')), 29.13 and 29.49 (2 C; C(2',5')), 43.46 and 44.00 (2 C; C(3''',5''')), 47.09 and 47.38 (CH₂N), 57.41 and 57.86 (C(1')), 66.32 and 66.69 (2 C; C(2''',6''')), 106.64 and 107.32 (arom. C), 115.66 and 115.77 (CN), 120.12 and 120.43 (arom. C), 120.94 and 121.00 (arom. C), 122.45 and 122.60 (arom. C), 134.87 (arom. C), 138.24 and 138.35 (arom. C), 140.54 (arom. C), 151.95 and 152.06 (CCN), 163.47 and 163.69 (CN₃), 164.57 and 164.86 ppm (CN₃);

IR (ATR): $\tilde{\nu} = 2956$ (w), 2863 (w), 1631 (very w), 1557 (s), 1486 (s), 1444 (w), 1422 (w), 1355 (m), 1306 (w), 1235 (m), 1202 (w), 1112 (w), 1067 (w), 1019 (very w), 1001 (w), 973 (very w), 942 (w), 911 (very w), 848 (m), 804 (w), 760 (very w), 729 cm⁻¹ (w);

HR-ESI-MS: m/z (%): 406.2184 (23.3, [$M + H + 1$ (¹³C isotope nat. abundance)]⁺, calcd for C₂₁H₂₅N₈O⁺: 406.2179), 405.2151 (94.2, [$M + H$]⁺, calcd for C₂₁H₂₅N₈O⁺: 405.2146).

2.7.2.25 4-[Cyclopentyl(1*H*-indazol-5-ylmethyl)amino]-6-(4-morpholinyl)-1,3,5-triazine-2-carbonitrile (56c).



56c

A solution of **55c** (29 mg, 0.057 mmol) in 2,2,2-trifluoroethanol (0.29 mL) was stirred at 100 °C for 3 h according to GP-F. MPLC (SiO₂; cyclohexane/EtOAc 100:1 to 4:1) gave **56c** (15 mg, 0.037 mmol, 65%) as a white solid.

$R_f = 0.44$ (SiO₂; cyclohexane/EtOAc 1:1);

m.p. 111–113 °C;

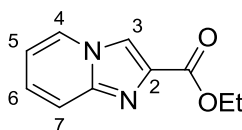
¹H NMR (400 MHz, CDCl₃): $\delta = 1.46$ – 1.96 (m, 17 H; (H–C(2', 3', 4', 5'), (CH₃)₃), 3.35–3.89 (br m, 8 H; (H–C(2''', 3''', 5''', 6''')), 4.73–5.13 (m, 3 H; H–C(1'), CH₂N), 7.33–7.39 (m, 1 H; arom. H), 7.44–7.50 (m, 1 H; H–C(4'')), 8.07–8.14 ppm (m, 2 H; arom. H and H–C(3''));

¹³C NMR (100 MHz, CDCl₃): $\delta = 23.72$ and 23.82 (2 C; C(3',4')), 28.32 (3 C; (CH₃)₃), 29.13 and 29.48 (2 C; C(2',5')), 43.45 and 44.02 (2 C; C(3''',5''')), 46.63 and 46.92 (CH₂N), 57.46 and 57.83 (C(1')), 66.36 and 66.73 (2 C; C(2''',6''')), 85.01 and 85.11 (C(CH₃)₃), 114.67 and 114.73 (arom. C), 115.56 and 115.76 (CN), 118.09 and 118.69 (C(4'')), 126.19 and 126.22 (arom. C), 127.66 and 128.12 (arom. C), 134.58 and 134.76 (arom. C), 139.03 and 139.10 (arom. C), 139.37 and 139.49 (arom. C), 149.28 (NCO₂), 151.98 and 152.08 (CCN), 163.54 and 163.70 (CN₃), 164.64 and 164.85 ppm (CN₃);

IR (ATR): $\tilde{\nu}$ = 2955 (s), 2859 (s), 1557 (s), 1485 (s), 1443 (w), 1423 (w), 1358 (m), 1306 (w), 1238 (m), 1205 (w), 1140 (very w), 1112 (w), 1067 (w), 1000 (w), 974 (very w), 941 (w), 909 (very w), 863 (w), 802 (w), 761 (very w), 729 cm^{-1} (m);

HR-ESI-MS: m/z (%): 406.2178 (26.9, $[M + H + 1$ (^{13}C isotope nat. abundance)] $^+$, calcd for $\text{C}_{21}\text{H}_{25}\text{N}_8\text{O}^+$: 406.2179), 405.2142 (100.0, $[M + H]^+$, calcd for $\text{C}_{21}\text{H}_{25}\text{N}_8\text{O}^+$: 405.2146).

2.7.2.26 Ethyl imidazo[1,2-a]pyridine-2-carboxylate (**57**).^[470]



57

A stirred solution of 2-aminopyridine (1.43 g, 15.0 mmol) in THF (34 mL) was treated dropwise with ethyl bromopyruvate at 24 °C. The resulting suspension was refluxed overnight. The white solid was filtered off, washed two times with cold THF (2 x 10 mL) and suspended in EtOAc (35 mL). The suspension was treated with saturated aqueous solution of NaHCO_3 (20 mL), then with aqueous solution of Na_2CO_3 (2 g in 5 mL) and stirred until the solid was fully dissolved. Layers were separated and the aqueous layer was extracted three times with EtOAc (3 x 30 mL). The organic extracts were combined, dried over anhydrous Na_2SO_4 and evaporated. MPLC (SiO_2 ; cyclohexane/EtOAc 5:3 to 1:100) gave **57** (1.89 g, 9.95 mmol, 66%) as an off-white solid.

R_f = 0.37 (SiO_2 ; 1% of NH_4OH in EtOAc);

m.p. 81–83 °C (^[470]: 82 °C)

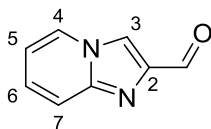
^1H NMR (400 MHz, CDCl_3): δ = 1.41 (t, J = 7.1 Hz, 3 H; CH_3), 4.43 (q, J = 7.1 Hz, 2 H; CH_2), 6.48 (dd, J = 6.8, 6.8 Hz, 1 H; H-C(5)), 7.21 (dd, J = 9.1, 6.8 Hz, 1 H; H-C(6)), 7.65 (d, J = 9.1 Hz, 1 H; H-C(7)), 8.11 (d, J = 6.8 Hz, 1 H; H-C(4)), 8.16 ppm (s, 1 H; H-C(3));

^{13}C NMR (100 MHz, CDCl_3): δ = 14.51 (CH_3), 61.21 (CH_2), 113.94 (arom. C), 116.98 (arom. C), 126.16 (arom. C), 126.23 (arom. C), 136.98 (C(2)), 145.35 (NCN), 163.38 ppm (CO_2);

IR (ATR): $\tilde{\nu}$ = 3151 (very w), 3109 (very w), 3054 (very w), 2983 (w), 2903 (very w), 1721 (very s), 1637 (w), 1538 (very w), 1524 (very w), 1485 (w), 1452 (very w), 1398 (very w), 1379 (w), 1353 (w), 1337 (very w), 1284 (w), 1263 (very w), 1194 (very s), 1149 (very w), 1132 (w), 1115 (m), 1022 (m), 970 (w), 918 (very w), 843 (w), 745 (very s), 623 cm^{-1} (very w);

HR-MALDI-MS: m/z (%): 404.1411 (21.1, $[2M + \text{Na} + 1 (^{13}\text{C} \text{ isotope nat. abundance})]^+$, calcd for $\text{C}_{20}\text{H}_{21}\text{N}_4\text{NaO}_4^+$: 404.1416), 403.1377 (100.0, $[2M + \text{Na}]^+$, calcd for $\text{C}_{20}\text{H}_{21}\text{N}_4\text{NaO}_4^+$: 403.1382), 381.1558 (82.3, $[2M + \text{H}]^+$, calcd for $\text{C}_{20}\text{H}_{21}\text{N}_4\text{O}_4^+$: 381.1558), 191.0815 (91.5, $[M + \text{H}]^+$, calcd for $\text{C}_{10}\text{H}_{11}\text{N}_2\text{O}_2^+$: 191.0816).

2.7.2.27 Imidazo[1,2-a]pyridine-2-carbaldehyde (**58**).^[453]



58

A solution of **57** (0.471 g, 2.45 mmol) in CH_2Cl_2 (12.3 mL) was cooled down to -78 °C and treated dropwise with a 1.1 M solution of DIBALH in cyclohexane (3.12 mL, 3.43 mmol). After stirring for 60 min at -78 °C, reaction was quenched carefully, by dropwise addition of a saturated La Rochelle solution (6.0 mL) and was left stirring and spontaneously warming for 15 min. The mixture was extracted with EtOAc (40 mL). The aqueous layer was extracted two more times with EtOAc (2 x 20 mL). Organic extracts were combined, dried over Na_2SO_4 and evaporated. MPLC (SiO_2 ; $\text{CH}_2\text{Cl}_2/\text{MeOH}$ 100:1 to 19:1) gave **58** (278 mg, 1.90 mmol, 78%) as a colorless oil.

R_f = 0.40 (SiO_2 ; $\text{CH}_2\text{Cl}_2/\text{MeOH}$ 10:1);

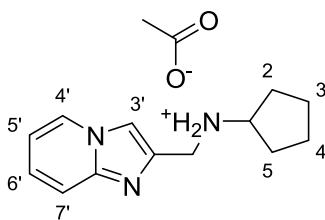
^1H NMR (400 MHz, CDCl_3): δ = 6.89 (dd, J = 6.8, 6.8 Hz, 1 H; H–C(5)), 7.26 (dd, J = 9.1, 6.8 Hz, 1 H; H–C(6)), 7.65 (d, J = 9.1 Hz, 1 H; H–C(7)), 8.14 (s, 1 H; H–C(3)), 8.16 (d, J = 6.8 Hz, 1 H; H–C(4)), 10.13 ppm (s, 1 H; CHO);

^{13}C NMR (100 MHz, CDCl_3): δ = 114.56 (arom. C), 115.67 (arom. C), 119.39 (arom. C), 126.68 (arom. C), 126.75 (arom. C), 143.76 (arom. C), 145.86 (arom. C), 188.03 ppm (CHO);

IR (ATR): $\tilde{\nu}$ = 3063 (w), 2798 (w), 2740 (very w), 2163 (very w), 1687 (very s), 1638 (m), 1539 (w), 1486 (w), 1452 (very w), 1391 (w), 1371 (w), 1350 (w), 1326 (w), 1279 (w), 1255 (w), 1205 (very w), 1167 (m), 1137 (m), 1012 (w), 982 (w), 916 (w), 835 (w), 819 (m), 782 (w), 752 (m), 734 (s), 646 (w), 621 cm^{-1} (very w);

HR-EI-MS: m/z (%): 146.0475 (100.0, $[M]^+$, calcd for $\text{C}_8\text{H}_6\text{N}_2\text{O}^+$: 146.0480), 145.0396 (25.8, $[M - 1]^+$, calcd for $\text{C}_8\text{H}_5\text{N}_2\text{O}^+$: 145.0397), 118.0526 (21.6, $[M - \text{CO}]^+$, calcd for $\text{C}_7\text{H}_6\text{N}_2^+$: 118.0531), 78.0336 (51.7, $[M - \text{C}_3\text{H}_2\text{NO}]^+$, calcd for $\text{C}_5\text{H}_4\text{N}^+$: 78.0339).

2.7.2.28 *N*-(Imidazo[1,2-*a*]pyridin-2-ylmethyl)cyclopentanaminium acetate (**59**).



59

A solution of **58** (221 mg, 1.50 mmol) and cyclopentylamine (0.150 mL, 1.50 mmol) in CH_2Cl_2 (15.0 mL) was stirred over 4 Å MS at 24 °C for 60 min. $\text{NaBH}(\text{OAc})_3$ (0.642 g, 3.00 mmol) was added and the mixture was stirred overnight. The mixture was diluted with EtOAc (30 mL) and the solids were filtered off. The filtrate was washed three times with saturated aqueous NaHCO_3 (3 x 10 mL), dried over anhydrous Na_2SO_4 and evaporated. MPLC (SiO_2 ; $\text{CH}_2\text{Cl}_2/\text{MeOH}$ 7:3) gave **59** (262 mg, 0.952 mmol, 63%) as a colorless oil.

$R_f = 0.22$ (SiO₂; CH₂Cl₂/MeOH 2:1);

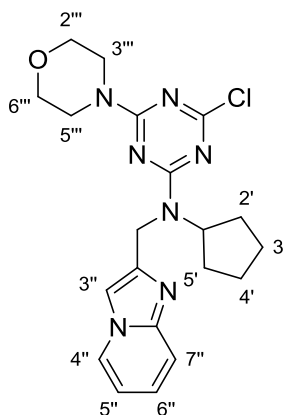
¹H NMR (400 MHz, CDCl₃): $\delta = 1.49$ – 2.00 (m, 11 H; H–C(2, 3, 4, 5), CH₃), 3.30 (m, 1 H; H–C(1)), 4.08 (s, 2 H; CH₂), 6.44 (br s, 2 H; NH₂), 6.76 (dd, $J = 6.8, 6.8$ Hz, 1 H; H–C(5')), 7.16 (dd, $J = 9.1, 6.8$ Hz, 1 H; H–C(6')), 7.54 (d, $J = 9.1$ Hz, 1 H; H–C(7')), 7.70 (s, 1 H; H–C(3')), 8.06 ppm (d, $J = 6.8$ Hz, 1 H; H–C(4'));

¹³C NMR (100 MHz, CDCl₃, based on HSQC): $\delta = 22.85$ (CH₃), 24.20 (2 C, C(3, 4)), 31.69 (2 C; C(2, 5)), 45.08 (CH₂N), 58.94 (C(1)), 111.33 (C(3')), 112.62 (C(5')), 117.28 (C(7')), 125.07 (C(6')), 125.94 (C(4')), 142.32 (arom. C), 145.22 (arom. C), 176.66 ppm (CO₂);

IR (ATR): $\tilde{\nu} = 3137$ (very w), 2948 (w), 2869 (w), 2601 (w), 1635 (w), 1533 (w), 1503 (m), 1453 (very w), 1402 (s), 1354 (w), 1332 (w), 1273 (w), 1230 (w), 1167 (very w), 1149 (w), 1125 (very w), 1033 (very w), 1009 (w), 911 (w), 756 (s), 740 (w), 651 (m), 617 cm⁻¹ (w);

HR-ESI-MS: m/z (%): 475.4145 (27.8), 419.3516 (31.2), 282.2791 (27.5), 217.1524 (20.8, [$M - C_2H_3O_2 + 1$ (¹³C isotope nat. abundance)]⁺, calcd for C₁₃H₁₈N₃⁺: 217.1529), 216.1494 (100.0, [$M - C_2H_3O_2$]⁺, calcd for C₁₃H₁₈N₃⁺: 216.1496), 131.0598 (85.6, [$M - C_5H_{10}N$]⁺, calcd for C₈H₇N₂⁺: 131.0604).

2.7.2.29 6-(4-Morpholinyl)-4-chloro-*N*-cyclopentyl-*N*-(imidazo[1,2-*a*]pyridin-2-ylmethyl)-1,3,5-triazin-2-amine (60).



60

A solution of **59** (264 mg, 0.95 mmol) in CH₂Cl₂ (9.5 mL) was treated with *i*Pr₂NEt (0.332 mL, 1.90 mmol) and then with cyanuric chloride (177 mg, 0.95 mmol) at 0 °C and stirred for 90 min at the same temperature. The solution was subsequently treated with *i*Pr₂NEt (0.166 mL, 0.95 mmol) and morpholine (0.084 mL, 0.95 mmol), and stirred overnight at 24 °C. The solution was concentrated and the residue dry loaded onto Celite. MPLC (SiO₂; CH₂Cl₂/MeOH 7:3) gave **60** (54 mg, 0.13 mmol, 14%) as a white solid.

$R_f = 0.33$ (SiO₂; EtOAc 100%);

m.p. 73-76 °C;

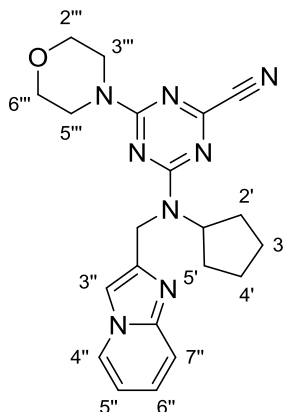
¹H NMR (400 MHz, CDCl₃): $\delta = 1.47$ – 1.95 (m, 8 H; H–C(2', 3', 4', 5')), 3.36 – 3.87 (m, 8 H; H–C(2''', 3''', 5''', 6''')), 4.73 – 5.18 (m, 3 H; H–C(1'), CH₂N), 6.68 – 6.77 (m, 1 H; H–C(5'')), 7.07 – 7.17 (m, 1 H; H–C(6'')), 7.27 (s, 1 H; H–C(3'')), 7.46 – 7.56 (m, 1 H; C(7'')), 7.97 – 8.05 ppm (m, 1 H; H–C(4''));

¹³C NMR (100 MHz, CDCl₃, based on HSQC): $\delta = 23.91$ and 23.96 (2 C, C(3', 4')), 29.17 and 29.47 (2 C; C(2', 5')), 42.25 and 42.57 (CH₂N), 43.91 and 43.97 (2 C; C(3''', 5''')), 56.75 and 57.68 (C(1')), 66.56 and 66.75 (2 C; C(2''', 6''')), 109.57 and 110.90 (C(3)), 112.25 and 112.29 (C(5'')), 117.09 and 117.30 (C(7'')), 124.33 and 124.51 (C(6'')), 125.65 and 125.69 (C(4'')), 144.41 and 144.70 (arom. C), 145.22 and 145.87 (arom. C), 164.39 and 164.65 (CN₃), 165.23 and 165.28 (CN₃), 169.39 and 169.53 ppm (CCIN₂);

IR (ATR): $\tilde{\nu} = 2956$ (w), 2859 (w), 1635 (very w), 1557 (s), 1483 (s), 1444 (m), 1422 (w), 1367 (w), 1343 (very w), 1293 (m), 1242 (m), 1186 (w), 1143 (very w), 1112 (w), 1059 (w), 1017 (very w), 990 (w), 968 (w), 897 (w), 856 (w), 812 (very w), 799 (w), 753 (w), 739 (w), 666 (w), 618 cm⁻¹ (very w);

HR-ESI-MS: m/z (%): 475.4143 (35.8), 419.3519 (39.3), 416.1787 (33.9, [$M + H + 2$]⁺, calcd for C₂₀H₂₅³⁷CIN₇⁺: 416.1775), 415.1833 (24.1, [$M + H + 1$]⁺, calcd for C₂₀H₂₅³⁶CIN₇⁺: 415.1838), 414.1806 (100.0, [$M + H$]⁺, calcd for C₂₀H₂₅³⁵CIN₇⁺: 414.1804), 274.2746 (23.5), 229.1225 (29.4), 105.0707 (22.3).

2.7.2.30 4-[Cyclopentyl(imidazo[1,2-a]pyridin-2-ylmethyl)amino]-6-(4-morpholinyl)-1,3,5-triazine-2-carbonitrile (61).



61

A solution of **60** (35 mg, 0.085 mmol) in DMSO (0.83 mL) was treated with KCN (18 mg, 0.27 mmol) and 18-crown-6 (1 mg, 4 μ mol) and heated for four days at 120 °C. The mixture was cooled down to 24 °C and diluted with EtOAc (4 mL). The suspension was washed four times with brine (4 x 1 mL). The solution was dried over anhydrous Na₂SO₄ and evaporated. FC (SiO₂; cyclohexane/EtOAc 1:1 to 100:1) gave **61** (16 mg, 0.040 mmol, 50%) as a white solid.

R_f = 0.33 (SiO₂; EtOAc 100%);

m.p. > 80 °C (decomp.);

¹H NMR (400 MHz, CDCl₃): δ = 1.46–2.00 (m, 8 H; H–C(2', 3', 4', 5')), 3.39–3.90 (m, 8 H; H–C(2''', 3''', 5''', 6''')), 4.76–5.18 (m, 3 H; H–C(1'), CH₂N), 6.71–6.79 (m, 1 H; H–C(5'')), 7.09–7.97 (m, 1 H; H–C(6'')), 7.27 and 7.45 (s, 1 H; H–C(3'')), 7.48–7.56 (m, 1 H; C(7'')), 7.98–8.05 ppm (m, 1 H; H–C(4''));

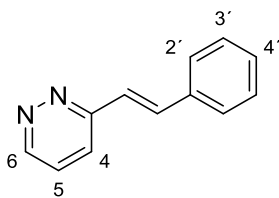
¹³C NMR (100 MHz, CDCl₃, based on HSQC): δ = 23.98 (2 C, C(3', 4')), 29.17 and 29.51 (2 C; C(2', 5')), 42.45 and 42.60 (CH₂N), 43.60 and 44.00 (2 C; C(3''', 5''')), 57.11 and 57.55 (C(1')), 66.51 and 66.77 (2 C; C(2''', 6''')), 109.47 and 110.80 (C(3'')), 112.30 and 112.35 (C(5'')), 115.80 (CN), 117.22 and 117.47 (C(7'')), 124.37 and 124.56 (C(6'')), 125.66 and 125.72 (C(4'')), 144.71

and 144.89 (arom. C), 144.99 and 145.55 (arom. C), 151.93 and 151.98 (CCN), 163.50 and 163.69 (CN₃), 164.32 and 164.41 ppm (CN₃);

IR (ATR): $\tilde{\nu}$ = 2956 (w), 2860 (w), 1557 (s), 1485 (s), 1444 (m), 1423 (w), 1356 (w), 1304 (w), 1246 (m), 1198 (w), 1142 (very w), 1113 (w), 1068 (w), 1018 (very w), 1002 (w), 971 (very w), 865 (w), 804 (w), 754 (w), 740 (m), 669 (very w), 641 cm⁻¹ (very w);

HR-ESI-MS: m/z (%): 406.2174 (26.8, [M + H + 1 (¹³C isotope natural abundance)]⁺, calcd for C₂₁H₂₅N₈O⁺: 406.2180), 405.2144 (100.0, [M + H]⁺, calcd for C₂₁H₂₅N₈O⁺: 405.2146).

2.7.2.31 (*E*)-3-Styrylpyridazine (**62**).^[471]



62

A mixture of 3-methylpyridazine (485 mg, 5.00 mmol), benzaldehyde (1.03 mL, 10.0 mmol) and ZnCl₂ (138 mg, 0.75 mmol) was stirred at 150 °C for 4 h. The mixture was cooled down and dry loaded onto Celite. MPLC (SiO₂; cyclohexane/EtOAc 1:1 to 1:100) gave **62** (342 mg, 1.88 mmol, 38%) as a pale brown solid.

R_f = 0.20 (SiO₂; cyclohexane/EtOAc 1:1);

m.p. 101-103 °C (^[471]: 100.5-101 °C);

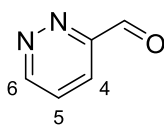
¹H NMR (400 MHz, CDCl₃): δ = 7.31–7.47 (m, 5 H; arom. H), 7.58–7.66 (m, 3 H; arom. H), 7.70 (d, J = 16.4 Hz, 1 H; trans-olefin H), 9.05 ppm (d, J = 4.9 Hz, 1 H; H–C(6));

¹³C NMR (100 MHz, CDCl₃): δ = 124.05 (C(2')), 125.29 (C(4)), 126.53 (C(4')), 127.48 (C(2')), 129.01 (C(3')), 129.21 (C(5)), 135.32 (C(1')), 136.05 (C(1')), 149.78 (C(6)), 158.39 ppm (C(3));

IR (ATR): $\tilde{\nu}$ = 1634 (w), 1578 (w), 1494 (w), 1434 (m), 1383 (w), 1251 (w), 1212 (w), 1074 (w), 1005 (w), 966 (m), 865 (w), 805 (m), 737 (m), 687 cm^{-1} (m);

HR-EI-MS: m/z (%): 182.0824 (32.0, $[M]^+$, calcd for $\text{C}_{12}\text{H}_{10}\text{N}_2^+$: 182.0844), 181.0763 (100.0, $[M - \text{H}]^+$, calcd for $\text{C}_{12}\text{H}_9\text{N}_2^+$: 181.0760).

2.7.2.32 Pyridazine-3-carbaldehyde (**63**).^[472]



63

A solution of **62** (302 mg, 1.64 mmol) in 1,4-dioxane (8.2 mL) was treated with 4% OsO_4 in H_2O (0.614 mL, 0.10 mmol), NaIO_4 (1.43 g, 6.56 mmol) and 2,6-lutidine (0.380 mL, 3.28 mmol) at 24 °C for 2 days. The solids were filtered off, washed with THF (2 x 5 mL), and the filtrate was concentrated under reduced pressure. The residue was dissolved in CH_2Cl_2 (50 mL), dried over Na_2SO_4 and dry loaded onto Celite. FC (SiO_2 ; $\text{CH}_2\text{Cl}_2/\text{MeOH}$ 99:1 to 90:1) gave **63** (103 mg, 0.953 mmol, 58%) as a colorless oil.

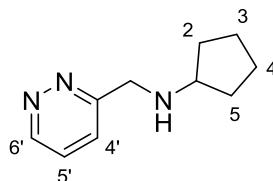
R_f = 0.39 (SiO_2 ; $\text{CH}_2\text{Cl}_2/\text{MeOH}$ 10:1);

^1H NMR (400 MHz, CDCl_3): δ = 7.70 (dd, J = 8.4, 5.0 Hz, 1 H; H-C(5)), 8.07 (d, J = 8.4 Hz, 1 H; H-C(4)), 9.38 (d, J = 5.0 Hz, 1 H; H-C(6)), 10.41 ppm (s, 1 H; CHO);

^{13}C NMR (100 MHz, CDCl_3): δ = 124.34 (C(4)), 127.46 (C(5)), 153.77 (C(6)), 155.53 (C(3)), 192.35 ppm (CHO);

IR (ATR): $\tilde{\nu}$ = 3057 (w), 2880 (w), 1994 (very w), 1701 (very s), 1573 (w), 1432 (w), 1401 (w), 1356 (m), 1254 (m), 1181 (w), 1154 (w), 1102 (very w), 1073 (w), 1053 (w), 1009 (s), 991 (m), 748 (m), 673 (m), 633 cm^{-1} (w);

HR-EI-MS: m/z (%): 108.0321 (95.0, $[M]^+$, calcd for $\text{C}_5\text{H}_4\text{N}_2\text{O}^+$: 108.0324), 80.0364 (36.6, $[M - \text{CO} + \text{H}]^+$, calcd for $\text{C}_4\text{H}_4\text{N}_2^+$: 80.0374), 53.0255 (100.0), 52.0184 (30.9), 51.0223 (43.3).

2.7.2.33 *N*-(Pyridazin-3-ylmethyl)cyclopentanamine (**64**).**64**

A solution of **63** (82 mg, 0.75 mmol) and cyclopentylamine (75 μ L, 0.75 mmol) in CH_2Cl_2 (7.5 mL) was stirred over 4 Å MS at 24 °C for 60 min. $\text{NaBH}(\text{OAc})_3$ (321 mg, 1.50 mmol) was added and the mixture was stirred overnight. The mixture was treated with saturated aqueous K_2CO_3 (7.5 mL), diluted with EtOAc (15 mL) and the solids were filtered off. The aqueous layer was extracted with EtOAc (2 x 15 mL). The combined organic extracts were dried over anhydrous Na_2SO_4 and evaporated. FC (SiO_2 ; $\text{CH}_2\text{Cl}_2/\text{MeOH}$ 10:1) gave an acetate salt which was subsequently partitioned between EtOAc (100 mL) and 1M KOH (30 mL). The organic layer was dried over anhydrous Na_2SO_4 , concentrated under reduced pressure and dried *in vacuo* to afford the free base **64** (76 mg, 0.43 mmol, 57%) as a pale brown oil.

$R_f = 0.17$ (SiO_2 ; $\text{CH}_2\text{Cl}_2/\text{MeOH}$ 10:1);

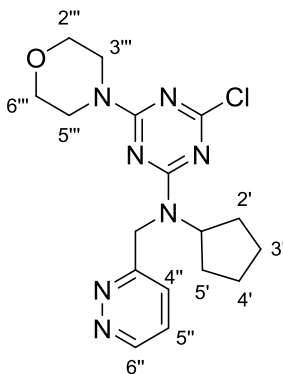
^1H NMR (400 MHz, CDCl_3): $\delta = 1.34\text{--}1.92$ (m, 9 H; H-C(2, 3, 4, 5), H-N), 3.11–3.15 (m, 1 H; H-C(1)), 4.09 (s, 2 H; CH_2), 7.43 (dd, $J = 8.4, 4.9$ Hz, 1 H; H-(5')), 7.55 (d, $J = 8.4$ Hz, 1 H; H-(4')), 9.08 ppm (d, $J = 4.9$ Hz, 1 H; H-(6'));

^{13}C NMR (100 MHz, CDCl_3): $\delta = 24.17$ (2 C, C(3, 4)), 33.31 (2 C, C(2, 5)), 52.58 (CH_2N), 59.84 (C(1)), 126.30 (C(4')), 126.65 (C(5')), 150.44 (C(6')), 162.45 ppm (C(3'));

IR (ATR): $\tilde{\nu} = 3293$ (very w), 3050 (very w), 2950 (w), 2865 (w), 1711 (w), 1581 (w), 1554 (very w), 1435 (w), 1397 (very w), 1362 (very w), 1281 (very w), 1169 (very w), 1124 (very w), 1076 (very w), 999 (very w), 838 (very w), 791 (m), 755 cm^{-1} (w).

HR-ESI-MS: m/z (%): 178.1341 (23.4, $[M + \text{H}]^+$, calcd for $\text{C}_{10}\text{H}_{16}\text{N}_3^+$: 178.1339), 110.0706 (100.0, $[M - \text{C}_5\text{H}_9 + 2\text{H}]^+$, calcd for $\text{C}_5\text{H}_8\text{N}_3^+$: 110.0713).

2.7.2.34 4-Chloro-*N*-cyclopentyl-6-(4-morpholinyl)-*N*-(pyridazin-3-ylmethyl)-1,3,5-triazin-2-amine (65).



65

A solution of **64** (72 mg, 0.40 mmol) in CH_2Cl_2 (4.0 mL) was treated with $i\text{Pr}_2\text{NEt}$ (70 μL , 0.40 mmol) and then with cyanuric chloride (75 mg, 0.40 mmol) at 0 °C and stirred for 60 min at the same temperature. The solution was subsequently treated with $i\text{Pr}_2\text{NEt}$ (70 μL , 0.40 mmol) and morpholine (35 μL , 0.40 mmol), and left stirring for 3 h at 24°C. The solution was concentrated under reduced pressure. MPLC (SiO_2 ; cyclohexane/EtOAc 1:1 to 1:100) gave **65** (82 mg, 0.22 mmol, 55%) as an off-white solid.

$R_f = 0.23$ (SiO_2 ; EtOAc 100%);

m.p. 67-70 °C;

^1H NMR (400 MHz, CDCl_3 , based on HSQC): $\delta = 1.37\text{--}2.00$ (m, 8 H; H-C(2', 3', 4', 5')), 3.23–3.91 (m, 8 H; H-C(2''', 3''', 5''', 6''')), 4.84–5.31 (m, 3 H; H-C(1'), CH_2N), 7.21–7.49 (m, 2 H; H-C(5''), H-C(4'')), 9.01–9.11 ppm (m, 1 H; H-(6''));

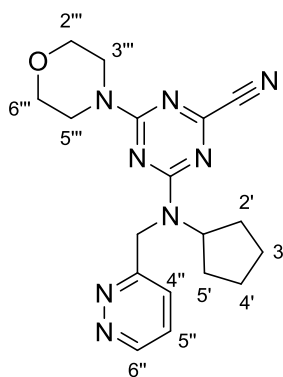
^{13}C NMR (100 MHz, CDCl_3 , based on HSQC): $\delta = 23.69$ and 23.82 (2 C, C(3', 4')), 29.16 and 29.48 (2 C; C(2', 5')), 43.77 and 44.01 (2 C; C(3''', 5''')), 46.96 and 47.32 (CH_2N), 56.73 and 57.75 (C(1')), 66.45 and 66.72 (2 C; C(2''', 6''')), 124.18 and 124.95 (C(4'')), 125.89 and 126.66

(C(5'')), 150.25 and 150.48 (C(6'')), 161.85 and 162.02 (C(3'')), 164.16 and 164.64 (CN₃), 165.53 and 165.76 (CN₃), 169.53 and 169.75 ppm (CClN₂);

IR (ATR): $\tilde{\nu}$ = 2957 (w), 2858 (w), 1558 (s), 1483 (s), 1437 (m), 1366 (w), 1343 (very w), 1299 (m), 1239 (m), 1202 (very w), 1186 (very w), 1112 (w), 1063 (w), 990 (w), 969 (w), 899 (w), 857 (w), 799 (m), 746 (very w), 611 cm⁻¹ (very w);

HR-ESI-MS: m/z (%): 378.1631 (33.2, [M + H + 2]⁺, calcd for C₁₇H₂₃³⁷CIN₇O⁺: 378.1618), 377.1684 (22.5, [M + H + 1]⁺, calcd for C₁₇H₂₃³⁶CIN₇O⁺: 377.1681), 376.1655 (94.3, [M + H]⁺, calcd for C₁₇H₂₃³⁵CIN₇O⁺: 376.1647).

2.7.2.35 4-[Cyclopentyl(pyridazin-3-ylmethyl)amino]-6-(4-morpholinyl)-1,3,5-triazine-2-carbonitrile (**66**).



66

A solution of **65** (82 mg, 0.22 mmol) in DMSO (2.15 mL) was treated with KCN (16 mg, 0.24 mmol) and 18-crown-6 (3 mg, 0.01 mmol) and heated for 2 days at 100 °C. The mixture was cooled down to 24 °C and diluted with EtOAc (4 mL). The suspension was partitioned between 10 mL EtOAc and 2.15 mL of brine. The organic layer was washed with brine (3 x 2 mL), dried over anhydrous Na₂SO₄ and concentrated under reduced pressure. RP-HPLC (column: Merck LiChroCART® 250-4, Lichrospher 100, RP-18, 5 μm; H₂O/MeCN gradient (%MeCN): 10% for 2 min; 10% to 50% for 15min; 50% for 6 min; 50% to 90% for 4 min) gave **66** (8 mg, 0.02 mmol, 9%) as a white solid.

$R_f = 0.23$ (SiO₂; EtOAc 100%);

m.p. > 50 °C (decomp.);

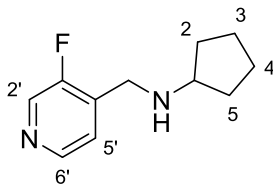
¹H NMR (400 MHz, CDCl₃): $\delta = 1.44$ – 1.98 (m, 8 H; H–C(2', 3', 4', 5')), 3.28 – 3.89 (m, 8 H; H–C(2''', 3''', 5''', 6''')), 4.83 – 5.26 (m, 3 H; H–C(1'), CH₂N), 7.27 – 7.52 (m, 2 H; H–C(5''), H–C(4'')), 9.06 – 9.19 ppm (m, 1 H; H–(6''));

¹³C NMR (100 MHz, CDCl₃, based on HSQC): $\delta = 23.73$ and 23.79 (2 C, C(3', 4')), 29.22 and 29.52 (2 C; C(2', 5')), 43.49 and 44.07 (2 C; C(3''', 5''')), 47.14 and 47.27 (CH₂N), 57.07 and 57.55 (C(1')), 66.37 and 66.69 (2 C; C(2''', 6''')), 115.48 and 115.58 (CN), 124.69 and 126.58 (C(4'')), 127.07 – 127.45 (m, C(5'')), 149.95 – 150.30 (m, C(6'')), 151.94 and 152.13 (CCN), 161.68 and 161.85 (C(3'')), 163.28 and 163.64 (CN₃), 164.72 and 164.87 ppm (CN₃);

IR (ATR): $\tilde{\nu} = 2957$ (w), 2858 (w), 1559 (s), 1486 (s), 1439 (m), 1361 (w), 1304 (w), 1242 (m), 1203 (w), 1112 (m), 1068 (w), 1001 (w), 970 (w), 860 (w), 804 (m), 737 (very w), 633 cm⁻¹ (very w);

HR-ESI-MS: m/z (%): 427.2565 (35.5), 368.2018 (25.9, [$M + H + 1$ (¹³C isotope nat. abundance)]⁺, calcd for C₁₈H₂₃N₈O⁺: 368.2023), 367.1990 (100.0, [$M + H$]⁺, calcd for C₁₈H₂₃N₈O⁺: 367.1989), 299.1367 (24.2, [$M - C_5H_9 + H$]⁺, calcd for C₁₃H₁₅N₈O⁺: 299.1363).

2.7.2.36 *N*-[(3-Fluoropyridin-4-yl)methyl]cyclopentanamine (**67a**).



67a

A solution of 3-fluoroisonicotinaldehyde (190 mg, 1.50 mmol) in CH₂Cl₂ (15.0 mL) was treated with cyclopentylamine (150 μ L, 1.50 mmol) over 4 Å MS at 24 °C for 60 min and then with NaBH(OAc)₃ (642 mg, 3.00 mmol). The mixture was quenched with saturated aqueous K₂CO₃

adjusted to pH = 14 (20 mL), partitioned with EtOAc (40 mL) and decanted off from molecular sieves sediment. The aqueous layer was extracted with EtOAc (2 x 30 mL). The combined organic extracts were dried over anhydrous Na₂SO₄ and evaporated. MPLC (SiO₂; CH₂Cl₂/MeOH 20:1 to 9:1) gave an acetate salt which was subsequently partitioned between Et₂O (40 mL) and 1M KOH (10 mL) and the basic aqueous layer was extracted with Et₂O (2 x 40 mL). The organic extracts were dried over anhydrous Na₂SO₄, and evaporated to afford the pure free base **67a** (140 mg, 0.721 mmol, 48%) as a colorless oil.

$R_f = 0.30$ (SiO₂; CH₂Cl₂/MeOH 10:1);

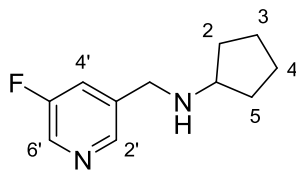
¹H NMR (400 MHz, CDCl₃): $\delta = 1.16\text{--}1.94$ (m, 9 H; H-C(2, 3, 4, 5), H-N), 3.03–3.16 (m, 1 H; H-C(1)), 3.85 (s, 2 H; CH₂N), 7.36 (m, 1 H; H-C(5')), 8.35–8.40 ppm (m, 2 H; H-C(2', 6'));

¹³C NMR (100 MHz, CDCl₃, based on HSQC): $\delta = 24.16$ (2 C, C(3, 4)), 33.29 (2 C; C(2, 5)), 44.93 (CH₂N), 59.42 (C(1)), 124.27 (d, ³ $J_{CF} = 2.1$ Hz, 1 C; C(5')), 136.62 (d, ² $J_{CF} = 12.8$ Hz, 1 C; C(4')), 137.79 (d, ² $J_{CF} = 24.3$ Hz, 1 C; C(2')), 145.95 (d, ⁴ $J_{CF} = 5.01$ Hz, 1 C; C(6')), 158.27 ppm (d, ¹ $J_{CF} = 254.7$ Hz, 1 C; C(3'));

¹⁹F NMR (376 MHz, CDCl₃): $\delta = -133.71$ ppm (F-C(3'));

IR (ATR): $\tilde{\nu} = 3291$ (very w), 3040 (very w), 2952 (w), 2866 (w), 1607 (very w), 1565 (very w), 1490 (w), 1453 (very w), 1344 (very w), 1280 (very w), 1242 (m), 1192 (w), 1119 (very w), 1054 (very w), 969 (very w), 944 (very w), 907 (very w), 834 (m), 789 (very w), 715 (w), 613 cm⁻¹ (w);

HR-ESI-MS: m/z (%): 369.3513 (20.0), 338.3416 (26.2), 283.2825 (21.0), 282.2794 (91.8), 195.1293 (41.6, [M + H]⁺, calcd for C₁₁H₁₆FN₂⁺: 195.1292), 127.0666 (42.3, [M - C₅H₉ + 2H]⁺, calcd for C₆H₈FN₂⁺: 127.0666).

2.7.2.37 *N*-[(5-Fluoropyridin-3-yl)methyl]cyclopentanamine (**67b**).**67b**

A solution of 5-fluoronicotinaldehyde (190 mg, 1.50 mmol) in CH_2Cl_2 (15.0 mL) was treated with cyclopentylamine (150 μL , 1.50 mmol) and with $\text{NaBH}(\text{OAc})_3$ (642 mg, 3.00 mmol), according to GP-G. MPLC (SiO_2 ; $\text{CH}_2\text{Cl}_2/\text{MeOH}$ 10:1 + 1% Et_3N) gave the pure free base **67b** (211 mg, 1.09 mmol, 72%) as a colorless oil.

$R_f = 0.32$ (SiO_2 ; $\text{CH}_2\text{Cl}_2/\text{MeOH}$ 5:1);

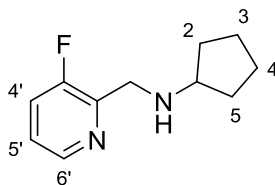
^1H NMR (400 MHz, CDCl_3): $\delta = 1.26\text{--}1.94$ (m, 9 H; H-C(2, 3, 4, 5), H-N), 3.04–3.15 (m, 1 H; H-C(1)), 3.81 (s, 2 H; CH_2N), 7.41–7.48 (m, 1 H; H-C(4')), 8.32 (d, $^3J_{\text{HF}} = 2.8$ Hz, 1 H; H-C(6')), 8.38 ppm (s, 1 H; H-C(2'));

^{13}C NMR (100 MHz, CDCl_3 , based on HSQC): $\delta = 24.12$ (2 C, C(3, 4)), 33.23 (2 C; C(2, 5')), 49.32 (d, $^4J_{\text{CF}} = 1.0$ Hz, 1 C; CH_2N), 59.47 (C(1)), 122.63 (d, $^2J_{\text{CF}} = 17.9$ Hz, 1 C; C(4')), 136.83 (d, $^2J_{\text{CF}} = 23.3$ Hz, 1 C; C(6')), 138.16 (d, $^3J_{\text{CF}} = 2.8$ Hz, 1 C; C(3')), 145.49 (d, $^4J_{\text{CF}} = 3.7$ Hz, 1 C; C(2')), 159.80 ppm (d, $^1J_{\text{CF}} = 256.5$ Hz, 1 C; C(5'));

^{19}F NMR (376 MHz, CDCl_3): $\delta = -127.48$ ppm (F-C(5'));

IR (ATR): $\tilde{\nu} = 3287$ (very w), 2951 (w), 2866 (w), 1601 (very w), 1579 (w), 1460 (w), 1429 (m), 1365 (very w), 1342 (very w), 1297 (very w), 1264 (w), 1222 (very w), 1146 (w), 1112 (very w), 1025 (very w), 965 (very w), 876 (w), 739 (w), 700 cm^{-1} (m);

HR-ESI-MS: m/z (%): 369.3517 (20.0), 338.3419 (21.0), 282.2790 (63.5), 279.1871 (26.1), 195.1296 (81.5, $[M + \text{H}]^+$, calcd for $\text{C}_{11}\text{H}_{16}\text{FN}_2^+$: 195.1292), 127.0664 (60.2, $[M - \text{C}_5\text{H}_9 + 2\text{H}]^+$, calcd for $\text{C}_6\text{H}_8\text{FN}_2^+$: 127.0666), 110.0400 (49.2, $[M - \text{C}_5\text{H}_{10}\text{N}]^+$, calcd for $\text{C}_6\text{H}_5\text{FN}^+$: 110.0401).

2.7.2.38 *N*-[(3-Fluoropyridin-2-yl)methyl]cyclopentanamine (**67c**).**67c**

A solution of 3-fluoropyridine-2-carbaldehyde (316 mg, 2.50 mmol) in CH_2Cl_2 (15.0 mL) was treated with cyclopentylamine (250 μL , 2.50 mmol) and $\text{NaBH}(\text{OAc})_3$ (1.07 g, 5.00 mmol), according to GP-G. MPLC (SiO_2 ; $\text{CH}_2\text{Cl}_2/\text{MeOH}$ 10:1 + 1% Et_3N) gave the pure free base **67c** (328 mg, 1.69 mmol, 68%) as pale brown liquid.

$R_f = 0.30$ (SiO_2 ; $\text{CH}_2\text{Cl}_2/\text{MeOH}$ 5:1);

^1H NMR (400 MHz, CDCl_3): $\delta = 1.30\text{--}1.98$ (m, 8 H; H-C(2, 3, 4, 5)), 2.18 (s, 1 H; H-N), 3.05–3.18 (m, 1 H; H-C(1)), 3.96 (s, 2 H; CH_2N), 7.14–7.22 (m, 1 H; H-C(5')), 7.29–7.37 (m, 1 H; H-C(4')), 8.34–8.40 ppm (m, 1 H; H-C(6'));

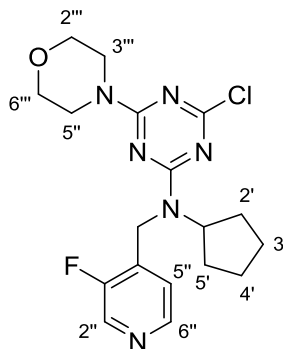
^{13}C NMR (100 MHz, CDCl_3 , based on HSQC): $\delta = 24.29$ (2 C, C(3, 4)), 33.29 (2 C; C(2, 5)), 47.40 (CH_2N), 59.62 (C(1)), 122.70 (d, $^2J_{\text{CF}} = 19.1$ Hz, 1 C; C(4')), 123.22 (d, $^3J_{\text{CF}} = 3.7$ Hz, 1 C; C(5')), 145.05 (d, $^4J_{\text{CF}} = 5.3$ Hz, 1 C; C(6')), 148.21 (d, $^2J_{\text{CF}} = 15.7$ Hz, 1 C; C(2')), 157.54 ppm (d, $^1J_{\text{CF}} = 256.2$ Hz, 1 C; C(3'));

^{19}F NMR (376 MHz, CDCl_3): $\delta = -126.55$ ppm (F-C(3'));

IR (ATR): $\tilde{\nu} = 2952$ (w), 2866 (w), 1602 (very w), 1572 (very w), 1444 (m), 1346 (w), 1244 (w), 1219 (very w), 1162 (w), 1121 (very w), 1088 (w), 968 (very w), 870 (w), 798 (m), 719 cm^{-1} (m);

HR-ESI-MS: m/z (%): 195.1292 (36.8, $[M + \text{H}]^+$, calcd for $\text{C}_{11}\text{H}_{16}\text{FN}_2^+$: 195.1292), 127.0654 (100.0, $[M - \text{C}_5\text{H}_9 + 2\text{H}]^+$, calcd for $\text{C}_6\text{H}_8\text{FN}_2^+$: 127.0666).

2.7.2.39 4-Chloro-*N*-cyclopentyl-*N*-[(3-fluoropyridin-4-yl)methyl]-6-(4-morpholinyl)-1,3,5-triazin-2-amine (68a).



68a

A solution of cyanuric chloride (57 mg, 0.31 mmol) in anhydrous MeCN (1.50 mL) was treated dropwise with a solution of *i*Pr₂NEt (214 μL, 1.22 mmol) and morpholine (27 μL, 0.31 mmol) in anhydrous MeCN (0.75 mL) at -20 °C and subsequently with a solution of **67a** (60 mg, 0.31 mmol) in anhydrous MeCN according to GP-H. MPLC (SiO₂; cyclohexane/EtOAc 9:1 to 7:3) gave **68a** (24 mg, 0.061 mmol, 20%) as a pale brown oil.

$R_f = 0.42$ (SiO₂; cyclohexane/EtOAc 2:1);

¹H NMR (400 MHz, CDCl₃): $\delta = 1.15$ – 2.05 (m, 8 H; H–C(2', 3', 4', 5')), 3.29–3.94 (m, 8 H; H–C(2''', 3''', 5''', 6''')), 4.66 and 4.79 (s, 2 H; CH₂N), 4.85–5.20 (m, 1 H; H–C(1')), 6.96–7.09 (m, 1 H; H–C(5'')), 8.26–8.34 (m, 1 H; H–C(6'')), 8.38–8.44 ppm (m, 1 H; H–C(2''));

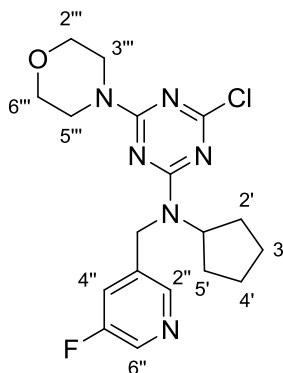
¹³C NMR (100 MHz, CDCl₃, based on HSQC): $\delta = 23.69$ and 23.79 (2 C, C(3', 4')), 29.13 and 29.42 (2 C; C(2', 5')), 39.85 and 39.90 (CH₂N), 43.69 and 44.02 (2 C; C(3''', 5''')), 56.71 and 57.44 (C(1')), 66.42 and 66.72 (2 C; C(2''', 6''')), 122.37 and 122.85 (C(5'')), 135.39–135.87 (m, 1 C; C(4'')), 137.23–137.73 (m, 1 C; C(2'')), 145.45–146.08 (m, 1 C; C(6'')), 157.33 ppm (d, ¹*J*_{CF} = 254.3 Hz, 1 C; C(3'')); 164.26 and 164.63 (CN₃), 165.48 and 165.91 (CN₃), 169.69 and 169.72 ppm (CCIN₂);

¹⁹F NMR (376 MHz, CDCl₃): $\delta = -133.38$ and -132.93 ppm (F–C(3''));

IR (ATR): $\tilde{\nu}$ = 2959 (w), 2859 (w), 1554 (s), 1482 (s), 1444 (m), 1414 (m), 1357 (w), 1299 (w), 1284 (w), 1239 (m), 1190 (w), 1112 (w), 1064 (w), 1018 (very w), 991 (w), 969 (w), 950 (w), 901 (w), 830 (w), 801 (m), 729 (w), 646 (very w), 605 cm^{-1} (very w);

HR-ESI-MS: m/z (%): 395.1571 (35.9, $[M + H + 2]^+$, calcd for $\text{C}_{18}\text{H}_{23}^{37}\text{ClN}_6\text{O}^+$: 395.1571), 394.1633 (24.9, $[M + H + 1]^+$, calcd for $\text{C}_{18}\text{H}_{23}^{36}\text{ClFN}_6\text{O}^+$: 394.1634), 393.1602 (100.0, $[M + H]^+$, calcd for $\text{C}_{18}\text{H}_{23}^{35}\text{ClFN}_6\text{O}^+$: 393.1600), 282.2794 (28.3).

2.7.2.40 4-Chloro-*N*-cyclopentyl-*N*-[(5-fluoropyridin-3-yl)methyl]-6-(4-morpholinyl)-1,3,5-triazin-2-amine (68b).



68b

A solution of cyanuric chloride (151 mg, 0.81 mmol) in anhydrous MeCN (4.1 mL) was treated dropwise with a solution of *i*Pr₂NEt (566 μL , 3.24 mmol) and morpholine (72 μL , 0.81 mmol) in anhydrous MeCN (2.0 mL) at -20 °C and subsequently with a solution of **67b** (159 mg, 0.81 mmol) in anhydrous MeCN (2.0 mL) according to GP-H. MPLC (SiO_2 ; cyclohexane/EtOAc 19:1 to 7:3) gave **68b** (122 mg, 0.311 mmol, 38%) as a pale brown oil.

R_f = 0.23 (SiO_2 ; cyclohexane/EtOAc 2:1);

¹H NMR (400 MHz, CDCl_3): δ = 1.35–2.02 (m, 8 H; H–C(2', 3', 4', 5')), 3.29–3.97 (m, 8 H; H–C(2''', 3''', 5''', 6''')), 4.65 and 4.77 (s, 2 H; CH_2N), 4.80–5.23 (m, 1 H; H–C(1')), 7.15–7.31 (m, 1 H; H–C(4'')), 8.26–8.40 ppm (m, 2 H; H–C(2'', 6''));

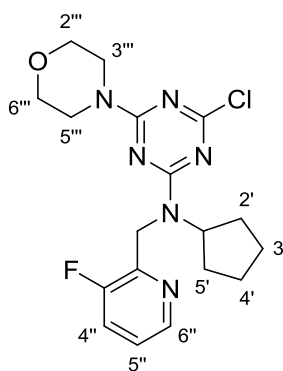
^{13}C NMR (100 MHz, CDCl_3 , based on HSQC): $\delta = 23.68$ and 23.79 (2 C, C(3', 4')), 29.27 and 29.51 (2 C; C(2', 5')), 43.59 – 44.28 (3 C; C(3''', 5''')), CH_2N , 56.91 and 57.70 (C(1')), 66.40 and 66.76 (2 C; C(2''', 6''')), 120.47 – 122.04 (m, 1 C; C(4'')), 136.27 – 137.41 (m, 2 C; arom. C), 143.79 – 144.55 (m, 1 C; arom. C), 159.74 (d, $^1J_{\text{CF}} = 255.9$ Hz, 1 C; C(5'')); 164.34 and 164.63 (CN_3), 165.51 and 165.80 (CN_3), 169.69 and 171.07 ppm (CCIN_2);

^{19}F NMR (376 MHz, CDCl_3): $\delta = -126.95$ and -126.88 ppm (F–C(5''));)

IR (ATR): $\tilde{\nu} = 2925$ (w), 2853 (w), 1556 (s), 1483 (s), 1430 (m), 1350 (w), 1299 (m), 1254 (w), 1238 (m), 1203 (very w), 1186 (very w), 1163 (very w), 1113 (m), 1063 (w), 1023 (w), 992 (w), 969 (m), 930 (very w), 898 (w), 857 (w), 812 (very w), 800 (m), 739 (very w), 729 (very w), 699 (w), 668 (very w), 631 cm^{-1} (very w);

HR-ESI-MS: m/z (%): 577.4189 (20.2), 567.4308 (21.5), 566.9292 (57.6), 566.4274 (73.1), 453.8454 (54.9), 453.3438 (100.0), 395.1577 (33.5, $[M + H + 2]^+$, calcd for $\text{C}_{18}\text{H}_{23}^{37}\text{ClN}_6\text{O}^+$: 395.1571), 394.1632 (21.1, $[M + H + 1]^+$, calcd for $\text{C}_{18}\text{H}_{23}^{36}\text{ClFN}_6\text{O}^+$: 394.1634), 393.1598 (96.0, $[M + H]^+$, calcd for $\text{C}_{18}\text{H}_{23}^{35}\text{ClFN}_6\text{O}^+$: 393.1600).

2.7.2.41 4-Chloro-*N*-cyclopentyl-*N*-[(3-fluoropyridin-2-yl)methyl]-6-(4-morpholinyl)-1,3,5-triazin-2-amine (68c).



68c

A solution of cyanuric chloride (224 mg, 1.20 mmol) in anhydrous MeCN (6.0 mL) was treated dropwise with a solution of *i*Pr₂N₂Et (839 μL , 4.80 mmol) and morpholine (106 μL , 1.20 mmol)

in anhydrous MeCN (3.0 mL) at -20 °C and subsequently with a solution of **67c** (235 mg, 1.20 mmol) in anhydrous MeCN (3.0 mL) according to the GP-H. MPLC (SiO₂; cyclohexane/EtOAc 19:1 to 7:3) gave **68c** (223 mg, 0.568 mmol, 47%) as a colorless oil.

¹H NMR (400 MHz, CDCl₃): δ = 1.40–2.09 (m, 8 H; H–C(2', 3', 4', 5')), 3.18–3.93 (m, 8 H; H–C(2''', 3''', 5''', 6''')), 4.63–5.27 (m, 3 H; H–C(1'), CH₂N), 7.09–7.19 (m, 1 H; H–C(5'')), 7.24–7.35 (m, 1 H; H–C(4'')), 8.25–8.33 ppm (m, 1 H; H–C(6''));

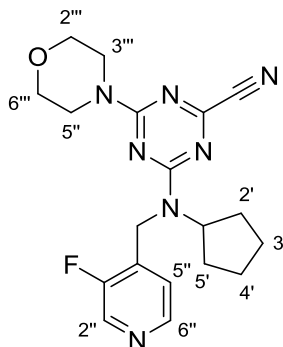
¹³C NMR (100 MHz, CDCl₃, based on HSQC): δ = 23.79 and 24.04 (2 C, C(3', 4')), 29.21 and 29.58 (2 C; C(2', 5')), 42.93–43.08 (CH₂N), 43.65–43.90 (2 C; C(3''', 5''')), 56.85 and 57.47 (C(1')), 66.51 and 66.75 (2 C; C(2''', 6''')), 122.05–122.63 (m, 1 C; C(4'')), 122.80–123.19 (m, 1 C; C(5'')), 144.73–145.19 (m, 1 C; C(6'')), 146.28–146.78 (m, 1 C; C(2'')), 155.82–158.78 (m, 1 C; C(3'')), 164.14 and 164.57 (CN₃), 164.94 and 165.51 (CN₃), 169.06 and 169.28 ppm (CCIN₂);

¹⁹F NMR (376 MHz, CDCl₃): δ = -126.38 and -125.98 ppm (F–C(3''));

IR (ATR): $\tilde{\nu}$ = 2958 (w), 2854 (w), 1555 (s), 1483 (s), 1440 (m), 1384 (very w), 1359 (w), 1298 (m), 1240 (m), 1238 (m), 1187 (very w), 1151 (very w), 1113 (m), 1093 (w), 1063 (w), 1018 (very w), 991 (w), 970 (w), 948 (w), 900 (w), 854 (w), 799 (m), 733 (very w), 720 (very w), 668 (w), 649 (very w), 627 cm⁻¹ (very w);

HR-ESI-MS: m/z (%): 566.9292 (36.0), 566.4274 (52.4), 453.8451 (39.5), 453.3435(69.2), 395.1570 (35.5, [M + H + 2]⁺, calcd for C₁₈H₂₃³⁷ClN₆O⁺: 395.1571), 394.1624 (24.7, [M + H + 1]⁺, calcd for C₁₈H₂₃³⁶ClFN₆O⁺: 394.1634), 393.1593 (100.0, [M + H]⁺, calcd for C₁₈H₂₃³⁵ClFN₆O⁺: 393.1600).

2.7.2.42 4-{Cyclopentyl[(3-fluoropyridin-4-yl)methyl]amino}-6-(morpholin-4-yl)-1,3,5-triazine-2-carbonitrile (69a).



69a

A solution of **68a** (148 mg, 0.377 mmol) in DMSO (3.0 mL) was treated with KCN (27 mg, 0.41 mmol) and DABCO (42 mg, 0.38 mmol) and heated for 18 h at 80 °C. The mixture was cooled down to 24 °C, diluted with EtOAc, washed with brine three times, dried over anhydrous Na₂SO₄ and concentrated under reduced pressure. MPLC (SiO₂; cyclohexane/EtOAc 100:0 to 70:30 within 20 min) gave **69a** (30 mg, 0.078 mmol, 21%) as a light brown oil.

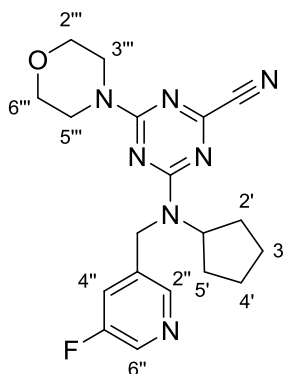
$R_f = 0.33$ (SiO₂; cyclohexane/EtOAc 4:1);

¹H NMR (400 MHz, CDCl₃): $\delta = 1.36$ – 2.00 (m, 8 H; H–C(2', 3', 4', 5')), 3.31–3.92 (m, 8 H; H–C(2''', 3''', 5''', 6''')), 4.66 and 4.78 (s, 2 H; CH₂N), 4.82–5.24 (m, 1 H; H–C(1')), 6.95–7.02 (m, 1 H; H–C(5'')), 8.27–8.33 (m, 1 H; H–C(6'')), 8.38–8.44 ppm (m, 1 H; H–C(2''));

¹³C NMR (100 MHz, CDCl₃, based on HSQC): $\delta = 23.71$ and 23.76 (2 C, C(3', 4')), 29.11 and 29.42 (2 C; C(2', 5')), 39.83 and 40.10 (d, ³ $J_{CF} = 5.3$ Hz; CH₂N), 43.22–44.28 (m, 2 C; C(3''', 5''')), 57.04 and 57.23 (C(1')), 66.23–66.92 (m, 2 C; C(2''', 6''')), 115.44 and 115.59 (CN), 122.18 and 122.48 (s; C(5'')), 134.98 and 135.17 (d, ³ $J_{CF} = 11.8$ Hz; C(4'')), 137.62 and 137.77 (d, ⁴ $J_{CF} = 23.4$ Hz; C(2'')), 145.83 and 145.95 (d, ² $J_{CF} = 5.1$ Hz; C(6'')), 152.07 (1 C; CN₂), 157.33 (d, ¹ $J_{CF} = 254.4$ Hz, 1 C; C(3'')); 163.38 and 163.67 (CN₃), 164.63 and 164.04 ppm (CN₃);

¹⁹F NMR (376 MHz, CDCl₃): $\delta = -133.29$ and -132.97 ppm (F–C(3''));

2.7.2.43 4-{Cyclopentyl[(5-fluoropyridin-3-yl)methyl]amino}-6-(morpholin-4-yl)-1,3,5-triazine-2-carbonitrile (69b).



69b

A solution of **68b** (122 mg, 0.311 mmol) in DMSO (3.0 mL) was treated with KCN (27 mg, 0.41 mmol) and DABCO (35 mg, 0.31 mmol) and heated for 18 h at 80 °C. The mixture was cooled down to 24 °C, diluted with EtOAc, washed with brine three times, dried over anhydrous Na₂SO₄ and concentrated under reduced pressure. MPLC (SiO₂; cyclohexane/EtOAc 100:0 to 95:5 within 30 min) gave **69b** (23 mg, 0.060 mmol, 19%) as a green oil.

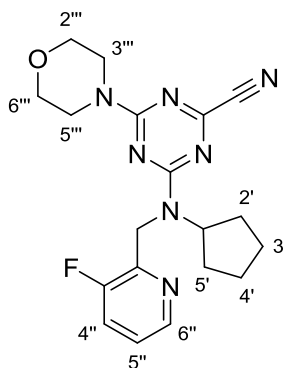
$R_f = 0.50$ (SiO₂; cyclohexane/EtOAc 1:1);

¹H NMR (400 MHz, CDCl₃): $\delta = 1.37\text{--}1.99$ (m, 8 H; H-C(2', 3', 4', 5')), 3.32–3.91 (m, 8 H; H-C(2''', 3''', 5''', 6''')), 4.65 and 4.77 (s, 2 H; CH₂N), 4.80–5.20 (m, 1 H; H-C(1')), 7.13–7.25 (m, 1 H; H-C(4'')), 8.26–8.39 (m, 1 H; H-C(6'') and H-C(2''));

¹³C NMR (100 MHz, CDCl₃, based on HSQC): $\delta = 23.69$ and 23.76 (2 C, C(3', 4')), 29.23 and 29.51 (2 C; C(2', 5')), 43.37–43.79 (m, 2 C; C(3''', 5''')), 43.90–44.31 (m, 1C; CH₂N), 57.25 and 57.48 (C(1')), 66.14–66.98 (m, 2 C; C(2''', 6''')), 115.48 and 115.60 (CN), 120.75 and 121.34 (d, ²J_{CF} = 18.6 Hz; C(4'')), 136.38–137.24 (m, 1 C; C(6'')), 143.98–144.18 (m, 1 C; C(2'')), 152.06 (1 C; CN₂), 159.72 (d, ¹J_{CF} = 257.2 Hz; C(5'')); 163.45 and 163.65 (CN₃), 164.65 and 164.91 ppm (CN₃);

¹⁹F NMR (376 MHz, CDCl₃): $\delta = -126.79$ and -126.68 ppm (F-C(5''));

2.7.2.44 4-{Cyclopentyl[(3-fluoropyridin-2-yl)methyl]amino}-6-(morpholin-4-yl)-1,3,5-triazine-2-carbonitrile (69c).



69c

A solution of **68c** (223 mg, 0.568 mmol) in DMSO (3.0 mL) was treated with KCN (41 mg, 0.62 mmol) and DABCO (64 mg, 0.57 mmol) and heated for 16 h at 80 °C. The mixture was cooled down to 24 °C, diluted with EtOAc, washed with brine three times, dried over anhydrous Na₂SO₄ and concentrated under reduced pressure. MPLC (SiO₂; cyclohexane/EtOAc 100:0 to 70:30 within 30 min) gave **69c** (110 mg, 0.287 mmol, 51%) as a colorless oil.

$R_f = 0.50$ (SiO₂; cyclohexane/EtOAc 1:1);

¹H NMR (400 MHz, CDCl₃): $\delta = 1.43$ – 1.81 and 1.82 – 2.04 (m, 8 H; H–C(2', 3', 4', 5')), 3.26 – 3.90 (m, 8 H; H–C(2'', 3'', 5'', 6'')), 4.75 and 4.90 (s, 2 H; CH₂N), 4.92 – 5.22 (m, 1 H; H–C(1')), 7.13 – 7.21 (m, 1 H; H–C(6'')), 7.28 – 7.39 (m, 1 H; H–C(4'')), 8.27 – 8.34 ppm (m, 1 H; H–C(5''));

¹³C NMR (100 MHz, CDCl₃, based on HSQC): $\delta = 23.69$ and 23.79 (2 C, C(3', 4')), 29.13 and 29.42 (2 C; C(2', 5')), 39.85 and 39.90 (CH₂N), 43.69 and 44.02 (2 C; C(3'', 5'')), 56.71 and 57.44 (C(1')), 66.42 and 66.72 (2 C; C(2'', 6'')), 115.72 and 115.82 (CN), 122.38 and 122.62 (d, ² $J_{CF} = 18.5$ Hz; C(4'')), 123.11 and 123.29 (d, ³ $J_{CF} = 3.5$ Hz; C(5'')), 144.95 and 145.14 (d, ⁴ $J_{CF} = 5.4$ Hz; C(6'')), 146.10 and 146.23 (d, ² $J_{CF} = 9.0$ Hz; C(2'')), 151.64 and 151.84 (1 C; CN₂), 157.36 (d, ¹ $J_{CF} = 257.0$ Hz; C(3'')); 163.31 and 163.67 (CN₃), 164.13 and 164.68 ppm (CN₃);

¹⁹F NMR (376 MHz, CDCl₃): $\delta = -126.53$ and -126.10 ppm (F–C(3''));

3 References

- [1] A. Mullard, *Nat. Rev. Drug Discov.* **2014**, *13*, 877–877.
- [2] J. P. Hughes, S. Rees, S. B. Kalindjian, K. L. Philpott, *Br. J. Pharmacol.* **2011**, *162*, 1239–1249.
- [3] J. C. Kendrew, G. Bodo, H. M. Dintzis, R. G. Parrish, H. Wyckoff, D. C. Phillips, *Nature* **1958**, *181*, 662–666.
- [4] A. Ilari, C. Savino, *Methods Mol. Biol.* **2008**, *452*, 63–87.
- [5] E. Persch, O. Dumele, F. Diederich, *Angew. Chem. Int. Ed.* **2015**, *54*, 3290–3327.
- [6] R. Baron, J. A. McCammon, *Annu. Rev. Phys. Chem.* **2013**, *64*, 151–175.
- [7] P. W. Snyder, J. Mecinovic, D. T. Moustakas, S. W. Thomas, M. Harder, E. T. Mack, M. R. Lockett, A. Héroux, W. Sherman, G. M. Whitesides, *Proc. Natl. Acad. Sci. U. S. A.* **2011**, *108*, 17889–17894.
- [8] W. N. Lipscomb, N. Sträter, *Chem. Rev.* **1996**, *96*, 2375–2434.
- [9] H. Birkedal-Hansen, W. G. I. Moore, M. K. Bodden, L. J. Windsor, B. Birkedal-Hansen, A. DeCarlo, J. A. Engler, *Crit. Rev. Oral Biol. Med.* **1993**, *4*, 197–250.
- [10] R. Rebolledo-Rios, S. Bandari, C. Wilms, S. Jakushev, A. Vortkamp, K. Grobe, D. Hoffmann, *PLoS Comput. Biol.* **2014**, *10*, e1003707.
- [11] M. Wickström, R. Larsson, P. Nygren, J. Gullbo, *Cancer Sci.* **2011**, *102*, 501–508.
- [12] J. J. V McMurray, *Eur. J. Heart Fail.* **2015**, *17*, 242–247.
- [13] B. P. Roques, M.-C. Fournié-Zaluski, M. Wurm, *Nat. Rev. Drug Discov.* **2012**, *11*, 292–310.
- [14] C. L. Yeager, R. A. Ashmun, R. K. Williams, C. B. Cardellicchio, L. H. Shapiro, A. T. Look, K. V Holmes, *Nature* **1992**, *357*, 420–422.
- [15] S. C. Prajapati, S. S. Chauhan, *FEBS J.* **2011**, *278*, 3256–3276.
- [16] P. K. Baral, N. Jajčanin-Jozić, S. Deller, P. Macheroux, M. Abramić, K. Gruber, *J. Biol. Chem.* **2008**, *283*, 22316–22324.

- [17] G. A. Bezerra, E. Dobrovetsky, R. Viertlmayr, A. Dong, A. Binter, M. Abramic, P. Macheroux, S. Dhe-Paganon, K. Gruber, *Proc. Natl. Acad. Sci. U. S. A.* **2012**, *109*, 6525–6530.
- [18] B. E. Hast, D. Goldfarb, K. M. Mulvaney, M. A. Hast, P. F. Siesser, F. Yan, D. N. Hayes, M. B. Major, *Cancer Res.* **2013**, *73*, 2199–2210.
- [19] Y. Yamamoto, J. I. Hashimoto, M. Shimamura, T. Yamaguchi, T. Hazato, *Peptides* **2000**, *21*, 503–508.
- [20] T. Chiba, Y.-H. Li, T. Yamane, O. Ogikubo, M. Fukuoka, R. Arai, S. Takahashi, T. Ohtsuka, I. Ohkubo, N. Matsui, *Peptides* **2003**, *24*, 773–778.
- [21] V. Thanawala, V. J. Kadam, R. Ghosh, *Curr. Drug Targets* **2008**, *9*, 887–894.
- [22] C. Chang, Z. Werb, *Trends Cell Biol.* **2001**, *11*, 37–43.
- [23] D. F. Seals, S. A. Courtneidge, *Genes Dev.* **2003**, *17*, 7–30.
- [24] K. Brew, H. Nagase, *Biochim. Biophys. Acta - Mol. Cell Res.* **2010**, *1803*, 55–71.
- [25] R. Khokha, A. Murthy, A. Weiss, *Nat. Rev. Immunol.* **2013**, *13*, 649–665.
- [26] N. M. Hooper, *FEBS Lett.* **1994**, *354*, 1–6.
- [27] C. C. Häse, R. A. Finkelstein, *Microbiol. Rev.* **1993**, *57*, 823–837.
- [28] B. Holmquist, B. L. Vallee, *J. Biol. Chem.* **1974**, *249*, 4601–4607.
- [29] B. L. Vallee, D. S. Auld, *Biochemistry* **1990**, *29*, 5647–5659.
- [30] D. Xu, H. Guo, *J. Am. Chem. Soc.* **2009**, *131*, 9780–9788.
- [31] A. V. Kilshtain, A. Warshel, *Proteins* **2009**, *77*, 536–550.
- [32] G. A. Pinto, P. W. Tardioli, R. Y. Cabrera-Padilla, C. M. A. Galvão, R. C. Giordano, R. L. C. Giordano, *Biochem. Eng. J.* **2008**, *39*, 328–337.
- [33] S. Wu, C. Zhang, D. Xu, H. Guo, *J. Phys. Chem. B* **2010**, *114*, 9259–9267.
- [34] M. W. Y. Szeto, J. I. Mujika, J. Zurek, A. J. Mulholland, J. N. Harvey, *J. Mol. Struct. THEOCHEM* **2009**, *898*, 106–114.
- [35] R. Breslow, D. Wernick, *J. Am. Chem. Soc.* **1976**, *98*, 259–261.
- [36] R. Breslow, D. L. Wernick, *Proc. Natl. Acad. Sci. U. S. A.* **1977**, *74*, 1303–1307.

- [37] A. C. Hausrath, B. W. Matthews, *Acta Crystallogr. D. Biol. Crystallogr.* **2002**, *58*, 1002–1007.
- [38] K. Titani, M. A. Hermodson, L. H. Ericsson, K. A. Walsh, H. Neurath, *Biochemistry* **1972**, *11*, 2427–2435.
- [39] C. Kooi, P. A. Sokol, *J. Med. Microbiol.* **1996**, *45*, 219–225.
- [40] A. de Kreijg, G. Venema, B. van den Burg, *J. Biol. Chem.* **2000**, *275*, 31115–31120.
- [41] H. Ooshima, H. Mori, Y. Harano, *Biotechnol. Lett.* **1985**, *7*, 789–792.
- [42] B. W. Matthews, J. N. Jansonius, P. M. Colman, B. P. Schoenborn, D. Dupourque, *Nat. New Biol.* **1972**, *238*, 37–41.
- [43] N. D. Rawlings, A. J. Barrett, *Biochem. J.* **1993**, *290*, 205–218.
- [44] J. Blumberger, G. Lamoureux, M. L. Klein, *J. Chem. Theory Comput.* **2007**, *3*, 1837–1850.
- [45] S. Kunugi, H. Hirohara, N. Ise, *Eur. J. Biochem.* **1982**, *124*, 157–163.
- [46] J. Feder, L. R. Brougham, B. S. Wildi, *Biochemistry* **1974**, *13*, 1186–1189.
- [47] Y. Ohta, Y. Ogura, A. Wada, *J. Biol. Chem.* **1966**, *241*, 5919–5925.
- [48] J. B. Bjarnason, J. W. Fox, *Methods Enzymol.* **1995**, *248*, 345–368.
- [49] W. Bode, F.-X. Gomis-Rüth, W. Stöckler, *FEBS Lett.* **1993**, *331*, 134–140.
- [50] H. E. Van Wart, H. Birkedal-Hansen, *Proc. Natl. Acad. Sci. U. S. A.* **1990**, *87*, 5578–5582.
- [51] J. W. Becker, A. I. Marcy, L. L. Rokosz, M. G. Axel, J. J. Burbaum, P. M. Fitzgerald, P. M. Cameron, C. K. Esser, W. K. Hagmann, J. D. Hermes, *Protein Sci.* **1995**, *4*, 1966–1976.
- [52] S. Ohlig, U. Pickhinke, S. Sirko, S. Bandari, D. Hoffmann, R. Dreier, P. Farshi, M. Götz, K. Grobe, *J. Biol. Chem.* **2012**, *287*, 43708–43719.
- [53] S. Ellis, J. M. Nuenke, *J. Biol. Chem.* **1967**, *242*, 4623–4629.
- [54] J. Mallen-St Clair, C. T. N. Pham, S. A. Villalta, G. H. Caughey, P. J. Wolters, *J. Clin. Invest.* **2004**, *113*, 628–634.
- [55] C. Lee, H. Snyder, **1982**, *257*, 12043–12050.
- [56] M. Abramić, M. Zubanović, L. Vitale, *Biol. Chem. Hoppe-Seyler* **1988**, *369*, 29–38.

- [57] M. Smyth, G. O’Cuinn, *J. Neurochem.* **1994**, *63*, 1439–1445.
- [58] J. Hashimoto, Y. Yamamoto, H. Kurosawa, K. Nishimura, T. Hazato, *Biochem. Biophys. Res. Commun.* **2000**, *273*, 393–397.
- [59] T. H. Jones, A. Kapralou, *Anal. Biochem.* **1982**, *119*, 418–423.
- [60] J. I. Vandenberg, G. F. King, P. W. Kuchel, *Biochim. Biophys. Acta* **1985**, *846*, 127–134.
- [61] J. I. Vandenberg, G. F. King, P. W. Kuchel, *Arch. Biochem. Biophys.* **1985**, *242*, 515–522.
- [62] C. Mazzocco, K. M. Fukasawa, A. A. Raymond, J. Puiroux, *Eur. J. Biochem.* **2001**, *268*, 4940–4949.
- [63] M. Baršun, N. Jajčanin, B. Vukelić, J. Špoljarić, M. Abramić, *Biol. Chem.* **2007**, *388*, 343–348.
- [64] S. Simaga, D. Babić, M. Osmak, J. Ilić-Forko, L. Vitale, D. Milicić, M. Abramić, *Eur. J. Cancer* **1998**, *34*, 399–405.
- [65] S. Simaga, D. Babić, M. Osmak, M. Sprem, M. Abramić, *Gynecol. Oncol.* **2003**, *91*, 194–200.
- [66] Y. Shimamori, Y. Watanabe, Y. Fujimoto, *Biochem. Med. Metab. Biol.* **1988**, *40*, 305–310.
- [67] T. Vanha-Perttula, *Clin. Chim. Acta.* **1988**, *177*, 179–195.
- [68] N. C. Kar, C. M. Pearson, *Clin. Chim. Acta.* **1978**, *82*, 185–192.
- [69] V. K. Hopsu-Havu, C. T. Jansén, *Arch. Klin. Exp. Dermatol.* **1969**, *235*, 53–62.
- [70] H. Sato, K. Kimura, Y. Yamamoto, T. Hazato, *Masui.* **2003**, *52*, 257–263.
- [71] A. A. Swanson, R. M. Davis, J. K. McDonald, *Curr. Eye Res.* **1984**, *3*, 287–291.
- [72] Y. Liu, J. T. Kern, J. R. Walker, J. A. Johnson, P. G. Schultz, H. Luesch, *Proc. Natl. Acad. Sci. U. S. A.* **2007**, *104*, 5205–5210.
- [73] I. Ohkubo, Y. H. Li, T. Maeda, Y. Yamamoto, T. Yamane, P. G. Du, K. Nishi, *Biol. Chem.* **1999**, *380*, 1421–1430.
- [74] F. Alba, J. C. Arenas, M. A. Lopez, *Peptides* **1995**, *16*, 325–329.
- [75] M. Abramić, D. Schleuder, L. Dolovcak, W. Schröder, K. Strupat, D. Sagi, J. Peter-Katalini, L. Vitale, *Biol. Chem.* **2000**, *381*, 1233–1243.

-
- [76] C. Mazzocco, K. M. Fukasawa, P. Auguste, J. Puiroux, *Eur. J. Biochem.* **2003**, *270*, 3074–3082.
- [77] S. A. Chan, K. Toursarkissian, J. P. Sweeney, T. H. Jones, *Biochem. Biophys. Res. Commun.* **1985**, *127*, 962–968.
- [78] Y. Watanabe, Y. Kumagai, Y. Fujimoto, *Chem. Pharm. Bull.* **1990**, *38*, 246–248.
- [79] E. Reits, J. Neijssen, C. Herberts, W. Benckhuijsen, L. Janssen, J. W. Drijfhout, J. Neefjes, *Immunity* **2004**, *20*, 495–506.
- [80] U. Tisljar, A. J. Barrett, *Biochem. J.* **1990**, *267*, 531–533.
- [81] I. A. York, A. X. Y. Mo, K. Lemerise, W. Zeng, Y. Shen, C. R. Abraham, T. Saric, A. L. Goldberg, K. L. Rock, *Immunity* **2003**, *18*, 429–440.
- [82] H. E. Moore, E. L. Davenport, E. M. Smith, S. Muralikrishnan, A. S. Dunlop, B. A. Walker, D. Krige, A. H. Drummond, L. Hooftman, G. J. Morgan, et al., *Mol. Cancer Ther.* **2009**, *8*, 762–770.
- [83] A. A. Ferrando, A. M. Pendás, E. Llano, G. Velasco, R. Lidereau, C. López-Otín, *J. Biol. Chem.* **1997**, *272*, 33298–33304.
- [84] D. B. Constam, A. R. Tobler, A. Rensing-Ehl, I. Kemler, L. B. Hersh, A. Fontana, *J. Biol. Chem.* **1995**, *270*, 26931–26939.
- [85] F. M. Cunha, D. A. Berti, Z. S. Ferreira, C. F. Klitzke, R. P. Markus, E. S. Ferro, *J. Biol. Chem.* **2008**, *283*, 24448–24459.
- [86] J. W. Wright, A. J. Bechtholt, S. L. Chambers, J. W. Harding, *Peptides* **1996**, *17*, 1365–1371.
- [87] I. Moeller, S. Y. Chai, I. Smith, R. Lew, F. A. Mendelsohn, *Clin. Exp. Pharmacol. Physiol. Suppl.* **1998**, *25*, S68–71.
- [88] H. L. Rittner, A. Brack, C. Stein, *Br. J. Anaesth.* **2008**, *101*, 40–44.
- [89] C. S. Dale, R. de L. Pagano, V. Rioli, *Mem. Inst. Oswaldo Cruz* **2005**, *100*, 105–106.
- [90] I. Saito, T. Saruta, T. Eguchi, K. Kondo, R. Nakamura, S. Matsuki, *Acta Endocrinol.* **1978**, *89*, 132–141.
- [91] S. Mazumder, I. Nath, M. M. Dhar, *Immunol. Lett.* **1993**, *35*, 33–38.
- [92] R. E. Faith, H. J. Liang, N. P. Plotnikoff, A. J. Murgo, N. F. Nimeh, *Nat. Immun. Cell Growth Regul.* **1987**, *6*, 88–98.

- [93] F. Fraioli, A. Fabbri, L. Gnessi, L. Silvestroni, C. Moretti, F. Redi, A. Isidori, *Ann. N. Y. Acad. Sci.* **1984**, 438, 365–370.
- [94] M. M. Nieto, S. L. E. Guen, B. L. Kieffer, B. P. Roques, F. Noble, *Neuroscience* **2005**, 135, 305–313.
- [95] N. C. Ebner, M. Horta, T. Lin, D. Feifel, H. Fischer, R. A. Cohen, *Front. Aging Neurosci.* **2015**, 7, 1–7.
- [96] A. S. Heimann, I. Gomes, C. S. Dale, R. L. Pagano, A. Gupta, L. L. de Souza, A. D. Luchessi, L. M. Castro, R. Giorgi, V. Rioli, et al., *Proc. Natl. Acad. Sci. U. S. A.* **2007**, 104, 20588–20593.
- [97] L. E. Eiden, *Cell. Mol. Neurobiol.* **1987**, 7, 339–352.
- [98] A. Dray, M. Perkins, *Trends Neurosci.* **1993**, 16, 99–104.
- [99] M. Paul, A. Poyan Mehr, R. Kreutz, *Physiol. Rev.* **2006**, 86, 747–803.
- [100] A. Reaux-Le Goazigo, X. Iturrioz, C. Fassot, C. Claperon, B. P. Roques, C. Llorens-Cortes, *Curr. Hypertens. Rep.* **2005**, 7, 128–134.
- [101] P. Moi, K. Chan, I. Asunis, A. Cao, Y. W. Kan, *Proc. Natl. Acad. Sci. U. S. A.* **1994**, 91, 9926–9930.
- [102] H. C. Hurst, *Protein Profile* **1995**, 2, 101–168.
- [103] J. W. Kaspar, S. K. Niture, A. K. Jaiswal, *Free Radic. Biol. Med.* **2009**, 47, 1304–1309.
- [104] S. K. Niture, J. W. Kaspar, J. Shen, A. K. Jaiswal, *Toxicol. Appl. Pharmacol.* **2010**, 244, 37–42.
- [105] A. A. Shukla, M. Jain, S. S. Chauhan, *FEBS J.* **2010**, 277, 1861–1875.
- [106] G. A. Bezerra, E. Dobrovetsky, R. Viertlmayr, A. Dong, A. Binter, M. Abramic, P. Macheroux, S. Dhe-Paganon, K. Gruber, *Proc. Natl. Acad. Sci. U. S. A.* **2012**, 109, 6525–6530.
- [107] J. Mansfeld, *Industrial Enzymes*, Springer Netherlands, Dordrecht, **2007**.
- [108] P. R. Gerber, K. Moeller, *J. Comput. Aided. Mol. Des.* **1995**, 9, 251–268.
- [109] D. A. Dougherty, *Acc. Chem. Res.* **2013**, 46, 885–893.
- [110] M. S. Marshall, R. P. Steele, K. S. Thanthiriwatte, C. D. Sherrill, *J. Phys. Chem. A* **2009**, 113, 13628–13632.

- [111] X. Xiu, N. L. Puskar, J. A. P. Shanata, H. A. Lester, D. A. Dougherty, *Nature* **2009**, *458*, 534–537.
- [112] B. Salopek-Sondi, B. Vukelić, J. Špoljarić, Š. Šimaga, D. D. Vujaklija, J. Makarević, N. Jajčanin, M. Abramić, J. Spoljarić, S. Simaga, et al., *Biol. Chem.* **2008**, *389*, 163–167.
- [113] M. A. Holmes, D. E. Tronrud, B. W. Matthews, *Biochemistry* **1983**, *22*, 236–240.
- [114] H. Burgi, J. Dunitz, E. Shefter, *J. Am. Chem. ...* **1973**, *587*, 5065–5067.
- [115] H. B. Buergi, J. D. Dunitz, *Acc. Chem. Res.* **1983**, *16*, 153–161.
- [116] M. Honda, H. Okutsu, T. Matsuura, T. Miyagi, Y. Yamamoto, T. Hazato, H. Ono, *Jpn. J. Pharmacol.* **2001**, *87*, 261–267.
- [117] E. Y. Blishchenko, O. V Sazonova, O. A. Kalinina, O. N. Yatskin, M. M. Philippova, A. Y. Surovoy, A. A. Karelin, V. T. Ivanov, *Peptides* **2002**, *23*, 903–910.
- [118] E.-L. Glämsta, B. Meyerson, J. Silberring, L. Terenius, F. Nyberg, *Biochem. Biophys. Res. Commun.* **1992**, *184*, 1060–1066.
- [119] D. De Bundel, I. Smolders, R. Yang, A. L. Albiston, Y. Michotte, S. Y. Chai, *Neurobiol. Learn. Mem.* **2009**, *92*, 19–26.
- [120] M. A. Sentandreu, F. Toldrá, *J. Agric. Food Chem.* **2000**, *48*, 5014–5022.
- [121] S. Dhanda, H. Singh, J. Singh, T. P. Singh, *Protein Expr. Purif.* **2007**, *52*, 297–305.
- [122] K. Fukasawa, K. M. Fukasawa, M. Kanai, S. Fujii, J. Hirose, M. Harada, *Biochem. J.* **1998**, *329*, 275–282.
- [123] K. R. Lynn, *Int. J. Biochem.* **1991**, *23*, 47–50.
- [124] Y. Shimamori, Y. Watanabe, Y. Fujimoto, *Chem. Pharm. Bull.* **1986**, *34*, 3333–3340.
- [125] T. Akiyama, S. Harada, F. Kojima, Y. Takahashi, C. Imada, Y. Okami, Y. Muraoka, T. Aoyagi, T. Takeuchi, *J. Antibiot.* **1998**, *51*, 553–559.
- [126] D. Agić, M. Hranjec, N. Jajčanin, K. Starčević, G. Karminski-Zamola, M. Abramić, *Bioorg. Chem.* **2007**, *35*, 153–169.
- [127] H.-J. Böhm, G. Klebe, *Angew. Chem. Int. Ed.* **1996**, *35*, 2588–2614.
- [128] R. E. Babine, S. L. Bender, *Chem. Rev.* **1997**, *97*, 1359–1472.
- [129] International Human Genome Sequencing Consortium, *Nature* **2004**, *431*, 931–945.

- [130] H. Kubinyi, *Curr. Opin. Drug Discov. Devel.* **1998**, *1*, 4–15.
- [131] J. H. Van Drie, M. S. Lajiness, *Drug Discov. Today* **1998**, *3*, 274–283.
- [132] W. P. Walters, M. T. Stahl, M. A. Murcko, *Drug Discov. Today* **1998**, *3*, 160–178.
- [133] C. R. Beddell, P. J. Goodford, F. E. Norrington, S. Wilkinson, R. Wootton, *Br. J. Pharmacol.* **1976**, *57*, 201–209.
- [134] P. J. Goodford, *J. Med. Chem.* **1984**, *27*, 558–564.
- [135] T. A. Steitz, M. L. Ludwig, F. A. Quioco, W. N. Lipscomb, *J. Biol. Chem.* **1967**, *242*, 4662–4668.
- [136] D. W. Cushman, H. S. Cheung, E. F. Sabo, M. A. Ondetti, *Biochemistry* **1977**, *16*, 5484–5491.
- [137] W. G. J. Hol, *Angew. Chem. Int. Ed.* **1986**, *25*, 767–778.
- [138] M. D. Walkinshaw, *Med. Res. Rev.* **1992**, *12*, 317–72.
- [139] M. L. West, D. P. Fairlie, *Trends Pharmacol. Sci.* **1995**, *16*, 67–75.
- [140] P. Y. Lam, P. K. Jadhav, C. J. Eyermann, C. N. Hodge, Y. Ru, L. T. Bacheler, J. L. Meek, M. J. Otto, M. M. Rayner, Y. N. Wong, *Science* **1994**, *263*, 380–384.
- [141] F. H. Allen, O. Kennard, R. Taylor, *Acc. Chem. Res.* **1983**, *16*, 146–153.
- [142] A. D. Tinoco, A. Saghatelian, *Biochemistry* **2011**, *50*, 7447–7461.
- [143] A. L. Vaccarino, A. J. Kastin, *Peptides* **2000**, *21*, 1975–2034.
- [144] D. E. Kohan, N. F. Rossi, E. W. Inscho, D. M. Pollock, *Physiol. Rev.* **2011**, *91*, 1–77.
- [145] F. Boccardo, D. Amoroso, *Chemotherapy* **2001**, *47 Suppl 2*, 62–77.
- [146] H. G. Boman, *Annu. Rev. Immunol.* **1995**, *13*, 61–92.
- [147] R. A. Wiley, D. H. Rich, *Med. Res. Rev.* **1993**, *13*, 327–384.
- [148] D. W. Cushman, H. S. Cheung, E. F. Sabo, M. A. Ondetti, *Am. J. Cardiol.* **1982**, *49*, 1390–1394.
- [149] J. Hughes, T. W. Smith, H. W. Kosterlitz, L. A. Fothergill, B. A. Morgan, H. R. Morris, *Nature* **1975**, *258*, 577–580.
- [150] D. Smith, J. F. Griffin, *Science* **1978**, *199*, 1214–1216.

- [151] A. Giannis, T. Kolter, *Angew. Chem. Int. Ed.* **1993**, *32*, 1244–1267.
- [152] K. H. Hsieh, T. R. LaHann, R. C. Speth, *J. Med. Chem.* **1989**, *32*, 898–903.
- [153] E. J. Corey, J. O. Link, *J. Am. Chem. Soc.* **1992**, *114*, 1906–1908.
- [154] P. W. Schiller, G. Weltrowska, T. M. Nguyen, C. Lemieux, N. N. Chung, B. J. Marsden, B. C. Wilkes, *J. Med. Chem.* **1991**, *34*, 3125–3132.
- [155] H. Yanagisawa, S. Ishihara, A. Ando, T. Kanazaki, S. Miyamoto, H. Koike, Y. Iijima, K. Oizumi, Y. Matsushita, T. Hata, *J. Med. Chem.* **1987**, *30*, 1984–1991.
- [156] U. Nagai, K. Sato, R. Nakamura, R. Kato, *Tetrahedron* **1993**, *49*, 3577–3592.
- [157] K. Sato, U. Nagai, *J. Chem. Soc. Perkin Trans. 1* **1986**, 1231.
- [158] D. S. Kemp, T. P. Curran, J. G. Boyd, T. J. Allen, *J. Org. Chem.* **1991**, *56*, 6683–6697.
- [159] R. Sarabu, K. Lovey, V. S. Madison, D. C. Fry, D. N. Greeley, C. M. Cook, G. L. Olson, *Tetrahedron* **1993**, *49*, 3629–3640.
- [160] A. B. Smith, T. P. Keenan, R. C. Holcomb, P. A. Sprengeler, M. C. Guzman, J. L. Wood, P. J. Carroll, R. Hirschmann, *J. Am. Chem. Soc.* **1992**, *114*, 10672–10674.
- [161] A. M. Lincoff, R. M. Califf, E. J. Topol, *J. Am. Coll. Cardiol.* **2000**, *35*, 1103–1115.
- [162] R. Hirschmann, P. A. Sprengeler, T. Kawasaki, J. W. Leahy, W. C. Shakespeare, A. B. Smith, *J. Am. Chem. Soc.* **1992**, *114*, 9699–9701.
- [163] M. J. Fisher, B. Gunn, C. S. Harms, A. D. Kline, J. T. Mullaney, A. Nunes, R. M. Scarborough, A. E. Arfsten, M. A. Skelton, S. L. Um, et al., *J. Med. Chem.* **1997**, *40*, 2085–2101.
- [164] B. K. Blackburn, A. Lee, M. Baier, B. Kohl, A. G. Olivero, R. Matamoros, K. D. Robarge, R. S. McDowell, *J. Med. Chem.* **1997**, *40*, 717–729.
- [165] R. Hirschmann, K. C. Nicolaou, S. Pietranico, J. Salvino, E. M. Leahy, P. A. Sprengeler, G. Furst, C. D. Strader, A. B. Smith, *J. Am. Chem. Soc.* **1992**, *114*, 9217–9218.
- [166] M. Miyamoto, N. Yamazaki, A. Nagaoka, Y. Nagawa, *Ann. N. Y. Acad. Sci.* **1989**, *553*, 508–510.
- [167] G. L. Olson, H. C. Cheung, E. Chiang, V. S. Madison, J. Sepinwall, G. P. Vincent, A. Winokur, K. A. Gary, *J. Med. Chem.* **1995**, *38*, 2866–2879.
- [168] R. B. Silverman, M. W. Holladay, *The Organic Chemistry of Drug Design and Drug Action*, Elsevier, **2014**.

- [169] J. Gante, *Synthesis* **1989**, 405–413.
- [170] H. Han, K. D. Janda, *J. Am. Chem. Soc.* **1996**, *118*, 2539–2544.
- [171] R. J. Simon, R. S. Kania, R. N. Zuckermann, V. D. Huebner, D. A. Jewell, S. Banville, S. Ng, L. Wang, S. Rosenberg, C. K. Marlowe, *Proc. Natl. Acad. Sci. U. S. A.* **1992**, *89*, 9367–9371.
- [172] S. Ren, E. J. Lien, *Prog. Drug Res.* **1998**, *51*, 1–31.
- [173] A. G. Tomasselli, R. L. Heinrikson, *Biochim. Biophys. Acta - Protein Struct. Mol. Enzymol.* **2000**, *1477*, 189–214.
- [174] A. M. J. Wensing, N. M. van Maarseveen, M. Nijhuis, *Antiviral Res.* **2010**, *85*, 59–74.
- [175] C. L. Waller, G. R. Marshall, *J. Med. Chem.* **1993**, *36*, 2390–2403.
- [176] R. Natesh, S. Schwager, E. Sturrock, K. Acharya, *Nature* **2003**, *421*, 551–554.
- [177] S. H. Ferreira, *Br. J. Pharmacol. Chemother.* **1965**, *24*, 163–169.
- [178] Y. S. Bakhle, *Nature* **1968**, *220*, 919–921.
- [179] D. W. Cushman, M. A. Ondetti, *Hypertension* **1991**, *17*, 589–592.
- [180] F. A. Quioco, W. N. Lipscomb, *Adv. Protein Chem.* **1971**, *25*, 1–78.
- [181] L. D. Byers, R. Wolfenden, *Biochemistry* **1973**, *12*, 2070–2078.
- [182] R. Chirumamilla, R. Marchant, P. Nigam, *J. Chem. Technol. Biotechnol.* **2001**, *76*, 123–127.
- [183] R. N. Patel, A. Banerjee, L. J. Szarka, *J. Am. Oil Chem. Soc.* **1996**, *73*, 1363–1375.
- [184] R. Natesh, S. L. U. Schwager, H. R. Evans, E. D. Sturrock, K. R. Acharya, *Biochemistry* **2004**, *43*, 8718–8724.
- [185] J. J. Woessner, *FASEB J* **1991**, *5*, 2145–2154.
- [186] W. K. Hagmann, M. W. Lark, J. W. Becker, *Annu. Rep. Med. Chem.* **1996**, *31*, 231–240.
- [187] I. Schechter, A. Berger, *Biochem. Biophys. Res. Commun.* **1967**, *27*, 157–162.
- [188] T. Stams, J. C. Spurlino, D. L. Smith, R. C. Wahl, T. F. Ho, M. W. Qoronfleh, T. M. Banks, B. Rubin, *Nat. Struct. Biol.* **1994**, *1*, 119–123.

- [189] J. C. Spurlino, A. M. Smallwood, D. D. Carlton, T. M. Banks, K. J. Vavra, J. S. Johnson, E. R. Cook, J. Falvo, R. C. Wahl, T. A. Pulvino, *Proteins* **1994**, *19*, 98–109.
- [190] J. J. Chen, Y. Zhang, S. Hammond, N. Dewdney, T. Ho, X. Lin, M. F. Browner, A. L. Castelhana, *Bioorg. Med. Chem. Lett.* **1996**, *6*, 1601–1606.
- [191] M. F. Browner, W. W. Smith, A. L. Castelhana, *Biochemistry* **1995**, *34*, 6602–6610.
- [192] B. Lovejoy, A. Cleasby, A. M. Hassell, K. Longley, M. A. Luther, D. Weigl, G. McGeehan, A. B. McElroy, D. Drewry, M. H. Lambert, *Science* **1994**, *263*, 375–377.
- [193] M. A. Phillips, R. Fletterick, W. J. Rutter, *J. Biol. Chem.* **1990**, *265*, 20692–20698.
- [194] J. R. Porter, N. R. A. Beeley, B. A. Boyce, B. Mason, A. Millican, K. Millar, J. Leonard, J. R. Morphy, J. P. O’Connell, *Bioorg. Med. Chem. Lett.* **1994**, *4*, 2741–2746.
- [195] B. E. Tomczuk, M. R. Gowravaram, J. S. Johnson, D. Delecki, E. R. Cook, A. K. Ghose, A. M. Mathiowetz, J. C. Spurlino, B. Rubin, D. L. Smith, et al., *Bioorg. Med. Chem. Lett.* **1995**, *5*, 343–348.
- [196] J. R. Morphy, N. R. A. Beeley, B. A. Boyce, J. Leonard, B. Mason, A. Millican, K. Millar, J. P. O’Connell, J. Porter, *Bioorg. Med. Chem. Lett.* **1994**, *4*, 2747–2752.
- [197] K. T. Chapman, P. L. Durette, C. G. Caldwell, K. M. Sperow, L. M. Niedzwiecki, R. K. Harrison, C. Saphos, A. J. Christen, J. M. Olszewski, V. L. Moore, et al., *Bioorg. Med. Chem. Lett.* **1996**, *6*, 803–806.
- [198] G. B. Fields, *Matrix Biol.* **2015**, *44-46*, 239–246.
- [199] D. Herries, *Biochem. Educ.* **1985**, *13*, 146.
- [200] M. H. O’Leary, M. D. Kluetz, *J. Am. Chem. Soc.* **1972**, *94*, 3585–3589.
- [201] H. Umezawa, T. Aoyagi, H. Morishima, S. Kunimoto, M. Matsuzaki, M. Hamada, T. Takeuchi, *J. Antibiot.* **1970**, *23*, 425–427.
- [202] H. Umezawa, *Annu. Rev. Microbiol.* **1982**, *36*, 75–99.
- [203] L. T. J. Delbaere, G. D. Brayer, *J. Mol. Biol.* **1985**, *183*, 89–103.
- [204] I. V Kurinov, R. W. Harrison, *Protein Sci.* **1996**, *5*, 752–758.
- [205] M. T. Stubbs, W. Bode, *Thromb. Res.* **1993**, *69*, 1–58.
- [206] F. Markwardt, *Proteolytic Enzymes*, Elsevier, **1970**.

- [207] T. J. Rydel, K. G. Ravichandran, A. Tulinsky, W. Bode, R. Huber, C. Roitsch, J. W. Fenton, *Science* **1990**, *249*, 277–280.
- [208] T. J. Rydel, A. Tulinsky, W. Bode, R. Huber, *J. Mol. Biol.* **1991**, *221*, 583–601.
- [209] W. Bode, D. Turk, A. Karshikov, *Protein Sci.* **1992**, *1*, 426–471.
- [210] P. C. Weber, S.-L. Lee, F. A. Lewandowski, M. C. Schadt, C.-H. Chang, C. A. Kettner, *Biochemistry* **1995**, *34*, 3750–3757.
- [211] R. Kikumoto, Y. Tamao, T. Tezuka, S. Tonomura, H. Hara, K. Ninomiya, A. Hijikata, S. Okamoto, *Biochemistry* **1984**, *23*, 85–90.
- [212] J. Stürzebecher, F. Markwardt, B. Voigt, G. Wagner, P. Walsmann, *Thromb. Res.* **1983**, *29*, 635–642.
- [213] D. W. Banner, P. Hadvary, *J. Biol. Chem.* **1991**, *266*, 20085–20093.
- [214] H. Brandstetter, D. Turk, H. W. Hoeffken, D. Grosse, J. Stürzebecher, P. D. Martin, B. F. P. Edwards, W. Bode, *J. Mol. Biol.* **1992**, *226*, 1085–1099.
- [215] D. Turk, J. Stürzebecher, W. Bode, *FEBS Lett.* **1991**, *287*, 133–138.
- [216] T. Matsuzaki, C. Sasaki, H. Umeyama, *J. Biochem.* **1988**, *103*, 537–543.
- [217] G. Danaei, M. M. Finucane, Y. Lu, G. M. Singh, M. J. Cowan, C. J. Paciorek, J. K. Lin, F. Farzadfar, Y.-H. Khang, G. A. Stevens, et al., *Lancet* **2011**, *378*, 31–40.
- [218] R. E. van Genugten, D. H. van Raalte, M. Diamant, *Diabetes. Obes. Metab.* **2012**, *14*, 101–111.
- [219] E. Matteucci, O. Giampietro, *Curr. Med. Chem.* **2011**, *18*, 4753–4760.
- [220] D. M. Ashworth, B. Atrash, G. R. Baker, A. J. Baxter, P. D. Jenkins, D. M. Jones, M. Szelke, *Bioorg. Med. Chem. Lett.* **1996**, *6*, 1163–1166.
- [221] D. J. Augeri, J. A. Robl, D. A. Betebenner, D. R. Magnin, A. Khanna, J. G. Robertson, A. Wang, L. M. Simpkins, P. Taunk, Q. Huang, et al., *J. Med. Chem.* **2005**, *48*, 5025–37.
- [222] J. A. Robl, L. G. Hamann, *Accounts in Drug Discovery*, Royal Society Of Chemistry, Cambridge, **2010**.
- [223] E. Shaw, *Adv. Enzymol. Relat. Areas Mol. Biol.* **1990**, *63*, 271–347.
- [224] E. Shaw, *J. Protein Chem.* **1984**, *3*, 109–120.
- [225] H.-H. Otto, T. Schirmeister, *Chem. Rev.* **1997**, *97*, 133–172.

- [226] M. H. O’Leary, M. Urberg, A. P. Young, *Biochemistry* **1974**, *13*, 2077–2081.
- [227] B. M. Wagner, R. A. Smith, P. J. Coles, L. J. Copp, M. J. Ernest, A. Krantz, *J. Med. Chem.* **1994**, *37*, 1833–1840.
- [228] I. G. Kamphuis, J. Drenth, E. N. Baker, *J. Mol. Biol.* **1985**, *182*, 317–329.
- [229] K. Takio, T. Towatari, N. Katunuma, D. C. Teller, K. Titani, *Proc. Natl. Acad. Sci. U. S. A.* **1983**, *80*, 3666–3670.
- [230] E. Schröder, C. Phillips, E. Garman, K. Harlos, C. Crawford, *FEBS Lett.* **1993**, *315*, 38–42.
- [231] R. A. Smith, L. J. Copp, S. L. Donnelly, R. W. Spencer, A. Krantz, *Biochemistry* **1988**, *27*, 6568–6573.
- [232] J. O. Westerik, R. Wolfenden, *J. Biol. Chem.* **1972**, *247*, 8195–8197.
- [233] S. A. Thompson, P. R. Andrews, R. P. Hanzlik, *J. Med. Chem.* **1986**, *29*, 104–111.
- [234] V. Ehmke, E. Winkler, D. W. Banner, W. Haap, W. B. Schweizer, M. Rottmann, M. Kaiser, C. Freymond, T. Schirmeister, F. Diederich, *ChemMedChem* **2013**, *8*, 967–975.
- [235] B. T. Mott, R. S. Ferreira, A. Simeonov, A. Jadhav, K. K.-H. Ang, W. Leister, M. Shen, J. T. Silveira, P. S. Doyle, M. R. Arkin, et al., *J. Med. Chem.* **2010**, *53*, 52–60.
- [236] V. Ehmke, J. E. Q. Quinsaat, P. Rivera-Fuentes, C. Heindl, C. Freymond, M. Rottmann, R. Brun, T. Schirmeister, F. Diederich, *Org. Biomol. Chem.* **2012**, *10*, 5764–5768.
- [237] T.-C. Liang, R. H. Abeles, *Arch. Biochem. Biophys.* **1987**, *252*, 626–634.
- [238] J. B. Moon, R. S. Coleman, R. P. Hanzlik, *J. Am. Chem. Soc.* **1986**, *108*, 1350–1351.
- [239] C. A. Lewis, R. Wolfenden, *Biochemistry* **1977**, *16*, 4890–4895.
- [240] J. T. Palmer, D. Rasnick, J. L. Klaus, D. Bromme, *J. Med. Chem.* **1995**, *38*, 3193–3196.
- [241] I. D. Kerr, J. H. Lee, C. J. Farady, R. Marion, M. Rickert, M. Sajid, K. C. Pandey, C. R. Caffrey, J. Legac, E. Hansell, et al., *J. Biol. Chem.* **2009**, *284*, 25697–25703.
- [242] E. J. Lien, H. Gao, L. L. Lien, *Prog. Drug Res.* **1994**, *43*, 43–86.
- [243] C. Jensen, P. Herold, H. R. Brunner, *Nat. Rev. Drug Discov.* **2008**, *7*, 399–410.
- [244] V. S. Kitchen, C. Skinner, K. Ariyoshi, E. A. Lane, I. B. Duncan, J. Burckhardt, H. U. Burger, K. Bragman, A. J. Pinching, J. N. Weber, *Lancet* **1995**, *345*, 952–955.

- [245] L. J. Hyland, T. A. Tomaszek, T. D. Meek, *Biochemistry* **1991**, *30*, 8454–8463.
- [246] A. Y. Kovalevsky, A. A. Chumanevich, F. Liu, J. M. Louis, I. T. Weber, *Biochemistry* **2007**, *46*, 14854–14864.
- [247] K. Suguna, E. A. Padlan, C. W. Smith, W. D. Carlson, D. R. Davies, *Proc. Natl. Acad. Sci. U. S. A.* **1987**, *84*, 7009–7013.
- [248] M. N. G. James, A. R. Sielecki, K. Hayakawa, M. H. Gelb, *Biochemistry* **1992**, *31*, 3872–3886.
- [249] D. H. Rich, *J. Med. Chem.* **1985**, *28*, 263–273.
- [250] R. Bott, E. Subramanian, D. R. Davies, *Biochemistry* **1982**, *21*, 6956–6962.
- [251] M. W. Holladay, F. G. Salituro, D. H. Rich, *J. Med. Chem.* **1987**, *30*, 374–383.
- [252] F. G. Salituro, N. Agarwal, T. Hofmann, D. H. Rich, *J. Med. Chem.* **1987**, *30*, 286–295.
- [253] D. H. Rich, E. T. O. Sun, E. Ulm, *J. Med. Chem.* **1980**, *23*, 27–33.
- [254] D. H. Rich, E. Sun, J. Singh, *Biochem. Biophys. Res. Commun.* **1977**, *74*, 762–767.
- [255] I. Katoh, T. Yasunaga, Y. Ikawa, Y. Yoshinaka, *Nature* **1987**, *329*, 654–656.
- [256] P. M. Fitzgerald, B. M. McKeever, J. F. VanMiddlesworth, J. P. Springer, J. C. Heimbach, C. T. Leu, W. K. Herber, R. A. Dixon, P. L. Darke, *J. Biol. Chem.* **1990**, *265*, 14209–14219.
- [257] W. J. Greenlee, P. K. S. Siegl, *Annu. Rep. Med. Chem.* **1992**, *27*, 59–68.
- [258] V. Dhanaraj, C. G. Dealwis, C. Frazao, M. Badasso, B. L. Sibanda, I. J. Tickle, J. B. Cooper, H. P. Driessen, M. Newman, C. Aguilar, *Nature* **1992**, *357*, 466–472.
- [259] M. A. Navia, P. M. Fitzgerald, B. M. McKeever, C. T. Leu, J. C. Heimbach, W. K. Herber, I. S. Sigal, P. L. Darke, J. P. Springer, *Nature* **1989**, *337*, 615–620.
- [260] A. Wlodawer, M. Miller, M. Jaskólski, B. K. Sathyanarayana, E. Baldwin, I. T. Weber, L. M. Selk, L. Clawson, J. Schneider, S. B. Kent, *Science* **1989**, *245*, 616–621.
- [261] M. Jaskolski, A. G. Tomasselli, T. K. Sawyer, D. G. Staples, R. L. Heinrikson, J. Schneider, S. B. H. Kent, A. Wlodawer, *Biochemistry* **1991**, *30*, 1600–1609.
- [262] S. H. Reich, M. Melnick, J. F. Davies, K. Appelt, K. K. Lewis, M. A. Fuhry, M. Pino, A. J. Trippe, D. Nguyen, H. Dawson, *Proc. Natl. Acad. Sci. U. S. A.* **1995**, *92*, 3298–3302.

- [263] S. H. Reich, M. Melnick, M. J. Pino, M. A. Fuhry, A. J. Trippe, K. Appelt, J. F. Davies, B. W. Wu, L. Musick, *J. Med. Chem.* **1996**, *39*, 2781–2794.
- [264] M. Melnick, S. H. Reich, K. K. Lewis, L. J. Mitchell, D. Nguyen, A. J. Trippe, H. Dawson, J. F. Davies, K. Appelt, B. W. Wu, et al., *J. Med. Chem.* **1996**, *39*, 2795–2811.
- [265] N. A. Roberts, J. A. Martin, D. Kinchington, A. V Broadhurst, J. C. Craig, I. B. Duncan, S. A. Galpin, B. K. Handa, J. Kay, A. Kröhn, *Science* **1990**, *248*, 358–361.
- [266] A. Krohn, S. Redshaw, J. C. Ritchie, B. J. Graves, M. H. Hatada, *J. Med. Chem.* **1991**, *34*, 3340–3342.
- [267] B. F. Lundt, N. L. Johansen, A. Vølund, J. Markussen, *Int. J. Pept. Protein Res.* **2009**, *12*, 258–268.
- [268] R. Geiger, W. König, *Protection of Functional Groups in Peptide Synthesis*, Elsevier, **1981**.
- [269] S. C. Nigama, A. Mann, M. Taddei, C.-G. Wermutha, *Synth. Commun.* **1989**, *19*, 3139–3142.
- [270] P. G. M. Wuts, T. W. Greene, *Greene's Protective Groups in Organic Synthesis*, John Wiley & Sons, **2012**.
- [271] T. Morwick, M. Hrapchak, M. DeTuri, S. Campbell, *Org. Lett.* **2002**, *4*, 2665–2668.
- [272] H. A. Staab, K. Wendel, *Org. Synth.* **1968**, *48*, 44.
- [273] A. K. Ghosh, K. Xi, K. Ratia, B. D. Santarsiero, W. Fu, B. H. Harcourt, P. A. Rota, S. C. Baker, M. E. Johnson, A. D. Mesecar, *J. Med. Chem.* **2005**, *48*, 6767–6771.
- [274] E. J. Corey, a. Venkateswrlu, *J. Am. Chem. Soc.* **1972**, *94*, 6190–6191.
- [275] E. J. Corey, T. K. Schaaf, W. Huber, U. Koelliker, N. M. Weinshenker, *J. Am. Chem. Soc.* **1970**, *92*, 397–398.
- [276] A. K. Ghosh, G. Bilcer, C. Harwood, R. Kawahama, D. Shin, K. A. Hussain, L. Hong, J. a. Loy, C. Nguyen, G. Koelsch, et al., *J. Med. Chem.* **2001**, *44*, 2865–2868.
- [277] A. Bartoszewicz, M. Kalek, J. Nilsson, R. Hiresova, J. Stawinski, *Synlett* **2008**, 0037–0040.
- [278] A. El-Faham, F. Albericio, *Chem. Rev.* **2011**, *111*, 6557–6602.
- [279] H. Schröder, G. A. Strohmeier, M. Leybold, T. Nuijens, P. J. L. M. Quaedflieg, R. Breinbauer, *Adv. Synth. Catal.* **2013**, *355*, 1799–1807.

- [280] F. G. Bordwell, *Acc. Chem. Res.* **1988**, *21*, 456–463.
- [281] J. Choy, S. Jaime-Figueroa, L. Jiang, P. Wagner, *Synth. Commun.* **2008**, *38*, 3840–3853.
- [282] S. Minegishi, H. Mayr, *J. Am. Chem. Soc.* **2003**, *125*, 286–295.
- [283] T. Kanzian, T. A. Nigst, A. Maier, S. Pichl, H. Mayr, *European J. Org. Chem.* **2009**, *2009*, 6379–6385.
- [284] A. Nadin, J. M. Sánchez López, J. G. Neduveilil, S. R. Thomas, *Tetrahedron* **2001**, *57*, 1861–1864.
- [285] B. E. Haug, D. H. Rich, *Org. Lett.* **2004**, *6*, 4783–4786.
- [286] I. Horiuti, M. Polanyi, *Trans. Faraday Soc.* **1934**, *30*, 1164.
- [287] M. Poterała, J. Plenkiewicz, *Tetrahedron: Asymmetry* **2011**, *22*, 294–299.
- [288] D. X. Hu, M. O'Brien, S. V Ley, *Org. Lett.* **2012**, *14*, 4246–4249.
- [289] Q. Zhang, H. Ren, G. L. Baker, *Beilstein J. Org. Chem.* **2014**, *10*, 1365–1371.
- [290] W. Zhang, M. L. Bolla, D. Kahne, C. T. Walsh, *J. Am. Chem. Soc.* **2010**, *132*, 6402–6411.
- [291] E. K. Jaffe, *Bioorg. Chem.* **2004**, *32*, 316–325.
- [292] R. Vallinayagam, H. Bertschy, Y. Berger, V. Wenger, R. Neier, *Synthesis* **2007**, 3731–3735.
- [293] J. Ivkovic, C. Lembacher-Fadum, R. Breinbauer, *Org. Biomol. Chem.* **2015**, *13*, 10456–10460.
- [294] R. Hili, S. Baktharaman, A. K. Yudin, *European J. Org. Chem.* **2008**, *2008*, 5201–5213.
- [295] D. Gryko, J. Chałko, J. Jurczak, *Chirality* **2003**, *15*, 514–541.
- [296] M. T. Reetz, *Chem. Rev.* **1999**, *99*, 1121–1162.
- [297] A. Fässler, G. Bold, H. Steiner, *Tetrahedron Lett.* **1998**, *39*, 4925–4928.
- [298] B. E. Maryanoff, M. N. Greco, H. C. Zhang, P. Andradegordon, J. a Kauffman, K. C. Nicolaou, a J. Liu, P. H. Brungs, *J. Am. Chem. Soc.* **1995**, *117*, 1225–1239.
- [299] G. Bringmann, J.-P. Geisler, *Synthesis* **1989**, 608–610.
- [300] F. A. Davis, T. Ramachandar, J. Chai, E. Skucas, *Tetrahedron Lett.* **2006**, *47*, 2743–2746.

- [301] T. Moriwake, S. Hamano, S. Saito, S. Torii, *Chem. Lett.* **1987**, 2085–2088.
- [302] J. R. Luly, J. F. Dellaria, J. J. Plattner, J. L. Soderquist, N. Yi, *J. Org. Chem.* **1987**, *52*, 1487–1492.
- [303] A. Gołębowski, J. Jurczak, U. Jacobsson, *Tetrahedron* **1987**, *43*, 3063–3066.
- [304] J. R. Luly, C. N. Hsiao, N. BaMaung, J. J. Plattner, *J. Org. Chem.* **1988**, *53*, 6109–6112.
- [305] M. Falorni, G. Giacomelli, A. Porcheddu, M. Taddei, *J. Org. Chem.* **1999**, *64*, 8962–8964.
- [306] R. Hili, A. K. Yudin, *J. Am. Chem. Soc.* **2006**, *128*, 14772–14773.
- [307] F. Coelho, G. Diaz, C. a. Abella, W. P. Almeida, *Synlett* **2006**, 435–439.
- [308] B. Soto-Cairolí, J. J. de Pomar, J. A. Soderquist, *Org. Lett.* **2008**, *10*, 333–336.
- [309] J.-A. Fehrentz, B. Castro, *Synthesis* **1983**, 676–678.
- [310] T. Yasuma, S. Oi, N. Choh, T. Nomura, N. Furuyama, A. Nishimura, Y. Fujisawa, T. Sohda, *J. Med. Chem.* **1998**, *41*, 4301–4308.
- [311] Y. Hamada, T. Shioiri, *Chem. Pharm. Bull.* **1982**, *30*, 1921–1924.
- [312] A. W. Konradi, S. J. Kemp, S. F. Pedersen, *J. Am. Chem. Soc.* **1994**, *116*, 1316–1323.
- [313] J. Jurczak, D. Gryko, E. Kobrzycka, H. Gruza, P. Prokopowicz, *Tetrahedron* **1998**, *54*, 6051–6064.
- [314] M. E. Sergeev, V. B. Pronin, T. L. Voyushina, *Synlett* **2005**, 2802–2804.
- [315] M. Ocejó, J. L. Vicario, D. Badía, L. Carrillo, E. Reyes, *Synlett* **2005**, 2110–2112.
- [316] C. K. Jung, M. J. Krische, *J. Am. Chem. Soc.* **2006**, *128*, 17051–17056.
- [317] R. P. Sharma, M. G. Gore, M. Akhtar, *J.C.S. Chem. Commun.* **1979**, 875–877.
- [318] A. Ito, R. Takahashi, Y. Baba, *Chem. Pharm. Bull.* **1975**, *23*, 3081–3087.
- [319] K. E. Rittle, C. F. Homnick, G. S. Ponticello, B. E. Evans, *J. Org. Chem.* **1982**, *47*, 3016–3018.
- [320] H. A. Staab, *Azolides in Organic Synthesis and Biochemistry Azolides in Organic Synthesis and Biochemistry*, **2002**.
- [321] H. Kathri, C. H. Stammer, *J.C.S. Chem. Comm.* **1979**, 79–80.

- [322] H. N. Khatri, C. H. Stammer, M. M. Bradford, R. A. McRorie, *Biochem. Biophys. Res. Commun.* **1980**, *96*, 163–167.
- [323] O. Krebs, R. J. K. Taylor, *Org. Lett.* **2005**, *7*, 1063–1066.
- [324] K. Ishigai, H. Fuwa, K. Hashizume, R. Fukazawa, Y. Cho, M. Yotsu-Yamashita, M. Sasaki, *Chem. Eur. J.* **2013**, *19*, 5276–5288.
- [325] A. Arlt, S. Benson, S. Schulthoff, B. Gabor, A. Fürstner, *Chem. Eur. J.* **2013**, *19*, 3596–3608.
- [326] Y. E. Jad, G. a. Acosta, S. N. Khattab, B. G. de la Torre, T. Govender, H. G. Kruger, A. El-Faham, F. Albericio, *Org. Biomol. Chem.* **2015**, *13*, 2393–2398.
- [327] M. Kunishima, A. Kitao, C. Kawachi, Y. Watanabe, S. Iguchi, K. Hioki, S. Tani, *Chem. Pharm. Bull.* **2002**, *50*, 549–550.
- [328] H. Hibino, Y. Nishiuchi, *Tetrahedron Lett.* **2011**, *52*, 4947–4949.
- [329] M. A. Elsayy, C. Hewage, B. Walker, *J. Pept. Sci.* **2012**, *18*, 302–311.
- [330] A. Dondoni, D. Perrone, T. Semola, *Synthesis* **1995**, 181–186.
- [331] S. Popovic, H. Bieräugel, R. J. Detz, A. M. Kluwer, J. A. A. Koole, D. E. Streefkerk, H. Hiemstra, J. H. van Maarseveen, *Chem. Eur. J.* **2013**, *19*, 16934–16937.
- [332] A. G. Myers, B. Zhong, M. Movassaghi, D. W. Kung, B. a. Lanman, S. Kwon, *Tetrahedron Lett.* **2000**, *41*, 1359–1362.
- [333] D. G. Piotrowska, *Tetrahedron: Asymmetry* **2002**, *13*, 2509–2512.
- [334] J. N. Denis, A. Correa, A. E. Greene, *J. Org. Chem.* **1991**, *56*, 6939–6942.
- [335] W. Wu, J. Xie, Y. Xuan, *J. Chem. Res.* **2008**, *2008*, 344–346.
- [336] W. Wu, J. Xie, D. Xie, *Russ. J. Inorg. Chem.* **2010**, *55*, 384–389.
- [337] N. London, D. Movshovitz-Attias, O. Schueler-Furman, *Structure* **2010**, *18*, 188–199.
- [338] R. Téllez-Sanz, L. García-Fuentes, C. Barón, *FEBS Lett.* **1998**, *423*, 75–80.
- [339] H. Lu, R. Gautier, M. D. Donakowski, Z. Liu, K. R. Poepelmeier, *Inorg. Chem.* **2014**, *53*, 537–542.
- [340] N. Basarić, S. S. Thomas, V. B. Bregović, N. Cindro, C. Bohne, *J. Org. Chem.* **2015**, *80*, 4430–4442.

- [341] V. Y. Torbeev, K. Mandal, V. A. Terechko, S. B. H. Kent, *Bioorg. Med. Chem. Lett.* **2008**, *18*, 4554–4557.
- [342] X.-M. Chen, X.-C. Huang, M.-L. Tong, Y.-X. Tong, S. W. Ng, *Aust. J. Chem.* **1997**, *50*, 865.
- [343] T. Hori, T. Kumasaka, M. Yamamoto, T. Nonaka, N. Tanaka, Y. Hashimoto, T. Ueki, K. Takio, *Acta Crystallogr. Sect. D Biol. Crystallogr.* **2001**, *57*, 361–368.
- [344] M. J. Loferer, C. S. Tautermann, H. H. Loeffler, K. R. Liedl, *J. Am. Chem. Soc.* **2003**, *125*, 8921–8927.
- [345] J. Li, Y. Deng, S. Jie, B.-G. Li, *J. Organomet. Chem.* **2015**, *797*, 76–82.
- [346] M. M. Ibrahim, A. Mosa, *Arab. J. Chem.* **2014**, *7*, 672–679.
- [347] R. E. Vandebroucke, C. Libert, *Nat. Rev. Drug Discov.* **2014**, *13*, 904–27.
- [348] L. A. Hardegger, B. Kuhn, B. Spinnler, L. Anselm, R. Ecabert, M. Stihle, B. Gsell, R. Thoma, J. Diez, J. Benz, et al., *Angew. Chem. Int. Ed.* **2011**, *50*, 314–318.
- [349] O. Dumele, D. Wu, N. Trapp, N. Goroff, F. Diederich, *Org. Lett.* **2014**, *16*, 4722–4725.
- [350] O. Dumele, N. Trapp, F. Diederich, *Angew. Chem. Int. Ed.* **2015**, *54*, 12339–12344.
- [351] D. Chandler, *Nature* **2005**, *437*, 640–647.
- [352] K. A. Dill, T. M. Truskett, V. Vlachy, B. Hribar-Lee, *Annu. Rev. Biophys. Biomol. Struct.* **2005**, *34*, 173–99.
- [353] C. Lalli, A. Trabocchi, G. Menchi, A. Guarna, *Synlett* **2008**, 189–192.
- [354] T. Ohshima, Y. Hayashi, K. Agura, Y. Fujii, A. Yoshiyama, K. Mashima, *Chem. Commun.* **2012**, *48*, 5434–5436.
- [355] S. K. Taylor, N. D. Ide, M. E. Silver, M. L. Stephan, *Synth. Commun.* **2001**, *31*, 2391–2397.
- [356] M. Chalid, H. J. Heeres, A. A. Broekhuis, *J. Appl. Polym. Sci.* **2012**, *123*, 3556–3564.
- [357] C. A. Lipinski, F. Lombardo, B. W. Dominy, P. J. Feeney, *Adv. Drug Deliv. Rev.* **2001**, *46*, 3–26.
- [358] G. R. Bickerton, G. V Paolini, J. Besnard, S. Muresan, A. L. Hopkins, *Nat. Chem.* **2012**, *4*, 90–98.
- [359] P. Leeson, *Nature* **2012**, *481*, 455–456.

- [360] M. Drag, M. Bogyo, J. A. Ellman, G. S. Salvesen, *J. Biol. Chem.* **2010**, 285, 3310–3318.
- [361] A. Byzia, A. Szeffler, L. Kalinowski, M. Drag, *Biochimie* **2015**, DOI 10.1016/j.biochi.2015.09.035.
- [362] M. M. Nachlas, T. P. Goldstein, A. M. Seligman, *Arch. Biochem. Biophys.* **1962**, 97, 223–231.
- [363] J.-A. Fehrentz, B. Castro, *Synthesis* **1983**, 676–678.
- [364] B. Wollinsky, L. Ludwig, A. Hamacher, X. Yu, M. U. Kassack, S.-M. Li, *Bioorg. Med. Chem. Lett.* **2012**, 22, 3866–3869.
- [365] E. a. Jares-Erijman, C. P. Bapat, A. Lithgow-Bertelloni, K. L. Rinehart, R. Sakai, *J. Org. Chem.* **1993**, 58, 5732–5737.
- [366] C. L. Moore, D. D. Leatherwood, T. S. Diehl, D. J. Selkoe, M. S. Wolfe, *J. Med. Chem.* **2000**, 43, 3434–3442.
- [367] M. Uyanik, M. Akakura, K. Ishihara, *J. Am. Chem. Soc.* **2009**, 131, 251–262.
- [368] D. J. Morris, a. S. Partridge, C. V. Manville, D. T. Racys, G. Woodward, G. Docherty, M. Wills, *Tetrahedron Lett.* **2010**, 51, 209–212.
- [369] J. Ahlfors, K. Mekouar, *WO2009140765A1*, **2009**.
- [370] T. James, I. Simpson, J. A. Grant, V. Sridharan, A. Nelson, *Org. Lett.* **2013**, 15, 6094–6097.
- [371] M. Nakamura, H. Miyashita, M. Yamaguchi, Y. Shirasaki, Y. Nakamura, J. Inoue, *Bioorg. Med. Chem.* **2003**, 11, 5449–5460.
- [372] B. Schmidt, S. Hauke, N. Mühlenberg, *Synthesis* **2014**, 46, 1648–1658.
- [373] R. I. McDonald, G. W. Wong, R. P. Neupane, S. S. Stahl, C. R. Landis, *J. Am. Chem. Soc.* **2010**, 132, 14027–14029.
- [374] J. Bondebjerg, Z. Xiang, R. M. Bauzo, C. Haskell-Luevano, M. Meldal, *J. Am. Chem. Soc.* **2002**, 124, 11046–11055.
- [375] A. Boeijen, J. van Ameijde, R. M. J. Liskamp, *J. Org. Chem.* **2001**, 66, 8454–8462.
- [376] G. Chennakrishnareddy, B. Vasantha, N. Narendra, V. V. Sureshbabu, *Int. J. Pept. Res. Ther.* **2011**, 17, 185–191.
- [377] M. Harder, B. Kuhn, F. Diederich, *ChemMedChem* **2013**, 8, 397–404.

- [378] A. Pecina, M. Lepšík, D. Hnyk, P. Hobza, J. Fanfrlík, *J. Phys. Chem. A* **2015**, *119*, 1388–1395.
- [379] M. J. Langton, Y. Xiong, P. D. Beer, *Chem. Eur. J.* **2015**, DOI: 10.1002/chem.201504236.
- [380] S. Scheiner, *Acc. Chem. Res.* **2013**, *46*, 280–288.
- [381] G. E. Garrett, G. L. Gibson, R. N. Straus, D. S. Seferos, M. S. Taylor, *J. Am. Chem. Soc.* **2015**, *137*, 4126–4133.
- [382] S. P. Thomas, D. Jayatilaka, T. N. Guru Row, *Phys. Chem. Chem. Phys.* **2015**, *17*, 25411–25420.
- [383] M. Harder, M. A. Carnero Corrales, N. Trapp, B. Kuhn, F. Diederich, *Chem. Eur. J.* **2015**, *21*, 8455–8463.
- [384] L. M. Salonen, M. C. Holland, P. S. J. Kaib, W. Haap, J. Benz, J.-L. Mary, O. Kuster, W. B. Schweizer, D. W. Banner, F. Diederich, *Chem. Eur. J.* **2012**, *18*, 213–222.
- [385] B. S. Lauber, L. A. Hardegger, A. K. Asraful, B. A. Lund, O. Dumele, M. Harder, B. Kuhn, R. A. Engh, F. Diederich, *Chem. Eur. J.* **2015**, DOI: 10.1002/chem.201503552.
- [386] S. H. Jungbauer, S. M. Huber, *J. Am. Chem. Soc.* **2015**, *137*, 12110–12120.
- [387] Y. Takeda, D. Hisakuni, C.-H. Lin, S. Minakata, *Org. Lett.* **2015**, *17*, 318–321.
- [388] P. Mentrangolo, G. Resnati, T. Pilati, R. Liantonio, F. Meyer, *J. Polym. Sci. Part A Polym. Chem.* **2007**, *45*, 1–15.
- [389] W. Wang, W. Yang, R. Guo, S. Gong, *CrystEngComm* **2015**, *17*, 7663–7675.
- [390] P. Ball, *Nature* **2008**, *452*, 291–292.
- [391] P. Wernet, D. Nordlund, U. Bergmann, M. Cavalleri, M. Odelius, H. Ogasawara, L. A. Näslund, T. K. Hirsch, L. Ojamäe, P. Glatzel, et al., *Science* **2004**, *304*, 995–999.
- [392] E. Arunan, G. R. Desiraju, R. A. Klein, J. Sadlej, S. Scheiner, I. Alkorta, D. C. Clary, R. H. Crabtree, J. J. Dannenberg, P. Hobza, et al., *Pure Appl. Chem.* **2011**, *83*, 1637–1641.
- [393] J. Finkelstein, *Nature* **2009**, *460*, 813–813.
- [394] K. J. Waldron, J. C. Rutherford, D. Ford, N. J. Robinson, *Nature* **2009**, *460*, 823–830.
- [395] S. H. A. M. Leenders, R. Gramage-Doria, B. de Bruin, J. N. H. Reek, *Chem. Soc. Rev.* **2015**, *44*, 433–448.

- [396] S. V Aradhya, M. Frei, M. S. Hybertsen, L. Venkataraman, *Nat. Mater.* **2012**, *11*, 872–876.
- [397] E. Weisberg, P. W. Manley, W. Breitenstein, J. Brüggem, S. W. Cowan-Jacob, A. Ray, B. Huntly, D. Fabbro, G. Fendrich, E. Hall-Meyers, et al., *Cancer Cell* **2005**, *7*, 129–141.
- [398] F. R. Fischer, W. B. Schweizer, F. Diederich, *Angew. Chem. Int. Ed.* **2007**, *46*, 8270–8273.
- [399] E. Piatnitski, R. Flowers, K. Deshayes, *Chem. Eur. J.* **2000**, *6*, 999–1006.
- [400] T. Ritschel, P. C. Kohler, G. Neudert, A. Heine, F. Diederich, G. Klebe, *ChemMedChem* **2009**, *4*, 2012–2023.
- [401] B. Kuhn, J. E. Fuchs, M. Reutlinger, M. Stahl, N. R. Taylor, *J. Chem. Inf. Model.* **2011**, *51*, 3180–3198.
- [402] P. Metrangolo, G. Resnati, *Chem. Eur. J.* **2001**, *7*, 2511–2519.
- [403] Y. N. Imai, Y. Inoue, I. Nakanishi, K. Kitaura, *J. Comput. Chem.* **2009**, *30*, 2267–2276.
- [404] E. A. Meyer, R. K. Castellano, F. Diederich, *Angew. Chem. Int. Ed.* **2003**, *42*, 1210–1250.
- [405] C. Bissantz, B. Kuhn, M. Stahl, *J. Med. Chem.* **2010**, *53*, 5061–5084.
- [406] L. M. Salonen, M. Ellermann, F. Diederich, *Angew. Chem. Int. Ed.* **2011**, *50*, 4808–4842.
- [407] C. D. Sherrill, T. Takatani, E. G. Hohenstein, *J. Phys. Chem. A* **2009**, *113*, 10146–10159.
- [408] E. G. Hohenstein, C. D. Sherrill, *J. Phys. Chem. A* **2009**, *113*, 878–886.
- [409] R. M. Meighan, R. H. Cole, *J. Phys. Chem.* **1964**, *68*, 503–508.
- [410] C. J. Helal, Z. Kang, X. Hou, J. Pandit, T. A. Chappie, J. M. Humphrey, E. S. Marr, K. F. Fennell, L. K. Chenard, C. Fox, et al., *J. Med. Chem.* **2011**, *54*, 4536–4547.
- [411] J. M. Sternberg, *Parasite Immunol.* **2004**, *26*, 469–476.
- [412] M. Wery, J. Burke, *Trans. R. Soc. Trop. Med. Hyg.* **1972**, *66*, 332–333.
- [413] V. Jamonneau, S. Ravel, A. Garcia, M. Koffi, P. Truc, C. Laveissière, S. Herder, P. Grébaud, G. Cuny, P. Solano, *Ann. Trop. Med. Parasitol.* **2004**, *98*, 329–337.
- [414] J. Lapierre, M. Coste, *Ann. Parasitol. Hum. comparée* **1963**, *38*, 757–782.
- [415] J. H. McKerrow, E. Sun, P. J. Rosenthal, J. Bouvier, *Annu. Rev. Microbiol.* **1993**, *47*, 821–853.

- [416] L. Redecke, K. Nass, D. P. DePonte, T. A. White, D. Rehders, A. Barty, F. Stellato, M. Liang, T. R. M. Barends, S. Boutet, et al., *Science* **2013**, 339, 227–230.
- [417] Z. B. Mackey, T. C. O'Brien, D. C. Greenbaum, R. B. Blank, J. H. McKerrow, *J. Biol. Chem.* **2004**, 279, 48426–48433.
- [418] C. R. Caffrey, E. Hansell, K. D. Lucas, L. S. Brinen, A. Alvarez Hernandez, J. Cheng, S. L. Gwaltney, W. R. Roush, Y.-D. Stierhof, M. Bogoyo, et al., *Mol. Biochem. Parasitol.* **2001**, 118, 61–73.
- [419] S. Scory, C. R. Caffrey, Y. D. Stierhof, A. Ruppel, D. Steverding, *Exp. Parasitol.* **1999**, 91, 327–333.
- [420] I. D. Kerr, P. Wu, R. Marion-Tsukamaki, Z. B. Mackey, L. S. Brinen, *PLoS Negl. Trop. Dis.* **2010**, 4, DOI: 10.1371/journal.pntd.0000701.
- [421] A. C. Storer, R. Ménard, *Perspect. Drug Discov. Des.* **1996**, 6, 33–46.
- [422] V. Ehmke, J. E. Q. Quinsaat, P. Rivera-Fuentes, C. Heindl, C. Freymond, M. Rottmann, R. Brun, T. Schirmeister, F. Diederich, *Org. Biomol. Chem.* **2012**, 10, 5764–5768.
- [423] V. Ehmke, C. Heindl, M. Rottmann, C. Freymond, W. B. Schweizer, R. Brun, A. Stich, T. Schirmeister, F. Diederich, *ChemMedChem* **2011**, 6, 273–278.
- [424] C. Grundmann, A. Kreuzberger, *J. Am. Chem. Soc.* **1955**, 77, 44–48.
- [425] A. Gulevskaya, B. Maes, C. Meyers, *Synlett* **2007**, 71–74.
- [426] V. N. Charushin, S. G. Alexeev, O. N. Chupahkin, H. C. Van Der Plas, *Advances in Heterocyclic Chemistry Volume 46*, Elsevier, **1989**.
- [427] A. Rykowski, D. Branowska, M. Makosza, P. Van Ly, *J. Heterocycl. Chem.* **1996**, 33, 1567–1571.
- [428] W. W. Paudler, T.-K. Chen, *J. Heterocycl. Chem.* **1970**, 7, 767–771.
- [429] C. Grundmann, *Angew. Chem. Int. Ed.* **1963**, 2, 309–323.
- [430] D. L. Boger, *Chem. Rev.* **1986**, 86, 781–793.
- [431] N. Saracoglu, *Tetrahedron* **2007**, 63, 4199–4236.
- [432] R. V Patel, Y.-S. Keum, S. W. Park, *Mini Rev. Med. Chem.* **2014**, 14, 768–789.
- [433] F. P. L. Lim, A. V Dolzhenko, *Eur. J. Med. Chem.* **2014**, 85, 371–390.

- [434] B. T. Mott, R. S. Ferreira, A. Simeonov, A. Jadhav, K. K.-H. H. Ang, W. Leister, M. Shen, J. T. Silveira, P. S. Doyle, M. R. Arkin, et al., *J. Med. Chem.* **2010**, *53*, 52–60.
- [435] C. A. M. Afonso, N. M. T. Lourenco, A. de A. Rosatella, *Molecules* **2006**, *11*, 81–102.
- [436] M. Cheung, A. Bloor, J. A. Stafford, *J. Org. Chem.* **2003**, *68*, 4093–4095.
- [437] J.-H. Sun, C. A. Teleha, J.-S. Yan, J. D. Rodgers, D. A. Nugiel, *J. Org. Chem.* **1997**, *62*, 5627–5629.
- [438] G. Luo, L. Chen, G. Dubowchik, *J. Org. Chem.* **2006**, *71*, 5392–5395.
- [439] F. Crestey, V. Collot, S. Stiebing, S. Rault, *Synthesis* **2006**, 3506–3514.
- [440] C. L. Habraken, P. Cohen-Fernandes, *J. Org. Chem.* **1971**, *36*, 3084–3086.
- [441] W. M. Welch, C. E. Hanau, W. M. Whalen, *Synthesis* **1992**, 937–939.
- [442] A. Bunnell, C. O'Yang, A. Petrica, M. J. Soth, *Synth. Commun.* **2006**, *36*, 285–293.
- [443] C. Rüchardt, V. Hassmann, *Liebigs Ann.* **1980**, 908–927.
- [444] T. Yoshida, N. Matsuura, K. Yamamoto, M. Doi, K. Shimada, T. Morie, S. Kato, *Heterocycles* **1996**, *43*, 2701–2712.
- [445] L. Baiocchi, G. Corsi, G. Palazzo, *Synthesis* **1978**, 633–648.
- [446] P. Jacobson, L. Huber, *Ber. Dtsch. Chem. Ges.* **1908**, *41*, 660–671.
- [447] R. A. Bartsch, I.-W. Yang, *J. Heterocycl. Chem.* **1984**, *21*, 1063–1064.
- [448] F. Crestey, V. Collot, S. Stiebing, S. Rault, *Tetrahedron* **2006**, *62*, 7772–7775.
- [449] F. Hervens, H. G. Viehe, *Angew. Chem. Int. Ed.* **1973**, *12*, 405–406.
- [450] Y. Shoji, Y. Hari, T. Aoyama, *Tetrahedron Lett.* **2004**, *45*, 1769–1771.
- [451] J. T. Thurston, J. R. Dudley, D. W. Kaiser, I. Hechenbleikner, F. C. Schaefer, D. Holm-Hansen, *J. Am. Chem. Soc.* **1951**, *73*, 2981–2983.
- [452] R. J. Sundberg, D. J. Dahlhausen, G. Manikumar, B. Mavunkel, A. Biswas, V. Srinivasan, F. King, P. Waid, *J. Heterocycl. Chem.* **1988**, *25*, 129–137.
- [453] O. Chavignon, J. C. Teulade, M. Madesclaire, A. Gueiffier, Y. Blache, H. Viols, J. P. Chapat, G. Dauphin, *J. Heterocycl. Chem.* **1992**, *29*, 691–697.
- [454] M. Murakami, M. Hajima, F. Takami, M. Yoshioka, *Heterocycles* **1990**, *31*, 2055–2064.

- [455] N. R. Cullum, A. H. M. Renfrew, D. Rettura, J. A. Taylor, J. M. J. Whitmore, A. Williams, *J. Am. Chem. Soc.* **1995**, *117*, 9200–9205.
- [456] J. Shakes, C. Raymond, D. Rettura, A. Williams, *J. Chem. Soc. Perkin Trans. 2* **1996**, 1553–1557.
- [457] S. Saure, *Chem. Ber.* **1950**, *83*, 335–340.
- [458] M. Coenen, *Liebigs Ann.* **1960**, *633*, 78–91.
- [459] A. H. Moustafa, S. A. El-Abbady, R. A. Jones, *J. Heterocycl. Chem.* **1981**, *18*, 1461–1463.
- [460] F. Brotzel, B. Kempf, T. Singer, H. Zipse, H. Mayr, *Chem. Eur. J.* **2007**, *13*, 336–345.
- [461] J. M. Andrés, R. Pedrosa, A. Pérez-Encabo, *Tetrahedron Lett.* **2006**, *47*, 5317–5320.
- [462] O. Diels, *Ber. Dtsch. Chem. Ges.* **1899**, *32*, 691–702.
- [463] S. Ludewig, M. Kossner, M. Schiller, K. Baumann, T. Schirmeister, *Curr. Top. Med. Chem.* **2010**, *10*, 368–382.
- [464] C. Chipot, R. Jaffe, B. Maigret, D. A. Pearlman, P. A. Kollman, *J. Am. Chem. Soc.* **1996**, *118*, 11217–11224.
- [465] F. L. Gervasio, R. Chelli, P. Procacci, V. Schettino, *J. Phys. Chem. A* **2002**, *106*, 2945–2948.
- [466] E. Fischer, J. Tafel, *Liebigs Ann.* **1885**, *227*, 303–340.
- [467] E. Georgarakis, H. Schmid, H.-J. Hansen, *Helv. Chim. Acta* **1979**, *62*, 234–270.
- [468] R. Blunt, A. J. Eatherton, V. Garzya, M. P. Healy, J. Myatt, R. A. Porter, *WO2011012622A1*, **2011**.
- [469] G. Anilkumar, S. B. Rosenblum, S. Venkatraman, F. G. Njoroge, J. A. Kozlowski, *WO2009032125A1*, **2009**.
- [470] Y. Rival, G. Grassy, G. Michel, *Chem. Pharm. Bull.* **1992**, *40*, 1170–1176.
- [471] H.-H. Perkampus, T. Bluhm, *Tetrahedron* **1972**, *28*, 2099–2110.
- [472] G. Heinisch, A. Mayrhofer, *Monatsh. Chem.* **1977**, *108*, 213–224.

4 Abbreviations

4-PDS	Di(4-pyridyl)disulfide
ACE	Angiotensin-I-converting Enzyme
ADAM	A Disintegrin And Metalloproteinase
AE	Acyl-Enzyme (intermediate)
AIBN	2,2'-Azobis(2-methylpropionitrile)
AIDS	Acquired Immunodeficiency Syndrome
APN	Aminopeptidase N
AT ₄	Angiotensin Receptor 4
ATR	Attenuated Total Reflectance
BMS	Bristol Myers Squibb
Boc	<i>tert</i> -Butyl-oxycarbonyl
CAM	Cerium Ammonium Molybdate
Cbz	Carboxybenzyl
CDI	1,1'-Carbonyldiimidazole
COSY	Correlation Spectroscopy
CPA	Carboxypeptidase A
DABCO	1,4-Diazabicyclo[2,2,2]octane
DCI	3,4-Dichloroisocoumarin
DCM	Dichloromethane

DFP	Diisopropylfluorophosphate
DIBAL-H	Diisobutylaluminium Hydride
DMAP	<i>N,N</i> -Dimethylaminopyridine
DMF	<i>N,N</i> -Dimethylformamide
DMSO	Dimethyl sulfoxide
DPP1	Dipeptidyl Peptidase-1
DPP3	Dipeptidyl Peptidase-3
DTNB	5,5'-Dithiobis-(2-nitrobenzoic acid) (Ellman's reagent)
ECM	Extracellular Matrix
EDTA	Ethylenediaminetetraacetic acid
ee	Enantiomeric Excess
EGTA	Ethyleneglycol-bis(2-aminoethylether)tetraacetic acid
EI	Electron Impact
EM-1	Endomorphin-1
EM-2	Endomorphin-2
EP	Enzyme-Product (complex)
ES	Enzyme-Substrate (complex)
ESI	Electrospray Ionization
Ets-1	E26 Transformation-specific (transcription factor)
EXSY	Exchange Spectroscopy
FDA	Food and Drug Administration
FID	Flame Ionization Detector

Fmoc	Fluorenylmethyloxycarbonyl
GC	Gas Chromatography
GLP-1	Glucagon-like Peptide-1
HATU	1-[Bis(dimethylamino)methylene]-1H-1,2,3-triazolo[4,5-b]pyridinium 3-oxid hexafluorophosphate
HBTU	2-(1 <i>H</i> -Benzotriazol-1-yl)-1,1,3,3-tetramethyluronium hexafluorophosphate
hCatL	Human Cathepsin L
hDPP3	Human Dipeptidyl Peptidase-3
HER	(<i>R</i>)-Hydroxyethylene Pseudopeptide
HFC	Human Fibroblast Collagenase
HFG	Human Fibroblast Gelatinase
HIV	Human Immunodeficiency Virus
HIV-1	Human Immunodeficiency Virus type 1
HMBC	Heteronuclear Multiple Bond Correlation
HNC	Human Neutrophil Collagenase
HOBt	1-Hydroxybenzotriazole
HPLC-MS	High Performance Liquid Chromatography – Mass Spectrometry
HR-EI-MS	High Resolution Electron Impact Mass Spectrometry
HR-ESI-MS	High Resolution Electrospray Ionization Mass Spectrometry
HR-MALDI-MS	High Resolution Matrix Assisted Laser Desorption Ionization Mass Spectrometry
HRMS	High Resolution Mass Spectrometry

HSQC	Heteronuclear Single Quantum Coherence
HTS	High Throughput Screening
ICE	Interleukin-1-beta Converting Enzyme
IMR 32	Human neuroblastoma cell line
IP	Intellectual Property
IR	Infrared
ITC	Isothermal Calorimetry
KEAP1	Kelch-like ECH-associated Protein 1
LDA	Lithium Diisopropylamide
LiHMDS	Lithium Hexamethyldisilazide
m.p.	Melting Point
MALDI	Matrix Assisted Laser Desorption Ionization
MMP	Matrix Metalloprotease
MP2	Møller-Plesset 2
MPLC	Medium Pressure Liquid Chromatography
MS	Multiple Sclerosis
MSD	Mass Selective Detector
MWD	Multiple Wavelength Detector
NBS	<i>N</i> -Bromosuccinimide
NCI	National Cancer Institute
NEM	<i>N</i> -Ethylmaleimide
NEP	Neutral Endopeptidase, Neprilysin

NMR	Nuclear Magnetic Resonance
NOE	Nuclear Overhauser Effect
Nrf2	Nuclear factor (erythroid-derived 2)-like 2
<i>p</i> CMB	<i>p</i> -Chloromercuribenzoic acid
<i>p</i> CMBS	<i>p</i> -Chloromercuribenzenesulfonic acid
PCMPS	<i>p</i> -Chloromercuriphenylsulfonic acid
<i>p</i> CMS	<i>p</i> -Chloromercuriphenylsulfate
PDB	Protein Data Bank
PDB	Protein Data Bank
<i>p</i> HMB	<i>p</i> -Hydroxymercuribenzoate
PMSF	Phenylmethanesulfonylfluoride
PPACK	D-Phenylalanylprolylarginylchloromethyl ketone
QED	Quantitative Estimate of Drug-Likeness
QM/MM	Quantum Mechanics/Molecular Mechanics
RGD	Arginine-Glycine-Aspartate
RP-HPLC	Reverse Phase High Performance Liquid Chromatography
RT	Room Temperature
SAR	Structure-activity Relationship
SARS	Severe Acute Respiratory Syndrome
SGPA	<i>Streptomyces griseus</i> protease A
SHE	(S)-Hydroxyethylene Pseudopeptide
tACE	Testicular Angiotensin-I-converting Enzyme

TbCatB	<i>Trypanosoma brucei</i> Cathepsin B
TBDPSCI	<i>tert</i> -Butyldiphenylsilyl Chloride
TBS	<i>tert</i> -Butyldimethylsilyl
TBSCI	<i>tert</i> -Butyldimethylsilyl Chloride
TBTU	2-(1 <i>H</i> -Benzotriazol-1-yl)-1,1,3,3-tetramethyluronium tetrafluoroborate
TFA	Trifluoroacetic Acid
THF	Tetrahydrofuran
TI	Transition Intermediate
TIMP	Tissue Inhibitor of Metalloproteinase
TIPSCI	Triisopropylsilyl Chloride
TLC	Thin Layer Chromatography
TOF	Time of Flight
TPCK	Tosylphenylalanylchloromethyl ketone
TS1	Transition State 1
TS2	Transition State 2
USD	United States Dollar
UV	Ultraviolet
UV	Ultraviolet
ZBF	Zinc-binding Function
β NA	β -Naphthylamide

5 Appendix

5.1 Bibliographic Data

This thesis contains 334 pages, 78 figures, 73 schemes, 19 tables and 472 references.

5.2 Curriculum Vitae

Jakov Ivković, born in Livno, Bosnia and Herzegovina, 13.02.1983

Professional experience

- 2014 (Jul – Dec)** *Research stay*
(ETH Zurich, Department of Chemistry and Applied Biosciences,
Laboratory of Organic Chemistry, Diederich Group, Zurich, Switzerland)
- 2011 – 2015** *PhD thesis* (PhD Program DK Molecular Enzymology, Graz University of
Technology, Institute of Organic Chemistry, Graz, Austria)
- 2011 (Apr – Aug)** *Research fellow* (Rudjer Boskovic Institute, Department of Organic
Chemistry and Biochemistry, Laboratory of Synthetic Organic Chemistry,
Zagreb, Croatia)
- 2009 – 2011** *R&D chemist* (Teva Pharmaceutical Industries Ltd., Pliva Croatia, TAPI
R&D, Zagreb, Croatia)

Education

- 2009 (Jan – Jul)** *Diploma thesis* (University of Zagreb, Faculty of Science, Department of
Chemistry, Zagreb, Croatia)
- 1998 – 2002** *High school* (V. Gimnazija, Zagreb, Croatia)

Awards

“Award for the Best Talk” at NAWI Graz Chemistry DocDays 2015.

Conferences and presentations

- “ISACS16 Challenges in Chemical Biology 2015“, ETH, Zurich, Switzerland, June 2015, poster presentation;
- “NAWI Graz Chemistry Doc Days 2015“, Graz, Austria, oral presentation;
- “Graduate Seminar 2014“, DK Molecular Enzymology, Graz, Austria, May 2014, oral presentation;
- “Austrian Peptide Symposium“, Graz University of Technology, Graz, Austria, December 2013, poster presentation;
- “ISACS11 Challenges in Chemical Biology 2013“, MIT, Boston, MA, USA, July 2013, poster presentation;
- “Enzymes and Signals“ joint research summit of the DK Molecular Enzymology (Graz) and the DK Molecular Mechanisms in Cell Signaling (Vienna), Graz, December 2012, oral presentation.

Memberships

Royal Society of Chemistry (since 2013)

Croatian Chemical Society (since 2002)

5.3 List of Publications

5. “A Rapid and Efficient One-pot Method for the Reduction of *N*-Protected α -Amino Acids to Chiral α -Amino Aldehydes Using CDI/DIBAL-*H*” J. Ivković, C. Lembacher-Fadum, R. Breinbauer, *Org. Biomol. Chem.* **2015**, *13*, 10456–10460.
4. “More Than Just a Halogenase: Modification of Fatty Acyl Moieties by a Trifunctional Metal Enzyme” S. M. Pratter, J. Ivković, R. Birner-Grünberger, R. Breinbauer, K. Zangger, G. Straganz, *ChemBioChem* **2014**, *15*, 567–574.
3. “Development of Small-molecule Inhibitors Targeting Adipose Triglyceride Lipase” N. Mayer, M. Schweiger, M. Romauch, G. F. Grabner, T. O. Eichmann, E. Fuchs, J. Ivković, C. Heier, I. Mrak, A. Lass, G. Höfler, C. Fledelius, R. Zechner, R. Zimmermann, R. Breinbauer, *Nat. Chem. Biol.* **2013**, *9*, 785–787.
2. “Excited State Intramolecular Proton Transfer (ESIPT) From Phenol to Carbon in Selected Phenyl-naphthols and Naphthylphenols” N. Basarić, N. Došlić, J. Ivković, Y. H. Wang, J. Veljković, K. Mlinarić-Majerski, P. Wan, *J. Org. Chem.* **2013**, *78*, 1811–1823.
1. “Very Efficient Generation of Quinone Methides Through Excited State Intramolecular Proton Transfer to a Carbon Atom” N. Basarić, N. Došlić, J. Ivković, Y. H. Wang, M. Mališ, P. Wan, *Chem. Eur. J.* **2012**, *18*, 10617–10623.